Climate Monitoring and Diagnostics Laboratory

No. 23

Summary Report 1994-1995

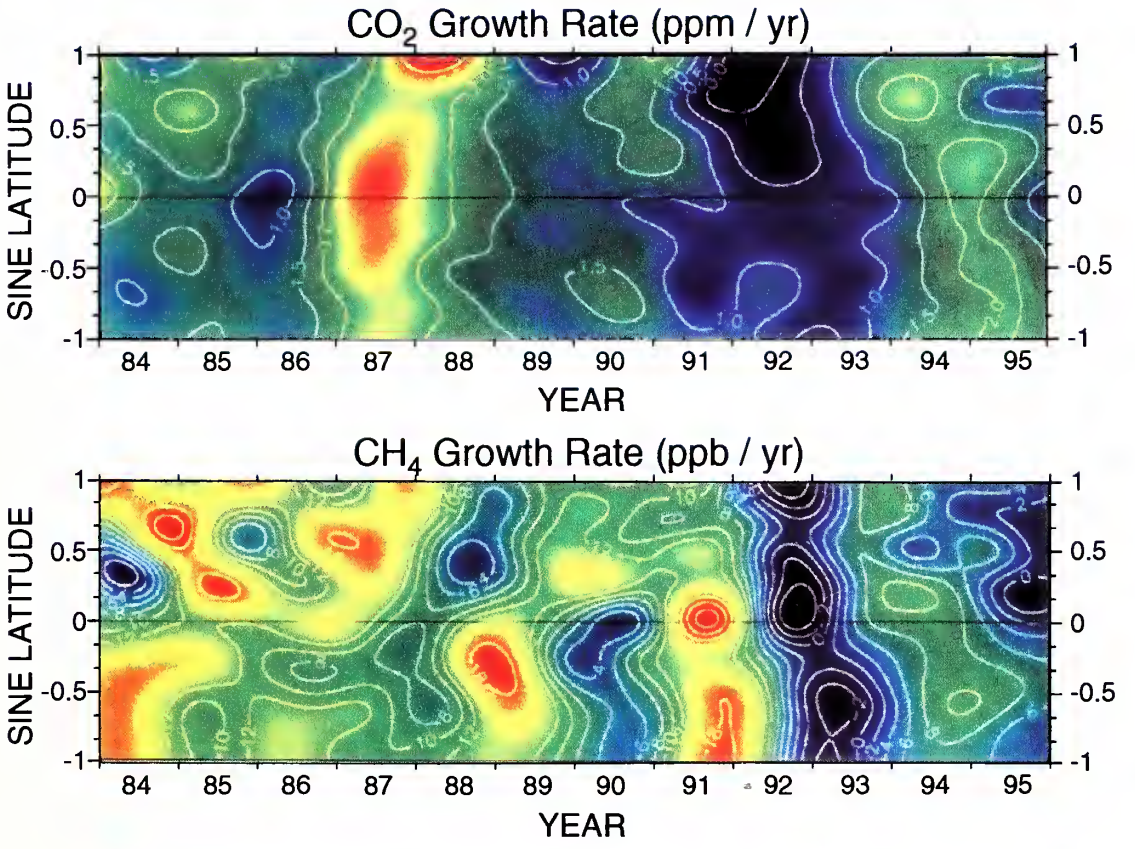

U.S. Department of Commerce
National Oceanic and Atmospheric Administration
Environmental Research Laboratories

Cover: Contour plots showing the temporal and spatial variations in the atmospheric increases of carbon dioxide (CO_2, upper panel) and methane (CH_4, lower panel). The cooler colors (blue, violet, black) represent periods of lower than average growth rates and the warmer colors (yellow, orange, red) represent high growth rate periods. These plots are derived from measurements of thousands of samples collected at the CMDL Cooperative Air Sampling Network sites. The variations in the growth rates of these climatically important gases are due to interannual variations in the imbalances between sources and sinks, and also to variations in atmospheric transport. Because the major sources and sinks for CO_2 and CH_4 are different, their patterns of growth rate variations are usually dissimilar. An exception to this is the period of low, and even negative growth rates of both gases in 1992-1993, a period when anomalous low temperatures were observed. These observations provide powerful constraints on attempts to model the global carbon cycle. [*This figure was created by Ken Masarie and Catherine McIntosh.*]

Climate Monitoring and Diagnostics Laboratory No. 23

Summary Report 1994-95

David J. Hofmann, Editor
James T. Peterson, Editor
Rita M. Rosson, Assistant Editor

Boulder, Colorado

September 1996

U.S. DEPARTMENT OF COMMERCE
Michael Kantor, Secretary

National Oceanic and Atmospheric Administration
D. James Baker, Under Secretary for Oceans and Atmosphere/Administrator

Environmental Research Laboratories
James L. Rasmussen, Director

NOTICE

Mention of a commercial company or product does not constitute an endorsement by NOAA Environmental Research Laboratories. Use for publicity or advertising purposes of information from this publication concerning proprietary products or the tests of such products is not authorized.

For sale by the National Technical Information Service, 5285 Port Royal Road
Springfield, VA 22161

Preface

The Climate Monitoring and Diagnostics Laboratory (CMDL) is located in Boulder, Colorado, with observatories in Barrow, Alaska; Mauna Loa, Hawaii; Cape Matatula, American Samoa; and South Pole, Antarctica. It is one of twelve components of the Environmental Research Laboratories (ERL) within the Office of Oceanic and Atmospheric Research (OAR) of the National Oceanic and Atmospheric Administration (NOAA). CMDL conducts research related to atmospheric constituents that are capable of forcing change in the climate of the earth through modification of the atmospheric radiative environment, for example greenhouse gases and aerosols, and those that may cause depletion of the global ozone layer.

This report is a summary of activities of CMDL for calendar years 1994 and 1995. It is the 23rd consecutive report issued by this organization and its Air Resources Laboratory/Geophysical Monitoring for Climatic Change predecessor since formation in 1972. From 1972 through 1993 (numbers 1 through 22), reports were issued annually. However, with this issue we begin a 2-year reporting cycle, which stems from a need to most efficiently use the time and financial resources of our staff and laboratory and from a general trend towards electronic media. In this respect, CMDL has developed a comprehensive internet home page during the past 2 years. There you will find information about our major groups and observatories, latest events and press releases, publications, data availability, and personnel. Numerous data graphs and ftp data files are available. The URL address is http://www.cmdl.noaa.gov. Information (program descriptions, accomplishments, publications, plans, data access, etc.) on CMDL parent organizations can best be obtained via the internet. Their URL addresses are ERL: http://www.erl.noaa.gov; OAR: http://www.oar.noaa.gov; NOAA: http://www.noaa.gov.

In 1995, Eldon Ferguson retired from federal service and from the CMDL Director's position that he held from the formation of the Laboratory in 1990. On a personal note, we extend to him our best wishes for the future and our thanks for scientific guidance and direction in the past. In 1996, David Hofmann, the CMDL Chief Scientist since 1990, was appointed Director of CMDL.

This report is organized into the following major sections:

1. Observatory, Meteorology, and Data Management
2. Carbon Cycle
3. Aerosols and Radiation
4. Ozone and Water Vapor
5. Nitrous Oxide and Halocompounds
6. Cooperative Programs

These are followed by a list of CMDL staff publications for 1994-1995.

Inquiries and/or comments are welcomed and should be addressed to:

Director, R/E/CG
NOAA/Climate Monitoring and Diagnostics Laboratory
325 Broadway
Boulder, CO 80303-3328
(303) 497-6074
e-mail: hofmann@cmdl.noaa.gov

Eldon E. Ferguson, Climate Monitoring and Diagnostics Laboratory Director, 1990-1995.

Contents

Preface iii
CMDL Organization, 1995 ix
CMDL Staff, 1995 x
CMDL Station Information xi

1. Observatory, Meteorology, and Data Management Operations 1
   1.1. Mauna Loa Observatory 1
      1.1.1. Operations 1
      1.1.2. Programs 2
   1.2. Barrow Observatory 9
      1.2.1. Operations 9
      1.2.2. Programs 9
   1.3. Samoa Observatory 12
      1.3.1. Operations 12
      1.3.2. Programs 12
   1.4. South Pole Observatory 14
      1.4.1. Operations 15
      1.4.2. Programs 14
   1.5. Meteorological Measurements 17
      1.5.1. Station Climatologies 17
      1.5.2. Meteorology Operations 24
   1.6. Data Management 26
   1.7. References 28

2. Carbon Cycle 29
   2.1. Overview 29
   2.2. Carbon Dioxide 29
      2.2.1. In Situ Carbon Dioxide Measurements 29
      2.2.2. Flask Sample Carbon Dioxide Measurements 30
      2.2.3. Carbon Dioxide Reference Gas Calibrations 31
      2.2.4. Measurements of Stable Isotopes of CO_2 33
      2.2.5. The Airkit Sampler 34
      2.2.6. Calibration of Measurements of Stable Isotopes of CO_2 34
   2.3. Methane 35
      2.3.1. In Situ Methane Measurements 35
      2.3.2. Discrete Sample Measurements of Methane 37
      2.3.3. Measurement of $^{13}C/^{12}C$ of Methane 39
   2.4. Carbon Monoxide 39
      2.4.1. In Situ Carbon Monoxide Measurements 39
      2.4.2. Flask Measurements of Carbon Monoxide 40
      2.4.3. The MAPS Program 42
      2.4.4. Carbon Monoxide Standards 42
   2.5. Flask Measurements of SF_6/N_2O 42
   2.6. Measurements on Tall Towers 43
   2.7. Automated Aircraft Sampling 45
   2.8. Data Management 47
   2.9. Data Integration 47
   2.10. Three-Dimensional Inverse Modeling 47
   2.11. References 48

3. Aerosols and Radiation 50
3.1. Aerosol Monitoring 50
3.1.1. Scientific Background 50
3.1.2. Experimental Methods 50
3.1.3. Annual Cycles 51
3.1.4. Long-Term Trends 53
3.1.5. Results From 1994-1995 53
3.1.6. Aircraft Observations 56
3.1.7. Lidar Measurements at Mauna Loa 59
3.2. Solar and Thermal Atmospheric Radiation 60
3.2.1. Baseline Monitoring Activities 60
3.2.2. Solar Radiation Calibration Facility 62
3.2.3. Aerosol Optical Depth Remote Sensing 62
3.2.4. Mauna Loa UV Spectroradiometer 63
3.2.5. MLO Broadband UV 65
3.2.6. BSRN 65
3.2.7. WMO GAW Stations 65
3.2.8. Volcanic Radiative Fording and Induced Global Cooling 65
3.2.9. BRW Surface Radiation and Meteorological Measurements 66
3.3. References 67

4. Ozone and Water Vapor 69
4.1. Continuing Programs 69
4.1.1. Total Ozone Observations 69
4.1.2. Umkehrs 70
4.1.3. Surface and Tropospheric Ozone 71
4.1.4. Ozonesondes 74
4.1.5. Atmospheric Water Vapor 76
4.1.6. Atmospheric Transport 76
4.2. Special Projects 77
4.2.1. The Mauna Loa Ozone Profile Intercomparison 77
4.2.2. Ozone Vertical Profiles Over the North Atlantic 77
4.2.3. Water Vapor and Ozone Profiles at McMurdo, Antarctica 78
4.2.4. Flow Patterns for SMO Described with Clustered Trajectories 80
4.3. References 82

5. Nitrous Oxide and Halocompounds 84
5.1. Continuing Programs 84
5.1.1. Introduction 84
5.1.2. Flask Samples 84
5.1.3. RITS Continuous Gas Chromatograph Systems 87
5.1.4. LEAPS 89
5.1.5. Chlorofluorocarbon Alternative Measurements Program 90
5.1.6. Gravimetric Standards 95
5.2. Aircraft GC Project: SHOE/MAESA Mission 96
5.2.1. Overview 96
5.2.2. Transport in the Lower Stratosphere 96
5.2.3. Bromine Budget 99
5.3. LACE 101
5.4. Ocean Project: BLAST Cruises 101
5.5. STEALTH Project: Automated Four-Channel Field Gas Chromatographs 103
5.5.1. Overview 103
5.5.2. Tower GC at WITN in Cooperation with CCG 104

5.6. Measurement of Air From South Pole Firn 105
5.7. References 109

6. Cooperative Programs 112
Evaluation of Arctic Meteorological Buoys
G.F. Appell 112
Asian Transport of Aerosols to Mauna Loa Observatory, Spring 1994
T.A. Cahill and K.D. Perry 114
Ultrahigh Resolution Infrared Solar Spectra From Mauna Loa Observatory: New Results
S.J. David, F.J. Murcray, A. Goldman, and R.D. Blatherwick 117
A Preliminary Comparison of $\delta^{13}C$ Measurements in CO_2 From Mace Head, Ireland
A. Gaudry, P. Monfray, M. Trolier, C. Flehoc, P. Ciais, and S.G. Jennings 119
Measurement of Short Period Magnetic Pulsations at Barrow: A Key Location in the STEP Polar Network
K. Hayashi 122
Total Nitrate Variation at Mauna Loa
B.J. Huebert and L. Zhuang 123
Radionuclides in Surface Air at BRW, MLO, SMO, and SPO During 1994 and 1995
J. Kada and C.G. Sanderson 126
Global Distribution of Chloroform in the Marine Boundary Layer
M.A.K. Khalil and R.A. Rasmussen 128
NSWC Pt. Barrow Geomagnetic Observatory
D.S. Lenko, J.F. Scarzello, and D. Taylor 130
Exposure Experiment, South Pole
J.E. Mak, C.A.M. Brenninkmeijer, and J.R. Southon 131
Investigation of the Transfer Function Between Snow and Atmosphere Concentrations of Hydrogen Peroxide at South Pole
J.R. McConnell and R.C. Bales 132
NDSC Stratospheric Ozone-Temperature-Aerosol Lidar
I.S. McDermid, E.W. Sirko, and T.D. Walsh 134
Antarctic UV Spectroradiometer Monitoring Program: Contrasts in UV Irradiance at the South Pole and Barrow, Alaska
T. Mestechkina, C.R. Booth, J.R. Tusson IV, and J.C. Ehramjian 135
Gamma Radionuclide Deposition at SMO During Recent French Nuclear Weapons Testing on South Pacific Atolls
M. Monetti 138
Early Morning UV-B During the 1994-1995 Record Low Ozone at Mauna Loa
P.J. Neale, D.L. Correll, V.R. Goodrich, and D.R. Hayes, Jr. 140
Advanced Global Atmospheric Gases Experiment (AGAGE)
R.G. Prinn, R.F. Weiss, F.N. Alyea, D.M. Cunnold, P.J. Fraser, L.P. Steele, and P.G. Simonds 142
The $^{13}C/^{12}C$ of Atmospheric Methane
P. Quay, J. Stutsman, and D. Wilbur 144
Aerosol Measurements on American Samoa
D.L. Savoie and J.M. Prospero 146
An Operational Intercalibration Experiment Between CMDL and CSIRO to Measure Several Atmospheric Trace Species
L.P. Steele, R.J. Francey, R.L. Langenfelds, C.E. Allison, M.P. Lucarelli, P.P. Tans, E.J. Dlugokencky, T.J. Conway, P.C. Novelli, K.A. Masarie, J.W.C. White, and M. Trolier 148
USGS Barrow Observatory
J. Townshend 150

The New ANSTO Radon Detector at MLO
S. Whittlestone 151
A comparison of CO_2 and $^{13}/^{12}C$ Seasonal Amplitudes in the Northern Hemisphere
T.P. Whorf, C.D. Keeling, and M. Wahlen 153

7. Publications and Presentations by CMDL Staff, 1994-1995 157

CMDL Organization, 1995

The CMDL organization structure features five research areas organized according to scientific discipline as follows: (1) Carbon Cycle; (2) Nitrous Oxide and Halocompounds; (3) Ozone and Water Vapor; (4) Aerosols and Radiation; and (5) Observatory Operations. At the end of 1995, the laboratory staff consisted of 46 civil service personnel (excluding part-time student assistants), 34 CIRES/University of Colorado personnel, and two NOAA Corps officers as well as several visitors and people on special appointments.

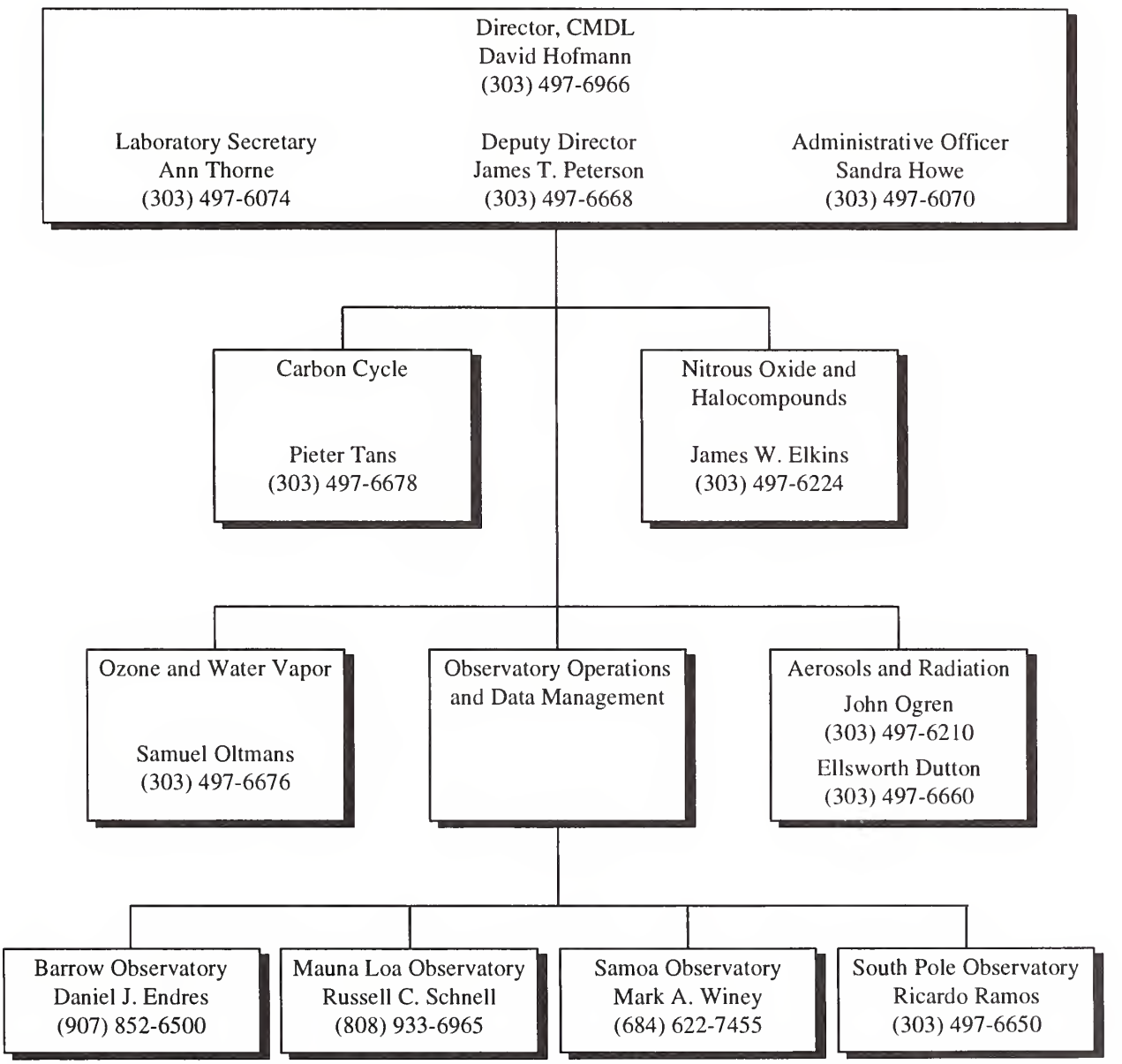

CMDL Staff, 1995

Director's Office

David Hofmann, Director
James T. Peterson, Deputy Director
Sandra Howe, Administrative Officer
Ann Thorne, Secretary
Rita Rosson, Editorial Assistant
Denise Theede, Program Support Technician
Kay Villars, Administrative Assistant

Special Projects

Mark Bieniulis, CIRES
Bradley Halter, CIRES
Thomas Mefford, CIRES
Kenneth Thaut, Electronic Technician
Patrick Sheridan, CIRES
Eldon Ferguson, Guest Scientist

Aerosols and Radiation Division

Ellsworth Dutton, Meteorologist
John Ogren, Physical Scientist
Jill Foose, Secretary
Sharon Anthony, CIRES
Michael Bergin, DOE Post Doc.
Barry Bodhaine, Meteorologist
Paul Breding, CIRES
Rudy Haas, Mathematician
Wen Huang, Physical Science Aid
Thomas Kotsines, Engineering Technician
David Longenecker, CIRES
Lynn McInnes, NRC Post Doc.
Brian Mohr, CCHE Intern
Charles Myers, Engineering Aid
Donald Nelson, Meteorologist
James Rattling Leaf, AISES Intern
Jay Shah, CIRES
Herman Sievering, Guest Worker
Ryan Spackman, CIRES
Robert Stone, CIRES
Shad Thaxton, CIRES
James Wendell, Electronic Technician
Brett Wightman, Physical Science Aid

Ozone and Water Vapor Division

Samuel Oltmans, Physicist
Jill Foose, Secretary
Kirsten Borbe, CIRES
Mark Clark, CIRES
Robert Evans, CIRES
Eric Hackathorn, Engineering Aid
Joyce Harris, Physical Scientist
Bryan Johnson, CIRES
Gloria Koenig, Physical Scientist
Walter Komhyr, CIRES
Jeffrey Lathrop, Physical Scientist
Micheal O'Neill, CIRES
Dorothy Quincy, CIRES
Holger Vömel, CIRES
Byron Wells, Physical Science Aid

Carbon Cycle Division

Pieter Tans, Chief
Debra Hansen , Secretary
Peter Bakwin, Physicist
Thomas Conway, Research Chemist
Wyatt Coy, CIRES
Richard Dissly, NRC Post Doc.
Ed Dlugokencky, Research Chemist
Scott Durelle, CCHE Intern
James Frelinger, Engineering Aid
Laurie Geller, CIRES Student
Douglas Guenther, CIRES
Michael Hahn, Physical Science Aid
Duane Kitzis, CIRES
Patricia Lang, Physical Scientist
Kenneth Masarie, CIRES
John Miller, CIRES
Paul Novelli, Res. Chemist
Constance Prostko-Bell, CIRES
Michel Ramonet, Guest Scientist
Kirk Thoning, Physicist
Tom Treloar, CIRES
Michael Trolier, INSTAAR
Lee Waterman, Research Chemist
Ni Zhang, CIRES
Conglong Zhao, CIRES

Nitrous Oxide and Halocarbons Division

James Elkins, Chief
Debra Hansen, Secretary
Thomas Baring, CIRES
James Butler, Research Chemist
Andrew Clarke, CIRES
Nicholas Condon, CIRES
Matthew Dicorleto, CIRES
Raymond Dunn, CIRES
Geoffrey Dutton, CIRES
Arnold Hayden, CIRES
Dale Hurst, NRC Associate
Bryan Jordan, C.U. Work Study
Frank Lee, AISES Intern
Jürgen Lobert, CIRES
Loreen Lock, C.U. Work Study
Michele McCarthy, C.U. Work Study
Lynn McInnes, NRC Post Doc.
Fred Moore, CIRES
Richard Myers, Physical Science Technician
Michael Perry, C.U. Work Study
Robin Sam, CIRES
Thomas Swanson, CIRES
Thayne Thompson, Physicist
Michael Volk, CIRES
Shari Yvon, DOE Post Doc

Observatory Operations Division

Bernard Mendonca, Chief
Linda Sachetti, Secretary

Daniel Endres, Station Chief, **Barrow**
Malcom Gaylord, Electronic Engineer

Russell Schnell, Director, **Mauna Loa**
Judith Pereira, Program Support Technician
John Barns, Physical Scientist
John Chin, Physicist
Darryl Kuniyuki, Electronic Engineer
Leslie Pajo, Data Clark
Steven Ryan, Physical Scientist
Robert Uchida, Electronic Technician
Alice Wall, Physical Science Aid
Alan Yoshinaga, Chemist

Mark Winey, Station Chief, **Samoa**
Alexis Brown, Environmental Engineer
Gerald Yung, Elect. Engineer

Ricardo Ramos, NOAA Corps, **South Pole**
Jeffrey Otten, Engineering Technician
Thomas Jacobs, NOAA Corps
Katherine, McNitt, NOAA Corps

CMDL Station Information

Name:	**Barrow (BRW)**	**Mauna Loa (MLO)**
Latitude:	71.323	19.539
Longitude:	156.609	155.578
Elevation:	8 m	3397 m
Time Zone:	GMT -9	GMT -10
Office Hours:	8:00 am-5:00 pm	8:00 am-5:00 pm
Telephone		
Office hours:	(907) 852-6500	(808) 961-3788
Fax:	(907) 852-4622	(808) 961-3789
Postal Address:	Officer in Charge NOAA/ERL/CMDL Pouch 8888 Barrow, AK 99723	U.S. Dept. of Commerce NOAA - Mauna Loa Observatory P.O. Box 275 Hilo, Hl 96720
Freight Address:	Same as above	U.S. Dept. of Commerce NOAA - Mauna Loa Observatory 154 Waianuenue Ave. Hilo, Hl 96720

Name:	**Samoa (SMO)**	**South Pole (SPO)**
Latitude:	-14.232	-89.997
Longitude:	170.563	-102.0
Elevation:	77 m	2841 m
Time Zone:	GMT -11	GMT +12
Office Hours:	8:00 am-5:00 pm	8:00 am - 5:00 pm
Telephone:		
Office hours:	011 (684) 622-7455	Relayed through CMDL Boulder
After hours:	011 (684) 699-9953	
Fax:	011 (684) 699-4440	
Postal Address:	U.S. Dept. of Commerce NOAA - CMDL Samoa Observatory P.O. Box 2568 Pago Pago, American Samoa 96799	Officer in Charge NOAA/CMDL Clean Air Facility S-257 South Pole, Antarctica PSC 468 Box 402 FPO AP 96598-5402
Freight Address:	Same as above	Same as above

1. Observatory, Meteorology, and Data Management Operations

1.1. Mauna Loa Observatory

R. C. Schnell and the MLO Staff

1.1.1. Operations

Mauna Loa Observatory (MLO) continues to evolve in the scope of the measurements conducted, the way in which data are recorded and transmitted, and the number and form of the buildings on the site. With installation of the majority of the Network for the Detection of Stratospheric Change (NDSC) instrumentation completed at MLO, remote monitoring of stratospheric ozone concentrations, temperatures, and water vapor has become routine. At the surface, ultraviolet (UV) radiation is now monitored in a program that is designed and operated in a manner to set the world standard. Over the past 2 years essentially all the instruments of the core MLO continuous measurement programs, as well as the NDSC instruments, were connected to the Internet. In a number of cases these instruments are controlled and adjusted from locations other than Hawaii.

Four new structures have been added to the MLO site over the past 2 years: a 3.7 m × 7.3 m building for the microwave ozone and microwave water vapor instruments, a similar building to accommodate visitors and their programs, a 3.7 m × 4.9 m tank storage building appended to the main observatory, and the Global Oscillation Network Group (GONG) 2.4 m × 6 m instrumented container. The GONG program, operated by the University of Arizona on space at MLO, is a study of the sun's core. The old Atomic Energy Commission (AEC) building was refurbished and a roof catchment water supply and a sink added.

A new Network for the Detection of Stratospheric Change (NDSC) building, which was to be erected on the 4-acre (16,187 m^2) parcel to the east of the main MLO site, has been scaled back to a smaller structure to be erected south of the main observatory building. If all goes to plan, this 306.6 m^2 building will be completed by December 1996.

At the Hilo facility, the refurbishing of the electronics shop and the addition of air conditioning to the room were major improvements as was the addition of an elevator linking the basement to the rest of the building. Installation of the FTS2000 telephone system in the Hilo offices with connections to the MLO site has reduced monthly telephone costs and expanded the number of lines available. MLO and cooperative/visitor programs now use 29 telephone lines in addition to the Internet. A note on Hilo's rain: Although Hilo has a reputation for having a lot of rain, in 1995 it had 2.5 m less than in 1994. But 1994 was a special year. On one day in August at sea level, Hilo had 45 cm of rain in 8 hours (greater amounts fell at higher elevations). In September, it had 50 cm in 7 hours.

At the Cape Kumukahi, Hawaii (KUM) site, grid electric power was added to the tower, with a distribution panel providing 110 V, 220 V and recreational vehicle (RV) circuits. A 15 m × 15 m area was graded, filled, and security fenced to provide a site for mobile trailers and vans for future short-term research projects. The KUM tower now has four air sample lines running from near the top (18 m) to the base. Two of these lines are used for weekly trace gas and oxygen flask sampling and are purged continuously. No aerosol or radiation measurements are conducted at KUM at present.

The largest nonroutine research activity of the past 2 years was the Mauna Loa Ozone Profile Intercomparison (MLO3) program, summer 1995, in which various NDSC ozone-profiling instruments were intercompared. Preparations for the program included the construction of a building to house the University of Massachusetts Millitech microwave ozone profiler; installation of the NOAA/NIWA multispectra, UV radiometer system; and preparation of a pad area for two 16.7 m-long National Aeronautics and Space Administration/Goddard Space Flight Center (NASA/GSFC) ozone lidar trailers. The Jet Propulsion Laboratories (JPL) ozone lidar, also part of the study, had been in full operation at MLO for more than a year prior to the intercomparison. World standard Dobson no. 83, secondary standard no. 65, and the MLO station Dobson were operated prior to, and during, the intercomparison. During a 3-week intensive study period in August, daily ozonesonde launches were conducted from Hilo. Some balloons carried three ozonesondes to determine the variability between instruments.

Ancillary MLO3 measurements included aerosol/temperature profiles with the NOAA lidars, infrared multispectral measurements with the University of Denver Fourier Transform Interferometer (FTIR) spectrometer, and twice-daily measurements from radiosondes launched from Hilo. A number of passes of a satellite carrying aerosol and ozone measurement instruments occurred during the intensive study period.

In the staff arena, an MLO physical scientist spent from June to December 1994 at the Australian Baseline Station, Cape Grim, Tasmania, in an exchange with the Technical Officer from Cape Grim. All parties concerned, and their families, found the experience to be beneficial. The Technical Officer helped improve the MLO sulfate (SO_2) measurement program and quickly became a valued member of the MLO mountain crew. MLO recommends similar exchanges in the future. A staff member new to MLO in January 1995 has responsibilities for managing data flow and data archiving, and has rapidly become a valued addition and a capable computer operator.

In May 1994, a motorcyclist was killed during a race on the MLO road when his brakes locked and he missed a turn in the road. This event, and the fact that the organizer of the weekly commercial bike rides down MLO was also killed in an unrelated bicycle accident in Kona, have dramatically reduced bicycle traffic on the MLO road.

MLO was host to about 960 visitors in 1994-1995. Countries represented were from Japan, China, Canada, Germany, Burkina-Faso, Switzerland, France, Togo, Australia, Brazil, Russia, Iran, England, Denmark, Samoa, Mexico, Singapore, Italy, Holland, New Zealand, Norway, and Sweden. These visitors were in addition to guests from 21 states. Most of these visitors were given a guided tour and many left with at least one color reprint of the most up-to-date CMDL data plots MLO had available.

Visitors to MLO from NOAA's higher level administrative community included the NOAA Administrator; NOAA Deputy Under Secretary; NOAA Associate Under Secretary; Director, Sustainable Development and Intergovernmental Affairs; outgoing Deputy Director, Environmental Research Laboratories (ERL); newly appointed Deputy Director, ERL; and Director, Oceans and Atmospheric Research Programs Office.

Mauna Loa Mountain is still inflating and carbon dioxide (CO_2) gas releases from the summit caldera persist which means that an eruption may occur within a few years. Therefore, an escape plan and an equipment removal list have been drawn up. In essence, most equipment valued over $10,000 per item will be removed when it is predicted that lava will inundate MLO within 12 hours.

1.1.2. PROGRAMS

Table 1.1 summarizes the programs in operation or terminated at MLO during 1994-1995. Relevant details of note on the respective programs are as follows:

Carbon Dioxide

The CMDL Siemens Ultramat-3 infrared (IR) CO_2 analyzer and the Scripps Institution of Oceanography (SIO) Applied Physics IR CO_2 analyzer were operated in parallel without major problems throughout 1994 and 1995. Routine maintenance and calibrations were undertaken on both instruments as scheduled. An electronic engineer from SIO upgraded the SIO CO_2 data acquisition system in 1994. Data are now recorded on a Brown strip chart recorder and stored on a personal computer (PC) hard disk and a floppy disk, which are mailed to SIO weekly. The CMDL CO_2 data acquisition system was modified on November 28, 1995, through the replacement of the original Control and Monitoring System (CAMS) data logger with a Unix CMDL Carbon Cycle Group (CCG) system connected to the Internet. Through computers in Boulder and in Hilo operators are able to monitor operation of the CO_2 analyzer and plot CO_2 concentrations in near-real time. The CCG has the capability of modifying the CO_2 measurement control software from Boulder. The venerable CO_2 strip chart recorder is now used only for viewing the weekly standard gas calibrations and weekly maintenance procedures.

Outgassing from the volcanic vents at the Mauna Loa caldera and along the northeast rift zone at Mauna Loa continued to cause periodic observable disturbances in some of the CO_2 data records. As in prior years, these venting events occurred mostly between midnight and 0800 (local standard time (LST) of the following day, during the downslope wind regime. The erratic CO_2 concentration data resulting from these venting events were easily identified by visually scanning chart records or by utilizing a computerized data screening procedure, and thus they have been separated from the clean-air record without difficulty. Such venting episodes were detected mainly on the basis of criteria for CO_2 concentration,

TABLE 1.1. Summary of Measurement Programs at MLO in 1994-1995

Program	Instrument	Sampling Frequency
Gases		
CO_2	Siemens Ultramat-3 IR analyzer†	Continuous
	0.5-L glass flasks, through analyzer	1 pair wk^{-1}
CO	Trace Analytical RGA3 reduction gas analyzer no. R5†	Continuous
CO_2, CH_4, CO, ^{13}C, ^{18}O of CO_2	2.5-L glass flasks, MAKS pump unit*	1 pair wk^{-1}
	3-L evacuated glass flasks‡	1 pair wk^{-1}
CH_4	Carle automated GC no. 6 (removed 11/95)	1 sample $(24\ min)^{-1}$
	HP6890GC† (began 11/95)	Continuous
	AIRKIT pump unit, 2.5-L glass flasks‡ (began 5/95)	1 pair wk^{-1}
SO_2	TECO model 435 pulsed-florescence analyzer† (began 6/94)	Continuous

TABLE 1.1. Summary of Measurement Programs at MLO in 1994-1995—Continued

Program	Instrument	Sampling Frequency
Gases - Continued		
Surface O_3	Dasibi ozone meter†	Continuous
Total O_3	Dobson spectrophotometer no. 76†	3 day^{-1}, weekdays
O_3 profiles	Dobson spectrophotometer no. 76† (automated Umkehr method)	2 day^{-1}
	Balloonborne ECC sonde	1 wk^{-1}
N_2O, CFC-11, CFC-12, CFC-113, CH_3CCl_3, CCl_4	300-mL stainless steel flasks	1 sample wk^{-1}
N_2O, CFC-11, CFC-12, CFC-113, CH_3CCl_3, CCl_4, SF_6, HCFC-22, HCFC-141b, HCFC-142b, CH_3Br, CH_3Cl, CH_2Cl_2, $CHCl_3$, C_2HCl_3, C_2Cl_4, H-1301, H-1211, H-2402, HFC-134a	850-mL stainless steel flasks	1 sample wk^{-1}
CFC-11, CFC-12, CFC-113, N_2O, CCl_4, CH_3CCl_3	HP5890 automated GC†	1 sample h^{-1}
N_2O	Shimadzu automated GC†	1 sample h^{-1}
Radon	Two-filter system	Continuous integrated 30-min samples
Aerosols		
Condensation nuclei	Pollak CNC	1 day^{-1}
	TSI CNC†	Continuous
Optical properties	Four-wavelength nephelometer†: 450, 550, 700, 850 nm three-wavelength nephelometer: 450, 550, 700 nm	Continuous
Aerosol light absorption (black carbon)	Aethalometer†	Continuous
Stratospheric and upper tropospheric aerosols	Lidar: 694.3 nm, 532 nm†	1 profile wk^{-1}
Solar Radiation		
Global irradiance	Eppley pyranometers with Q, OG1, and RG8 filters†	Continuous
Direct irradiance	Eppley pyrheliometer with Q filter†	Continuous
	Eppley pyrheliometer with RG8 filter†	
	Eppley pyrheliometer with Q, OG1, RG2, and RG8 filters†	3 day^{-1}
	Eppley/Kendall active cavity radiometer†	1 mo^{-1}
Diffuse irradiance	Eppley pyrgeometer with shading disk and Q filter†	Continuous
UV solar radiation	Yankee Environmental UVB pyranometer (280-320 nm)†	Continuous
Terrestrial (IR) radiation	Global downwelling IR pyrgeometer†	Continuous
Turbidity	J-202 and J-314 sunphotometers with 380-, 500-, 778-, 862 nm narrowband filters	3 day^{-1}, weekdays
	PMOD three-wavelength sunphotometer†: 380, 500, 778 nm; narrowband	Continuous
Column water vapor	Two wavelength tracking sunphotometer: 860, 940 nm†	Continuous
Meteorology		
Air temperature	Aspirated thermistor, 2-, 9-, 37-m heights†	Continuous
	Max.-min. thermometers, 2-m height	1 day^{-1}
Air temperature (30-70 KM)	Lidar	1 profile wk^{-1}
Temperature gradient	Aspirated thermistors, 2-, 9-, 37-m heights†	Continuous
Dewpoint temperature	Dewpoint hygrometer, 2-m height†	Continuous
Relative humidity	TSL 2-m height†	Continuous
Pressure	Capacitance transducer†	Continuous
	Mercurial barometer	5 wk^{-1}

TABLE 1.1. Summary of Measurement Programs at MLO in 1994-1995—Continued

Program	Instrument	Sampling Frequency
Meteorology - Continued		
Wind (speed and direction)	8.5-, 10-, and 38-m heights†	Continuous
Precipitation	Rain gauge, 20-cm	5 wk^{-1}
	Rain gauge, 20-cm§	1 wk^{-1}
	Rain gauge, tipping bucket†	Continuous
Total precipitable water	Foskett IR hygrometer†	Continuous
Precipitation Chemistry		
pH	pH meter	wk^{-1}
Conductivity	Conductivity bridge	wk^{-1}
Cooperative Programs		
CO_2 (SIO)	Applied Physics IR analyzer†	Continuous
CO_2, ^{13}C, N_2O (SIO)	5-L evacuated glass flasks*	1 pair wk^{-1}
CO_2, CO, CH_4, $^{13}C/^{12}C$ (CSIRO)	Pressurized glass flask sample	1 mo^{-1}
CH_4, CH_3CCl_3, CH_3Cl, F-22, F-12, F-11, F-113, CO, CO_2, N_2O, $CHCl_3$, CCl_4 (OGIST)	Pressurized stainless steel flasks*	3 wk^{-1}
O_2 analyses (SIO)	5-L glass flasks through tower line and pump unit*	3 $(2\ mo)^{-1}$
O_2 analyses (URI)	3-L glass flasks through tower line and pump unit	2 $(2\ mo)^{-1}$
CH_4 ($^{13}C/^{12}C$) (Univ. of Washington)	35-L evacuated flask	2 mo^{-1}
Total suspended particulates (DOE)	High-volume sampler	Continuous (1 filter wk^{-1})
Ultraviolet radiation (Smithsonian)	Eight-wavelength UV radiometer: 290-325 nm; narrowband	Continuous
Ultraviolet radiation (Univ. of Hawaii)	Robertson-Berger UV radiometer (erythema)†	Continuous
Solar aureole intensity (CSU)	Multi-aperture tracking photometer: 2, 5, 10, 20, 30° fields of view (discontinued 9/94)	Continuous
Precipitation collection (DOE)	Exposed collection pails	Integrated monthly sample
Aerosol chemistry (Univ. of Calif.-Davis)	Programmed filter sampler	Integrated 3-day sample, 1 continuous and 1 downslope sample $(3\ days)^{-1}$
Sulfate, nitrate, aerosols (Univ. of Hawaii)	Filter system	Daily, 2000-0600 LST
Radon (ANSTO)	Aerosol scavenging of Rn daughters† (2-filter system after 4/95)	Continuous; integrated 30-min samples
Network for Detection of Stratospheric Change (NDSC)		
Ultraviolet radiation (NOAA and NIWA, New Zealand)	UV spectrometer (290-450 nm), 1 nm resolution†	Continuous
Stratospheric ozone profile, 20-70 km (Univ. of Mass, Amherst)	Microwave spectroscopy, Millitech Corp, 110.8 GH_z	3 profiles h^{-1}
Stratospheric ozone profiles (15-55 km), temperature (15-80 km), aerosol profiles (15-40 km) (JPL)	UV lidar†	3-4 profiles/wk^{-1}
Solar spectra (Univ. of Denver)	FTIR spectrometer, automated†	5 wk^{-1}

All instruments are at MLO unless indicated.
*MLO and Kumukahi.
†Data from this instrument recorded and processed by microcomputers.
‡Kumukahi only.
§Kulani Mauka

variability, and wind sector. The criterion for the CO_2 standard deviation screening was 1.0 ppm, which is the value suggested by *Thoning et al.* [1989].

The monthly occurrences of observable outgassing from volcanic vents on Mauna Loa for 1994 and 1995 are listed in Table 1.2, and the annual number of events for the past years are listed in Table 1.3. A paper was published in the American Geophysical Union (AGU) *Monograph No. 92* concerning the outgassing history of Mauna Loa volcano as recorded in the MLO data record [*Ryan*, 1995]. In early 1993, the CO_2 emissions from the summit, as measured at MLO, began to increase after undergoing a steady exponential decline since the last eruption in 1984. The distribution of volcanic CO_2 with wind direction suggests that there is a new CO_2 source just outside the summit cauldera, high on the southwest rift. The average plume CO_2 concentration continued to increase through the end of 1995. Condensation nuclei and SO_2 in the volcanic plume also began to increase during this period. These changes may be an early precursor to the next eruption of Mauna Loa, which continues to inflate and which has produced a slightly greater frequency of shallow summit earthquakes since 1993.

The weekly CO_2, methane (CH_4), and other gas sampling programs, using flasks at MLO and at KUM, were carried out according to schedule throughout the year, without major problems. An AIRKIT sampling pump unit upgraded from the MAKS pump unit began its weekly operation on May 8, 1995, at KUM only. The flask types used and sampling procedure were the same as for the MAKS method.

Carbon Monoxide

A Trace Analytical RGA3 reduction gas analyzer for the continuous measurement of carbon monoxide (CO) mixing ratios was installed in May 1992 and continued to work well throughout 1995. The analyzer was replaced with a new, but essentially identical, unit on November 28, 1995, in an upgrade program. On the same date, system operations and chromatographic data logging were switched to a Hewlett Packard (HP) 35900E analog-digital converter system. This new installation is connected to the MLO-site Unix workstation. The system operates without using chart paper. Chromatograms stored on the workstation hard disk may be displayed on the computer monitor.

Methane

The Carle automated gas chromatograph (GC) system, Carle 6, was in continuous operation throughout the period providing CH_4 data from a grab air sample taken every 24 minutes. On November 28, 1995, the Carle 6 was replaced with the HP6890 GC, which is considered the best commercial GC available in the market. The system uses nitrogen carrier gas instead of helium, which has improved sensitivity in the measurement. A new analog-digital converter, HP35900E, which has the capacity of obtaining better precision, has replaced the original HP3393 integrator. The new CH_4 GC system is paperless; the chromatograms are stored in the CCG hard disk and can be displayed on the CH_4 computer monitor at the observatory.

The CH_4 data continued to show clearly defined cycles of varying frequencies. The typical diurnal cycle was well correlated with upslope and downslope winds, with the marine boundary layer air having the higher CH_4 concentrations. Multiday or synoptic-scale CH_4 cycles were also observed, which apparently relate to different air mass source regions.

Sulfur Dioxide

An SO_2 monitoring program was developed in house during the spring of 1994, with measurements beginning at MLO on June 1, 1994. The measurement system is built around a TECO 435 pulsed-florescence analyzer with a PC controlling flows, monitoring temperatures and humidities, and acquiring data. The system runs on hourly cycles consisting of a 20-minute sample of ambient air through a Teflon line at 4 m, followed by a 10-minute zero-air sample, a 20-minute sample of air from a high-volume polyvinyl chloride (PVC) line at 34 m, and another 10-minute zero-air sample. A one-point, 1.2-ppb calibration is performed for 10 minutes every 12 hours by injecting a 10-ppm SO_2-in-air standard into the 1000 L min^{-1} high-volume flow. A six-point calibration is automatically run every 10 days over a range of concentrations between 125 ppt and 5 ppb. Injecting the calibration gas into the ambient air sample allows us to measure the effect of humidity on the loss of SO_2 in the sampling system. It also allows the use of a stable ppm-level calibration gas to perform sub-ppb calibrations.

The system had a 95% data recovery rate in 1994-1995, with most of the downtime caused by an intermittent failure of the computer hard drive. Several system modifications were made, including the addition of humidity and temperature sensors in January and February of 1995. Data graphs are available over the Internet in Hilo in near-real time.

One-minute-average measurements of zero air had a standard deviation of 35 ppt, yielding a 1-hour detection limit of about 10 ppt. The nightly average clean-air

TABLE 1.2. Estimated Mauna Loa Venting Episodes (Total Time in Hours) at MLO in 19994 and 1995*

Jan.	Feb.	March	April	May	June	July	August	Sept.	Oct.	Nov.	Dec.	Year
						1994						
2	3	0	1	0	2	0	4	1	3	4	4	24
						1995						
0	0	0	1	1	1	0	2	1	0	3	†	9

*Criteria: CO_2 SD ≥1.0 ppm; wind direction sector 135°-225°; wind speed ≥1.35 m s^{-1}.
†No data due to new system installation.

TABLE 1.3. CO_2 Venting Events From 1988 Through 1995

Year	Total Time (Hours)
1988	200
1989	84
1990	48
1991	26
1992	23
1993	28
1994	24
1995	9*

*No data for December due to new system installation.

baseline concentration of SO_2 at MLO as measured through the 4-m Teflon intake varied between 10 and 30 ppt. The high-volume PVC intake lost 5 to 10 ppt of SO_2 through dry deposition, and began to experience hygroscopic losses at relative humidities above 40%. During "Asian dust" events, which bring high concentrations of radon and anthropogenic gases, the SO_2 concentration increased to as much as 100 ppt. The volcanic plume from Mauna Loa (detected by high variability in the CO_2 concentration) contained up to 500 ppt SO_2 and had an SO_2 to CO_2 ratio of about 10^{-4}. The largest source of SO_2 was Kilauea volcano located 1 km above sea level on the south slope of Mauna Loa. Traces of its eruptive plume were frequently transported to MLO in the daytime upslope winds, producing SO_2 concentrations that occasionally exceed 50 ppb. On 15% of the nights in 1995, SO_2 from Kilauea was detected at concentrations between 100 ppt and 25 ppb in the downslope winds between midnight and 0700 LST.

Ozone Monitoring

The 1994-1995 MLO ozone monitoring program consisted of three measurement foci: continuous MLO surface ozone monitoring using a Dasibi model 1003-AH UV-absorption ozone monitor; total ozone three times a day and Umkehr ozone profile measurements two times a day using a computer-based automated Dobson instrument (Dobson no. 76); and ozone profile measurements based on weekly ascents of balloonborne electrochemical concentration cell (ECC) ozonesondes released from the National Weather Service (NWS) station at the Hilo airport.

Ozonesondes were launched weekly whenever supplies were available from Boulder. In 1994 there were 45 ozonesonde flights. In 1995 there were 52 ozonesonde flights, which included an intensive period in August when daily flights were launched during an NDSC intercomparison with the Dobson ozone spectrophotometer, two ozone lidar systems, a microwave ozone profiler, and a variety of related instruments operated at MLO.

Halocarbons and Nitrous Oxide

The Radiatively Important Trace Species (RITS) system for measuring halocarbons and nitrous oxide had its semiannual maintenance in March 1994 and August 1994. Besides the normal checks, precision checks and round-robin tank measurements were undertaken. System software was upgraded in August and a watchdog timer installed to cut down on computer lockups.

In May 1995 a new computer system was installed. At that time the watchdog timer was removed because it never worked well, and Channel A was connected to P5 (AR/CH_4) to curb the CO_2 effect. In October 1995, new file transfer protocol (FTP) 4.0 software was installed and a more extensive hardware check of the GCs was carried out. During both of these major maintenance undertakings, round-robin tank measurements were made and precision checks completed. In general, the operation of the RITS computer has improved over the previous years with the installation of the new unit.

Radon

By the end of 1995, the CMDL Department of Energy (DOE) radon program had collected 5 complete years of data. The radon instrument has performed reliably, the only problems being a broken drive belt and periodic replacement of the filter paper roll. A radon calibration source was purchased in 1995, and the instrument calibration was found to be within 5% of the source value. Daily average radon between 0000 and 0700 LST is shown in Figure 1.1, along with a 90-day running mean. The principal source of radon is soil. Radon has a half-life of 3.8 days. The amount of atmospheric radon reaching Mauna Loa during baseline conditions is a function of both the amount of continental radon injected into the free troposphere and its travel time across the Pacific Ocean. The yearly radon cycles seen in Figure 1.1 are similar to those measured for dust particles and anthropogenic gases and aerosols at MLO. There is a late-winter/spring maximum that is caused by the fast transport of air coming from Asia, and a late-summer/autumn minimum that occurs when air has spent long periods over the tropical Pacific. The 5-year record is beginning to show interannual variability. The average radon concentrations in the spring of 1991 and 1992 were higher than those of later years.

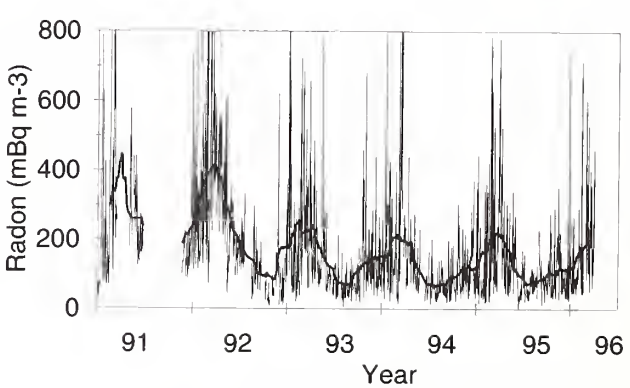

Fig. 1.1. Daily average radon at MLO measured by the CMDL-DOE radon instrument between 0000 and 0700 LST (downslope air) with a 90-point running mean (darker line). The annual peaks in the mean define the spring Asian dust season when fast air transport brings continental air and Gobi Desert dust to the observatory.

The mean annual cycle of radon varied from a high of 270 mBq m^{-3} in March to a low of 70 mBq m^{-3} in August. This is a factor of 4, which is two radon half-lives or about 7.5 days. If the seasonal variation in radon is entirely due to variations in air mass transport time across the Pacific, it follows that the average transit time of continental air to MLO is 1 week less in the spring than in late summer.

Aerosol Monitoring

Condensation nucleus counter. The Thermo Systems Incorporated (TSI) unit is a continuous-expansion condensation nucleus counter (CNC) in which condensation occurs in butyl alcohol vapor in a chamber and single-particle counting statistics are used as a basis for calculating condensation nuclei (CN) concentrations. The instrument has continued to display higher counts than the Pollak CNC since its return from the manufacturer in 1991.

Nephelometer. The four-wavelength nephelometer continues to run without too much downtime. A three-wavelength nephelometer with much better resolution was installed and activated in April 1994. These two units will operate in parallel for a couple of years sampling the same air stream before the older instrument will be retired.

Aethalometer. The aethalometer performed satisfactorily during 1994-1995. A new computer and program was set up in September 1994. A dual-head pump was installed in November 1994 to increase the air sample flow rate.

Lidar. Ruby lidar (694 nm) observations of stratospheric aerosols were continued throughout 1994-1995, adding to the MLO lidar database extending back to late 1974. The only significant modification to the instrument, following the major changes in 1993 (486 computer for data acquisition and automatic control of the laser), was rotating the entire lidar 90° in the building in April 1995. This was undertaken to provide more room for the new YAG lidar described below in this section. The lidar reorientation resulted in the ruby lidar telescope being positioned closer to the outgoing beam (from 122 cm to 79 cm), thereby increasing the low-altitude signal strength. The data are still being acquired with the 10-MHz, 8-bit Biomation unit and the operating conditions (PMT voltages, data-taking delays, number of shots) are unchanged.

Data analysis was improved to better account for signal-induced noise generated by the strong signal at low altitudes. A nonlinear fit of the signal background improved the aerosol profile between 30 and 45 km where it should converge to zero (backscatter ratio of one). The same extinction-to-backscatter ratio (50) and standard atmosphere that have been used in the past were maintained. The entire record of aerosol profiles is not currently available in a database, although the integrated backscatter is. Reanalysis of raw signals from 1984 to 1990 to add to the overall database was started in 1995 and has continued to the present.

In March 1994 the first aerosol profiles were taken with the new Nd:YAG laser-based lidar. The laser (Spectra Physics GCR-6, 30 Hz) emits 39 W at 1064 nm and has frequency doubling and tripling to produce 532 nm and 355 nm wavelengths. The 532 nm wavelength is the only wavelength used for measurements. A single mirror (61-cm diameter) focuses light onto a liquid light guide that carries the illumination to three PMT detectors. The detectors are electronically gated at low altitudes to reduce signal-induced noise. All channels are photon counted and have dynamical ranges of 10 MHz. Channel one detects the full signal for stratospheric and mesospheric altitudes and channel two detects a few percent of the signal for the troposphere. A third channel detects a Raman-shifted wavelength from nitrogen to obtain molecular density in the presence of aerosols. Besides producing a much better measurement than the ruby lidar, the new system is largely built with equipment that is readily available and serviceable. A second 61-cm mirror was installed for detection of the 1064 nm wavelength in the future.

The aerosol analysis for the new system is quite similar to the ruby lidar procedures (with changes in Rayleigh scattering cross sections) but simpler because of the much larger dynamic range of the electronics. A significant difference in the systems is that the Nd:YAG lidar obtains accurate data above the aerosol layer (35-45 km), which may then be used as an aerosol-free altitude. The ruby lidar analysis assumes an aerosol-free reference altitude below that altitude (around 15 km), which is not always a valid assumption. The Nd:YAG measurement is now used to correct the reference for the ruby lidar. The 532 nm signal is also used to measure atmospheric temperatures from 33 to 70 km by assuming the ideal gas law, hydrostatic equilibrium, and pure Rayleigh scattering. The temperature is initialized at 80 km using a MAP85 model calculated for 19.5°N with seasonal dependence.

See sections 3.1.2-3.1.7 for results of the observations.

Solar Radiation

The set of solar radiation instruments at MLO remained unchanged from previous years. In March 1994 the Physikalisch-Meteorologisches Observatorium Davos (PMOD) (World Radiation Center) sunphotometer filters were exchanged and their spectral characteristics measured in Boulder. Hand-held sunphotometers continued to be calibrated at MLO, with 34 calibrations performed in 1994 and 38 made in 1995.

In September 1995, a new data acquisition and control system was installed in the solar dome. The system is based on an HP data acquisition unit and a personal computer, and is tied to the Internet. It automatically operates the dome shutter and adjusts the azimuthal position of the dome based on calculations of the sun position and feedback from a shaft encoder on the dome drive motor. After overcoming a few initial problems, the system has performed well.

UV Radiation Monitoring

In July 1995 a spectral UV monitor was installed at MLO. The instrument was originally developed and

operated at the National Institute for Water and Atmosphere (NIWA) in Lauder, New Zealand, and then moved to MLO when a newer instrument was built to replace it. The monitor measures the global UV spectrum between 290 and 450 nm in 0.2 nm steps with a bandpass of 1.15 nm. It is calibrated with mercury and standard lamps every week. An absolute standard lamp calibration is made several times per year. Early results from this program are presented in section 3 of this *Summary Report.*

Computers/Network

Many changes to the MLO network/computer systems have occurred during the 1994-1995 period, both in the number of computers in the network and the sophistication of the operation. The "nerves" of the mountain system were expanded with the installation of fiber optic lines connecting the main building to the Radon Building, Solar Dome, University of Denver FTIR and NOAA/NIWA UV Building, Microwave Ozone Building, National Center for Atmospheric Research/High Altitude Observatory (NCAR/HAO) Facility, GONG Observatory site, and the new Visitor Building. At the Hilo site, fiber optic lines were installed to link NCAR/HAO's Hilo office and the Smithsonian Institution Observatory to MLO's Internet server.

To control the overall network, two Windows NT servers were installed as nodes, one at the Hilo office and the other at the MLO mountain site. "Trusts" were created with the NT server in CMDL, Boulder, which in effect allows the MLO and CMDL network administrators access to some of each other's network control software. This facilitates data transfer for the ozonesonde, surface ozone, and solar dome programs.

CMDL measurement programs and projects connected to the network in 1994-1995 include the aethalometer, SO_2, radon, RITS, carbon cycle species, and the NOAA/NIWA UV systems. NDSC programs added were the University of Denver FTIR and the University of Massachusetts microwave ozone system. The JPL lidar group, already on the network from the previous year, added six more computers to the network.

Other groups affiliated with the MLO facility also enhanced their network utilization as NCAR/HAO added six computers at the mountain site and one at Hilo, GONG added two computers, and the Smithsonian Observatory added two computers and a printserver.

MLO computers for the staff have all been upgraded to 486s and Pentiums (six 486s and four Pentiums), and two 486 computers were installed at the observatory, one for staff and one for visitor programs. Surge protection devices and UPSs were installed at all locations to protect servers, computers, and other network devices.

New telephone and data lines were installed in 1995 giving MLO access to the Centernet and FTS2000. This resulted in an increase of eight voice and data lines split between MLO and Hilo at no increase in monthly expenses.

An MLO home page located at http://mloserv.mlo.hawaii.gov has been set up on the Internet. This page contains some information on the observatory, staff, and a few data plots.

Software upgrades were numerous and varied; some of interest to users of MLO data and the MLO network: the VAX was upgraded with a newer operating system and other software, a server was set up for remote prints, and an anonymous FTP set up for public file transfers. Excursion software has been upgraded for use with Windows 95.

The operating system for client machines is slowly being converted from Windows For Workgroups to Windows 95. Eudora is now being used for e-mail by the entire staff because it is much easier to use than the VAX mailer. The Time and Attendance program has been upgraded twice over the past 2 years. A network monitoring program has been implemented to aid in troubleshooting the network. PCanywhere is being used for testing the remote control of a test computer with the view of developing methods of controlling more routine MLO functions from a keyboard in Hilo.

MLO receives trajectory plots and meteorological data on a daily basis from Boulder automatically over the Internet. Radiosonde data from NWS are being archived weekly on our VAX. A small electronic database has been created for MLO publications, which includes scanned abstracts.

Meteorology

The old meteorological system and the planetary boundary layer (PBL) Met system were deactivated and removed in October 1993. They were replaced with a computer-based system, the "New Met System," which measures temperatures at the 2-, 9-, and 37-m levels, dewpoint at the 2-m level, and wind speeds and directions at the 8.5-, 10-, and 38-m levels. This new system has operated unaltered and with high reliability to date.

Precipitation Chemistry

The MLO modified program of precipitation chemistry collection and analyses was continued throughout 1994-1995 within the basic MLO operational routine. This program consists of collection of a weekly integrated precipitation sample from the Hilo NWS station and collection of precipitation event samples at MLO. Analyses of these samples are undertaken in the Hilo laboratory for pH and conductivity.

Cooperative Programs

MLO Cooperative Programs are listed in Table 1.1. In September 1994 the Colorado State University (CSU) sunphotometer program was discontinued. The Australian Nuclear Science and Technology Organization (ANSTO) radon monitor underwent a major upgrade in April 1995 which resulted in an increase in sensitivity, a decrease in the response time, simpler operation, and more reliable performance.

1.2. Barrow Observatory

D. Endres

1.2.1. Operations

Data collection continued at the Barrow Observatory, Barrow Alaska (BRW) without any major interruptions during 1994-1995. Data collection system upgrades improved the quality of data for several programs and allowed remote access to data by personnel in Boulder. A second 486 computer was added to the station inventory allowing access to the Internet and, by using PC/TCP software, allowing access to email. The Control and Monitoring System (CAMS) units reached the end of their useful life and replacement data acquisition systems were installed.

The future of the distant early warning (DEW) Line site remains in question with the only certainty being a reduction in personnel. At this time it is uncertain how changes may affect operations at BRW. Assurances were given by the Air Force that any changes made at the DEW Line will have the smallest possible impact on the observatory while meeting the changing needs of the Air Force.

For the second time in the 23-year history of BRW, the exterior of the main building was painted during the summer of 1994. Plans are still in the works for other much needed upgrades to the building. A new pump enclosure was built at the end 1995 to help the sound abatement program at the observatory. Sound levels were measured at 85 dB at one time and have been reduced to 66 dB. A further reduction is expected when the enclosure is finished and all pumps are installed. On two separate occasions snow and/or ice blocked the sampling stack and had to be cleaned. Cleaning was done by removing the cap at the bottom of the stack and tapping the stack near the top with a long pole. This dislodged the blockage and allowed the normal volume of air to pass through the stack.

A change in personnel occurred in April 1994 when the technician left for a position in Boulder. A replacement arrived shortly before his departure and assumed the technician duties in a very smooth transition. The station chief celebrated his tenth year at BRW during 1994 and in 1995 was asked to serve on the Barrow Restoration Advisory Board. This Board is concerned with the cleanup of toxic waste spills by the Navy and the Air Force at the old National Arctic Research Laboratory site and the DEW Line site.

Vehicles ran well with the sole exception of a cracked piston in one of the snow machines. It was repaired and the snow machine was returned to service without interruption to the daily routine. The Naval Surface Warfare Center donated a snow machine to the station in the summer of 1995.

The NOAA housing was connected to the city water supply during the summer of 1995. Water no longer must be hauled in by truck; the storage tank at the CMDL unit will be removed.

During 1994-1995 BRW was visited by 158 registered guests. Among these were Congressional staff members, the NOAA Administrator, and researchers from China, Japan, and Russia. There were several visits by personnel from the National Science Foundation (NSF), the Arctic Research Consortium of the U.S. (ARCUS), and the U.S. Air Force and Navy.

1.2.2. Programs

Aerosols

The Thermo Systems Incorporated (TSI) condensation nucleus counter (CNC) uses butyl alcohol to saturate particles and passes them through a laser diode to count CN. The instrument continued to run well throughout the year. Problems were found, however, in noise levels in the signal. There appears to be a possible ground loop problem causing noise on the Campbell Scientific, Inc. (CSI) data recorder. On two separate occasions the optics and air path were cleaned of debris buildup and the alcohol was drained due to moisture absorption.

The nephelometer measures backscatter at four wavelengths. It ran well this period except for the ball valve in the blower system. A shaft made of inferior plastic broke and the change between filtered air and ambient air could not take place. Station personnel machined a new part at the local high school and the unit was returned to operation the next day. Problems with the noise mentioned above was also found in the nephelometer signal.

Solar Radiation

The CSI data acquisition system (DAS) operated well all year with the only problem being a shorted input channel. Signal lines were moved to another terminal and the data flow continued with only a minor interruption.

Blowers were installed on the pyranometers and pyrgeometers during 1994. They ran well during the 1994-1995 season and helped keep the snow and ice from building up on the domes. The air flow across the domes and the dry BRW air combined to sublimate any ice buildup that did occur.

Instruments are taken off line each year in November and installed again in February of the following year. During this downtime any calibrations that are needed are performed in Boulder and repairs made as needed. During the 1995 winter season, all instruments were returned to Boulder with the exception of the up-facing and down-facing pyrgeometer infrared instruments which were left online. The filter wheel normal incidence pyrheliometer (NIP), normally kept in the Dobson dome, was also returned to Boulder.

Carbon Cycle

Carbon Dioxide Nondispersive Infrared Analyzer. The Siemens Ultramat 5-E continues to be the station instrument and ran well the entire period. Data trends continue to show the normal seasonal variations in BRW data. Highs of up to 370 ppm and lows to 340 ppm were noted.

A static discharge damaged the electronics in the Linseis chart recorder. The recorder was taken out of service for approximately 3 weeks while replacement parts were ordered.

Future plans call for replacing the CAMS DAS with a Hewlett Packard (HP) UNIX-based workstation. The strip chart recorder will be taken out of service as well. These changes are being planned for sometime during the spring of 1996.

Methane. A Carle GC uses flame ionization to measure CH_4. Data is recorded by an HP integrator and stored on floppy disks. Noise in the data for a short time was the only problem encountered.

Data trends continue as in past years with data ranging between highs of over 1950 ppbv and lows of 1750 ppbv. Growth exhibited a slightly negative trend in 1994.

Carbon Monoxide. A Trace Analytical gas chromatograph (GC) has been in continuous operation since 1991. CO mixing ratios range between approximately 150 ppbv and 250 ppbv. Flask data are available since 1990.

The system ran well during the entire period with no significant downtime. Data are measured by an HP A/D, processed on an HP integrator, recorded on an HP floppy disk drive, and sent to Boulder for final analysis.

Flask Samples. Flask samples were collected as scheduled based on availability of flasks. The carbon dioxide (CO_2), methane (CH_4), carbon monoxide (CO) and isotopic data from the flask samples can be found in sections 2 and 5 of the report. No major problems were encountered.

Meteorology

A new data collection system was installed during April 1994. The new system replaces the aging CAMS DAS and is a ruggedized 486 computer rack mounted for ease of use. Metrabyte modules are used as an interface between the sensors and DAS. The new system was connected to the BRW local area network (LAN) and data are available to the CMDL Meteorological group on demand. Data are transferred to Boulder once per day and a quick look for quality control assures a higher level of confidence in the data.

Calibrations are performed twice each year, once in the spring and once in the fall, to assure correct operation of all sensors. Temperature probes are checked and corrected, if needed, to 0.2°C. Alignment of the wind sensor is checked and the speed accuracy is traceable to NIST standards.

CAMS

As mentioned previously, the MET CAMS was replaced during April 1994. The aerosol solar radiation (ASR) CAMS was replaced during 1993. The only programs still running on CAMS are the CO_2 and the Dasibi. Plans call for replacing the CO_2 early in 1996. The CAMS system has had minimal problems during its entire 10-year lifetime, but parts have become too hard to find and a replacement needed to be found.

Ozone

Surface Ozone. Surface ozone, as measured by the Dasibi, continues to be one of the long-term staples of the BRW measurement regime. The Dasibi was temporarily affected by the blockage of the stack with snow. A new display and logic board was installed when the old board malfunctioned. Otherwise the system ran without major problems.

Dobson. BRW continues to operate Dobson no. 91. Long-term trends in the data continue as in past years with seasonal highs in the spring and lows occurring in the fall. Values in April can be as high as 440 Dobson Units (DU) and lows in September can be as low as 290 DU. The Dobson is not run during the winter months due to lack of sunlight, but the calibration regime is continued to assure proper functioning when the sun rises the next year. Observations are usually made from February until October.

Nitrous Oxide and Halocarbons

Gas Chromatographs. The HP DAS was replaced with a 486-based system during the summer of 1995. The new system was connected to the LAN and allows access to the data by Boulder personnel. The new system is considerably more reliable than the HP computer used in the past. New data handling schemes are possible that were not with the HP-based system. The GC's remain unchanged. Currently there is an HP-5890 and a Shimadzu GC-8A onsite running every half hour, alternating between calibration gas and ambient air.

Flask Samples. Flask samples were collected as scheduled and available. Data show a very distinct leveling of the chlorofluorocarbon-11 and -12 (CFC) mixing ratio. This is attributed to the Montreal Protocol, which phases out production of certain CFCs. A detailed list of the chemicals analyzed by the CMDL Nitrous Oxide and Halocompounds Group (NOAH) can be found in Table 1.4.

Cooperative Projects

A comprehensive list of all BRW cooperative projects and affiliation is given in Table 1.4. Only projects with special problems or unusual occurrences are mentioned here.

TABLE 1.4. Summary of Measurement Programs at BRW in 1994-1995

Program	Instrument	Sampling Frequency
Gases		
CO_2	Siemens Ultramat 5E analyzer	Continuous
	3-L glass flasks	1 pair wk^{-1}
	0.5-L glass flasks, through analyzer	1 pair wk^{-1}
CO_2, CH_4, CO, and $^{13}C/^{12}C$ and $^{18}O/^{16}O$ of CO_2	0.5-L glass flasks, P^3 pump unit	1 pair wk^{-1}
CH_4	Carle automated GC	1 sample $(12\ min)^{-1}$
Surface O_3	Dasibi ozone meter	Continuous
Total O_3	Dobson spectrophotometer no. 91	3 day^{-1}
CO_2	Siemens Ultramat 5E analyzer	Continuous
N_2O, CFC-11, CFC-12, CFC-113, CH_3CCl_3, CCl_4	300-mL stainless steel flasks	1 sample mo^{-1}

TABLE 1.4. Summary of Measurement Programs at BRW in 1994-1995—Continued

Program	Instrument	Sampling Frequency
Gases - Continued		
N_2O, CFC-11, CFC-12, CFC-113, CH_3CCl_3, CCl_4, SF_6, HCFC-22, HCFC-141b, HCFC-142b, CH_3Br, CH_3Cl, CH_2Cl_2, $CHCl_3$, C_2HCl_3, C_2Cl_4, H-1301, H-1211, H-2402, HFC-134a	850-mL stainless steel flasks	1 sample mo^{-1}
CFC-11, CFC-12, CFC-113, N_2O CCl_4, CH_3CCl_3	HP5890 automated GC	1 sample h^{-1}
N_2O	Shimadzu automated GC	1 sample h^{-1}
CO	Trace Analytical GC	1 sample $(6\ min)^{-1}$
Aerosols		
Condensation nuclei	Pollak CNC	1 day^{-1}
	T.S.I. CNC	Continuous
Optical properties	Four-wavelength nephelometer	Continuous
Black carbon	Aethalometer	Continuous
Solar Radiation		
Global irradiance	Eppley pyranometers with Q and RG8 filters	Continuous
Direct irradiance	Tracking NIP	Continuous
	Eppley pyrheliometer with Q, OG1 RG2, and RG8 filters	Discrete
Albedo	Eppley pyranometer	Continuous
Terrestrial (IR) Radiation		
Upwelling and downwelling	Eppley pyrgeometers	Continuous
Meteorology		
Air temperature	Thermistor, 2 levels	Continuous
	Max.-min. thermometers	1 day^{-1}
Dewpoint temperature	Dewpoint hygrometer	Continuous
Pressure	Capacitance transducer	Continuous
	Mercurial barometer	Discrete
Wind (speed and direction)	R.M. Young aerovane	Continuous
Precipitation	Rain gauge, tipping bucket	
Cooperative Programs		
Total surface particulates (DOE)	High-volume sampler (1 filter wk^{-1})	Continuous
Precipitation gauge (USDA)	Nipher shield, Alter shield, 2 buckets	1 mo^{-1}
Magnetic fields (USGS)	3-Component fluxgate magnetometer and total field proton magnetometer	Continuous
	Declination/inclination magnetometer sample	6 sets mo^{-1}
Various trace gases (OGIST)	Stainless steel flasks	1 set wk^{-1} (3 flasks set^{-1})
CO_2, ^{13}C, N_2O (SIO)	5-L evacuated glass flasks	1 pair wk^{-1}
CH_4 (Univ. of Calif., Irvine)	Various stainless steel flasks	1 set $(3\ mo)^{-1}$
Earthquake detection (Univ. of Alaska)	Seismograph	Continuous, check site 1 wk^{-1}
$^{13}CH_4$ ($^{13}C/^{12}C$) (Univ. of Washington)	35-L stainless steel flasks	1 $(2\ wk)^{-1}$
^{14}CO (Univ. of Washington)	A150 aluminum cylinders filled to 2000 psi	1 $(3\ wk)^{-1}$
UV monitor (NSF)	UV spectrometer	1 scan per 0.5 hour
Magnetic fields (NAVSWC)	^3He sensors	Continuous
Sound Source (DOE)	RASS	1 hr^{-1}
Ice Buoys (NOS)	Ice buoys	Continuous
O_2 in air (Univ. of Rhode Island)	3-L glass flasks	1 pair $(2\ wk)^{-1}$
Magnetic micropulsations (Univ. of Tokyo)	Magnetometer and cassette recorder	Continuous
Aerosol chemistry (Univ. of Alaska)	High-volume sampler	3 wk^{-1}

DOE/ARM. The Department of Energy (DOE) Atmospheric Radiation Measurement (ARM) Laboratory is planning a long-term program of atmospheric radiation monitoring to collect data for use in climate models. The largest single unknown is the effect of cloud cover on the climate. BRW has been chosen as one of three sites worldwide to monitor these variables. Since late 1993, in cooperation with the North Slope Borough, Department of Wildlife Management, DOE has been testing an active Radio Acoustic Sounding System (RASS). Its impact on wildlife near the site is monitored.

NOAA/Navy Joint Ice Center. In *CMDL Summary Report No. 22* a brief discussion of this project was given. Since that time new buoys and a new DAS have been added to the project. Phone access to the data is now possible. This project has yielded much useful data as to the type of buoy and the problems encountered with arctic deployment.

University of Tokyo. A new data recorder was installed in 1995 and this project was reactivated. The recorder, with high gain amplifiers, is connected to a set of three search coil sensors that point to magnetic north, magnetic east, and vertical. Magnetic micropulsations of 0.001-5 Hz are recorded and the tapes are sent to the University of Tokyo for analysis of magnetic storm effects. Each week during the tape change, a time check to the nearest second is performed and the system is checked during the week for proper functioning.

University of Alaska, Fairbanks. A trace metals project was reactivated this time period. This is the reactivation of the former University of Rhode Island (URI) filter project discontinued in 1988. A filter is connected to a hi-vol pump and samples are collected three times per week. Filters are sent to the University of Alaska where they are stored for future analysis for trace metals associated with arctic haze. At the present time no analysis is being performed.

1.3. Samoa Observatory

M. Winey

1.3.1. Operations

The environmental engineer position with the Samoa Observatory, American Samoa (SMO) was vacated in October 1995 after 2 years of service. The replacement electronic engineer was selected with arrival due in 1996.

Internet access for the SMO local area network (LAN) was made possible by the installation of a modem router; however, e-mail services will be the only feature taken advantage of due to the high cost of a phone call and the poor quality of the telephone lines in Samoa. Hopes were high when the phone company replaced the old cable that runs 915 m from the observatory to the main phone line; unfortunately, there was no noticeable improvement.

Due to ongoing deterioration of the remote Ekto sampling building, plans were made to replace it with a permanent, concrete wall structure. This new building will be just a little larger than the old one and located as close as possible to the existing walk-up tower. Construction began in November 1995 with an expected completion date of June 1996.

Termites continued to be a problem at house T-7. The garage was torn down and replaced with a carport because termites devoured most of the old structure. The house was also infested and had to be fumigated again; this slows down the feeding process but does not stop it.

Both of the aging observatory vehicles were replaced with new trucks. This resulted in much less time being spent by the staff dealing with the constant vehicle problems.

The standby generator allowed the observatory to continue operation through many blackouts. No major problems were encountered and the small ones were easily handled by the staff.

The observatory continues to be a favorite tourist attraction because of the beautiful views. The observatory is also a favorite with local science teachers who bring their classes on field trips. Visitors are always welcomed and given a tour if they wish to learn more about the observatory's function.

1.3.2. Programs

Table 1.5 summarizes the programs at SMO for 1994-1995. Further descriptions of some of the programs follow.

Carbon Dioxide

The Siemens analyzer has traditionally been one of the most trouble-free instruments at SMO. However, when it broke down and defied local attempts to fix it, the analyzer made a round trip to Boulder for repair and was back in service in less than a month.

The air-intake line on the mast broke in 1994 and again in 1995. The problem is probably wind-induced vibration in the tubing thus causing it to crack.

The AirKit flask air sampler was put into service for an intercomparison with the older Martin and Kitzis Sampler (MAKS) unit. Eventually the MAKS unit will be retired in favor of the AirKit's built-in condenser that removes moisture from the air.

Surface Ozone

The Dasibi began the period in good condition with the Control and Monitoring System (CAMS) still responsible for the digital data collection. CAMS had a few problems that were eventually dealt with but a fair amount of data will have to be entered by hand from the chart recording. A new PC-based data system was received, but several problems prevented it from being hooked up.

In May 1995 the Dasibi overheated and blew some circuits; onsite repair was not feasible, therefore, a replacement was obtained. Unfortunately, the replacement was also a used instrument with its own set of troubles. As of the end of 1995, the Dasibi was not working properly.

TABLE 1.5. Summary of Measurement Programs at SMO in 1994-1995

Program	Instrument	Sampling Frequency
Gases		
CO_2	Siemens Ultramat-5E analyzer	Continuous
CO_2, CH_4	0.5-L glass flasks, through analyzer	1 pair wk^{-1}
	2.5-L glass flasks, MAKS pump unit	1 pair wk^{-1}
CO_2, CH_4, CO, and ^{13}C, ^{18}O of CO_2	2.5-L glass flasks, AirKit	1 pair wk^{-1}
Surface O_3	Dasibi ozone meter	Continuous
Total O_3	Dobson spectrophotometer no. 42	4 day^{-1}
N_2O, CFC-11, CFC-12, CFC-113, CH_3CCl_3, CCl_4	300-mL stainless steel flasks	1 sample wk^{-1}
N_2O, CFC-11, CFC-12, CFC-113, CH_3CCl_3, CCl_4, SF_6, HCFC-22, HCFC-141b, HCFC-142b, CH_3Br, CH_3Cl, CH_2Cl_2, $CHCl_3$, C_2HCl_3, C_2Cl_4, H-1301, H-1211, H-2402, HFC-134a	850-mL stainless steel flasks	1 sample wk^{-1}
CFC-11, CFC-12, CFC-113, N_2O, CCl_4, CH_3CCl_3	HP5890 automated GC	1 sample h^{-1}
N_2O	Shimadzu automated GC	1 sample h^{-1}
Aerosols		
Condensation nuclei	Pollak CNC	1 day^{-1}
	TSI CNC	Continuous
Solar Radiation		
Global irradiance	Eppley pyranometers with Q and RG8 filters	Continuous
Direct irradiance	Eppley pyrheliometer with Q filter	Continuous
	Eppley pyrheliometer with Q, OG1, RG2, and RG8 filters	Discrete
Diffuse irradiance	Eppley pyrgeometer with shading disk and Q filter	Continuous
Meteorology		
Air temperature	Thermistors (2)	Continuous
Dewpoint temperature	Polished mirror	Continuous
Pressure	Capacitance transducer	Continuous
	Mercurial barometer	1 wk^{-1}
Wind (speed and direction)	Bendix Aerovane	Continuous
Precipitation	Rain gauge, tipping bucket	Continuous
	Rain gauge, plastic bulk	1 day^{-1}
Cooperative Programs		
CO_2, ^{13}C, N_2O (SIO)	5-L evacuated glass flasks	1 set wk^{-1} (3 flasks set^{-1})
GAGE project: CFC-11, CFC-12, N_2O, CH_3CCl_3, CCl_4 (SIO)	HP5880 gas chromatograph	1 h^{-1}
Various trace gases (OGIST)	Stainless steel flasks	1 set wk^{-1} (3 flasks set^{-1})
Bulk deposition (DOE)	Plastic bucket	Continuous (1 bucket mo^{-1})
	Ion exchange column	Continuous (1 filter mo^{-1}
Total suspended particulates (DOE)	High-volume sampler	Continuous (1 filter wk^{-1})
Total suspended particulates (SEASPAN)	High-volume sampler	Continuous (1 filter wk^{-1})
CH_4,($^{13}C/^{12}C$ ratio) (Univ. of Wash.)	30-L pressurized cylinder	Biweekly
Light hydrocarbons (UCI)	1-L evacuated stainless steel flasks	3-4 flasks qtr^{-1}
O_2 (URI)	2.5-L glass flasks	2 pair mo^{-1}
O_2 (SIO)	3-L glass flasks	2 sets mo^{-1} (3 flasks set^{-1})

SIO - Scripps Institution of Oceanography
OGIST - Oregon Graduate Institute of Science and Technology
UCI - University of California, Irvine
URI - University of Rhode Island

Total Ozone

The Dobson worked well with only one small problem when the high voltage power supply had to be replaced.

The data acquisition program was updated and continues to work well.

The dome is aging fast in the corrosive sea-air and will have to be replaced soon.

Ozonesonde Balloons

Ozonesonde balloon launches were restarted in August 1995 after a break of several years. At the airport the National Weather Service made their balloon inflation facility available, including the use of hydrogen gas to fill the balloons. Releases were made weekly.

Nitrous Oxide and Halocompounds

The old Hewlett Packard (HP) data acquisition computer was replaced with a PC-based system. This was done in May 1995. Some problems were solved and some new ones were born. The good news was that system crashes were almost completely eliminated. The most perplexing problem was a lack of readable chromatograms. Good data was being produced and saved but for some reason the printouts were no good.

The new computer came with a network board and software installed, however, reliable communication has yet to be achieved. This could be due to the long, 200 m run of coaxial cable from the main building to the remote site where the computer is located.

As in the past, several site visits were made by CMDL personnel from Boulder. This regular, close attention is one good reason why this program is so successful.

Aerosols

In January 1995 data acquisition was switched from CAMS to the new solar radiation system. This was a big improvement.

The Pollak performed well for the most part; the only problems encountered were with the ammeter. Apparently these ammeters are becoming scarce and servicing old ones is a delicate operation.

The main blower that provides the steady flow of air from the top of the pipe to the instruments inside failed. The failure was not noticed for several months. A new blower was installed April 1994.

With the construction of a new sampling building in November 1995, occasional heavy activity near the air intake for the aerosol instruments had a noticeable effect on the data.

Solar Radiation

A new data acquisition system was installed January 1995. This was a major improvement with several benefits including 24-hour access via modem to real time data. Another benefit was the elimination of the chore of packaging and mailing the data to Boulder.

An Eppley pyrgeometer with a Q dome and a shading disk mounted to a tracker to measure diffuse irradiance was put online August 1995.

Meteorology

A major overhaul of the meteorological system occurred in July 1994. A new data acquisition system was installed and all of the old sensors were replaced with new ones. As with the new solar radiation system, data will be available in Boulder at any time via modem. Unfortunately, this convenient feature was hampered by the poor quality of the telephone communication system in Samoa.

The new system performed flawlessly for several months then gradually became afflicted by resets and hangups. This problem was never satisfactorily solved; the most likely suspect was excessive noise on the 485-communication line connecting all the sensors to the computer.

CAMS

By the end of 1995, carbon dioxide (CO_2) was the only program still using CAMS for data acquisition. The CO_2 CAMS unit has done a fine job but some day it too will be retired in favor of a more modern system.

Cooperative Programs

SIO GC. The Scripps Institution of Oceanography (SIO) gas chromatograph (GC) Nafion dryer used to dry the incoming air sample was upgraded. The new system is self-recharging thus eliminating the chore of replacing cartridges periodically.

SEASPAN. The SEAREX South Pacific Aerosol Network (SEASPAN) wind sensor cable was replaced with a new one; the old one had several splices that were suspected of degrading the signal. The wind speed transducer was also upgraded.

DOE. The Department of Energy (DOE) wet/dry rooftop collection bucket was replaced with an ion exchange column in August 1995. At the same time, the frequency at which samples were shipped out was increased to once per week. This was done in response to the decision in France to resume nuclear testing at Muroroa Atoll near Tahiti.

1.4. South Pole Observatory

T. Jacobs

1.4.1. Operations

The CMDL South Pole Observatory (SPO) is located at the geographic South Pole at an elevation of 2835 m above sea level with an average temperature of -49°C. SPO is part of Amundsen Scott Station, which is managed by the National Science Foundation (NSF) Office of Polar Programs.

Most CMDL projects are housed in the Clean Air Facility (CAF), an elevated building located upwind of the main South Pole Station. Construction of a replacement facility began in October 1995; the new building should be complete and ready for occupation by January 1997. Because the surface wind at the South Pole blows predominantly from the grid northeast, the SPO "Clean Air Sector" includes the area grid north of the CAF between grid 340 degrees and grid 110 degrees. Excursions into the Clean Air Sector are generally prohibited, with few exceptions.

SPO's meteorological instruments are mounted on the walk-up Met. Tower, which was located 100 m from the eastern side of the CAF. In November of 1995 the tower was moved to accommodate construction of the new CAF.

Operations for the balloon program take place in three locations: the main station science building, the cargo arch, and the Balloon Inflation Tower (BIT). The cargo arch is used to inflate plastic balloons, that are too large to inflate and launch from the BIT.

Amundsen Scott Station is supplied by air. Because airplanes can only land at the Pole during the relatively warm months of October through February, the station is physically "closed" for 8 months each year. A midwinter "airdrop" took place in June of 1994 and 1995. Air samples collected during the austral winter cannot be returned for analysis until the following spring. Data are transferred digitally via satellite throughout the year. In January 1994, Amundsen Scott Station established a satellite link to the Internet, greatly facilitating the transfer of data.

During 1994 and 1995 there were occasional power outages and frequent "brownouts" because of an increasing demand for electrical power at the Pole. Within the CAF, science demands continue to exceed the "clean" power supplied by the building's uninteruptable power supply (UPS).

The University of Rome lidar was replaced by a similar instrument, owned and operated by the University of lllinois.

1.4.2. PROGRAMS

Table 1.6 is a summary of the measurement programs at SPO during 1994 and 1995. Operational highlights are as follows.

Carbon Cycle

The Siemens continuous carbon dioxide (CO_2) analyzer ran continuously without significant problems. Sample flask pairs were filled through the analyzer once per week and through a portable Martin and Kitzis Sampler (MAKS) unit twice per month.

Aerosols

The Meteorology Research, Inc. (MRI) four-wavelength nephelometer "hung" occasionally for unknown reasons. Discrete observations with the Pollak condensation nucleus counter (CNC), taken twice daily, generally agreed, as expected, with data from the Thermo Systems Inc. (TSI) CNC.

Solar and Terrestrial Radiation

During the summer, all Eppley pyranometers, pyrgeometers, and the tracking normal incidence phyrheliometer (NIP) ran continuously without significant problems. Discrete observations with the filter wheel NIP took place three times daily during especially clear conditions. In November 1995, a pyranometer equipped with a sun blocking disk was installed on the roof of the CAF. After sunset each March, the short-wave instruments were taken off-line for the winter.

Ozone and Water Vapor

The Dasibi ultraviolet absorption ozone monitor ran continuously without remarkable problems. Discrete observations with the Dobson ozone spectrophotometer took place three times daily during the summer and again during the darkest winter months using the full moon as a light source.

The ozonesonde program ran well during 1994 and 1995. Rubber balloons were launched from the balloon inflation tower (BIT) platform; the larger plastic balloons were inflated in the cargo arch and launched from the cargo yard. Launches usually occurred once per week except during the months of stratospheric ozone depletion (August-November) when the schedule was increased to every 3 days and then to every other day.

Nitrous Oxides and Halocarbons

The two Shimadzu Mini-2 electron capture gas chromatographs were inspected and upgraded in January 1994 and November 1994. Sample flask pairs were filled with ambient air twice per month whenever flasks were available.

Meteorology

The meteorology system was upgraded in January 1994 with all new sensors and a new data acquisition system. Manual weather observations took place daily at midnight universal time (UT).

Data Acquisition

The aerosol Control and Monitoring System (CAMS) unit was taken off-line during summer 1994.

Cooperative Programs

SIO. The Scripps Institution of Oceanography (SIO) conducts long-term monitoring of CO_2, $^{13}C/^{12}C$ ratio, and N_2O. Twice per month, three evacuated glass flasks were exposed to ambient air.

SIO. Three glass flasks were pressurized with ambient air on the first and fifteenth of each month for the long-term monitoring of O_2 and N_2.

DOE. The Department of Energy (DOE)conducts long-term monitoring of the spatial and temporal distribution of specific and anthropogenic radionuclides in surface air. The DOE pump ran continuously without significant problems; filters were replaced each week.

OGIST. Oregon Graduate Institute of Science and Technology (OGIST) monitors seasonal trends in the amount of chlorine-and bromine-containing trace gases in the Antarctic. Two flasks per week were filled with ambient air.

CSIRO. CSIRO monitors the ratio $^{13}C/^{12}C$ in atmospheric CO_2 for use in a 2-D global carbon cycle model. One glass flask was pressurized with ambient air every 2 weeks.

SUNY. Five air-filled cylinders remained on platforms approximately 800 m downwind of the main station for the quantification of the production rate of radiocarbon by galactic cosmic rays. The cylinders were inspected and cleared of snow once per month; no other operations were required for State University of New York (SUNY) . .

University of Arizona. An unsuccessful attempt was made to run a continuous meter during the winter of 1994 for the monitoring of H_2O_2 in the air/snow interface. In the summer of 1994 CMDL began collecting surface snow and micropit snow samples once per week.

TABLE 1.6. Summary of Measurement Programs at SPO in 1994-1995

Program	Instrument	Sampling Frequency
Gases		
CO_2	Siemans IR analyzer	Continuous
CO_2, CH_4	2.5-L glass flasks, through analyzer	1 pair twice mo^{-1}
	2.5-L glass flasks, MAKS pump unit	1 pair twice mo^{-1}
Surface O_3	Dasibi ozone meter	Continuous
Total O_3	Dobson spectrophotometer no. 82	3 day^{-1}
Ozone profiles	Balloonborne ECC sonde	1 wk^{-1}, summer, autumn, winter; 1 (3 day)$^{-1}$, spring
Water vapor	Balloonborne sonde	10 times yr^{-1}
N_2O, CFC-11, CFC-12, CFC-113, CH_3CCl_3, CCl_4	300-mL stainless steel flasks	1 sample mo^{-1}
N_2O, CFC-11, CFC-12, CFC-113, CH_3CCl_3, CCl_4, SF_6, HCFC-22, HCFC-141b, HCFC-142b, CH_3Br, CH_3Cl, CH_2Cl_2, $CHCl_3$, C_2HCl_3, C_2Cl_4, H-1301, H-1211, H-2402, HFC-134a	850-mL stainless steel flasks	1 sample mo^{-1}
CFC-11, CFC-12, CFC-113, N_2O, CH_3CCl_3, CCl_4	Shimadzu automated GCs	1 sample h^{-1}
Aerosols		
Condensation nuclei	Pollack CNC	2 day^{-1}
	TSI CNC	Continuous
Optical properties	Four-wavelength nephelometer	Continuous
Solar Radiation		
Global irradiance	Eppley pyranometers with Q and RG8 filters	Continuous, summer
	Eppley pyranometer with Q filter	Continuous, summer
	Net radiometer	Continuous, summer
Direct irradiance	Eppley pyrheliometer with Q, OG1, RG2, and RG8 filters	2 day^{-1}
	Eppley pyrheliometers with Q and RG8 filters	Continuous, summer
Albedo	Eppley pyranometers with Q and RG8 filters filters, downward facing	Continuous, summer
Terrestrial (IR) Radiation		
Upwelling and downwelling	Eppley pyrgeometers	Continuous
Meteorology		
Air temperature	Platinum resistor, 2- and 20-m heights	Continuous
Pressure	Capacitance transducer	Continuous
	Mercurial barometer	1 time wk^{-1}
Wind (speed and direction)	Bendix Aerovane	Continuous
Frost-point temperature	Hygrometer	Continuous
Cooperative Programs		
CO_2, ^{13}C, N_2O (SIO)	5-L evacuated glass flasks	2 mo^{-1} (3 flasks sample^{-1})
Total surface particulates (DOE)	High-volume sampler	Continuous (4 filters mo^{-1})
Various trace gases (OGIST)	Stainless-steel flasks	1 week^{-1} (2 flasks set $^{-1}$), summer only
Interhemispheric $^{13}C/^{14}C$ (CSIRO)	5-L glass flasks	1 or 2 flasks mo^{-1}
O_2, N_2 (Scripps)	Air sampling pump and flasks	1 mo^{-1} (3 flasks set^{-1})
H_2O_2 (Univ. of Arizona)	Snow sample collection	1 time wk^{-1}
Isotope production (SUNY)	Pressurized cylinders	N/A; checked once mo^{-1}

1.5. METEOROLOGICAL MEASUREMENTS

T. MEFFORD (EDITOR), M. BIENIULIS,
B. HALTER, AND J. PETERSON

1.5.1. STATION CLIMATOLOGIES

Introduction

The climatology of surface meteorological observations at the four CMDL observatories is based on hourly average measurements of the resultant wind direction and speed, barometric pressure, ambient and dewpoint temperatures, and the precipitation amount. The 19-year station climatologies are an important record for the interpretation of measured values of aerosols, trace gases, atmospheric turbidity, and long-term changes in the records themselves. The records also serve to outline periods of local contamination. The sensors in use were selected for their high accuracy and their ability to withstand the extreme conditions of the polar region. Data is recorded as 1-minute average values so that the variability within the hourly averages can be determined. To the extent that is practical, World Meteorological Organization (WMO) siting standards [*WMO*, 1969] are followed. Thermometers are also positioned at the top of the sampling towers at BRW, MLO, and SPO to measure the temperature gradient to determine the stability of the surface boundary layer.

The Control and Monitoring System (CAMS) was replaced with a PC-based meteorological data acquisition system at BRW in April 1994, MLO in October 1993, SMO in June 1994, and SPO in January 1994. A detailed description of the new data acquisition system can be found in [*Peterson and Rosson*, 1994]. Table 1.7 describes the sensor disposition as of December 31, 1995.

Barrow

Descriptions of the BRW station and its climate are given in previous CMDL Summary Reports [e.g., *DeLuisi*, 1981]. Wind roses of hourly average resultant wind direction and speed are presented in 16 direction classes and 4 speed classes (Figure 1.2). Winds from the "clean air" sector, north-northeast to southeast occurred 58.8% of the time in 1994 and 62.8% in 1995 as compared to 62.1% for the 17-year climatology period of 1977 through 1993 (Figure 1.3). Wind speeds that were greater than 10 ms^{-1} for 1994 (9.1%) and 1995 (6.8%) were both lower than the 17-year climatology (12.1%). The average speed of 5.5 ms^{-1} in 1994 (Table 1.8) was the second lowest average while the 5.0 ms^{-1} in 1995 set the lowest average in the 19 years at the station. This could have been caused by lowering of the new anemometer to 9.5 m from 16.5 m on April 15, 1994, when the new system was installed.

The average temperature of -13.1°C in 1994 was 0.5°C colder than the 17-year average (Table 1.8). In 1995, the average of -11.4°C was 1.2°C warmer than the 17-year average. June 1994 set a new record low temperature and December 1994 tied its lowest record. In 1995, April tied its record high and September set a new record high. A temperature of -44.4°C set the new record low temperature for March. The barometric pressure for 1994 was close to normal; however, 1995 was 2.0 hPa above the 17-year average. The summertime precipitation measured 85 mm in 1994 and 53 mm in 1995.

Mauna Loa

The climatology of MLO is best understood when it is considered in two distinctive wind direction regimes, the night (downslope) period (1800-0559 Hawaiian Standard Time (HST)) and the day (upslope) period (0600-1759 HST). The 17-year night and day wind roses illustrate the two distinct wind patterns (Figure 1.4).

Night Regime. The 17-year wind rose (Figure 1.4) shows that 91.2% of all winds observed had a southerly component. The percentage of occurrence of southerly winds in 1994 was 94.2% (Figure 1.5) and 90.9% in 1995 (Figure 1.6). Pressure gradient controlled winds (WS≥10 ms^{-1}) from predominately westerly and south-easterly

TABLE 1.7. CMDL Meteorological Sensor Deployment December 31, 1995

	BRW		MLO		SMO		SPO	
Sensor	Serial No.	Elevation, m	Serial No.	Elevation, m	Serial No.	Elevation, m	Serial No.	Elevation, m
Primary anemometer†	14584	10.5	13864	10.0	15945	13.7	14583	10.0
Secondary anemometer†			13865	38.2				
Pressure transducer‡	374199	9.5	374198	3398.4	374200	78.5	358960	2841.0
Mercurial barometer	641	9.5	278	3398.4	961	78.5	215	2841.0
Air temperature A§		2.2		2.0		14.0		2.0
Air temperature B§¶		16.3		37.4				22.0
Air temperature C**		2.0		2.0		12.8		2.0
Dewpoint temperature	G0001	2.0	G0004	2.0	G0008	12.8	G0007	2.0
Rain gauge		~4		0.8		~4		

†Propeller Anemometer, model no. 05105, R. M. Young Company, Traverse City, Michigan.

‡Pressure Transducer, model no. 270, Setra Systems, Acton Massachusetts. Heights of all pressure sensors are given with respect to MSL.

§Platinum Resistance Probe, Logan 4150 Series, Logan Enterprises, Liberty, Ohio.

¶Thermometer, positioned at the top of the local sampling tower to facilitate an estimation of boundary layer stability.

**Hygrothermometer, Technical Services Laboratory model no. 1088-400, Fort Walton Beach, Florida.

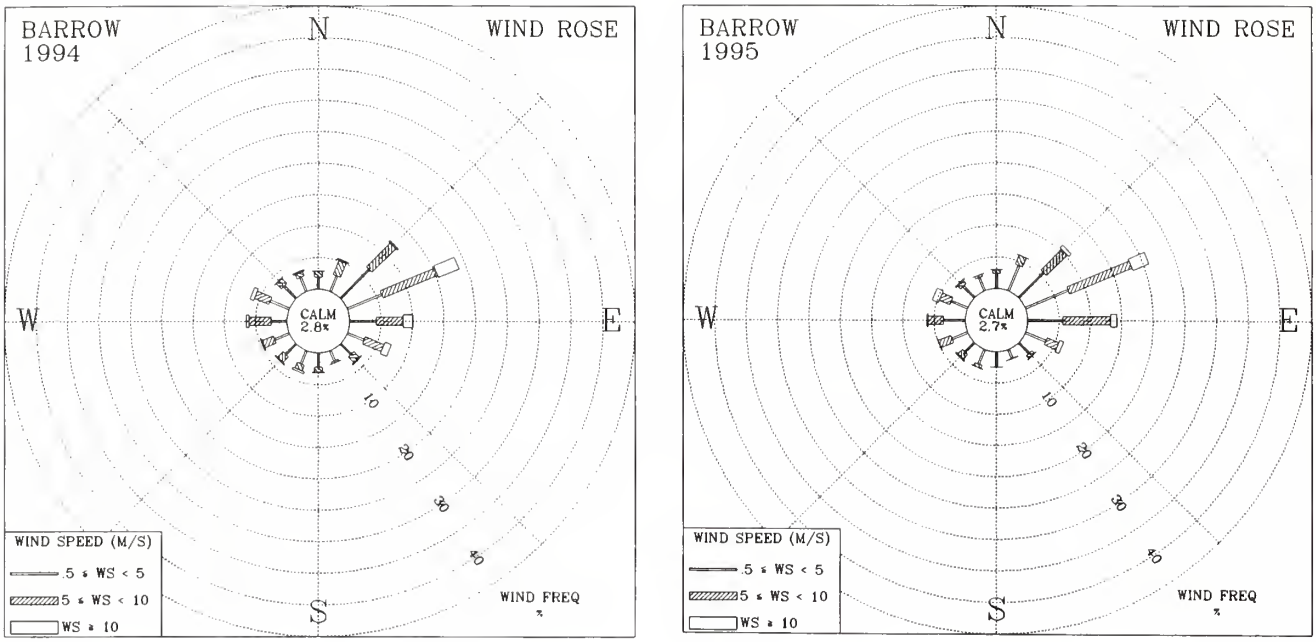

Fig. 1.2. Wind rose of surface winds for BRW for 1994 (left) and 1995 (right). The distribution of resultant wind direction and speed are given in units of percent occurrence. Wind speed is displayed as a function of direction in three speed classes.

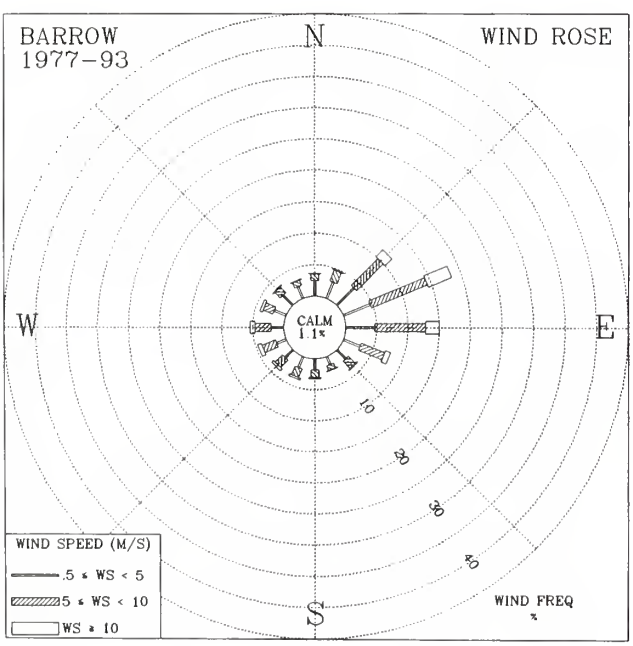

Fig. 1.3. Wind rose of surface winds for BRW for 1977-1993. The distribution of resultant wind direction and speed are given in units of percent occurrence for the 17-year period. Wind speed is displayed as a function of direction in three wind classes.

directions occurred 5.0% of the time in 1994 and 8.4% in 1995 while the 17-year record shows a 6.1% occurrence. The annual average wind speed for both 1994 and 1995 was not significantly different from the long-term mean (Tables 1.9 and 1.10). The upslope or northerly component winds (north-northwest through east-northeast) that occurred 2.0% of the time in 1994 and 1.9% in 1995, are the result of daytime, upslope flow extending into the early evening hours.

Day Regime. The 1994 and 1995 wind roses (Figures 1.5 and 1.6) indicate that winds from the west-northwest through east-northeast occurred 58.4% and 55.4% of the time respectively, compared with the expected occurrence of 58.5% indicated by the 17-year climatology. Pressure gradient controlled winds ($WS \geq 10$ ms^{-1}) occurred 4.1% of the time in 1994 and 8.7% in 1995 while the 17-year average shows an expected occurrence of 5.7%. In 1994, the pressure gradient winds, which are usually associated with storms, followed the expected pattern of fewer occurrences during the day regime. In 1995, these winds had approximately the same number of occurrences in the day and night regimes. The day wind rose is more uniformly distributed in the light wind classes than the night wind rose. This is due to the occurrence of variable wind directions during the transition periods at dawn and dusk, most of which are included in this regime.

The average ambient temperature for 1994 and 1995 (Tables 1.9 and 1.10), combining both the day and night records, was 7.8°C and 8.4°C respectively, both considerably higher than the long-term average of 7.0°C. September 1995 set a new record high temperature for the

TABLE 1.8. BRW 1994 and 1995 Monthly Climate Summary

	Jan.	Feb.	March	April	May	June	July	Aug.	Sept.	Oct.	Nov.	Dec.	Year
							1994						
Prevailing wind direction	ENE	ESE	ENE	ENE	ENE	W	E	ESE	NE	ENE	ENE	NE	ENE
Average wind speed ($m\ s^{-1}$)	8.8	7.2	5.9	4.2	6.1	4.0	4.3	5.0	5.6	4.3	6.0	4.4	5.5
Maximum wind speed* ($m\ s^{-1}$)	17	20	13	13	12	9	12	13	14	13	19	14	20
Direction of max. wind* (deg.)	67	95	73	72	64	270	90	231	264	71	66	210	95
Average station pressure (hPa)	1028.5	1026.5	1016.1	1020.1	1014.6	1011.3	1010.0	1009.2	1012.3	1009.5	1006.9	1006.5	1014.3
Maximum pressure* (hPa)	1050	1050	1036	1036	1025	1023	1024	1030	1027	1022	1032	1025	1050
Minimum pressure* (hPa)	1003	1003	995	1006	998	1001	995	995	998	991	980	987	980
Average air temperature (°C)	-23.0	-23.2	-28.1	-17.8	-7.7	-0.3	3.6	5.5	-3.2	-13.0	-22.9	-27.2	-13.1
Maximum temperature* (°C)	-14	-2	-11	-2	2	9	17	20	7	-3	-6	-7	20
Minimum temperature* (°C)	-35	-36	-40	-33	-18	-11	-3	-3	-12	-31	-36	-44	-44
Average dewpoint temperature (°C)	-26.0	-25.6	-30.9	-19.7	-9.1	-1.3	2.5	3.7	-5.0	-14.4	-25.1	-29.7	-15.1
Maximum dewpoint temperature (°C)	-16	-4	-13	-4	0	8	11	15	7	-3	-7	-7	15
Minimum dewpoint temperature (°C)	-38	-39	-43	-36	-19	-12	-3	-9	-13	-34	-40	-48	-48
Precipitation (mm)	0	0	0	0	2	1	15	48	3	0	0	16	85
							1995						
Prevailing wind direction	ENE	E	ENE	ENE	ENE	NE	E	ENE	ENE	ENE	ENE	ENE	ENE
Average wind speed ($m\ s^{-1}$)	4.8	5.1	5.4	5.2	5.4	3.8	5.1	4.3	5.7	6.6	4.2	4.8	5.0
Maximum wind speed* ($m\ s^{-1}$)	13	16	15	13	13	9	12	9	13	14	16	16	16
Direction of max. wind* (deg.)	104	50	112	226	58	258	74	246	72	64	292	72	50
Average station pressure (hPa)	1010.4	1025.5	1023.6	1014.9	1017.5	1012.7	1012.4	1011.2	1011.2	1013.3	1020.7	1019.8	1016.0
Maximum pressure* (hPa)	1025	1042	1040	1024	1036	1028	1022	1025	1030	1025	1036	1034	1042
Minimum pressure* (hPa)	986	1002	1002	997	1003	1000	1003	999	990	1001	1001	1002	986
Average air temperature (°C)	-24.3	-26.8	-27.4	-13.7	-4.5	1.2	2.8	1.7	1.7	-7.2	-15.1	-24.5	-11.4
Maximum temperature* (°C)	-4	-7	-3	2	2	16	17	14	16	-1	-2	-12	17
Minimum temperature* (°C)	-44	-46	-44	-35	-11	-6	-2	-3	-4	-27	-29	-35	-46
Average dewpoint temperature (°C)	-26.6	-29.4	-29.9	-15.2	-4.9	-0.9	0.9	1.4	0.4	-8.9	-16.1	-26.2	-12.8
Maximum dewpoint temperature (°C)	-5	-8	-3	0	0	0	11	10	10	-2	-2	-12	11
Minimum dewpoint temperature (°C)	-49	-50	-49	-37	-12	-7	-6	-5	-6	-28	-31	-37	-50
Precipitation (mm)	0	0	0	1	0	15	28	5	3	0	0	0	53

Instrument heights: wind, 10.5 m; pressure, 9.5 m (MSL); air temperature, 2.2 m; dewpoint temperature, 2.0 m. Wind and temperature instruments are on a tower 25 m northeast of the main building.

*Maximum and minimum values are hourly averages.

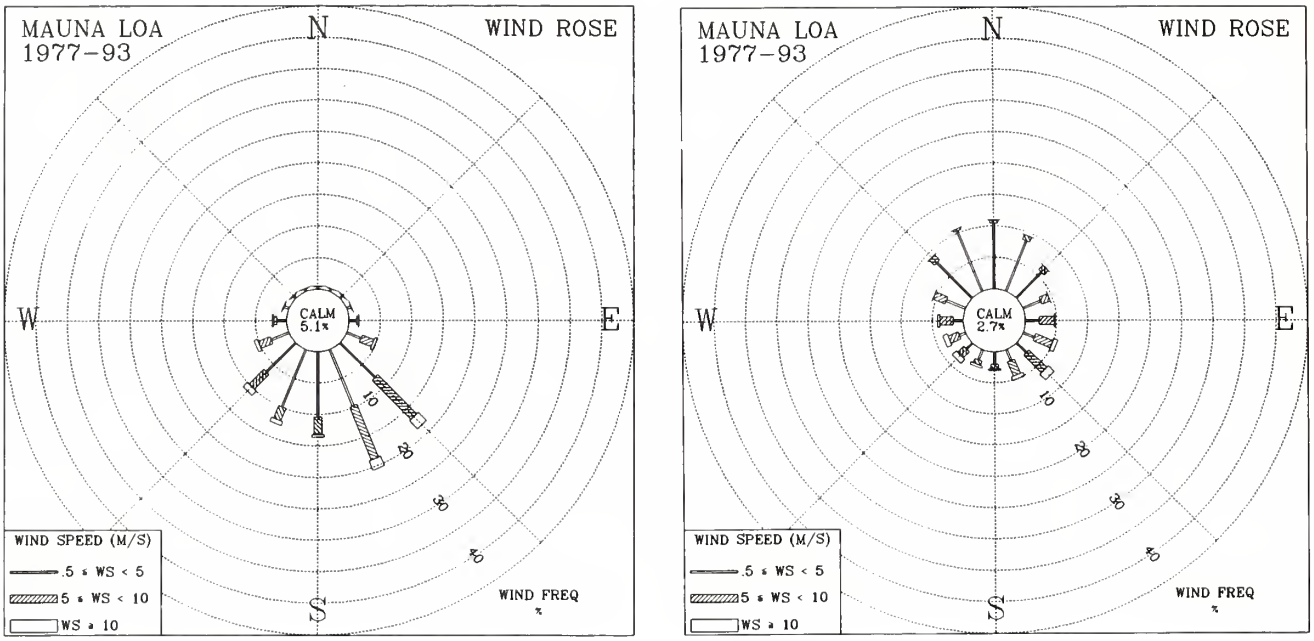

Fig. 1.4. Wind roses of the surface winds for MLO for 1977-1993 night (left) and day (right). The distribution of resultant wind direction and speed are given in units of percent occurrence for the 17-year period. Wind speed is displayed as a function of direction in three speed classes.

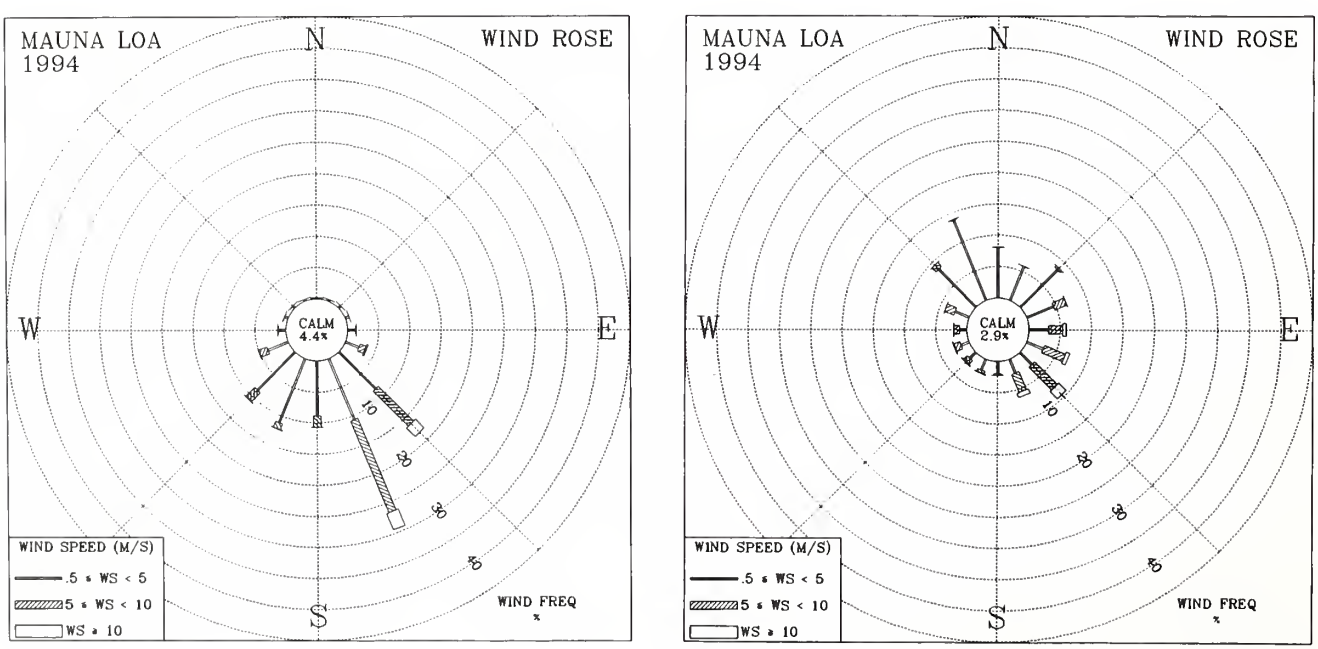

Fig. 1.5. Wind roses of the surface winds for MLO for 1994 night (left) and day (right). The distribution of resultant wind direction and speed are given in units of percent occurrence. Wind speed is displayed as a function of direction in three speed classes.

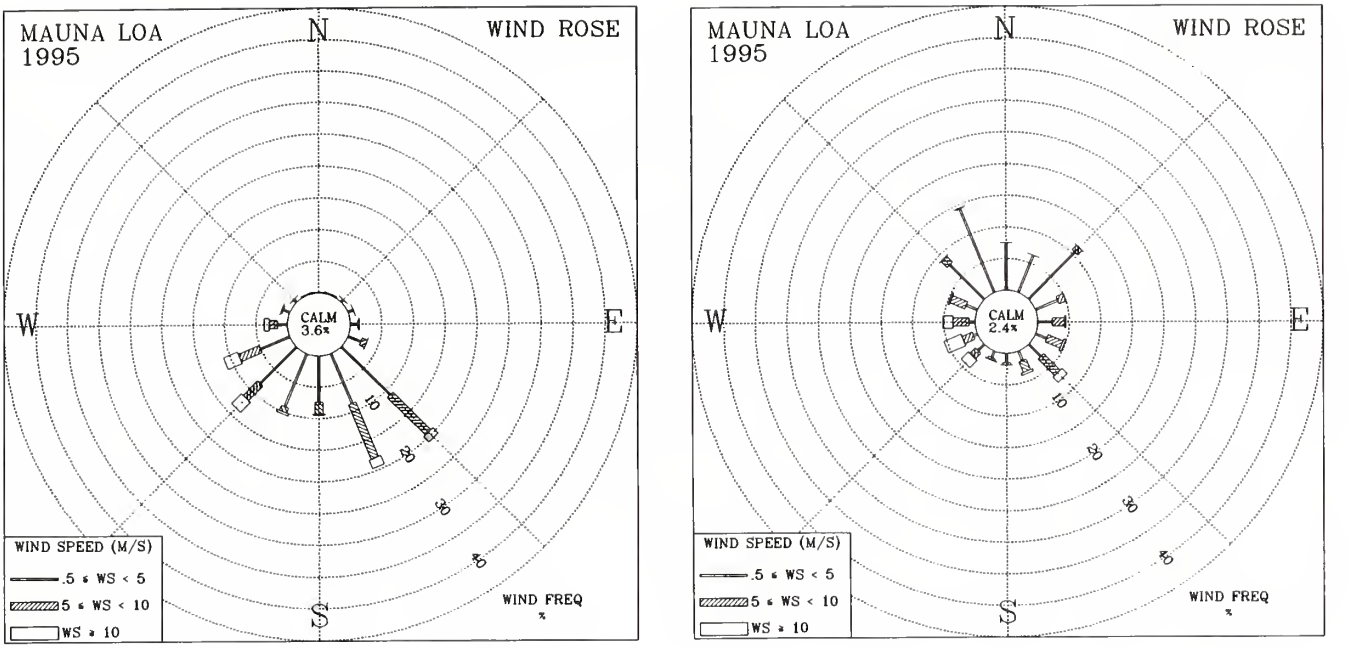

Fig. 1.6. Wind roses of the surface winds for MLO for 1995 night (left) and day (right). The distribution of resultant wind direction and speed are given in units of percent occurrence. Wind speed is displayed as a function of direction in three speed classes.

month. The January 1994 and November 1995 average wind speeds set new minimums for the month. The barometric pressure for 1994 and 1995 (679.7 hPa and 680.0 hPa respectively) were both lower than the long-term average pressure of 680.5 hPa. July 1994 and March 1995 each tied its record minimum pressure for those months and April 1995 set a new record minimum for the month. The precipitation amounts for 1994 and 1995 (438 mm and 188 mm respectively) were both significantly lower than the long-term average amount of 500 mm. The 1995 amount is the lowest amount ever received at the station.

Samoa

A comparison of SMO's 1994 and 1995 wind roses (Figure 1.7) to that of the 17-year period (Figure 1.8) shows a lower percentage (57.7%) of "clean air" sector winds (north-northwest through southeast) in 1994 while 1995 shows a higher percentage (61.2%) than the long-term average of 59.8%. The occurrence of winds in the 10 ms^{-1} or greater class was 6.7% in 1994 and 3.9% in 1995 while the expected occurrence based on the 17-year record is 4.9%. The average wind speed for both 1994 and 1995, 4.8 ms^{-1} (Table 1.11) is close to normal. The monthly average for May 1995 set a new minimum record for the month.

The average ambient temperature for 1994 and 1995 was 27.3°C and 27.0°C respectively, which are both very close to the 17-year average of 27.1°C. Five new record highs were set in 1994 that occurred during the months of February through June with a new record low occurring during the month of June. In 1994, temperatures during the first 7 months were above their monthly means and the other 5 months were below their respective monthly means. The average barometric pressure for 1994 and 1995 (Table 1.11) was 1.2 hPa and 1.9 hPa above the 17-year average of 999.3 hPa at Cape Matatula respectively. The months of January and June in 1995 both tied the record maximum pressure for the month. The amount of precipitation in 1994 measured near normal amounts during the first 6 months of the year while the last 6 months were wetter than normal. In 1995, the precipitation amount was again near normal for the first 6 months; however, the last 6 months were drier than normal.

South Pole

The distribution of the surface wind direction in 1994 and 1995 (Figure 1.9) shows a higher percentage of "clean air" sector (grid north-northwest through east-southeast) winds (95.0%) in 1994 while 1995 showed a lower percentage (92.4%) from the than the 17-year average (93.9%) (Figure 1.10). A lower percentage of winds in the 10 ms^{-1} class (3.5% in 1994 and 3.1% in 1995) were observed as compared to the 17-year average (4.0%). The average wind speeds for 1994 and 1995 were very close to the long-term average of 5.4 ms^{-1}. May 1995 tied its maximum wind speed record. The monthly average wind speed for January 1995 set a new minimum for the month.

The average temperature for 1994 (-49.5°C) and 1995 (-49.7°C) were both colder than the 17-year average of -49.0°C. September 1994 set a new record maximum and July 1995 tied its record maximum temperature for the month. January 1995 tied its record minimum temperature for the month. The minimum temperature of -74°C for 1994 occurred in May and September while the minimum of -77°C in 1995 occurred in September. The annual average station pressures for 1994 (679.7 hPa) and 1995 (679.6 hPa) (Table 1.12) were both above the 17-year average of 679.1 hPa. June 1994 tied its record high pressure for the month and July 1995 set a new record high pressure.

TABLE 1.9. MLO 1994 Monthly Climate Summary

	Jan.	Feb.	March	April	May	June	July	Aug.	Sept.	Oct.	Nov.	Dec.	Year
							Night						
Prevailing wind direction	SW	SW	SW	SSE	SSE	SSE	SSE	SSE	SSE	SSE	SSE	SSE	SSE
Average wind speed (m s^{-1})	3.7	4.3	4.8	4.1	4.4	3.4	5.9	4.1	3.9	3.3	5.4	6.5	4.5
Maximum wind speed* (m s^{-1})	12	12	13	12	13	10	16	14	13	9	13	17	17
Direction of max. wind* (deg.)	248	241	129	150	148	157	153	154	155	166	158	143	143
Average station pressure (hPa)	678.1	677.9	679.1	679.6	680.2	680.4	680.6	680.9	680.0	679.6	679.8	680.3	679.7
Maximum pressure* (hPa)	682	682	684	683	683	684	683	684	683	683	682	684	684
Minimum pressure* (hPa)	675	673	672	676	678	678	677	678	677	676	677	677	672
Average air temperature (°C)	4.0	3.7	4.7	5.5	6.5	7.1	7.7	7.1	6.7	6.5	4.8	6.0	5.9
Maximum temperature* (°C)	10	9	12	11	12	15	13	13	11	10	10	11	15
Minimum temperature* (°C)	0	0	0	1	1	2	4	3	3	3	1	2	0
Average dewpoint temperature (°C)	-16.7	-8.6	-14.3	-17.6	-13.5	-11.1	-6.1	-3.7	-3.9	-12.1	-9.0	-22.8	-11.7
Maximum dewpoint temperature (°C)	4	5	4	4	7	9	8	9	8	6	4	-3	9
Minimum dewpoint temperature (°C)	-32	-24	-30	-29	-30	-29	-24	-16	-18	-29	-29	-32	-32
Precipitation (mm)	38	23	22	0	0	1	13	4	7	0	31	0	140
							Day						
Prevailing wind direction	NW	NNW	NW	NNW	NNW	NNW	ESE	NNW	NNW	NNW	SE	SE	NNW
Average wind speed (m s^{-1})	3.9	4.3	4.4	3.5	3.7	2.8	5.0	3.7	3.1	2.7	4.5	5.8	4.0
Maximum wind speed* (m s^{-1})	12	12	15	13	13	8	15	13	11	10	13	16	16
Direction of max. wind* (deg.)	259	214	104	141	153	106	142	147	152	160	142	124	124
Average station pressure (hPa)	678.1	677.9	679.1	679.7	680.3	680.6	680.8	681.0	679.9	679.6	679.7	680.3	679.8
Maximum pressure* (hPa)	682	683	684	683	682	684	683	683	683	683	683	684	684
Minimum pressure* (hPa)	675	673	672	677	678	678	677	678	677	676	677	677	672
Average air temperature (°C)	7.3	6.5	8.3	9.8	10.6	11.2	11.4	11.2	10.3	10.4	7.9	10.2	9.7
Maximum temperature* (°C)	12	13	16	15	15	17	16	15	15	15	14	16	17
Minimum temperature* (°C)	0	0	0	2	3	4	5	4	4	3	1	2	0
Average dewpoint temperature (°C)	-11.7	-5.7	-8.9	-9.6	-6.1	-4.4	-1.6	-0.3	0.6	-5.9	-4.6	-18.4	-6.5
Maximum dewpoint temperature (°C)	6	6	6	8	8	9	9	9	10	8	7	2	10
Minimum dewpoint temperature (°C)	-32	-24	-30	-28	-28	-27	-22	-18	-21	-26	-27	-31	-32
Precipitation (mm)	29	42	38	0	0	10	19	56	58	12	34	0	298

Instrument heights: wind, 10.0 m; pressure, 3398.4 m (MSL); air temperature, 2.0 m; dewpoint temperature, 2.0 m. Wind and temperature instruments are on a tower 15 m southwest of the main building.

*Maximum and minimum values are hourly averages.

TABLE 1.10. MLO 1995 Monthly Climate Summary

	Jan.	Feb.	March	April	May	June	July	Aug.	Sept.	Oct.	Nov.	Dec.	Year
							Night						
Prevailing wind direction	SE	WSW	WSW	SW	SE	SE	SSE	SE	SSE	SE	SSE	SSE	SE
Average wind speed (m s^{-1})	5.4	7.0	6.5	6.1	4.5	4.4	3.8	3.9	3.5	4.3	3.8	4.4	4.8
Maximum wind speed* (m s^{-1})	17	15	16	16	13	12	11	11	11	15	13	14	17
Direction of max. wind* (deg.)	249	241	224	224	241	164	169	164	141	140	152	160	249
Average station pressure (hPa)	680.0	677.4	678.7	678.4	680.2	681.1	680.6	680.3	680.9	680.1	680.4	680.8	679.9
Maximum pressure* (hPa)	683	681	684	682	684	684	683	683	684	684	684	684	684
Minimum pressure* (hPa)	677	673	669	672	677	678	678	678	678	677	677	676	669
Average air temperature (°C)	5.8	4.2	5.7	5.7	6.5	8.8	8.1	7.3	8.5	6.9	5.6	5.5	6.6
Maximum temperature* (°C)	11	11	13	11	11	14	14	13	14	13	10	11	14
Minimum temperature* (°C)	1	-1	-1	0	2	5	2	2	3	1	2	1	-1
Average dewpoint temperature (°C)	-12.8	-15.0	-15.0	-12.5	-12.7	-15.9	-11.2	-13.1	-15.2	-14.7	-5.5	-12.3	-13.0
Maximum dewpoint temperature (°C)	5	3	1	5	8	7	8	7	7	6	6	6	8
Minimum dewpoint temperature (°C)	-30	-38	-30	-32	-28	-25	-24	-27	-28	-29	-24	-31	-38
Precipitation (mm)	5	18	5	1	1	0	3	0	0	0	12	3	49
							Day						
Prevailing wind direction	WSW	WNW	W	NNW	NNW	NE	NE	NE	NE	NNW	NNW	NNW	NNW
Average wind speed (m s^{-1})	5.1	7.1	6.5	6.5	4.7	3.8	3.6	3.5	3.1	3.8	3.0	3.4	4.5
Maximum wind speed* (m s^{-1})	17	14	17	16	13	10	14	12	13	13	13	12	17
Direction of max. wind* (deg.)	248	297	233	233	251	144	148	155	125	147	155	234	248
Average station pressure (hPa)	680.0	677.5	678.8	678.4	680.3	681.2	680.8	680.5	681.0	680.2	680.3	680.7	680.0
Maximum pressure* (hPa)	683	682	684	682	684	683	684	683	684	683	684	685	685
Minimum pressure* (hPa)	677	673	670	673	677	678	678	678	678	677	678	676	670
Average air temperature (°C)	9.4	7.6	9.7	9.7	10.6	13.0	11.7	11.2	12.2	10.5	8.9	9.0	10.3
Maximum temperature* (°C)	16	15	17	15	16	17	16	17	19	17	14	15	19
Minimum temperature* (°C)	1	-1	1	2	3	7	5	4	5	2	2	2	-1
Average dewpoint temperature (°C)	-10.4	-10.9	-10.6	-7.9	-4.7	-7.7	-2.8	-3.8	-5.8	-7.1	-2.2	-7.7	-6.8
Maximum dewpoint temperature (°C)	5	4	6	6	9	8	9	10	9	7	8	6	10
Minimum dewpoint temperature (°C)	-30	-38	-30	-30	-26	-24	-22	-27	-26	-29	-23	-31	-38
Precipitation (mm)	7	16	7	10	11	0	8	16	9	10	25	19	140

Instrument heights: wind, 10.0 m; pressure, 3398.4 m (MSL); air temperature, 2.0 m; dewpoint temperature, 2.0 m. Wind and temperature instruments are on a tower 15 m southwest of the main building.

*Maximum and minimum values are hourly averages.

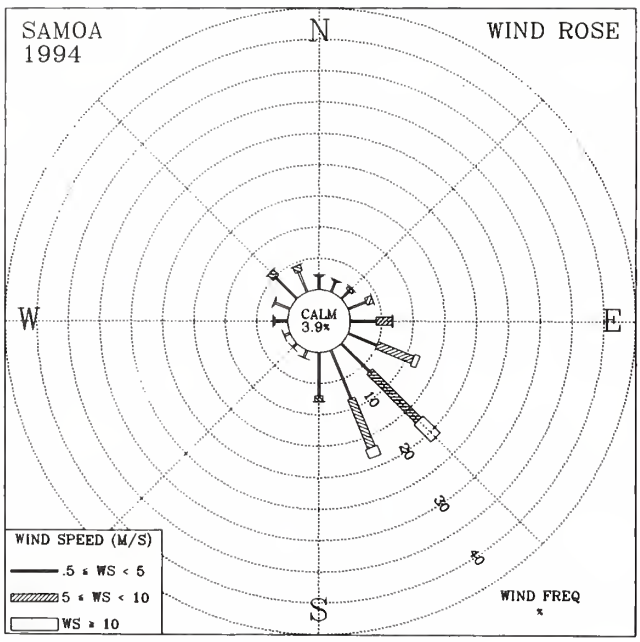

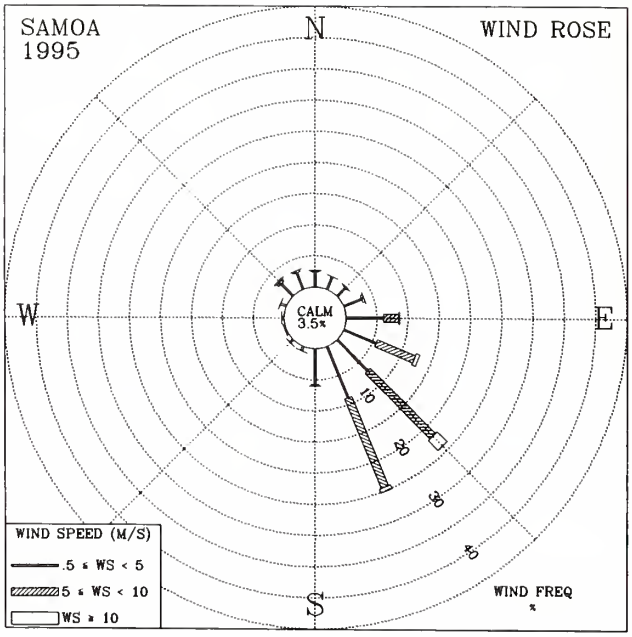

Fig. 1.7. Wind rose of surface winds for SMO for 1994 (left) and 1995 (right). The distribution of resultant wind direction and speed are given in units of percent occurrence. Wind speed is displayed as a function of direction in three speed classes.

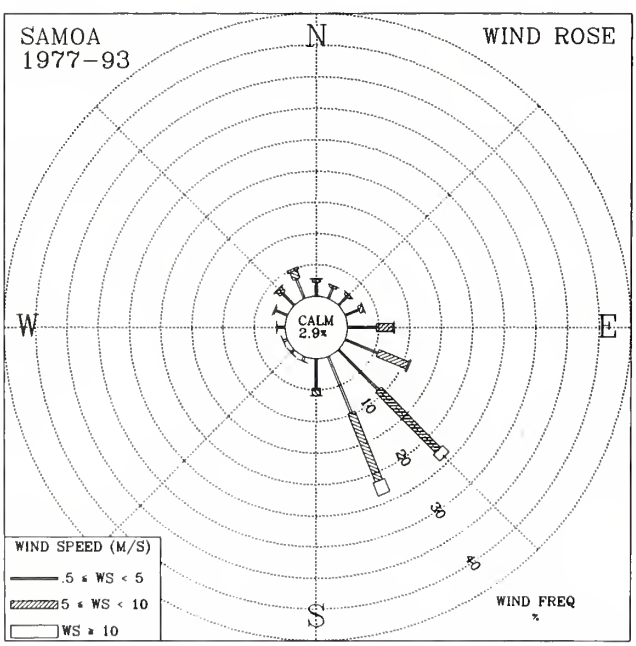

Fig. 1.8. Wind rose of surface winds for SMO for 1977-1993. The distribution of resultant wind direction and speed are given in units of percent occurrence for the 17-year period. Wind speed is displayed as a function of direction in three speed classes.

1.5.2. Meteorology Operations

New Dewpoint Sensors and Electronics Upgrade

Three new hygrothermometers and transmit logic boards from Technical Services Laboratory (TSL) were purchased for the BRW, SMO, and SPO observatories. The model 1088-400 replaced the model 1063-104 at BRW in August 1995, at SMO in December 1995, and at SPO in November 1995. The new model hygrothermometer was installed at MLO when the new data acquisition was initially installed in October 1993. The upgrade improvements include tighter tolerances in the electronic components for greater data accuracy, better radiation shielding of the temperature sensors, and a higher volume of ambient air flow past the temperature sensors to minimize the effects of heat buildup in the sensor housing.

SPO Meteorological Sampling Tower Relocation and Sensor Recalibrations

Prior to moving the meteorological sampling tower, all of the SPO meteorological sensors listed in Table 1.7, except for the Setra pressure transducer, were removed and located on the grid north (upwind) railing of the clean air facility (CAF). The alignment of the wind direction sensor was approximate. From November 9 through November 22, 1995, the tower was disassembled, moved from a location at approximately 100 m along a grid 110° from the current CAF to a location approximately 183 m grid northeast of the CAF, and reassembled. The new location will put the tower approximately 91 m at grid 340° from

TABLE 1.11. SMO 1994 and 1995 Monthly Climate Summary

	Jan.	Feb.	March	April	May	June	July	Aug.	Sept.	Oct.	Nov.	Dec.	Year
							1994						
Prevailing wind direction	SE	NW	SSE	NW	SE	SSE	SE	SE	SSE	SE	SE	SSE	SE
Average wind speed (m s^{-1})	3.8	3.1	3.5	3.7	4.6	6.5	5.5	7.3	4.8	3.7	6.5	4.0	4.8
Maximum wind speed* (m s^{-1})	9	8	14	14	12	13	13	15	11	12	14	11	15
Direction of max. wind* (deg.)	310	140	334	315	144	138	146	145	112	113	138	151	145
Average station pressure (hPa)	998.7	999.3	999.5	999.1	1001.0	1001.8	1001.2	1002.8	1002.7	1001.8	1000.3	997.8	1000.5
Maximum pressure* (hPa)	1003	1003	1004	1003	1005	1006	1004	1007	1007	1005	1004	1003	1007
Minimum pressure* (hPa)	991	996	992	994	996	998	998	997	999	998	994	992	991
Average air temperature (°C)	28.7	29.5	29.1	28.2	27.7	26.9	26.3	25.5	25.9	26.4	26.8	27.3	27.3
Maximum temperature* (°C)	35	37	36	36	34	34	29	27	28	29	29	30	37
Minimum temperature* (°C)	23	23	24	23	21	23	23	23	23	23	23	24	21
Average dewpoint temperature (°C)	23.2	23.5	23.8	23.6	22.4	22.8	23.0	21.7	22.8	24.0	23.8	25.0	23.3
Maximum dewpoint temperature (°C)	26	25	26	26	25	25	26	25	25	26	26	27	27
Minimum dewpoint temperature (°C)	21	22	22	20	20	19	18	15	17	21	20	23	15
Precipitation (mm)	215	121	181	288	283	84	233	200	65	299	201	332	2503
							1995						
Prevailing wind direction	SSE	SE	ESE	SSE	SSE	SE	SE	SE	SE	SSE	SSE	E	SSE
Average wind speed (m s^{-1})	5.9	3.1	3.2	3.1	3.4	6.6	6.1	6.1	6.9	5.7	4.1	2.1	4.8
Maximum wind speed* (m s^{-1})	14	10	8	10	12	11	15	13	13	13	12	6	15
Direction of max. wind* (deg.)	322	138	323	118	156	153	124	164	130	130	87	64	124
Average station pressure (hPa)	998.7	1000.1	1000.6	1000.0	1001.0	1002.9	1002.5	1002.9	1003.7	1001.8	1000.2	999.0	1001.2
Maximum pressure* (hPa)	1005	1004	1005	1003	1004	1007	1006	1007	1007	1006	1005	1005	1007
Minimum pressure* (hPa)	992	995	996	997	997	999	999	999	1000	998	995	995	992
Average air temperature (°C)	27.2	27.7	27.8	27.3	27.1	27.2	26.8	26.4	26.4	26.3	26.8	27.6	27.0
Maximum temperature* (°C)	29	30	29	30	30	29	28	30	29	28	29	30	30
Minimum temperature* (°C)	24	24	24	23	23	24	24	23	23	24	23	25	23
Average dewpoint temperature (°C)	23.9	24.4	24.6	23.9	24.0	23.4	23.5	23.3	22.7	22.9	23.9	23.8	23.7
Maximum dewpoint temperature (°C)	26	27	26	26	26	26	25	25	25	25	26	27	27
Minimum dewpoint temperature (°C)	21	21	22	20	22	20	21	20	17	20	22	21	17
Precipitation (mm)	288	128	192	258	183	85	143	273	119	103	149	39	1960

Instrument heights: wind, 13.7 m; pressure, 78.5 m (MSL); air temperature, 14.0 m; dewpoint temperature, 12.8 m. Wind and temperature instruments are on Lauagae Ridge, 110 m northeast of the main building.

*Maximum and minimum values are hourly averages.

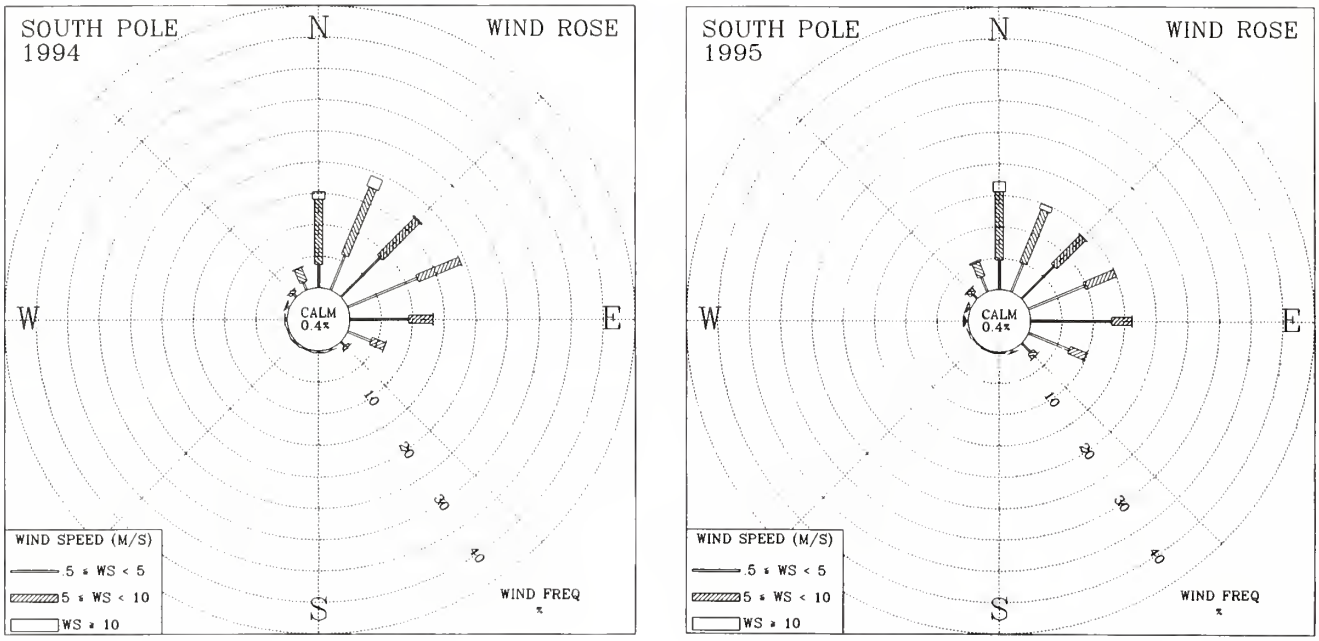

Fig. 1.9. Wind rose of surface winds for SPO for 1994 (left) and 1995 (right). The distribution of resultant wind direction and speed are given in units of percent occurrence. Wind speed is displayed as a function of direction in three speed classes.

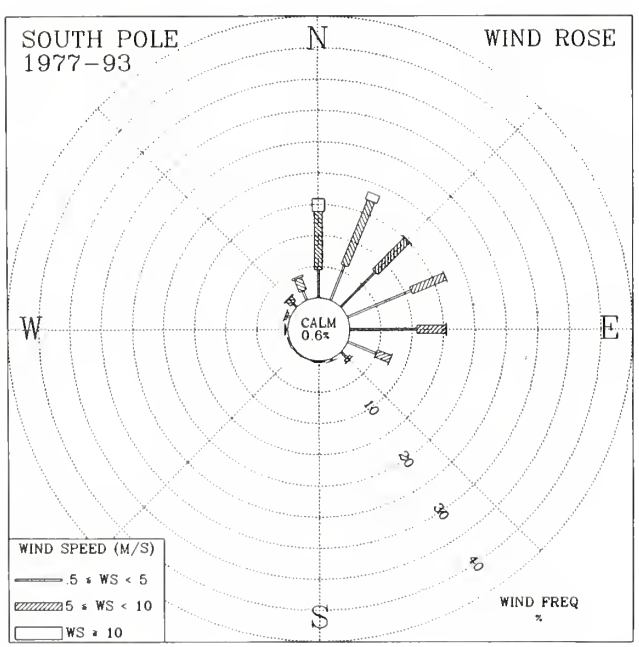

Fig. 1.10. Wind rose of surface winds for SPO for 1977-1993. The distribution of resultant wind direction and speed are given in units of percent occurrence for the 17-year period. Wind speed is displayed as a function of direction in three speed classes.

the new CAF. Nearly two full 2-m sections were buried under snow at the old location. The increase in snow height at the old location was 267 mm per year on average since 1983. The move resulted in a gain of 3 to 3.4 m of tower height and an ability to use all 24 m of the tower. During this time, the new TSL 1088-400 hygrothermometer was put into operation and calibrated. The platinum resistance probes (RTDs) were calibrated by using an ice bath at 0°C. From November 22 through December 2, 1995, a new cable for the RS-485 data communications line was prepared, and hardware for the AC power and the meteorological sensors was installed on the tower at the new location. The azimuth orientation of the anemometer was set by using a solar azimuth alignment tool and tables of solar position. Table 1.13 describes the sensor heights before and after the move of the sampling tower.

1.6. Data Management

During 1994, the meteorological data acquisition system operated 96.9% of the time and during 1995 operated 93.8% of the time. The meteorological data acquisition system gathers data from sensors that operate continuously at each of the four CMDL observatories. The performance was monitored by comparing the number of data points recorded against that expected for the year. Table 1.14 shows the performance of each system during 1994 and 1995. Due to the remoteness of the observatories, power outages are common and the main reason for data loss.

TABLE 1.12. SPO 1994 and 1995 Monthly Climate Summary

	Jan.	Feb.	March	April	May	June	July	Aug.	Sept.	Oct.	Nov.	Dec.	Year
							1994						
Prevailing wind direction	N	ENE	N	E	N	NE	ENE	NE	E	NNE	NNE	ENE	NNE
Average wind speed (m s^{-1})	5.3	4.7	6.2	4.7	5.8	6.2	6.0	5.8	6.6	5.7	4.3	3.4	5.4
Maximum wind speed* (m s^{-1})	11	10	12	10	13	14	12	12	13	10	9	7	14
Direction of max. wind* (deg.)	359	5	13	40	7	214	20	359	30	17	25	116	214
Average station pressure (hPa)	688.3	680.0	674.7	681.9	674.8	691.2	675.4	670.9	676.8	677.3	685.1	680.9	679.7
Maximum pressure* (hPa)	697	687	684	696	693	705	691	687	697	693	693	690	705
Minimum pressure* (hPa)	679	669	664	666	661	677	660	653	651	663	675	672	651
Average air temperature (°C)	-28.3	-44.0	-53.7	-57.3	-58.3	-54.9	-62.5	-58.5	-56.9	-51.3	-37.4	-28.7	-49.5
Maximum temperature* (°C)	-23	-35	-37	-38	-35	-37	-45	-37	-31	-34	-27	-22	-22
Minimum temperature* (°C)	-37	-55	-64	-70	-74	-68	-72	-73	-74	-63	-47	-34	-74
Average dewpoint temperature (°C)	-31.3	-51.1	-59.5	-62.2	-59.3	-59.7	-65.9	-61.0	-56.7	-57.3	-44.5	-34.1	-52.6
Maximum dewpoint temperature (°C)	-24	-42	-42	-42	-39	-41	-50	-41	-34	-38	-33	-26	-24
Minimum dewpoint temperature (°C)	-52	-63	-71	-71	-71	-71	-71	-71	-71	-70	-56	-41	-71
Precipitation (mm)	0	0	0	0	0	0	0	0	0	0	0	0	0
							1995						
Prevailing wind direction	E	N	NNE	N	ESE	E	NE	E	ESE	ENE	N	N	N
Average wind speed (m s^{-1})	3.0	5.1	5.7	6.2	5.8	5.1	6.2	5.4	4.8	6.6	5.3	3.6	5.2
Maximum wind speed* (m s^{-1})	7	10	11	13	14	10	15	12	11	13	10	8	15
Direction of max. wind* (deg.)	351	22	23	340	9	4	28	36	6	11	3	6	28
Average station pressure (hPa)	681.9	682.1	682.0	676.6	671.9	680.5	686.2	676.3	671.4	679.3	683.7	683.6	679.6
Maximum pressure* (hPa)	691	692	690	691	688	697	705	695	685	692	693	692	705
Minimum pressure* (hPa)	675	673	670	655	662	666	673	660	662	669	673	678	655
Average air temperature (°C)	-31.3	-40.3	-52.6	-58.3	-59.0	-58.6	-55.6	-61.8	-64.6	-48.9	-37.9	-27.3	-49.7
Maximum temperature* (°C)	-24	-28	-40	-44	-37	-39	-34	-49	-50	-31	-27	-20	-20
Minimum temperature* (°C)	-38	-51	-66	-74	-76	-72	-68	-74	-77	-66	-49	-33	-77
Average dewpoint temperature (°C)	-38.2	-46.0	-58.1	-63.8	-65.6	-63.7	-61.7	-70.1	-71.8	-54.3	-42.3	-31.1	-54.7
Maximum dewpoint temperature (°C)	-27	-32	-44	-49	-42	-43	-37	-54	-55	-35	-30	-23	-23
Minimum dewpoint temperature (°C)	-47	-60	-73	-81	-85	-79	-75	-81	-86	-73	-55	-37	-86
Precipitation (mm)	0	0	0	0	0	0	0	0	0	0	0	0	0

Instrument heights: wind, 10.0 m; pressure, 2841 m (MSL); air temperature, 2.0 m; dewpoint temperature, 2.0 m. Wind and temperature instruments were on a tower 100 m grid east-southeast of the CAF until November 9, 1995, when the tower was moved to a location 183 m grid northeast of the CAF.

*Maximum and minimum values are hourly averages.

TABLE 1.13. SPO Sensor Instrument Heights Before and After Tower Move

Instrument	Height Before Move (m)	Height After Move (m)
Primary anemometer	10.0	10.0
Pressure transducer	2841.0	2841.0
Air temperature A	1.1	2.0
Air temperature B	20.0	22.0
Air temperature C	1.6	2.0
Dewpoint temperature	1.6	2.0
Non-aspirated temperature	1.4	2.0

Heights are in meters above snow surface, except for barometric pressure, which is with respect to MSL.
Refer to Table 1.7 for sensor information.

TABLE 1.14. CMDL Meteorological Operations Summary, 1994-1995

Station	Expected Number of Data Points	Percent Data Capture	Number of Missing Data Points
	1994		
BRW	3,006,720*	99.08%	27,678
MLO	6,832,800	94.48%	377,222
SMO	1,955,520†	99.27%	14,215
SPO	3,985,920‡	94.95%	201,128
	1995		
BRW	4,204,800	99.40%	25,115
MLO	6,832,800	95.85%	283,394
SMO	3,679,200	84.08%	585,716
SPO	4,204,800	95.88%	173,093

*Expected number of data points as of April 15, 1994.
†Expected number of data points as of June 21, 1994.
‡Expected number of data points as of January 20, 1994.

Hardware failure, system restarts, and system maintenance are the other reasons for data loss. At BRW, during the winter periods, rime, snow, and ice occasionally would build up on the sensors and have to be removed by station personnel. At MLO, high winds caused electrostatic buildup in the wind direction module at 38 m. High winds also caused damage to the 38 m anemometer nose cone and propeller shaft assembly. At SMO, the hygrothermometer failed. The biggest cause of data loss was due to the buildup of corrosion on the sensor connector pins and moisture getting into the RS-485 communications line. This produced noise in the communications that the data acquisition system was not able to handle. At SPO the fuse in the meteorological crate, which houses the Setra pressure transducer and the module for the non-aspirated platinum resistance probe, blew several times due to station power failures. The plastic junction box for the anemometer, which houses a circuit board, disintegrated due to the extreme cold of SPO. Periods of high winds at SPO caused static buildup along the sensors and data lines. The solution was to temporarily disconnect the AC power that would reset the modules. On at least two separate occasions, the static buildup damaged electrical components, requiring their replacement with spare parts on hand at the station.

Data is transferred to Boulder on a daily basis via the Internet. Preliminary hourly averages of wind direction and speed, barometric pressure, ambient and dewpoint temperature, and precipitation amounts are sent to the station personnel. Each month a climatic summary is prepared from edited data and distributed within CMDL and to each of the observatories.

Recently, parts for the aerosol solar radiation (ASR), CO2, and MO3 CAMS have become very difficult to purchase. As a result, CAMS is in the process of being decommissioned. Since 1993, the CAMS system has been gradually replaced with more sophisticated data acquisition systems. These new systems are also gradually getting on the Internet so that the data can be transferred to Boulder more quickly than was possible with the CAMS system.

Acknowledgment. We wish to thank Gary Herbert and Ken Thaut (both retired) who were responsible for the installation of the new meteorological data acquisition systems at MLO in 1993, BRW, SMO, and SPO in 1994, and for their dedication to the CMDL meteorology program.

1.7. References

DeLuisi, J. (ed.), *Geophysical Monitoring for Climatic Change No. 9 Summary Report 1980*, 163 pp., NOAA Environmental Research Laboratories, Boulder, CO 1981.

Peterson, J.T., and R.M. Rosson (eds.), *Climate Monitoring and Diagnostics Laboratory No. 22 Summary Report 1993*, 152 pp., NOAA Environmental Research Laboratories, Boulder, CO, 1994.

Ryan, S., Quiescent outgassing from Mauna Loa Volcano 1958-1994, in *Mauna Loa Revealed: Structure, Composition, History, and Hazards, Geophysical Monograph 92*, edited by J.M. Rhodes and J.P. Lockwood, Am. Geophys. Union, Washington, D.C., 95-115, 1995.

Thoning, K.W., P.P. Tans, and W.D. Komhyr, Atmospheric carbon dioxide at Mauna Loa Observatory, 2, Analysis of the NOAA GMCC data, 1974-1985, *J. Geophys. Res.*, 95(D6), 8549-8565, 1989.

World Meteorological Organization (WMO), *Guide to Meteorological Instrumentation and Observing Practices, No. 8, Tech. Paper 3*, 347 pp., World Meteorological Organization, Geneva, 1969.

2. Carbon Cycle

P.P. Tans (Editor), P.S. Bakwin, T.J. Conway, R.W. Dissly, E.J. Dlugokencky, L.S. Geller, D.W. Guenther, D.F. Hurst, D.R. Kitzis, P.M. Lang, K.A. Masarie, J.B. Miller, P.C. Novelli, C. Prostko-Bell, M. Ramonet, K.W. Thoning, M. Trolier, L.S. Waterman, N. Zhang, and C. Zhao

2.1. Overview

The overall goal of the work by the Carbon Cycle Group (CCG) is to improve our understanding of what determines the atmospheric burden of the major trace gases involved in the carbon cycle: CO_2, CH_4, and CO. Concern about global climate change, and possible future management of the problem, is the driving force behind the work. The anthropogenic influence on all three gas species is large, but natural cycles are involved as well.

Two methods were employed from the start of the Geophysical Monitoring for Climatic Change program, the forerunner of CMDL. Continuous measurements in remote clean air locations, namely the four CMDL observatories, and the collection of weekly or bi-weekly discrete flask samples in pairs, also at remote clean air locations. Initially the samples were analyzed only for CO_2. Methane was added in 1983, CO in 1988, isotopic ratios of CO_2 (in collaboration with the University of Colorado/Institute for Arctic and Alpine Research (CU/INSTAAR)) in 1990.

Information on the sources and sinks of the trace gases is obtained from their rates of increase and from their spatial distributions. The link between sources and observed mixing ratios is provided by numerical models of atmospheric transport operating in both two and three dimensions. Since we are working "backwards" from observed concentrations, this problem is in the class of so-called inverse problems. The greatest limitation is sparseness of data, especially in regions close to important sources and sinks. Therefore the Carbon Cycle Group has gradually expanded the spatial coverage of the cooperative air sampling network, as well as added isotopic ratio measurements since different sources/sinks may be characterized by distinctive isotopic "signatures."

To overcome the limitation of having only measurements from the marine boundary layer, remote from many important source areas, two new approaches were initiated. One is to continuously measure a number of chemical species and atmospheric physical properties at different heights on very tall towers. Mixing ratios in the continental planetary boundary layer are highly variable and their interpretation is more difficult, requiring much more auxiliary data, than the "traditional" marine air samples. The second new approach is to obtain discrete air samples from low-cost airplanes in automated fashion from the boundary layer up to about 8 km altitude. These samples are then sent back to the laboratory in Boulder for analysis. The use of this method, especially over North America, will be greatly expanded to provide significant regional-scale constraints on the budgets of carbon species.

The global air samples also provide a unique resource for narrowing the uncertainties of additional atmospheric problems. In collaboration with the Nitrous Oxide And Halocompounds (NOAH) group of CMDL, the species N_2O (a greenhouse gas) and SF_6 were added to the suite of flask measurements, and other species are under investigation. The development of a method to routinely measure the $^{13}C/^{12}C$ ratio of CH_4, in collaboration with INSTAAR, is at an advanced stage.

Since the global coverage of our sampling is unmatched, CMDL plays an active role in bringing together the measurements from many different laboratories around the world. Towards this end, measurements of field samples as well as reference gas standards are intercompared. The link with the Commonwealth Scientific and Industrial Research Organization (CSIRO) in Australia is particularly strong in this regard. For CO_2 and CO, calibrated reference gases are provided under the auspices of the World Meteorological Organization (WMO). At the "product" end, a common database for CO_2 has been assembled without significant calibration or methodological discrepancies, incorporating the measurements of a number of laboratories, called GLOBALVIEW-CO2. Its intended use is for three-dimensional (inverse) modeling. Plans are to maintain and enlarge the database, as well as assemble similar ones for CH_4, isotopic ratios, etc.

Data records and monthly means can be obtained for each site from the CMDL World Wide Web page (www.cmdl.noaa.gov); the ftp file server's "pub" directory (ftp.cmdl.noaa.gov), from the WMO World Data Center for Greenhouse Gases (Tokyo), and from the Carbon Dioxide Information Analysis Center (Oak Ridge, Tennessee).

2.2. Carbon Dioxide

2.2.1. In Situ Carbon Dioxide Measurements

The mixing ratio of atmospheric CO_2 was measured with continuously operating nondispersive infrared (NDIR) analyzers at the four CMDL observatories during 1994 and 1995 as in previous years. Monthly and annual mean CO_2 concentrations (in the WMO 1993 mole fraction scale (X93)) are given in Table 2.1. These values are provisional, pending final calibrations of station standards. Preliminary selected monthly average CO_2 mixing ratios for the entire record through 1995 are plotted versus time for the four observatories in Figure 2.1.

The CO_2 in situ systems operated during 1994 and 1995 at 94.0% and 91.2% at BRW; 94.2% and 95.1% at MLO; 91.0% and 78.7% at SMO; and 90.9% and 92.9% at SPO. The maximum percentage expected is 95.8% based on missing data due to reference gas calibrations during the year. The majority of the loss of data at SMO in 1995 was due to a failure in the CO_2 NDIR analyzer in November that lasted until late December.

A new data acquisition and control system was installed at MLO in December 1995. This system uses a Hewlett-Packard Unix workstation for controlling not only the CO_2 NDIR measurements, but the CH_4 and CO in situ gas chromatograph systems as well. Data are downloaded from MLO to Boulder daily over the Internet, as well as recorded on optical disks at MLO for backup. New data

TABLE 2.1. Provisional 1994 and 1995 Monthly Mean CO_2 Mixing Ratios From Continuous Analyzer Data (micromol/mol, abbreviated as ppm, relative to dry air WMO X85 mole fraction scale)

Month	BRW	MLO	SMO	SPO
		1994		
Jan.	361.83	358.01	357.00	355.48
Feb.	363.76	358.82	357.37	355.45
March	365.04	359.74	357.10	355.51
April	364.26	361.13	357.35	355.63
May	364.07	361.49	356.76	355.76
June	362.76	360.60	357.02	356.04
July	354.37	359.20	357.60	356.46
August	349.03	357.23	357.32	357.14
Sept.	350.41	355.44	357.33	357.52
Oct.	357.37	355.89	357.63	357.56
Nov.	360.80	357.42	358.16	357.52
Dec.	364.28	358.74	358.59	357.40
Year	359.83	358.64	357.44	356.46
		1995		
Jan.	364.49	359.74	358.54	357.22
Feb.	366.13	360.59	359.30	357.23
March	366.27	361.59	359.31	357.40
April	366.60	363.05	359.03	357.40
May	365.78	363.56	359.43	357.63
June	364.01	363.08	359.28	357.87
July	356.53	361.57	359.50	358.35
Aug.	351.49	358.91	359.31	358.78
Sept.	355.24	357.94	359.17	359.10
Oct.	357.90	357.78	359.47	359.29
Nov.	363.80	359.21	359.89	359.39
Dec.	366.94	360.45	360.15	359.40
Year	362.10	360.62	359.36	358.26

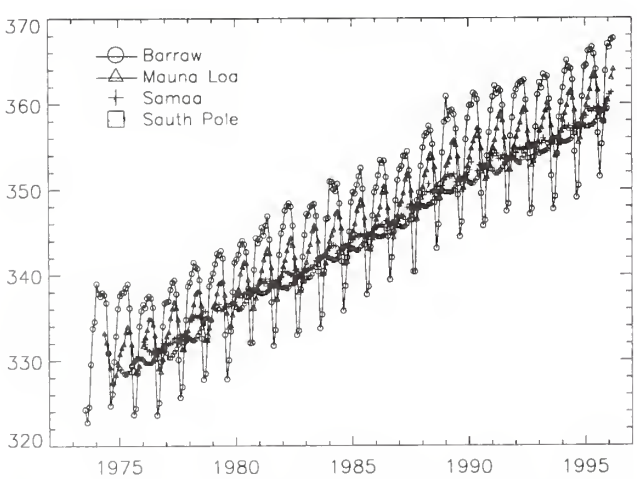

Fig. 2.1. Preliminary selected monthly mean CO_2 mixing ratios expressed in micromol/mol at the four CMDL observatories

acquisition and control systems will be installed at the remaining observatories during 1996.

In addition to the new data system, the CO_2 NDIR analyzer was fitted with smaller optical cells, 60 mm in length compared with the original 180 mm length cells. The glass H_2O cryotrap was relocated between the inlet air pumps and the gas manifold with a smaller auxiliary cryotrap added in between the gas manifold and the NDIR analyzer. With this setup, the first cryotrap dried only the ambient air samples, and the second cryotrap dried the reference gases and the dried ambient air. The volume of gas that the reference gases need to flush away after each gas change was greatly reduced so that lower flow rates were possible. The flow rate was reduced to ~150 cc min^{-1} from 300 cc min^{-1}.

2.2.2. Flask Sample Carbon Dioxide Measurements

Measurements of the distribution and variations of atmospheric CO_2 continued during 1994 and 1995 using samples collected throughout the CMDL global air sampling network. In January and February 1994, sampling began at Easter Island, Chile (29°09'S, 109°26'W; site code: EIC) and Ny-Alesund, Svalbard (78°54'N, 11°53'E; ZEP), respectively. The flask sampling at Easter Island is through the cooperation of the Chilean Meteorological Service. Ny-Alesund is a collaboration with the Stockholm University in situ CO_2 measurement program and is intended to study the North Atlantic/subarctic marine sink for CO_2. In September 1994, flask sampling began near Ushuaia, Argentina (54°52'S, 68°29'W; TDF) in support of the new Global Atmosphere Watch (GAW) observatory. In October 1994, sampling was initiated at Constanta, Romania (44°10'N, 28°41'E; BSC) on the western shore of the Black Sea, and the sampling program on Terceira Island, Azores (38°46'N, 27°23'W; AZR) was revived after a 2-year interruption. In September 1995 flask sampling began at Assekrem, Algeria (23°11' N, 5°25'E; ASK) in cooperation with the GAW observatory at Tamanrasset, Algeria. Finally, in November 1995 CCG began receiving samples collected in the Negev Desert, Israel (31°08'N, 34°53'E; WIS) in cooperation with the Weizmann Institute of Science. These new sites are shown with the rest of the air sampling network in Figure 2.2. Annual mean mixing ratios for 41 sites for 1993, 1994, and 1995 are given in Table 2.2. The 1995 values are based on preliminary editing and data selection.

Air samples were collected in evacuated flasks at 5 degree latitude intervals over the Pacific Ocean aboard the *California Star* (OPC) during 1993 through 1995. In 1995 sampling began on a second ship, the *Brisbane Star* (OPB). Annual averages calculated from merged data from both ships (POC) are given for 14 latitude intervals in Table 2.3. Flask samples were also collected from ships in the South China Sea (SCS). Annual averages for seven 3 degree latitude intervals are given in Table 2.4.

The globally-averaged CO_2 growth rate determined from the air sampling network data is shown in Figure 2.3. The CO_2 growth rate declined from a high of ≈2.6 µmol (abbreviated ppm) per year in 1987 to a low of ≈0.6 ppm yr^{-1} in 1992. The growth rate in 1994 was above the 1981-1995 average of ≈1.4 ppm yr^{-1}, and in 1995 the growth rate was still above the decadal average.

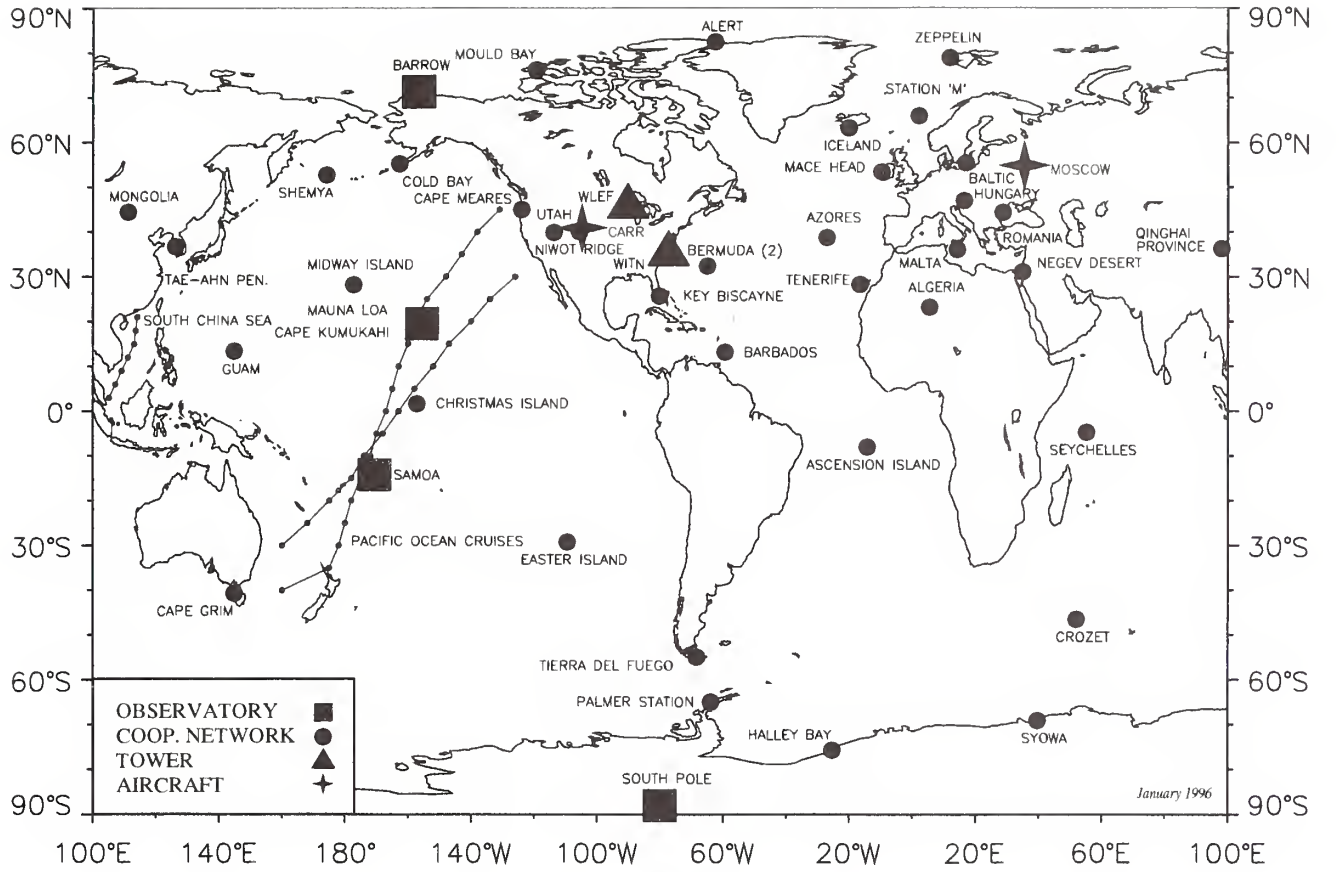

Fig. 2.2. Network of continuing measurements by the Carbon Cycle Group.

A two-dimensional model was developed to use the flask CO_2 data, together with measurements of the $^{13}C/^{12}C$ ratio in CO_2 from the same air samples, to partition CO_2 sources and sinks into terrestrial and marine components as a function of latitude [*Ciais et al.*, 1995a]. An application of this model to data through 1993 attributed a large fraction of the northern hemisphere sink to the terrestrial biosphere [*Ciais et al.*, 1995b]. This is an important result because it is not known which processes account for this sink and also because carbon stored as biomass has the potential to be returned to the atmosphere on short time scales. A preliminary application of the model through 1995 shows that the total global CO_2 sink in 1992 was a factor of 2 larger than in 1995. This analysis also showed significant interannual variations in both the marine and terrestrial components of this sink.

2.2.3. Carbon Dioxide Reference Gas Calibrations

The calibration of CO_2-in-air reference gas tanks continued in 1995; 407 tanks were calibrated using the NDIR analyzer. All CO_2-in-air reference gas tanks used by CMDL are filled with clean dry ambient air from Niwot Ridge, Colorado, in aluminum tanks.

A manometric system was developed for performing primary calibrations of the absolute mole fraction of CO_2 in a carrier (air) gas. The manometric apparatus itself is principally made of glass. It consists essentially of a 6-L glass flask connected by means of a manifold to a 10-mL glass small volume. A pressure gauge of quartz spiral Bourdon tube type as a primary manometer in the manometric system is used to measure the CO_2 and the carrier gas pressures precisely. The apparatus is enclosed in an oven. The temperature of the oven is uniform and controlled to an accuracy of 0.01°C during the calibration process. The quartz spiral pressure gauge is regularly calibrated with a dead-weight pressure calibration tester.

To begin the manometric calibrating process the glass manometric chamber, including the 6-L large volume, the manifold, and 10-mL volume, are evacuated to a residual pressure of less than 1 millitorr. A sample of air from a cylinder to be analyzed is dried at -70°C to remove water vapor and then fills the evacuated glass chamber to the ambient pressure. After the sample air in the chamber has come to equilibrium, the temperature is measured by platinum resistance thermometers, and pressure is measured by the quartz spiral gauge. The sample air from the chamber is then slowly pumped out through two liquid nitrogen traps, freezing out CO_2, N_2O, and residual water vapor. Upon completion of the extraction, the CO_2 frozen in the traps is dried with a dry ice-alcohol mixture and then transferred to the small 10 mL volume by placing liquid nitrogen around it. After the 10-mL small volume containing the collected pure CO_2 (and N_2O) is thawed, the temperature and pressure are continuously measured

TABLE 2.2. Provisional 1993-1995 Annual Mean CO_2 Mixing Ratios From Network Sites

Code	Station	CO_2 (ppm) 1993	1994	1995
ALT	Alert, N.W.T., Canada	357.7	359.8	361.1
ASC	Ascension Island	355.8	357.3	359.2
AZR	Terceira Island, Azores	[ ]	[ ]	359.5
BAL	Baltic Sea	359.9	361.9	364.4
BME	Bermuda (east coast)	356.8	358.8	361.3
BMW	Bermuda (west coast)	357.3	359.8	361.0
BRW	Barrow, Alaska	358.2	359.6	361.9
BSC	Constanta, Romania		[ ]	364.6
CBA	Cold Bay, Alaska	357.8	359.1	361.4
CGO	Cape Grim, Tasmania	354.5	356.1	357.9
CHR	Christmas Island	357.4	[ ]	[ ]
CMO	Cape Meares, Oregon	358.5	361.7	[ ]
CRZ	Crozet Island	355.3	356.9	357.9
EIC	Easter Island, Chile		355.7	357.6
GMI	Guam, Mariana Islands	356.6	358.5	360.6
GOZ	Gozo Island, Malta	[ ]	359.6	362.2
HBA	Halley Bay, Antarctica	355.1	356.9	358.1
HUN	Hegyhatsal, Hungary	[ ]	362.2	366.6
ICE	Vestmanaeyjar, Iceland	357.3	359.0	360.1
IZO	Izana Observatory, Tenerife	357.5	358.6	361.4
KEY	Key Biscayne, Florida	358.4	359.3	362.1
KUM	Cape Kumukahi, Hawaii	357.1	359.1	360.9
MBC	Mould Bay, Canada	357.8	359.9	361.3
MHT	Mace Head, Ireland	356.7	358.6	360.7
MID	Midway Island	357.5	359.2	360.9
MLO	Mauna Loa, Hawaii	356.9	358.5	360.6
NWR	Niwot Ridge, Colorado	357.4	359.5	361.2
PSA	Palmer Station, Antarctica	355.1	356.4	358.1
QPC	Qinghai Province, China	357.3	359.3	[ ]
RPB	Ragged Point, Barbados	356.7	358.0	360.2
SEY	Mahe Island, Seychelles	356.0	356.5	358.1
SHM	Shemya Island, Alaska	357.7	360.6	360.9
SMO	American Samoa	355.6	357.4	359.2
SPO	South Pole, Antarctica	354.8	356.2	357.7
STM	Ocean Station M	357.5	359.2	360.4
SYO	Syowa Station, Antarctica	354.5	356.1	358.1
TAP	Tae-ahn Peninsula, S. Korea	360.4	361.2	363.6
TDF	Tierra del Fuego, Argentina		[ ]	[ ]
UTA	Wendover, Utah	[ ]	361.2	361.2
UUM	Ulaan Uul, Mongolia	357.1	359.3	360.3
ZEP	Ny-Alesund, Svalbard		359.2	361.0

Square brackets indicate insufficient data to calculate annual mean.

The 1994 and 1995 annual means have been adjusted upward by 0.25 ppm to correct for a systematic loss of CO_2 in the flask analysis apparatus.

while equilibrium is reached. Because the volume ratio of the small and the large volumes is known accurately, the molar ratio of the CO_2 in the original air sample can be calculated with the virial equation of state, taking real gas compressibility into account, and correcting for the N_2O contribution.

From December 1995 to February 1996, the CO_2 concentrations of three cylinders with CO_2-in-air mixtures were determined by the manometric calibration system. The results of the tests are presented in Table 2.5. For

TABLE 2.3. Provisional 1993-1995 Annual Mean CO_2 Mixing Ratios from Pacific Ocean Cruises

Latitude	CO_2 (ppm) 1993	1994	1995
30°N	357.7	359.4	360.8
25°N	357.7	359.5	361.4
20°N	357.1	359.6	361.0
15°N	357.6	359.7	360.7
10°N	357.8	359.2	361.1
5°N	357.7	359.5	361.0
Equator	357.5	359.1	360.6
5°S	357.0	358.9	360.4
10°S	356.7	358.3	360.2
15°S	356.2	357.8	359.5
20°S	355.8	358.1	359.0
25°S	355.4	357.6	358.5
30°S	355.4	356.9	358.4
35°S	355.5	357.0	358.6

TABLE 2.4. Provisional 1993-1995 Annual Mean CO_2 Mixing Ratios from South China Sea

Latitude	CO_2 (ppm) 1993	1994	1995
21°N	361.1	360.4	362.0
18°N	360.2	360.3	362.2
15°N	357.8	360.2	362.3
12°N	359.9	360.0	361.2
9°N	357.9	359.9	362.3
6°N	357.9	359.8	361.5
3°N	359.2	359.8	361.1

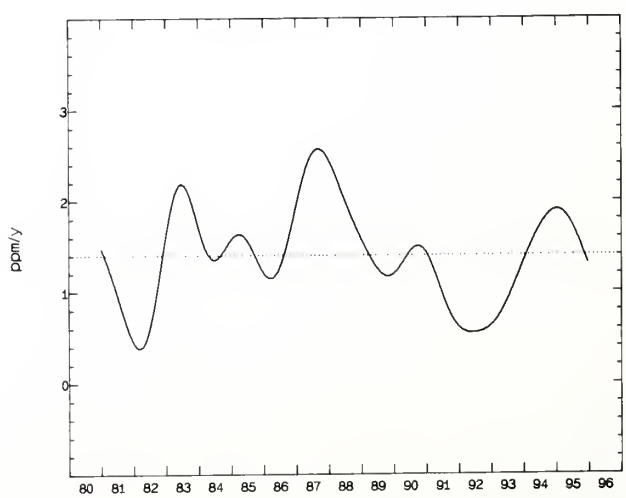

Fig. 2.3. Global CO_2 growth rate.

TABLE 2.5. Results of Tests Using Manometric Calibration System

Date	Cylinder Serial No.	Manometric CO_2	Average	Standard Deviation	NDIR	Difference (NDIR-MANO)
Dec. 6, 1995	71568	386.33				
Dec. 6, 1995	71568	386.30				
Dec. 8, 1995	71568	386.37	386.33	0.035	386.25	-0.08
Feb. 1, 1996	56797	352.67				
Feb. 2, 1996	56797	352.78				
Feb. 5, 1996	56797	352.83				
Feb. 13, 1996	56797	352.62				
Feb. 16, 1996	56797	352.77				
Feb. 17, 1996	56797	352.77				
Feb. 19, 1996	56797	352.76				
Feb. 20, 1996	56797	352.62				
Feb. 20, 1996	56797	352.77				
Feb. 21, 1996	56797	352.63				
Feb. 21, 1996	56797	352.89	352.74	0.090	352.77	0.03
Feb. 23, 1996	114997	314.97				
Feb. 24, 1996	114997	314.95				
Feb. 26, 1996	114997	315.02				
Feb. 28, 1996	114997	314.90				
Feb. 28, 1996	114997	315.02				
Feb. 29, 1996	114997	315.08	314.99	0.063	315.05	0.06

CO_2 concentrations in µmol/mol.

comparison, the CO_2 mole fractions measured by a NDIR analyzer using reference gases calibrated by the Scripps Institution of Oceanography (SIO) are also shown in the table. The reproducibility of the manometric system indicated in Table 2.5 as the standard deviation is about ±0.06 µmol for a total of 20 measurements. The largest mean difference of measurements between the NDIR and the manometric system is 0.08 µmol for the three CO_2-in-air mixture cylinders.

2.2.4. Measurements of Stable Isotopes of CO_2

Since 1990, the Stable Isotope Laboratory at INSTAAR has been measuring the stable isotopic composition of CO_2 from flask samples from the CMDL global air sampling network. The natural ratio of ^{13}C to ^{12}C is about 1.1% everywhere, but biogeochemical processes (such as photosynthesis or atmosphere-ocean exchange) can sustain small but readily measurable differences in that ratio between different carbon reservoirs. For example, plants discriminate against ^{13}C during photosynthetic uptake, therefore the $^{13}C/^{12}C$ ratio in plant carbon (and, by derivation, in soils and fossil fuels) is depleted relative to the atmosphere, typically by about 20‰ (per mil, or parts per thousand)—which in turn leaves the atmosphere subtly enriched in ^{13}C. Observing such a ^{13}C signature allows exchanges of CO_2 with the biosphere to be distinguished from oceanic fluxes because the latter do not carry a significant isotopic signature [e.g., *Keeling et al.*, 1995]. The ^{18}O composition of atmospheric CO_2 ultimately derives from its equilibration with liquid water, providing a link between the global carbon and hydrologic cycles. For example, CO_2 exposed to water within the leaves of plants, but diffusing out of the leaf before being incorporated, carries the isotopic signature of leaf water back to the atmosphere. Because CO_2 "remembers" the ^{18}O signature of the water reservoir it has most recently visited, this tracer may prove to be useful in quantifying the gross annual uptake of CO_2 by photosynthesis and its release by respiration.

INSTAAR currently measures $\delta^{13}C$ (the normalized difference between the isotopic ratios of a sample and standard) and $\delta^{18}O$ in CO_2 for almost all of the CMDL network flasks, having begun with a selection of only six sites and two ships in 1990. The growth of the effort, reflected by the number of sites and flasks measured each year, is shown in Figure 2.4. Each measurement is made by first cryogenically extracting CO_2 from about 750 standard cm^3 of dried air, then measuring the relative abundance of isotopic species of masses 44, 45, and 46 using a triple-collector isotope-ratio mass spectrometer [*Trølier et al.*, 1996]; precisions of 0.03‰ and 0.06‰ are obtained for $\delta^{13}C$ and $\delta^{18}O$ respectively. Small numerical corrections account for the presence of N_2O trapped with CO_2 and for the presence of isotopic species including ^{17}O. The isotopic data are fully integrated into the Carbon Cycle Group's trace gas data base.

A sample of the isotope data is given in Figure 2.5, which shows time series of CO_2 mixing ratio, $\delta^{13}C$, and $\delta^{18}O$ from Barrow, Alaska, from 1990 through 1995. There is a striking anticorrelation between the seasonal cycles of mixing ratio and $\delta^{13}C$, reflecting the strong influence of the annual cycle of photosynthesis and respiration imposed on the atmosphere by the terrestrial biosphere in the northern hemisphere. Whereas the mixing ratio shows an increasing long-term trend due to the use of fossil fuels, the trend of $\delta^{13}C$ is to lighter values, reflecting the depletion in ^{13}C of fossil fuel relative to the atmosphere. The seasonal cycle of $\delta^{18}O$ lags behind CO_2 and $\delta^{13}C$, and while its interannual variability shows no steady trend, it can change its level dramatically from year to year, most likely because of the large exchanges of CO_2 between biosphere and atmosphere that are subject to efficient oxygen isotope exchange.

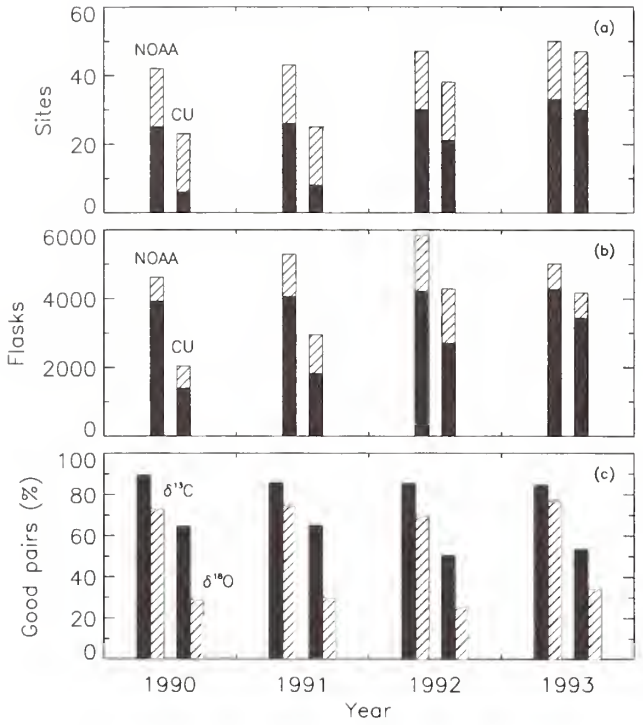

Fig. 2.4. Statistics of the isotope measuring effort. The extent of the NOAA CO_2 monitoring program is shown for comparison. Solid bars represent land sites, hatched bars represent latitude bands from shipboard sampling. (a) Number of sites measured during each year. (b) Number of flasks analyzed each year. (c) Percentage of "good" flask pairs for $\delta^{13}C$ and $\delta^{18}O$.

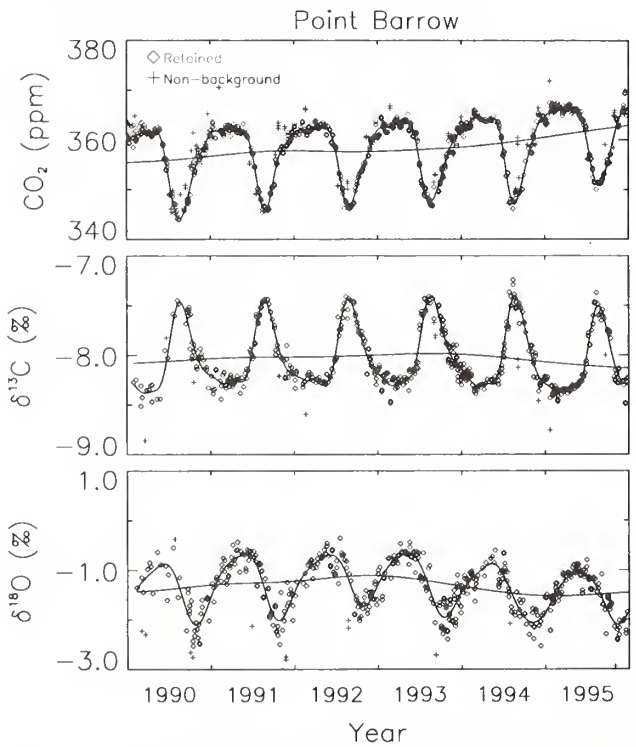

Fig. 2.5. Time series of CO_2 (upper panel), $\delta^{13}C$ of CO_2 (middle panel), and $\delta^{18}O$ (lower panel) from Point Barrow, Alaska.

The INSTAAR isotope data were recently described in detail [*Trolier et al.*, 1996]. The INSTAAR $\delta^{13}C$ time series, though beginning only in 1990, were used in concert with the longer $\delta^{13}C$ time series from Cape Grim, Australia, obtained by CSIRO, to identify a global flattening of the long-term $\delta^{13}C$ trend during 1988-1992 [*Francey et al.*, 1995a]. The decadal average trend observed during the 1980s, about 0.025‰ yr^{-1}, was apparently offset during these years by anomalously high uptake of CO_2 by the global biosphere. Similarly, the INSTAAR $\delta^{13}C$ data, supplemented by CSIRO data from the southern hemisphere, definitively identify a strong northern hemisphere biospheric sink equivalent to nearly half the annual anthropogenic source during 1992 and 1993 [*Ciais et al.*, 1995b]. Interpretive work using the $\delta^{18}O$ data is underway. In addition to these scientific analyses, the measurements are actively intercompared with other atmospheric monitoring laboratories measuring CO_2 isotopic composition [*Francey et al.*, 1995b; *Gaudry et al.*, 1996].

INSTAAR recently obtained a more precise isotope-ratio mass spectrometer, a VG Optima, for analyzing the CMDL flasks. The instrument is currently being tested and it will come on-line for flask analysis during 1996. This instrument will be devoted entirely to analysis of atmospheric samples and will allow us to focus more attention on calibration. It is expected that the Optima will improve the analytical precision by about a factor of 3.

2.2.5. The Airkit Sampler

Field testing of a new prototype air sampling apparatus began at SMO in September 1994 and Cape Kumukahi, Hawaii (KUM) in May 1995. The new Airkit (Air Kitzis sampler) differs from the currently used MAKS (Martin and Kitzis Sampler) in two important ways: (1) It has a thermoelectrically cooled condenser to remove water vapor from the air stream, and (2) It has a microprocessor to control the sampling process so that collecting the sample is more automated and less subject to operator error. The effect of drying the air sample is most dramatic for the measurement of $^{18}O/^{16}O$ in CO_2 (Figures 2.6 and 2.7). In samples collected at humid, tropical locations without drying, the $^{18}O/^{16}O$ measurements are highly variable and consistently more depleted in ^{18}O due to the exchange of oxygen atoms between CO_2 and H_2O molecules. It was established through systematic tests at INSTAAR [*Gemery*, 1993] that the exchange takes place during storage in the flasks when the relative humidity of the air sample is above 50%. Overlapped sampling with the Airkit and MAKS at SMO and KUM shows that this effect is eliminated with the Airkit and that the measurement of other species is not affected by the drying (Table 2.6). The pair agreement improves from 0.73‰ (1σ) to 0.09‰.

2.2.6. Calibration of Measurements of Stable Isotopes of CO_2

The INSTAAR stable isotope data are reported as isotopic composition relative to VPDB-CO_2 for both $\delta^{13}C$ and $\delta^{18}O$. Calibration of this record has two distinct facets. The first relies on comparatively precise intercomparisons of samples of CO_2 extracted from air. Carbon dioxide from individual flask samples is always

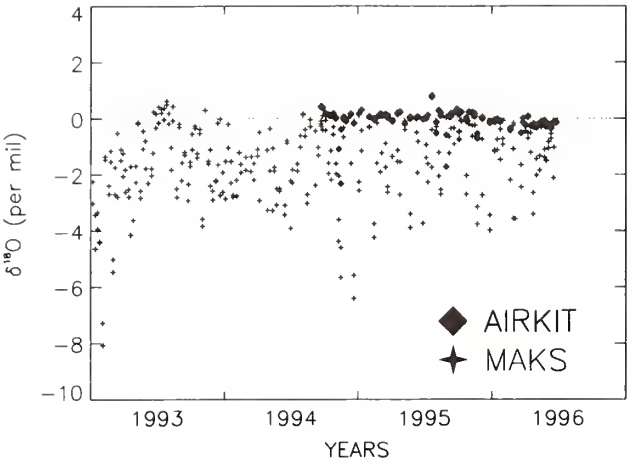

Fig. 2.6. Oxygen-18 in flask samples from Cape Matatula, Samoa. The majority of the "wet" samples were rejected due to poor pair agreement. The few fortuitously retained pairs tend to be isotopically "light." Since samples have been dried with the Airkit, however, a first glimpse of the true $\delta^{18}O$ signature of CO_2 at equatorial latitudes from the CMDL network has been seen.

compared with CO_2 from a "working reference" cylinder. The isotopic composition of the working reference cylinder itself is currently tracked on a monthly basis by comparison with a suite of secondary reference cylinders. The second facet of calibration consists of the comparison of the isotopic scale established by the reference cylinders to accepted international standards ("absolute" calibration). These measurements require the comparison of CO_2 derived from different materials using different preparation systems and to date have been subject to larger uncertainties. Both carbonate standards (NBS-19, NBS-20, and INSTAAR laboratory standards) and water standards (V-SMOW, SLAP, and laboratory standards) have been used for absolute calibrations.

Comparisons among the reference cylinders, though few in the early years of the program, have expanded to provide a fairly strong constraint on the consistency of the

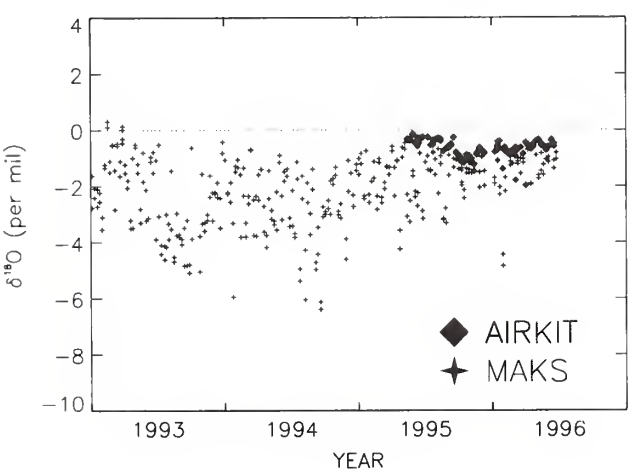

Fig. 2.7. Oxygen-18 in flask samples from Cape Kumukahi, Hawaii. The comparison between Airkit and MAKS is very similar to Samoa.

TABLE 2.6. Comparison of Airkit to MAKS Sampler

			Airkit Minus MAKS		
Site	Species	No. Pairs	Average	Standard Deviation	Units
KUM	CO_2	31	-0.07	0.40	ppm
SMO	CO_2	48	-0.04	0.18	ppm
KUM	CH_4	33	0.19	1.99	ppb
SMO	CH_4	53	0.42	2.35	ppb
KUM	CO	28	-2.01	2.49	ppb
SMO	CO	53	0.05	1.19	ppb
KUM	$\delta^{13}C$	29	0.02	0.05	permil
SMO	$\delta^{13}C$	47	0.02	0.14	permil
KUM	$\delta^{18}O$	7	0.67	0.82	permil
SMO	$\delta^{18}O$	15	1.08	1.06	permil

Summary of the differences between retained pairs for simultaneous Airkit and MAKS samples. There are no significant differences between Airkit samples and the MAKS samples except for $\delta^{18}O$, where the retained MAKS pairs are considerably depleted in ^{18}O at both KUM and SMO.

working reference gas scales for $\delta^{13}C$ and $\delta^{18}O$. Working reference gas cylinders are used for up to 3 years; transitions between working reference cylinders provide the unfortunate possibility of a step shift in calibration. Such shifts could be too subtle to detect by too-seldom and too-noisy comparisons with carbonates and waters but can be tracked by other cylinders (provided, of course, that the suite of cylinders is not drifting in parallel).

Figure 2.8 shows a summary of the calibration data available for the INSTAAR isotope data for $\delta^{13}C$ and $\delta^{18}O$. The central feature of these plots are the scales defined by the sequence of working reference gases shown by solid lines plotted for each cylinder during its lifetime. This scale determines the values that are assigned to individual flask samples. Dotted lines represent the cylinders' values outside their period of use as the working reference. The relative values of any two working reference cylinders are determined by extensive inter-comparison preceding the transition. Also shown are the values for the working cylinders determined from other reference gases (open symbols) and carbonate or water standards (closed symbols); error bars (1σ) are shown where more than one determination is made in a month. Uncertainties clearly persist, particularly for the absolute assignment of the $\delta^{18}O$ scale. The assigned scales are to some extent based on subjective evaluations of the reliability of different calibration methods. However, drifts and step shifts within the working reference scales seem unlikely beyond (pessimistically) 0.02U‰ for $\delta^{13}C$ and 0.04‰ for $\delta^{18}O$.

2.3. Methane

2.3.1. In Situ Methane Measurements

Quasi-continuous in situ measurements of atmospheric CH_4 continued at MLO and BRW. Details of the measurement techniques and analysis of the in situ data through early 1994 were published in late 1995 [*Dlugokencky et al.*, 1995]. Daily averaged CH_4 mole fractions (in nanomol/mol or 10^{-9} mole/mole; abbreviated ppb) are plotted in Figure 2.9 for BRW (a) and MLO (b).

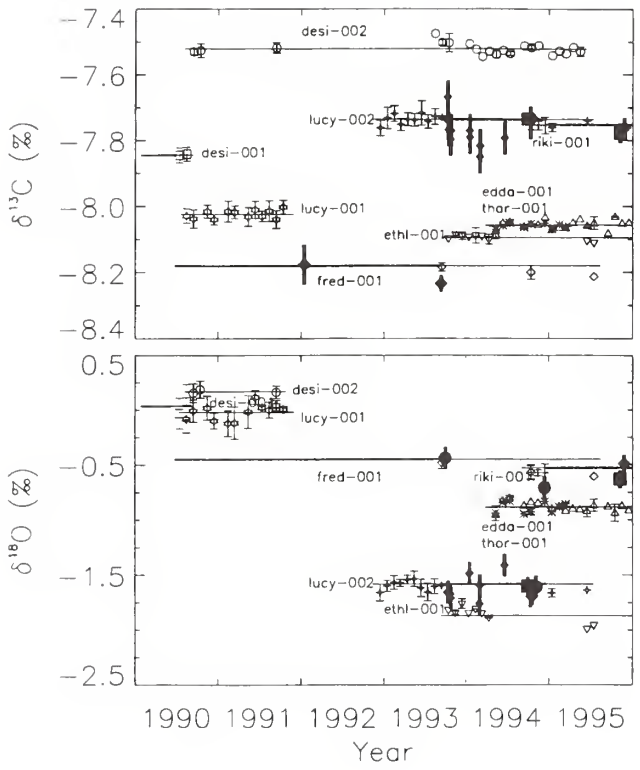

Fig. 2.8. Calibration of the NOAA-CU data set. The upper panel shows calibrations for $\delta^{13}C$, the lower for $\delta^{18}O$. Reference gases are identified by cylinder name. Monthly means of calibrations of reference gases are plotted using open symbols; where more than one determination was made in a month, error bars are plotted at twice the standard deviation of the monthly values. Mean values for working reference gases are plotted as thick solid lines, for secondary reference gases as thin lines. Calibrations of the working reference scale using primary isotope reference materials are plotted as solid symbols (NBS-19, squares; NBS-20, diamonds; SMOW, circles).

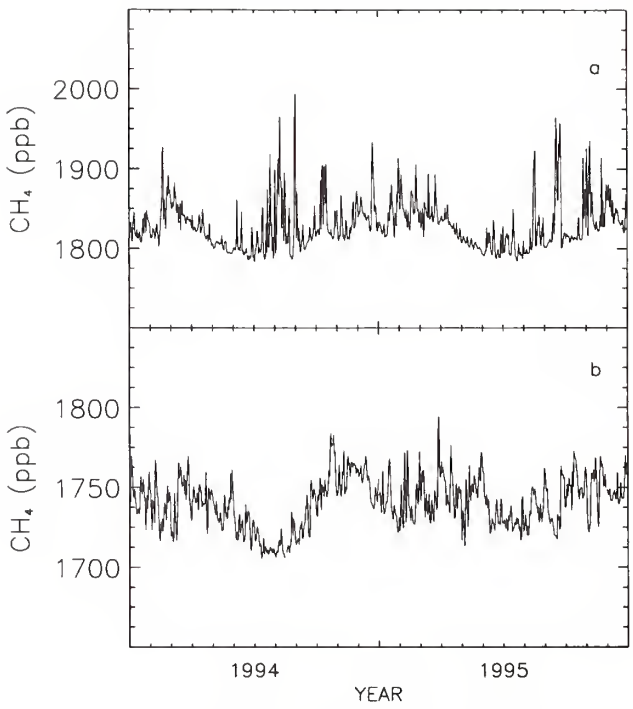

Fig. 2.9. Daily mean CH_4 mixing ratios in 10^{-9} mole/mole (abbreviated ppb) for (a) BRW and (b) MLO for 1994 and 1995. The data have not been selected for meteorological conditions, but have undergone a quality control step to ensure that the analytical instrument was working optimally when they were obtained [*Masarie et al.*, 1991].

The data have been edited for instrument malfunction using a rule-based expert system [*Masarie et al.*, 1991], but were not selected for meteorological conditions. High CH_4 values at BRW are due to emissions from local sources. Limitations of the unselected data sets have been discussed previously [*Dlugokencky et al.*, 1995].

Previously it was reported that the precision of the measurements (~0.2%) was limited in part by variations in laboratory temperature which affects the flow rate of H_2 to the FID [*Peterson and Rosson*, 1993]. On December 1, 1995, a new analytical system was installed at MLO ushering in a new era of high precision in situ CH_4 measurements at MLO. Main components of the system are an HP 6890 GC with FID, an HP 35900E analog-to-digital converter (A/D), a temperature controlled box for the sample valve, and a HP UNIX workstation. A similar system will be installed at Barrow during Spring 1996.

The gas chromatography has not changed significantly from what was used previously, except that the carrier gas was switched to N_2 to improve sensitivity. Two columns are used to separate CH_4 from air, and flame ionization is used for detection. Column head pressure and flow rates for the FID gases are controlled electronically by the GC. The signal from the FID is amplified by an electrometer and sent to the A/D. Previously the A/D was included in a stand-alone integrator. The new HP 35900E A/D is 24-bit (versus 16 bit for the integrator), so it does not limit the measurement precision.

Integration is now done on the UNIX workstation using an algorithm developed by SIO and incorporated into a program developed by the Carbon Cycle Group called GCPLOT. This program allows integration and display of chromatograms, and it is a powerful diagnostic that can be used to troubleshoot problems with the CH_4 chromatography and GC system. This integration system is also paperless; about 1-month's worth of chromatograms are stored on the workstation hard disk, and these can be displayed on the computer monitor with GCPLOT. A typical chromatogram is shown in Figure 2.10. The peak at about 78 seconds is the air disturbance. The CH_4 peak response (at retention time = 124 seconds), from the baseline to the top of the peak, is ~16.8 mV. Peak-to-peak noise is ~8 μV. Previously, peak height was used to calculate CH_4 mole fractions since height resulted in about a factor of 3 better precision than peak area response. With the new integration algorithm, peak area yields slightly better precision than height; therefore, peak area is now being used as the quantitative measure of CH_4 peak response. Using area is preferable to height because it gives a linear response over a larger range of mixing ratios. The mole fractions are calculated as before; the peak area

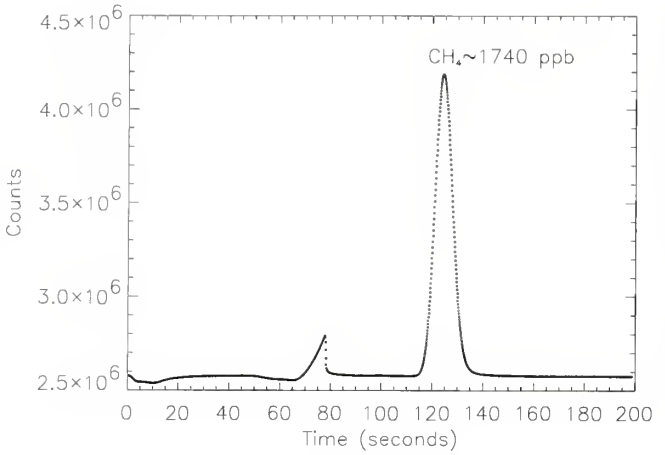

Fig. 2.10. Typical CH_4 chromatogram from MLO obtained with the new analysis system. A/D sampling rate was 10 Hz. On the y-axis, there are 10^5 counts mV^{-1}. Signal-to-noise is ~2000, based on a peak height of 16.8 mV and peak-to-peak noise of ~8μV. The retention time for CH_4 is 124.3 seconds, and the full-width-at-half-max is 8 seconds.

from the sample is ratioed to the average peak area of the bracketing standard gas injections. This ratio is then multiplied by the assigned value for the standard gas cylinder. By only using the injections of standard gas, this calculation can be used to assess the instrument precision as described in the following paragraph.

The preceding improvements have lead to an overall improvement in precision at MLO of a factor of 4. Typical relative precision is 0.04 to 0.07% (or <1 ppb CH_4 for ambient levels of about 1700 ppb). In Figure 2.11, relative differences between measurements of standard gas and the assigned value for the standard gas cylinder ("Relative Precision") are plotted for a 24-hour period. The relative precision for this day (assessed as 1σ) was 0.03% (0.6 ppb).

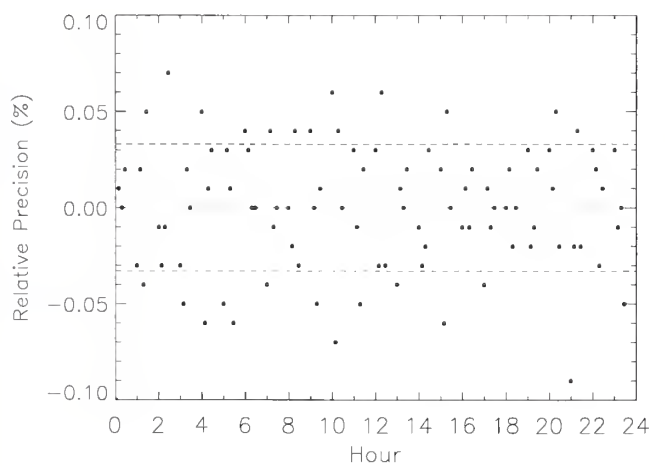

Fig. 2.11. Relative measurement precision, assessed as the difference between measurements of standard gas and the assigned value of the standard gas cylinder, plotted for a 24-hour period. The relative instrument precision on this day, based on 1σ for each measurement of reference gas, was 0.03% (plotted as the dashed lines). This corresponds to a precision, in mole fraction, of ±0.6 ppb for each measurement.

The new system is controlled by a program run on the UNIX workstation. This program chooses between ambient and standard gas flows from the stream selection valve, switches the gas sample valve to start the run, and records the digitized chromatogram. A VXI bus acts as the interface between the UNIX workstation and other system components. Various other programs that can be used to look at the results are also available at the workstation.

2.3.2. Discrete Sample Measurements of Methane

During 1994-1995, the determination of the global distribution of atmospheric CH_4 continued from 46 sampling sites of the Carbon Cycle Group's cooperative air sampling network. Provisional annual mean values for 1994-1995 are given in Table 2.7.

The effects of the eruption of Mt. Pinatubo on the growth rates of trace species such as CH_4, CO_2, CO, and N_2O still remain an area of great interest to our group. Studies of perturbations in growth rate that are associated with a specific event such as the eruption can be a useful tool in understanding the trace gas budgets. The eruption of Mt. Pinatubo on June 15, 1991, injected 20 Mt SO_2 and 3-5 km^3 of ash into the upper troposphere and lower stratosphere, and CH_4 and CO mixing ratios in the tropics immediately increased. The increased growth rates were short-lived as CH_4 [*Dlugokencky et al.*, 1994a] and CO [*Novelli et al.*, 1994] growth rates showed dramatic decreases later during 1992 and 1993.

In Figure 2.12a, CH_4 zonal means for the latitude zone 30-90°S are plotted (open triangles) along with a function fitted to the zonal means (dashed line) of the form:

$$f(t) = a_1 + a_2 t + a_3 t^2 + \sum_{i=1}^{4} [a_{2i+2} \sin(2\pi i t) + a_{2i+3} \cos(2\pi i t)]. \quad (1)$$

Equation (1) is used to approximate (or model) the average trend and seasonal cycle for atmospheric CH_4. Starting in late 1991, there is a significant departure of the "model" from the zonal means. The solid line is the deseasonalized trend (see *Dlugokencky et al.*, 1994b for details of the curve fitting process). Its derivative, the instantaneous CH_4 growth rate, is shown in Figure 2.12b. The largest perturbation in CH_4 growth rate observed in this time series was during late-1991 and early 1992.

The CH_4 growth rate is due to a relatively small imbalance between sources and sinks; therefore, the perturbation in 1991 could be due to either a change in one or more sources or a change in the sink. The major sink for CH_4 is reaction with hydroxyl radical

$$OH + CH_4 \rightarrow H_2O + CH_3 . \quad (2)$$

In the clean marine troposphere, most OH formation is initiated through photolysis of O_3 to give electronically excited oxygen atoms

$$O_3 + h\nu\ (330 \geq \lambda \geq 290\ nm) \rightarrow O(^1D) + O_2 . \quad (3)$$

TABLE 2.7. Provisional 1994 and 1995 Annual Mean CH_4 Mixing Ratios From the Air Sampling Network

Code	Station	1994 CH_4 (ppb)	1995 CH_4 (ppb)
ALT	Alert, N.W.T., Canada	1809.8	1811.3
ASC	Ascension Island	1684.0	1690.4
AZR	Terceira Island, Azores	[ ]	1783.2
BAL	Baltic Sea	1828.6	1853.7
BME	Bermuda (east coast)	1773.1	1780.5
BMW	Bermuda (west coast)	1765.3	1771.0
BRW	Barrow, Alaska	1821.4	1822.3
CBA	Cold Bay, Alaska	1801.9	1804.2
CGO	Cape Grim, Tasmania	1671.8	1679.8
CMO	Cape Meares, Oregon	1788.5	[ ]
CRZ	Crozet Island	[ ]	1679.3
GMI	Guam, Mariana Islands	1731.3	1741.2
GOZ	Dwejra Point, Gozo, Malta	1798.2	1804.2
HUN	Hegyhatsal, Hungary	1853.3	1870.7
ICE	Heimaey, Iceland	1799.1	1806.8
ITN	WITN, Grifton, N. Carolina	1817.1	1817.0
IZO	Izaña Observatory, Tenerife	1754.0	1757.2
KEY	Key Biscayne, Florida	1751.1	1765.1
KUM	Cape Kumukahi, Hawaii	1753.7	1756.8
LEF	WLEF, Park Falls, Wisconsin	[ ]	1825.4
MBC	Mould Bay, Canada	1812.0	1816.8
MHT	Mace Head, Ireland	1793.2	1792.3
MID	Midway Island	1763.5	1772.8
MLO	Mauna Loa, Hawaii	1736.7	1739.7
NWR	Niwot Ridge, Colorado	1764.9	1774.0
PSA	Palmer Station, Antarctica	1672.4	1679.1
QPC	Qinghai Province, China	1777.8	1782.2
RPB	Ragged Point, Barbados	1740.5	1740.2
SEY	Mahé Island, Seychelles	1696.3	1700.7
SHM	Shemya Island, Alaska	1801.4	1804.8
SMO	American Samoa	1679.3	1684.8
SPO	South Pole, Antarctica	1671.2	1678.1
STM	Ocean Station M	1803.2	1807.0
SYO	Syowa Station, Antarctica	1671.5	1678.9
TAP	Tae-ahn Peninsula, S. Korea	1830.5	1821.3
UTA	Wendover, Utah	1779.1	1783.7
UUM	Ulaan Uul, Mongolia	1802.1	1803.0
ZEP	Ny-Alesund, Svalbard	1806.1	1815.2

Square brackets indicate insufficient data to calculate annual mean.

Most $O(^1D)$ is quenched to ground state O atoms, but a small fraction reacts with water,

$$O(^1D) + H_2O \rightarrow 2OH \, . \qquad (4)$$

The photolysis rate coefficient for formation of $O(^1D)$, $jO_3(O(^1D))$, is a function of the actinic flux in the appropriate wavelength region, the ozone cross section, and the quantum yield (for $O(^1D)$ formation). Anything that affects the flux of radiation in the wavelength region $330 \geq \lambda \geq 290$ nm, also affects the CH_4 sink.

The large increase in CH_4 growth rate in 1991 is consistent with decreased actinic flux in the wavelength region 290-330 nm due to UV absorption by SO_2 and enhanced scattering by sulfate aerosols. In Figure 2.13, the change in $jO_3(O(^1D))$ calculated with a radiative transfer model is plotted. Initially, direct absorption of UV radiation by SO_2 lead to a 12% decrease in $jO_3(O(^1D))$.

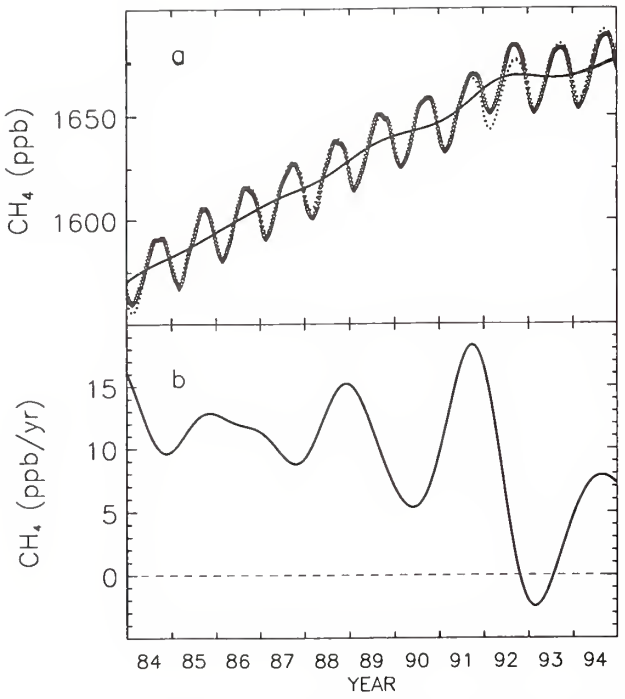

Fig. 2.12. (a) Zonally-averaged CH_4 mixing ratios for 30-90°S (symbols). The dashed line is a function (Eq. (1)) fitted to the zonal means to approximate the long-term trend and average seasonal cycle. The solid line is the deseasonalized trend; it is a combination of the polynomial in Eq. (1) and the result of the 650-day cutoff filter. (b) Instantaneous, smoothed growth rate for atmospheric CH_4 in the latitude zone 30-90°S. The curve is calculated as the derivative of the solid curve in (a).

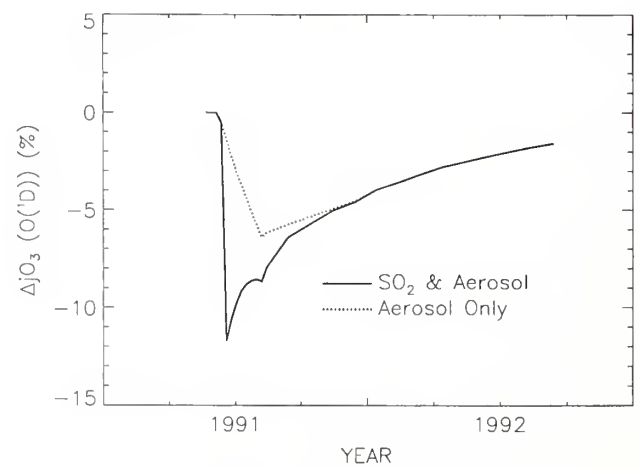

Fig. 2.13. Relative change in $jO_3(O(^1D))$ after the eruption of Mt. Pinatubo. The solid line includes the effects of direct absorption by SO_2 and scattering by sulfate aerosol; the dotted line includes aerosol only. The change is plotted relative to a 10-year climatological background.

This effect was relatively short-lived due to the short lifetime (~30 days) for SO_2. Later, UV scattering from sulfate aerosol produced by oxidation of the SO_2 maintained lower than normal values for j for more than 1 year after the eruption. It is suggested that the decreased UV flux led to a decreased steady-state concentration of atmospheric OH in the tropics and midlatitudes of the southern hemisphere, and this led to the observed perturbation in CH_4 growth rate.

Of more general interest are the far reaching effects of the eruption of Mt. Pinatubo on trace gas budgets. In the case of CH_4, it has been suggested previously that Mt. Pinatubo resulted in initially enhanced growth rates during 1991 and early 1992. Cooler temperatures resulting from the eruption [*Dutton and Christy*, 1992] also likely led to decreased CH_4 emissions from natural wetlands in the northern hemisphere [*Hogan and Harriss*, 1994], which in turn may have been largely responsible for the large observed decrease in CH_4 growth rate during late-1992 and 1993 in the high northern latitudes. This is consistent with isotopic measurements of CO_2 that suggest that the biosphere was a larger than normal sink for fossil CO_2 during 1992 and 1993 through either increased photosynthesis or decreased respiration [*Ciais et al.*, 1995b], either of which could result from short-term variations in temperature or precipitation as a result of the eruption.

2.3.3. Measurement of $^{13}C/^{12}C$ of Methane

Although many sources of CH_4 have been identified, the uncertainty in individual source terms remains large. In order to explain trends in the CH_4 growth rate, such as the period of almost no growth in 1992 and 1993 [*Dlugokencky et al.*, 1994a,b] a more precise understanding of the CH_4 budget is needed. The global measurement of the stable carbon isotopes of CH_4 ($\delta^{13}C$) afford an excellent means of furthering our understanding of the CH_4 budget. The three primary processes that produce CH_4 (bacterial fermentation, fossil fuel extraction, and biomass burning) all have different characteristic isotopic "signatures." Thus, global measurement of $\delta^{13}C$ used together with a transport and chemistry model will allow for a more accurate characterization of sources than is currently possible.

A system is under development for the automated analysis of small (20 mL) air samples for $\delta^{13}C$. The technique employed is gas chromatography coupled with isotope-ratio mass spectrometry. Methane is chromatographically extracted from air, cryofocused, combusted to produce CO_2, and then admitted to the mass spectrometer. The total analysis time, including reference gas analysis, is less than 30 minutes per sample. The automation, small sample size, and short analysis time are key design elements so that these isotopic measurements may be easily incorporated into our cooperative air sampling network.

For our sample, the shot-noise limited precision would be 0.01‰; therefore, the goal of a precision of 0.1‰ is attainable even with such a small sample size. To date, our best precision for five replicate samples of air from Niwot Ridge is 0.16‰ (one standard deviation) (Figure 2.14).

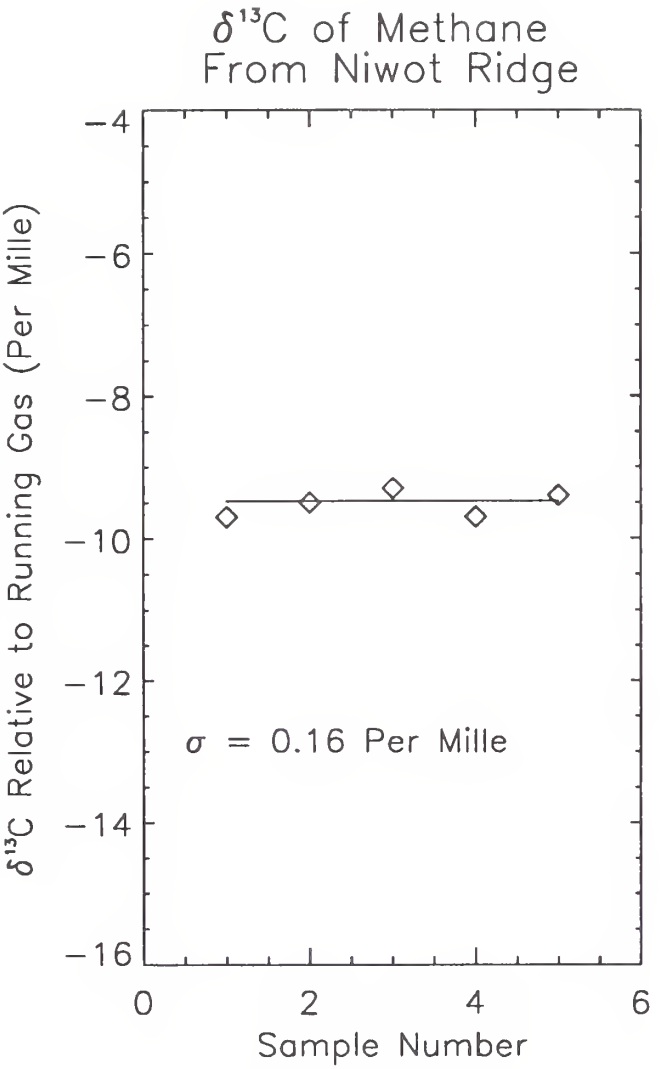

Fig. 2.14. Reproducibility of repeated measurements of ^{13}C of methane in the same air.

2.4. Carbon Monoxide

2.4.1. In Situ Carbon Monoxide Measurements

In situ measurements of CO continued at BRW and MLO during 1994 and 1995. For the analysis, a Reduction Gas Analyzer (RGA) (Trace Analytical, Inc.) was used. This measures CO using the gas chromatography-mercuric oxide reduction technique (previously described in *Peterson and Rosson*, 1993). The instruments operating at both observatories are identical and provided CO concentrations for four to five air samples per hour. The CO content of air samples was quantified by comparison to standards that reflected the range of concentrations seen at each site: 80 to 220 ppb at BRW and 60 to 180 ppb at MLO. All standards were referenced to the CMDL CO reference scale

[*Novelli et al.*, 1991]. To account for a nonlinear detector response common to the RGAs, a 3-point linear calibration (three standards) was used. This approach fits a linear regression to the two standards closest in instrument response to that of the sample, the regression coefficient, then used to calculate the sample CO mixing ratio.

Preliminary CO hourly-average mixing ratios measured at BRW and MLO during 1994 and 1995 are presented in Figure 2.15. These data have not been filtered for instrument performance or selected for background conditions. Work is currently underway to develop an expert system, based upon chromatographic parameters, that will automatically identify and flag periods when the instrument was not operating satisfactorily. The unselected time series, show features of the local and regional atmosphere. The timing of the seasonal cycles agrees well with that previously reported at these sites [*Seiler et al.*, 1976; *Novelli et al.*, 1992]. Maximum CO mixing ratios occur in late winter/early spring and the minimum occurs in summer. Periods of low variability are interrupted by short-term increases or decreases. These events reflect both the impact of local sources and the transport of air parcels from other locations.

The annual mean CO mixing ratio determined from the in situ measurements made at BRW during 1994 and 1995 were 141.9 and 138.6 nanomol/mol, abbreviated as ppb, respectively. The annual means at MLO were 88.9 and 88.4 ppb. Breaks in the time series of about 2 weeks extent, occurred at MLO in 1995 due primarily to problems related to data storage. In spite of the high frequency variation seen in the in situ record, the annual average CO mixing ratios agree well with those determined from weekly flask samples that are collected to represent background conditions (Table 2.8).

Comparison of CO mixing ratios determined using the in situ measurements to those measured from weekly flask samples provide a means to assure the quality of the former. There is strong confidence in the flask measurements because CMDL has better control over the characteristics of the analytical system and the stability of the CO standards used for flask analysis. Figure 2.16 compares CO mixing ratios measured in weekly flask samples of air to the corresponding hourly mean mixing ratio determined in situ. The results from the two sampling approaches agree well (r^2 values > 0.97). There is no significant difference between the flask concentrations and those measured in situ at BRW. However, the slight positive Y intercept in the regression of the MLO data suggests a small positive offset. It is unlikely that this is due to the calibration gases, because all standards were referenced against the CMDL working standards. If the instrument zero has increased (as observed before with these instruments) and is not accounted for, the calculated in situ CO mixing ratios could be slightly underestimated.

TABLE 2.8. Preliminary 1994 and 1995 Mean CO Mixing Ratios From Land Sites

Code	Station	Annual Mean CO (ppb) 1994	1995
ALT	Alert, Canada	140.6	126.4
ASC	Ascension Island	74.0	74.0
BAL	Baltic Sea	177.2	175.7
BME	Bermuda (East)	126.1	122.4
BMW	Bermuda (West)	124.0	117.4
BRW	Pt. Barrow, Alaska	141.6	131.3
CBA	Cold Bay, Canada	139.5	126.5
CGO	Cape Grim, Tasmania	51.3	51.7
CHR	Christmas Island	73.9	[ ]
CMO	Cape Meares, Oregon	151.0	[ ]
EIC	Easter Island, Chile	55.6	57.7
GMI	Marianas Island, Guam	90.5	94.5
GOZ	Gozo, Malta	169.3	165.0
HUN	Hegyhatsal, Hungary	225.1	241.1
ICE	Vestmanaeyjar, Iceland	137.4	[ ]
ITN	Grifton, N. Carolina	182.0	171.6
IZO	Izana, Tenerife	103.9	101.1
KEY	Biscayne, Florida	103.1	[ ]
KUM	Cape Kumukahi, Hawaii	110.7	102.2
MBC	Mold Bay, Canada	140.0	129.3
MHT	Mace Head, Ireland	137.2	124.1
MID	Midway Island	116.9	116.3
MLO	Mauna Loa, Hawaii	95.1	90.2
NWR	Niwot Ridge, Colorado	121.7	119.2
PSA	Palmer Station	[ ]	48.6
QPC	Qinghai Prov., China	131.2	127.8
RPB	Ragged Point, Barbados	93.9	89.7
SEY	Seychelles	82.4	79.2
SMO	American Samoa	58.1	57.7
SYO	Syowa, Antarctica	47.9	NA
TAP	Tae-ahn Peninsula, S. Korea	226.1	204.4
UTA	Wendover, Utah	132.2	123.4
UUM	Ulaan Uul, Mongolia	161.6	141.4
ZEP	Ny-Alesund, Spitzbergen	[ ]	132.6

Square brackets indicate insufficient data to calculate an annual mean.
NA indicates annual mean not yet available.

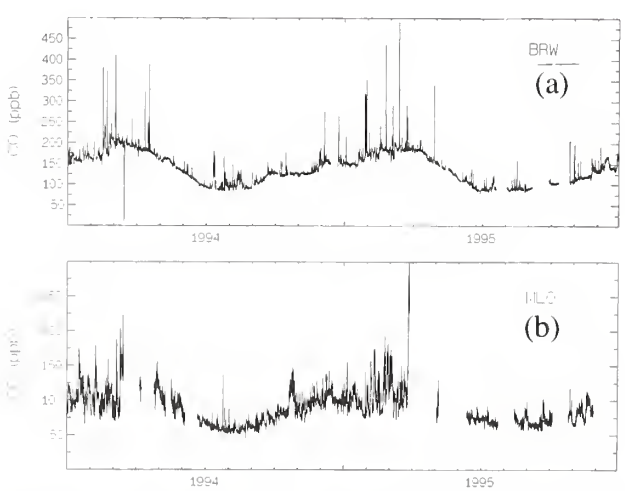

Fig. 2.15. Preliminary in situ hourly average CO mixing ratios during 1994-1995 at (a) BRW and (b) MLO.

2.4.2. Flask Measurements of Carbon Monoxide

Carbon monoxide mixing ratios were measured in a subset of flasks collected as part of the cooperative air sampling network. It was previously reported [*Novelli et al.*, 1992] that the stability of CO in a container is dependent upon the flask materials and geometry. Only

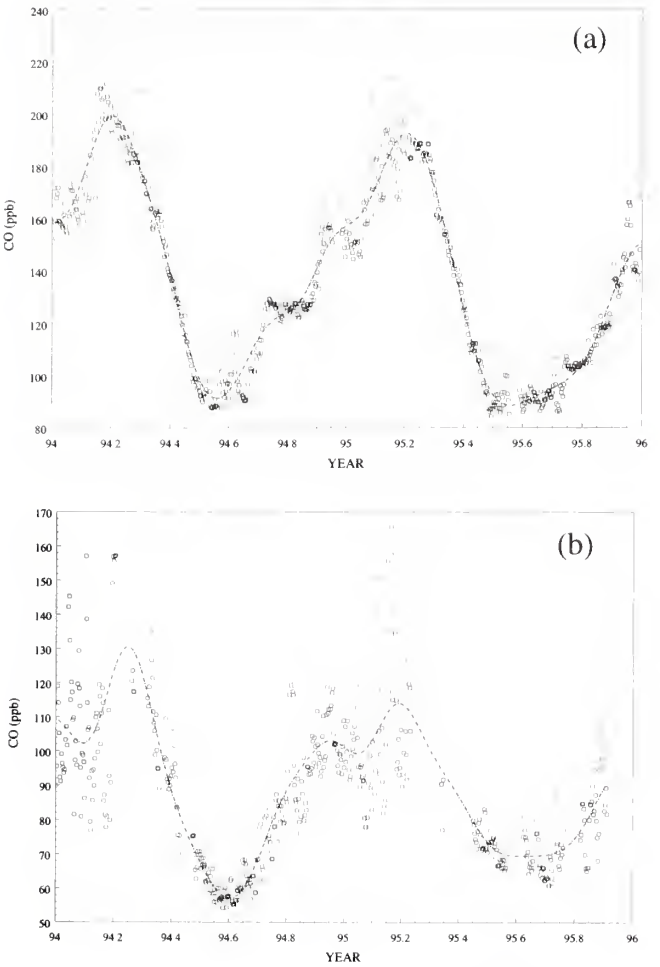

Fig. 2.16. Comparison of CO hourly averages measured in situ to those measured using flask sampling at (a) BRW and (b) MLO.

glass flasks fitted with glass piston stopcocks were used to measure CO. Over the lifetime of the CO program, the number of sampling locations has gradually increased as new sites in the network are started and the type of flasks used at older sites are converted to glass flasks for CO measurements. Analysis of air from flasks for CO and H_2 were made on a semiautomated RGA. The response characteristics of the instrument used for flask analysis were nonlinear for CO over the range of atmospheric values. Therefore, a multipoint calibration (six to eight standards) was used to quantify the sample CO content [*Peterson and Rosson*, 1993; *Novelli et al.*, 1994]. The precision of the CO method, estimated as the difference of mixing ratios determined for each flask in a simultaneously collected pair of flasks, was typically better than 2 ppb. A data selection routine flagged flask pairs having a difference of greater than 3 ppb. As before, hydrogen was referenced to an arbitrary scale. A set of H_2 standards was prepared using gravimetric methods in collaboration with the NOAH Group. The H_2 working standards are now being evaluated against the gravimetric standards.

Table 2.8 provides the land-based sites at which CO was measured in 1994 and 1995, and, whenever possible, the 1994 and 1995 annual mean values for these sites are shown. Samples for CO were also collected on trans-Pacific and South China Sea cruises; the annual mean CO mixing ratios are presented in Tables 2.9 and 2.10. These mean values were calculated from a curve fit to the total time series [*Thoning et al.*, 1989].

Over the past several years new sites located near areas of human activity have been added to the CMDL air sampling network and these are expected to represent the regionally-polluted atmosphere. Comparison of these sites to "background" sites located at similar latitude illustrates the impact of economic development on atmospheric composition and are important constraints on models of global trace gas budgets. The difference in CO levels at two sites in Europe: Mace Head, Ireland (MHT), and the middle of the Baltic Sea (BAL), show the effect of human activities on regional-scale surface CO levels. MHT is a coastal site (53°20'N, 9°54'W), and winds are typically off the north Atlantic. BAL, located about 2000 km to the northeast (55°30'N, 16°40'E), is polluted from combustion of fossil fuels in Europe. Carbon monoxide time series

TABLE 2.9. Preliminary 1994 and 1995 Mean CO Mixing Ratios From Combined Pacific Ocean Cruises

	Annual Mean CO (ppb)	
Site	1994	1995
N35	119.3	123.3
N30	125.4	114.2
N25	108.6	[]
N20	106.6	100.1
N15	105.4	96.4
N10	89.6	83.5
N05	70.2	73.5
000	66.1	66.3
S05	65.4	66.5
S10	63.3	61.9
S15	58.0	58.1
S20	58.5	55.8
S25	55.6	54.9
S30	52.2	54.5
S35	[ ]	55.1

A description of the CMDL shipboard measurement program is given in *Lang et al.* [1992]. Typically samples are collected at a frequency of one per 1.5-2 weeks.

TABLE 2.10. Preliminary 1994 and 1995 Mean CO Mixing Ratios From South China Sea Cruise

	Annual Mean CO (ppb)	
Site	1994	1995
N21	190.0	[ ]
N18	147.3	[ ]
N15	147.3	172.0
N12	138.5	[ ]
N9	142.8	130.9
N6	145.9	126.0
N3	145.3	126.4

Approximately four samples per month were collected in each latitude bin.

measured at BAL is much noisier and mixing ratios are consistently higher than at MHT. In winter, CO mixing ratios at BAL are often 100 ppb greater than those at MHT, while in the summer the difference is 25 to 75 ppb. At BAL carbon dioxide (CO_2), another combustion product, was also enhanced relative to mixing ratios observed at MHT. However, there are also times when the CO and CO_2 differences between the two sites are quite small, suggesting that BAL experiences periods of relatively unpolluted air.

Similarly, comparison of CO mixing ratios measured as part of the shipboard sampling programs in the Pacific and in the South China Sea (Tables 2.9 and 2.10) show the effects of human activities on CO in the boundary layer. Whereas the Pacific cruises sample air representative of the background marine boundary layer, the SCS cruises encounter pollution from the highly developed coast of southeastern Asia. CO mixing ratios along coastal Asia are typically 50 to 100% greater than those found in the Pacific. At the lower latitude SCS sites, isentropic back-trajectories suggested that during periods in October 1994, air was transported to these sites from areas in the southern hemisphere where fires had been observed. The high levels of CO seen in these regions may then result from both fossil fuel combustion in industrialized areas plus emission of CO from biomass burning in less developed areas.

2.4.3. The MAPS Program

As part of the CMDL collaboration with the Measurement of Air Pollution from Satellites (MAPS) program (National Aeronautics and Space Administration-Langley Research Center), nearly real-time data from BRW and MLO were provided to the MAPS team during April and October 1994. Because the MAPS instrument provides a maximum signal in the middle troposphere [*Reichle et al.*, 1990], measurements from mountain sites above the boundary layer were used as a quick test of the radiances measured by the space-borne instrument and the associated retrieval calculations. During March to November 1994, a CO instrument was installed at Niwot Ridge, Colorado, and the CMDL aircraft program flew vertical profiles above the site during the MAPS missions. These data have proved very valuable in the validation of the MAPS measurements. The MAPS measurements have also been compared with other ground based and aircraft measurements supported by a program of reference gas standard intercomparisons (section 2.4.4). CMDL coordinated the correlative measurements team for the 1994 flights of MAPS. This team provided MAPS with CO data from more than 60 sites worldwide. These data were used to validate measurements made by MAPS and to provide a unique picture of CO in the lower troposphere during April and October 1994.

2.4.4. Carbon Monoxide Standards

The primary CMDL CO standards were prepared gravimetrically during 1988-1989 and then propagated to a set of working standards [*Novelli et al.*, 1991]. These working standards were re-evaluated using a new set of gravimetric standards in March 1992. Comparisons of values assigned to working standards using the original gravimetrics, those produced in 1992, and the working standards themselves, suggest that the accuracy of propagation and stability of the scale has been within about 1% [*Novelli et al.*, 1994].

It is now well known that CO standards used by one laboratory can be significantly different from those used in another [*Weeks et al.*, 1989]. Therefore, it has been difficult to combine CO measurements made by different laboratories. Under the MAPS program, an inter-comparison of CO measurements made by 11 laboratories in 8 countries was organized. The round-robin inter-comparison was organized with four standards having approximate mixing ratios of 50, 100, 150, and 200 ppb in air (levels that represent the range of global CO mixing ratios in the unpolluted atmosphere). The experiment began in July 1993 and was completed in October 1995. The participating laboratories used either gas chromatography with HgO reduction detection or gas filter correlation radiometry and standards from several sources, including CMDL, National Institute of Standards Technology (NIST), the Fraunhofer Institute (Germany), and the Chemical Instrument Testing Institute (Japan). Differences between participants ranged to 20%. These could not be explained solely by differences in calibration gases and indicate the effect of different calibration procedures and instrument configuration on the results.

2.5. Flask Measurements of SF_6/N_2O

This project is a collaborative effort between the CCG and NOAH groups within CMDL funded by the Atmospheric Chemistry Project of NOAA's Climate and Global Change Program. A custom built gas chromatograph-electron capture detection (GC-ECD) system was installed to measure N_2O and SF_6 in the air samples collected from the CCG air sampling network. This GC uses technology developed in the NOAH Group, which is the same as that used for the tower GCs and ACATS-IV (see *Elkins, et al.*, 1996, for further instrumental details). Near the end of 1995 this system was used to analyze flasks from a subset of sites in the CCG network; eventually all of the sites in the network will be phased in.

A primary goal of the N_2O measurement program is to gain a better understanding of the budget of this compound. Both the natural and the anthropogenic sources of N_2O are poorly quantified, and the effectiveness of in situ field measurements is limited due to the extremely heterogeneous nature of N_2O emissions. These CCG flask measurements will complement the already existing background measurements made by NOAH in several ways: The CCG network has more continental sites that will give a closer look at the land-based N_2O sources. The CCG network also includes regular ocean cruise sampling that will help us better understand the oceanic source of N_2O and the effect that El Niño/QBO phenomenon has on this natural N_2O source. More generally, the increased spatial coverage of the CCG network will improve our ability to use inverse modeling techniques to derive N_2O sources and sinks on a more regional level, as has been done for CO_2 [*Tans, et al.*, 1989; 1990].

There are several motivations for the SF_6 flask measurement program. (For more details on SF_6 sources, analysis, calibration, and CMDL references, see the NOAH section 5.1.2 of this report). The global mean growth rate of this strong greenhouse gas will be elucidated from the

NOAH baseline station flask sampling. With the CCG flask measurements, however, the more detailed variations in this compound's atmospheric distribution can be looked at. Because of its extreme inertness in the atmosphere and its well-understood sources, SF_6 is a nearly ideal tracer of atmospheric dynamics. To this end, the SF_6 flask data can be used to help keep track of interannual variations in interhemispheric mixing and to better characterize the "geographical history" of the air masses being sampled at our CCG network sites. Since it is a purely anthropogenic compound, the spatial and temporal variations that are observed in SF_6 will aid in the ability to interpret the variations that are observed in the carbon gases and N_2O, which all have a combination of biogenic and anthropogenic sources. Initial findings show that, as expected, the continental sites (such as HUN, UTA, LEF; see Table 2.7 for acronyms) have SF_6 levels that are on average ≈0.2 picomol/mol (abbreviated as ppt) higher than the marine sites (which are at ≈3.5 ppt), and some of our coastal and near shore sites (MHT, RPB, BME) show regular incursions of polluted continental air.

Long-term flask storage tests were conducted for N_2O using our standard glass flasks with Teflon o-rings filled with humidified air. After 1 year, a loss of ≈1.0 ppb of N_2O was measured most likely due to slow diffusion into the flasks' Teflon o-ring. Because the goal is to try to discern gradients about 1-3 ppb, this may rule out the use of N_2O data from flasks that have a long delay time between sample collection and analysis, primarily high latitude southern hemisphere sites. Similar long-term storage tests for SF_6 are currently being conducted.

2.6. Measurements on Tall Towers

The Carbon Cycle Group initiated the Tall Towers Program as a component of the effort to incorporate regionally representative continental sampling sites into the global network of CO_2, CH_4, and CO observations. The CCG approach is to utilize the tallest existing towers (television transmitters up to 610 m) to get away from the influence of sources and sinks in the immediate vicinity of the tower in order to examine the sources of variance of CO_2, CH_4,, and CO mixing ratios in the continental boundary layer. These sources of variance include atmosphere/biosphere exchange, boundary layer dynamics, horizontal transport, fossil fuel and biomass combustion, and other anthropogenic sources (e.g., landfills, wastewater treatment, and natural gas leakage for CH_4).

Observations of CO_2 mixing ratio at the WITN TV tower (610 m) in eastern North Carolina began in June 1992 and are ongoing. A description of the site and surrounding area, and of the experimental setup is given and initial results are discussed in *Bakwin et al.* [1995]. Measurements are carried out at 51, 123, and 496 m above the ground. Daily mean CO_2 mixing ratios at each of the three measurement levels on the North Carolina tower and smooth curve fits to the data [*Thoning et al.*, 1989] are shown in Figure 2.17. A seasonal cycle of 15-20 ppm amplitude is apparent in the daily mean data from 496 m but is damped in measurements made closer to the ground. The seasonal cycle of CO_2 near the ground is masked by a large diurnal cycle driven by photosynthesis and respiration [*Bakwin et al.*, 1995]. The nighttime buildup of CO_2 near the ground due to respiration, is especially pronounced in summer and "fills in" the seasonal

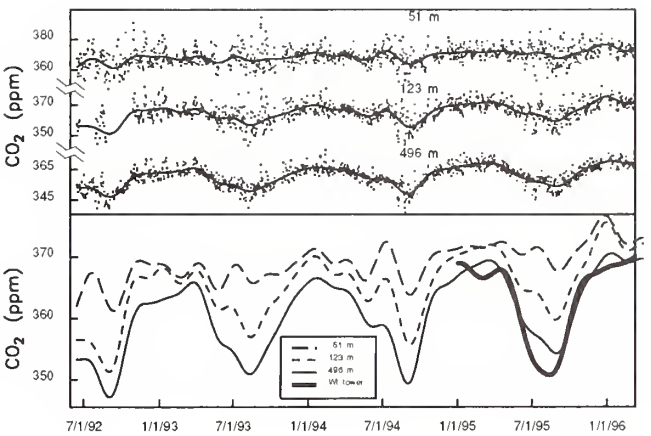

Fig. 2.17. Daily mean CO_2 mixing ratios at 51, 123, and 496 m on the North Carolina tower. In the top panel the data for each day are shown as points, and the vertical axes for each observation height are offset. In the lower panel the smooth curve fits are plotted on the same scale for comparison. The smooth curve fit to daily mean data from 396 m above the ground on the Wisconsin tower is also shown.

drawdown of CO_2. Observations well above the level of the nocturnal inversion, as can be obtained from tall towers, are necessary to quantify CO_2 mixing ratios typical of the whole planetary boundary layer (PBL).

To determine the annual growth rate for CO_2 mixing ratios at the 496 m level, a trend curve is fitted through the data in Figure 2.17 as described by *Thoning et al.* [1989]. The annual growth rates for 1993, 1994, and 1995 were found to be 1.7, 2.0, and 2.0 ppm yr^{-1}, respectively. These growth rates are larger by about 0.3-0.6 ppm yr^{-1} than those for the whole northern hemisphere in each year. The reason for this accumulation of CO_2 over the region, relative to the whole northern hemisphere, is not known.

In October 1994 CCG began observations of CO, CH_4, N_2O, and a suite of halocompounds at 51, 123, and 496 m on the North Carolina tower by automated in situ gas chromatography. The GC design and operating parameters are discussed in section 5.2.2 of the 1993 CMDL Summary Report [*Peterson and Rosson*, 1994]. Measurements of N_2O and halocompounds are discussed in Section 5.2.4 of this report. Figure 2.18 shows daily mean CH_4 and CO mixing ratios for 496 m plotted with flask data from Bermuda, giving a comparison of the continental tower site with a "background" marine site at approximately the same latitude. Mixing ratios of CO at the tower are consistently 40-60 ppb higher than at Bermuda, likely reflecting fossil fuel combustion sources proximate to the tower. Emission of CO and CO_2 from the average mix of fossil fuel combustion in the United States occurs with a molar ratio of around 0.020 (20 ppb/ppm) [*Bakwin et al.*, 1994; J. Logan, Harvard University, personal communication, 1993], so our observations indicate that CO_2 mixing ratios at the tower are enhanced year-round by roughly 2-3 ppm relative to "background" air due to regional fossil fuel combustion. Mixing ratios of CH_4 at the tower are enhanced by 20-60 ppb throughout the year, probably also mainly due to anthropogenic sources [*Bakwin et al.*, 1995].

In October 1994 measurements began at the WLEF TV transmitter tower in northern Wisconsin (45.95°N,

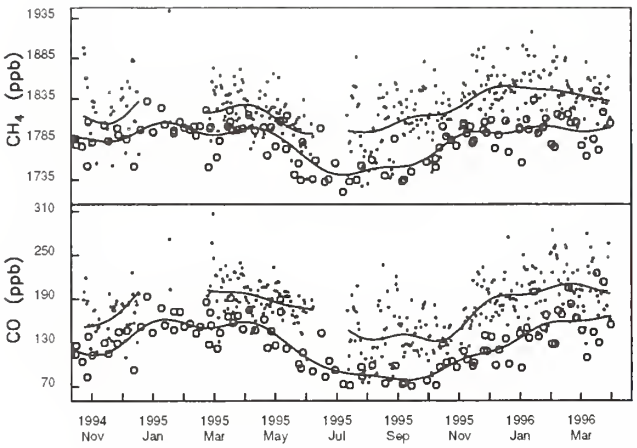

Fig. 2.18. Daily mean CH_4 and CO mixing ratios at 496 m on the North Carolina tower (points) and flask data from the CCG Bermuda sites BME and BMW (open circles). Each time series is fit with a smooth curve as described by *Thoning et al.* [1989].

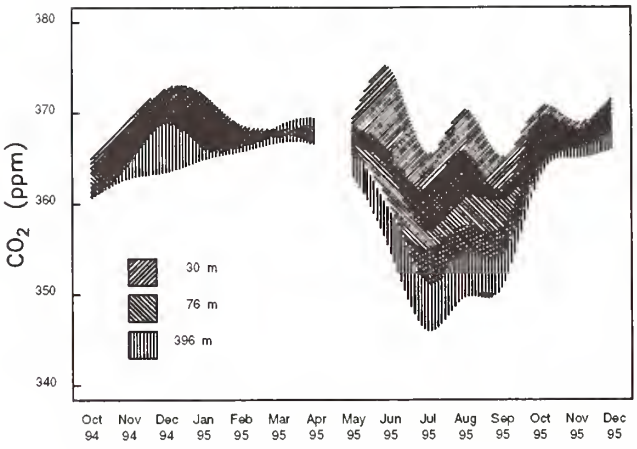

Fig. 2.19. Shaded regions indicate the inner 50% of daily average CO_2 mixing ratios for each month from 30, 76, and 396 m on the Wisconsin tower.

90.28°W, base height 472 m above sea level). The tower is 447 m tall and is located in the Chequamegon National Forest. The region is a heavily forested zone of low relief. The Chequamegon National Forest covers an area of about 3250 km^2, and the dominant forest types are mixed northern hardwoods (850 km^2), aspen (750 km^2), and lowlands and wetlands (600 km^2). Much of the area was logged, mainly for pine, during 1860-1920 and has since regenerated (J. Isebrands, USDA Forest Service, personal communication, 1994). The regional population density is very low, and there is limited industry.

Carbon dioxide mixing ratios are measured at 11, 30, 76, 122, 244, and 396 m above the ground. Wind speed and direction, temperature, and humidity at 76, 122, and 396 m, and barometric pressure, rainfall, incident photosynthetically active radiation (PAR) and net radiation at the surface. Intermittently (so far) vertical fluxes of CO_2 are also measured at 76 and 396 m using eddy correlation. The flux measurements have been discontinuous because of instrumental problems, but steps have recently been taken to improve reliability.

In June 1995 an automated GC was installed at the Wisconsin tower for measurements of CH_4 and CO. The method of analysis is similar to that used at the North Carolina tower (Table 5.3 of *Peterson and Rosson* [1994]), and every 30 minutes one measurement is obtained at each of 30, 76, and 396 m above the ground.

The smooth curve fit to the Wisconsin tower CO_2 daily mean mixing ratios from 396 m above the ground is shown in Figure 2.17 to allow comparison with the North Carolina tower. Mixing ratios at the Wisconsin and North Carolina towers are similar in winter, but the summertime draw-down is 3-4 ppm deeper and at least 1 month narrower at Wisconsin. The inner 50% (by month) of daily averages for CO_2 data from 30, 76, and 396 m is displayed in Figure 2.19, and monthly statistics for CH_4 and CO on the Wisconsin tower are presented in Figure 2.20.

Figure 2.21 shows an example of CO_2, CH_4, and CO mixing ratios, and CO_2 fluxes at the Wisconsin tower for September 1-2, 1995. During the daytime the PBL is well mixed to heights well above the top of the tower (e.g., 1400-1600 m on these 2 days, W. Angevine, NOAA Aeronomy Laboratory, unpublished data) and the trace gas mixing ratios show little vertical gradient. At night a shallow inversion forms and CO_2 and CH_4 mixing ratios increase rapidly near the ground due to surface sources. Surface fluxes of CO_2 calculated from data obtained for 76 and 396 m are generally in good agreement. The eddy fluxes show net uptake of CO_2 by the forest in the afternoon of up to around 0.4 ppm m s^{-1} or 7 kg (C) ha^{-1} h^{-1}. At night the forest releases CO_2 as is also indicated by the vertical profiles. In the future, plans are to measure CO_2 fluxes continuously and to be able to determine the annual net CO_2 balance of the forest. Some additional results from the flux measurements are presented by *Davis et al.* [1996].

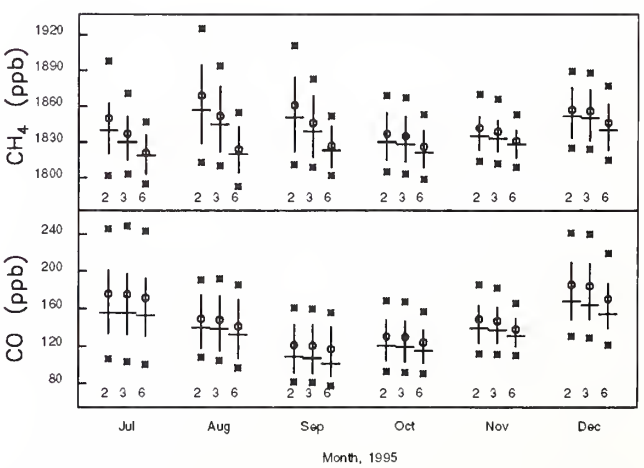

Fig. 2.20. Monthly statistics of CO and CH_4 measurements at the Wisconsin tower. Circles and asterisks are means ±1 standard deviation. The crosses indicate medians (horizontal bars) and upper and lower quartiles (vertical bars). The numbers across the bottom of the plot indicate sampling level (2, 3, and 6 refer to 30, 76, and 396 m, respectively).

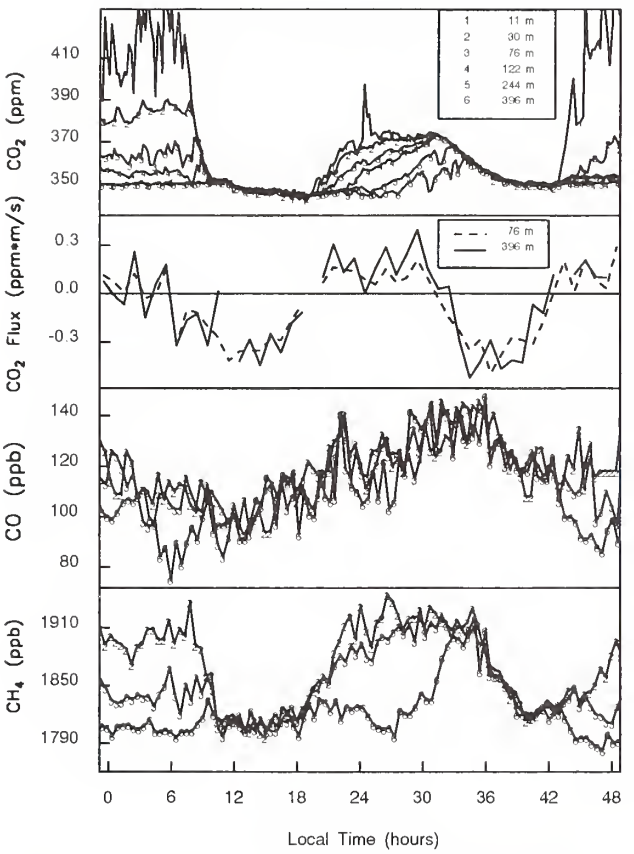

Fig. 2.21. Time series of mixing ratios and surface fluxes of CO_2 and mixing ratios of CO and CH_4 measured on the WLEF tower in Wisconsin on September 1-2, 1995. Surface fluxes are calculated from eddy correlation measurements at 76 and 396 m above the ground. Mixing ratio measurements made below those levels are used to account for divergence of the fluxes in the vertical.

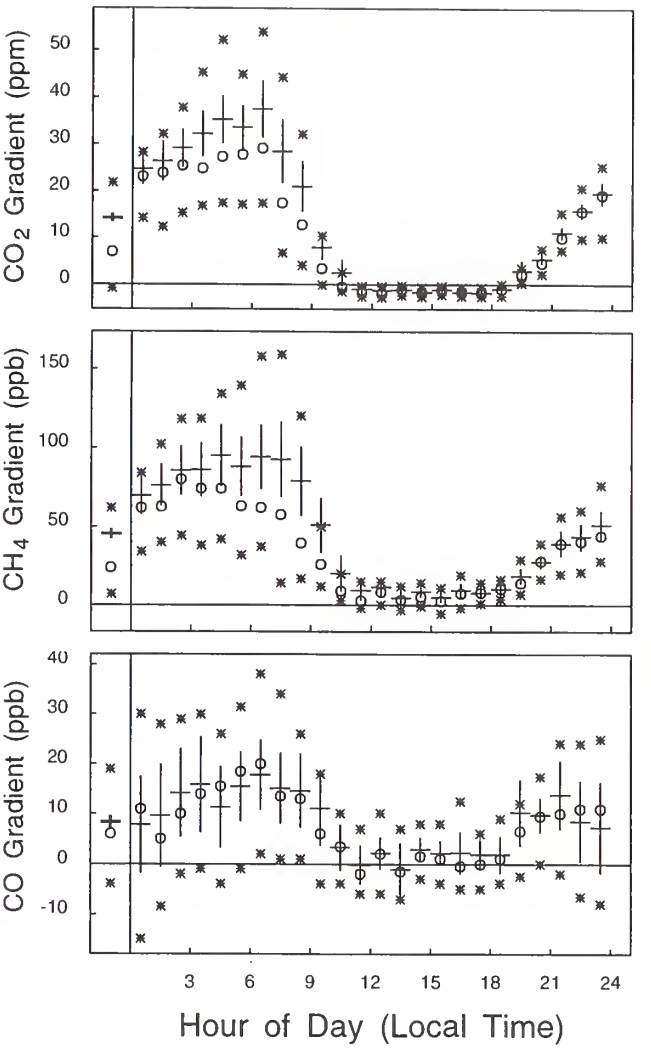

Fig. 2.22. Statistics of vertical gradients (30 m-396 m) for CO_2, CH_4, and CO, binned by hour, for August 1995. Crosses indicate means (horizontal bars) ± the 95% confidence interval (vertical bars), circles indicate medians, and asterisks indicate upper and lower quartiles. The leftmost panel on each plot gives statistics for the mean daily vertical gradients.

Figures 2.22 and 2.23 show statistics for mixing ratio gradients between 30 m and 396 m, binned by hour of the day, for CO_2, CH_4, and CO at the Wisconsin tower during August and December 1995, respectively. The gradients typically increase throughout the night as emissions accumulate in the shallow nocturnal PBL (below 396 m). In August the maximum mean gradients for CO_2, CH_4,, and CO are 37 ppm, 95 ppb, and 18 ppb, respectively. If the nocturnal increase in CO in summer is attributed solely to fossil fuel combustion emissions with a CO/CO_2 of 0.02 (mol/mol), then less than 1 ppm of the nocturnal accumulation of CO_2 can be attributed to fossil fuel combustion. The CO/CO_2 for emissions from the burning of forest biomass in North America is typically larger (0.15-0.25 [*Hegg et al.*, 1990]). Hence, >95% of the CO_2 that accumulates in the nocturnal stable layer in summer is biogenic (respiration). In December the maximum gradients for CO_2 and CH_4 are much smaller, only about 2 ppm and 17 ppb, but the maximum gradient for CO (28 ppb) is larger than in August. These observations likely reflect the nearly complete shutdown of biogenic sources of CO_2 and CH_4 in winter. Mixing ratio gradients for CO may be higher in winter due to increased combustion activity and shallower mixing depths for the nocturnal PBL than in summer.

The winter-summer comparison of vertical gradients indicates that the main source of CH_4 in the region surrounding the Wisconsin tower is biogenic (Figure 2.21). Future plans are to determine CH_4 fluxes at the Wisconsin tower using measurements of CO_2 fluxes (by eddy correlation) and vertical profiles of CO_2 and CH_4. In contrast, our results for the North Carolina tower imply that the main regional CH_4 sources are associated with anthropogenic activity [*Bakwin et al.*, 1995].

2.7. Automated Aircraft Sampling

The aircraft sampling project has been in continuous operation at the Carr, Colorado [40.9°N, 104.8°W] site since November 1992. Until April 1995, profiles of 20 samples each were taken on a biweekly basis. After April,

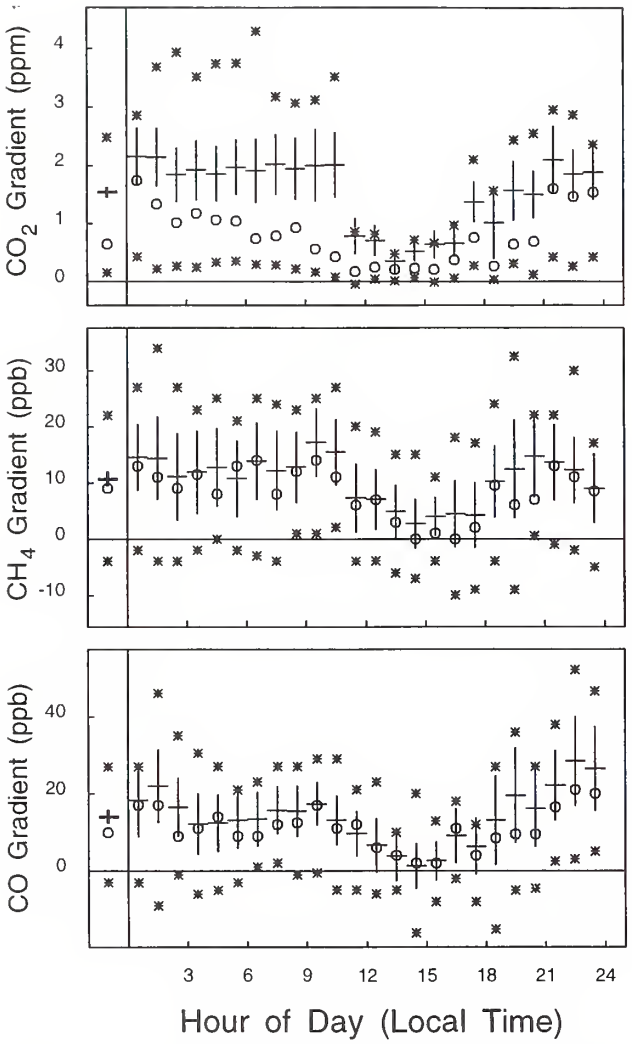

Fig. 2.23. Statistics of vertical gradients (30 m-396 m) for CO_2, CH_4, and CO, binned by hour, for December 1995. Symbols are the same as for Figure 2.22.

profiles were scheduled on a weekly basis to investigate improved signal to noise from the increased data rate and to gain experience with the logistics of more frequent flights. Approximately 30 flights were made in 1995 alone. An additional change was the use of a Cessna Model T210 aircraft beginning in June 1995 that increased the profile height to 7.9 km typical (9.1 km maximum). An example of a smoothed-curve fit to a profile altitude interval from the last 3 years of data is shown in Figure 2.24. Although the plot shows a good seasonal cycle and trend, the irregularities in the fit and outliers in the data are a reminder of the difficulty in measuring continental air masses and the complexities of individual profiles.

Also in 1995, collaboration began with the Aviaecocentre group in Moscow, Russia, to fly the CCG automated sampling system on a Russian Air Force twin-turboprop AN-24. The project acquired six profiles between June and the end of the year at altitudes from 0.3 to 6.1 km at a location about 100 km southeast of Moscow (54.9°N, 35.5°E). Meteorology and air mass back-

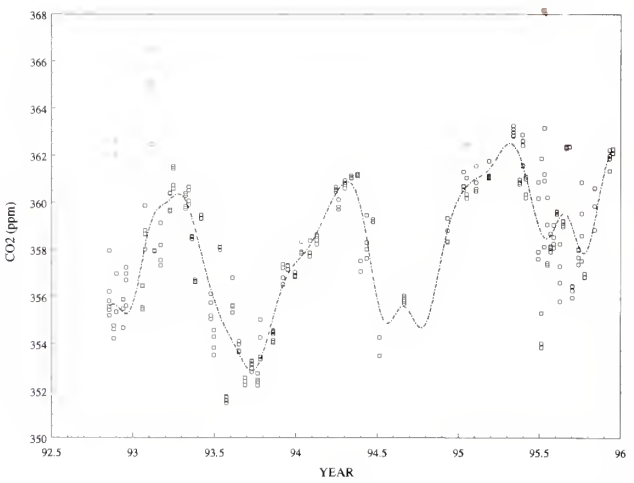

Fig. 2.24. Carbon dioxide in samples obtained between 3-4 km above Carr, Colorado.

trajectory data were also recorded. A typical profile from the Moscow site is shown in Figure 2.25. The Russian collaborators are working to develop a climatology for the site that can be correlated with the long-term carbon data. It is expected that this work will continue at least through August 1996.

All of the sampling was performed with the automated sampling package developed by the Carbon Cycle Group. This package continues to evolve with experience and the testing of various components. A newer version of the package uses a more compact valve-actuator system so that each flask can be equipped with two valves and flushed more thoroughly and reliably than evacuated flasks. An internal Global Positioning System receiver was also included in the package for fully automatic operation.

As part of this research and development effort, year-long sample storage tests were performed on our "standard" 2.5-L glass flasks equipped with Teflon o-rings, to measure the trend of trace gas variability. Over a 12-month period, the tests show a 0.4 ppm loss of CO_2, a 0.5 ppb gain of CH_4 (not significant), a 7.2 ppb gain of CO, a 5.7 ppb gain of H_2 (not significant), and a 1.1 ppb loss of

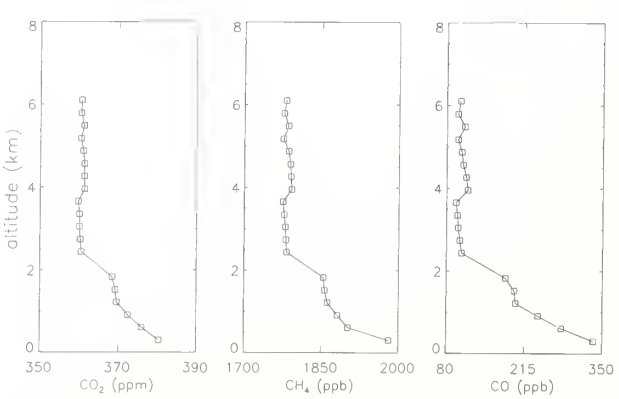

Fig. 2.25. Vertical profiles of trace species over Yuchonov, Russia, near Moscow, on November 14, 1995.

N_2O. These trends imply that the trace gas mixing ratio drift within the sample flask is easily less than the analysis limits if the samples are stored for a month or less, which is our normal operating procedure.

2.8. Data Management

The long-term flask data management strategy adopted in 1992 (see *Peterson and Rosson* [1993] for a detailed description) maintains a sampling history for over 85,000 ambient air samples and 23,000 special samples, and grows at a rate of ~7000 samples per year. Analysis and processing information is maintained for a suite of measurements that includes CO_2, CH_4, CO, H_2, SF_6, N_2O, and the stable isotopes of CO_2. The present database management strategy has several important features. While individual measurement projects retain a degree of independence, they are inextricably linked by way of the database, making multiple-species comparisons reliable and straightforward. Because the database employs UNIX text files as a storage format, database access does not require specialized software; files can be readily viewed using a variety of operating system commands and off-the-shelf software tools. Software written for the statistical and graphical analysis of flask measurement data can be species independent because the format is identical for different species, providing powerful tools to a greater number of flask programs.

Database maintenance includes regular integrity checks designed to verify consistency throughout the database and to ensure the adequacy of security precautions. Although the current strategy is working well, it is anticipated that the approach will continue to evolve to meet the growing needs as both the sampling network expands and new projects are added. Recently, the need to log procedural changes or equipment modifications into a central repository was recognized so that complete histories of analytical systems or projects can be readily reconstructed. In response, software tools are being developed that will maintain a meta-database, e.g., a database containing information about the data, that will complement our existing strategy.

2.9. Data Integration

Measurement records from the cooperative air sampling network are frequently used to constrain two- and three-dimensional transport models that derive plausible source/sink scenarios of CO_2 [*Tans et al.*, 1989; *Ciais et al.*, 1995a,b] and CH_4 [*Fung et al.*, 1991]. Interpretation of these scenarios is limited to large spatial scales and relatively short time scales due to the sparsity of sampling sites and the lack of temporal continuity among observations from different locations. In an attempt to reduce uncertainty in model-derived carbon budget scenarios due to the limitations of the observations, a procedure was developed that addresses these issues. Data extension [*Masarie and Tans*, 1995] attempts to extend the knowledge gained during a limited period of measurements beyond the period itself producing a record with no discontinuities. Extrapolated and interpolated values are derived using information about (1) the behavior of the record itself that can be described by its average seasonal cycle and long-term trend, and (2) the average behavior of the record relative to other CMDL measurement records that are nearby in latitude. The result is a set of records containing measured data and extrapolated and interpolated values. To improve the spatial resolution of the observations, high precision CO_2 measurement records from many laboratories were extended and integrated with considerable effort to ensure compatibility with respect to methodology and calibration.

During the past year, the Cooperative Atmospheric Data Integration Project for Carbon Dioxide was created with the ongoing aim of producing a globally-consistent CO_2 database with unprecedented spatial resolution and temporal continuity. Flask and continuous data from the CMDL programs comprise the bulk of the database, but measurement records contributed by other laboratories in Australia, Canada, China, France, Germany, Hungary, Italy, Japan, New Zealand, and the United States have enhanced the spatial and temporal coverage and have provided unique opportunities to compare overlapping independent records. This effort has resulted in the first release of GLOBALVIEW-CO2, the most complete atmospheric CO_2 database yet available (Internet access by way of anonymous FTP to ftp.cmdl.noaa.gov, Path: ccg/co2/GLOBALVIEW).

With the framework of a global CO_2 database in place, ways to enhance the methods used to extend and integrate records from different laboratories are being explored. Data extension techniques will become more robust with the addition of updated and new measurements records. Data integration techniques will be enhanced by using information resulting from the comparisons of overlapping measurement records. Furthermore, frequent comparisons will improve the quality of the original data. Beginning in 1991, for example, a subset of CMDL air samples collected at Cape Grim, Tasmania, was routed through the CSIRO/DAR Global Atmospheric Sampling Laboratory in Aspendale where they were analyzed for CO_2 and a host of other trace gas species [*Peterson and Rosson*, 1994]. This subset was then returned to Boulder where the same air was analyzed for a suite of trace gas species including CO_2. Results from this ongoing intercomparison will complement calibration and methodology considerations and further validate the integration of measurements from the two laboratories. Similar intercomparisons with other laboratories may be a necessary step to fully justify the merging of independent measurement programs. Data extension and integration techniques are now being applied to other trace gas species such as CH_4, CO, and the stable isotopes of CO_2. It is anticipated that GLOBALVIEW-13CO2 and GLOBALVIEW-CH4 will be available in the near future.

2.10. Three-Dimensional Inverse Modeling

In order to reconcile the contemporary budget of CO_2, and to understand by which processes this gas is absorbed by the ocean and/or by the terrestrial biosphere, it is of first importance to identify which regions are gaining or losing CO_2. In past years, several inverse calculations were performed to estimate the north/south gradient of net sources from the observed zonal mean concentrations [*Tans et al.*, 1989; *Enting et al.*, 1991; *Ciais et al.*, 1995a,b; *Bousquet et al.*, 1996; *Law et al.*, 1996]. The observational network has grown significantly in the last

decade, and the present framework is designed to go beyond the interpretation of the north/south gradient. In the present work, the goal is to study the feasibility of a 3-D inversion to assess the net fluxes over large regional scales. For this, about 25 continental and oceanic regions were defined. For each of them a forward simulation was made using a normalized source and the TM2 model [*Heimann*, 1995]. The linear combination of separate sources providing the best fit to the observations is calculated using the singular value decomposition technique.

Before applying this method to real data, modeled data were defined from a forward simulation using a global flux distribution as realistic as possible [*Ramonet*, 1994]. Different subsets of these modeled data were used to recalculate the initial flux distribution over each postulated source. This methodology allows study of the influence of the surface and/or tropospheric network resolution and the contribution of new monitoring sites. The first results showed that the annual fluxes were resolved at ±0.2 GtC yr^{-1} when a network of as few as 144 regularly spaced surface sites was used. The errors of the deduced fluxes strongly increase when the number of regularly spaced surface sites is reduced to 50. Using the same locations as the CMDL network, there are additional problems due to a lack of an observational site over large continental areas, especially over South America. Preliminary results show that the error for this region can be largely reduced by adding a surface site in Central Brazil.

In the work described previously, the implicit assumption of perfectly simulated transport is made. It is known that simulation of the transport is one of the sources of uncertainty in inverse calculations [*Rayner and Law*, 1995]. To take into account the error induced by the transport models, the NCAR Community Climate Model (CCM2) will be used to calculate the modeled data and the TM2 for the normalized sources. There will then be an estimate of how sensitive the results are to the transport calculations of different models. In the near future plans are to use the additional information provided by isotopic ratios $^{13}CO_2/^{12}CO_2$ and to apply the inverse method to the measurements smoothed in time.

2.11. References

Bakwin, P.S., P.P. Tans, and P.C. Novelli, Carbon monoxide budget in the Northern Hemisphere, *Geophys. Res. Lett.*, 21, 433-436, 1994.

Bakwin, P.S., P.P. Tans, C. Zhao, W. Ussler, III, and E. Quesnell, Measurements of carbon dioxide on a very tall tower, *Tellus*, 47B, 535-549, 1995.

Bousquet, P., P. Ciais, P. Monfray, Y. Balkanski, M. Ramonet, and P.P. Tans, Influence of two different atmospheric transport models on inferring sources and sinks of atmospheric CO_2, *Tellus*, in press, 1996.

Ciais, P., P.P. Tans, J.W.C. White, M. Trolier, R.J. Francey, J.A. Berry, D.R. Randall, P.J. Sellers, J.G. Collatz, and D.S. Schimel, Partitioning of ocean and land uptake of CO_2 as inferred by $\delta^{13}C$ measurements from the NOAA CMDL global air sampling network, *J. Geophys. Res.*, 100, 5051-5070, 1995a.

Ciais, P., P.P. Tans, M. Trolier, J.W.C. White, and R.J. Francey, A large northern hemisphere terrestrial CO_2 sink indicated by the $^{13}C/^{12}C$ ratio of atmospheric CO_2, *Science*, 269, 1098-1102, 1995b.

Davis, K.J., P.S. Bakwin, C. Zhao, W.M. Angevine, and D.F. Hurst, Monitoring regional forest-atmosphere exchanges of carbon dioxide, in *Proceedings of the 22nd Conference on Forest and Agricultural Meteorology*, American Meteorological Society 76th Annual Meeting, January 1996, Atlanta, Georgia, pp. 302-305, 1996.

Dlugokencky, E.J., L.P. Steele, P.M. Lang, and K.A. Masarie, Atmospheric methane at Mauna Loa and Barrow observatories: Presentation and analysis of in situ measurements, *J. Geophys. Res.*, 100, 23,103-23,113, 1995.

Dlugokencky, E.J., K.A. Masarie, P.M. Lang, P.P. Tans, L.P. Steele, and E.G. Nisbet, A dramatic decrease in the growth rate of atmospheric methane in the northern hemisphere during 1992, *Geophys. Res. Lett.*, 21, 45-48, 1994a.

Dlugokencky, E.J., L.P. Steele, P.M. Lang, and K.A. Masarie, The growth rate and distribution of atmospheric methane, *J. Geophys. Res.*, 99, 17021-43, 1994b.

Dutton, E.G., and J.R. Christy, Solar radiative forcing at selected locations and evidence for global lower tropospheric cooling following the eruptions of El Chichón and Pinatubo, *Geophys. Res. Lett.*, 19, 2313-2316, 1992.

Elkins, J.W., D.W. Fahey, J.M. Gilligan, G.S. Dutton, T.J. Baring, C.M. Volk, R.E. Dunn, R.C. Myers, S.A. Montzka, P.R. Wamsley, A.H. Hayden, J.H. Butler, T.M. Thompson, T.H. Swanson, E.J. Dlugokencky, P.C. Novelli, D.F. Hurst, J.M. Lobert, S.J. Cicora, R.J. McLaughlin, T.L. Thompson, R.H. Winkler, P.J. Fraser, L.P. Steele, M.P. Lucarelli, Airborne gas chromatograph for in situ measurements of long lived species in the upper troposphere and lower stratosphere, *Geophys. Res. Lett.*, 23(4), 347-350, 1996.

Enting, I.G., and J.V. Mansbridge, Latitudinal distribution of sources and sinks of CO_2: Results of an inversion study, *Tellus*, 43(B), 156-170, 1991.

Francey, R.J., P.P. Tans, C.E. Allison, I.G. Enting, J.W.C. White and M. Trolier, Changes in oceanic and terrestrial uptake since 1982, *Nature*, 373, 326-330 (1995a).

Francey, R.J., C.E. Allison, L.P. Steele, R.L. Langenfelds, E.D. Welch, J.W.C. White, M. Trolier, P.P. Tans, and K.A. Masarie, Intercomparison of stable isotope measurements of CO_2, in *Climate Monitoring and Diagnostics Laboratory, No. 22: Summary Report 1994*, edited by J.T. Peterson and R.M. Rosson, pp. 106-110, NOAA Environmental Research Laboratories, Boulder, CO, 1995.

Fung, I., J. John, J. Lerner, E. Matthews, M. Prather, L.P. Steele, and P.J. Fraser, Three-dimensional model synthesis of the global methane cycle, *J. Geophys. Res.*, 96, 13,033-13,065, 1991.

Gaudry, A., M. Trolier, C. Flehoc, P. Ciais, S.G. Jennings and P. Monfray, A preliminary comparison of $\delta^{13}C$ measurements in CO_2 from Mace Head, Ireland, in *Climate Monitoring and Diagnostics Laboratory No. 24: Summary Report 1994-1995*, edited by D. Hofmann, J.T. Peterson, and R.M. Rosson, this issue.

Gemery, P.A., Investigation of the sources of deviation in oxygen isotope measurements made on atmospheric carbon dioxide, M.A. thesis, 157 pp., Univ. of Colorado, Boulder, CO, 1993.

Hegg, D.A., L.F. Radke, P.V. Hobbs, R.A. Rasmussen, and P.J. Riggan, Emissions of some trace gases from biomass fires, *J. Geophys. Res.*, 95, 5669-5675, 1990.

Heimann, M., The global atmospheric tracer model TM2, *Technical Report No. 10*, 53 pp., edited by D. Klimarechenzentrum, Max-Planck-Institut für Meteorologie, Germany, 1995.

Hogan, K.B. and R.C. Harriss, Comment on "A dramatic decrease in the growth rate of atmospheric methane in the northern hemisphere during 1992," by E.J. Dlugokencky et al., *Geophys. Res. Lett.*, 21, 2445-2446, 1994.

Keeling, C.D., T.P. Whorf, M. Wahlen, and J. van der Plicht, Interannual extremes in the rate of rise of atmospheric carbon dioxide since 1980, *Nature*, 375, 666-669 (1995).

Lang, P.M., L.P. Steele, L.S. Waterman, R.C. Martin, K.A. Masarie, and E.J. Dlugokencky, NOAA/CMDL atmospheric methane data for the period 1983-1990 from shipboard flask sampling, *NOAA Tech. Memo. ERL CMDL-4*, 88 pp., Environmental Research Laboratories, Boulder, CO, 1992.

Law, R.M., and I. Simmonds, The sensitivity of deduced CO_2 sources and sinks to variations in transport and imposed surface concentrations, *Tellus*, in press, 1996.

Masarie, K.A., L.P. Steele, and P.M. Lang, A rule-based expert system for evaluating the quality of long-term in situ, gas chromatographic measurements of atmospheric methane, *NOAA Tech. Memo. ERL CMDL-3*, 37 pp., Environmental Research Laboratories, Boulder, CO, 1991.

Masarie, K.A., and P.P. Tans, Extension and integration of atmospheric carbon dioxide data into a globally consistent measurement record, *J. Geophys. Res.* 100, 11,593-11,610, 1995.

Novelli, P.C., L.P. Steele, and J.W. Elkins, The development and evaluation of a gravimetric reference scale for measurements of atmospheric carbon monoxide, *J. Geophys. Res.*, 96, 13,109-13,121, 1991.

Novelli, P.C., P. Steele, and P.P. Tans, Mixing ratios of carbon monoxide in the troposphere, *J. Geophys. Res.*, 97, 20,731-20,750, 1992.

Novelli, P.C., J.E. Collins, Jr., R.C. Myers, G.W. Sachse, and H.E. Scheel, Re-evaluation of the NOAA/CMDL carbon monoxide reference scale and comparisons to CO reference gases at NASA-Langley and the Fraunhofer Institute, *J. Geophys. Res.*, 99, 12,833-12,839, 1994.

Peterson, J.T., and R.M. Rosson, *Climate Monitoring and Diagnostics Laboratory, No. 21, Summary Report 1992*, Environmental Research Laboratories, Boulder, CO, 131 pp., 1993.

Peterson, J.T., and R.M. Rosson, *Climate Monitoring and Diagnostics Laboratory, No. 22, Summary Report 1993*, Environmental Research Laboratories, Boulder, CO, 152 pp., 1994.

Ramonet, M., Modelisation du transport atmospherique du dioxyde de carbone dans l'hemisphere sud, PhD. thesis, Univ. of Paris VII, 295 pp., 1994.

Rayner, P.J., and R.M. Law, A comparison of modelled responses to prescribed CO_2 sources, *Tech. Paper No. 36,* CSIRO/DAR Australia, 84 pp., 1995.

Reichle, H.G., Jr., V.S. Connors, J.A. Holland, R.T. Sherrill, H.A. Wallio, J.C. Casas, E.P. Condon, B.B. Gormsen, and W. Seiler, The distribution of middle tropospheric carbon monoxide during early October 1994, *J. Geophys. Res.*, 95, 9845-9856, 1990.

Seiler, W., H. Giehl, and H. Ellis, A method for the monitoring of background CO and the first results of continuous registrations on the Mauna Loa Observatory, *WMO Spec. Environ. Rep., 10,* 31-39, World Meteorological Organization, Geneva, 1976.

Tans, P.P., T.J. Conway, T. Nakazawa, Latitudinal distribution of the sources and sinks of atmospheric carbon dioxide derived from surface observations and an atmospheric transport model, *J. Geophys. Res.*, 94(4), 5151-5172, 1989.

Tans, P.P, I.Y. Fung, T. Takahashi, Observational constraints of the global atmospheric CO_2 budget, *Science*, 247, 1431-1438, 1990.

Thoning, K.W., P.P. Tans, and W.D. Komhyr, Atmospheric carbon dioxide at Mauna Loa Observatory, 2, Analysis of the NOAA GMCC data 1974-1985, *J. Geophys. Res.*, 94, 8549-8576, 1989.

Trolier, M., J.W.C. White, P.P Tans, K.A. Masarie and P.A. Gemery, Monitoring the isotopic composition of atmospheric CO_2: Measurements from the NOAA global air sampling network, *J. Geophys Res.*, in press, 1996.

Weeks, I.A., I.E. Galbally, P.J. Fraser, and G. Matthews, Comparison of the carbon monoxide standards used at Cape Grim and Aspendale, in, *Baseline Atmospheric Program 1987*, edited by B.W. Forgan and G.P. Ayers, pp. 21-25, Australian Government Department of Science and Technology, Canberra, Australia, 1989.

3. Aerosols and Radiation

3.1. Aerosol Monitoring

J. Ogren (Editor), S. Anthony, J. Barnes, M. Bergin, W. Huang, L. McInnes, C. Myers, P. Sheridan, S. Thaxton, and J. Wendell

3.1.1. Scientific Background

Aerosol particles affect the radiative balance of earth both "directly," by scattering and absorbing solar and terrestrial radiation, and "indirectly," through their action as cloud condensation nuclei (CCN) with subsequent effects on the microphysical and optical properties of clouds. Evaluation of the climate forcing by aerosols, defined here as the perturbation of the earth's radiation budget induced by the presence of airborne particles, requires knowledge of the spatial distribution of the particles, their optical and cloud-nucleating properties, and suitable models of radiative transfer and cloud physics. Obtaining a predictive relationship between the aerosol forcing and the physical and chemical sources of the particles additionally requires regional and global-scale chemical process, and physical transformation and transport models for calculating the spatial distributions of the major chemical species that control the optical and cloud-nucleating properties of the particles. Developing and validating these various models requires a diverse suite of in situ and remote observations of the aerosol particles on a wide range of spatial and temporal scales.

Aerosol measurements began at the CMDL baseline observatories in the mid-1970s as part of the Geophysical Monitoring for Climate Change (GMCC) program. The objective of these "baseline" measurements was to detect a response, or lack of response, of atmospheric aerosols to changing conditions on a global scale. Since the inception of the program, scientific understanding of the behavior of atmospheric aerosols has improved considerably. One lesson learned is that residence times of tropospheric aerosols are generally less than 1 week and that human activities primarily influence aerosols on regional/ continental scales rather than global scales. In response to this increased understanding and to more recent findings that anthropogenic aerosols create a significant perturbation in the earth's radiative balance on regional scales [*Charlson et al.*, 1992; *National Research Council*, 1996], CMDL expanded its aerosol research program to include regional aerosol monitoring stations. The goals of this regional-scale monitoring program are to characterize means, variabilities, and trends of climate-forcing properties of different types of aerosols, and to understand the factors that control these properties.

A primary hypothesis to be tested by NOAA's aerosol research program is that the climate forcing by anthropogenic sulfate will change in response to future changes in sulfur emissions. The forcing is expected to decrease in and downwind of the United States as a result of emission controls mandated by the Clean Air Act, while continued economic development in China and other developing countries is expected to lead to an increased forcing in and downwind of those areas. Testing this hypothesis will require a coordinated research program involving modeling, monitoring, process, and closure studies. This report describes the observations that CMDL is conducting towards this goal.

CMDL's measurements provide ground truth for satellite measurements and global models, as well as key aerosol parameters for global-scale models (e.g., scattering efficiency of sulfate particles, hemispheric backscattering fraction). An important aspect of this strategy is that the chemical measurements are linked to the physical measurements through simultaneous, size-selective sampling, which allows the observed aerosol properties to be connected to the atmospheric cycles of specific chemical species.

3.1.2. Experimental Methods

Extensive aerosol properties monitored by CMDL include the total particle number concentration (N_{tot}), aerosol optical depth (δ), and components of the aerosol extinction coefficient at one or more wavelengths (total scattering σ_{sp}, backwards hemispheric scattering σ_{bsp}, and absorption σ_{ap}). At the regional sites, size-resolved impactor and filter samples (submicrometer and supermicrometer size fractions) are obtained for gravimetric and chemical (ion chromatograph) analyses. All size-selective sampling, as well as the measurements of the components of the aerosol extinction coefficient at the regional stations, is performed at a low, controlled relative humidity (<40%) to eliminate confounding effects due to changes in ambient relative humidity. Data from the continuous sensors are screened to eliminate contamination from local pollution sources. At the regional stations, the screening algorithms use measured wind speed, direction, and total particle number concentration in real-time to prevent contamination of the chemical samples. Algorithms for the baseline stations use measured wind speed and direction to exclude data that are likely to have been locally contaminated.

Prior to 1995, data from the baseline stations were manually edited to remove spikes from local contamination. For the 1995 baseline data an automatic editing algorithm was applied in addition to manual editing of local contamination spikes. For the baseline stations (Barrow (BRW), Mauna Loa (MLO), South Pole (SPO), and Samoa (SMO)), as well as Sable Island, data are automatically removed when the wind direction is from local sources of pollution (such as generators and buildings) as well as when the wind speed is less than a threshold value (0.5-1 ms^{-1}). In addition, Mauna Loa data for upslope conditions (1800-1000 UTC) are excluded since the airmasses do not represent "background" free tropospheric air for this case. A summary of the data editing criteria is given in Table 3.1.

Integrating nephelometers are used to determine the light scattering coefficient of the aerosol. These instruments operate by illuminating a fixed sample volume from the side and observing the amount of light that is scattered by particles and gas molecules in the direction of a photomultiplier tube. The instrument integrates over scattering angles of 7-170°. Depending on the station, measurements are performed at one, three, or four wave-

TABLE 3.1. Data Editing Summary for NOAA Baseline and Regional Stations

Station	Editing	Clean Sector
South Pole	a,b,c	0° < WD < 110°, 330° < WD < 360°
Samoa	a,b,c	0° < WD < 165°, 285° < WD < 360°
Mauna Loa	a,b,c,d	90° < WD < 270°
Barrow	a,b,c	0° < WD < 130°
Sable Island	a,b,c	0° < WD < 35°, 85° < WD < 360°
Niwot Ridge	a	
Bondville	a	

WD; Wind direction
a-Manual removal of local contamination spikes
b-Automatic removal of data not in clean sector
c-Automatic removal of data for low wind speeds
d-Removal of data for upslope wind conditions

lengths in the visible and near-infrared. Newer instruments allow determination of the hemispheric backscattering coefficient by using a shutter to prevent illumination of the portion of the instrument that yields scattering angles less than 90°. A particle filter is inserted periodically into the sample stream to measure the light scattered by gas molecules, which is subtracted from the total scattered signal to determine the contribution from the particles alone. The instruments are calibrated by filling the sample volume with a gas of known scattering coefficient; carbon dioxide (CO_2) is used for high sensitivity instruments, while dichlorodifluoromethane (CFC-12) is used for the few single-wavelength, lower sensitivity instruments still in use.

The aerosol light absorption coefficient is determined with a continuous light absorption photometer. This instrument continuously measures the amount of light transmitted through the filter. The rate of decrease of transmissivity, divided by the sample flow rate, is directly proportional to the light absorption coefficient of the particles. Newer instruments have been calibrated in terms of the difference of light extinction and scattering in a long-path extinction cell for laboratory test aerosols. Instruments at the baseline stations ("aethalometers") have been calibrated by the manufacturer in terms of the equivalent amount of black carbon, from which the light absorption coefficient is calculated assuming a mass absorption efficiency of the calibration aerosols of 10 $m^2\ g^{-1}$.

Particle number concentration is determined with a CN counter that exposes the particles to a high supersaturation of butanol vapor. This causes the particles to grow to a size where they can be detected optically and counted. The instruments in use have lower particle-size detection limits of 10-20 nm diameter.

Summaries of the extensive measurements obtained at each site are given in Tables 3.2 and 3.3. Table 3.4 lists the intensive aerosol properties that can be determined from the directly-measured extensive properties. These properties are used in chemical transport models to determine the radiative effects of the aerosol concentrations calcuated by the models. Inversely, these properties are used by algorithms for interpreting satellite remote-sensing data to determine aerosol amounts based on measurements of the radiative effects of the aerosol.

Information and data from the aerosol group at CMDL are available on the Internet via FTP and World Wide Web servers. Recently processed data, file format specifications, documents summarizing data processing and flow, and clean processed data presented in hourly-averaged files for all years of station operation are available via anonymous FTP to ftp.cmdl.noaa.gov, directory "aerosol." In addition to the above, the CMDL World Wide Web server at http://www.cmdl.noaa.gov supplies online plots of recently processed aerosol data and hypertext links to various related documents (including this one).

3.1.3. Annual Cycles

The annual cycles of selected extensive and intensive properties are illustrated in Figure 3.1a-d. The data are presented in the form of box-whisker plots that summarize the distribution of values: the box ranges from the lower to upper quartiles, with a central bar at the median value, while the whiskers extend to the 5th and 95th percentiles. The statistics are based on hourly averages of each parameter for each month of the year, as well as for the entire year ("ANN").

In general, changes in long-range transport patterns dominate the annual cycles. For BRW, the highest values of σ_{sp} are observed during the spring because of the long-range transport of pollution from lower latitudes ("Arctic haze"). The BRW CN record shows a more variable semiannual cycle, with a maximum that usually coincides with the maximum in σ_{sp} and a secondary maximum in late summer or early fall. The secondary maximum in late summer is thought to be caused by local oceanic emissions of dimethyl sulfide (DMS) gas that are eventually converted to sulfate aerosol [*Radke et al.*, 1990]. For MLO, the highest σ_{sp} values occur in the springtime,

TABLE 3.2. CMDL Baseline Aerosol Monitoring Stations (Status as of January 1996)

Category	Baseline Arctic	Baseline Tropical Free Troposphere	Baseline Marine	Baseline Antarctic
Location	Point Barrow	Mauna Loa	American Samoa	South Pole
Status	Operational 1976	Operational 1974	Operational 1977	Operational 1974
Sample RH	Uncontrolled	Uncontrolled	Uncontrolled	Uncontrolled
Sample Size Fractions	Uncontrolled	Uncontrolled	Uncontrolled	Uncontrolled
Optical measurements	$\sigma_{sp}(4\lambda)$, $\sigma_{ap}(1\lambda)$	$\sigma_{sp}(4\lambda)$, $\sigma_{sp}(3\lambda)$, $\sigma_{ap}(1\lambda)$, $\delta(6\lambda)$	$\sigma_{sp}(4\lambda)$	$\sigma_{sp}(4\lambda)$
Microphysical measurements	N_{tot}	N_{tot}	N_{tot}	N_{tot}
Chemical measurements	none	none	none	none

TABLE 3.3. CMDL Regional Aerosol Monitoring Sites (Status as of January 1996)

Category	Perturbed Marine	Perturbed Continental	Perturbed Continental	Clean Continental	Clean Marine
Location	Sable Island, Nova Scotia	Bondville, Illinois	K'puszta, Keszcemet, Hungary	Niwot Ridge, Colorado	Cheeka Peak, Washington
Designator	WSA	BND	KPO	NWR	CPO
Latitude	+43.933	+40.053	+46.967	+40.036	+48.30
Longitude	+060.007	+088.372	-019.550	+105.534	+124.62
Elevation (m)	5	230	180	3020	480
Responsible institute	NOAA/CMDL	NOAA/CMDL	U. Veszprem, Hungary	NOAA/CMDL	U. Washington
Collaborating institute	Atmospheric Environment Service, Canada, NOAA/PMEL	University of Illinois; Illinois State Water Survey	NOAA/CMDL	U. Colorado, Boulder; Colorado State U., Fort Collins	NOAA/CMDL
Status	Operational August 1992	Operational July 1994	Operational September 1994	Site feasibility measurements began November 1993	Operational, May 1993
Sample RH	RH < 40%	RH < 40%	RH < 40%	Uncontrolled	RH < 40%
Sample Size Fractions	D < 1 μm 1 < D < 10 μm	D < 1 μm 1 < D < 10 μm	D < 1 μm	Uncontrolled	D < 1 μm 1 < D <10 μm
Optical measurements	$\sigma_{sp}(3\lambda)$, $\sigma_{ap}(1\lambda)$, $\sigma_{bsp}(3\lambda)$, $\delta(4\lambda)$	$\sigma_{sp}(1\lambda)$	$\sigma_{sp}(1\lambda)$, $\sigma_{ap}(1\lambda)$, $\delta(4\lambda)$	$\sigma_{sp}(1\lambda)$	$\sigma_{sp}(3\lambda)$, $\sigma_{bsp}(3\lambda)$, $\sigma_{ap}(1\lambda)$
Microphysical measurements	N_{tot}	N_{tot}	N_{tot}	N_{tot}, n(D)	N_{tot}, n(D)
Chemical measurements	Major ions, mass	Major ions, mass	Major ions	None	Major ions, mass

TABLE 3.4. Intensive Aerosol Properties Derived From the CMDL Network

Properties	Description
$\mathring{a}$	The angstrom exponent, defined by the power-law $\sigma_{sp} \propto \lambda^{-\mathring{a}}$, describes the wavelength-dependence of scattered light. In the figures below, $\mathring{a}$ is calculated from measurements at 550 and 700 nm wavelength. Situations where the scattering is dominated by submicrometer particles typically have values around 2, while values close to 0 occur when the scattering is dominated by particles larger than a few microns in diameter.
$\tilde{\omega}_0$	The aerosol single-scattering albedo, defined as $\sigma_{sp}/(\sigma_{ap} + \sigma_{sp})$, describes the relative contributions of scattering and absorption to the total light extinction. Purely scattering aerosols (e.g., sulfuric acid) have values of 1, while very strong absorbers (e.g., elemental carbon) have values around 0.3.
g, b	Radiative transfer models commonly require one of two integral properties of the angular distribution of scattered light (phase function): the asymmetry factor g or the hemispheric backscatter fraction b. The asymmetry factor is the cosine-weighted average of the phase function, ranging from a value of -1 for entirely backscattered light to +1 for entirely forward-scattered light. The hemispheric backscatter fraction b is σ_{bsp}/σ_{sp}.
α_i	The mass scattering efficiency for species i, defined as the slope of the linear regression line relating σ_{sp} and the mass concentration of the chemical species, is used in chemical transport models to evaluate the radiative effects of each chemical species prognosed by the model. This parameter has typical unites of $m^2\ g^{-1}$.

caused by the the long-range transport of pollution and mineral dust from Asia. Little seasonality is seen in CN concentrations at MLO, however, indicating that the smallest particles (<0.1 μm diameter), which usually dominate the CN concentration, are not enriched during these long-range transport events. Little seasonality is seen in the results from SMO, while at SPO the high σ_{sp} levels observed in the late winter are due to the long-range transport of sea salt in the upper troposphere from stormy regions near the Antarctic coast to the interior of the continent.

Previous reports describing the baseline aerosol data sets include BRW: *Bodhaine* [1989] and *Quakenbush and Bodhaine* [1986]; MLO: *Massey et al.* [1987]; SMO: *Bodhaine and DeLuisi* [1985]; and SPO: *Bodhaine et al.* [1986, 1987] and *Bodhaine and Shanahan* [1990].

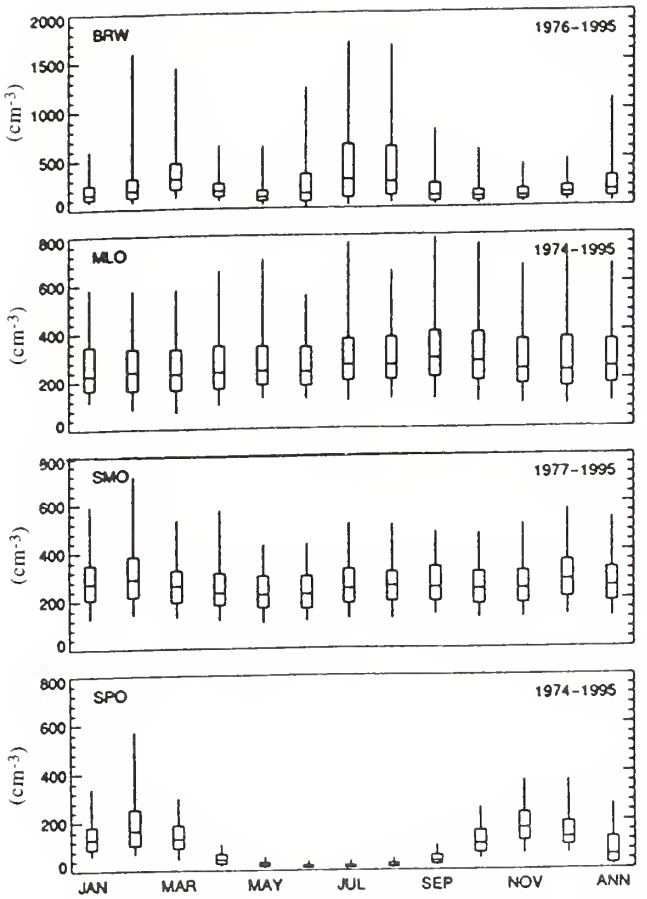

Fig. 3.1a. Annual cycles of CN concentration for baseline stations at BRW, MLO, SMO, and (SPO Monthly median values are shown. Box-whisker plots illustrate the upper and lower quartiles (box), and 5th and 95th percentiles (whiskers). Values representing the entire year period, for all years, are also presented (ANN).

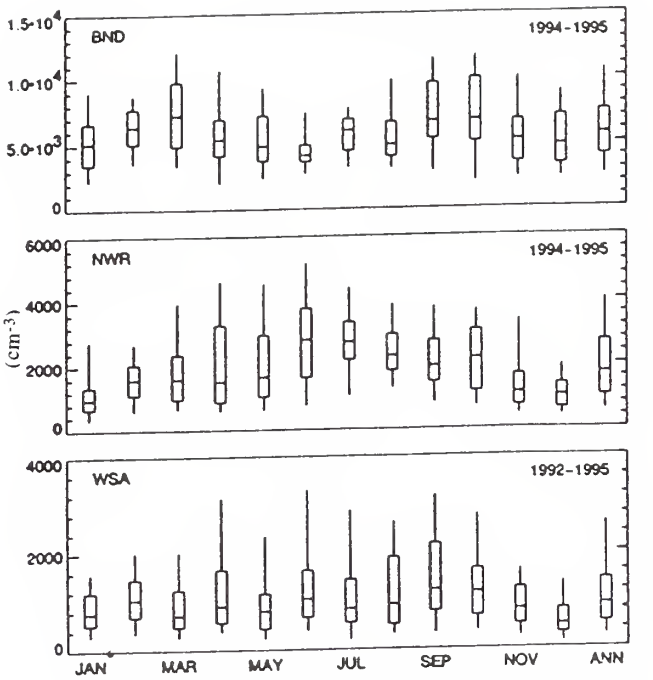

Fig. 3.1b. Annual cycles of CN concentration for regional stations at Bondville, Illinois (BND), Niwot Ridge, Colorado (NWR), and Sable Island, Nova Scotia (WSA).

Based on only 2-3 years of measurements, the annual cycles for the regional stations are very uncertain, therefore, it is premature to discuss the causes of the observed variability. The proximity of the regional sites to North American pollution sources is apparent in the results, however, with monthly median values that in some cases are over 2 orders of magnitude higher compared to values from the baseline stations.

3.1.4. Long-Term Trends

Long-term trends in CN concentration, σ_{sp}, and angstrom exponent are plotted in Figure 3.2a-c for the baseline stations. The trends are plotted for the annual geometric average as well as for the geometric averages for the months with the lowest and highest median values observed in the annual cycle plots. Interpretation of the results are complicated by two changes in instrumentation: (a) replacement of the nephelometer at MLO in 1985 and (b) the replacement of the CN counters with butanol-based instruments at MLO in 1988; at SPO in 1989; at BRW in1990; and SMO in 1992. The two types of CN counters have different lower-size detection limits, which means that any change in the long-term record will depend on the presence of particles not detected by one of the counters. This is the likely cause for the fact that obvious step changes in CN concentration are seen at MLO and SPO, but not at BRW and SMO.

As discussed in the 1988 Summary Report [*Elkins and Rosson*, 1989], σ_{sp} values at MLO were generally higher since the installation of the new nephelometer in 1985 and have not reached the low values previously observed in winter. The increasing trend in σ_{sp} at MLO is caused by higher winter values in the latter part of the record and the reason is believed to be instrumental. A modern, high-sensitivity three-wavelength nephelometer was deployed at MLO in 1994, and future comparison of the results from the two nephelometers is expected to quantify any biases introduced by the older, less-sensitive instrument. All data reported here are from the older instrument, however.

3.1.5. Results From 1994-1995

Daily Mean Values of Aerosol Properties

Figures 3.3a-g show the daily mean values at each monitoring station for total number concentration (CN), aerosol scattering coefficient at 550 nm (σ_{sp}) and the angstrom exponent for the 550/700 nm wavelength pair from January 1, 1994, to December 31, 1995. Significant day-to-day variability in CN concentration, aerosol scattering coefficient, and angstrom exponent can be seen in the figures. The daily variability of these parameters is due to several factors, including changes in local meteorology,

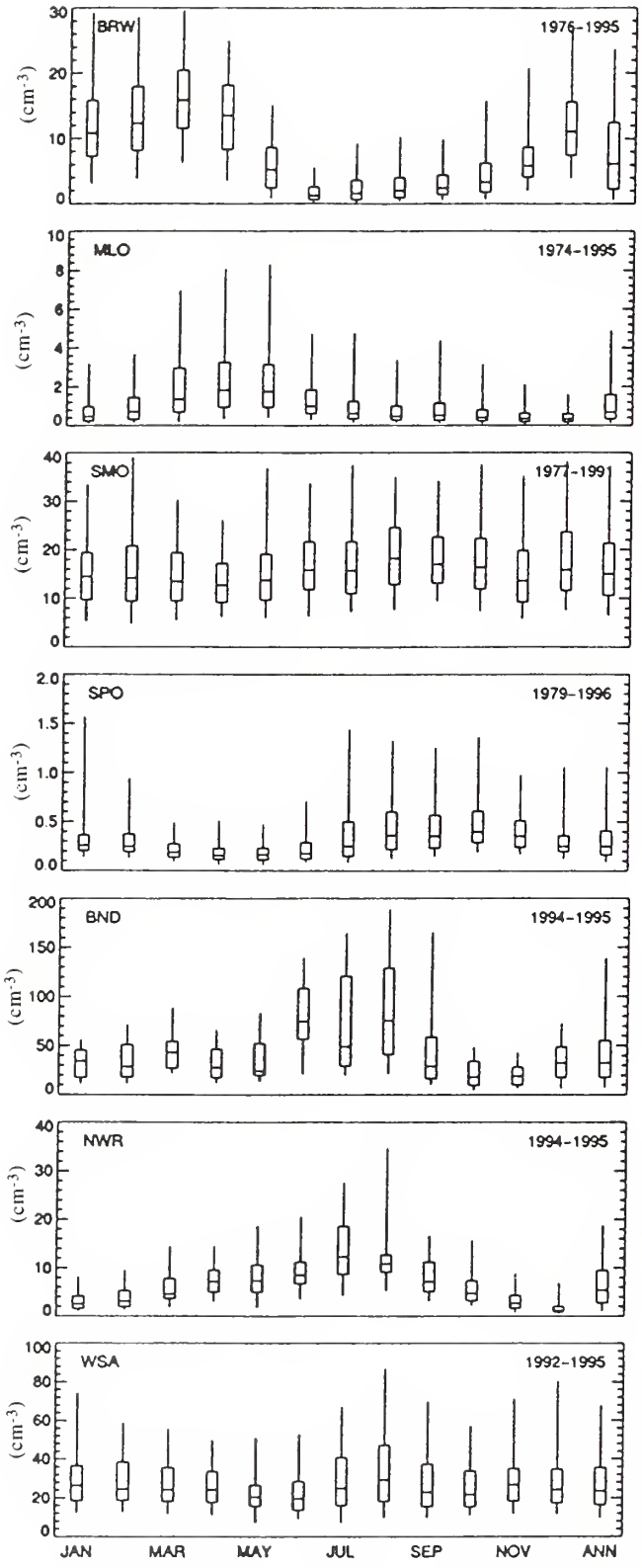

Fig. 3.1c. Annual cycles of σ_{sp} at 550 nm for baseline stations at BRW, MLO, SMO, and SPO and for regional stations at BND, NWR, and WSA.

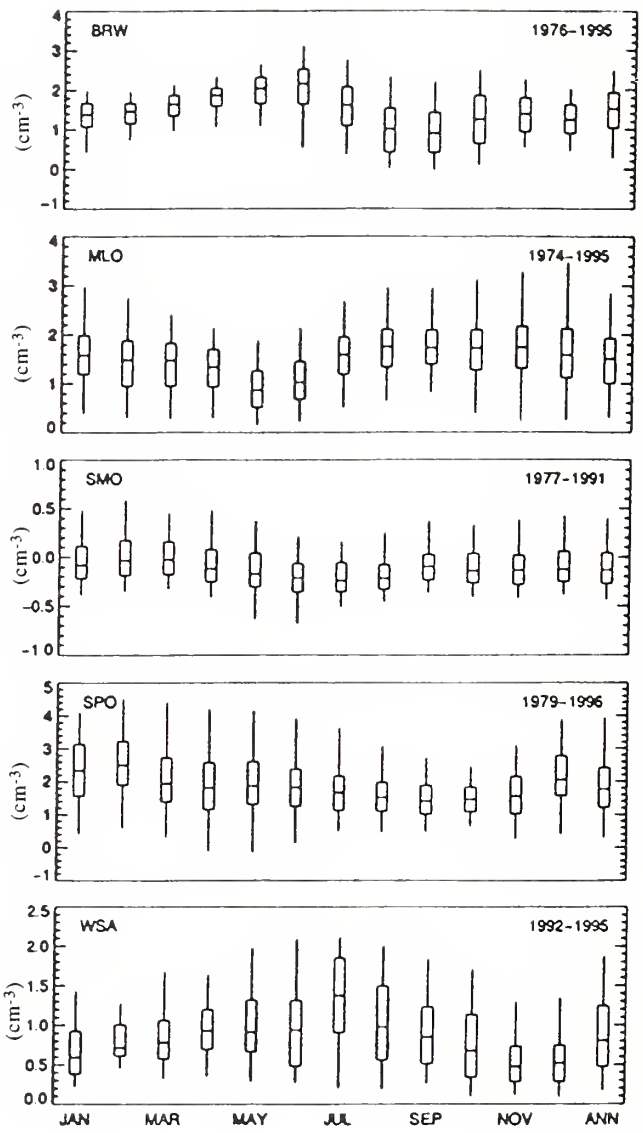

Fig. 3.1d. Annual cycles of angstrom exponent (å, 550/700 nm) for baseline and regional stations.

aerosol sources, transport time from source regions, and processing of aerosols during transport. It is worthwhile to point out that the data editing procedure for 1995, as seen in the CN plots from the edited stations, results in a more stringent acccptance of data. This can be clearly seen in the Barrow CN plot that shows significantly more breaks in the 1995 data because of the rejection of a greater amount of data compared with the previous year. The more rigorous approach to data screening for 1995 and after, generally results in less day-to-day variability in the CN concentrations, which is likely becaue of the fact that data resulting from local pollution are more completely excluded.

Aerosol Intensive Properties

Figure 3.4 shows box/whisker plots of the variability in the daily averages of three different intensive aerosol

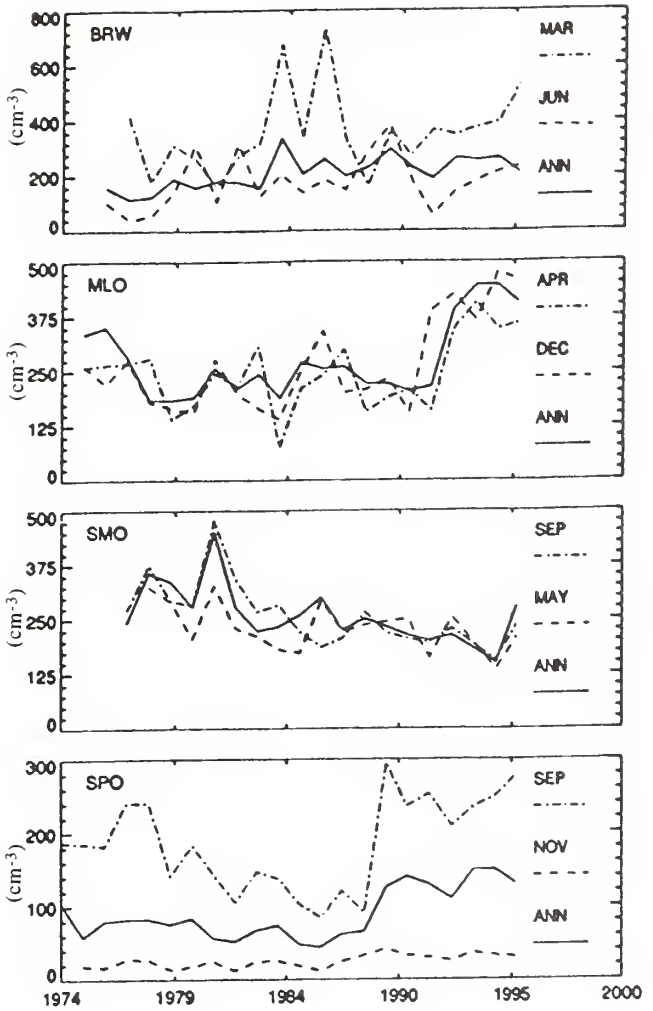

Fig. 3.2a. Long-term trends in CN concentration for baseline stations, showing months with the lowest and highest median values, and annual averages for each year (ANN).

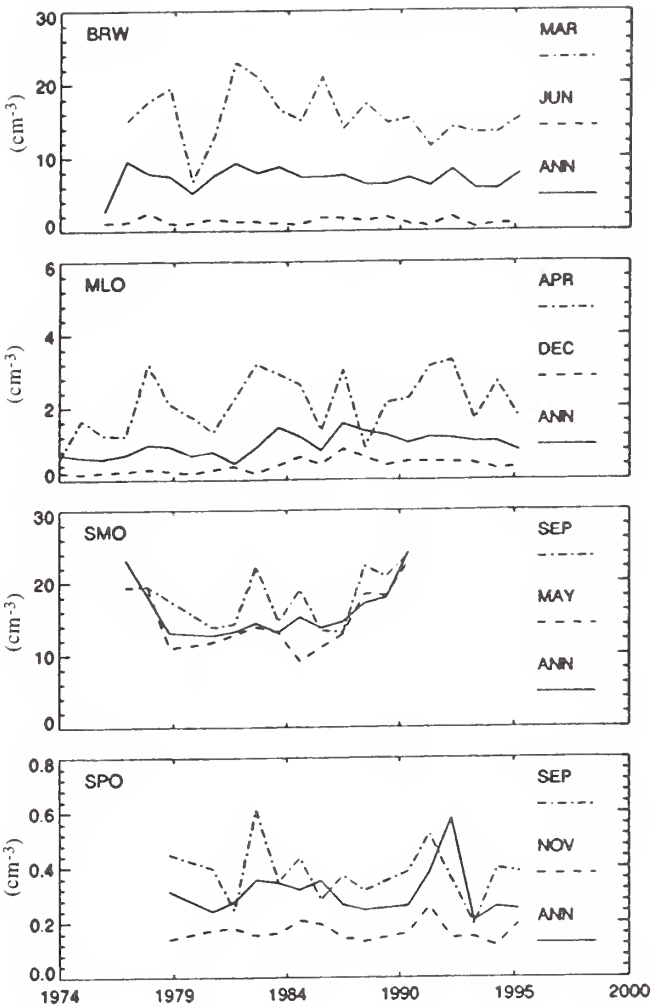

Fig. 3.2b. Long-term trends σ_{sp} at 550 nmfor baseline stations, showing months with the lowest and highest median values and annual averages.

properties measured at Sable Island: the angstrom exponent (550/700 nm wavelength pair) for submicrometer particles, the fraction of scattering caused by submicrometer particles, and the fraction of the light that is scattered into the backwards hemisphere. The data were classified into three cases: "clean" conditions when both N_{tot} and σ_{sp} (550 nm, $D_p < 1$ μm) are below the lower quartile for the entire data set, "dirty" conditions in which N_{tot} and σ_{sp} are above the upper quartile, and all "other" periods that do not meet the previously defined criteria (for example periods with low N_{tot} and high σ_{sp} values). For comparison, the fine/total scattering fraction is plotted for Bondville (BND) (data for the other intensive properties are not available at BND prior to 1996). It can be seen that the values of the angstrom exponent increase for more polluted periods suggesting that the submicrometer aerosol shifts systematically towards smaller particles as the degree of pollution increases. This is also reflected in size-segregated measurements of light scattering, which show that a larger fraction of the total scatter is due to the submicrometer aerosol as the air becomes more polluted, reaching a median value of 84% at BND. In the cleanest cases at Sable Island, only 28% (median value) of the light scattering is caused by submicrometer particles; the remainder is presumably caused by larger sea salt particles. Submicrometer particles contribute a larger fraction to the total for each quartile at Bondville, suggesting the continental aerosol is always heavily influenced by fine aerosol pollution. Aerosol number concentrations and values of σ_{sp} for the submicrometer aerosol are consistently higher at Bondville than at Sable Island (Figure 3.1b,c). The backscatter fraction, on the other hand, exhibits relatively little dependence on the degree of pollution.

Linear regression of the angstrom exponent with the fraction of submicrometer scattering (Figure 3.5) demonstrates that the two variables are highly correlated, suggesting that most of the variance in the angstrom exponent is controlled by the relative abundance of submicrometer particles. This challenges the traditional notion that the angstrom exponent can be interpreted as the slope of a power-law aerosol size distribution and better supports a bimodal model of the size distribution where the

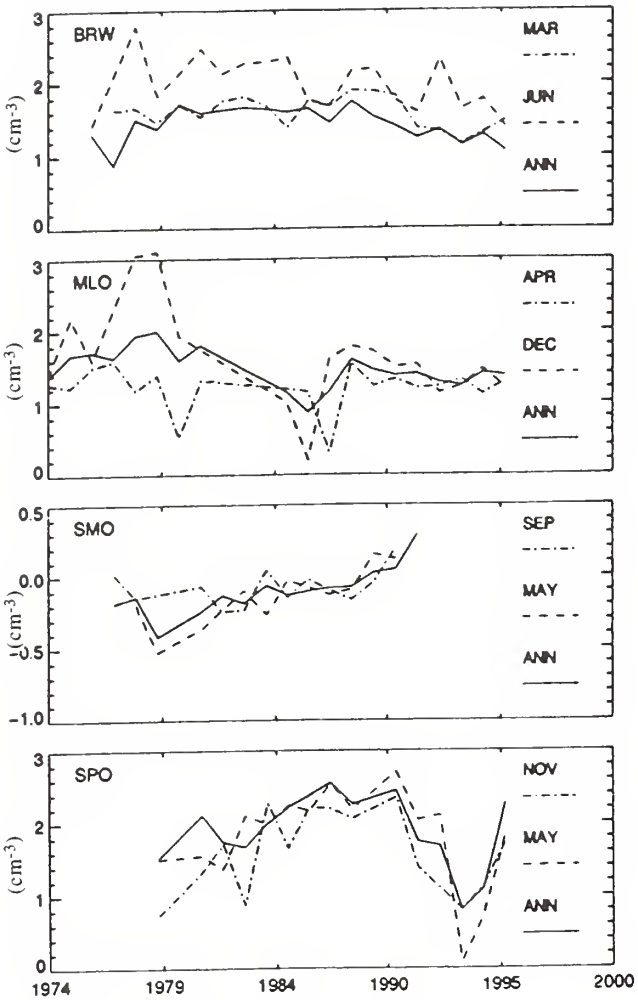

Fig. 3.2c. Long-term trends for å (550/700 nm) for baseline stations, showing months with the lowest and highest median values and annual averages.

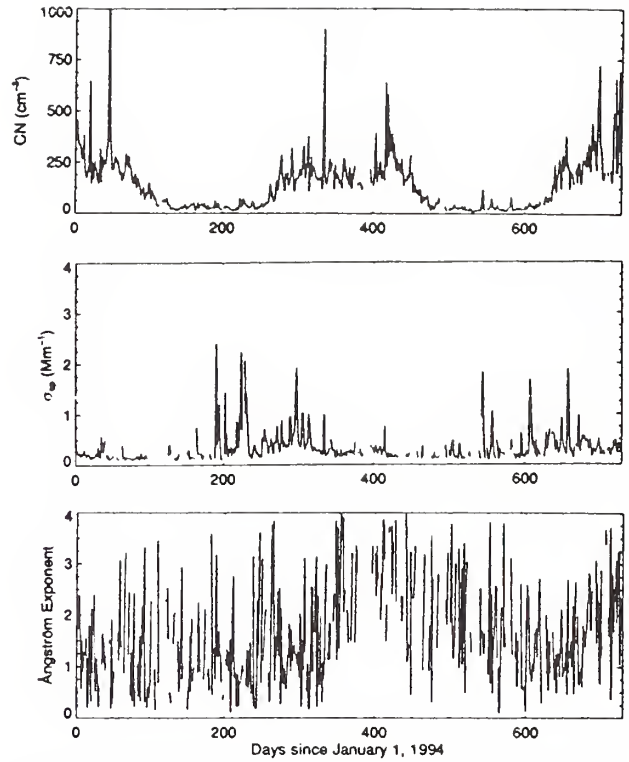

Fig. 3.3a. Daily means of aerosol properties (CN concentration, σ_{sp}, and å) for SPO for 1994, 1995.

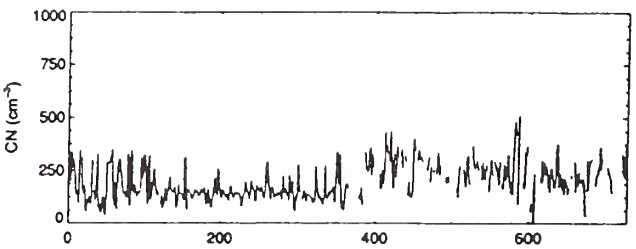

Fig. 3.3b. Daily means of CN concentration for SMO for 1994, 1995.

angstrom exponent is a measure of the relative amounts of material in the two modes.

3.1.6. Aircraft Observations

A special version of the CMDL aerosol instrumentation package used at the regional aerosol monitoring sites was developed for use on research aircraft. This effort was undertaken to extend our measurement capability into the vertical dimension and to greatly increase geographic coverage as well. This airborne aerosol package includes a three-wavelength nephelometer with backscatter shutter, a light absorption photometer, a condensation nucleus counter, and a multi-filter sampler, all interfaced to a laptop computer for instrument control and data logging. As is done on the ground, the sample air is heated as necessary to maintain a relative humidity below 40%, and multijet impactors are used to restrict the size-range of particles sampled (on the aircraft, only particles smaller than 1 µm aerodynamic diameter are sampled). Additionally, wing-mounted probes permit the determination of aerosol-size distributions. These instruments constitute a comprehensive airborne aerosol measurement platform capable of determining a wide suite of aerosol chemical, optical, and microphysical properties.

Measurements of the optical properties of submicrometer aerosol particles were measured from the NOAA WP-3D Orion research aircraft during the summer 1995 Southern Oxidants Study. The majority of the flights were in the midwest and southeastern United States at altitudes below 5 km and provide a survey of the vertical and horizontal variability of the aerosols that dominate the direct aerosol radiative forcing of climate. Some flights were conducted over Colorado, allowing comparison of these aerosol properties between the humid East and arid West. Figure

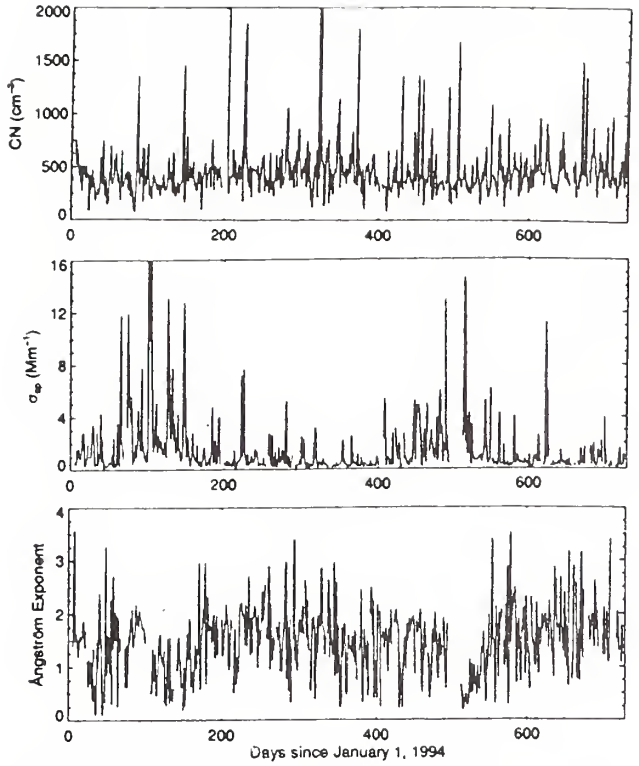

Fig. 3.3c. Daily means of aerosol properties for MLO for 1994, 1995.

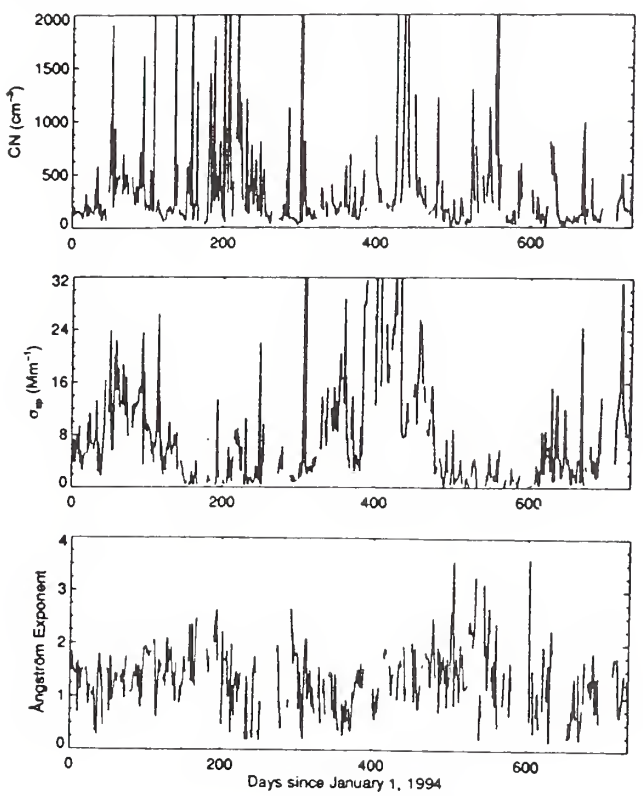

Fig. 3.3d. Daily means of aerosol properties for BRW for 1994, 1995.

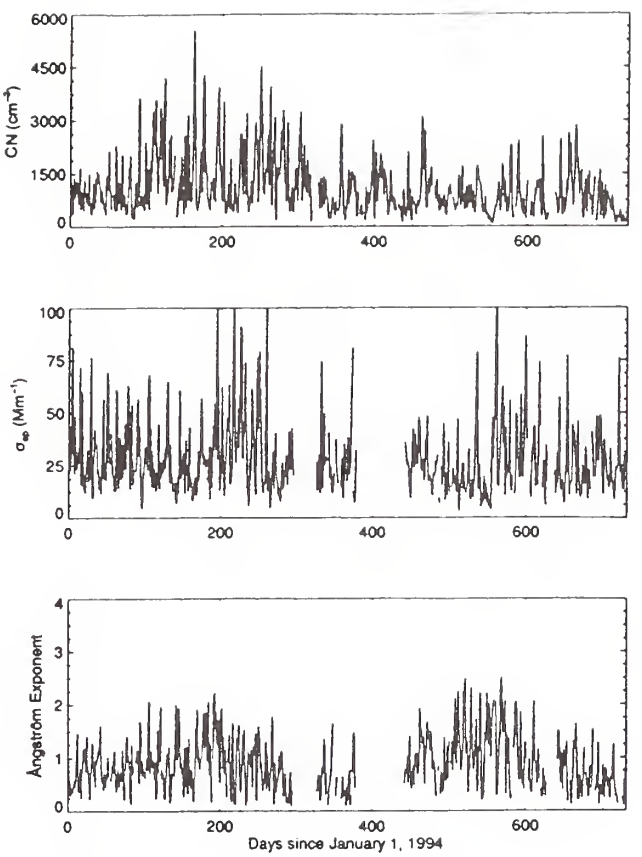

Fig. 3.3e. Daily means of aerosol properties for WSA for 1994, 1995.

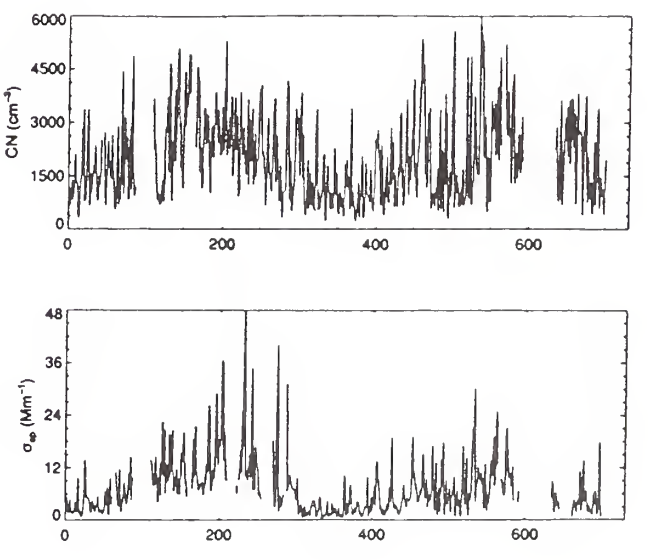

Fig. 3.3f. Daily means of aerosol properties for NWR 1994, 1995.

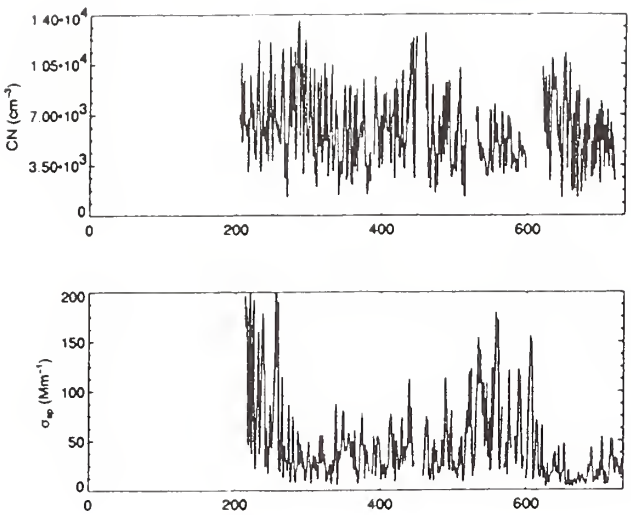

Fig. 3.3g. Daily means of aerosol properties for BND 1994, 1995.

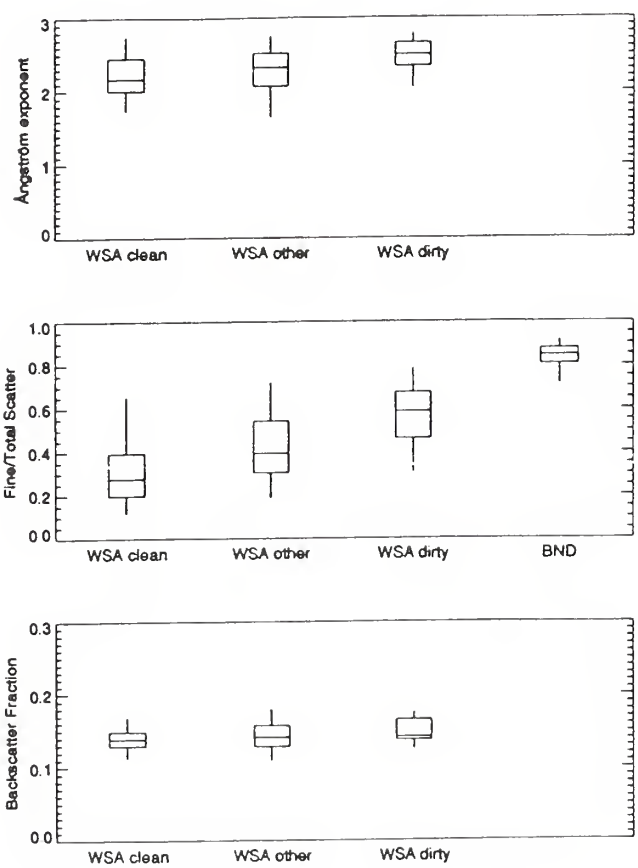

Fig. 3.4. Aerosol intensive properties (å, fraction of submicrometer scattering, and backscatter fraction) for WSA and BND. The data from Sable Island were separated according to clean, dirty, and other cases.

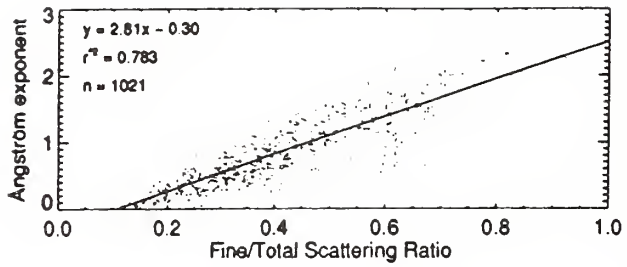

Fig. 3.5. Linear regression of å versus the fraction of submicrometer scattering for WSA.

3.6 shows the vertical profiles measured over Colorado of $\mathring{a}$, $\tilde{\omega}_o$, b, and σ_{sp} (denoted by B_{sp} in the figure legend). The data in Figure 3.6 were obtained over a large area of the state, and some of the variations are due to horizontal inhomogeneity. Nevertheless, the results show fairly constant values of $\tilde{\omega}_o$, b, and $\mathring{a}$ throughout the lower troposphere. The increased variability above 5 km results from the very low (and hence imprecise) values of the primary measured variables, leading to large variations in parameters that are defined as ratios of the primary variables. The single-scattering albedo varies in the range 0.88-0.95, and the hemispheric backscattering fraction is 0.15-0.18.

A similar vertical profile over the southeastern United States is seen in Figure 3.7 in spite of much higher values of light scattering (note the scale change for σ_{sp}) than were observed over Colorado. Once again, values at the higher altitudes are much less reliable because of the low values of the scattering and absorption coefficients. In the boundary layer, the single-scattering albedo is 0.95 and the hemispheric backscattering fraction is 0.11. These values are somewhat different from the values obtained over Colorado, suggesting systematic differences in aerosol composition and size distribution in the two regions. However, the differences may also be due to day-to-day variations in the aerosol. Figure 3.8 shows the horizontal variability observed in the boundary layer on the transit flight from Colorado to Tennessee. As was the case for the vertical dimension, the derived parameters ($\tilde{\omega}_o$, b, $\mathring{a}$) are relatively constant in spite of large changes in the primary measured variables.

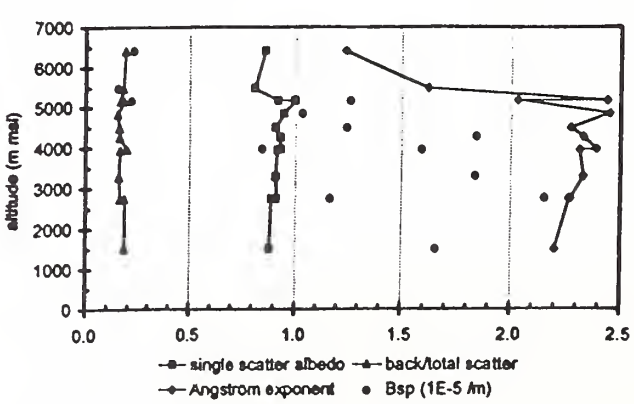

Fig. 3.6. Vertical profile of aerosol properties over Colorado, June 6, 1995.

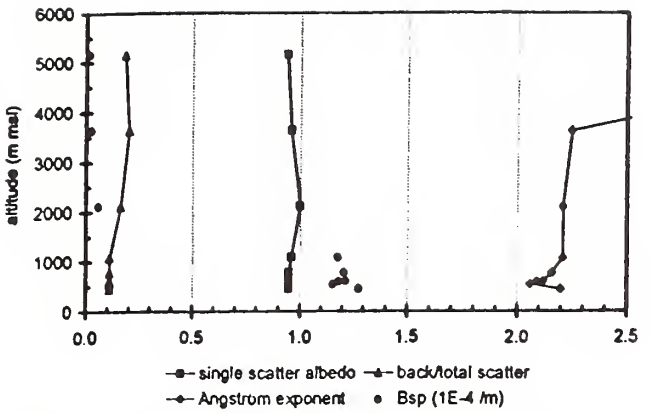

Fig. 3.7. Vertical profile of aerosol properties over the southeastern United States July 1, 1995.

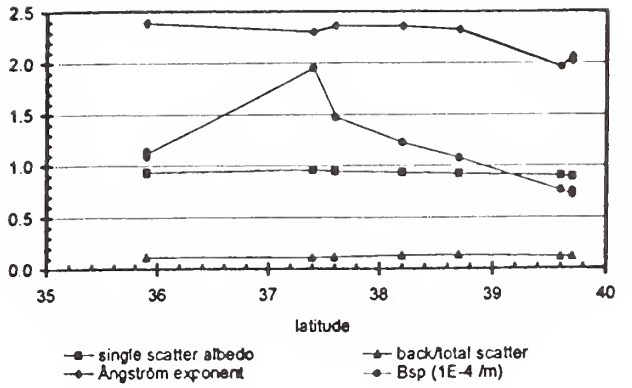

Fig. 3.9. North-south transect, midwest United States July 10, 1995.

Finally, Figure 3.9 shows the latitudinal variability that was observed in the boundary layer over the mid-western U.S. (Tennessee-Indiana), where the values of $\tilde{\omega}_0$ and b are identical to the boundary layer values shown in Figure 3.8. Slightly more variability is seen in the single-scattering albedo (0.89-0.96), but the hemispheric backscattering fraction is once again nearly constant (0.12). In all four cases, the angstrom exponent stays in the range 2.0-2.5. Although instrumental noise is a limiting factor, the observed variability in $\mathring{a}$ may be due to variations in the aerosol size distribution with the larger values of $\mathring{a}$ corresponding to cases with smaller particle sizes.

Taken as a whole, the results of this study yield values for the single-scattering albedo in the range 0.88-0.96, with more variation observed from day-to-day than from place-to-place (horizontally or vertically). Similar conclusions can be drawn for the hemispheric backscattering fraction (0.11-0.18) and the angstrom exponent (2.0-2.5), although b in the boundary layer was always below 0.13 except for the one vertical profile over Colorado. Although it is difficult to draw general conclusions from a 1-month study, the results suggest that ground-based measurements of the light scattering and absorption coefficients of submicrometer, continental particles can be used to derive values of the single-scattering albedo, hemispheric backscattering fraction, and angstrom exponent representative of the dry aerosol throughout the lower troposphere.

3.1.7. Lidar Measurements at Mauna Loa

Vertical profiles of tropospheric and stratospheric aerosols are regularly determined at MLO with two different lidar systems. Section 1.1.2 (Aerosol Monitoring, page 7, this report) describes the instruments and analysis techniques, and the new Nd:YAG lidar.

The integrated aerosol backscatter (IABS) data at 694 nm in Figure 3.10 show that no volcanic eruptions injected large amounts of aerosols that were detectable in the stratosphere at MLO latitudes in 1994-1995. The decay of Mt. Pinatubo's aerosols continued, and by the end of 1995, the lowest levels of IABS in the past 16 years were in evidence. A small increase and decay in stratospheric aerosols just prior to the Mt. Pinatubo eruption may have been related to the eruption of Kelut which was observed by the Stratospheric Aerosol and Gas Experiment (SAGE) instrument. A similar small increase in the IABS data in the fall of 1994 may be observed in Figure 3.11 at 532 nm and 694 nm. The 532-nm data are from the new Nd:YAG

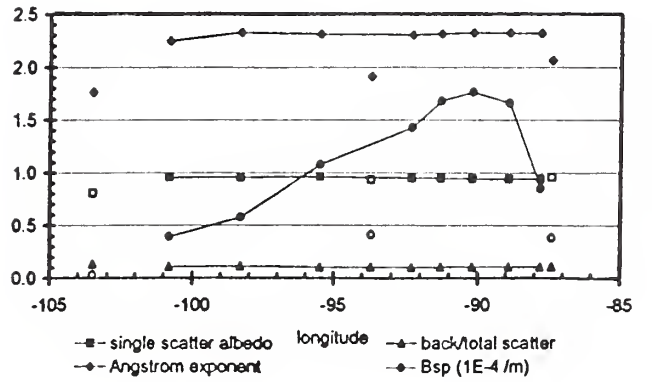

Fig. 3.8. East-west transect, Colorado to Tennessee, June 19, 1995. Open symbols denote free tropospheric measurements.

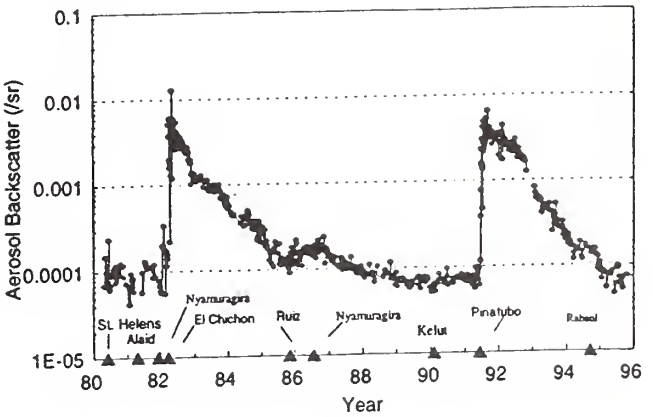

Fig. 3.10. Integrated aerosol backscatter for 1980-1995 at 694 nm (ruby lidar) from 15.8 to 33 km.

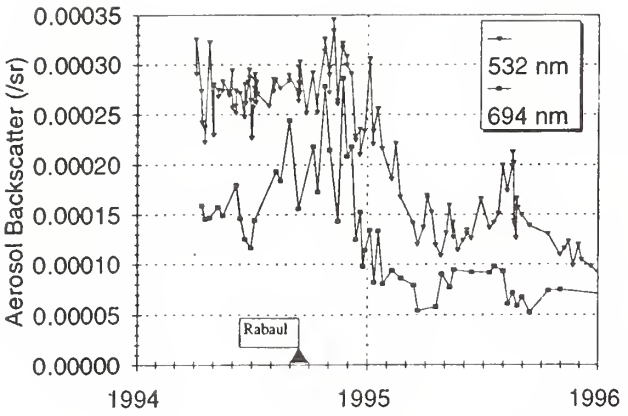

Fig. 3.11. Integrated aerosol backscatter for 1994-1995 at 532 and 694 nm (ruby lidar) from 15.8 to 33 km.

lidar. This increase coincides with an eruption of Rabaul in New Guinea. The increase abruptly disappears in December 1994 coincident with the air mass above the observatory switching abruptly from tropical to midlatitude air.

In September 1994 the Lidar In-space Technology Experiment (LITE) was flown in the Space Shuttle. The lidar made aerosol measurements at 1064, 532, and 355 nm from the upper stratosphere into the troposphere. LITE observing times were concentrated over the Atlantic and Europe, but during two overflights of MLO, correlative measurements were made at 532 nm. For the first overflight (September 14), the profiles agree well throughout the stratosphere. On the second flight (September 16) the profiles agree (within calculated error) below 23 km. However, the MLO lidar observed higher aerosol backscatter at elevations from 23 to 33 km although the MLO lidar exhibited the same general features in the profile as the satellite instruments.

The MLO lidars, as part of the Network for the Detection of Stratospheric Change (NDSC), participated in an aerosol analysis intercomparison (August 1995) conducted within the lidar group of NDSC to validate the analysis methods used by NDSC lidars. In the study, raw signals and radiosonde data were provided to participants to be used in their respective analysis routines. Preliminary results show good agreement between MLO analysis and the benchmark data.

Atmospheric temperature profiles have been measured with the MLO lidar over altitudes from 33 to 70 km beginning in July 1994. A blind intercomparison of temperature profiles made between the NOAA lidar and three other NASA lidars during the MLO3 campaign was undertaken in August 1995; the results and analysis have not been released to date.

3.2. Solar and Thermal Atmospheric Radiation

E. Dutton (Editor), B. Bodhaine, R. Haas, D. Longenecker, D. Nelson, R. Stone, and J. Wendell

3.2.1. Baseline Monitoring Activities

The CMDL surface radiation monitoring project began in 1973 with the intent to provide supporting information for baseline climate monitoring activities and to determine trends and variations in the surface radiation budget induced by changing atmospheric composition because of anthropogenic activity. Then, trends predicted in the measured radiation quantities due to anthropogenic sources were near or below the level of detectability for the available instrumentation. However, other sources of variability in the surface radiation budget were also not adequately known or understood; thus the measurements could contribute to the most basic understanding of the natural and changing surface radiation budget. Such contributions included definition of diurnal and annual cycles, effects of cloudiness, variation on daily to decadal time scales, effects of major volcanic eruptions, unexpectedly high concentrations of anthropogenic pollution in the Arctic, effects of constituent variations on narrowband irradiance (e.g., ozone and ultraviolet (UV) changes), and possible anthropogenic modification to cloudiness. In addition to research conducted by CMDL, the surface radiation measurements contribute to several global data bases. Global data bases are needed to evaluate the radiation and energy budget necessary to diagnose the climatic time scale general circulation of the atmosphere. Observations also contribute to satellite-based projects where surface measurements serve to verify spot estimates and to allow features of the intervening atmosphere to be deduced. A major goal of the monitoring program is to obtain a record, as long and complete as possible, of surface radiation parameters which will permit examination of the record for all scales of natural and modified variability. Of particular interest is the determination of the magnitude, representativeness, and possible consequences of any observed changes. To this end, the CMDL radiation group maintains complete and continuous surface radiation budget observations at several globally diverse sites with various ancillary supporting observations. The following describes those projects, particularly recent changes and results.

CMDL Baseline Observatories

The four main CMDL baseline observatories have been involved in the radiation project since the early 1970s. The different environments and conditions among the sites have resulted in different programs evolving at each site. The basic measurements made at all sites include both the downward global and direct components of solar radiation. By late 1995, solar diffuse radiation measurements had been added to each of the sites permitting more accurate determination of global radiation from the sum of vertical direct and diffuse. Broadband thermal infrared measurements were added in the last 10 years. At sites where the surrounding terrain is representative of a larger regional area (SPO and BRW), the upward solar and thermal infrared irradiances are also measured. The solar radiation records acquired at these sites constitute some of the longest known U.S. records of their kind acquired under research conditions. In 1994 a major upgrade to the observing network was accomplished with the conversion to a commercial data-logging system that provides 13-bit accuracy and precision, resistance and voltage measurements, and onsite processing of the data. The raw data are routinely transmitted over phone lines or Internet to the central data processing facility in Boulder where data editing, final calibrations, graphical inspection, and archiving are performed.

Basic Measurements

The basic measurements currently conducted at each of the four baseline observatories for the past 20 years include normal-direct and downward-broadband solar irradiance, downward solar irradiance in the 0.695 μm to 2.8 μm band, and wideband spectral direct solar irradiance. Downward broadband thermal irradiance measurements were added at BRW, MLO, and SPO in more recent years as well as upwelling irradiance measurements at SPO and BRW. The wideband spectral direct observations are obtained manually under clear sky conditions while the others are sampled at 1 Hz with 3-minute averages recorded on computer media. Preliminary data from all CMDL radiation sites are generally available on the Internet within a few days of acquisition in the radiation section on the CMDL Home Page (www.cmdl.noaa.gov).

Filter Wheel NIP

The wideband spectral direct solar irradiance measurements are made with a filter wheel normal incidence pyrheliometer (FWNIP). The data from these observations are compared to a higher spectral resolution radiative transfer model [*Bird and Riordan*, 1986]. The model is based on Beer's law and has only one level (surface). The aerosol optical depth and precipitable water are adjusted within the model to obtain a best match with the FWNIP observations. This provides a low precision, but a relatively stable estimate of mean visible aerosol optical depth and water vapor at the four baseline observatories. The accuracy of the method of obtaining aerosol optical depth and water vapor is limited by the dependence on the absolute values of the extraterrestrial solar spectrum and instrument calibration, unlike typical applications in sunphotometery. The aerosol data record from this observational project is shown through 1995 (Figure 3.12).

MLO Apparent Transmission

The transmission of direct broadband solar irradiance through the atmosphere above MLO is monitored using a quantity known as the apparent transmission. This quantity is computed by taking the average of three ratios of direct solar irradiance where each ratio is the quotient of the irradiance at an integer air mass divided by the irradiance at the next smaller integer air mass as first defined by *Ellis and Pueschel* [1971] and used by *Dutton et al.* [1985] and others. The apparent transmission is stable over time because it is independent of a radiometer calibration value and also, therefore, quite sensitive to small changes in transmission that can be due to aerosols, ozone, or water vapor. Previous studies [*Bodhaine et al.*, 1981; *Dutton et al.*, 1985] have shown that in monthly averages, aerosols tend to dominate observed changes in the apparent transmission such that the major observed excursions in the record given in Figure 3.13, are because of aerosols. The major observable features in Figure 3.13 are the effects of several volcanoes, particularly Agung in 1963, El Chichón in 1982, Mt. Pinatubo in 1991, and an annual oscillation caused primarily by the springtime transport of Asian aerosol over the site [*Bodhaine et al.*, 1981]. Figure 3.13 is complete through 1995 and most recently shows that the recovery from the eruption of Mt. Pinatubo was not yet complete in 1995. The fact that the MLO apparent transmission record still indicates a Mt. Pinatubo residual

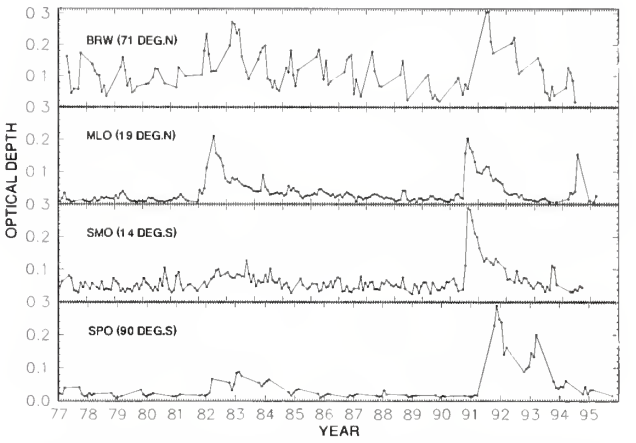

Fig. 3.12. Monthly average aerosol optical depth as determined from the filter wheel NIP for the four primary observatories. Note that these derived values are not as accurate as determined by some other techniques but are inherently stable and relatively complete over the period of record as compared to other attempts to remotely sense these quantities at these stations.

is evidence of the sensitivity of the measurement since it is known from other measurements by CMDL and others, that the optical depth of Mt. Pinatubo in 1995 was very low (about 0.005 at 500 nm).

Boulder Atmospheric Observatory (BAO) Tower

Observations of upwelling and downwelling solar and thermal irradiances at the top of the 300-m BAO tower, located near Erie, Colorado, began in 1985. Nearly continuous observations of these quantities, hourly resolution until 1992 and 3-minute thereafter, have been maintained since 1985. The data provide a unique view of surrounding agricultural land in that the data are more representative than typical surface-based solar radiation budget observations. The data from the site were used in

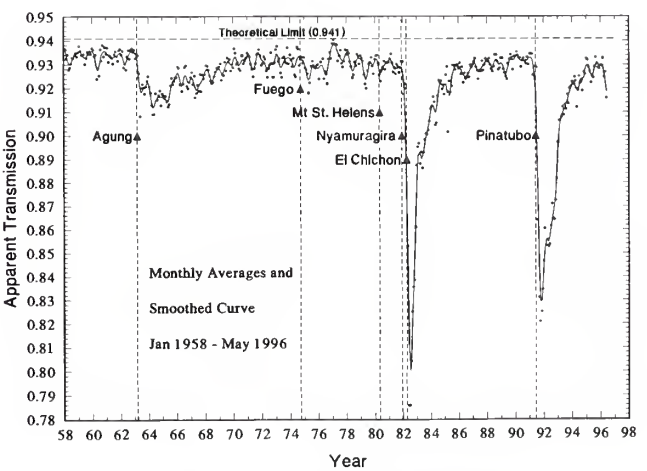

Fig. 3.13. Monthly average apparent solar transmission above Mauna Loa, Hawaii. The effects of major volcanic eruptions and the annual transport of Asian aerosol is most evident.

several recent publications [*Nemesure et al.,* 1994; *Cess et al.,* 1995; *Dutton and Cox,* 1995; *Garrett and Prata,* 1996; and several earlier papers]. Since 1990, observa-tions of direct solar and downwelling solar irradiances have been made near the base of the tower. This site has contributed data to the World Climate Research Program (WCRP) Baseline Surface Radiation Network (BSRN).

Kwajalein

Observations of direct solar, downwelling solar, and thermal IR irradiance began in Kwajalein in 1989. Kwajalein is a small, <4 km^2, island in the tropical Pacific. Data obtained at this location are virtually free of any effects of the island and, therefore, are often taken as representative of the open ocean in that region. Data from Kwajalein were used in several recent publications including *Dutton* [1993], *Whitlock et al.* [1995], and *Bishop et al.* [1996]. Substantial upgrades to the Kwajalein radiation measurement array are planned for 1996 including spectral direct and diffuse, broadband diffuse, disk-shaded pyrgeometer, UV-B, Photo-synthetically Active Radiation (PAR), and improved solar tracking capability. Data from Kwajalein have been submitted to the BSRN data archive.

Bermuda

Observations of downwelling solar and thermal IR began on the east end of Bermuda in 1990 on the National Aeronautics and Space Administration (NASA) tracking station site. The rather small size and elongated shape of the island in the lower midlatitude westerlies is believed to have a minimal influence on the irradiance measurements, although some clouds of orographic origin are known to exist there in the summer months under certain synoptic meteorological conditions. Data from Bermuda were submitted to the BSRN data archive and have been used by *Whitlock et al.* [1995] and *Bishop et al.* [1996] in satellite comparison and validation studies.

3.2.2. Solar Radiation Calibration Facility

Routine Operations

Calibration support for the four CMDL baseline observatories and the BSRN sites at Kwajalein, Bermuda, and BAO during 1994 and 1995 was carried out by the CMDL Solar Radiation Calibration Facility (SRCF). Calibrations and characterizations of pyranometers and pyrheliometers were performed as needed, and field exchanges of recalibrated instruments were completed. Improved diffuse-sky measurements were implemented at the SRCF with the addition of ventilated tracking disk systems designed for the Eppley automated solar trackers used by CMDL. The improved diffuse measurements, together with automated cavity operation for the collection of solar direct beam data, have enabled more accurate characterizations and calibration procedures requiring accurate determination of solar components (direct beam and diffuse sky).

Standards Activities

The CMDL reference cavity radiometers were compared with reference cavities from other organizations during 1994 and 1995. A cavity intercomparison was held at the National Renewable Energy Laboratory in Golden, Colorado, October 8-10, 1994. In 1995 the CMDL references were taken to the World Radiation Center in Davos, Switzerland, for participation in the WMO-sponsored eighth International Pyrheliometer Comparison (IPCVIII). These comparisons are typically conducted every 5 years and allow reference instruments from all of the WMO regions to document their performance relative to a standard group of instruments maintained at the World Radiation Center. Seventy-seven reference instruments from 37 countries participated in IPCVIII from September 25 to October 13, 1995. Participation in IPCVIII of the CMDL reference cavities (TMI67502 and AHF28553) maintains the historical traceability of the NOAA standards to the World Radiometric Reference maintained in Davos and the World Radiation Center. All solar radiation measurements made by CMDL are thus traceable to the world reference.

Instrument Development Activities

Efforts began during 1995 to add observational capability to the BSRN sites at Kwajalein, Bermuda, and BAO. Dual ventilated shade disk systems were acquired, tested, and deployed to BAO during 1995 with installation at Bermuda and Kwajalein scheduled for early 1996. The dual shade disk systems attach to the Eppley solar trackers and enable a pyranometer and pyrgeometer to be continuously shaded and ventilated. Improvements in solar tracking accuracy for these sites was also achieved by implementing a more accurate solar position algorithm in the tracker control program, precision leveling of the solar tracker during installation and setup, and a solar position detector designed and built by CMDL was added to the solar tracker. Tracking accuracies of better than 0.1 degrees are achievable with these improvements. These improvements are scheduled for installation at the Kwajalein, Bermuda, and BAO sites in 1996. In addition, software was added to the tracker control computer that allows remote access to the tracker control program via modem. This capability, together with the solar position detector data, will allow monitoring of tracker performance at the remote sites and tracker control from Boulder if necessary. Installation of an automated self-calibrating cavity radiometer system in the refurbished MLO solar dome was also completed during the latter part of 1995. A new Eppley automated cavity system was purchased for this application with the goal of incorporating its operation and control in the dome control computer system. When this is completed, continuous direct-solar-beam data will be available from MLO in addition to the NIP data that have been collected since 1958.

Special Projects

In addition to the routine CMDL monitoring support for the four baseline observatories. The SRCF provided support, resources, training, and logistics assistance in other areas such as the World Meteorological Organization/Global Environmental Fund/Global Atmos-pheric Watch (WMO/GEF/GAW) baseline station network.

3.2.3 Aerosol Optical Depth Remote Sensing

Remote sensing of aerosol optical depth is carried out in several projects in CMDL. Derivation of low precision aerosol optical depth from wideband filtered pyrheliometer observations is described in a previous section. Traditional narrow-band sunphotometery measurements are

currently made routinely at MLO and Sable Island, Nova Scotia. The CMDL radiation group also maintains a few calibrated handheld sunphotometers of an older but reliable design for use in various short-term field programs. Such field programs have recently included, ACE-1, TOGA CORE, Antarctic dry valley studies, Arctic aircraft flights, and visits to BSRN sites. CMDL will begin to deploy commercial versions of the Multi-Filter Rotating Shadowband Radiometer (MFRSR) from which not only can spectral optical depth be derived but also spectral diffuse and total spectral irradiance fields. As part of a world-wide aerosol optical depth network, the GAW and BSRN programs are awaiting delivery of several multi-channel sunphotometers from the WRC.

The automated solar observatory at MLO, which houses the primary CMDL sunphotometer, was upgraded during 1995. The antiquated computers used for dome control and data acquisition were replaced with a single 486-PC. The dome operates, as before, opening and closing each day with both the internal spar and dome tracking the sun while constantly monitoring precipitation and wind speed to determine shutdown conditions. Instruments on the spar include the CMDL PMOD01 sunphotometer, two dual-channel water vapor meters, an active cavity radiometer, and a backup pyrheliometer. Aerosol optical depth data are obtained at three wavelengths: 380, 500, and 778 nm. One value per day per wavelength is derived from the Langley plot technique. The most recent summary of data from this project was given by *Dutton et al.* [1994].

3.2.4. Mauna Loa UV Spectroradiometer

A research-grade UV spectroradiometer was installed at MLO in July 1995. Because Mauna Loa (mountain) extends above the marine boundary layer, and because of the diurnal upslope-downslope wind circulation, mornings at MLO often exhibit unusually clear skies, providing an excellent site for solar radiation measurements. The instrument described here was developed and operated by the National Institute for Water and Atmosphere at Lauder, New Zealand [*McKenzie et al.*, 1991, 1992].

The solar radiation measured at the earth's surface depends on the transmission of the atmosphere, the earth-sun distance, and the irradiance of the sun. The atmospheric transmission in the UV portion of the spectrum is controlled primarily by total ozone, and, since ozone is affected by anthropogenic influences, solar UV irradiance arriving at the earth's surface is controlled by both natural and anthropogenic effects. Ozone concentration, in turn, is also affected by changes in solar UV. The UV-A region of the spectrum (320-400 nm) is virtually unaffected by ozone absorption; the UV-B (280-320 nm) is strongly affected by variations in ozone; and the UV-C (<280 nm) is almost entirely absorbed before it reaches the surface. An excellent review of this subject was given by *Stamnes* [1993].

The data presented here are the first spectroradiometer measurements at MLO. Because of the long Dobson spectrophotometer ozone measurement record at MLO (1957-present), a unique opportunity now exists to obtain well-calibrated UV spectroradiometer measurements and to compare them with the ozone measurements. Past studies show that short-term variations of UV-B irradiance are inversely correlated with variations in total ozone [*McKenzie et al.*, 1991; *Hofmann et al.*, 1996].

A description of the MLO site and instrumentation, and the first 3 months of data are presented. Although this time period was insufficient to observe long-term trends, it is expected that sufficient variation will occur to observe the inverse relation between UV and ozone.

Instrumentation

The UV spectroradiometer, built around a commercially available Jobin-Yvon DH10 double monochromator, is interfaced with a computer to provide automatic control and data acquisition [*McKenzie et al.*, 1992]. A 17-mm diameter custom-made Teflon diffuser, designed to minimize cosine error, is mounted as a horizontal incidence receptor and views the whole sky. A shadow disk may be added in order to separate the diffuse and direct radiative components.

The spectral range of the instrument is 290-450 nm, and the bandpass is about 1 nm. The gratings are driven by a stepper motor under computer control, and a complete scan requires about 200 seconds. The irradiance signal is sampled every 0.2 nm using a photomultiplier as a detector. The instrument is mounted in a weatherproof insulated enclosure (painted white) located on a concrete pad at the MLO site. The interior of the enclosure is temperature controlled using a Peltier heater/cooler unit. The computer control and data logging system are located in a small building near the instrument.

Calibration of the spectroradiometer is performed onsite using a standard 1000-W FEL quartz-halogen lamp with calibration traceable to the National Institute of Standards. Calibrations are performed at approximately 6-month intervals using a precision optical bench. A stability test using a 45-W lamp and a wavelength check using a mercury lamp are performed weekly. The expected long-term accuracy of the spectroradiometer system is expected to be better than ±5%. A detailed error analysis for this instrument was given by *McKenzie et al.* [1992].

Observations

The spectroradiometer is programmed to begin measurements at dawn and perform scans at 5° solar zenith angle intervals throughout the day beginning and ending at 95°, except that during the middle of the day the system switches to a scan every 15 minutes. In addition, a scan is performed each midnight to give "dark" values.

A typical clear sky scan is shown in Figure 3.14. The solid curve gives total (direct + diffuse) irradiance for July 16, 1995, at a solar zenith angle of 45°. The long-dashed line shows the effective action spectrum accepted for calculating the erythema spectrum used to estimate the effect of UV radiation on human skin [*McKinlay and Diffey*, 1987]. Note that the effective action spectrum is a dimensionless quantity normalized to 1 for $\lambda < 298$ nm. The short-dashed line in Figure 3.14 shows the erythemal spectrum for that scan, obtained by multiplying the total irradiance by the effective action spectrum. The erythema can then be calculated by integrating over the erythemal spectrum. In this example the erythema is 17.5 $\mu W\ cm^{-2}$. This is the quantity commonly measured by broadband instruments designed to monitor erythema. At smaller solar zenith angle, the irradiances can be much higher, and erythemal irradiances in excess of 45 $\mu W\ cm^{-2}$ have been measured at MLO.

For the following analyses, UV spectroradiometer data for 45° solar zenith angles were chosen for clear mornings

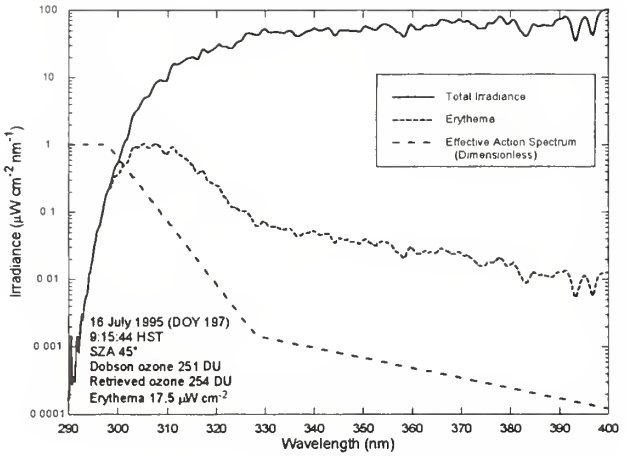

Fig. 3.14. Example of a Mauna Loa UV spectrum obtained on a clear morning (July 16, 1995) at a solar zenth angle of 45° (solid line). A point is plotted every 0.2 nm. Also shown is the erythema spectrum (short-dashed) for this scan obtained by weighting the UV spectrum by the effective action spectrum (EAS) (long-dashed). The EAS is a dimensionless quantity normalized to 1 for $\lambda < 298$ nm. The erythema for this scan is 17.5 μW cm^{-2}.

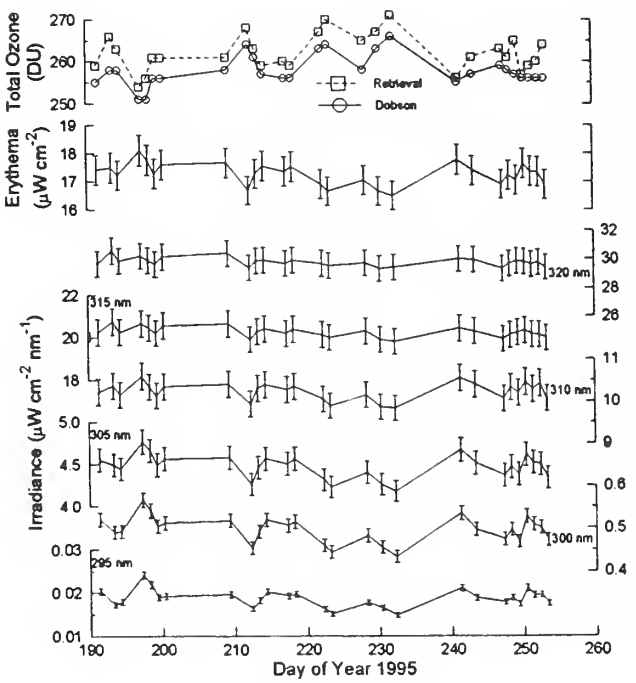

Fig. 3.15. One-nm averages of spectral irradiance on 27 clear sky mornings at MLO for selected wavelengths at a solar zenith angle of 45° (lower), corresponding erythema calculated using the EAS (middle), and total column Dobson ozone compared with ozone retrieved from the spectroradiometer data (top). The ozone retrieval uses I_{340}/I_{305} as described by *Stamnes et al.* [1991]. Error bars shown are 2-σ estimates including calibration, noise, and wavelength errors. Note that DOY 190 = July 9, 1995.

at MLO. Clear mornings at MLO were determined by examining other solar radiation records for MLO. For each scan, 1-nm averages were formed centered at each 1-nm wavelength. In order to quantify changes in UV related to changes in ozone, and to display data as a time series, all spectral irradiance data were adjusted for the eccentricity of the earth's orbit around the sun.

All Dobson spectrophotometer total ozone data were taken directly from the MLO observer notes. Retrieved ozone values were obtained from the UV spectroradiometer data using the method of *Stamnes et al.* [1991], which uses the irradiance ratio I_{340}/I_{305} to infer total ozone. Erythemal radiation data were obtained from the spectroradiometer data by applying the effective action spectrum weighting function and integrating over wavelength as discussed previously.

Analyses

The radiative amplification factor (RAF) is defined as the percent change of UV irradiance divided by the percent change of total ozone, a quantity that was introduced to estimate the effects of ozone depletion on the incident UV radiation. In this work, RAFs were calculated using the power law formulation from *Madronich* [1993]: RAF = $-\Delta\ln(I)/\Delta\ln(O_3)$, where I is UV irradiance.

Referring again to Figure 3.14, it is seen that irradiance decreases by 5 orders of magnitude over the wavelength range 290-320 nm. All of the variability seen in the data is real and some of it is due to solar structure, such as the obvious calcium lines between 390 and 400 nm. As discussed previously, the 290-320 nm range is most strongly influenced by atmospheric ozone.

Figure 3.15 shows a time series over the period DOY 192-253, 1995, of 1-nm means of UV irradiance data for a solar zenith angle of 45° over the 295- to 320-nm wavelength band (5-nm intervals). Only data for clear days are shown, giving 27 data points; however, the individual data points are connected by straight lines for continuity. Although this 3-month time series is not long enough to show a significant trend, significant variations in both UV irradiance and total ozone occurred. During this time period, stability tests showed that the instrument was operating well within the expected limits of calibration uncertainty. The error bars show estimated 2-σ errors that include calibration, noise, and wavelength errors calculated similar to that shown by *McKenzie* [1982]. The calculated erythema radiation correlates strongly with irradiance at the shorter wavelengths as expected. Total ozone values retrieved from the spectroradiometer data correlate well with Dobson total ozone but show a systematic difference of about 4 Dobson Units. However, this is better than 2% agreement and could be improved by optimizing the retrieval algorithm for MLO. RAFs, shown as a function of wavelength in Figure 3.16, are negligible for wavelengths longer than about 325 nm and increase for shorter wavelengths. This erythema RAF of about 1.4 for MLO is larger than the values of 1.1-1.2 reported for other locations [*McKenzie et al.*, 1991] but is not significantly different because of the large error bars.

Based on the previous discussion of the MLO UV spectroradiometer program, the following can be concluded: (a) The UV spectroradiometer has operated properly at MLO and is producing excellent data within expected calibration limits. The CMDL program plans to

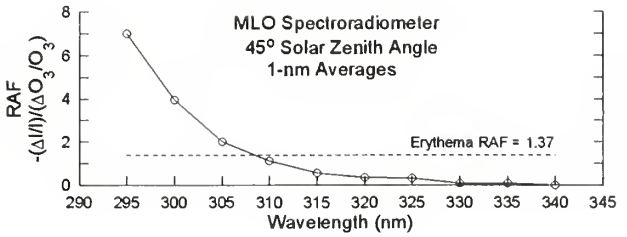

Fig. 3.16. Radiative amplification factor (RAF) as a function of wavelength. Note that the erythema RAF is 1.37, equivalent to a wavelength of about 308 nm.

continue these measurements as a long-term project in an effort to detect any possible long-term UV spectral trends and to relate these to ozone trends. (b) UV irradiance variations are strongly correlated (inversely) with Dobson total ozone variations, with the highest correlation coefficients at the shortest wavelengths. Erythema calculated from the spectroradiometer is also strongly correlated with ozone. (c) The RAFs of about 1.4 measured at MLO are higher than those previously measured at other sites but may not be significant because of the large error bars. (d) In this limited data set, no significant UV irradiance trend is evident.

3.2.5. MLO Broadband UV

A UV broadband horizontal incidence instrument (Yankee UVB-1, SN 950208) was installed at MLO on July 7, 1995. This instrument was interfaced with the station solar radiation data acquisition system to provide 3-minute mean data. The UVB-1 has a spectral response over the wavelength range 280-330 nm and uses a fluorescent phosphor to convert UV light to visible light, which is then detected by a solid-state photodiode. All optical components are thermally stabilized at 45°C using a thermostatically controlled heater. The UVB-1 will undergo annual factory calibrations, and its calibration will be checked by comparison with the MLO spectro-radiometer that commenced measurements at the site at about the same time. The performance of the broadband UV radiometer relative to the spectral measurements will be used to assess the information content of broadband UV measurements at other CMDL sites.

3.2.6. BSRN

CMDL has established an active role in the management of the WCRP BSRN. In addition to supplying data from five CMDL sites to the BSRN archive, CMDL provides the international manager for the program. BSRN is intended to acquire and supply surface radiation data of superior quality for global energy budget and satellite studies. Several instrumentation upgrades are still required at the CMDL observatories to fully comply with BSRN specifications. Recent improvements to the CMDL radiation sites that move in the direction of more complete BSRN compliance are new data loggers and tracking shadow disks for pyranometers and pyrgeometers. In addition, observations of wideband UV-B and PAR as well as spectral diffuse/total irradiance were added at some sites and will be added to more as funding and manpower allow. Considerable effort is put into data processing and analysis for the purpose of passing final data on to the BSRN archive.

3.2.7. WMO GAW Stations

The CMDL radiation project participated in an effort to establish surface solar radiation programs at the GAW observatories. This effort involved the development of solar radiation monitoring systems, calibration capability, and personnel training for five sites. By the end of 1995, four of the five GAW sites had operational solar radiation monitoring programs. The four operational sites are located in Algeria, China, Tierra del Fuego, and Indonesia. A fifth site in Brazil is under preparation. Each site is equipped with pyrheliometers and pyranometers to monitor direct solar beam, global horizontal and diffuse-sky radiation, plus an automated cavity radiometer system for calibration. All sensors for the GAW sites were characterized and compared to CMDL standards prior to deployment to each site and site calibrations are performed using an automated cavity radiometer that enables the sites to maintain traceability to the absolute scale and the world radiometric reference. Instrumentation for the site was purchased with funds through the World Bank, Global Environmental Fund. Personnel from each site were trained in Boulder for a period of 1 month and some assistance from Boulder was provided in establishing some of the sites. Three of the four sites have been visited by CMDL personnel (China, Tierra del Fuego, and Indonesia); future collaboration between CMDL and these new monitoring sites is anticipated. Data from the sites is under the control of the individual site scientists and are to be sent to GAW archives and to Boulder for inspection and brief analysis.

3.2.8. Volcanic Radiative Forcing and Induced Global Cooling

The zonal mean global radiative forcing due to the eruptions of El Chichón (1982) and Mt. Pinatubo (1991) was computed based on near global coverage aerosol optical depth estimates made from satellite [*Dutton and Cox*, 1995]. These events provide two case studies of the viability of our global observational network and our ability to assess the impact of a major radiation budget altering event. Aerosol optical properties were derived from Mie inverted aerosol size distributions based on surface measured spectral aerosol optical depth. Comparisons between optical properties derived from Mie inversions and those using in situ measured size distributions show little difference between the two in computed volcanic radiative forcing. The computed global zonal mean radiative forcing was used in a simple global thermal mass model to estimate the hemispheric tropospheric cooling, with close agreement to Microwave Sounding Unit (MSU) temperature observations following Mt. Pinatubo, but with poor agreement after El Chichón. The anomalous sea-surface temperature conditions of 1982-1983 are most likely responsible for the thermal model's failure to track observed temperatures. Previously, *Dutton and Christy* [1992] suggested that the observed volcanic aerosol and radiative forcing following El Chichón and Mt. Pinatubo might be responsible for observed (MSU) and predicted [*Hansen et*

al., 1992] global cooling following these two major eruptions.

3.2.9. BRW Surface Radiation and Meteorological Measurements

Measured surface radiation budget components for BRW have been compiled for 1994. From hourly-averaged data, daily and monthly means were produced and merged with ancillary meteorological data for each year, and monthly statistics were computed. These data were published by *Stone et al.* [1996] which also contains a description of CMDL's monitoring program at BRW and the data processing techniques used. Tables of daily values, monthly statistical summaries, and corresponding plots show annual cycles of several measured and derived radiation variables collated with meteorological data. These data include the four components that constitute the net surface radiation balance, i.e., the upward and downward solar (or shortwave) and the upward and downward thermal infrared (or longwave) irradiances and also direct-beam solar irradiance and surface albedo, derived from the ratio of the reflected to incident radiation. Figure 3.17 is a sample of the data for 1994 showing daily mean time series of the net surface radiation components, the direct beam irradiance, and derived quantities. Daily average total-sky cover, averaged from three hourly National Weather Service (NWS) observations made in Barrow, is also included. Coincident meteorological data

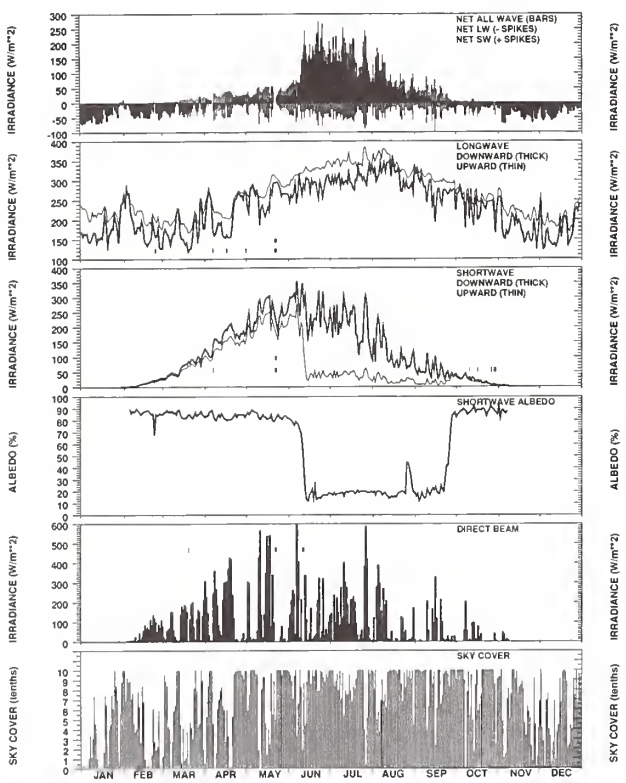

Fig. 3.17. Daily average surface irradiance (W m^{-2}) observations and sky cover (cloudiness in tenths of total sky), for Barrow, Alaska, 1994.

(not shown) are displayed similarly in the report to facilitate correlative analyses. In addition to the printed report, the 1992, 1993, and 1994 daily data are accessible digitally through the Internet via connection to the CMDL World Wide Web home page.

Radiation measurements at BRW show a dramatic increase in net irradiance each spring in late May or early June coinciding with the maximum average daily solar gain at the surface. Snow melt typically occurs during the second week in June [*Dutton and Endres,* 1991] evidenced by a dramatic decrease in surface albedo (Figure 3.17). Monthly mean net radiation generally peaks in July, which tends to be the least cloudy of summer months. The downwelling thermal irradiance reaches a maximum, on average, during August, which is typically the cloudiest summer month and often the warmest. The data acquisition section (1.5) of this Summary Report gives a description of the BRW meteorology program as well as climate summaries for 1994 and 1995.

Year-to-year variations in the net radiation balance at BRW are found to be greatest during the winter months when the longwave components dominate and day-to-day values correlate well with transient weather events. Increased cloudiness, relatively warm temperatures, and westerly winds weaken the surface-based temperature inversion and warm the surface. In fact, clouds tend to radiatively warm the surface most of the year when it is snow covered. Clear periods during winter are coldest and are usually associated with (northeasterly) outflow of air from a quasi-persistent polar anticyclone and relatively calm winds resulting in strong surface-based temperature inversions [*Kahl,* 1990].

Understanding the links between conditions at BRW and the central Arctic, such as ice distributions in the Beaufort and Chukchi Seas and/or the frequency of cyclones in the central Arctic [e.g., *Serreze et al.,* 1995; *Maslanik et al.,* 1996] is the focus of ongoing research. For instance, an inspection of the 1992-1994 sky-cover record compared with *Kahl's* [1990] analysis suggests that spring cloudiness has increased significantly in recent years. Because clouds can dramatically influence radiative flux at the surface at this time of year, the net radiation balance may also be affected. A comparison of the 1992-1994 BRW radiation measurements with an earlier record [*Maykut and Church,* 1973] suggests that this has occurred [*Stone et al.,* 1996]. In turn, these changes may be associated with decreasing sea ice concentrations upwind of Barrow [*Maslanik et al.,* 1996] and/or regionally changing circulation patterns that affect the Arctic hydrologic cycle [e.g., *Serreze, et al.,* 1995]. Only through continuous monitoring of polar processes and analyses of correlative data sets will we begin to understand the complicated feedback mechanisms that determine polar climates; these in turn affect global circulation patterns [*Fletcher,* 1970].

BRW is strategically situated to investigate Arctic climate interactions because it is sensitive to processes that occur throughout the region. Useful discussions on how synoptic-scale systems influence the Barrow climate are given in *Halter and Peterson* [1981], *Halter and Harris* [1983], and *Harris and Kahl* [1994]. CMDL will continue its monitoring efforts as part of the BSRN [*Wielicki et al.,* 1995]. In addition, the U.S. Department of Energy (DOE) is constructing a Cloud and Radiation Testbed (CART) facility nearby as part of their Atmospheric Radiation Measurement (ARM) Program [*Wielicki et al.,* 1995;

Stokes and Schwartz, 1994], and an ambitious field experiment to investigate the Surface Heat Budget of the Arctic (SHEBA) is being organized to take place in the Beaufort Sea. The addition of DOE/ARM remote sensing and other sophisticated ground-based instruments in the vicinity of BRW will greatly enhance our ability to assess the unique radiative properties of the Arctic atmosphere and thus improve parameterizations needed for model studies. In addition, through comparative analyses of the combined BRW, DOE/ARM, and SHEBA data sets, critical aspects of Arctic climate will be further investigated.

3.3. REFERENCES

Bishop, J.K.B., W.B. Rossow, and E.G. Dutton, Clouds, aerosols, and the temporal and spatial variability of surface solar irradiance. *J. Geophys. Res.,* in press, 1996.

Bodhaine, B.A., Barrow surface aerosol: 1976-1987, *Atmos. Environ.*, 23(11), 2357-2369, 1989.

Bodhaine, B.A., and J.J. DeLuisi, An aerosol climatology of Samoa, *J. Atmos. Chem.*, 3, 107-122, 1985.

Bodhaine, B.A., J.J. DeLuisi, J.M. Harris, P. Houmere, and S. Bauman, Aerosol measurements at the South Pole, *Tellus*, 38B, 223-235, 1986.

Bodhaine, B.A., J.J. DeLuisi, J.M. Harris, P. Houmere, and S. Bauman, PIXE analysis of South Pole aerosol, in *Nuclear Instruments and Methods in Physics Reserach*, B22, pp. 241-247, Elsevier, Holland, 1987.

Bodhaine, B.A., B.G. Mendonca, J.M. Harris, and J.M. Miller, Seasonal variations in aerosols and atmospheric transmission at Mauna Loa Observatory, *J. Geophys. Res.*, 86(C8), 7395-7398, 1981.

Cess, R.D.,M.H. Zhang, P. Minnis, L. Corsetti, E.G. Dutton, B.W. Forgan, D.P. Garber, W.L. Gates, J.J. Hack, E.F. Harrison, X. Jing, J.T. Kiehl, C.N. Long, J.-J. Morcrett, G.L. Potter, V. Ramanathan, B. Subasilar, C.H. Whitlock, D.F. Young, and Y. Zhou, Absorption of solar radiation by clouds: Observations versus models, *Science,* 267, 496-499, 1995.

Charlson, R.J., S.E. Schwartz, J.M. Hales, R.D. Cess, J.A. Coakley, Jr., J.E. Hansen, and D.J. Hofmann, Climate forcing by anthropogenic aerosols, *Science,* 255, 423-430, 1992.

Dutton, E.G., An extended comparison between LOWTRAN7-computed and observed broadband thermal irradiances: Global extreme and intermediate surface conditions, *J. Atmos. Ocean. Tech.,* 10, 326-336, 1993.

Dutton, E.G. and S.K. Cox, Tropospheric radiative forcing from El Chichón and Mt. Pinatubo: Theory and observations, *Colorado State University, Dept. of Atmos. Science Paper No. 586*, Fort Collins, CO, 209 pp., 1995.

Dutton, E.G., and D.J. Endres, Date of snowmelt at Barrow, Alaska, U.S., *Arc. Alp. Res.*, 23(1), 115-119, 1991.

Dutton, E.G. and J.R. Christy, Solar and radiative forcing at selected locations and evidence for global lower tropospheric cooling following the eruptions of El Chichón and Pinatubo, *Geophys. Res. Lett.*, 23, 2313-2316, 1992.

Dutton, E.G., J.J. DeLuisi, and A.P. Austring, Interpretation of Mauna Loa atmospheric transmission relative to aerosols, using photometric precipitable water amounts, *J. Atmos. Chem.,* 3, 53-68, 1985.

Dutton, E.G., P. Reddy, S. Ryan, and J.J. DeLuisi, Features and effects of aeosol optical depth observed at Mauna Loa, Hawaii: 1982-1992, *J. Geophys. Res.*, 99(D4), 8295-8306, 1994.

Elkins, J.W., and R.M. Rosson (Eds.), *Geophysical Monitoring for Climatic Change No. 17, Summary Report 1988*, 142 pp., NOAA Air Resources Laboratory, Boulder, CO, 1989.

Fletcher, J.O., Polar ice and the global climate machine, *Bull. Atomic. Sci.*, 40-47, 1970.

Ellis, H.T., and R.F. Pueschel, Solar radiation: Absence of air pollution trends at Mauna Loa, *Science*, 172, 845-346, 1971.

Garratt, J. R., and A.J. Prata, Downwelling longwave fluxes at continental surfacaes-a comparison of observations with GCM simulations and implications for the global land-surface radiation budget, *J. Clim.*, 9(3), 646-655, 1996.

Halter, B.C., and J.M. Harris, On the variability of atmospheric carbon dioxide concentration at Barrow, Alaska during winter, *J. Geophys. Res.*, 88, 6858-6864, 1983.

Halter, B.C., and J.T. Peterson, On the variability of atmospheric carbon dioxide concentration at Barrow, Alaska during summer, *Atmos. Environ.,* 15, 1391-1399, 1981.

Hansen, J.E., A. Lacis, R. Ruedy, and M. Sato, Potential climate impact of Mount Pinatubo eruption, *Geophys. Res. Lett.*, 19, 215-218, 1992.

Harris, J.M., and J.D.W. Kahl, Analysis of 10-day isentropic flow patterns for Barrow, Alaska: 1985-1992, *J. Geophys. Res.*, 99(D12), 25,845-25,855, 1994.

Hofmann, D.J., S.J. Oltmans, G.L. Koenig, B.A. Bodhaine, J.M. Harris, J.A. Lathrop, R.C. Schnell, J. Barnes, J. Chin, D. Kuniyuki, S. Ryan, R. Uchida, A. Yoshinaga, P.J. Neale, D.R. Hayes, Jr., V.R. Goodrich, W.D. Komhyr, R.D. Evans, B.J. Johnson, D.M. Quincy, and M. Clark, Record low ozone at Mauna Loa Observatory during winter 1994-1995: A consequence of chemical and dynamical synergism? *Geophys. Res. Lett.*, 23, 1533-1536, 1996.

Kahl, J.D., Characteristics of the low-level temperature inversion along the Alaskan Arctic coast, *Int. J. Climatol.,* 10, 537-548, 1990.

Madronich, S., *The Atmosphere and UV-B Radiation at Ground Level, in Environmental UV Photobiology*, edited by A. R. Young et al., Plenum Press, New York, 1-39, 1993.

Maslanik, J.A., M.C. Serreze, and R.G. Barry, Recent decreases in summer Arctic ice cover and linkages to anomalies in atmospheric circulation, *Geophys. Res. Lett.*, submitted, 1996.

Maykut, G.A., and P.E. Church, Radiation climate of Barrow, Alaska, 1962-66, *J. Appl. Meteorol.*, 12, 620-628, 1973.

McKenzie, R. L., W. A. Matthews, and P. V. Johnston, The relationship between erythemal UV and ozone, derived from spectral irradiance measurements, *Geophys. Res. Lett.*, 18, 2269-2272, 1991.

McKenzie, R. L., P. V. Johnston, M. Kotkamp, A. Bittar, and J. D. Hamlin, Solar ultraviolet spectroradiometry in New Zealand: Instrumentation and sample results from 1990, *Appl. Opt.*, 31, 6501-6509, 1992.

McKinlay, A.F., and B.L. Diffey, A reference action spectrum for ultraviolet induced erythema in human skin, *J. Int. Comm. Illum.*, 6, 17-22, 1987.

National Research Council (NRC), Aerosol Radiative Forcing and Climate Change, in *Panel on Aerosol Radiative Forcing and Climate Change, Board on Atmospheric Sciences and Climate, Commission on Geosciences, Environment, and Resources*, National Academy Press, Washington, D.C., 161 pp., 1996.

Nemesure, S., R.D. Cess, E.G. Dutton, J.J. DeLuisi, Z. Li, and H.G. Leighton, Impact of the shortwave radiation budget of the surface-atmosphere system for snow-covered surfaces, *J. Clim.*, 7, 579-585, 1994.

Quakenbush, T.K., and B.A. Bodhaine, Surface aerosols at the Barrow GMCC observatory: Data from 1976 through 1985, *NOAA Data Rep. ERL ARL-10*, 230 pp., NOAA Air Resources Laboratory, Silver Spring, MD, 1986.

Radke, L.F., C.A. Brock, R.J. Ferek, and D.J. Coffman, Summertime arctic hazes, paper A52B-03 presented at the American Geophysical Union Fall Annual Meeting, San Francisco, December 3-7, 1990.

Serreze, M.C., J.A. Maslanik, J.R. Key, R.F. Kokaly, and D.A. Robinson, Diagnosis of record minimum in Arctic sea ice area during 1990 and associated snow cover extremes, *Geophys. Res. Lett.*, 22(16), 2183-2186, 1995.

Stamnes, K., The stratosphere as a modulator of ultraviolet radiation into the biosphere, in *Surveys of Geophysics*, 14, Kluwer, Netherlands, 167-186, 1993.

Stamnes, K., J. Slusser, and M. Bowen, Derivation of total ozone abundance and cloud effects from spectral irradiance measurements, *Appl. Opt.*, 30, 4418-4426, 1991.

Stokes, G.M., and S.E. Schwartz, The Atmospheric Radiation Measurement (ARM) Program: Programmatic background and design of the cloud and radiation test bed, *Bull. Amer. Meteorol. Soc.*, 75, 1201-1221, 1994.

Stone, R.S., T. Mefford, E.G. Dutton, D. Longenecker, B. Halter, and D. Endres, Barrow, Alaska, surface radiation and meteorological measurements: January 1992 to December 1994, *NOAA Data Report, ERL CMDL-11*, NOAA Environmental Research Laboratories, Boulder, CO, 81 pp., 1996.

Whitlock, C.H., T.P. Charlock, W.F. Staylor, R.T. Pinker, I. Laszlo, A. Ohmura, H. Gilgen, T. Konzelman, R.C. DiPasquale, C.D. Moats, S.R. LeCroy, and N.A. Ritchey, First global WCRP shortwave surface radiation budget dataset, *Bull. Amer. Meteorol. Soc.*, 76, 905-922, 1995.

Wielicki, B.A., R.D. Cess, M.D. King, D.A. Randall, and E.F. Harrison, Mission to planet earth: Role of clouds and radiation in climate, *Bull. Amer. Meteorol. Soc.*, 76(11), 2125-2153, 1995.

4. Ozone and Water Vapor

S. Oltmans (Editor), D. Hofmann, J. Harris, B. Johnson, R. Evans, G. Koenig, J. Lathrop, M. O'Neill, H. Vömel, D. Quincy, W. Komhyr, M. Clark, and E. Hackathorn

4.1. Continuing Programs

4.1.1. Total Ozone Observations

Total ozone observations continued throughout 1994 and 1995 at 15 of the 16 stations that comprise the U.S. Dobson spectrophotometer network (Table 4.1). Of the 16 stations, 5 were operated by CMDL personnel, 5 by NWS, 2 are domestic cooperative stations, and 4 are foreign cooperative stations. All stations are either fully or semiautomated. In addition, a Brewer spectrophotometer was operated on a nearly continuous basis at Boulder.

The Peruvian station was still out of operation at the end of 1995, although a new baseline monitoring station is under construction. Operations will likely start in late 1996. In May 1995 the Fresno instrument and shelter were moved 30 miles southwest of Hanford, California. The Bismarck instrument and shelter were moved about 150 m in August 1994.

Provisional daily total ozone amounts applicable to local apparent noon for the stations listed in Table 4.1 were archived at the World Ozone Data Center (WODC), 4905 Dufferin Street, Ontario M3H 5T4, Canada, in *Ozone Data for the World*. Table 4.2 lists the monthly mean total ozone amounts measured at the various stations for 1994 and 1995. (Monthly means are computed for stations where observations were made on at least 10 days each month.).

Ten Dobson ozone spectrophotometers in the CMDL network as well as 29 others were calibrated during 1994 and 1995. Tables 4.3 list all the instruments calibrated and the resulting calibration difference expressed as a percent ozone difference. This percent difference is between ozone calculated from the test and the standard instrument measurements with the ADDSGQP observation type at a μ value of 2, and a total ozone value of 300 Dobson Units (DU), before any repair or calibration adjustment is made. The table also lists the place of the calibration and the standard instrument used.

The Mauna Loa Observatory, Hawaii (MLO) instrument D076 failed mechanically in February 1994. This automated instrument was repaired and back in service in May 1994. During the repair the left side mirror was replaced due to a deteriorating surface.

CMDL participated in an international Dobson spectrophotometer calibration at Izaña Observatory (Tenerife, Spain) in June 1994 and at Arosa, Switzerland (LKO) in July 1995 as part of its role as the World Center for Dobson Calibrations. Instruments for Mexico City, Mexico; Comodoro Rivadavia, Argentina; and Montevideo, Uruguay, were calibrated in Boulder during this period. A representative from the Czech Hydrological and Meteorological Institute assisted with the latter two instruments. These were new instruments from Ealing Opto-Electronics.

Reevaluation of more than 400 station-years of total ozone data from 25 CMDL (and its predecessor organizations) Dobson spectrophotometer stations was completed in 1995. Corrections were based on field instrument calibrations made throughout the years with World Primary Standard Dobson Instrument no. 83 [*Komhyr et al.*, 1989]. This instrument's long-term ozone measurement precision has been maintained since the early 1960s at ±1% by means of Langley calibration

TABLE 4.1. U.S. Dobson Ozone Spectrophotometer Station Network for 1994-1995

Station	Period of Record	Instrument No.	Agency
Bismarck, North Dakota	Jan. 1, 1963-present	33	NOAA
Caribou, Maine	Jan. 1, 1963-present	34	NOAA
Wallops Is., Virginia	July 1, 1967-present	38	NOAA; NASA
SMO	Dec. 19, 1975-present	42	NOAA
Tallahassee, Florida	May 2, 1964-Nov. 30, 1989; Nov. 1, 1992-present	58	NOAA; Florida State University
Boulder, Colorado	Sept. 1, 1966-present	61	NOAA
Fairbanks, Alaska	March 6, 1984-present	63	NOAA; University of Alaska
Lauder, New Zealand	Jan. 29, 1987-present	72	NOAA; DSIR
MLO	Jan. 2, 1964-present	76	NOAA
Nashville, Tennessee	Jan. 2, 1963-present	79	NOAA
Perth, Australia	July 30, 1984-present	81	NOAA; Australian Bureau Meteorology
SPO	Nov. 17, 1961-present	82	NOAA
Haute Provence, France	Sept. 2, 1983-present	85	NOAA; CNRS
Huancayo, Peru	Feb. 14, 1964-Dec. 31, 1992	87	NOAA; IGP
BRW	June 6, 1986-present	91	NOAA
Fresno, California	June 22, 1983-March 13, 1995	94	NOAA
Hanford, California	March 15, 1995-present	94	NOAA

TABLE 4.2. Provisional 1994 Monthly Mean Total Ozone Amounts (M-Atm-CM)

Station	Jan.	Feb.	March	April	May	June	July	Aug.	Sept.	Oct.	Nov.	Dec.
					1994							
Bismarck, North Dakota	361	367	372	351	327	322	319	302	286	294	286	300
Caribou, Maine	340	382	390	377	369	338	324	324	316	299	293	304
Wallops Is., Virginia	320	343	347	325	355	327	309	302	292	281	255	270
SMO	241	242	244	237	237	241	240	244	244	248	251	242
Tallahassee, Florida	289	291	306	308	338	321	322	299	-	-	241	269
Boulder, Colorado	321	331	333	341	315	295	299	280	277	274	265	276
UAF-GI, Alaska	-	[371]	420	408	380	347	312	278	-	-	-	-
Lauder, New Zealand	277	267	262	265	289	315	337	361	370	360	341	302
MLO	244	256	-	-	279	271	268	265	258	256	238	220
Nashville, Tennessee	321	323	339	328	334	322	313	304	296	277	252	276
Perth, Australia	266	262	265	257	269	291	294	300	309	317	307	278
SPO	266	253	[245]	[231]	[277]	[231]	[239]	[226]	-	132	269	316
Haute Provence, France	326	373	314	382	352	332	320	305	311	295	273	293
Huancayo, Peru	Station closed											
BRW	-	-	457	445	379	346	310	293	-	-	-	-
Fresno, California	314	324	325	332	333	303	305	292	-	269	275	280
					1995							
Bismarck, North Dakota	334	358	341	347	347	321	311	282	286	290	292	297
Caribou, Maine	349	382	357	372	348	323	320	304	302	-	311	325
Wallops Is., Virginia	307	344	316	325	316	323	312	297	288	267	299	284
SMO	242	243	243	244	243	247	245	250	259	262	251	251
Tallahassee, Florida	267	282	284	288	302	313	302	308	294	266	277	263
Boulder, Colorado	296	290	304	328	325	299	281	276	284	270	276	275
UAF-GI, Alaska	-	[349]	365	367	341	326	300	302	268	326	-	-
Lauder, New Zealand	277	267	282	273	280	302	335	336	361	348	328	287
MLO	217	223	254	268	280	274	262	262	261	255	254	239
Nashville, Tennessee	321	323	339	328	334	322	313	304	296	277	252	276
Perth, Australia	272	257	268	276	268	282	295	292	312	311	306	273
SPO	287	270	[231]	[256]	[255]	[245]	[246]	[223]	-	120	192	257
Haute Provence, France	293	319	333	340	340	331	322	329	304	277	283	303
Huancayo, Peru	Station closed											
BRW	-	[354]	407	386	339	345	304	300	269	[260]	-	-
Handford, California	293	292	315	316	338	330	298	292	286	272	264	285

Monthly mean ozone values in square brackets are derived from observations made on fewer than 10 days per month.

observations conducted periodically at MLO and with standard lamps. Procedures used in reevaluating the data are described in detail in *Komhyr* [1993].

Seasonal and annual downward trends in ozone during 1979-1995, determined from the reevaluated data for five U.S. mainland stations (Caribou, Maine; Bismarck, North Dakota; Boulder, Colorado; Wallops Island, Virginia; and Nashville, Tennessee) and for MLO and Samoa Observatory, American Samoa (SMO), are shown in Table 4.4. Also included in the table are the ozone trends measured at Fresno, California, during 1985-1995. The statistical method used in determining the trends (G. C. Reinsel, University of Wisconsin-Madison) was similar to that employed by the 1988 Ozone Trends Panel [*WMO,* 1988] whereby solar cycle and ozone QBO effects are removed from the data. Note that the downward trend in ozone, averaged over the five contiguous U.S. stations with the longest records, is largest at -5.45% per decade for spring (March-May) months and smallest at -1.6% per decade for autumn (September to November) months. On an annual basis, the downward ozone trend at these sites averages -3.58% per decade. These trends exhibit a slight recovery from values determined from 1979-1993 data that encompassed record low ozone values over the U.S. during the winter of 1992-1993 [*Komhyr et al.*, 1994]. For the earlier time period, the average five-station downward ozone trend for spring months (not shown) was -5.79% per decade and -3.8% per decade on an annual basis. Downward trends in ozone measured nearer the equator at MLO and SMO are significantly smaller.

4.1.2. UMKEHRS

Umkehr observations made with the Automated Dobson Network instruments continued in 1994 and 1995 at Boulder; Haute Provence, France; Lauder, New Zealand; MLO; Perth, Western Australia; and at the University of Alaska's Geophysical Institute. Umkehr processing is set to resume early in 1996. Processing will begin with MLO, followed by Lauder and the other stations in a

TABLE 4.3. Dobson Ozone Spectrophotometers Calibrated in 1994-1995

Station	Instrument Number	Calibration Date	Calibration Correction (%)	Standard Number	Place
		1994			
Lisbon, Spain	D013	Aug. 2, 1990	+0.7%	65	Izaña Observatory
Oslo, Norway	D056	Aug. 21, 1986	+0.5%	65	Izaña Observatory
Potsdam, Germany	D064	Aug. 2, 1990	+0.6%	65	Izaña Observatory
Huancayo, Peru	D087	May 15, 1985	+0.9%	65	Izaña Observatory
Natal, Brazil	D093	May 20, 1986	+2.9%	65	Izaña Observatory
Buenos Aires, Argentina	D097	July 15, 1992	+0.1%	65	Izaña Observatory
El Arenosillo, Spain	D120	Aug. 9, 1990	+1.3%	65	Izaña Observatory
Ushuaia, Argentina	D131	None	N/A	65	Izaña Observatory
Tallahassee, Florida	D058	Sept. 9, 1991	-.3	83	Boulder
Boulder, Colorado	D061	Aug. 27, 1992	0.0%	65	Boulder
MLO	D076	June 13, 1993	N/A	83	Boulder
SPO	D080	May 26, 1988	0.5%	83	Boulder
BRW	D091	May 26, 1989	0.0%	83	Boulder
Fresno, California	D094	June 26, 1989	1.0%	83	Boulder
Mexico D.F Mexico	D098	August 1978	-0.3%	83	Boulder
		1995			
RA VI Spare	15	None	N/A	65	LKO Arosa
Vindeln, Sweden	30	May 10, 1990	+0.7%	65	LKO Arosa
United Kingdom	32	May 1995	N/A	65	LKO Arosa
Uccle, Belgium	40	Aug. 1, 1990	+2.0%	65	LKO Arosa
United Kingdom, Standard	41	Aug. 2, 1990	+1.2%	65	LKO Arosa
Sestola, Italy	48	Nov. 12, 1980	+2.4%	65	LKO Arosa
Bordeaux, France	49	July 10, 1990	+0.3%	65	LKO Arosa
Reykjavik, Iceland	50	Aug. 2, 1990	+1.1%	65	LKO Arosa
Arosa, Switzerland	62	Aug. 7, 1992	+1.7%	65	LKO Arosa
Belsk, Poland	84	Aug. 2, 1990	+0.2%	65	LKO Arosa
l'Obs. Haute Provence, France	85*	July 10, 1990	+0.7%	65	LKO Arosa
Denmark	92*	Aug. 2, 1990	+1.0%	65	LKO Arosa
Arosa, Switzerland	101	Aug. 2, 1990	+2.1%	65	LKO Arosa
Hohenpeissenberg, Germany	104	Aug. 2, 1990	+1.6%	65	LKO Arosa
Moscow, Russia	107	Aug. 5, 1990	+1.4%	65	LKO Arosa
Budapest, Hungary	110	Aug. 2, 1990	+0.5%	65	LKO Arosa
Tsukuba, Japan, Standard	116*	June 29, 1992	+0.6%	65	LKO Arosa
Bucharest, Romania	121	Aug. 5, 1990	Not consistent	65	LKO Arosa
Bismarck, North Dakota	D033	Oct. 1, 1993	+1.5	83	Boulder
Caribou, Maine	D034	Sept., 9, 1991	+0.3	83	Boulder
Wallops Island, Virginia	D038	Sept. 16, 1991	+1.0	83	Boulde
Nashville, Tennessee	D079	Aug. 14, 1991	+0.6	83	Boulder
Comodoro Rivadavia, Argentina	D133	New Dobson	N/A	83	Boulder
Montevideo, Uruguay	D134	New Dobson	N/A	83	Boulder

collaborative effort with the University of Alabama, Huntsville. Since the reprocessing of the total ozone from these stations will have been completed, the updated calibration tables and ozone values will be incorporated into the Umkehr processing. Under conditions of high stratospheric aerosol loading, which was the case following the eruption of Mt. Pinatubo, reliable ozone profiles can be obtained from the Umkehr technique only by correcting for aerosols. Such conditions prevailed through 1992 at most of the sites. The effort with University of Alabama, Huntsville, will include the application of proper aerosol corrections to the profile data.

4.1.3. Surface and Tropospheric Ozone

At least 20-year records of observation are now available for each of the four CMDL baseline sites. Records at Bermuda, Barbados, and Niwot Ridge are at least 5 years in length. At Westman Islands, Iceland, observations began in 1992. For several years, data were being obtained from Mace Head, Ireland, in a cooperative program as part of the Atmosphere/Ocean Chemistry Experiment (AEROCE). Data continues to be received from Mace Head but CMDL is no longer actively involved in that measurement program. The aging complement of surface

TABLE 4.4. Annual and Seasonal Trends January 1979-December 1993

Station	Latitude	Annual		Dec.-Feb.		March-May		June-Aug.		Sept.-Nov.	
		Trend	Std. Error	Trend	Std. Error	Trend	Std. Error	Trend	Std. Error	Trend	Std. Error
Caribou, Maine	46.9°N	-4.00	0.71	-4.84	1.73	-5.64	1.12	-3.34	0.79	-1.52	1.16
Bismarck, North Dakota	46.8°N	-3.30	0.63	-3.25	1.43	-5.69	1.01	-2.00	0.93	-1.62	0.95
Boulder, Colorado	40.0°N	-3.85	0.61	-3.97	1.23	-6.50	1.22	-2.68	0.75	-1.51	0.98
Wallops Is., Virginia	37.9°N	-3.67	0.68	-4.79	1.33	-4.77	1.28	-2.66	0.78	-2.10	1.18
Nashville, Tennessee	36.3°N	-3.09	0.70	-4.08	1.25	-4.62	1.35	-2.03	0.92	-1.23	1.22
Fresno, California*	36.8°N	-3.81	1.37	-3.18	2.00	-3.84	3.00	-3.52	1.71	-4.74	1.31
MLO	19.5°N	-0.53	0.77	-1.55	1.15	-0.51	1.44	-0.20	0.94	0.08	0.74
SMO	14.3°S	-1.66	0.66	-1.48	0.96	-2.13	0.80	-1.42	1.09	-1.61	0.85
Average over first five stations		-3.58		-4.19		-5.45		-2.54		-1.60	

ozone monitors, some of which are 20 years old, has experienced a number of breakdowns. Significant blocks of data were lost at Barbados and SMO during 1994 and 1995.

The extent to which tropospheric ozone may have changed since preindustrial times and over the past 20 years is of significant interest. Surface ozone measurements using modern instruments were made only during the past 25 years. Some quantitative measurements using wet chemical techniques were made in Europe in the 1950s [*Staehelin et al.*, 1994], and one set of measurements dates from the turn of the century [*Volz and Kley*, 1988]. These measurements show that over Europe ozone in the lower troposphere at least doubled from the beginning of the measurements to the early 1980s. Many of the more recent measurements (since 1970) show that at least over Europe, and probably over other areas in the midlatitudes of the northern hemisphere, tropospheric ozone continued to increase through the 1970s and early 1980s [*Oltmans et al.*, 1995]. An analysis of most of the recent data sets from surface stations (some located above the boundary layer) suggests that over at least the past decade there has been a significant slowing in tropospheric ozone growth at midlatitudes of the northern hemisphere [*Oltmans et al.*, 1995]. Most other regions show no evidence for tropospheric ozone increases over the past 20 years and in some cases, such as South Pole Observatory, Antarctica (SPO), significant decreases are evident.

The four CMDL baseline observatory surface ozone data records are among the longest available. The annual averages and long-term trends at each location are shown in Figure 4.1. The numerical trend displayed in the figure is a linear regression of the monthly mean observations. At Barrow Observatory, Barrow, Alaska (BRW) there was a significant upward trend prior to 1990, primarily due to summer increases. Smaller annual averages over the last 5 years have driven the trend downward to show an overall small but insignificant increase. The lower amounts in the 1990s are consistent with the results seen in the ozonesonde record at the Canadian stations [*Tarasick et al.*, 1995]. At MLO the overall record beginning in 1974 shows a small but significant increase. At the two

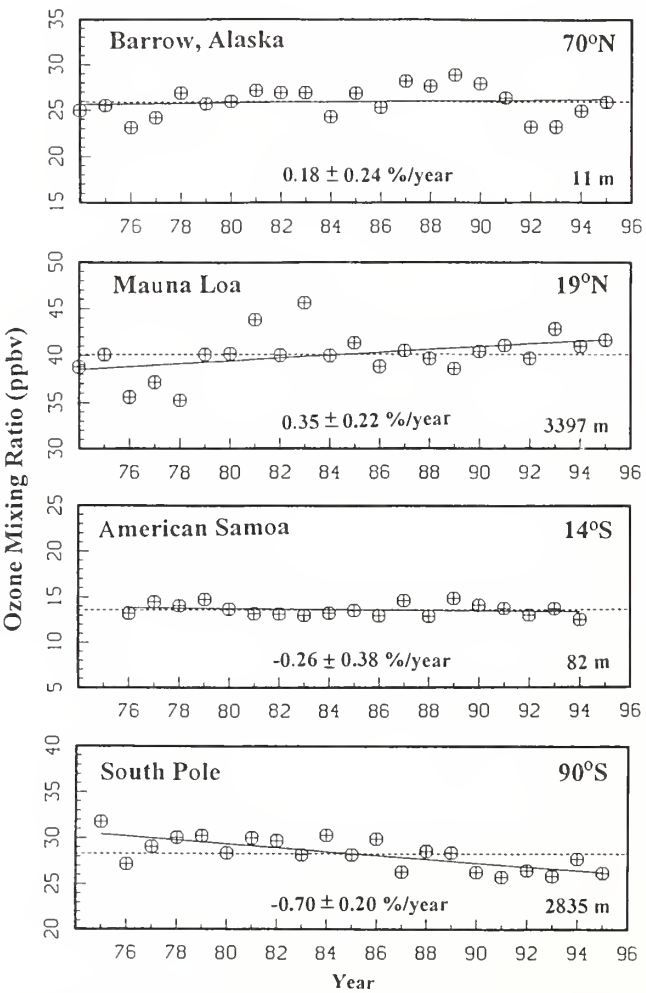

Fig. 4.1. Annual average surface ozone mixing ratios in parts per billion (ppbv) for BRW, MLO, SMO, and SPO. The solid line is a linear trend fit to the monthly anomalies. The trend and 95% confidence levels in percent per year are also shown.

southern hemisphere sites there are long-term decreases. At SMO this decrease is not significant but at SPO a large and significant decline is evident. This is most apparent after 1986. This decline at SPO was discussed in the 1993 Summary Report [*Peterson and Rosson*, 1994].

The monthly ozone means for each of the four CMDL baseline sites for the period of observation are given in Table 4.5. For MLO the means are for the hours 0000-0800 LST, which falls within the time of downslope flow at the observatory.

TABLE 4.5. Monthly Mean Surface Ozone Mixing Ratios (ppbv)

Year	Jan.	Feb.	March	April	May	June	July	Aug.	Sept.	Oct.	Nov.	Dec.
						BRW						
1973	-	-	22.3	15.8	15.6	19.3	15.1	18.8	23.3	30.8	30.2	34.8
1974	28.7	27.4	-	-	23.3	22.0	17.7	18.1	26.1	31.6	32.8	30.9
1975	27.4	29.9	32.7	22.5	23.4	23.7	19.7	19.2	23.0	30.3	28.3	26.3
1976	29.2	31.2	24.4	9.7	11.3	24.1	18.6	18.1	20.3	31.6	30.7	29.1
1977	31.3	32.9	20.8	9.7	20.2	24.5	21.1	20.8	22.4	25.6	33.6	28.0
1978	32.1	32.2	31.0	21.7	22.0	24.1	21.4	22.3	23.6	32.8	29.6	30.3
1979	33.9	31.1	22.6	19.7	25.1	22.5	18.9	18.5	21.1	33.2	32.2	29.3
1980	33.5	33.6	24.5	19.6	18.1	24.7	20.3	19.1	27.9	25.6	34.3	30.0
1981	30.5	27.9	24.5	23.8	26.9	26.1	19.8	23.2	26.2	31.3	34.6	30.9
1982	31.6	31.1	22.5	12.2	15.3	27.1	24.5	23.3	29.7	34.6	36.2	34.5
1983	27.9	34.2	25.9	21.6	21.4	20.4	23.6	22.4	28.2	33.5	30.8	33.0
1984	26.8	19.9	21.5	6.8	16.4	25.5	21.9	22.1	24.3	35.7	38.3	32.2
1985	31.8	28.7	-	-	20.2	28.0	21.2	25.0	28.8	31.4	33.0	33.4
1986	35.5	28.0	20.5	13.9	17.4	24.7	20.4	21.6	25.0	30.3	34.6	31.4
1987	31.1	27.2	22.0	15.0	24.0	30.9	23.3	25.6	31.1	32.5	38.8	36.4
1988	36.4	30.9	22.7	23.8	22.2	26.2	21.7	23.8	26.9	31.6	34.2	31.4
1989	30.2	36.8	32.9	24.6	20.2	24.3	19.9	21.0	31.4	34.8	35.0	35.8
1990	32.3	29.0	27.1	19.5	24.6	23.6	21.1	25.5	32.5	33.1	34.3	32.4
1991	31.6	30.2	16.8	14.3	29.4	25.4	24.4	31.6	28.3	27.5	29.8	27.3
1992	29.1	27.8	27.4	15.5	16.9	19.4	18.3	18.8	23.9	27.2	28.6	26.0
1993	26.1	26.5	14.7	17.5	20.6	22.4	16.3	19.1	24.1	29.1	30.3	31.8
1994	31.4	29.7	21.7	10.9	11.3	25.6	21.5	19.4	29.6	31.7	34.7	31.4
1995	33.0	28.5	18.0	18.8	22.4	27.6	20.5	21.3	25.4	35.1	32.2	28.0
						MLO						
1973	-	-	-	-	-	-	-	-	-	36.5	33.4	36.0
1974	34.5	42.8	51.8	51.8	49.6	40.8	38.0	31.5	31.2	31.9	29.6	31.9
1975	31.4	38.9	47.5	51.7	48.7	47.3	43.3	43.7	34.1	31.5	29.6	-
1976	37.3	41.6	36.7	41.2	39.3	35.6	32.2	30.0	25.6	30.9	39.3	37.5
1977	-	35.8	48.5	41.6	46.4	41.5	29.2	28.9	-	-	39.0	33.2
1978	36.1	39.2	45.0	49.2	37.2	31.8	33.5	29.2	31.9	28.8	27.7	33.6
1979	39.5	36.6	48.5	50.3	48.5	43.7	36.7	29.4	37.4	31.0	38.2	41.6
1980	41.0	42.1	45.0	53.8	47.1	42.0	35.8	38.6	27.4	36.8	38.4	34.5
1981	43.5	42.2	52.1	61.1	60.8	38.6	39.1	37.0	35.9	37.8	38.3	39.9
1982	35.1	40.7	48.8	52.5	54.3	39.3	31.6	30.2	32.4	32.9	36.7	45.7
1983	46.8	53.6	59.1	63.4	56.7	47.6	44.4	32.2	31.0	38.6	34.3	40.2
1984	40.4	40.5	48.4	-	47.1	46.8	37.8	33.8	36.9	31.0	31.8	37.6
1985	43.2	41.6	52.4	50.7	48.4	43.9	40.3	36.9	31.4	33.2	36.2	38.1
1986	39.9	40.0	43.2	46.4	47.2	45.4	31.3	38.7	24.3	38.1	30.2	41.6
1987	38.4	40.5	50.0	-	-	-	-	36.3	31.9	34.4	40.5	33.4
1988	44.8	43.3	50.3	53.1	47.5	32.3	41.2	33.5	34.2	30.0	29.5	36.1
1989	40.7	37.4	40.6	48.4	45.9	35.8	37.1	38.5	38.6	24.8	35.0	40.7
1990	37.8	38.3	49.6	52.0	55.0	43.3	36.7	35.3	30.5	38.1	28.8	39.6
1991	45.3	41.8	48.4	56.9	55.5	41.5	39.2	33.1	31.5	33.9	32.6	33.3
1992	40.2	42.8	53.8	61.0	46.9	49.5	38.8	30.6	26.3	24.9	29.2	32.2
1993	42.2	41.3	50.0	63.3	55.2	50.6	38.0	30.6	26.6	35.3	42.7	38.3
1994	43.3	37.5	48.5	57.9	48.7	35.4	30.1	29.8	33.5	41.4	40.5	45.5
1995	34.4	42.0	51.1	50.5	52.1	44.6	34.6	45.8	42.1	36.7	30.7	35.5

TABLE 4.5. Monthly Mean Surface Ozone Mixing Ratios (ppbv) - Continued

Year	Jan.	Feb.	March	April	May	June	July	Aug.	Sept.	Oct.	Nov.	Dec.
						SMO						
1976	9.9	9.1	8.8	8.3	11.2	13.5	17.6	21.7	17.9	15.2	12.4	13.2
1977	11.0	8.6	8.8	9.2	12.2	20.7	19.9	20.7	15.9	16.7	15.2	15.0
1978	10.2	9.2	9.2	8.4	13.6	15.9	22.8	15.9	17.7	18.6	13.9	13.3
1979	10.5	8.3	8.1	12.5	15.1	17.2	18.6	19.7	19.3	18.8	13.8	14.8
1980	9.8	7.9	8.5	11.6	15.1	19.3	16.8	21.8	17.7	-	11.4	9.7
1981	9.4	9.4	9.5	9.3	14.0	17.0	20.0	16.4	15.1	15.3	10.9	11.8
1982	8.2	9.1	6.7	7.3	14.0	16.9	16.7	16.1	20.2	13.5	17.0	12.2
1983	8.9	6.3	9.4	11.5	11.2	18.3	19.8	20.8	13.0	15.3	13.0	8.5
1984	7.4	7.1	8.0	5.7	17.3	18.4	18.7	17.6	14.5	17.2	14.7	-
1985	10.3	10.0	7.3	11.2	11.8	17.1	20.2	17.7	17.1	14.0	14.9	10.7
1986	8.4	8.6	8.4	7.2	-	14.0	20.3	21.3	14.5	16.6	12.9	12.7
1987	8.1	6.4	6.5	13.6	16.3	20.1	20.7	24.8	17.1	20.2	10.1	11.9
1988	7.4	8.4	8.1	9.9	11.8	13.9	21.6	17.1	18.3	15.8	13.3	9.1
1989	9.3	8.0	9.0	12.1	10.6	19.6	21.5	20.1	19.4	16.1	18.8	13.8
1990	11.4	11.1	11.3	10.8	16.7	16.1	20.0	19.3	13.4	12.7	13.2	13.2
1991	6.7	8.7	6.6	7.9	13.8	14.4	20.9	20.0	23.2	15.1	12.2	15.4
1992	12.2	-	12.1	-	11.7	18.5	15.2	13.7	12.2	13.9	13.0	9.9
1993	9.4	9.6	9.1	-	-	-	-	-	-	-	-	-
1994	8.9	8.3	9.4	6.9	12.7	18.0	18.1	22.5	13.6	10.1	13.7	8.0
						SPO						
1974	-	-	-	-	-	-	-	-	-	-	-	28.7
1975	24.6	25.7	24.9	29.4	35.7	34.9	35.3	34.4	35.1	36.2	33.9	31.6
1976	26.2	21.3	21.9	25.2	29.4	31.7	34.4	33.6	26.6	25.2	25.8	24.9
1977	23.5	22.0	21.5	26.7	31.5	33.1	34.2	36.0	33.1	29.9	26.7	30.8
1978	27.4	24.3	-	-	-	33.1	34.8	34.3	33.5	31.8	33.0	31.3
1979	25.1	22.2	23.6	29.6	33.1	34.7	37.9	34.5	33.1	34.4	-	25.1
1980	24.9	22.5	22.3	26.9	29.3	33.3	35.0	34.4	33.0	29.1	26.8	23.2
1981	21.3	19.6	20.1	24.6	29.0	32.5	35.3	37.7	37.8	37.6	35.3	29.5
1982	-	21.5	24.0	31.5	33.6	35.5	36.4	34.9	33.1	28.5	27.7	24.5
1983	21.3	20.5	21.2	27.3	30.6	33.1	34.3	32.7	33.4	30.6	27.8	25.6
1984	20.5	20.1	21.3	29.0	34.2	36.1	37.5	36.1	35.9	31.5	34.0	28.2
1985	22.7	19.3	22.0	24.4	30.5	36.6	36.7	34.4	32.3	28.3	26.7	24.8
1986	18.3	20.1	21.9	27.1	34.4	36.3	38.7	38.2	36.9	33.0	29.4	25.4
1987	20.0	17.8	19.3	23.5	28.0	30.9	29.7	-	-	-	24.4	26.0
1988	18.9	21.5	23.7	27.4	31.0	34.1	34.0	33.0	33.9	31.1	29.5	25.3
1989	22.9	19.7	18.7	25.4	35.3	35.4	36.2	36.0	35.5	24.2	28.6	23.4
1990	20.2	20.2	23.1	24.5	27.6	31.2	32.3	30.1	28.8	27.0	27.4	23.7
1991	23.8	19.9	18.9	23.8	26.8	30.9	31.8	34.1	27.7	27.2	22.8	22.1
1992	18.0	17.9	16.9	22.4	29.7	33.5	34.9	34.4	28.5	25.8	26.7	29.3
1993	23.4	20.1	17.5	23.1	26.4	29.7	30.7	30.3	29.1	27.5	29.7	22.9
1994	25.0	19.7	21.1	24.4	27.7	33.1	34.1	33.5	31.6	27.3	29.3	26.8
1995	25.3	18.0	18.0	19.8	24.0	28.3	34.5	33.0	21.8	26.3	29.2	26.4

Monthly means are computed from daily (24-hr) averages.

4.1.4. OZONESONDES

Table 4.6 summarizes the 1994-1995 CMDL ozonesonde project involvment. This includes supplying receiving stations and all ozonesonde supplies, training where needed, personnel launching ozonesondes at several of the sites, and final data processing.

The CMDL long-term stations at Boulder, Colorado; Hilo, Hawaii; and SPO, continued operating at one launch per week in 1994 and 1995, with SPO increasing to three per week during the ozone-hole period. The SPO minimum total ozone, measured by ozonesondes, reached 102 and 98 DU in 1994 and 1995, respectively. The minimum profiles and the predepletion profiles are shown in Figure 4.2. Severe depletion was observed in the 14-20 km region (nearly 100%) but did not extend down to the 10-14 km region as it did in 1993 when a record low of 91 DU was measured [*Hofmann et al.*, 1994]. This extended ozone-depletion layer in the lower stratosphere, observed in 1992 and 1993, was due to the effects of the Mt. Pinatubo volcanic aerosol layer [*Hofmann and Oltmans*, 1993]. By 1994, the Mt. Pinatubo volcanic layer had decayed to background levels over McMurdo Station, Antarctica [*Deshler et al.*, 1996].

TABLE 4.6. Summary of 1994-1995 Ozonesonde Projects

Ozonesonde Sites	1994 Totals	1994 Dates	1995 Totals	1995 Dates	Project
			Station (weekly)		
Boulder	52	Full year	52	Full year	NOAA long term
MLO	52	Full year	62	Full Year	NOAA long term + MLO3
SPO	69	Full year	69	Full Year	NOAA long term
McMurdo	65	Feb. 3-Dec. 25	6	Jan. 1-Feb. 12	NSF and NOAA
Tahiti	-		24	July 31-Dec. 29	PEM-Tropics
SMO	-		16	Aug. 1-Dec. 14	PEM-Tropics
			Intensives (~daily)		
Azores	30	May 5-June 3	42	June 2-July 27	AEROCE
Bermuda	10	Jan 21-May 31`	55	April 17-July 27	AEROCE
Maryland	-		12	April 13-May 16	AEROCE
Rhode Island	-		7	April 18-May 15	AEROCE
Newfoundland	-		20	April 12-Aug. 3	AEROCE
Nashville	-		14	June 27-July 21	Southern Oxidant Study
			Ship Cruises		
Indian Ocean	-		21	Feb. 12-April 14	NSF R/V *Malcom Baldrige*
Pacific Ocean	-		17	Oct. 17-Dec. 11	ACE R/V *Discoverer*
Totals	278		418		

PEM-Tropics - Pacific Exploratory Mission in the Tropics (a global tropospheric experiment).

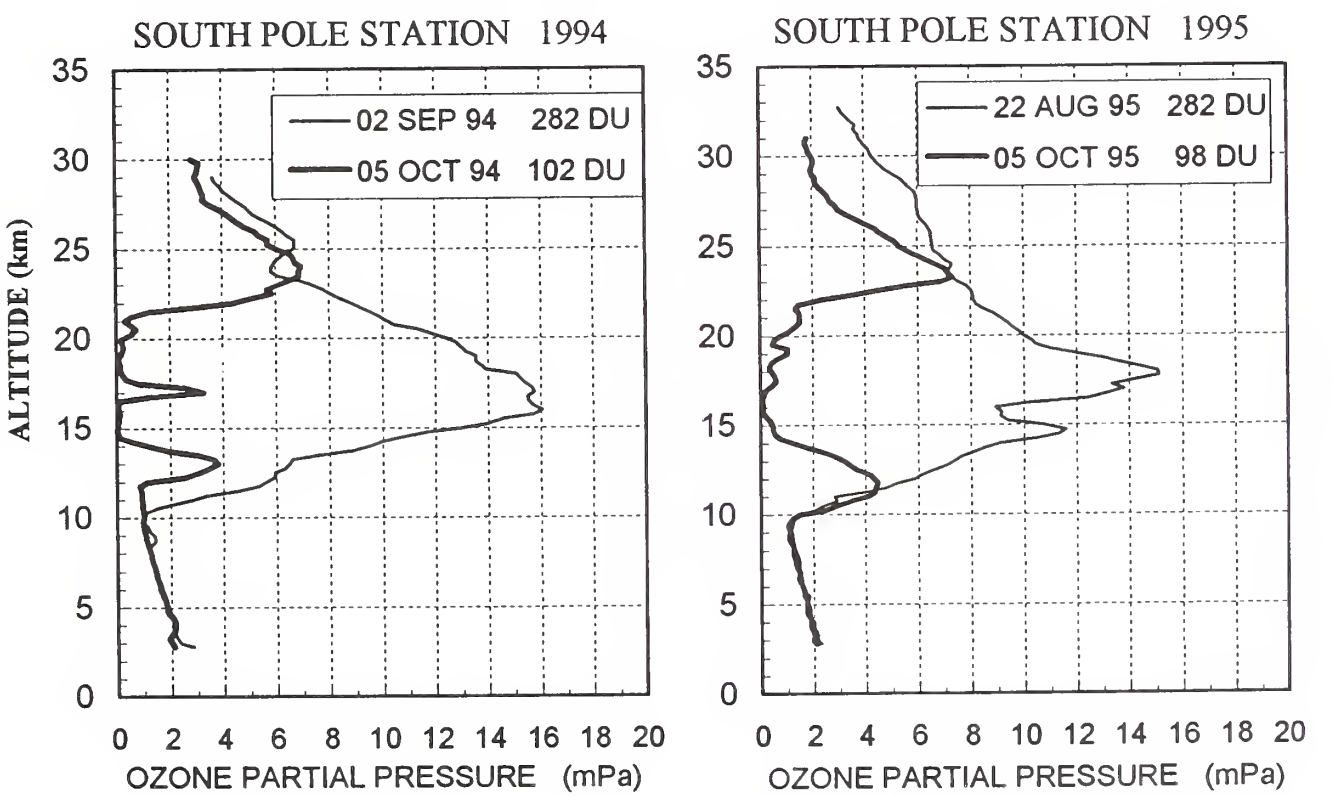

Fig. 4.2. Vertical profiles of ozone partial pressure in millipascals (mPa) at SPO during the ozone hole of 1994 and 1995. The lighter line represents the predepletion profile while the thicker line is the profile observed at the total ozone minimum.

NOAA was also involved in regular ozonesonde and water vapor measurements at McMurdo Station, Antarctica, from February to August 1994 during a winterover project designed to study the development of polar stratospheric clouds using balloonborne instruments. The University of Denver, University of Wyoming, and NOAA conducted balloon flights to measure ozone, water vapor, nitric acid, and particle concentration profiles during the austral summer, fall, and winter of 1994 prior to and during the development of polar stratospheric clouds and ozone depletion. An early sign of ozone depletion was observed in the June 1994 profile in the 12-20 km layer [*Vömel et al.*, 1995a] (section 4.2.3., this report). CMDL continued measuring ozone profiles on a weekly basis at McMurdo from November 1994 to February 1995. This was done in order to complete the first full year of ozonesonde profiles from McMurdo (February 1994-February 1995). The University of Wyoming launched ozonesondes during the ozone hole period from August to November 1994.

Weekly ozonesondes began at Tahiti and SMO in July 1995 as part of the Global Tropospheric Experiment Pacific Exploratory Mission in the Tropics (PEM-Tropics).

The intensive, short-term ozonesonde projects were all part of the AEROCE II and AEROCE III and the North Atlantic Regional Experiment (NARE). Ozone profiles were measured on a nearly daily basis from several sites (Table 4.6) in the spring and summer of 1994 and 1995 to investigate the sources (anthropogenic and natural) of high ozone layers in the troposphere over the north Atlantic Ocean region.

The 21 ozonesondes flown from the R/V *Malcom Baldrige* cruise in the Indian Ocean began near South Africa at ~30°S, 30°E and ended near Sri Lanka at ~7°N, 73°E. This was a preliminary study for the Indian Ocean Experiment (INDOEX) planned for January 1998 to study the chemical and radiative composition of the atmosphere over the Indian Ocean particularly in the region south of the Indian subcontinent. The Aerosol Characterization Experiment (ACE) R/V *Discoverer* cruise in the Pacific Ocean extended from ~31°N, 214°E to 45°S, 145°E. This set of measurements provided the first ozone profiles in a long cross section through the mid-Pacific.

4.1.5. Atmospheric Water Vapor

Monthly water vapor profile measurements continued at Boulder. As was noted earlier [*Oltmans and Hofmann*, 1995; *Ferguson and Rosson*, 1992], water vapor in the stratosphere over Boulder has increased significantly. The updated trend information is summarized in Table 4.7. As was reported in the past, the largest trends are seen in the lowest part of the stratosphere over Boulder (16-20 km). This change of about 0.8% yr^{-2} is somewhat less than reported earlier. This is primarily because the seasonal minimum which occurs in winter and early spring was somewhat lower than in recent years (Figure 4.3). This may be associated with enhanced transport from the tropics during early 1995. Lower stratospheric ozone amounts were also less than normal, indicative of tropical transport. Above 20 km the increase is about 0.5% yr^{-2}, which is consistent with the expected increase resulting from increasing CH_4 concentrations in the atmosphere.

4.1.6. Atmospheric Transport

CMDL supports various research efforts to verify sources and sinks of trace gases and aerosols. The CMDL isentropic transport model [*Harris and Kahl*, 1994] calculates trajectories at requested elevations, including those in the stratosphere. Trajectories may then be compared to data collected at the surface or data collected at elevation (sonde, aircraft, and lidar data). Variations in concentration may be linked to transport where applicable.

Trajectories were used to describe seasonal flow patterns to MLO [*Harris and Kahl*, 1990], SPO [*Harris*, 1992], and BRW [*Harris and Kahl*, 1994]. A similar study of SMO flow patterns is underway. Highlights of this study appear as a special project at the end of this section (4.2.4). These four studies summarize many years of trajectories for each observatory in order to understand the average flow patterns, their meteorological causes, and the range of yearly and seasonal variations. Knowledge of transport characteristics has led to a better understanding of seasonal patterns in MLO methane data [*Harris et al.*, 1992] and SMO carbon dioxide data [*Halter et al.*, 1988], among other constituents.

TABLE 4.7. 1981-1995 Water Vapor Mixing Ratios Over Boulder, Colorado

Level (km)	Mean (ppmv)	Standard Deviation (ppmv)	Number of Observations	Trend* (% yr^{-1})	95% Confidence† Interval (% yr^{-1})
10-12	60.46	40.27	137	1.47	2.60
12-14	12.23	6.97	137	1.34	1.88
14-16	4.68	1.04	137	.61	.87
16-18	3.90	.49	137	.78‡	.49
18-20	3.87	.35	136	.80‡	.35
20-22	4.08	.29	131	.48‡	.28
22-24	4.24	.30	125	.51‡	.29
24-26	4.34	.34	108	.55	.34

*The trends are computed for deseasonalized values.

†The 95% confidence interval is based on students t-distribution.

‡Significant at 95% confidence level.

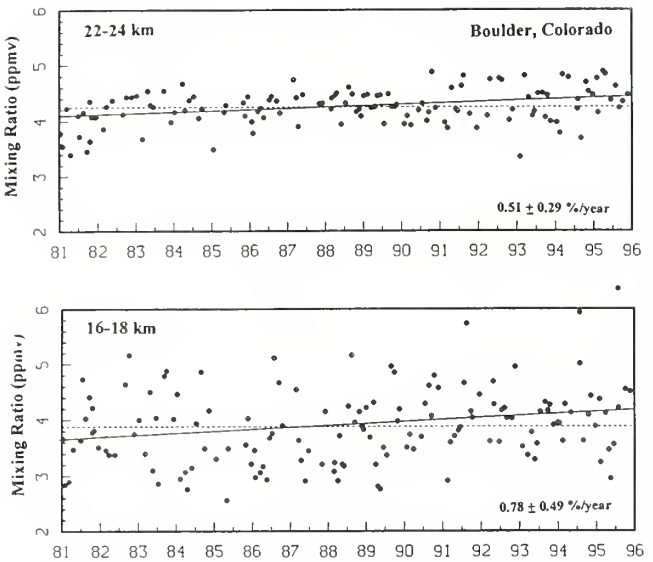

Fig. 4.3. Layer average water vapor mixing in parts per million (ppmv) at Boulder, Colorado, for the 16-18 km and 22-24 km layers. The dashed line is the overall mean and the solid line is the linear trend fitted to the monthly anomalies. The trend and 95% confidence levels in percent per year are also shown.

Information about the transport model (methodology, description of plots, and formats of data files) is available on the Internet at http://www.cmdl.noaa.gov/traj. This home page also serves as the distribution site for "real-time" trajectories. These are trajectories calculated from data downloaded twice a day as it becomes available from National Centers for Environmental Prediction (NCEP) (previously National Meteorological Center). For various CMDL baseline and regional observing sites, trajectories are thus provided within a day of when measurements are actually made. This capability will be expanded in the future to include any site on the globe. The trajectory home page also includes pointers to several archives of trajectory data.

4.2. Special Projects

4.2.1. The Mauna Loa Ozone Profile Intercomparison

From August 14 through September 1, 1995, the CMDL Ozone Group measured daily ozone profiles during the Network for the Detection of Stratospheric Change (NDSC) Stratospheric Ozone Profile Intercomparison (MLO3) held at Mauna Loa Observatory and Hilo, Hawaii. Participating groups in Hawaii included the JPL lidar, NASA Goddard lidar, NASA Langley Microwave, and NOAA umkehr and ozonesondes. All the remote sounding instruments were operating at MLO (3397 m). Seventeen electrochemical concentration cell (ECC) ozonesondes were launched from Hilo (11 m) to coincide with the evening MLO observations. Six of the balloons launched were carrying a new "triple" ozonesonde platform. The "triple" flights showed very good precision that can be seen in the August 30, 1995, profiles (Figure 4.4a). These profiles were fairly typical of all the triple flights with an average relative standard deviation of 2-4% in the lower troposphere (0-5 km) and in the stratosphere from 15 km to burst altitude (~35 km). The poorest precision was in the mid- to upper troposphere, where very low concentrations of ozone approach the background levels of the ozonesonde. In this region the relative standard deviation was as high as 20%.

Figure 4.4b shows the average ozonesonde profile from the August 30 flight, the lidar and microwave profiles, and a SAGE overpass ozone profile measurement. All of the profiles agreed very well above 15 km, except for the JPL lidar between 15 and 18 km. At the ozone peak, the ozonesonde profile is about 8-10% greater than the ground based instruments. The ozonesonde profiles measured during MLO3 were decreased by a maximum of 6% at burst altitude due to an observed increase in response to ozone as the 1% potassium iodide solution evaporates during the flight and becomes more concentrated. Additional testing has shown that the sonde may be reading even higher than the 6% correction. This would reduce the ozonesonde profile further resulting in less than 5% differences between the ozonesondes and ground based instruments.

4.2.2. Ozone Vertical Profiles Over the North Atlantic

As part of AEROCE and NARE, several intensive ozone vertical profiling campaigns were carried out. During these campaigns, ozonesondes are launched on a near daily schedule for periods of approximately 1 month. The focus of these intensive measurements is to describe the ozone variations throughout the troposphere over the North Atlantic and to relate the processes identified as being responsible for surface ozone variations with changes throughout the troposphere [*Oltmans and Levy*, 1992; *Moody et al.*, 1995]. The results, primarily from the 1993 and 1994 campaigns, have recently been prepared for publication [*Oltmans et al.*, 1996].

During spring 1995, an intensive series of measurements was made at Bermuda. Over the month the soundings were carried out and several profiles were also obtained at the University of Rhode Island and at the University of Maryland. These soundings on the east coast of the United States were made in order to look at the ozone content of air masses as they moved from the United States to Bermuda. The profiles from May 6, 1995, at Rhode Island and Maryland (Figures 4.5a and b) and for May 7 at Bermuda (Figure 4.5c) illustrate how such a system can produce high ozone amounts in the midtroposphere over the North Atlantic. At the more northerly location (Rhode Island), the upper troposphere from 8-11 km has ozone concentrations over 125 ppb (Figure 4.5a) and large ozone amounts (~85 ppb) extend down to 6.5 km. At Maryland (Figure 4.5b), on the other hand, the layer of elevated ozone over 100 ppb is confined to a relatively thin layer at about 7 km. On May 6 at Bermuda (profile not shown) ozone throughout the troposphere is 50-70 ppb. Early on May 7 at Bermuda (Figure 4.5c) there is a peak of ~120 ppb at about 6.5 km.

The Bermuda trajectories for May 7 (Figure 4.5d) show that for the 0000 UT arrival time, air had passed over the northeastern United States about 12 hours earlier at an altitude of 8 km. The larger ozone amounts seen at

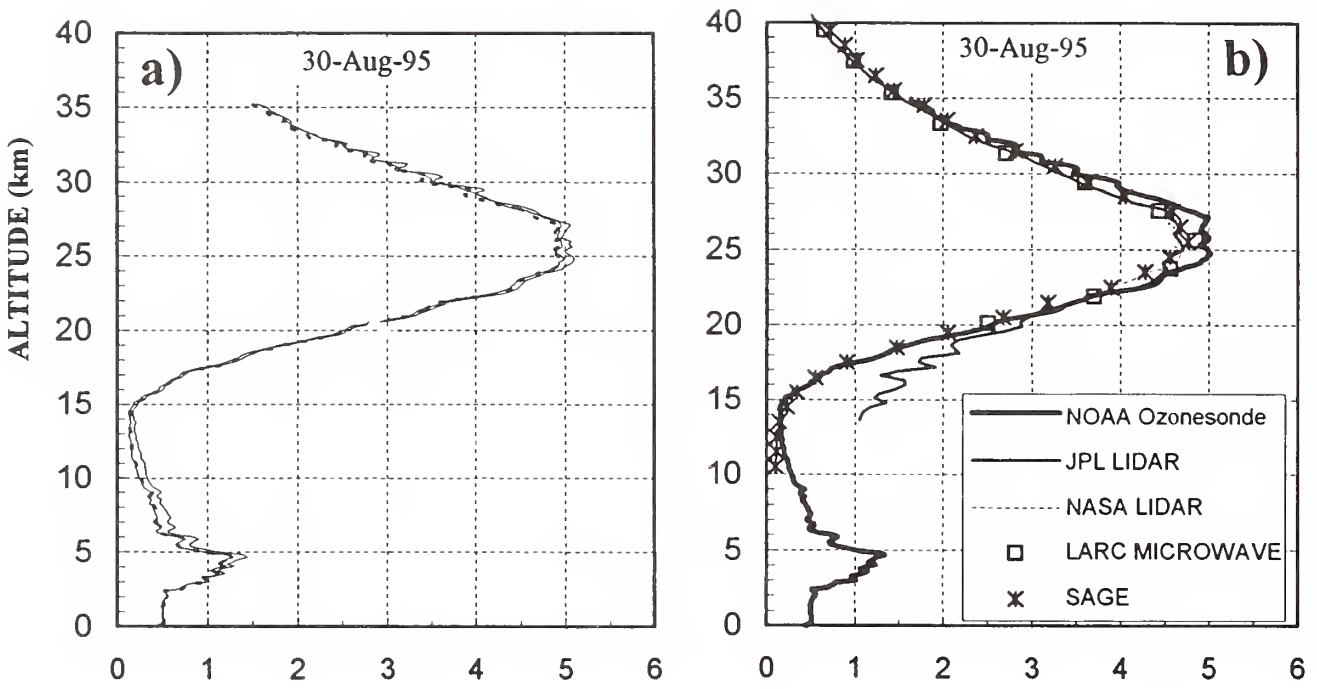

Fig. 4.4. (a) Three vertical profiles of ozone concentration (10^{12} cm^{-3}) measured by the August 30, 1995, triple ozonesonde flight. (b) The average of the triple ozonesonde profiles from (a) and the profiles of ozone concentration from the two MLO lidars and microwave ozone profilers and the coincident Stratospheric Aerosol and Gas Experiment II (SAGE II) satellite profile.

Maryland and Rhode Island (1400 Z on May 6) are clearly part of the same system producing the large ozone peak over Bermuda seen at 0100 Z at about 6.5 km. Air travels rapidly from near the Arctic Circle and descends over 2.5 km in just 2 days before reaching Bermuda. This meteorological pattern with flow behind the upper air trough brings air from a region where significant transfer of air from the stratosphere into the troposphere is likely to take place [*Merrill et al.*, 1996]. The presence of these layers of larger ozone concentration aloft at Bermuda and other sites over the North Atlantic are invariably associated with transport from higher altitudes and latitudes [*Oltmans et al.*, 1996]. These layers are also very dry, which is another indication that the air was mixed down from the stratosphere. It is likely that this process is an important source of ozone in the troposphere [*Oltmans et al.*, 1996].

During July 1995, intensive profiling campaigns were carried out at the Canary Islands, Azores, Bermuda, and Newfoundland. For each of these sites, ozone amounts near the surface are much smaller than are seen at the surface during the spring. In the middle and high troposphere, however, intrusions of large ozone amounts are common during the early summer and the peak values are larger than those seen in the spring [*Oltmans et al.*, 1996]. The presence of these layers of large ozone concentration is strongly tied to flow characteristics and water vapor amounts that demonstrate the stratospheric origin of these layers in a manner very similar to what is seen in the spring. Transfer of ozone-rich air from the stratosphere into the troposphere during the summer is significant.

4.2.3. Water Vapor and Ozone Profiles at McMurdo, Antarctica

The very cold temperatures of the Antarctic winter stratosphere lead to the formation of polar stratospheric clouds (PSCs). The formation of these clouds, particularly when temperatures reach the frost point of water (type II PSCs), leads to significant dehydration of the Antarctic stratosphere [*Vömel et al.*, 1995b; *Peterson and Rosson*, 1994]. In order to more completely describe and better understand the process of dehydration within the Antarctic stratospheric vortex, a program of 19 frost-point soundings was carried out at McMurdo between February and October 1, 1994. Each frost-point sounding was accompanied by an ozone vertical profile as well. In addition, ozonesondes were flown between the water vapor profile measurement times on about a one-per-week schedule. Measurements of PSC particles and nitric acid in the stratosphere were made by groups from the University of Wyoming and Denver University, respectively.

About the middle of June the coldest portions of the Antarctic stratospheric vortex reach the water vapor saturation temperature leading to rapid formation of ice crystals which fall with sufficient speed to rapidly dehydrate the stratosphere [*Vömel et al.*, 1995b]. By late July continuing into October (Figure 4.6), much of the stratosphere in the vortex between 12 and 20 km remains highly dehydrated. During this period of sustained dehydration, there does not appear to be significant continued removal of water vapor, and also little moisture

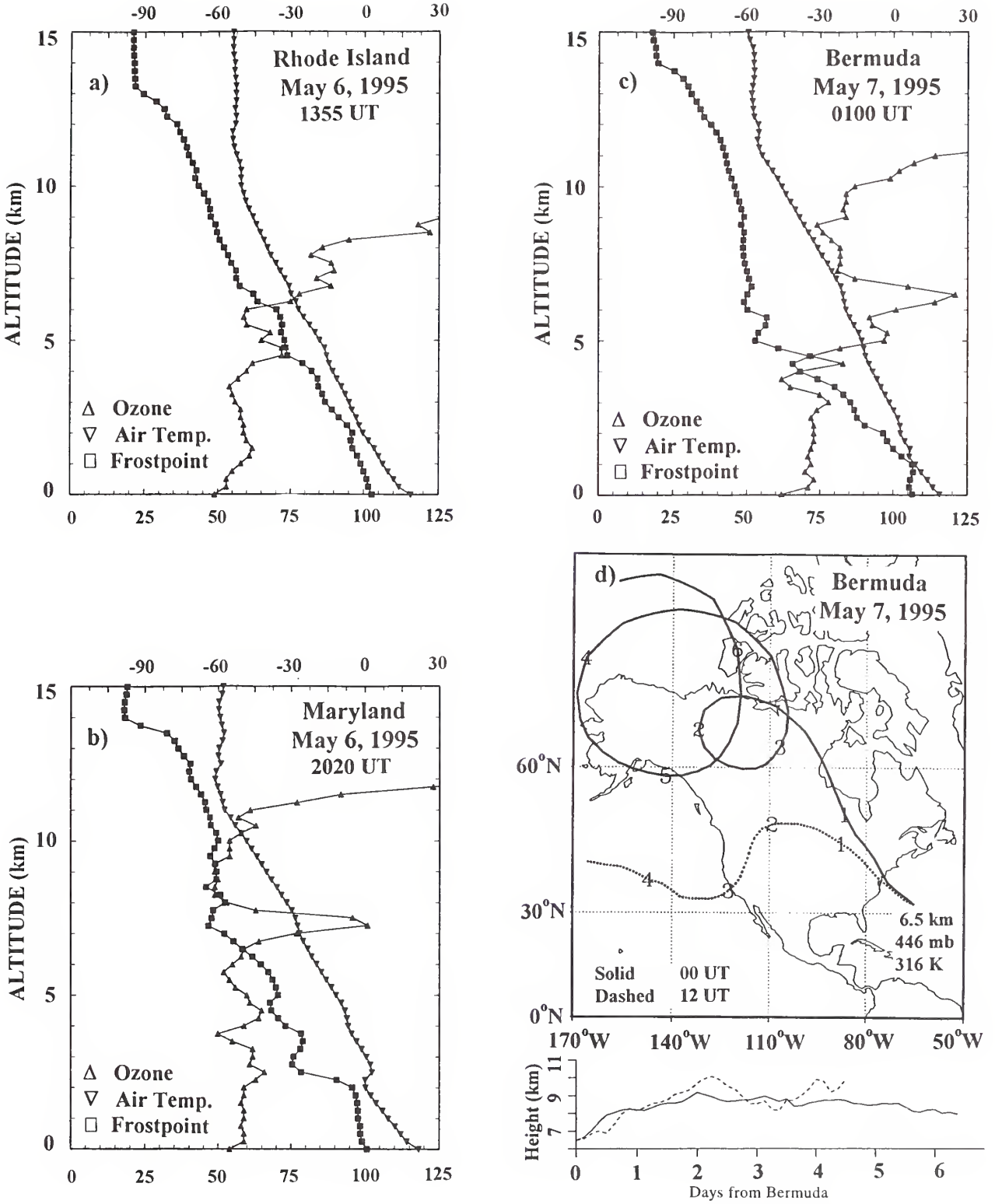

Fig. 4.5. Vertical profiles of ozone mixing ratio (ppbv), temperature (°C), and frost-point temperature (°C) at (a) University of Rhode Island for May 6, 1995, at 1355 UT, (b) University of Maryland for May 6, 1995, at 2020 UT, and (c) Bermuda Naval Air Station for May 7, 1995, at 0100 UT. (d) The isentropic back trajectories for May 7 at 0000 UT (solid line) and 1200 UT (dashed line) arriving at 6.5 km at Bermuda.

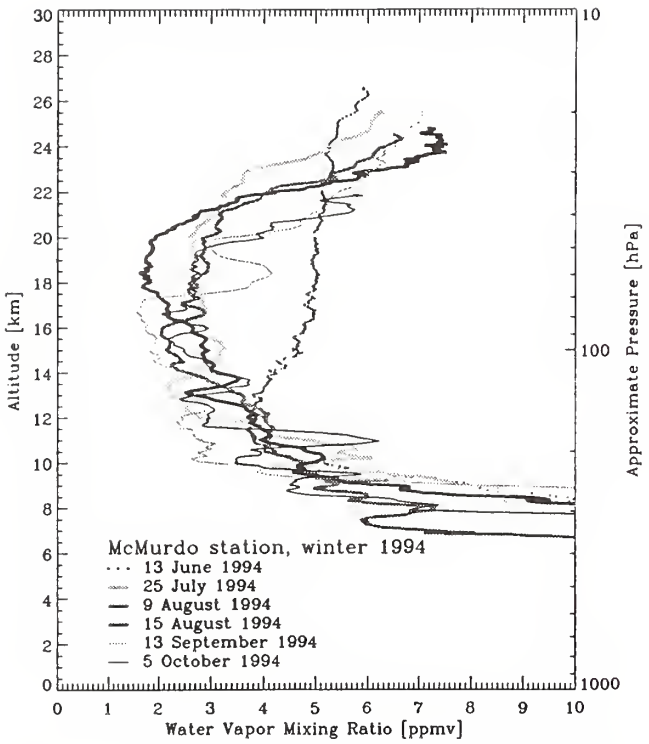

Fig. 4.6. Vertical profiles of water vapor mixing ratio at McMurdo, Antarctica, during the sustained dehydration period of the winter of 1994. The June 13, 1994, profile shows conditions before dehydration begins.

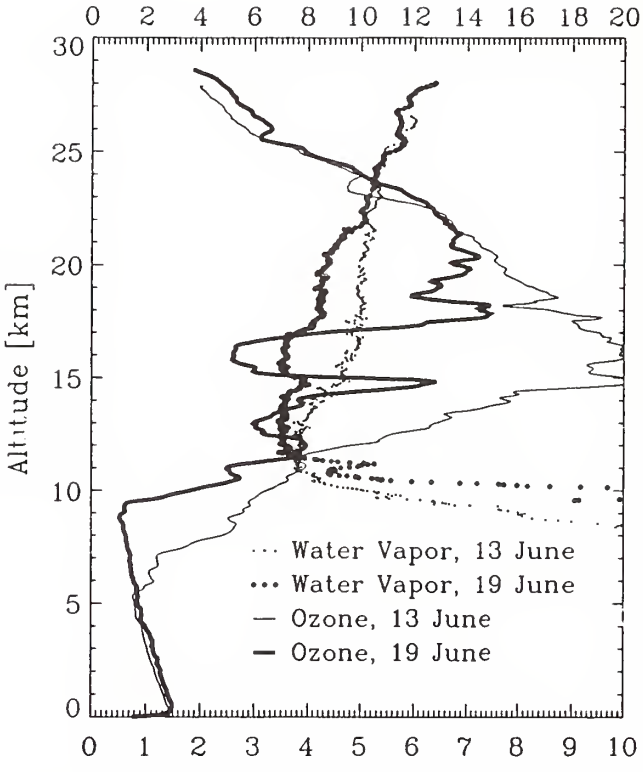

Fig. 4.7. Vertical profiles of ozone partial pressure (mPa) and ozone mixing ratio (ppmv) at McMurdo on June 13 and June 19, 1994. The June 19 case shows significant ozone depletion and dehydration between 11 and 24 km compared to the unperturbed June 13 profiles.

is added from outside the vortex. By the time the sun reappears over Antarctica, the air in the entire stratospheric vortex is highly processed and ozone depletion can take place over a broad geographical scale and through a significant depth.

Early in the dehydration process (June 19), an ozone profile was observed with significant depletion between 12 and 20 km (Figure 4.7). This depleted ozone layer corresponds very closely to the region where significant dehydration was first detected at McMurdo. Since it is dark over the Antarctic continent at this time, sufficient sunlight to allow ozone depletion can only be attained if the air parcel moves to a higher latitude after it is dehydrated and the air is significantly processed. The trajectory analysis [*Vömel et al.*, 1995a] shows that indeed the dehydrated and ozone-depleted parcel passes through the coldest temperatures over the continent and subsequently moves to a sunlit region near 50°S latitude. Furthermore, this analysis shows that significant ozone depletion can take place on a relatively short time scale. An analysis of the time when the observed air masses could have formed type II PSCs (ice particles) for the first time, limits the time scale for the observed ozone destruction to about 4 days [*Vömel et al.*, 1995a].

4.2.4. Flow Patterns for SMO Described with Clustered Trajectories

Ten years of isentropic trajectories (1986-1995) were calculated for SMO (14.25°S, 170.56°W) and were summarized for various time frames using cluster analysis.

Ten-day back isentropic trajectories were produced twice per day at 0000 and 1200 GMT arrival times. Trajectories were calculated to arrive at approximately 500 m asl, an elevation close to that of the observatory (77 m) and representative of the boundary layer. Input to the transport model consists of gridded meteorological data from the European Centre for Medium Range Weather Forecasts.

An earlier study by *Halter et al.* [1988] identified three distinct source regions contributing their signals to atmospheric measurements made at SMO, in particular those of carbon dioxide. Figures 4.8-4.10 show trajectories depicting transport from these three regions. Figure 4.8 shows trajectories arriving at SMO in the trade wind regime. At most, 1 km of descent is seen in this type of trajectory. Ten days back from SMO air parcels are in the remote southeastern Pacific, never reaching the South American continent. The second transport type is illustrated in Figure 4.9, which shows flow from southern

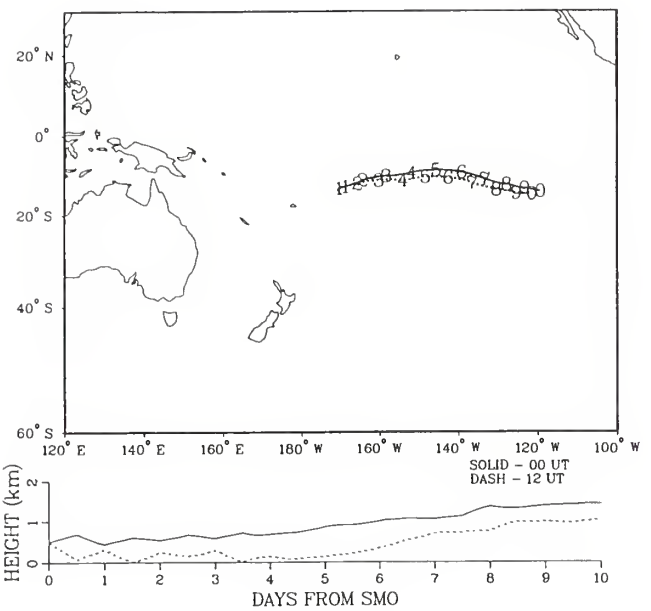

Fig. 4.8. Ten-day back isentropic trajectories arriving at SMO at 500 m on August 7, 1989, showing an example of trade wind type transport. The numbers along the trajectories give days back from SMO.

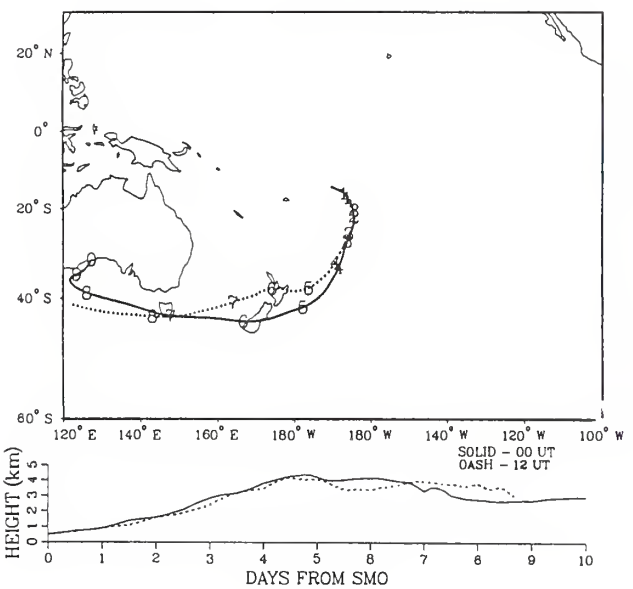

Fig. 4.9. Ten-day back isentropic trajectories arriving at SMO at 500 m on June 30, 1990, showing an example of transport from midlatitudes. The numbers along the trajectories give days back from SMO.

midlatitudes to SMO. This trajectory type may descend 3 km or more as it curves anticyclonically en route to SMO. Note that as air parcels descend in elevation, wind speeds decrease significantly. For this transport type, approach to SMO is often from the southeast. The third

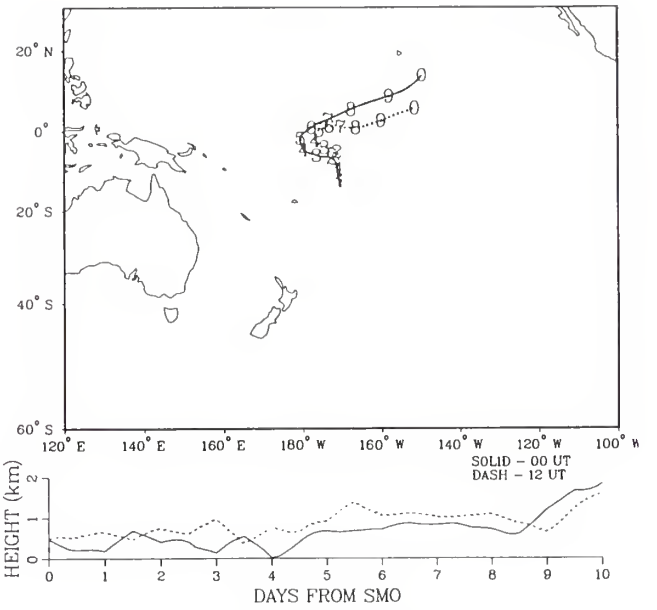

Fig. 4.10. Ten-day back isentropic trajectories arriving at SMO at 500 m on February 1, 1987, showing an example of transport from the northern hemisphere. The numbers along the trajectories give days back from SMO.

least frequent transport type brings air from the northern hemisphere to the observatory. Figure 4.10 shows trajectories with origins well beyond the equator. *Halter et al.* [1988] found that carbon dioxide transported to SMO in this manner was in phase with that measured at Kumakahi, Hawaii, although the amplitude of the signal was reduced. To quantify the frequency of SMO transport types, the complete set of trajectories was summarized using cluster analysis.

Cluster analysis is a multivariate statistical technique used here to group trajectories by shape and length. Each group or so-called cluster is represented by an average trajectory called the cluster mean. Figure 4.11 shows six cluster means derived for the entire 10-year period. Each cluster mean is marked with plus signs indicating the 1-day upwind intervals. At 10 days upwind, the cluster means are labeled with two numbers; the top number gives the percentage of trajectories that occurs in the cluster, and the bottom number identifies the cluster. The cluster identifiers (1-6) are used to distinguish one transport type from the other; the numbers themselves have no inherent significance and are not related from one clustering to the next.

Figure 4.11 gives a quantitative estimate of the frequency of each transport type. For example, the rapid transport from southern midlatitudes is represented by cluster 2 and cluster 3, with 2% and 7% frequency of occurrence, respectively. These two clusters differ in the average length of trajectory contained in the cluster, but both bring air parcels to SMO from elevations of 3 km or more. As a result of subsidence on approach to the observatory, wind speeds decrease significantly compared with their initial magnitudes several days earlier. A third cluster with transport from the south, cluster 4, exhibits much lower wind speeds, but shares the characteristics of

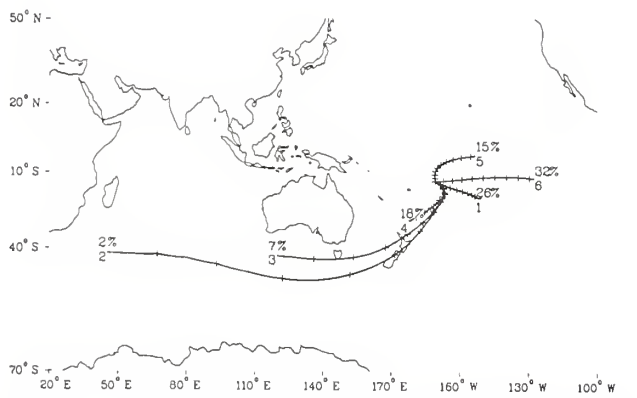

Fig. 4.11. Atmospheric flow patterns for SMO depicted by cluster-mean back trajectories arriving at 500 m asl for 1986-1995. Plus signs indicate 1-day upwind intervals. At 10 days upwind the cluster means are labeled with two numbers; the top number gives the percentage of trajectories that occurs in the cluster and the bottom number identifies the cluster.

10-day average origin south of 30°S and anticyclonic curvature on approach to SMO from the southeast. This cluster, comprising 18% of trajectories, has a mixed character because it contains some trajectories with tropical origins.

Clusters 1, 5, and 6 in Figure 4.11 contain trajectories that correspond to the easterly trade wind transport type. Cluster 5 trajectories have a northerly component on approach to SMO and occur 15% of the time. Cluster 6 trajectories approach from the due east 32% of the time. Cluster 1 trajectories have lower wind speeds, a southerly component, and occur 26% of the time.

Transport from the northern hemisphere occurs in cluster 5. This cluster also contains trajectories that do not cross the meteorological equator. To estimate the frequency of transport of true northern hemisphere air, the number of trajectories that had 10-day origins north of 5°N were counted. Trajectories of this transport type have frequency of 2-3% per year. They occur most often in February and March at about 10% frequency, but can also occur in December, January, and April though usually at lower frequency. The occurrence of transport from the northern hemisphere is quite variable from year to year with frequency in the two most likely months (February and March) ranging from 0 to 25%. Trajectories were also clustered by month in order to learn more about the seasonality of flow patterns at SMO. Figures 4.12a (January) and 4.12b (July) represent yearly extremes in flow patterns. The marked differences between these plots show a strong seasonality in SMO transport. Summer months are characterized by minimal flow from southern midlatitudes, a northerly component in some of the trade wind trajectories, and a cluster with trajectories approaching SMO from the northwest (for example, cluster 2, Figure 4.12a). Winter months are characterized by both easterly trades and strong flow from the south. In fact this "winter" pattern is present from May through November, with July having the highest frequency of strong southerly flow. Trade winds are evident during every month.

In terms of 10-day origins, air transported to SMO is predominantly from remote tropical-marine regions. The

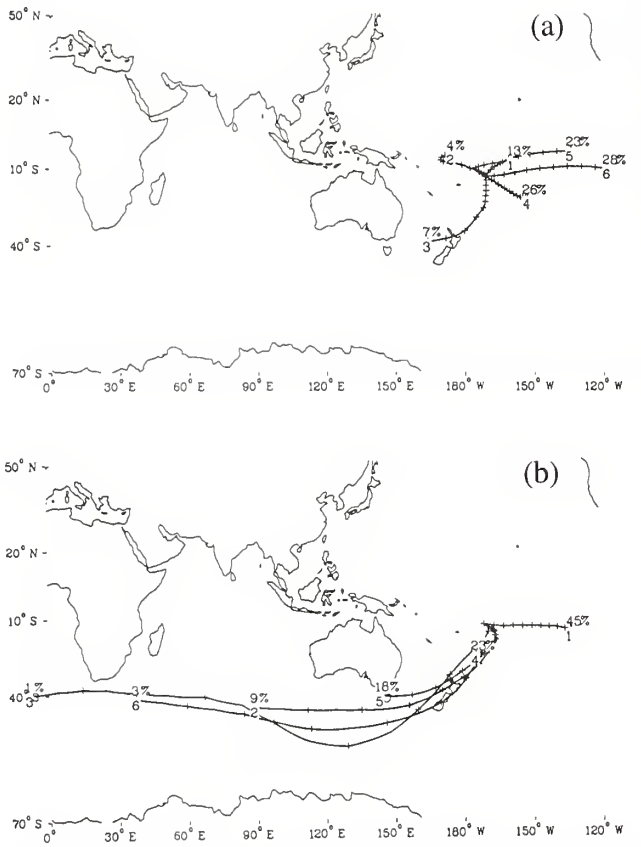

Fig. 4.12. Atmopsheric flow patterns at SMO for 1986-1995 depicted by cluster-mean back trajectories arriving at 500 m asl for (a) January and (b) July. Symbols are as in Figure 4.11.

frequency of such origins is about 50% in winter to 80% in summer. The remaining trajectories are from more southerly latitudes usually from elevations of 3 km or higher. Northern hemispheric air is transported to SMO at a rate of 2-3% per year, exclusively during the summer and fall months.

4.3. REFERENCES

Deshler, T., B.J. Johnson, D.J. Hofmann, and B. Nardi, Correlations between ozone loss and volcanic aerosol at altitudes below 14 km over McMurdo Station, Antarctica, *Geophys. Res. Lett.*, submitted, 1996.

Ferguson, E.E., and R. Rosson (Eds.), *Climate Monitoring and Diagnostics Laboratory, No. 20, Summary Report 1991*, 131 pp., NOAA Environmental Research Laboratories, Boulder, CO, 1992.

Halter, B.C., J.M. Harris, and T.J. Conway, Component signals in the record of atmospheric carbon dioxide concentration at American Samoa, *J. Geophys. Res.*, 93(D12), 15,914-15,918, 1988.

Harris, J.M., An analysis of 5-day midtropospheric flow patterns for the South Pole: 1985-1989, *Tellus*, 44B, 409-421, 1992.

Harris, J.M., and J.D. Kahl, A descriptive atmospheric transport climatology for the Mauna Loa Observatory, using clustered trajectories, *J. Geophys. Res.*, 95(D9), 13,651-13,667, 1990.

Harris, J.M., and J.D.W. Kahl, An analysis of 10-day isentropic flow patterns for Barrow, Alaska: 1985-1992, *J. Geophys. Res.*, 99(D12), 25,845-25,855, 1994.

Harris, J.M., P.P. Tans, E.J. Dlugokencky, K.A. Masarie, P.M. Lang, S. Whittlestone, and L.P. Steele, Variations in atmospheric methane at Mauna Loa Observatory related to long-range transport, *J. Geophys. Res.*, 97(D5), 6003-6010, 1992.

Hofmann, D.J., and S.J. Oltmans, Anomalous Antarctic ozone during 1992: Evidence for Pinatubo volcanic aerosol effects, *J. Geophys. Res.*, 98(D10), 18,555-18,561, 1993.

Hofmann, D.J., S.J. Oltmans, J.A. Lathrop, J.M. Harris, and H. Vömel, Record low ozone at the South Pole in the spring of 1993, *J. Geophys. Res.*, 21(6), 421-424, 1994.

Komhyr, W.D., *Dobson Data Re-Evaluation Handbook, Section II: Re-evaluation of instrument constants*, WMO Report No. 29, pp. II-1-II-82, edited by R.D. Hudson and W.G. Planet, World Meteorological Organization, Geneva, Switzerland, 1993.

Komhyr, W.D., R.D. Grass, and R.K. Leonard, Dobson spectrophotometer 83: A standard for total ozone measurements, 1962-1987, *J. Geophys. Res.*, 94(D7), 1847-9861, 1989.

Komhyr, W.D., R.D. Grass, R.D. Evans, R.K. Leonard, D.M. Quincy, D.J. Hofmann, and G.L. Koenig, Unprecedented 1993 ozone decrease over the United States from Dobson spectrophotometer observations, *Geophys. Res. Lett.*, 21(3), 201-204, 1994.

Merrill, J.T., J.L. Moody, S.J. Oltmans, and H. Levy II, Meteorological analysis of tropospheric ozone profiles at Bermuda, *J. Geophys. Res.*, in press, 1996.

Moody, J.L., S.J. Oltmans, H. Levy II, and J.T. Merrill, A chemical transport climatology of tropospheric ozone: Bermuda 1988-1991, *J. Geophys. Res.*, 100, 7179-7194, 1995.

Oltmans, S.J., and D.J. Hofmann, Increase in lower-stratospheric watervapor at a midlatitude Northern Hemisphere site from 1981-1994, *Nature*, 374, 146-149, 1995.

Oltmans, S.J., and H. Levy II, Diurnal, synoptic and seasonal variability of surface ozone over the western North Atlantic, *Nature*, 358, 392-394, 1992.

Oltmans, S.J., J.A. Lathrop, A.S. LeFohn, H. Levy II, H.E. Scheel, W.A. Matthews, and I. Galbally, Recent changes in tropospheric ozone from ozonesonde and surface ozone measurements, *IUGG XXI General Assembly*, B235, 1995.

Oltmans, S.J., H. Levy II, J. M. Harris, J.T. Merrill, J.L. Moody, J.A. Lathrop, W. Cuevas, M. Trainer, M.S. O'Neill, J.M. Prospero, H. Vömel, and B.J. Johnson, Summer and spring ozone profiles over the North Atlantic from Ozonesonde Measurements, *J. Geophys. Res.*, in press, 1996.

Peterson, J., and R. Rosson (Eds.), *Climate Monitoring and Diagnostics Laboratory, No. 21, Summary Report 1992*, 131 pp., NOAA Environmental Research Laboratories, Boulder, CO, 1993.

Peterson, J., and R. Rosson (Eds.), *Climate Monitoring and Diagnostics Laboratory, No. 22, Summary Report 1993*, 152 pp., NOAA Environmental Research Laboratories, Boulder, CO, 1994.

Staehelin, J., J. Thudium, R. Buehler, A. Volz-Thomas, and W. Graber, Trends in surface ozone concentrations at Arosa, Switzerland, *Atmos. Environ.*, 28, 75-87, 1994.

Tarasick, D.W., D.I. Wardle, J.B. Kerr, J.J. Bellefleur, and J. Davies, Tropospheric ozone trends over Canada: 1980-1993, *Geophys. Res. Lett.*, 22, 409-412, 1995.

Volz, A., and D. Kley, Evaluation of the Montsouris series of ozone measurements made in the nineteenth century, *Nature*, 332, 240-242, 1988.

Vömel, H., D.J. Hofmann, S.J. Oltmans, and J.M. Harris, Evidence for midwinter chemical ozone destruction over Antarctica, *Geophys. Res. Lett.*, 22(17), 2381-2384, 1995a.

Vömel, H., S.J. Oltmans, D.J. Hofmann, T. Deshler, and J.M. Rosen, The evolution of the dehydration in the Antarctic vortex, *J. Geophys. Res.*, 100, 13,919-13,926. 1995b.

World Meteorological Organization (WMO), Report of the International Ozone Trends Panel 1988, *Global Ozone Research and Monitoring Project Report No. 18*, WMO, Geneva, Switzerland, 194 pp., 1988.

5. Nitrous Oxide and Halocompounds

J.W. Elkins (Editor), J.H. Butler, T.M. Thompson, S.A. Montzka, R.C. Myers, J.M. Lobert, S.A. Yvon, P.R. Wamsley, F.L. Moore, J.M. Gilligan, D.F. Hurst (with CCG), A.D. Clarke, T.H. Swanson, C.M. Volk, L. T. Lock, L.S. Geller (with CCG), G.S. Dutton, R.M. Dunn, M.F. Dicorleto, T.J. Baring, and A.H. Hayden

5.1. Continuing Programs

5.1.1. Introduction

The Nitrous Oxide and Halocarbons Group was formed in 1986. In April 1995, the name was changed to Nitrous Oxide and Halocompounds Group (NOAH) to reflect the fact that noncarbon containing, halogenated gases such as sulfur hexafluoride (SF_6) are now an integral part of our program. The general mission of the group is to quantify the distributions as well as the magnitudes of the sources and sinks for atmospheric nitrous oxide (N_2O) and halocarbons that include the chlorofluorocarbons (CFCs), chlorinated solvents (CCl_4, CH_3CCl_3, etc.), hydrochlorofluorocarbons (HCFCs), hydrofluorocarbons (HFCs), methyl halides (CH_3Br, CH_3Cl, CH_3I), halons, and numerous other important ozone-depleting and greenhouse gases. Two chromatographic techniques, electron capture detector-gas chromatography (EC-GC) and gas chromatograph-mass spectrometer (GC-MS), are used primarily to detect these trace atmospheric species. NOAH samples air from ground-based stations, towers, ocean vessels, aircraft, and balloons to accomplish its mission. Achieving these goals requires the production and maintenance of reliable gas calibration standards that are supplied to laboratories throughout the world.

New sites for both the flask and in situ programs were added over the past 2 years. The location of these sites in the CMDL N_2O and Halocompounds Network are shown in Figure 5.1. In cooperation with the Carbon Cycle Group (CCG), two tower sites (WITN Tower, North Carolina (ITN) and WLEF Tower, Wisconsin (LEF)) were added to the in situ program to ascertain source strengths of gases near urban and forested areas. With a similar purpose, an in situ gas chromatograph (GC) system was started at Harvard Forest (HFM) in collaboration with Harvard University scientists. At Alert, Northwest Territories, Canada (ALT) and in cooperation with the Canadian Atmospheric Environment Services (AES) program, an in situ GC for measuring N_2O and SF_6 also was installed and operated in 1995. Monthly, and in some cases weekly, flask samples were collected at these new in situ sites. Another site within CMDL, Cape Kumakahi, Hawaii (KUM), was added to obtain flask measurements of air from the remote, tropical, northern hemispheric marine boundary layer. Combined with MLO, this should allow us to estimate vertical gradients of trace atmospheric halocarbons, particularly those that react readily with sunlight or tropospheric OH. Table 5.1 summarizes the geographic location and type of operations of eleven flask and nine in situ sampling sites.

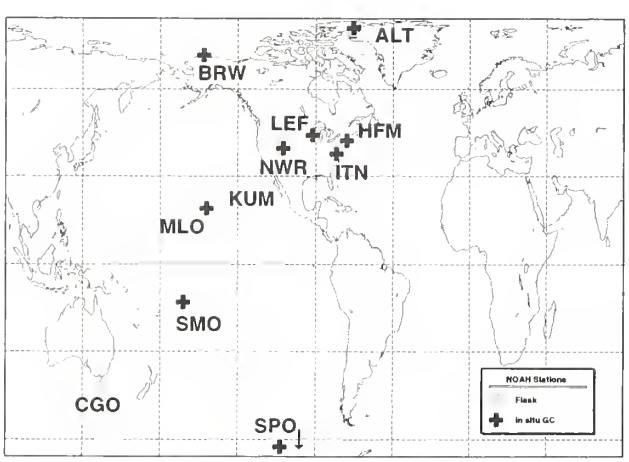

Fig. 5.1. Geographical locations of old and new stations in the NOAH flask (gray circles) and in situ (pluses) networks.

5.1.2. Flask Samples

Overview

NOAH's flask sampling and measurement program underwent a number of changes and improvements in 1994 and 1995. Most significant of these was the retirement of the "old" flask GC, a Hewlett-Packard (HP) Model 5710A GC-ECD, at the end of 1995 used for the measurement of CFC-12 (CCl_2F_2), CFC-11 (CCl_3F), and N_2O since inception of the old GMCC halocarbon monitoring program in 1973. This instrument, which operated in an almost entirely manual mode and for which data reduction was a cumbersome process, was replaced by the NOAH automated flask GC (OTTO). The OTTO GC, which began operation in 1992, analyzes samples for seven gases. A detailed comparison of mixing ratios of CFC-11, CFC-12, and N_2O from all stations between the old HP 5710A and OTTO GCs shows that the new OTTO GC gives better precision and close agreement with the older GC (Figure 5.2). The Whitey 300 mL-flasks were also removed from the sampling network. Over the past 10 years, the flask network was augmented with increasingly large flasks (0.85 L and 2.4 L) to accommodate the increased number of measurements and larger amounts of air required. The last Whitey flasks were filled at the end of 1995 at all stations except at the South Pole Observatory, Antarctica (SPO), which will not be able to return them until its reopening in the fall of 1996. Originally selected for sampling of stable CFCs and N_2O, the Whitey flasks, with their smaller volume and coarser internal surfaces, were also increasingly problematic for some of the more reactive gases such as methyl chloroform (CH_3CCl_3), carbon tetrachloride (CCl_4), and methyl bromide (CH_3Br) that were added to the suite of measurements over time. All flasks in the network are now 0.85-L Biospherics or 2.4-L Max Planck Institute (MPI) electropolished, stainless steel containers with Nupro metal-bellows (SS-4H) valves.

TABLE 5.1. Geographic and Network Information on NOAH Network Sites (In Order of Highest Latitude)

Code	Station	Latitude	Longitude	Elevations (m)	LST-GMT (hr)	Type
ALT	Alert, North West Territories. Canada*	82.45°N	62.52°W	210	-4	F,I
BRW	Pt. Barrow, Alaska	71.32°N	136.60°W	11	-9	F,I
LEF	WLEF tower, Wisconsin†	45.95°N	90.28°W	470	-6	F,I
HFM	Harvard Forest, Massachusetts‡	42.54°N	72.18°W	340	-5	F,I
NWR	Niwot Ridge, Colorado§	40.04°N	105.54°W	3013	-7	F,I
ITN	WITN tower, North Carolina†	35.37°N	77.39°W	9	-5	F,I
MLO	Mauna Loa, Hawaii	19.54°N	155.58°W	3397	-10	F,I
KUM	Cape Kumukahi, Hawaii	19.52°N	154.82°W	3	-10	F
SMO	Tuluila, American Samoa	14.23°S	170.56°W	77	-11	F,I
CGO	Cape Grim, Tasmania, Australia**	40.41°S	144.64°E	94	+10	F
SPO	South Pole, Antarctica	89.98°S	102.00°E	2841	+12	F,I

Cooperative sites (F = flasks, I = in situ) with:

*AES, in situ GC: Only N_2O and SF_6

†CCG. Flasks will be added to WLEF in 1996. The ACATS-II instrument ran as an in situ GC at WLEF for 1995.

‡Harvard University

§University of Colorado

**Commonwealth Scientific and Industrial Research Organization (CSIRO) and Bureau of Meteorology, Australia

Flasks are now filled to 376-505 kPa (40-60 psig) at all sites. Although this typically has not been a problem at sea level where the KNF Neuberger, Inc. pumps (Model UN05SV1) are rated to deliver 410 kPa (45 psi), samples collected at higher altitudes (SPO, Mauna Loa Observatory, Hawaii (MLO), Niwot Ridge, Colorado (NWR)) could only reach pressures around 273 kPa (25 psig), which today are barely enough gas for CMDL measurements. To accommodate this change, the inlets were reconfigured to the automated, in situ GCs to allow the Neuberger pumps to draw air from the pressurized portion of the inlet line. Although the inlet lines (Dekabon) and pumps (Air-Cadet, Cole-Palmer) contain plastic, they are kept clean by continuous flushing, 24 hours per day at 5-10 L min^{-1}. No noticeable difference was observed in the data as a result of making this change. Pumps and lines have been installed at NOAA sites, e.g., KUM, that do not support in situ GCs.

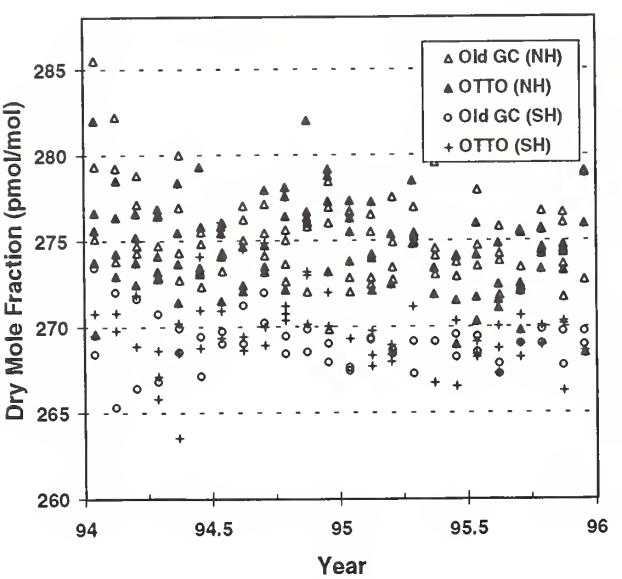

Fig. 5.2. Continuity of CFC-11 data from the old GC and automated flask GC (OTTO) during 1994-1995. Data are shown for sites in both hemispheres.

In addition to the routine, weekly sampling of flask pairs at the CMDL observatories and cooperative sampling sites, NOAH scientists also analyzed air in flasks collected during two cruises in 1994 (Bromine Latitudinal Air/Sea Transect (BLAST I and BLAST II); section 5.4 and SF_6 section) to obtain "snapshots" of the interhemispheric gradient of a number of gases and to support measurements made by in situ GCs onboard. These measurements included over 25 gases and involved all of NOAH laboratory instrumentation. Another project (section 5.6) involved the flask program for the analysis of air sampled from South Pole firn (compressed snow). This provided NOAH scientists with a unique opportunity to observe the N_2O and halocarbon content of air dating back to the end of the 19th century. Although the air was collected into glass flasks with Teflon o-rings, which in the past have caused some problems in the analysis of halocarbons, contamination was minimal for most gases in this instance. The success of these measurements prompted NOAH scientists to pursue similar analyses from firn air collected at Vostok and Greenland. Because of the number of investigators requiring air from the SPO flasks, sharing was limited. Consequently, the samples were analyzed only with the OTTO and Low Electron Attachment Potential Species (LEAPS) GCs, which require less sample than the GC-MS systems.

Finally, a number of changes were made in instrumentation, data acquisition, and data management for flask measurements that have improved the precision of some measurements, enhanced detection limits for others, and dramatically streamlined the processing of data. Today, data from samples run on OTTO and LEAPS can be

finalized and evaluated alongside all previous data within minutes following analysis.

Measurements by EC-GC

Improvements in Analysis. The precision of flask measurements by EC-GC has improved dramatically during 1994-1995. Modifications in sampling technique and sample introduction, full automation of CFC, N_2O, and chlorocarbon measurements, and installation of 24-bit interfaces for analyses by OTTO and LEAPS combined to yield analytical and sampling precisions about 0.1 ppt or less for LEAPS gases and on the order of tenths of a ppt for gases measured on OTTO.

The old Nelson Analytical, Inc. data acquisition and handling system on OTTO was replaced with entirely new hardware and software to allow more rapid and consistent processing of samples. The HP Model 210 computer was replaced with an IBM PC compatible 486, the 16-bit A/D converters were replaced with two HP 24-bit A/D boards for the PC, and the Rocky Mountain Basic software was replaced with the 1995 version of HP Chemstation software. Programs were written in Microsoft Visual Basic to consolidate the HP Chemstation output from each run of flasks, compute results, generate flags for erroneous or anomalous data, perform additional quality control tests, and load the results into a Microsoft Access data base. Currently, eight flasks can be run at once on OTTO, obtaining precise measurements of CFC-12, CFC-11, CFC-113, CH_3CCl_3, CCl_4, N_2O, and SF_6.

Results and Trends. The years 1994 and 1995 heralded the downturn in total chlorine, equivalent chlorine, and effective equivalent chlorine in the earth's troposphere [*Montzka et al.,* 1995b, 1996b]. Led by a marked drop in CH_3CCl_3, this suggested that the abundance of ozone-depleting halogen in the stratosphere could begin to decline in the near future. Other gases that began decreasing in abundance during this time include CFC-113, CCl_4, and, to a lesser extent CFC-11 (Figure 5.3). CFC-12 continued to increase in the atmosphere, although not in sufficient quantity to offset the losses in organic chlorine represented by the other compounds (Figure 5.3). As expected, the atmospheric abundances of CFC alternative compounds (HCFCs and HFCs) have been increasing at reasonably fast rates, although these gases contain relatively little chlorine and have shorter lifetimes than the CFCs ([*Montzka et al.,* 1993, 1994, 1996a,b]; section 5.1.5).

SF_6—An Important Tracer and Strong Greenhouse Gas

On a per molecule basis, SF_6 is one of the strongest greenhouse gases known, about 25,000 times greater than CO_2 [*Albritton et al.,* 1995]. It is solely anthropogenic in origin and used primarily for the insulation of high-voltage electrical equipment. With its increasing use and very long

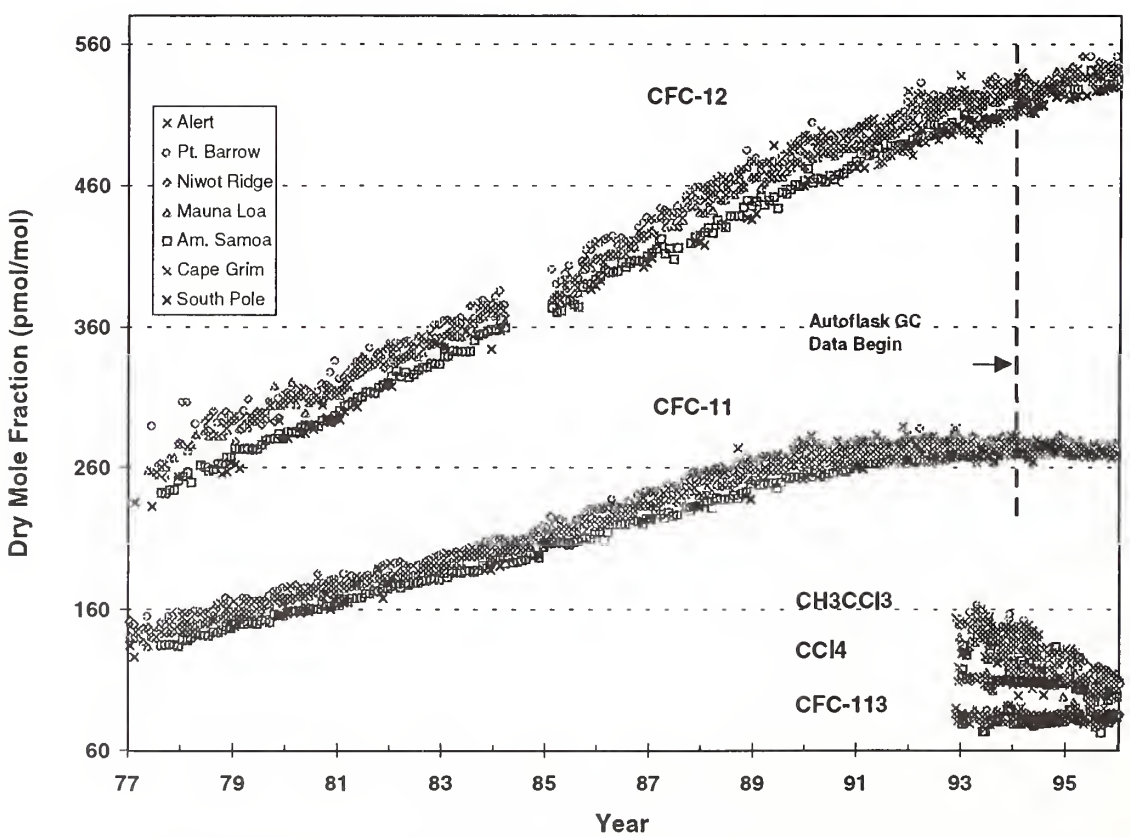

Fig. 5.3. CFCs and chlorocarbons measured on the old GC and OTTO in ppt versus time since 1977. The transition from old GC data to OTTO data for CFCs -11 and -12 is shown by a vertical, dashed line at the beginning of 1994. Noticeable are the tighter measurements of OTTO and the lack of an offset between the instruments. Also shown in proportion are the recent growth rates of the major, Class I ozone-depleting, chlorinated compounds and their narrowing interhemispheric gradients.

lifetime, SF_6 is rapidly accumulating in the atmosphere at ~7% yr^{-1}. In addition to its importance as a greenhouse gas, SF_6 is a nearly ideal tracer of atmospheric dynamics due to its well understood sources and long atmospheric lifetime of ~3200 years [*Ravishankara et al.*, 1993].

CMDL scientists recently began monitoring atmospheric SF_6 in weekly flask samples from all baseline stations and many CCG network sites as high-resolution latitudinal profiles during the 1994 BLAST ocean cruises [*Geller et al.*, 1994] as in situ stratospheric measurements from the Airborne Chromatograph for Atmospheric Tracers (ACATS) field missions [*Elkins et al.*, 1996], and as in situ measurements at Alert, Harvard Forest, and North Carolina [*Hurst et al.*, 1995]. SF_6 was measured with ECD-GC as described in *Elkins et al.* [1996]. Even though ambient levels of SF_6 are only ~3.5 ppt, it is possible to measure direct air injections (no sample preconcentration) to a precision of 1-3%. A suite of gravimetric SF_6 standards ranging from 3 to 108 ppt was developed in the NOAH Group. An intercalibration with the University of Heidelberg (Germany) showed CMDL measurements are less than 2% lower that the German calibration scale.

The long-term trend of SF_6 is illustrated in Figure 5.4, which shows NOAA data together with the University of Heidelberg data. These different data sets, collected and analyzed by different techniques, show good agreement. A northern hemispheric trend was fit to the combined Izaña and NWR data, because data from these two midlatitude sites are close to the latitudinally weighted hemispheric mean. Likewise, in the southern hemisphere, data from Antarctica and Cape Grim well represent the true southern hemisphere mean, therefore the southern hemisphere trend was fit to the Neumayer and Cape Grim data from the University of Heidelberg, and the SPO and Cape grim data from NOAA data. A preliminary estimate for the global trend (the average of the northern and southern hemispheric trends) shows a quadratic increase described by: $y = 3.43 - 0.2352 \times + 0.00487x^2$ (for x = (year - 1996); 0.23 ppt yr^{-1} (6.86% yr^{-1}). This trend, which is derived from the combined data sets, shows no significant difference from the trend derived from the University of Heidelberg data alone [*Maiss et al.*, 1996]. Figure 5.5 shows the high resolution latitudinal profiles of SF_6 collected over both the Pacific and Atlantic oceans on the BLAST cruises of 1994. Figure 5.5c also shows a mean latitudinal profile of SF_6 for November 1995 obtained from the flask sampling network. These profiles should not be taken as representative of an overall global distribution of SF_6 since they can vary seasonally.

5.1.3. RITS Continuous Gas Chromatograph Systems

Operations Update

A new watchdog timer turns the power off, then resets the computer, printer, and Nelson A to D boxes if a signal 1987 < year <1996). This yields a late 1995 growth rate of

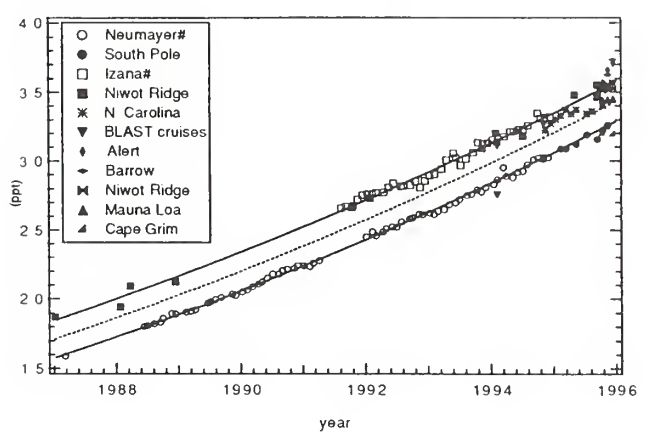

Fig. 5.4. Temporal trends of SF_6. CMDL data shown together with University of Heidelberg data [from *Maiss et al.*, 1996, marked in the figure legend as #]. The Heidelberg data has been adjusted to the CMDL calibration scale and binned into monthly means. The curve fitting is described in the text.

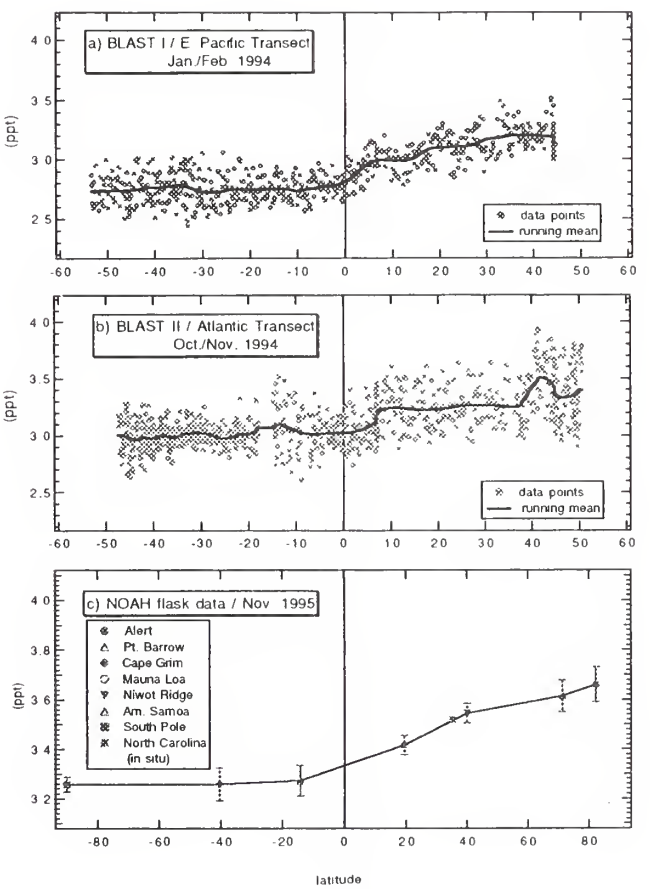

Fig. 5.5. Latitudinal profiles of atmospheric SF_6 (dry, ppt by mole fraction). (a) and (b) are in situ data from the marine boundary layer in 1994. (c) shows the monthly mean mixing ratios for November 1995 obtained from flask samples collected at seven sampling stations and from the in situ North Carolina data. Error bars represent ±1 standard deviation of the flask pair mixing ratios at each station.

is not received in a specified recurring period of time. This restarts data acquisition when station personnel are not present at night or on weekends and the system locks up. In June 1994 the hardware was installed at the Barrow Observatory, Alaska (BRW) in June and at MLO and Samoa Observatory, American Samoa (SMO) in August. At this same time a new function was added to the system software to decrease paper usage by the printer. A set of calibration gas and air chromatograms were printed only once a day prior to the arrival of the station personnel instead of continuous printouts. In August, system software was modified to include a menu-driven log for problems, failures, and changes to be easily documented. In the past such information was written on daily and weekly check lists and then typed into a database.

Original data acquisition and control computers, HP Model 9816s of mid-1980 vintage, were replaced in 1995 by 486 PCs. The software port from HP Basic to TransEra HTBasic running in Microsoft Windows 3.1 required only minor changes. This software upgrade was installed in April at NWR, in May at MLO and SMO, and in June at BRW. An additional feature of the new computers is network access. Data downloading, software upgrading, and determining equipment status is now possible over the Internet.

Alert

A single-channel GC equipped with an ECD and based on the STEALTH GC design (section 5.5) was built in 1995 and installed at ALT as part of a cooperative research agreement between CMDL and AES. Continuous instrument operation began in late August 1995 with two samples of ambient air analyzed each hour for N_2O and SF_6. These measurements augment the weekly flask samples taken at ALT since late 1987 and allowed detection of episodic pollution events. Of particular interest was the monitoring of polluted air that arrives at Alert from northern Asia and from the former Soviet Union.

Data Analysis

In response to observed depletion of stratospheric ozone, the 1987 Montreal Protocol on Substances That Deplete the Ozone Layer mandated a 50% reduction of chlorofluorocarbons and selected chlorinated solvent production over the next 10 years. In 1990 this was strengthened to a 100% phase out by the year 2000. An additional amendment in 1992 required a 75% reduction by 1994 and a complete ban by 1996. The chemical industry responded quickly with substitutes. Emissions have, therefore, generally been reduced in excess of expectations.

The global average CFC-11 tropospheric mixing ratio reached a maximum of 272 ppt in 1993 (Figure 5.6). The growth rate has now started to decline at -1 ppt yr^{-1}. Recently the interhemispheric difference declined by half, indicative of a long lifetime and a mostly northern hemisphere source that is diminishing quickly. In situ measurements of CFC-11 and CFC-12 are described in *Elkins et al.* [1993], and the data were recently updated in *Montzka et al.* [1996b].

CFC-12 growth continues to slow down with the end of 1995 growth rate about 6 ppt yr^{-1}. Because CFC-12's major use is in domestic, commercial, and industrial

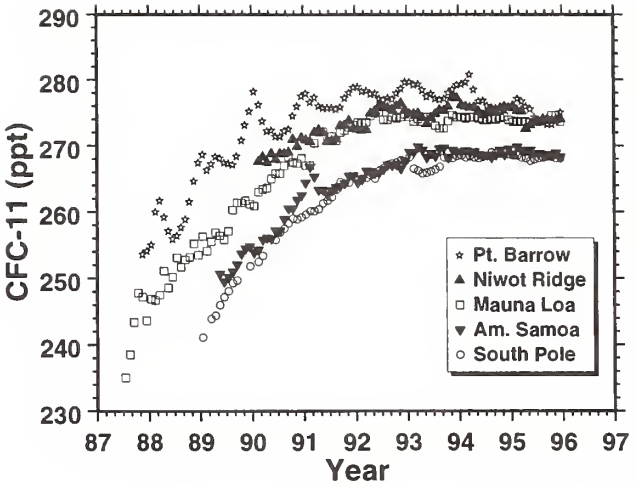

Fig. 5.6. Monthly average CFC-11 mixing ratios in ppt from the in situ GCs.

refrigeration and air conditioning, release to the atmosphere is slower than foam blowing, propellant, and solvent applications. Assuming a constant deceleration of -1.66 ppt yr^{-2}, CFC-12 is estimated to peak in the atmosphere in mid-1999 with a global-average tropospheric mixing ratio of 544 ppt (Figure 5.7 and 5.8).

Southern hemispheric mixing ratios of methyl chloroform peaked in 1992 and northern hemisphere mixing ratios peaked a little more than a year earlier (Figure 5.9). The time lag is similar to the known interhemispheric mixing time. The large north to south gradient before 1993 is indicative of very strong northern hemisphere sources. The rapid decrease in mixing ratios during phaseout shows the chemical has a short lifetime estimated at about 5 years [*Prinn et al.*, 1995].

The chlorinated solvent CCl_4, was used as the primary source (feed stock) for the chemical synthesis of all the chlorofluorocarbons. With their ban, this role has

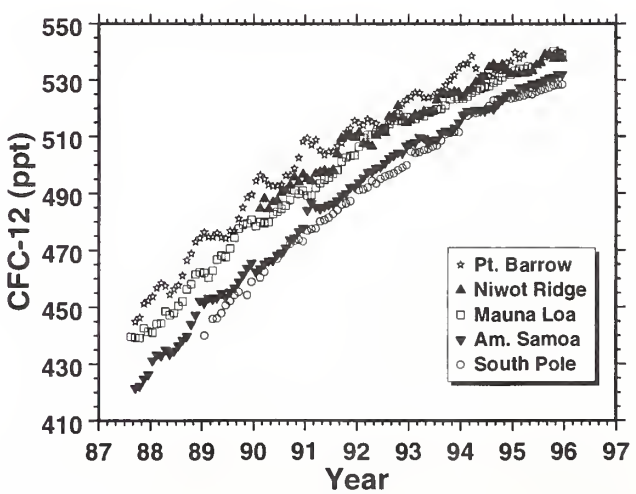

Fig. 5.7. Monthly average CFC-12 mixing ratios in ppt from the in situ GCs.

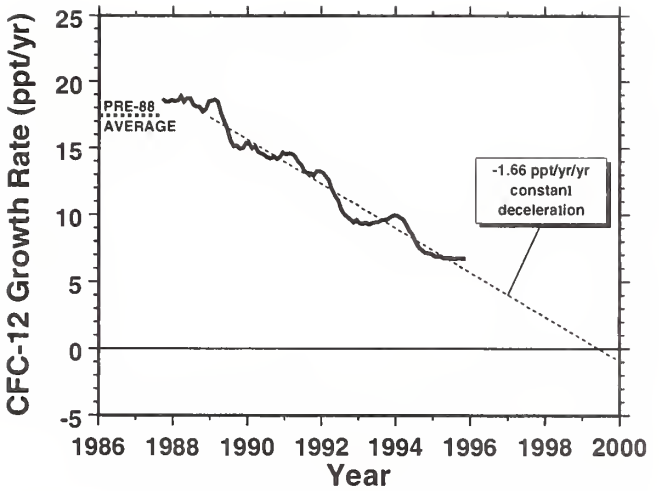

Fig. 5.8. A decrease in the global average growth rate of CFC-12 is projected to become zero in mid-1999.

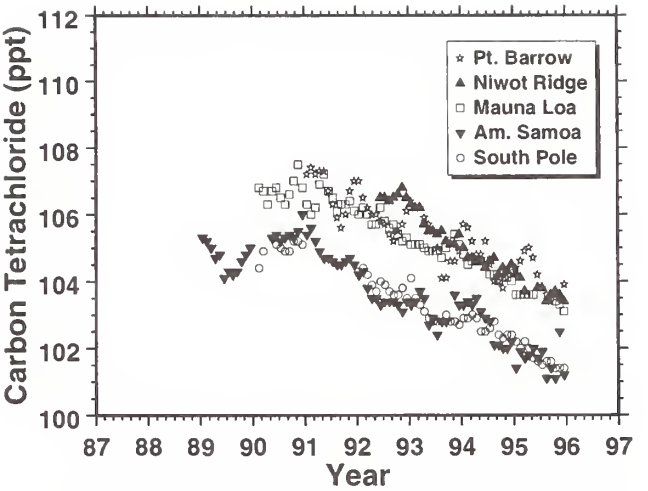

Fig. 5.10. Monthly average CCl_4 mixing ratios in ppt from the in situ GCs.

diminished significantly. Atmospheric mixing ratios were observed to be slowly decreasing at approximately -0.75 ppt yr^{-1} since 1991 (Figure 5.10). One unusual feature is the north to south gradient was near constant during this same period.

The methyl chloroform and carbon tetrachloride data were published in *Montzka et al.* [1996b]. The mixing ratios of both compounds are decreasing with time as a result of the Montreal Protocol.

N_2O continued to increase in the troposphere (Figure 5.11). The average global growth rate for 1995 was 0.61 ppb yr^{-1}.

5.1.4. LEAPS

Although precision of the Low Electron Attachment Potential Species (LEAPS) analyses was improved by an order of magnitude in 1992 with better chromatography (tenths to hundredths of a ppt; *Swanson et al.* [1993]; *Thompson et al.* [1994]), the system still operated with the old Nelson Analytical hardware and software. In 1994 this was replaced with a 24-bit A/D board and an IBM PC-compatible 386, and HP Chemstation software. New software was written for processing data and incorporating it into a Microsoft Access data base manager. As with data from OTTO, final LEAPS data are now available immediately following analysis.

Halons have not been produced by industry since January 1, 1994, except for some small exceptions; however, the mixing ratios of the three major halons (H-1211 or $CBrClF_2$, H-1301 or $CBrF_3$, and H-2402 or CBr_2F_4) in the troposphere continued to rise (Figure 5.12), because a considerable amount of halon remains stored in fire suppression systems. The growth rates are, however,

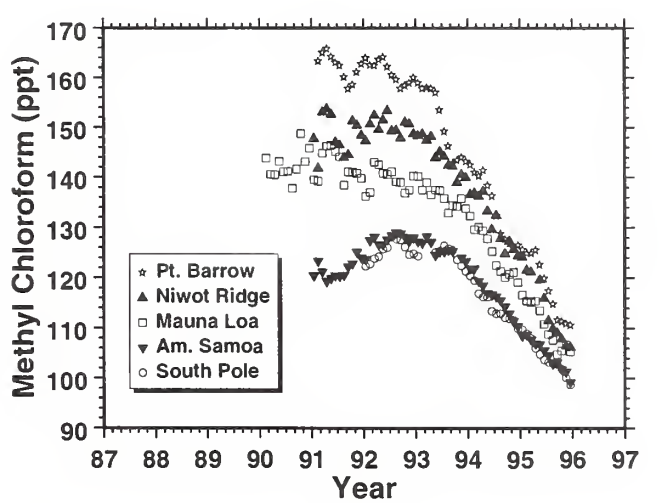

Fig. 5.9. Monthly average CH_3CCl_3 mixing ratios in ppt from the in situ GCs.

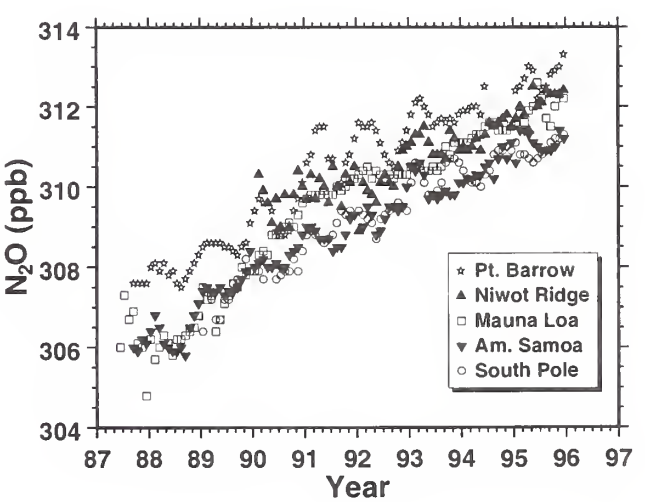

Fig. 5.11. Monthly average N_2O mixing ratios in ppb from the in situ GCs.

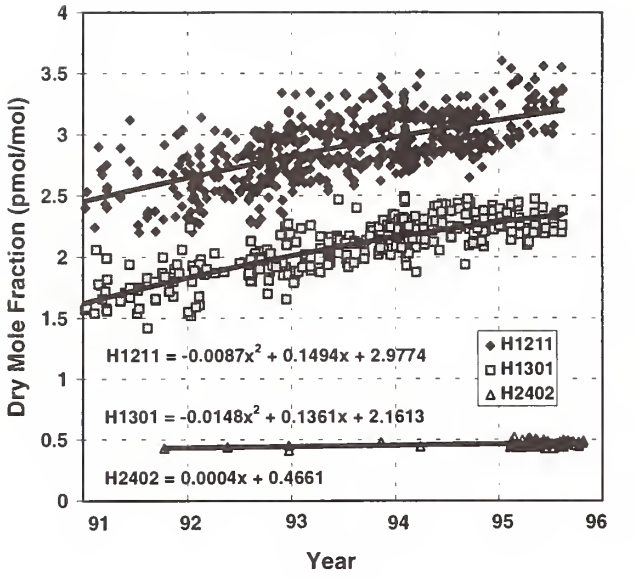

Fig. 5.12. Growth of halons in the atmosphere since 1991. Growth rates are given for January 1, 1994, thus approximating today's increase of stratospheric bromine from halons. Pre-1995 data for H-2402 are from the NOAA archive; all other measurements are from the flask network.

considerably lower now than during the 1970s and 1980s [*Butler et al.*, 1992].

5.1.5. Chlorofluorocarbon Alternative Measurements Program

Flask air analysis by GC-MS continued through 1994-1995. Mixing ratios of selected CFCs, HCFCs, HFCs, chlorinated hydrocarbons, brominated hydrocarbons, and halon-1211 were determined from air collected in flasks at the seven remote flask sampling observatories (four CMDL stations and three cooperative flask sampling locations). Toward the end of 1995, flask samples were also collected at three additional sites: KUM, ITN, and HFM.

During this period, analysis methods were developed on a second instrument for precise measurement of halocarbons such as HFCs at mixing ratios of ~0.1 ppt and higher. This was accomplished by using larger volumes of air per injection than in the original GC-MS instrument (up to 1 L of air per injection versus ~0.17 L in *Montzka et al.* [1993]). Detection of halocarbons in this second instrument is also performed with mass spectrometry. Larger flasks (2.4 L) were incorporated into the sampling network in early 1995 to allow for air analysis on this new instrument in addition to other instruments. With these changes and the development of the second GC-MS instrument, measurements of selected HFCs and additional HCFCs became possible in modern air starting in early 1995. Furthermore in 1995, enhanced sensitivity has allowed for the analysis of HFCs, HCFCs, and other halocarbons within archived air samples that were collected at NWR and other locations since 1987.

HCFC-22 ($CHClF_2$) Measurements

The most abundant HCFC, HCFC-22, increased in the global troposphere at a rate of 4.5% yr^{-1} (mean exponential rate estimated from flask samples collected between 1992 and 1996; Table 5.2, Figure 5.13a, and *Montzka et al.*, [1996b]). This rate represents a slower annual increase on a relative basis when compared to growth rates reported for time periods encompassing the 1980s and early 1990s [*Montzka et al.*, 1993; *Zander et al.*, 1994; *Irion et al.*, 1994; *Rinsland et al.*, 1996].

Informal exchange of flask air samples and standards in 1994-1995 with the National Center for Atmospheric Research (NCAR), the University of Bristol, England, and the Scripps Institution of Oceanography has suggested that consistent results (within 5%) can be obtained by chromatographic analysis of air even when different detectors are used (MS and O_2-doped ECD). These results are also reasonably consistent with surface mixing ratios inferred from long-path absorption studies [*Irion et al.*, 1994].

Emission estimates compiled by industry can be used to infer an atmospheric lifetime for HCFC-22. However, uncertainties associated with this exercise limit its usefulness for providing constraints to the global mean burden of the hydroxyl radical. With simple box-model calculations and emission estimates [*AFEAS*, 1995] (without adding additional emission to allow for unreported production), an atmospheric lifetime of 12 ± 2 years is estimated for HCFC-22 from CMDL data. This lifetime is consistent with 11.5 ± 0.7 years, which has been estimated for HCFC-22 based upon a comparison between measurements and model calculations of methyl chloroform [*Prinn et al.*, 1995].

HCFC-141b (CH_3CCl_2F) Measurements

Rapid atmospheric growth continues to be observed throughout both tropospheric hemispheres for HCFC-141b (Table 5.2, Figure 5.13c, *Montzka et al.* [1996b]). Mixing

TABLE 5.2. Annual Mean Growth Rate and Mean Tropospheric Burden (Mixing Ratio) for HCFCs and HFC-134a*, Mid-1994 and Mid-1995

	Mid-1994		Mid-1995	
Compound	Growth Rate, ppt yr^{-1}	Mixing Ratio, ppt	Growth Rate, ppt yr^{-1}	Mixing Ratio, ppt
HCFC-22	5.3	111.1	5.6	116.6
HCFC-142b	1.2	5.6	1.1	6.8
HCFC-141b	1.4	1.9	1.9	3.5
HFC-134a	~0.7†	N.D.‡	1.2	1.6

Global mean growth rates and mixing ratios estimated from polynomial fits to data binned by monthly, bimonthly, odd month, and even month periods, and by station. HCFC-22 growth of 4.5% yr^{-1} is estimated from an exponential fit to global mean data between 1992 and 1996.

*See Figure 5.13. Estimates reported here for HCFC-142b were corrected for an error in Table 1 of *Montzka et al.* [1996b].

†Estimated from mean of two cruises in 1994.

‡Not determined.

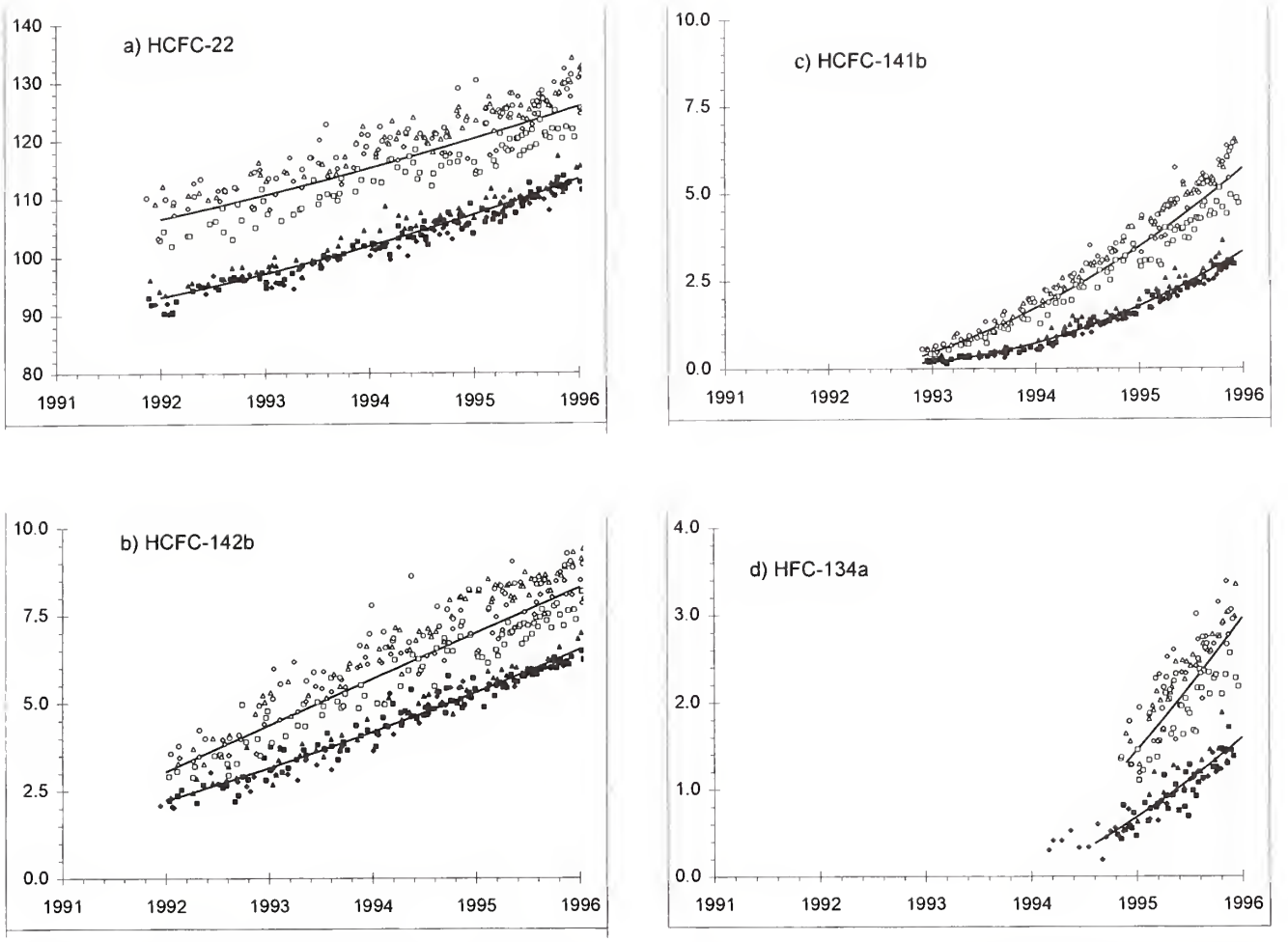

Fig. 5.13. Atmospheric dry mole fractions (ppt) determined since 1992 for the most abundant substitutes for ozone-depleting substances. Each point represents a mean of two simultaneously filled flasks from one of seven stations: ALT, open circles; BRW, open triangles; NWR, open diamonds; MLO, open squares; SMO, filled triangles; CGO, filled squares; SPO, filled diamonds. These data were obtained from the original GC-MS instrument (see text). Solid lines represent fits to hemispheric monthly means.

ratios have increased more than tenfold throughout the global troposphere since the beginning of 1993. Fairly good agreement was reported among different laboratories that have published measurements for this compound [*Montzka et al.*, 1994; *Schauffler et al.*, 1995; *Oram et al.*, 1995].

Preliminary emissions have been estimated recently for HCFC-141b by industry (P. Midgley, Alternative Fluorocarbon Environmental Acceptability Study (AFEAS), personal communication, 1996). At the beginning of 1993, the global tropospheric abundance estimated from the measurements was ~2.0 times greater than the burden estimated from these emissions. By the end of 1994, this ratio had decreased to between 1.3 and 1.4. The exact cause for this discrepancy is currently unknown; however, the difference (but not its time dependence) could be reconciled if emissions are a larger fraction of production than currently assumed. Some of this difference could also be explained by larger vertical gradients within the troposphere than assumed in the simple box-model calculation.

Whereas the atmospheric lifetime of HCFC-141b also influences ambient mixing ratios and affects the magnitude of the difference discussed here, mixing ratios are fairly insensitive to the lifetime chosen for HCFC-141b during the initial phase of use and emission. For example, if we were to consider a lifetime for HFC-141b of 20 years instead of the more accepted value of ~10 years [*WMO*, 1995], the ratio calculated for the end of 1994 would be 1.2-1.3 instead of 1.3-1.4.

Analysis of the CMDL air archive reveals fairly constant mixing ratios of 0.08 - 0.10 ppt for HCFC-141b from 1987 to 1990 (Figure 5.14). After 1990, the abundance increases to ~0.6 ppt in 1993, which is consistent with mixing ratios determined for the northern hemisphere from the flask program at that time [*Montzka et al.*, 1994]. These results are also similar to data reported by *Oram et al.* [1995] where fairly constant mixing ratios of 0.08 ± 0.01 ppt HCFC-141b were found in samples collected at Cape Grim between 1982 and 1991. A dramatic increase was observed at this southern hemispheric site in 1992 and 1993, or 1 to 2 years after that observed at NWR in the CMDL archive.

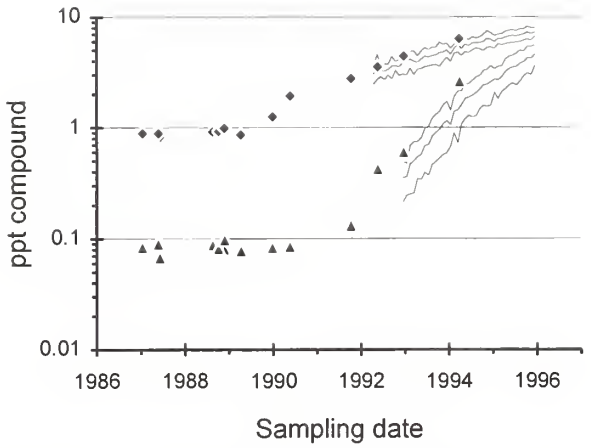

Fig. 5.14. Atmospheric dry mole fractions for HCFC-142b (filled diamonds) and HCFC-141b (filled triangles) in archived air samples as determined on the newer GC-MS instrument. Analyses of archived air were performed in early 1995. With the exception of samples filled in mid-1987, all samples were obtained from NWR or MLO. Samples collected in mid-1987 were obtained shipboard in both hemispheres. Solid lines represent hemispheric (northern always higher than southern) and global monthly means for HCFC-142b and HCFC-141b as determined from the data in Figures 5.13b and 5.13c.

HCFC-142b (CH_3CClF_2) Measurements

Rapid atmospheric growth was also observed for HCFC-142b during 1994-1995 (Table 5.2; Figure 5.13b; *Montzka et al.* [1996b]). Published results from ground-based air samples disagree by ~30%, with CMDL data [*Montzka et al.*, 1994] being higher than mixing ratios reported from the UEA [*Oram et al.*, 1995]. Accurate comparison with a few earlier measurements from NCAR [*Pollock et al.*, 1992; *Schauffler et al.*, 1993] is difficult because these earlier measurements were from air collected above 15 km in northern latitudes. However, from informal exchange of air samples and standards between CMDL and NCAR, and between CMDL and the University of Bristol, mixing ratios determined from these three independent laboratories are expected to span a range of approximately 10% (with CMDL results approximating the mean of the three laboratories: University of Bristol, NCAR, and CMDL).

It is also noted that the mixing ratio reported for HCFC-142b in Table 1 of *Montzka et al.* [1996b] is too high by approximately 6%. The revised growth estimate for 1995 is reduced by a larger percentage (Table 5.2). This error arose in determining the mixing ratio for HCFC-142b in an air sample used for reference in the analysis of flask samples in 1995. This correction does not affect mixing ratios reported or conclusions drawn in *Montzka et al.* [1994]. This error was corrected in public accessible data files (CMDL World Wide Web site) in July 1996.

Emissions estimated by industry from production figures [*AFEAS*, 1995] underestimate the atmospheric burden of HCFC-142b [*Montzka et al.*, 1994; *Oram et al.*, 1995] regardless of which measurements are considered accurate. *Oram et al.* [1995] have suggested that a portion of this discrepancy arises from non-negligible emission of HCFC-142b in the years before 1981, which is the first year for which industry emission estimates are available. Between 1992 and the end of 1995, mixing ratios deduced from these emissions appear to underestimate the atmospheric burden of HCFC-142b by a consistent factor of ~1.9 (CMDL scale).

Analysis of the CMDL NWR air archive in 1995 for HCFC-142b shows mixing ratios of between 0.9 and 1.0 ppt between 1987 and 1989 (Figure 5.14). This is approximately 1.3 times higher than reported by *Oram et al*, [1995] for this period at Cape Grim, and this difference is consistent with calibration differences as discussed above. After 1989, enhanced growth was observed at NWR. The rate of accumulation is believed to have accelerated at Cape Grim approximately 1 year later [*Oram et al.*, 1995].

HFC-134a (CH_2FCF_3) Measurements

Development of techniques for determining mixing ratios of halocarbons present in the atmosphere at ~1 ppt and higher were refined in 1995 on a second GC-MS instrument. This allowed for analysis of air samples for numerous HCFCs, HFCs, and other halocarbons. Archived samples were also analyzed to determine how the abundance of HFC-134a has changed over the past 10 years. Results from these analyses show that the abundance of HFC-134a in the northern hemisphere has risen from ~50 parts per quadrillion (ppq) in 1990 (the limit of detection for this instrument) to ~2.5 ppt in mid-1995 [*Montzka et al.*, 1996a]. Analysis of flask samples filled onboard ship during cruises in 1987, early 1994, and late 1994 show similar atmospheric increases. The abundance of HFC-134a approximately doubled in the time elapsed between the two 1994 cruises in both hemispheres. Cruise flask samples were filled and stored prior to analysis in early 1995 under dramatically different pressures and humidities than the archived samples filled at NWR. The consistency observed between archived samples from NWR and cruise flask samples suggests that the amount of HFC-134a has not been altered significantly during storage by container-related effects and that the measurements are likely representative of atmospheric abundances at the time of sampling.

Routine measurements of HFC-134a in flask samples filled at the CMDL observatories and cooperative sampling locations began in early 1995 (Figure 5.13d; [*Montzka et al.*, 1996a,b]). Mixing ratios for this HFC are increasing rapidly at all sampling locations. Although it is not possible to accurately estimate the growth rate from such a short data record, the increase observed between 1994 and 1996 is consistent with exponential growth at ~100% yr^{-1}.

In simultaneously-filled flasks, mixing ratios determined for HFC-134a were not significantly different. The amount of HFC-134a measured in flasks filled in parallel typically agreed to within 30 ppq and was <100 ppq for 95% of the flask pairs analyzed. Similarly, analysis precision (1 s.d.) for replicate injections of air from flasks collected after 1995 from the ground-based stations was typically <30 ppq (<2%) and was <100 ppq for 95% of the flasks analyzed. This consistency is expected for properly-filled flasks and for molecules not adversely affected by storage in flasks. Flasks received from ground-based stations after February 1, 1995, were analyzed an average of 23 days after sampling.

Preliminary emissions for HFC-134a have recently been estimated by industry (P. Midgley, personal communication, 1996). At the end of 1994, these

emissions overestimate the observed abundance of HFC-134a by only ~0.1 ppt (measured/calculated = ~0.8-0.9).

CMDL Instrument Comparison from Routine Flask Analyses

Beginning in early 1995, large flasks (2.4 L) were filled and analyzed at the stations on both GC-MS instruments. For the compounds shown in Table 5.3, mixing ratios were assigned to air samples based upon independent calibration of reference air with CMDL gravimetric standards. Comparisons of results obtained from these independent instruments can provide further estimates of measurement uncertainty for halocarbons at these low mixing ratios, especially because different analytical conditions are used in the two instruments. The second instrument incorporates a different analytical column (DB-1 versus DB-5), trapping of compounds at different temperatures on a different substrate (a section of alumina PLOT column at −80°C versus a length of uncoated fused silica at −140 to −150°C), and a different valving arrangement. Different mass fragments were monitored during air analysis on the different instruments to determine HCFC-22 mixing ratios (Table 5.3). Because different ions would likely be influenced to different degrees by any coeluting compounds, consistent results obtained with different ions gives additional confidence that these measurements are not affected by such potential chromatographic problems.

Good consistency is observed for measurements of HCFC-22, HCFC-142b, and HFC-134a from the two different instruments. These results suggest that potential problems associated with sample analysis (such as coelution or instrument-specific problems) are not influencing the results that are obtained for these halocarbons on either instrument. A small, consistent offset is apparent for HCFC-141b. The cause of this offset is currently unknown. Variability observed between instruments for measurements of HFC-134a is larger than for other compounds because measured mixing ratios in early 1995 were often near the detection limit on the older GC-MS instrument.

Measurements of Additional Chlorinated Compounds with GC-MS Instrumentation

Mixing ratios for numerous other compounds were determined from flasks during 1994-1995. Data for certain chlorinated hydrocarbons with atmospheric lifetimes of <1 year show dramatic seasonal cycles in both hemispheres (Figure 5.15). Minima for these compounds were observed shortly after midsummer in each hemisphere when loss rates were expected to be greater than at other times of the year.

TABLE 5.3. Results of Individual Flask Air Analysis on Two Different GC-MS Instruments*

	New Instrument to Old Instrument Ratio		Mass to Charge Ratio Ions Monitored	
Compound	Mean	Standard Deviation	New Instrument	Old Instrument
HCFC-141b	0.96	0.04	81	81
HCFC-142b	0.99	0.03	65	65
HCFC-22	1.00	0.03	67	51
HFC-134a	1.00	0.13	83	83

*Comparison based on ~150 flasks analyzed on both instruments in 1995.

Atmospheric Trends for Chlorine and Bromine Contained in Long-Lived Halocarbons

Chlorine and bromine catalyze reactions leading to the depletion of stratospheric ozone. Enhanced use of

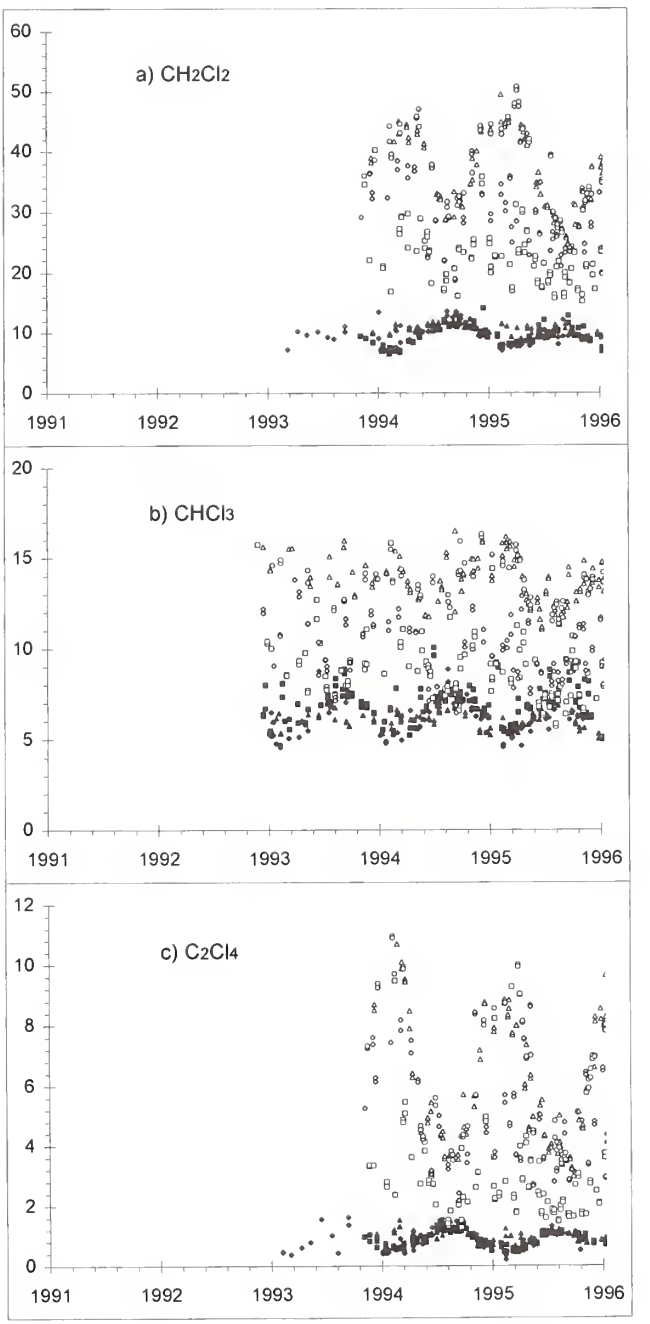

Fig. 5.15. Atmospheric dry mole fractions (ppt) for selected chlorinated compounds. Symbols are identical to those described in Figure 5.13. These data were obtained from flask air analyses on the original GC-MS instrument (see text). Mixing ratios reported are based on a preliminary calibration scale.

chlorine- and bromine-containing compounds by mankind has led to a steady increase in the abundance of chlorine and bromine in the atmosphere in recent time and to the depletion of stratospheric ozone [*WMO,* 1995]. Only bromine and chlorine-containing compounds that are relatively insoluble and have atmospheric lifetimes longer than a year can deliver significant amounts of halogen to the stratosphere. In 1994 the atmospheric abundance of Cl contained in these types of halocarbons was approximately five times greater than the burden estimated in the absence of anthropogenic emissions. Similarly, anthropogenic emissions of bromine-containing compounds have resulted in an atmospheric bromine abundance that is approximately twice that estimated for preindustrial times.

Model studies suggest that the tropospheric abundance of Cl will peak in the mid 1990s at 3.5-4.0 ppb if limits outlined in the most recent Copenhagen amendments to the Montreal Protocol are not exceeded. Not all nations have agreed to the restrictions set forth in the Protocol; in addition, evidence suggests that significant amounts of CFCs are currently produced illegally. Furthermore, developing countries are allowed a 10 year grace period on consumption restrictions under the Montreal Protocol. As a result, much uncertainty has remained regarding the timing and magnitude of peak halogen (Cl and Br) loading of the atmosphere.

In the NOAH Group, global tropospheric distributions and abundances are routinely determined for the most abundant, long-lived anthropogenic halocarbons. Measurements of the halogen burden in the troposphere can supply a reasonable estimate for the stratospheric halogen burden 3 to 5 years in the future [*WMO,* 1995]. Accordingly, the results provide estimates for the burden of ozone-depleting gases in the future stratosphere.

By accounting for the number of Cl atoms contained in the most abundant CFCs, HCFCs, chlorinated solvents, and halon-1211, it is estimated that the tropospheric abundance of Cl contained within these halocarbons peaked in early 1994 and is currently decreasing at a rate of 25 ppt yr^{-1} (Figure 5.16a; Table 5.4) [*Montzka et al.,* 1996b]. The current decrease is a dramatic turnaround from reported increases of 110 ppt yr^{-1} in 1989 and 60 ppt yr^{-1} in 1992 [*WMO,* 1995]. Most of the current decline in tropospheric Cl can be attributed to a decrease in the atmospheric abundance of CH_3CCl_3 (Figure 5.9) which has a relatively short atmospheric lifetime (~5 yr) [*Prinn et al.,* 1995]. The abundance of the major CFCs and chlorinated solvents were all stable or decreasing in 1995 with the exception of CFC-12. The abundance of CFC-12 continued to increase in mid-1995 at a rate of ~6 ppt yr^{-1} or approximately one-third the rate observed in the late 1980s (Figure 5.7 and 5.8). Increases in the abundance of HCFCs (HCFC-22, -142b, and -141b) accounted for growth in tropospheric chlorine of ~11 ppt per year in 1995 [*Montzka et al.,* 1996b]. After accounting for chlorine contributed from CH_3Cl, other chlorinated hydrocarbons (~700 ppt), and less abundant CFCs, it is estimated that the mean global chlorine loading of the troposphere peaked in 1994 at ~3.7 ppb.

Stratospheric ozone is destroyed through reactions of inorganic bromine and chlorine molecules. To estimate how the abundance of stratospheric inorganic halogen will change as a result of the observed trends for halocarbons in the troposphere, stratospheric degradation rates of halocarbons must be considered. Halogen release rates

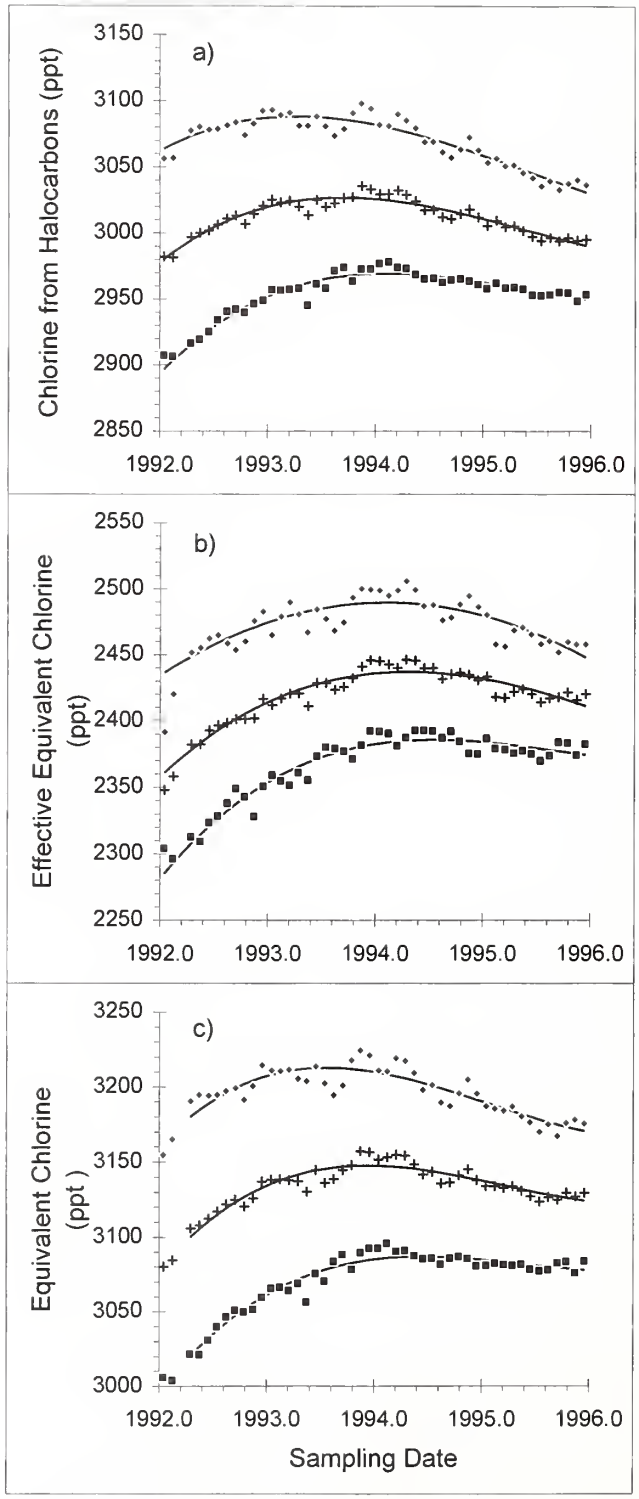

Fig. 5.16. (a) The amount of total chlorine, (b) effective equivalent chlorine (EECl) and (c) equivalent chlorine (ECl) contained within anthropogenic halocarbons: CFC-11, CFC-12, CFC-113, CH_3CCl_3, CCl_4, HCFC-22, HCFC-142b, HCFC-141b, halon-1211, and halon-1301. Data were binned by month and hemisphere (northern hemisphere, filled triangles; southern hemisphere, filled squares; global mean, plus symbols). Solid lines represent fits to monthly means.

TABLE 5.4. Mean Rate of Change Estimated for Mid-1995 From Measured Halocarbons (ppt yr^{-1})*

Compound	Global	NH	SH
Chlorine	-22	-30	-20
EECl	-23	-35	-16
ECl	-15	-22	- 8

*CFC-11, CFC-12, CFC-113, CH_3CCl_3, CCl_4, halon 1211, halon 1301, HCFC-22, HCFC-141b, HCFC-142b.

vary over altitude and latitude in the stratosphere, as does the efficiency for bromine to catalyze the destruction of stratospheric ozone when compared to chlorine (the alpha factor). Whereas bromine is estimated to be about 40 times more efficient than chlorine for destroying stratospheric ozone in the polar vortex [*WMO,* 1995], it may be as much as 100 times more efficient in the lower, midlatitude stratosphere [*Garcia and Solomon*, 1994]. In the following, the future reactive halogen burden is estimated for the lower, midlatitudinal stratosphere (effective equivalent chlorine, EECl) [*Daniel et al.,* 1995] and for the springtime, polar stratosphere (equivalent chlorine, ECl) with halogen release rates and alpha factors appropriate for each region. The abundance of halons increased over this period so that by considering higher estimates for alpha, the decline in EECl or ECl is underestimated.

The current mix and abundance of halocarbons within the troposphere ultimately will release fewer halogen atoms to the lower, midlatitudinal stratosphere than in previous years. The mean global tropospheric burden of halogen that will become inorganic halogen in the stratosphere reached a maximum in early 1994 and was declining in mid-1995 at 21 ± 8 ppt EECl yr^{-1}. (Figure 5.16b; Table 5.4; *Montzka et al.* [1996b]).

The actual rate of change for EECl in mid-1995 may be somewhat lower if the atmospheric abundance of methyl bromide has increased since 1992. However, limits to production outlined in the Copenhagen Amendments and production figures from the major global producers for 1991 and 1992 suggest anthropogenic methyl bromide emissions may have stabilized in the early 1990s. It is unlikely that an increase in methyl bromide over this period would have been large enough to offset the decrease reported here for EECl [*Montzka et al.,* 1996b].

For a mean transport time between the troposphere and lower, midlatitude stratosphere of 3-4 years [*Hall and Plumb*, 1994; *Fahey et al.,* 1995; *Boering et al.,* 1995], maximum levels of inorganic halogen are expected in the lower midlatitudinal stratosphere between 1997 and 1998. Modeling studies suggest that when stratospheric mixing ratios of reactive halogenated compounds begin declining, column-ozone abundance at midlatitudes will begin to recover [*WMO,* 1995]. However, because stratospheric ozone is influenced by other variables such as aerosol loading and temperature [*Solomon et al.,* 1996], the exact timing will also depend on how these variables change over this period.

To estimate the stratospheric abundance of ozone-depleting gases in the springtime polar vortex, equivalent chlorine (ECl) was calculated based upon CMDL tropospheric halocarbon measurements. The current mix and growth rates of these gases in the troposphere will result in lower ECl in the polar stratosphere in the future. In mid-1995 equivalent chlorine was decreasing at 18 ± 7 ppt ECl yr^{-1} (Figure 5.16c; Table 5.4; *Montzka et al.* [1996b]). It is unlikely that an increase in atmospheric methyl bromide in recent time would have been large enough to offset this decrease. Because transport of air from the lower troposphere to the polar stratosphere below ~25 km occurs in 3-5 years [*Prather and Watson*, 1990; *Pollock et al.,* 1992; *WMO,* 1995], or over a slightly longer period than to the lower, midlatitude stratosphere, levels of equivalent chlorine are expected to reach a maximum in the polar stratosphere between 1997-1999 and decline thereafter as long as current growth rates for halons and CFC-12 and the abundance of other CFCs and halocarbons continue to decline.

Although the abundance of reactive halogen in the polar stratosphere above Antarctica will decline when air currently within the troposphere reaches this region, springtime, total-column ozone levels will not increase there immediately. Ozone was nearly completely destroyed in the lower stratosphere above the Antarctic continent in springtime for the past 8 years [*WMO,* 1995]. Total-column ozone abundance within this region is expected to begin recovering only when mixing ratios of reactive halogenated compounds drop below those present in the late 1980s [*Prather and Watson,* 1990; *WMO,* 1995].

5.1.6. Gravimetric Standards

One of the strengths of NOAH is the ability to generate unique standards for "hot-topic" molecules with ease. Almost all of the NOAH standards are produced by actually weighing the individual components in air or by gravimetry. With maximum dilutions of 1:20,000 and accuracy's of better than 0.2%, two or four dilutions are sometimes required to produce standards at the ppt level. Not only does NOAH produce standards for internal use, but some of the clients have included other international and national research institutions. Some of this work over the past 2 years is summarized below.

Aluminum compressed gas cylinders are now being used with brass and stainless steel valves that have all-metal valve stems and seats. Materials such as KEL-F have a high absorption/desorption potential for gases such as 1,1,2-trichloro-1,2,2-trifluoroethane (CFC-113).

Five compressed gas cylinders containing pure reagent gases were analyzed for impurities using a CEC-103 mass spectrometer located at the National Institute of Standards and Technology (NIST) in Gaithersburg, Maryland. The results of the analyses indicated that the measured purity levels of the pure methane (CH_4), carbon monoxide (CO), carbon dioxide (CO_2), hydrogen (H_2), and nitrous oxide (N_2O) gases are consistent with the stated purity as specified by the gas supplier. These pure mixtures are being used to prepare gravimetric standards for CCG (CH_4, CO, CO_2, and H_2) and for NOAH (N_2O).

A total of 26 gravimetrically prepared CH_4 in air standards now exist for use by CCG. The nominal mixing ratios of the gas mixtures range from 32 ppb to 20 ppm. The standards are currently being studied for stability.

A suite of gravimetrically prepared sulfur hexafluoride (SF_6) in air standards were prepared for the first time this year. The standards were prepared with nominal mixing ratios ranging from 3 ppt to 110 ppt.

A suite of hydrogen (H_2) in air standards were also gravimetrically prepared for the first time this year. The mixing ratios of these standards range from approximately 450 ppb to 600 ppb.

HFC-134a in air standards were prepared in 1995 and were intercompared with existing HFC-134a standards prepared several years ago. The results confirm that the gas is stable over many years.

Several nine-component standards containing various methyl halide compounds were gravimetrically prepared primarily for the ocean and flask programs. The standards contain methyl bromide (CH_3Br), methyl chloride (CH_3Cl), methyl iodide (CH_3I), dibromomethane (CH_2Br_2), tribromomethane ($CHBr_3$), chlorodibromomethane ($CHBr_2Cl$), bromochloromethane (CH_2BrCl), chloroiodomethane (CH_2ICl), and diiodomethane (CH_2I_2). Nine two-component mixtures were initially prepared with mixing ratios at the ppb level. The pure liquids were handled under darkroom conditions with the use of a black-light source, because compounds with iodine are photochemically active and decompose quickly in sunlight and artificial light.

Existing CH_3CCl_3 and CCl_4 primary standards at the ppb level were compared to standards recently prepared to determine the stability of these gases over a number of years and to resolve a difference in sensitivity between several suites of ppt level standards that were prepared from the ppb standards. The mixing ratios range from 120 ppb to 760 ppb for CH_3CCl_3 and from 190 ppb to 950 ppb for CCl_4. The gases were analyzed using GC with a FID. The results of the analyses indicate that eight of nine CH_3CCl_3 standards and nine of nine CCl_4 standards are consistent to within ±2%.

5.2. Aircraft GC Project: ASHOE/MAESA Mission

5.2.1. Overview

A new four-channel GC, Airborne Chromatograph for Trace Atmospheric Species (ACATS-IV), was deployed for the first time in 1994 as part of the year-long Airborne Southern Hemisphere Ozone Experiment/Measurements for Assessing the Effects of Stratospheric Aircraft (ASHOE/MAESA) mission. ACATS-IV flew successfully on 24 flights spanning latitudes from 70°S to 60°N during four seasons. During ASHOE/MAESA, ACATS-IV was configured to measure ten different molecules. In addition to CFC-11, CFC-113, and CH_4 (compounds measured previously with a two-channel version of the instrument) ACATS-IV measured CH_3CCl_3, CCl_4, CFC-12, H-1211, N_2O, SF_6, and H_2. ACATS-IV provides an important set of tracer measurements for several different aspects of atmospheric research: (a) Dynamic and chemical models can be constrained by the wide range of these tracer's lifetimes (4.5-3200 years). (b) Halogens play an important role in stratospheric ozone destruction and ACATS-IV provides in situ stratospheric measurements of 80% of the chlorine containing species and the bromine containing compound, H-1211 which contains about 20% of the total organic tropospheric bromine. (c) Apart from tropical transport of water from the troposphere to the stratosphere, CH_4 oxidation is the largest source of stratospheric water, which has a large global warming potential. Simultaneous CH_4, hydrogen, and water measurements completely constrain the stratospheric hydrogen budget. (d) The age of stratospheric air is an important input to atmospheric models. SF_6 is a purely anthropogenic compound with no known tropospheric sinks, a stratospheric lifetime of 3200 years, and an approximately linear tropospheric growth rate that makes it an excellent indicator of the age of stratospheric air.

A complete instrument description can be found in a recent publication by *Elkins et al.* [1996]. The GC has been optimized for low ppt work and frequent sampling of 3-6 minutes by using an appropriate choice of separation columns, very sensitive ECDs, and 12-port gas sampling valves that permit heart-cutting the chromatogram (Figure 5.17). The measured tracers have a wide range of lifetimes that can be used to estimate a tropical-midlatitude exchange in the stratosphere as demonstrated in *Volk et al.* [1996]. The H-1211, SF_6, CFC-11, and CFC-12 measurements from ASHOE/MAESA have also been incorporated into a calculation that indicates the oldest stratospheric air measured by ACATS-IV has 17 ± 3 ppt of bromine and that all of the bromine resides in inorganic form.

5.2.2. Transport in the Lower Stratosphere

ACATS-IV observations in the lower tropical and midlatitude stratosphere during ASHOE/MAESA provide new information about mass exchange between the tropics and midlatitudes. Because of the profound impact of transport on the distribution of long-lived stratospheric constituents, the magnitude of such exchange is critical for prediction of ozone depletion by human activities. The sparse set of previous tropical in situ tracer data [*Goldan et al.*, 1980; *Murphy et al.*, 1993] and satellite observations of tracer and aerosol distributions [*Trepte and Hitchman*, 1992; *Randel et al.*, 1993; *Mote et al.*, 1996] have provided evidence for a subtropical "barrier" to horizontal exchange. These observations led to the suggestion that the stratosphere might be closer to a "tropical pipe" model [*Plumb*, 1996], in which tropical air ascends in isolation from midlatitude influence, than a "global diffuser" model [*Plumb and Ko*, 1992]. For the first time the ASHOE/MAESA campaign provided extensive tropical measurements of many tracers with local lifetimes ranging from less than 1 to 100 years. These data provide a powerful tool for quantifying the amount of transport across the subtropical barrier. A simple tropical tracer model was used to analyze ACATS data for CFC-11, CFC-12, CFC-113, CCl_4, CH_3CCl_3, halon-1211, and CH_4 along with measurements of N_2O, NO_y, and O_3 from three other instruments aboard the ER-2 [*Podolske and Loewenstein*, 1993; *Fahey et al.*, 1989; *Proffitt and McLaughlin*, 1983]. The observations during ASHOE/MAESA span latitudes from 60°N to 70°S and altitudes up to 21 km. The model considers the vertical evolution of a tropical tracer, including loss and production resulting from local photochemistry and entrainment of midlatitude air (due to isentropic mixing):

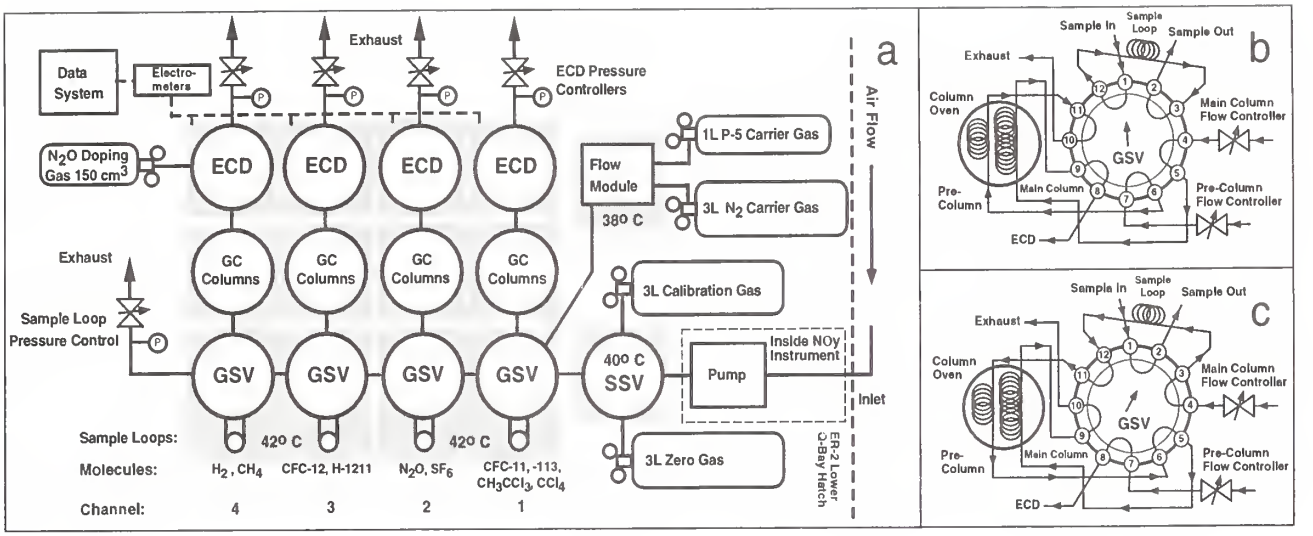

Fig 5.17. (a) Schematic of the ACATS-IV instrument showing pressure transducers (P), electron capture detectors (ECD), gas sampling valves (GSV), and the stream selection valve (SSV). Shaded areas are temperature-controlled zones where the temperatures for the GSV, SSV, and flow module are indicated. ECD and sample loop pressure controllers use a valve (MKS Instruments, Inc., Andover, Massachusetts) servo-controlled to a pressure gauge (Micro Gage, Inc., El Monte, California). The GC inlets for the calibration, carrier gases, and air sample have 10 μm screens to remove particles. (b) The first position of the 12-port GSV permits loading the sample loop, backflushing of the pre-column, and detection of the peaks of interest from the previous sample injection. (c) Turning the rotor of the 12-port GSV allows injection of the sample onto the columns and diversion of the column exhaust away from the ECD.

$$\frac{\partial \chi}{\partial \theta} Q = P - \frac{\chi}{\tau} - \gamma\chi - \frac{\chi - \chi_{mid}}{\tau_{in}} \qquad (1)$$

where χ and χ_{mid} are the mean tropical and midlatitude mixing ratios; θ is potential temperature used as vertical coordinate; $Q = d\theta/d\tau$ is the net diabatic heating rate, equivalent to vertical ascent rate; P is the photochemical production rate; τ is the lifetime for photochemical loss; γ is the long-term growth rate; and τ_{in} is a time scale for import of midlatitude air, the quantity to be determined by this analysis. Tropical ascent rates (Q) were obtained from published calculations [*Rosenlof*, 1995; *Eluszkiewicz et al.*, 1996]; chemical production and sinks for the species considered were calculated with a radiative transfer model [*Minschwaner et al.*, 1993] and a photochemical model [*Salawitch et al.*, 1994]; and long-term growth rates (γ) were derived from CMDL network data. Midlatitude mixing ratios were constrained from observations between 35° and 55° in both hemispheres. Tropical air was identified as the region equatorward of the sharp meridional gradient in the NO_y/O_3 ratio observed in the subtropics [*Murphy et al.*, 1993].

A qualitative impression of the isolation of the tropical ascent region can be gained by comparison of vertical profiles of tracer mixing ratios observed in the tropics to profiles calculated assuming unmixed ascent (unmixed profiles), i.e., solutions to Eq. (1) with $\tau_{in} = \infty$ (Figure 5.18). Observed profiles of the longer-lived species, N_2O and CFC-12, and also of CH_4 and NO_y (not shown) deviate noticeably from unmixed profiles, indicating mixing with photochemically aged midlatitude air. However, for CFC-113, CFC-11, and the shorter-lived species CH_3CCl_3, CCl_4, and halon-1211 (not shown), observed profiles fall within the uncertainty range of values calculated for unmixed ascent because their vertical profiles are controlled primarily by photochemical loss that dominates loss by mixing for these shorter-lived species.

Quantitative derivation of the rates of transport between the tropics and midlatitudes is best achieved by analyzing correlation diagrams of two species with disparate lifetimes [*Volk et al.*, 1996]. Differences in the slopes of correlations observed at midlatitudes and in the tropics provide a direct measure of exchange between the two regions if horizontal mixing is fast compared to photochemistry for one of the two species (but not both). As an example, for a given mixing ratio of N_2O, the shorter-lived species show lower abundances in the tropics than at midlatitudes because their loss processes are larger near ~20 km (Figure 5.19), whereas N_2O is not destroyed until the air reaches higher altitudes. Because the abundance of N_2O in the tropics is sensitive to isentropic mixing, however (Figure 5.18), the tropical correlations do not match the correlations calculated assuming unmixed ascent.

In order to derive the entrainment time (τ_{in}) from the correlation diagrams in Figure 5.19, we consider Eq. (1) for the tropical mixing ratios of two tracers X and Y:

$$\frac{\partial Y}{\partial X} = \frac{P_y - (\tau_y^{-1} + \gamma_y)Y - \tau_{in}^{-1}(Y - Y_{mid})}{P_x - (\tau_x^{-1} + \gamma_x)X - \tau_{in}^{-1}(X - X_{mid})} \qquad (2)$$

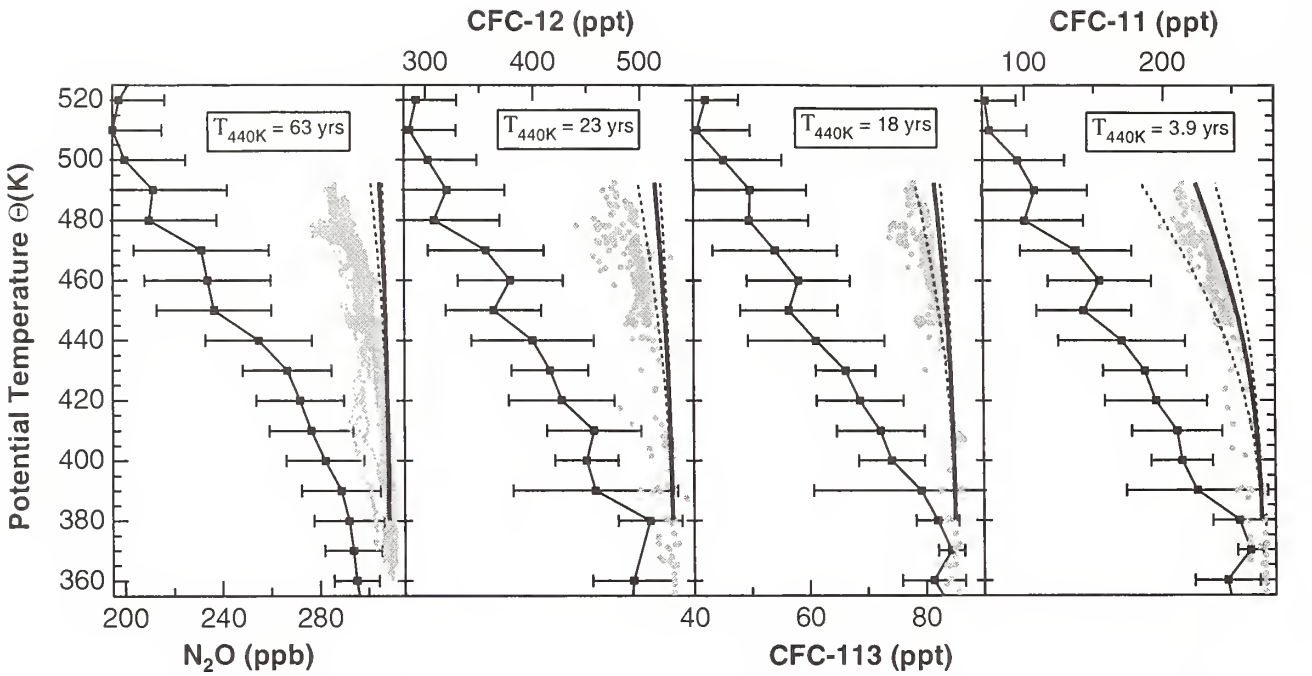

Fig. 5.18. Vertical profiles of mixing ratios of several long-lived trace species in the tropics (light filled circles) and at midlatitudes (dark filled squares) [*Volk et al.*, 1996]. For the midlatitudes the data was binned into 10K increments of potential temperature (θ); the profiles shown represent the bin averages and the error bars represent the standard deviation within each bin. Calculated tropical profiles are shown for unmixed ascent ($\tau_{in} = \infty$) (—) from θ = 380K (the mean tropical tropopause height) along with an uncertainty range induced by a 50% uncertainty in Q (---). Also indicated is the "effective lifetime" T ($=1/(\tau^{-1}+\gamma)$) at θ = 440 K (~19 km altitude) for each of the species.

Eq. (2), constrained by the mixing ratios for midlatitudes from observations and computed photochemical sources and sinks, is solved to calculate the tropical correlation Y(X) of two species; the entrainment time τ_{in} is treated as a free (altitude-independent) parameter. For each pair of tracers displayed in Figure 5.18, the value of τ_{in} is determined giving best agreement between the calculated tropical correlations (Figure 5.19) and the observations. The same procedure was also applied to correlation diagrams of the longer-lived species, CH_4, N_2O, CFC-12, CFC-113, and NO_y, versus O_3, which is shorter-lived (with a photochemical production time of only ~3.5 months at 19 km). Analysis of each correlation diagram yielded a mean for τ_{in} of 13.5 months, with an uncertainty of ~20%. This seasonally and vertically-averaged entrainment time is longer than the time scale for isentropic mixing at midlatitudes of less than 3 months [*Boering et al.*, 1995], confirming that mixing into the tropics is slow compared to mixing within midlatitudes. Because of the variability of the tropical correlations and the limited seasonal coverage, the data do not provide information on the dependence of τ_{in} with height.

Entrainment of air into the tropics is not necessarily balanced by poleward detrainment from the tropics. In the annual mean, the net mass flux out of the tropics (detrainment minus entrainment) must be balanced by the mean mass divergence within the tropics (that can be determined from the mean ascent rate):

$$\frac{\rho}{\tau_{out}} - \frac{\rho}{\tau_{in}} = -\frac{\partial}{\partial z}(\rho w) \qquad (3)$$

where τ_{out} is a time scale for export of air whose inverse is the detrainment rate; ρ is the air density; z is altitude; and w is the mean vertical velocity. Detrainment rates computed from Eq. (3) for the estimate of τ_{in} (13.5 months) and ascent velocities averaged over 24 months, show that over much of the altitude range considered, more air is exported from the tropics than is imported (Figure 5.20a). The corresponding detrainment time (τ_{out}) of less than ~6 months below 19 km and the morphology of decreasing detrainment with altitude is consistent with observations of the propagation of the seasonal cycles of CO_2 and H_2O from the tropics to midlatitudes [*Boering et al.*, 1995; *McCormick et al.*, 1993] and with studies of aerosol dispersal from the tropics [*Trepte and Hitchman*, 1992].

As shown in Figure 5.20b, for an entrainment time of 13.5 months, ~45% of air of extratropical origin accumulates in a tropical air parcel during its ~8 month ascent from the tropopause to 21 km. The large uncertainty range in this result (Figure 5.20b) results from the uncertainty of the ascent velocity. This substantial entrainment of midlatitude air into the tropical ascent region of the lower stratosphere implies that a significant fraction of NO_x (=NO + NO_2) and other effluents emitted

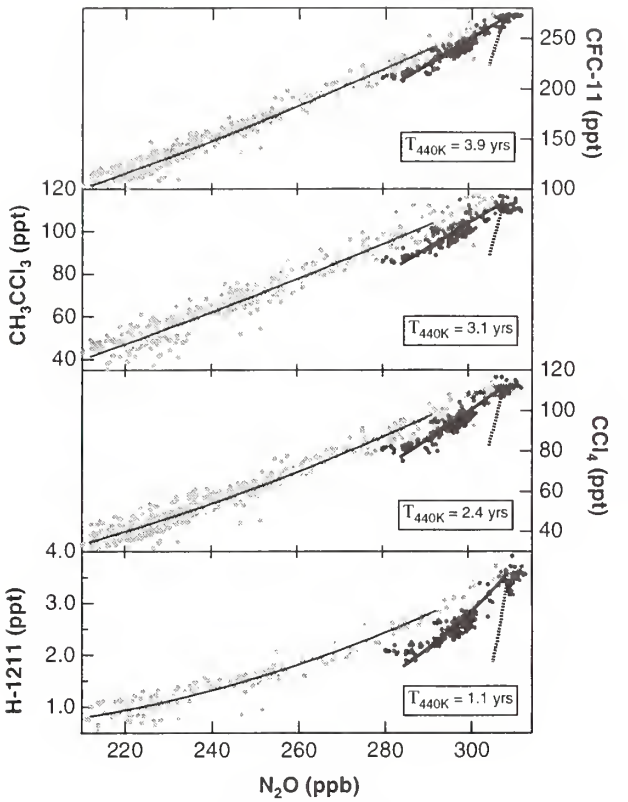

Fig 5.19. Correlations of mixing ratios for the shorter-lived species versus N_2O in the tropics (dark filled circles) and at midlatitudes (light filled circles) [Volk *et al.*, 1996]. Mean midlatitude correlations used in the model (long dash) were obtained from quadratic fits to the correlations. Calculated tropical correlations are shown for the unmixed case (τ_{in}= ∞) (short dash) and for a constant entrainment time τ_{in} that yielded the best agreement (in a least-squares sense) with the observed tropical correlations (long dash). Also indicated is the "effective lifetime" T (= $1/(\tau^{-1}+g)$) at θ = 440 K for each of the species.

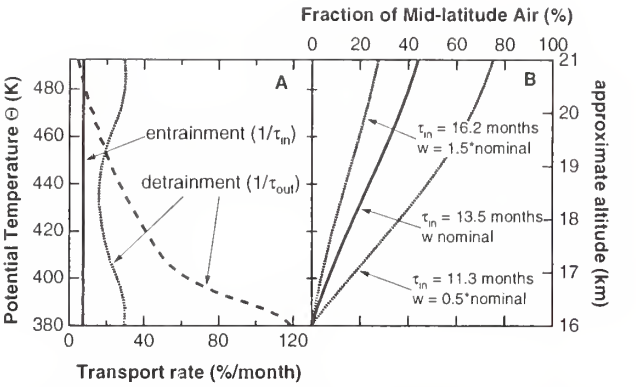

Fig 5.20. (a) Entrainment rate into and detrainment rates out of the tropics versus potential temperature, expressed as % of air within a tropical air volume (at a fixed altitude) entrained/detrained per month [*Volk et al.*, 1996]. Results are for τ_{in} =13.5 months and ascent rates from *Rosenlof* [1995] (short dash) and *Eluszkiewicz et al.* [1996] (dotted). The disagreement between the detrainment rates based on these two studies reflects differences in the vertical profiles of the ascent rates. (b) Fraction of midlatitude air within the tropics versus potential temperature for nominal (long dash) and extreme (dotted) values of τ_{in} and ascent rates w from *Rosenlof* [1995] as indicated.

from supersonic aircraft at midlatitudes between 16 and 23 km will likely reach the middle and upper stratosphere where enhancements in NO_x are expected to lead to reductions in ozone [*Stolarski et al.*, 1996].

While estimating the effects of human activity on ozone remains a task for multi-dimensional models of atmospheric transport and chemistry, the determination of the rates of transport and the fraction of midlatitude air within the tropical ascent region constitutes important tests for the accuracy of such models. Most current 2-D models do not reproduce steep meridional tracer gradients in the subtropics such as observed in the NO_y/O_3 ratio [*Murphy et al.*, 1993], suggesting they generally overestimate the magnitude of mixing between the tropics and midlatitudes. Tests with a particular two-dimensional model show that greater reductions of midlatitude ozone are calculated, improving agreement with observed trends, if mixing parameters are modified to simulate restricted exchange across the tropics [M.K.M. Ko, private communication, 1996]. Realistic representation of dynamical coupling between the tropical source and midlatitude sink regions of ozone may thus hold the key to understanding and reliably predicting the response of the stratospheric ozone layer to a variety of anthropogenic as well as natural perturbations.

5.2.3. Bromine Budget

Concern over bromine's contributions to stratospheric polar ozone loss [*McElroy et al.*, 1986] and potential for midlatitude ozone destruction [*Yung et al.*, 1980] has resulted in an international regulation of halons and methyl bromide. These bromine-containing compounds occur at much lower stratospheric mixing ratios than chlorine-containing compounds, but bromine is 40-100 times more efficient than chlorine at destroying ozone in the lower stratosphere [*WMO*, 1995]. In an effort to improve the understanding of brominated compounds in the stratosphere, the first real-time, in situ stratospheric measurements of the purely anthropogenic compound, $CBrClF_2$ (H-1211) [*Elkins et al.*, 1996] were obtained. Measurements of H-1211 and nine additional tracers were obtained in 1994 at latitudes ranging from 70°S to 60°N and to altitudes of 20 km as part of the ASHOE/MAESA mission. The complete H-1211 data set for ASHOE/MAESA is shown in Figure 5.21. These measurements were incorporated into a calculation of the total 1994 stratospheric bromine burden. The lower stratosphere was calculated to contain 17 ± 3 ppt of bromine in 1994 and that essentially all of the organic bromine had been converted to inorganic forms.

The total stratospheric bromine burden was calculated by summing the bromine content in the tropospheric organic bromine species with lifetimes long enough to allow their transport to the stratosphere. This approach assumed that the only source of stratospheric bromine is at the earth's surface. The organic bromine species included in the model are CH_3Br, H-1211, H-1301, CH_2Br_2, H-2402, and CH_2BrCl with November 1994 mixing ratios of 10.1, 3.3, 2.3, 1.1, 0.47, and 0.14 ppt respectively. The CMDL background site monitoring program provided a historical record of H-1211, H-1301, H-2402, and CH_2Br_2. The CH_3Br data were collected on transects of the Atlantic and Pacific Oceans in 1994 by CMDL researchers

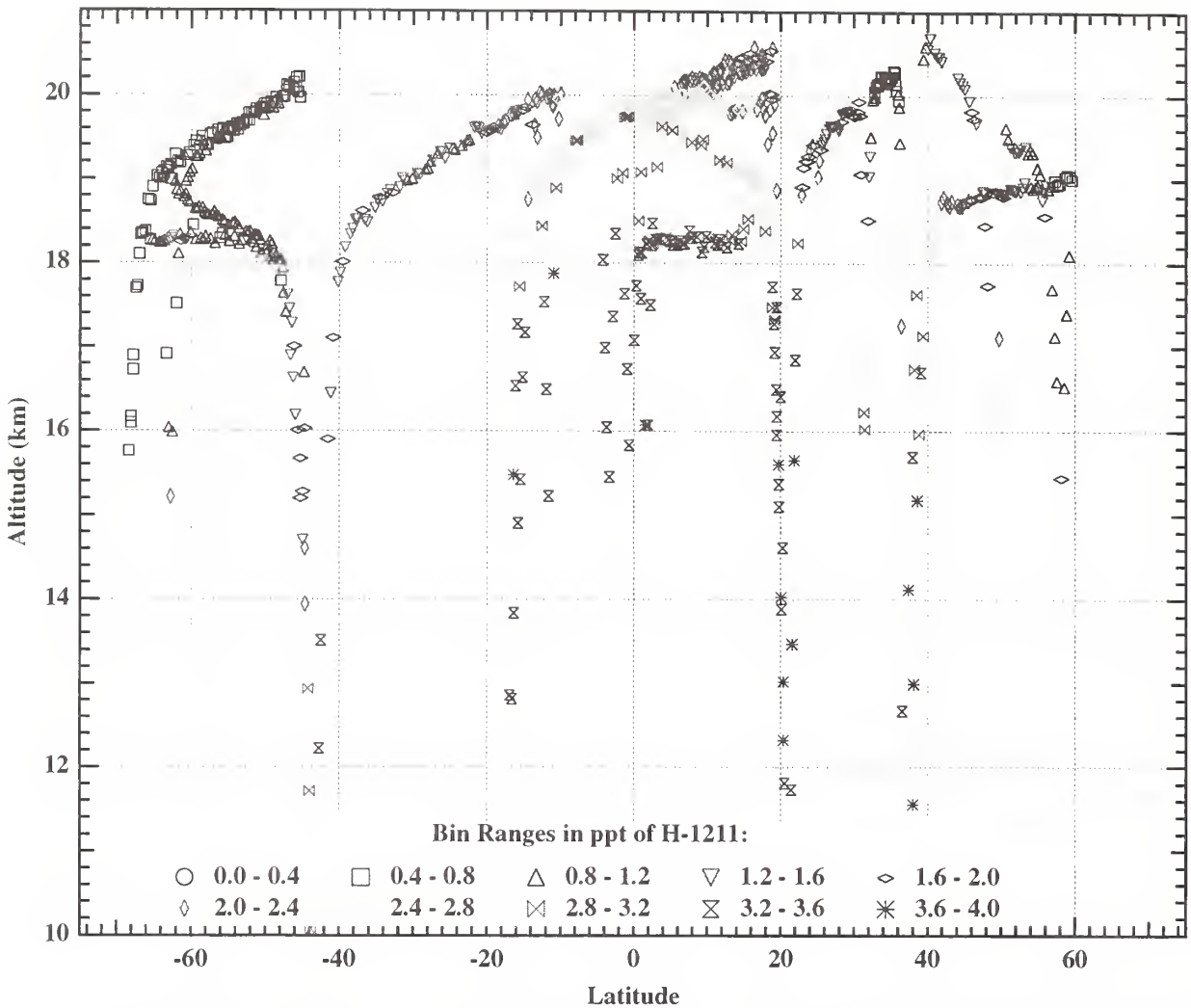

Fig. 5.21. Latitudinal profile of halon-1211 as a function of pressure (mb). ACATS-IV measurements of halon-1211 in ppt during ASHOE/MAESA.

[*Lobert et al.*, 1995]. The CH_2BrCl data are from Whole Air Sampler (WAS) measurements taken by researchers at NCAR in early 1995. Taking the weighted sum of the mixing ratios of these species yields the following equation for the total bromine contained in these species as a function of time.

$$\begin{aligned} &\text{Tropospheric } [CBr_y](t) = \\ &[CH_3Br] + [\text{H-1211}](t) + \\ &[\text{H-1301}](t) + 2[CH_2Br_2] + \\ &2[\text{H-2402}](t) + [CH_2BrCl] = \\ &8.64 + (0.2863t) + (-0.0235\ t^2) \end{aligned} \qquad (4)$$

where t is time in years measured from 1994. The tropospheric burden of these species provides an upper limit on the concurrent stratospheric bromine burden. ACATS-IV ASHOE/MAESA measurements of the sulfur hexafluoride (SF_6) mixing ratios are used to determine the age of the stratospheric air and thus, the total bromine present in the air being sampled.

Photolysis of the organic bromine species produces inorganic bromine species with the majority of the inorganic bromine in reactive forms. The partitioning of stratospheric bromine was calculated using the equation

$$\text{Total Bromine} = \text{Organic Bromine} + \text{Inorganic Bromine} \qquad (5)$$

where Total Br is determined as outlined previously. The only organic bromine species that ACATS-IV measured is H-1211, but from whole air sampler measurements from NCAR (Schauffler, private communication, 1996) and the University of California, Irvine (Blake, private communication, 1996), correlations were compiled of the unmeasured species with measured CFCs. These correlations are shown in Figure 5.22. These correlations permit an estimate of total organic bromine (Figure 5.23).

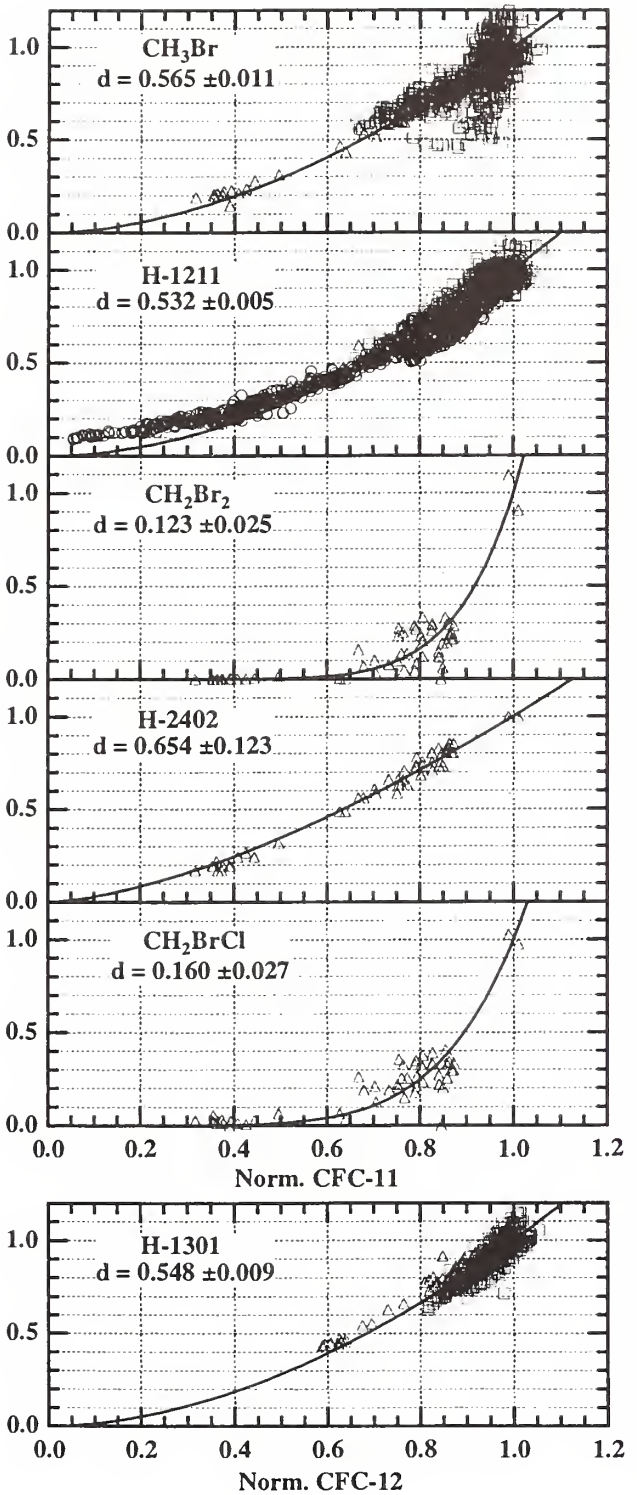

Fig. 5.22. Correlations of bromine-containing species with CFC-11. The longest-lived species, H-1301, is correlated with CFC-12. Each data set was normalized individually and then the complete data set for each species was fit with a function of the form $[X_n] = [CFC_n]^{(1/d)}$, where the subscript, n, represents a normalized quantity. The longest lived species, H-1301, is correlated with CFC-12. ACATS-IV data are shown by circles. NCAR data are denoted by triangles and UC-Irvine data are shown by squares.

The oldest air sampled by ACATS-IV during ASHOE/MAESA indicated that all of the stratospheric bromine was in inorganic forms.

5.3. LACE

A new project titled Lightweight Airborne Chromatograph Experiment (LACE) is a 2-channel GC designed to measure CFC-11, CFC-113, and SF_6. It was built to fly on a balloon and take data from altitudes up to 32 km. This will complement the lower altitude NASA ER-2 data, help solidify understanding of atmospheric dynamics, and provide a comparison for midlatitude and tropics chemistry. NOAH scientists used the ACATS-IV instrument as a starting point; however, several key differences have been introduced. The balloon's fast decent of 2.5 m s^{-1} imposes a faster data sample rate of 1 minute to acquire reasonable coverage of data every 150 m. Sample rates for the ACATS-IV instrument are currently 3 and 6 minutes with the exception of one recent flight where the new 1-minute chromatography (Figure 5.24) was successfully flown. Because of the higher altitude, clean air samples must be loaded from an ambient pressure of only 10 mb compared to an ambient pressure of 50 mb or higher for the ACATS instrument. Finally, in contrast to the ER-2's Q-bay, which is pressurized to a minimum of 300 mb and houses the ACATS instrument, the balloon platform required a self-pressurized, lighter-weight instrument that uses less power.

Problems solved in building this GC for a balloon platform were similar to those that will occur when placing an instrument in a remotely piloted aircraft (RPA) like Perseus. When an operational RPA becomes available, LACE can be easily modified for flight on this type of platform.

5.4. Ocean Project: BLAST Cruises

In 1994 the NOAH Group participated in two research cruises for the Bromine Latitudinal Air/Sea Transect (BLAST) project. The first cruise extended through the East Pacific between Seattle, Washington, and Punta Arenas, Chile, from January 26 to February 17, 1994; the second cruise was conducted between October 18 and November 21, 1994, heading through the Atlantic Ocean from Bremerhaven, Germany, to Punta Arenas, Chile (Figure 5.25). The main objective of these cruises was to gather data to ascertain the presence or absence of a potential oceanic source for methyl bromide (CH_3Br). Methyl bromide contributes about 50% to tropospheric organic bromine and, hence, has received considerable attention, particularly because its budget is currently not well understood [*Butler*, 1995, 1996; *Butler and Rodriguez*, 1996]. Frequently collected CH_3Br data from the two expeditions constitute the largest data set for oceanic CH_3Br to date and the first solid estimate of oceanic emission, production, and chemical degradation of the compound. It is concluded from these studies that the ocean is not a net source of CH_3Br but rather a net sink [*Lobert et al.*, 1995, 1996; *Butler et al.*, 1995]. Although CH_3Br is both produced and consumed everywhere in the surface ocean [*Butler*, 1994], the rate of consumption exceeds that of production in most waters sampled. Exceptions were coastal and coastally-influenced waters,

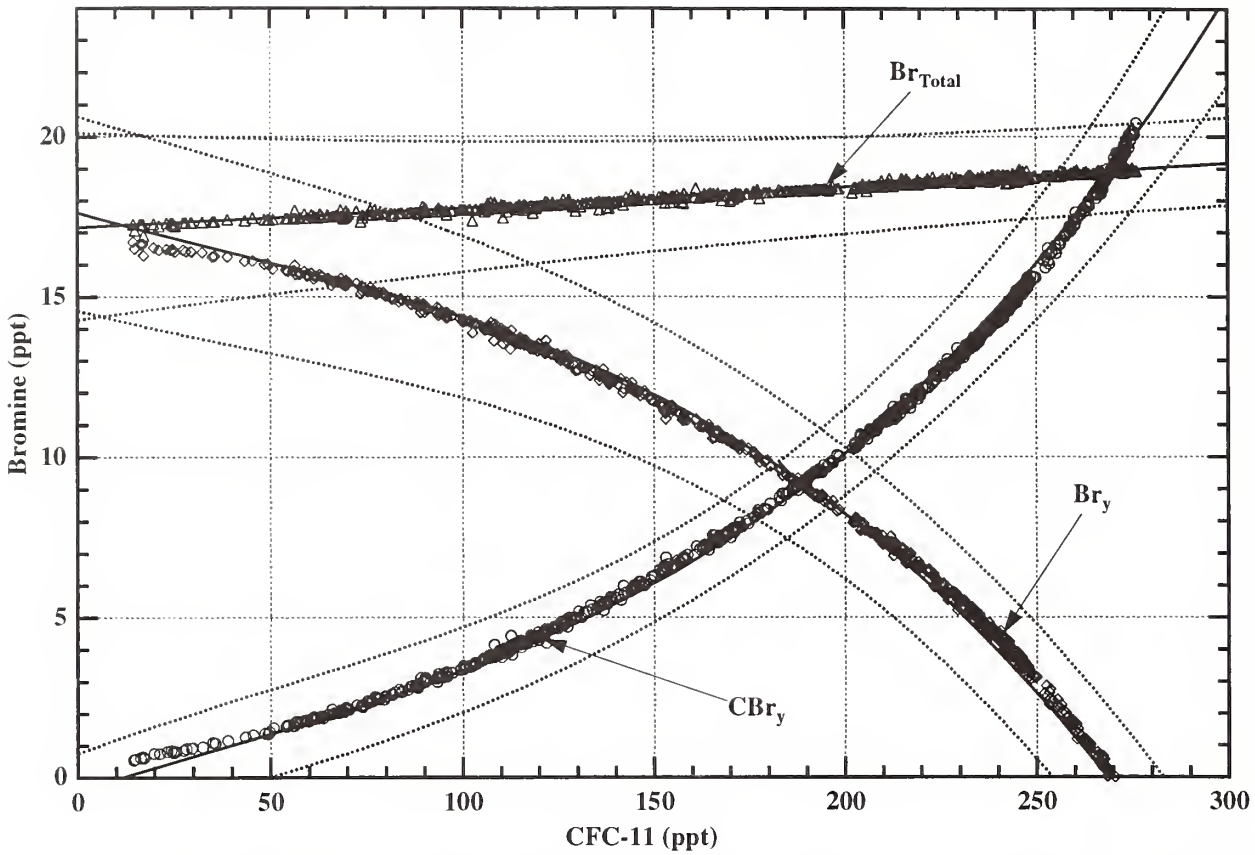

Fig. 5.23. Calculated results for the total stratospheric bromine, Br_{total}, (open triangles), and its partitioning into total organic CBr_y (open circles), and inorganic, Br_y (open diamonds), components. The dashed lines represent standard deviation windows.

which were typically supersaturated, and areas of open ocean upwelling, where CH_3Br saturation anomalies were close to zero. About 80% of the oceans are undersaturated in CH_3Br, representing a net annual sink of 8-22 Gg yr^{-1}.

CH_3Br data from the second cruise further supported NOAH conclusions from the first expedition. The latter results give greater strength to the global extrapolations of the first data set. Data from the two cruises are summarized in Table 5.5 and Figure 5.26.

The best estimate of the partial lifetime of atmospheric CH_3Br with respect to oceanic losses is 2.7 (2.4-6.5) years. This range was derived from a 40-year, global data set of sea surface temperatures and wind speeds [*Yvon and Butler*, 1996] (Figure 5.27). Data from the two expeditions suggested a shorter lifetime of CH_3Br of about 2.4 years. The difference between the two estimates is due to higher than average wind speeds encountered during the cruises. The estimated atmospheric lifetime, based upon combined atmospheric, soil, and oceanic losses, is now 0.8 years compared to earlier estimates of 1.8-2.1 years when the ocean was considered an insignificant sink, the soil sink [*Shorter et al.*, 1995] was unknown, and tropospheric OH concentrations were underestimated by 15% [*Prinn et al.*, 1995]. The oceanic sink correspondingly lowers ozone depletion potential estimates for CH_3Br by about one-third from earlier estimates.

TABLE 5.5. Results for Atmospheric and Oceanic CH_3Br From BLAST I and BLAST II Cruises

	BLAST I	BLAST II	Combined Estimate
Global mean (ppt)	9.8	10.4	10.1
NH mean (ppt)	11.2	11.7	11.5
SH mean (ppt)	8.6	9.4	9.0
Variability (ppt)	0.6	1.2	
ITCZ (°N)	4.1	6.4	
IHD (ppt)	2.65	2.31	2.48
NH/SH ratio	1.31	1.25	1.28
SA (%)	-15.7	-19.7	-18.4
P (Gg yr^{-1})	175	248	214
L (Gg yr^{-1}	-188	-267	-229
Net Flux (Gg yr^{-1})	-13.0	-18.7	-14.8

Measured global, northern hemispheric, and southern hemispheric means (NH and SH) and the observed interhemispheric tropical convergence zone (ITCZ), which was used to determine the hemispheric ratios. The net saturation anomaly (SA), the hemispheric ratios, and the interhemispheric difference (IHD) were calculated from the measurements. Finally, estimates of the oceanic production (P), oceanic loss (L), and the net oceanic flux of CH_3Br were added. The net satura-tion anomaly is the percent departure of CH_3Br in the surface ocean from equilibrium with the atmosphere. Negative numbers indicate fluxes from the atmosphere to the ocean. Variability is the residual standard deviation of a loess fit through all atmospheric measurements.

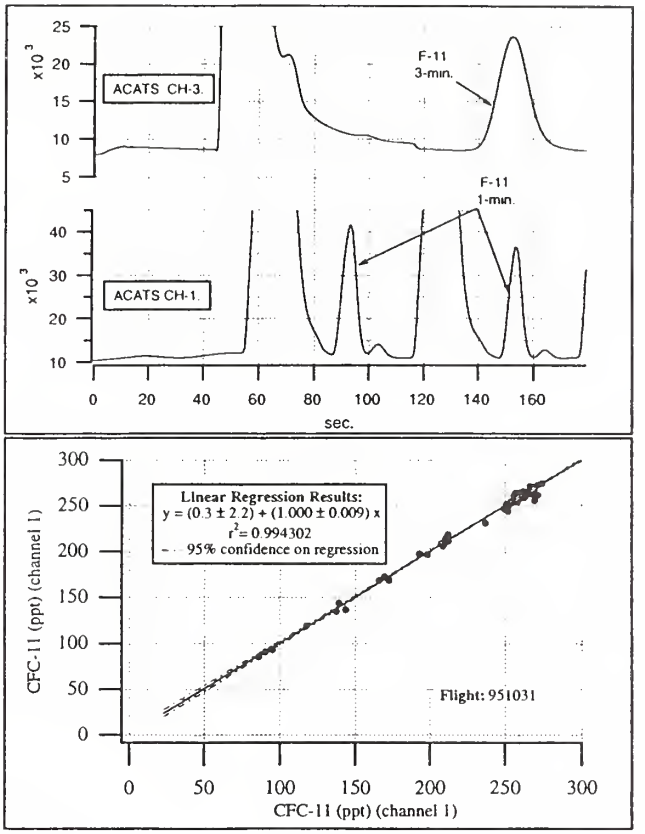

Fig. 5.24. Simultaneous 1- and 3-minute chromatograms and a correlation plot of the 1-minute CFC-11 versus the 3-minute CFC-11 data for this flight.

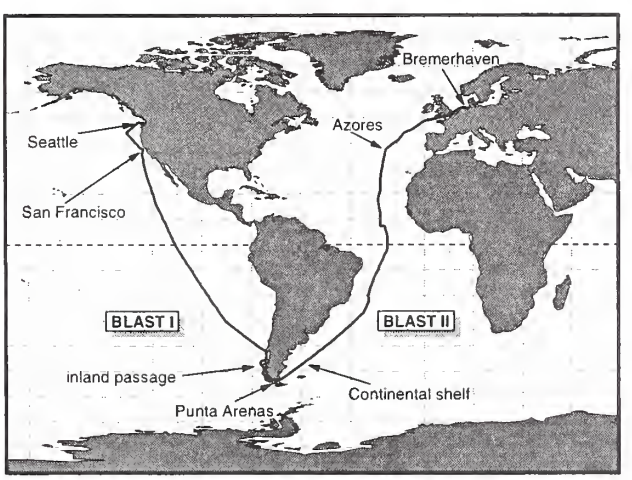

Fig. 5.25. Cruise tracks of both ocean missions. The cruises covered a diverse mixture of coastal waters, upwelling regions, large open ocean areas, and coastally influenced areas in the East Pacific and Atlantic oceans.

Concentrations of CFC-12, CH_3Br, and CH_3Cl in water column samples collected during BLAST II were higher within the mixed layer than at depth. Considering that oceanic CFC-12 originates from the atmosphere, this suggests that both CH_3Br and CH_3Cl have sources associated with the atmosphere or surface waters. Departures of CH_3Br and CH_3Cl concentrations from those of CFC-12 may result from chemical or biological in situ production or degradation of these gases.

Potential artifacts associated with sampling and analysis of CH_3Br and other compounds were investigated. These studies revealed significant problems associated with the measurement of CH_3Br from air stored in stainless steel flasks that have historically been used for measuring CH_3Br in the atmosphere. From a comparison between measurements made shipboard and from air stored in flasks, and from the reanalysis of air in flasks over time, it has been determined that CH_3Br in stainless steel flasks can be unstable and may increase or decrease with time. In addition, results for CH_3Br determined by GC-ECD can be compromised by some GC configurations [*Montzka et al.*, 1995a; *Lobert et al.*, 1996].

Besides CH_3Br, a suite of CFCs and methyl halides was measured during the cruises, and data for oceanic methyl chloride (CH_3Cl), methyl iodide (CH_3I), dibromomethane (CH_2Br_2), and bromoform ($CHBr_3$) are currently being finalized for publication.

5.5. STEALTH Project: Automated Four-Channel Field Gas Chromatographs

5.5.1. Overview

The STEALTH GC was installed at ALT, HFM, ITN, and LEF with different custom configurations for each client. The four-channel STEALTH GC will replace the old HP5920 GCs at the Radiatively Important Trace Species (RITS) stations (BRW, NWR, MLO, SMO, and SPO) and is currently being constructed and laboratory tested.

The data acquisition software and operating system of the STEALTH GC computer is being upgraded. NOAH is currently cooperating with personnel at Harvard University in the development of new data acquisition software for the PC-based UNIX operating system, QNX. QNX is a multitasking and multi-user operating system that will facilitate data acquisition, data retrieval, data archival, and real-time display. The airborne GC, ACATS-IV, is currently being configured to test the QNX data acquisition software. In 1996, NOAH scientists will implement the software on an ACATS-IV deployment and on the new STEALTH station GCs.

The STEALTH GC is an ECD/GC system based on technology developed on ACATS-IV and LACE. The first channel encompasses a Shimadzu mini-2E ECD and a Porapak Q packed column (Figure 5.28). This channel allows for the measurement of N_2O and SF_6. Channel two of the instrument uses a Valco ECD along with a Unibeads 2S packed column. This configuration is capable of measuring N_2O, CFC-12, H-1211, CFC-11, and CFC-113. The third channel also uses a Valco ECD and an OV-101 packed column and is used to measure CFC-11, CFC-113, $CHCl_3$, CH_3CCl_3, CCl_4, and C_2Cl_4 (perchloro-

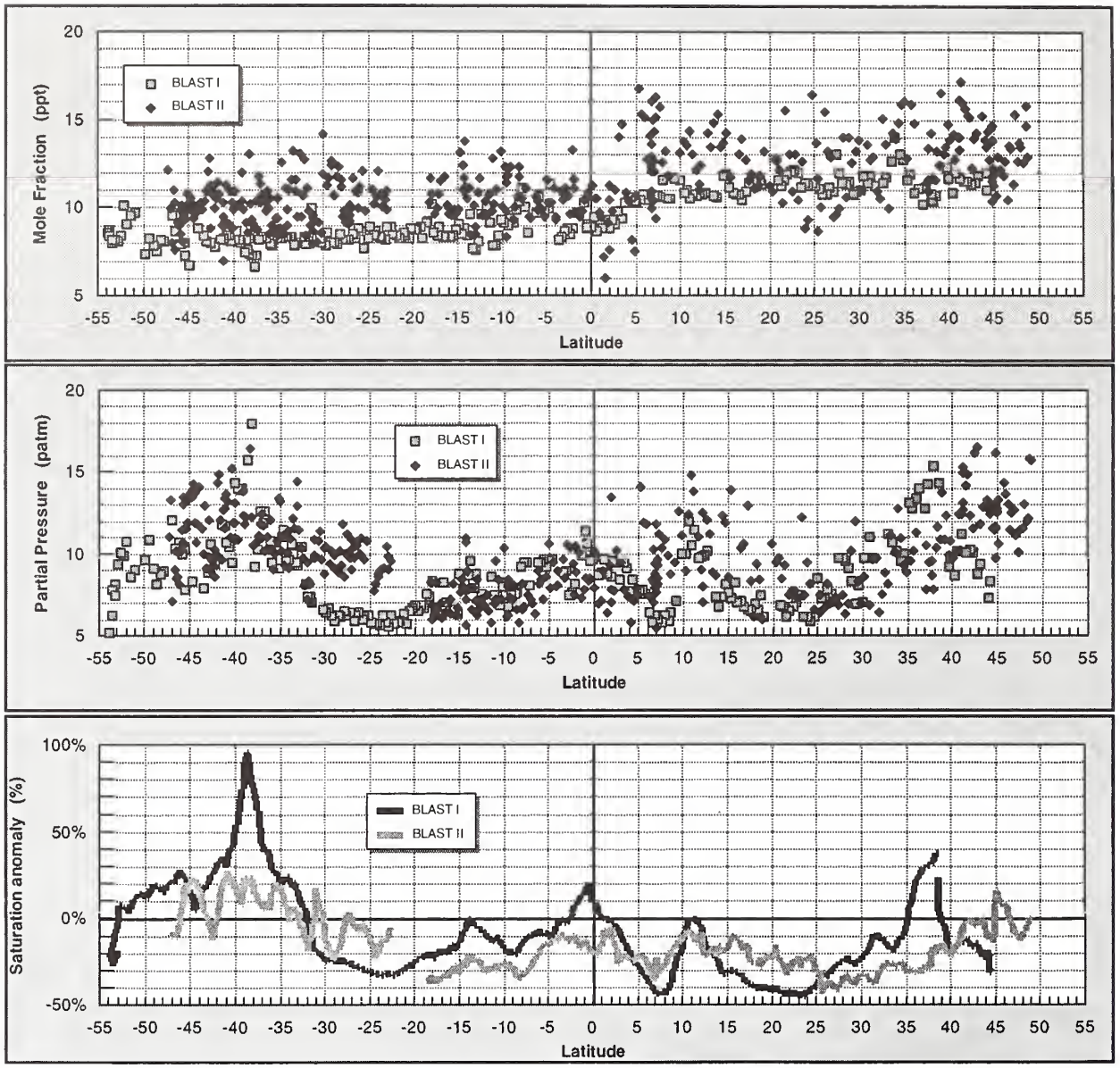

Fig, 5.26 Atmospheric CH_3Br, its partial pressure in the surface water, and the net saturation anomalies for both cruises.

ethylene, PCE). All of the aforementioned channels have been proven in other similar instruments that have been constructed and deployed to various sites.

Channel four, however, has just recently been developed and uses quite a different setup than the other three channels. This channel also uses a Valco ECD, but incorporates a GS Q capillary column rather than a packed column. This channel also uses a Neslab cryocooler which allows for the preconcentration trapping of the three trace gasses, HCFC-22, CH_3Cl, and CH_3Br being measured. With the current configuration of this channel, one is capable of measurements of better than 1% for HCFC-22, 0.5% for CH_3Cl, and 2% for CH_3Br. Figure 5.28d is a chromatogram of the newly developed fourth channel.

5.5.2. Tower GC at WITN in Cooperation with CCG

The GC and instruments that monitor CO_2 and ^{222}Rn are housed in a building adjacent to a tall tower (WITN) in rural North Carolina. Diaphragm pumps located in the building continuously draw air from 51, 123, and 496 m above ground through 1 cm i.d. Dekabon tubing affixed to the tower. Detailed descriptions of sample handling and drying, and initial results of CO_2 measurements at WITN were published [*Bakwin et al.*, 1995]. GC analyses of air from each sampling level and of two calibrated whole-air standards are performed hourly. Standards are stored at high pressure in "Aculife"-treated aluminum cylinders.

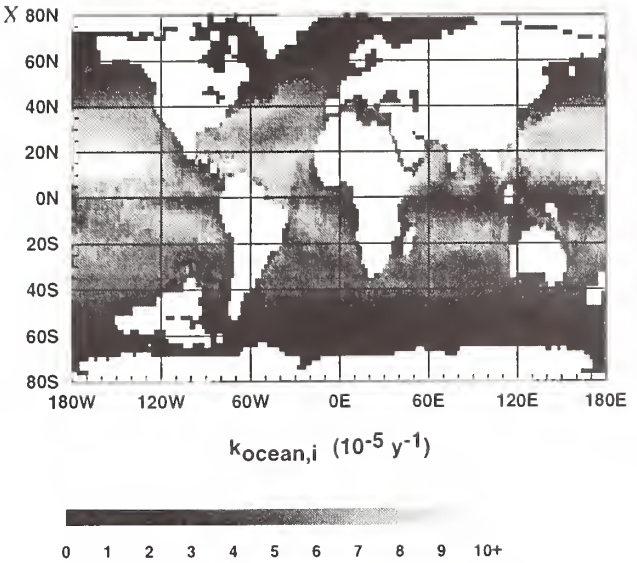

Fig. 5.27. Map of the global distribution of the rate constant ($k_{ocean,\ i}$) for the irreversible uptake of atmospheric methyl bromide (CH_3Br) by the ocean ($k_{ocean,\ i} = 1/\tau_{ocean,\ i}$; global τ_o = 2.7 years). This rate constant is computed with data from COADS for each cell on a 2° × 2° grid. Note that higher loss rates are found in the northern hemisphere in regions containing both high wind speeds and warm SST's.

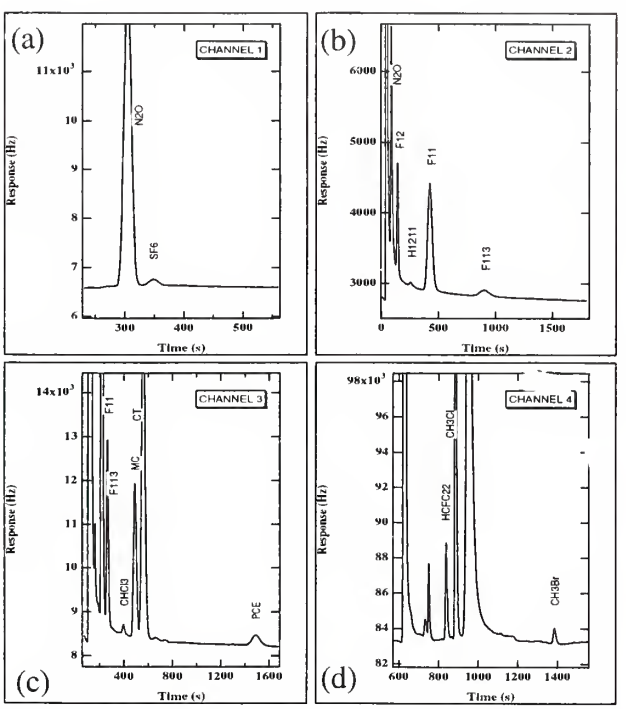

Fig. 5.28. Chromatograms of all four channels of the STEALTH GC that will replace the old RITS HP5890 GCs.

Chromatographic and housekeeping data are logged by a 486SX PC and archived on 1.2 Gb optical disks that are sent to the NOAH laboratory each week for analysis. Instruments and gas supplies are maintained by a technician who visits the site weekly .

Monthly statistics of mixing ratios for several halocompounds and N_2O at the WITN tower are presented in Figure 5.29. Statistics for each sampling height (51, 123, and 496 m) are denoted by 1, 2, and 3, respectively, along the bottom of each plot . For each month, the mean (circle) and standard deviation (distance between circle and asterisk) of the mixing ratios of each species generally decrease with increasing sample height. Variability in trace gas mixing ratios within the continental boundary layer is determined by sources, sinks, boundary layer dynamics, and horizontal transport. Since each species plotted in Figure 5.29 has solely ground-based sources, it is expected that mixing ratios and variability should be greatest near the ground. This effect is inflated at night by the accumulation of emissions from local, ground-based sources in the shallow nocturnal stable layer.

Figure 5.30 gives statistics for the 51-496 m mixing ratio gradients, binned by hour of day, of N_2O, CH_3CCl_3, and SF_6 for November 1995. Significant vertical gradients of N_2O and CH_3CCl_3 were observed at night, indicating these compounds were emitted by local, ground-based sources. In contrast, the insignificant accumulation of SF_6 in the nocturnal stable layer suggests an absence of local, ground-based sources. During the late morning and afternoon, convection rapidly mixes air from the ground to >500 m, and vertical gradients approach zero.

In studying regional emissions of trace gases, it is critical that the influences of local sources are minimized. At WITN, the boundary layer height during the night is typically <500 m. Hence, mixing ratio variability at 496 m during the nighttime is primarily driven by horizontal transport of polluted air to the site, and mixing ratios of long-lived species should reflect regional-scale emissions. Figure 5.31 shows the correlation of CH_3CCl_3 and C_2Cl_4 mixing ratios at 496 m between 2200-0900 EST during November 1995. An orthogonal distance regression through the data yields a slope of 0.62, which can be taken as the regional emission ratio of these two compounds. Using accurate (±5%) estimates of North American emissions of C_2Cl_4 [*McCulloch and Midgely*, 1996], CH_3CCl_3 emissions can be calculated. Using this methodology, emissions of halocompounds, especially those whose production and emissions are controlled by the Montreal Protocol, are monitored.

5.6. Measurement of Air From South Pole Firn

As part of a cooperative venture with scientists from the University of Rhode Island, Pennsylvania State University, and CCG, NOAH analyzed the contents of flasks filled with firn air from the SPO in early 1995 [*Battle et al.*, 1996].

The sampling system was designed so that large quantities of air could be pulled from discrete depths in the firn down to the firn-ice transition depth of 122 m. Because it was possible to obtain large amounts of air, flasks could be flushed adequately and filled for nearly routine air analyses in Boulder and elsewhere. Air at the bottom of the firn had a CO_2 age of about 100 years [*Battle et al.*, 1996].

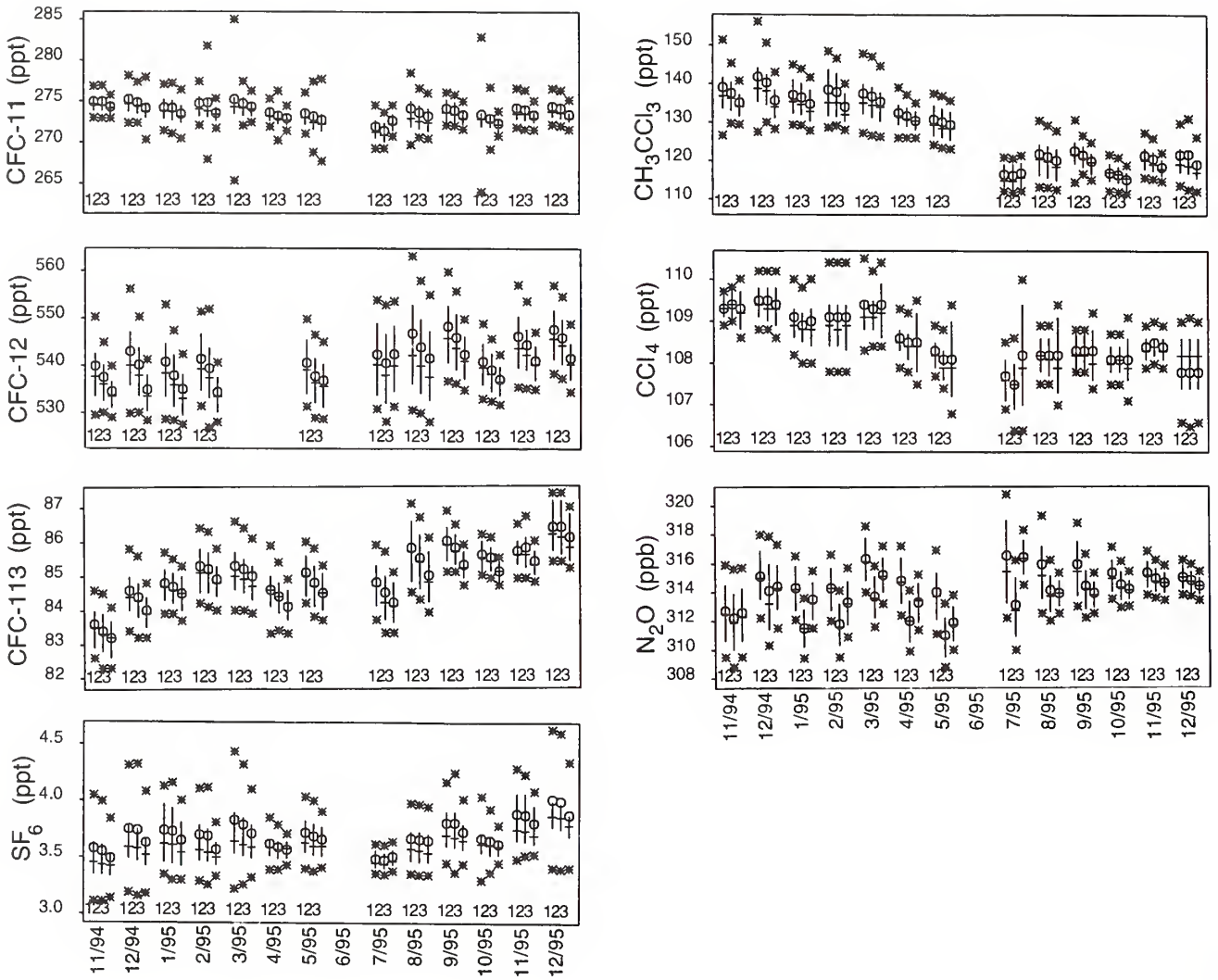

Fig. 5.29. Monthly statistics of CFC-11, CFC-12, CFC-113, methyl chloroform, carbon tetrachloride, nitrous oxide, and sulfur hexafluoride mixing ratios at the WITN tower. Crosses represent medians (horizontal bars) and interquartile range (vertical bars). Circles and asterisks are means and means ±1 standard deviation, respectively. The numbers across the bottom of each plot are the sampling level (1, 2, and 3 refer to 51, 123, and 496 m, respectively).

N_2O in these samples analyzed by NOAH forms a bridge between ice-core data, which typically are much less precise owing to sample handling procedures and small samples, and real-time, present-day measurements (Figure 5.32). These results suggest that preindustrial levels of N_2O in the atmosphere had to be about 280 ppb and that N_2O was increasing steadily through the latter part of the 20th century. The growth rate of atmospheric N_2O from 1904 through 1958 was 0.06 ± 0.01% yr^{-1} (95% confidence level); thereafter, it has increased at a rate of 0.22 ± 0.02% yr^{-1} (95% C.L.). N_2O covaried well with CO_2 throughout the profile, although the smoothness of the fit could be attributable to subsurface diffusion of the gases. Nevertheless, the overall trend of N_2O as a function of CO_2 was 0.50 ± 0.03 ppb N_2O ppm^{-1} CO_2^{-1} (95% confidence level, $r^2 = 0.98$).

Surprisingly these flasks, which were sealed with Teflon o-rings, did not cause significant contamination of most halocarbons. Consequently, depth profiles were obtained of CFCs, chlorocarbons, and bromocarbons representing air as far back as the late 19th century. (Dates assigned to halocarbons will be older than CO_2 in the same bolus of air owing to their slower rates of diffusion.) As shown in Figure 5.33, which is a close-up of the lower portion of the CFC-11 profile, the sampling and analytical precisions are on the order of tenths of a ppt. Small amounts of contamination are suggested in that the lowest values were still 2 ppt (<1% of today's atmosphere) and that two pairs of flasks showed higher levels of CFC-11 in some of the deepest firn. This latter contamination was probably caused by stress on the pump near the firn-ice transition zone where less air was available to pull, thus increasing

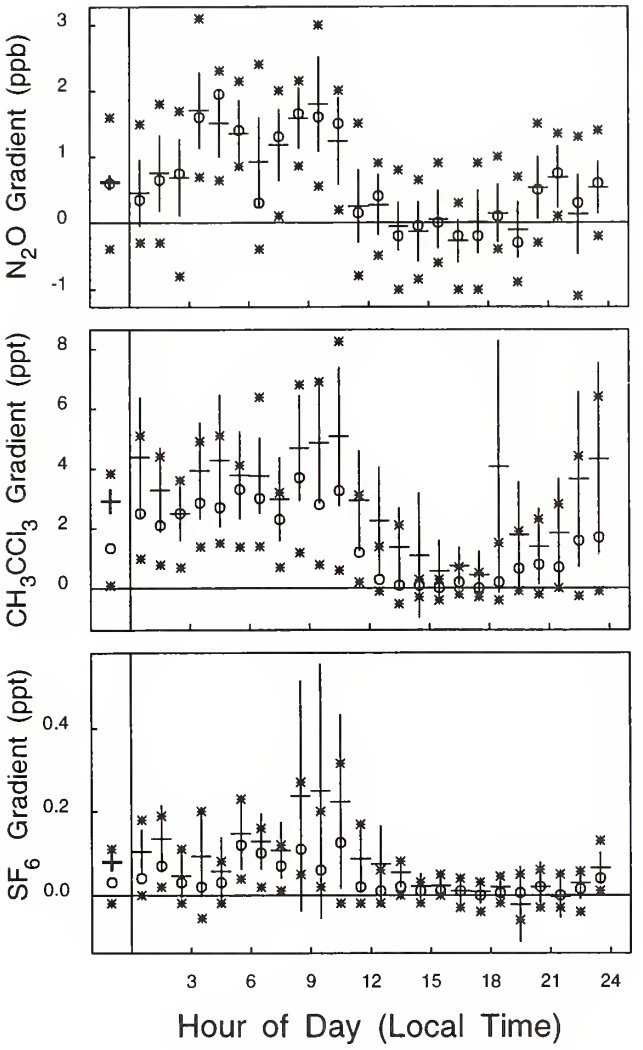

Fig. 5.30. Statistics of 51 m - 496 m mixing ratio gradients for N_2O, CH_3CCl_3, and SF_6, binned by hour, for November 1995. Crosses indicate means (horizontal bars) ± the 95% confidence interval (vertical bars). Circles represent medians, and asterisks indicate upper and lower quartiles. The left panel gives statistics of 51 m - 496 m gradients for the entire month.

the probability of sucking in unrepresentative air. This feature showed up in all of the gases, further suggesting contamination with modern air. Nevertheless, this level of contamination is not representative of the rest of the profile. Thus, we were able to obtain precise, but probably accurate, measurements at sub-ppt levels throughout most of the profile.

These results yield entire atmospheric histories for CFCs, halons, and other halocarbons of purely anthropogenic origin (Figures 5.33 through 5.37). They also showed atmospheric trends for gases of both natural and anthropogenic origin, such as CH_3Br, during a time when the human population, its agricultural output, and its industrial activity increased dramatically. These data demonstrate that natural sources of CFCs and halons are minimal at best and most likely nonexistent. Models of

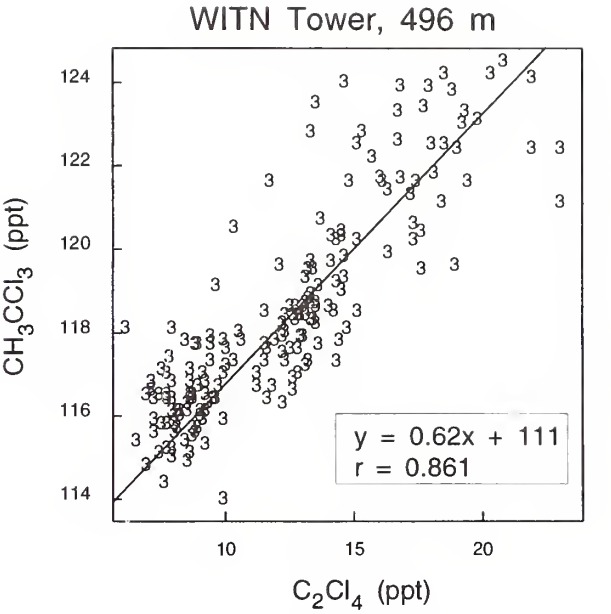

Fig. 5.31. Correlation between CH_3CCl_3 and C_2Cl_4 mixing ratios at 496 m between 2200 and 0900 (EST) during November 1995. The slope of an orthogonal distance regression (0.62) is taken as the regional emission ratio of these two compounds.

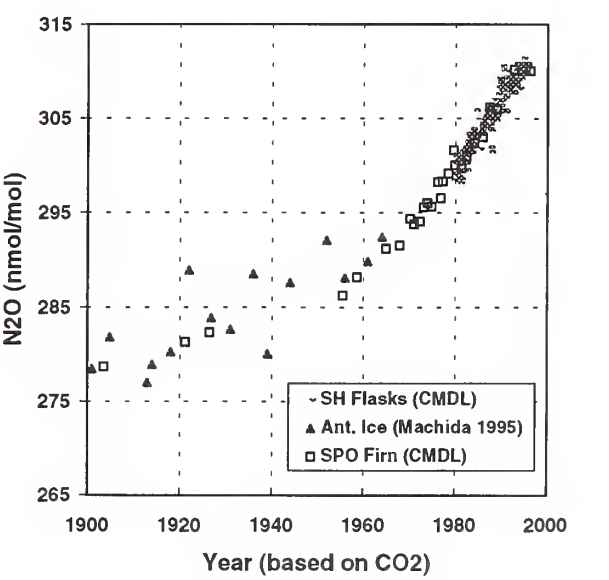

Fig. 5.32. History of atmospheric N_2O over the past century, derived from antarctic ice-core measurements [*Machida et al.*, 1995], real-time air measurements in the southern hemisphere (NOAH), and analyses of South Pole firn air (NOAH). Firn air ages are determined from correlation of CO_2 in the samples with the atmospheric CO_2 history of *Etheridge et al.* [1996]. Diffusivities of N_2O and CO_2 are assumed to be identical and ice core data of *Machida et al.* [1995] have been lowered by 1 ppb to conform to the CMDL scale.

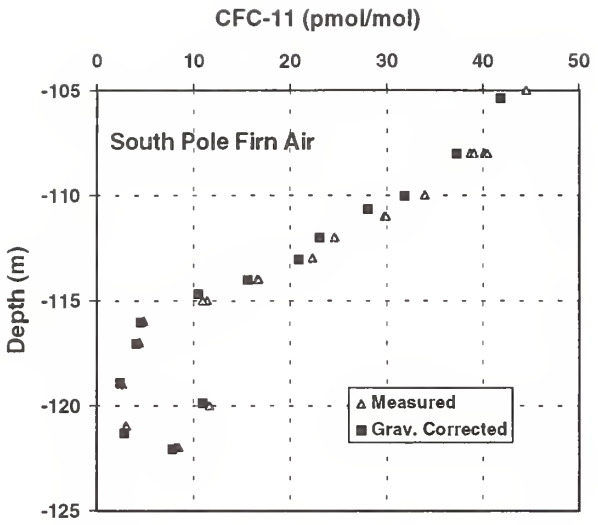

Fig. 5.33. CFC-11 in the lower portion of the firn at the South Pole. The high degree of precision is shown in the actual measurements (triangles), where two flasks were collected at each depth and plotted separately. Only at 108 m depth are these symbols distinguishable and there only because two pairs of flasks from this depth in two separate holes were analyzed. Flasks at 120 and 122 m were subjected to some contamination with modern air during sampling, probably owing to stress on the pump as the firn layers began to turn to ice. Also shown here is the effect of the gravitational correction for settling of CFC-11, which is a gas heavier than air. Again, the error is small.

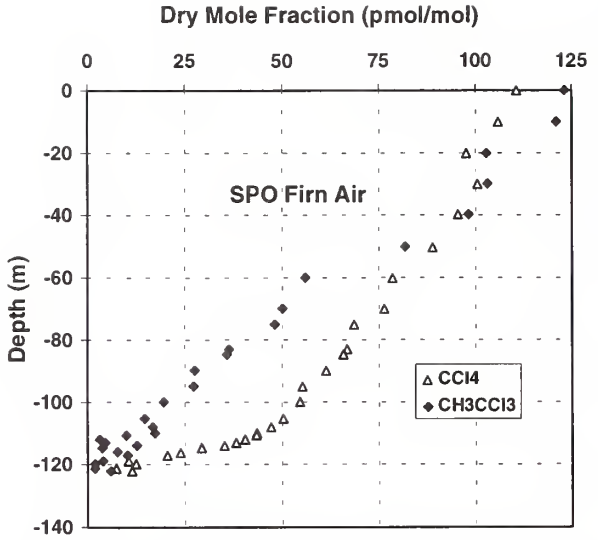

Fig. 5.35. Depth profiles of CCl_4 and CH_3CCl_3 in South Pole firn. There is some evidence of contamination of a few ppt in the CH_3CCl_3 data, although mole fractions of this compound came very close to zero near the bottom of the profile. Mole fractions of CCl_4 never fell below 10 ppt, suggesting either significant, specific contamination of this compound, a very early history of significant anthropogenic release, or a natural source.

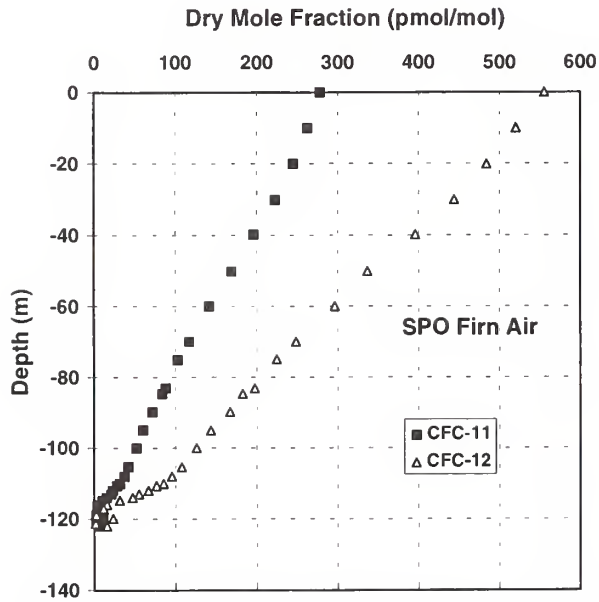

Fig. 5.34. Depth profiles of CFC -11 and -12 in South Pole firn air. Mole fractions of both gases near the bottom of the firn are less than 1% of the present day values, suggesting that natural sources are minimal or non-existent.

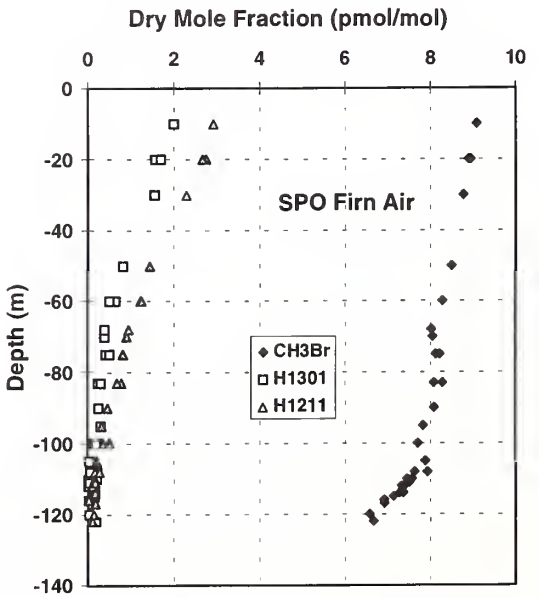

Fig. 5.36. Brominated gases in South Pole firn air. The anthropogenic halon mole fractions both drop to zero early in the profile. These gases were not introduced into the atmosphere in significant amounts until the 1970s. CH_3Br is about 6.5 ppt in air nominally dating back to about 1880.

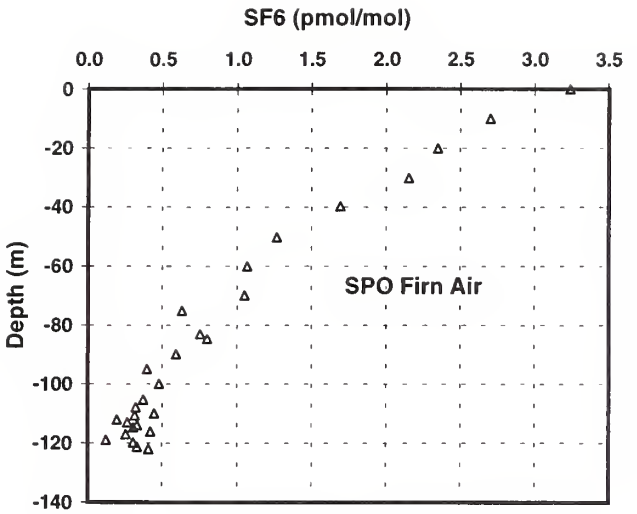

Fig. 5.37. SF_6 in South Pole firn air. Because of its small analytical peak on the GC, the detection limit for SF_6 in real air is around a few tenths of a ppt. Like the halons, this gas was not introduced into the atmosphere until the 1970s [*Maiss et al.*, 1996].

anthropogenic CFC emissions are supported by these findings, confirming the predominance of anthropogenic activity in the atmospheric budget of refractory, organic chlorine. The data for CFCs and the longer-lived organic chlorocarbons ultimately will be useful in dating oceanic water masses and isolated ground waters, providing atmospheric data where none existed before. Atmospheric CH_3Br in the southern hemisphere appears to have been about 25% lower at the turn of the century than it is today (Figure 5.36).

5.7. References

AFEAS (Alternative Fluorocarbon Environmental Acceptability Study), *Production, Sales and Atmospheric Release of Fluorocarbons Through 1993*, S & PS, Inc., Washington, D.C., 1995.

Albritton, D.L., R.G. Derwent, I.S.A. Isaken, M. Lal, D.J. Wuebbles, Trace gas radiative forcing indices, in *Climate Change 1994: Radiative Forcing of Climate Change and An Evaluation of the IPCC IS92 Emission Scenarios*, edited by J.T. Houghton, L.G.M. Filho, J. Bruce, H. Lee, B.A. Callander, E. Haites, N. Harris, and K. Maskell, 339 pp., Cambridge University Press, Cambridge, UK, 1995.

Bakwin, P.S., P.P Tans, C. Zhao, W. Ussler, III, and E. Quesnell, Measurements of carbon dioxide on a very tall tower, *Tellus*, 47B, 535-549, 1995.

Battle, M., M. Bender, T. Sowers, P. Tans, J. Butler, J. Elkins, J. Ellis, T. Conway, N. Zhang, P. Lang, and A. Clarke, Histories of atmospheric gases from the firn at South Pole. *Nature*, in press, 1996.

Boering, K.A., E.J. Hintsa, S.C. Wofsy, J.G. Anderson, B.C. Daube, A.E. Dessler, M. Loewenstein, M.P. McCormick, J.R. Podolske, E.M. Weinstock, and G.K. Yue, Measurements of stratospheric carbon dioxide and water vapor at northern midlatitudes: Implications for troposphere-to-stratosphere transport, *Geophys. Res. Lett.*, 22, 2737-2740, 1995.

Butler, J.H., The potential role of the ocean in regulating atmospheric CH_3Br, *Geophys. Res. Lett.*, 21, 185-189, 1994.

Butler, J.H., Methyl bromide under scrutiny. *Nature*, 376, 469-470, 1995.

Butler, J.H., Scientific uncertainties in the budget of atmospheric methyl bromide, *Atmos. Environ.*, 30(7), i-iii, 1996.

Butler, J.H., and J. Rodriguez, Methyl bromide in the atmosphere, in *The Methyl Bromide Issue*, edited by N. Price, London, Wiley and Sons, Ltd., in press, 1996.

Butler, J.H., J.W. Elkins, B.D. Hall, S.O. Cummings, and S.A. Montzka, A decrease in the growth rates of atmospheric halon concentrations, *Nature*, 359, 403-405, 1992.

Butler, J.H., Lobert J.M., S.A. Yvon, and L.S. Geller, The distribution and cycling of halogenated trace gases between the atmosphere and ocean, in *The Expedition Antarktis XII of RV "Polarstern" in 1994/95. Reports of Legs ANT XII/1 and 2*, edited by G. Kattner and K. Fuetterer, Alfred Wegener Institute for Polar and Marine Research, Bremerhaven, 1995.

Daniel, J.S., S. Solomon, and D.L. Albritton, On the evaluation of halocarbon radiative forcing and global warming potentials, *J. Geophys. Res.*, 100, 1271-1285, 1995.

Elkins, J.W., T.M. Thompson, T.H. Swanson, J.H. Butler, B.D. Hall, S.O. Cummings, D.A. Fisher, and A.G. Raffo, Decrease in the growth rates of atmospheric chlorofluorocarbons 11 and 12, *Nature*, 364, 780-783. 1993.

Elkins, J.W., D.W. Fahey, J.M. Gilligan, G.S. Dutton, T.J. Baring, C.M. Volk, R.E. Dunn, R.C. Myers, S.A. Montzka, P.R. Wamsley, A.H. Hayden, J.H. Butler, T.M Thompson, T.H. Swanson, E.J. Dlugokencky, P.C. Novelli, D.F. Hurst, J.M. Lobert, S.J. Cicora, R.J. McLaughlin, T.L. Thompson, R.H. Winkler, P.J. Fraser, L.P. Steele, M.P. Lucarelli, Airborne gas chromatograph for in situ measurements of long lived species in the upper troposphere and lower stratosphere, *Geophys. Res. Lett*, 23(4), 347-350, 1996.

Eluszkiewicz, J., D. Crisp, R. Zurek, L. Elson, E. Fishbein, L. Froidevaux, J. Waters, R.G. Grainger, A. Lambert, R. Harwood, and G. Peckham, Residual circulation in the stratosphere and lower mesosphere as diagnosed from microwave limb sounder data, *J. Atmos. Sci.*, 53, 217-240, 1996.

Etheridge, D.M., L.P. Steele, R.L. Langenfelds, R.J. Francey, J.M. Barnola, and V.I. Morgan, Natural and anthropogenic changes in atmospheric CO_2 over the last 1000 years from air in Antarctic ice and firn. *J. Geophys. Res.*, 101(D2), 4115-4128, 1996.

Fahey, D.W., J.W. Elkins, S.A. Montzka, R.C. Myers, G.S. Dutton, C.M. Volk, Mean age of the air mass: In situ measurements of stratospheric sulfur hexafluoride in 1994, *EOS*, 76, p. 130, 1995.

Fahey, D.W., D.M. Murphy, K.K. Kelly, M.K.W. Ko, M.H. Proffitt, C.S. Eubank, D.W. Ferry, M. Loewenstein, and K.R. Chan, Measurements of nitric oxide and total reactive nitrogen in the Antarctic stratosphere: Observations and chemical implications, *J. Geophys. Res.*, 94, 16,665-16,681, 1989.

Garcia, R.R., and S. Solomon, A New numerical model of the middle atmosphere 2. Ozone and related species, *J. Geophys. Res.*, 99, 12,937-12,951, 1994.

Geller, L., J. Lobert, J. Butler, R. Myers, J. Elkins, Latitudinal distribution of sulfur hexafluoride in and over the Atlantic and E. Pacific Oceans, *EOS*, 76, p. 17, 1994.

Goldan, P.D., W.C. Kuster, D.L. Albritton, and A.L. Schmeltekopf, Stratospheric $CFCl_3$, CF_2Cl_2, and N_2O height profile measurements at several latitudes, *J. Geophys. Res.*, 85, 413-423, 1980.

Hurst, D., L. Geller, P. Novelli, P. Bakwin, R. Myers, J. Elkins, Observations of sulfur hexafluoride from a very tall tower in the southeastern United States, *EOS*, 76, p. 70, 1995.

Hall, T. M., and R. A. Plumb, Age as a diagnostic of stratospheric transport, *J. Geophys. Res.*, 99, 1059-1070, 1994.

Irion, F.W., M. Brown, G.C. Toon, M.R. Gunson, Increase in atmospheric CHF_2Cl (HCFC-22) over Southern California from 1985 to 1990, *Geophys. Res. Lett.*, 21, 1723-1726, 1994.

Lobert, J.M., J.H. Butler, S.A. Montzka, L.S. Geller, R.C. Myers, and J.W. Elkins, A net sink for atmospheric methyl bromide in the East Pacific Ocean. *Science*, 267, 1002-1005, 1995.

Lobert, J. M., J. H. Butler, L. S. Geller, S. A. Yvon, S. A. Montzka, R. C. Myers, A. D. Clarke, J. W. Elkins, BLAST 94: Bromine Latitudinal Air Sea Transect 1994. Report on Oceanic Measurements of Methyl Bromide and Other Compounds, *NOAA Tech. Memo. ERL CMDL-10*, 39 pp., NOAA Environmental Research Laboratories, Boulder, CO, 1996.

Machida, T., T. Nakazawa, Y. Fujii, S. Aoki, and O. Watanabe, Increase in the atmospheric nitrous oxide concentration during the last 250 years, *Geophys. Res. Lett.*, 22(21), 2921-2924, 1995.

Maiss, M., L.P. Steele, R.J. Francey, P.J. Fraser, R.L. Langenfelds, N. B.A. Trivett, and I. Levin, Sulfur hexafluoride—a powerful new atmospheric trace, *Atmos. Environ.*, 30, 1621-1629, 1996.

McCormick, M.P., E.W. Chiou, L.R. McMaster, W.P. Chu, J.C. Larsen, D. Rind, and S. Oltmans, Annual variations of water vapor in the stratosphere and upper troposphere observed by the Stratospheric Aerosol and Gas Experiment II, *J. Geophys. Res.*, 98, 4867-4874, 1993.

McCulloch, A., and P. Midgely, The production and global distribution of emissions of trichloroethene, tetrachloroethene, and dichloromethane over the period 1988-1992, *Atmos. Env.*, 30, 601-608, 1996.

McElroy, M. B., R. J. Salawitch, S. C. Wofsy and J. A. Logan, Reductions of antarctic ozone due to synergistic interactions of chlorine and bromine, *Nature*, 321, 759-762, 1986.

Minschwaner, K., R.J. Salawitch, and M.B. McElroy, Absorption of solar radiation by O_2: Implications for O_3 and lifetimes of N_2O, $CFCl_3$, and CF_2Cl_2, *J. Geophys. Res.*, 98, 10,543-10,561, 1993.

Montzka, S.A., R.C. Myers, J.H. Butler, J.W. Elkins, and S.O. Cummings, Global tropospheric distribution and calibration scale of HCFC-22, *Geophys. Res. Lett.*, 20, 703-706, 1993.

Montzka, S.A., R.C. Myers, J.H. Butler, and J.W. Elkins, Early trends in the global tropospheric distribution of hydrofluorocarbon-141b and -142b, *Geophys. Res. Lett.*, 21, 2483-2486, 1994.

Montzka, S.A., J.H. Butler, J.W. Elkins, S. Yvon, A. Clarke, J. Lobert, and L. Lock, Difficulties associated with measuring atmospheric levels of methyl bromide and other methyl halides, *EOS*, 76, S160, 1995a.

Montzka, S.A., R.C. Myers, J.M. Butler, T.M. Thompson, J.W. Elkins, L.T. Lock, A.D. Clarke, T.H. Swanson, Changing trends in the global tropospheric abundance of CFCs, HCFC, HFCs, and chlorine in recent time, *EOS*, 76, F98, 1995b.

Montzka, S.A., R.C. Myers, J.H. Butler, J.W. Elkins, L.T. Lock, A.D. Clarke, A.H. Goldstein, Observations of HFC-134a in the remote troposphere, *Geophys. Res. Lett.*, 23, 169-172, 1996a.

Montzka, S.A., J.H. Butler, R.C. Myers, T.M. Thompson, T.H. Swanson, S.D. Clarke, L.T. Lock, J.W. Elkins, Decline in the tropospheric abundance of halogen from halocarbons, *Science*, 272, 1318-1322, 1996b.

Mote, P.W., K.H. Rosenlof, M.E. McIntyre, E.S. Carr, J.S. Kinnersley, H.C. Pumphrey, R.S. Harwood, J.R. Holton, J.M. Russell III, J.W. Waters, J.C. Gille, and K.K. Kelly, An atmospheric tape recorder: The imprint of tropical tropopause temperatures on stratospheric water vapor, *J. Geophys. Res.*, 101, 3989-4006, 1996.

Murphy, D.M., S.W. Fahey, M.H. Proffitt, S.C. Liu, K.R. Chan, C.S. Eubank, S.R. Kawa, and K.K. Kelly, Reactive nitrogen and its correlation with ozone in the lower stratosphere and upper troposphere, *J. Geophys. Res.*, 98, 8751-8773, 1993.

Oram, D.E., C.E. Reeves, S.A. Penkett, and P.J. Fraser, Measurements of HCFC-142b and HCFC-141b in the Cape Grim air archive: 1978-1993, *Geophys. Res. Lett.*, 22, 2741-2744, 1995.

Peterson, J.T., and R.M. Rosson (Eds.), *Climate Monitoring and Diagnostics Laboratory, No. 21, Summary Report 1992*, 131 pp., NOAA Environmental Research Laboratories, Boulder, CO, 1993.

Peterson, J.T., and R.M. Rosson (Eds.), *Climate Monitoring and Diagnostics Laboratory, No. 22, Summary Report 1993*, 152 pp., NOAA Environmental Research Laboratories, Boulder, CO, 1994.

Plumb, R.A., A "tropical pipe" model of stratospheric transport, *J. Geophys. Res.*, 101, 3957-3972, 1996.

Plumb, R.A., and M.K.W. Ko, Interrelationships between mixing ratios of long-lived stratospheric constituents, *J. Geophys. Res.*, 97, 10,145-10,156, 1992.

Podolske, J., and M. Loewenstein, Airborne tunable diode laser spectrometer for trace-gas measurement in the lower stratosphere, *Appl. Opt.*, 32, 5324-5333, 1993.

Pollock, W.H., L.E. Heidt, R.A. Lueb, J.F. Vedder, M.J. Mills, S. Solomon, On the age of stratospheric air and ozone depletion potentials in polar regions, *J. Geophys. Res.*, 97, 12,993-12,999, 1992.

Prather, M.J., and R.T. Watson, Stratospheric ozone depletion and future levels of atmospheric chlorine and bromine, *Nature*, 344, 729-734, 1990.

Prinn, R.G., R.F. Weiss, B.R. Miller, J. Huang, F.N. Alyea, D.M. Cunnold, P.J. Fraser, D.E. Hartley, and P.G. Simmonds, Atmospheric trends and lifetime of CH_3CCl_3 and global OH concentrations, *Science*, 269, 187-192, 1995.

Proffitt, M.H., and J. McLaughlin, Fast-response dual-beam UV absorption ozone photometer suitable for use on stratospheric balloons, *Rev. Sci. Instrum.*, 54, 1719-1728, 1983.

Randel, W.J., J.C. Gille, A.E. Roche, J.B. Kumer, J.L. Mergenthaler, J.W. Waters, E.F. Fishbein, and W.A. Lahoz, Stratospheric transport from the tropics to middle latitudes by planetary-wave mixing, *Nature*, 365, 533-535, 1993.

Ravishankara, A. R., S. Solomon, A.A. Turnipseed, R.F. Warren, Atmospheric lifetimes of long-lived halogenated species, *Science*, 259, 194-199, 1993.

Rinsland, C. P., E. Mahieu, R. Zander, M. R. Gunson, R. J. Salawitch, A. Y. Chang, A. Goldman, M. C. Abrams, M. M. Abbas, M. J. Newchurch, and F. W. Irion, Trends of OCS, HCN, SF_6, and $CHClF_2$ (HCFC-22) in the lower stratosphere from 1985 and 1994 atmospheric trace molecule spectroscopy experiment measurements near 30°N latitude, *Geophys. Res. Lett.*, in press, 1996.

Rosenlof, K.H., Seasonal cycle of the residual mean meridional circulation in the stratosphere, *J. Geophys. Res.*, 100, 5173-5191, 1995.

Salawitch, R.J., S.C. Wofsy, P.O. Wennberg, R.C. Cohen, J.G. Anderson, D.W. Fahey, R.S. Gao, E.R. Keim, E.L. Woodbridge, R.M. Stimpfle, J.P. Koplow, D.W. Kohn, C.R. Webster, R.D. May, L. Pfister, E.W. Gottlieb, H.A. Michelsen, G.K. Yue, M.J. Prather, J.C. Wilson, C.A. Brock, H.H. Jonsson, J.E. Dye, D. Baumgardner, M.H. Proffitt, M. Loewenstein, J.R. Podolske, J.W. Elkins, G.S. Dutton, E.J. Hintsa, A.E. Dessler, E.M. Weinstock, K.K. Kelly, K.A. Boering, B.C. Daube, K.R. Chan, and S.W. Bowen, The diurnal variation of hydrogen, nitrogen, and chlorine radicals: Implications for the heterogeneous production of HNO_2, *Geophys. Res. Lett.*, 21, 2251-2554, 1994.

Schauffler S.M., L.E. Heidt, W.H. Pollock, T.M. Gilpin, J.F. Vedder, S. Solomon, R.A. Lueb, and E.L. Atlas, Measurements of halogenated organic compounds near the tropical tropopause, *Geophys. Res. Lett.*, 22, 2567-2570, 1993.

Schauffler S.M., W.H. Pollock, E.L. Atlas, L.E. Heidt, and J.S. Daniel, Atmospheric distributions of HCFC 141b, *Geophys. Res. Lett.*, 22, 819-822, 1995.

Shorter, J.H., C.E. Kolb, P.M. Crill, R.A. Kerwin, R.W. Talbot, M.E. Hines, and R.C. Harriss, Rapid degradation of atmospheric methyl bromide in soils. *Nature*, 377, 717-719, 1995.

Solomon S., R. W. Portmann, R. R. Garcia, L. W. Thomason, L.R. Poole, and M. P. McCormick, The role of aerosol variations in anthropogenic ozone depletion at northern midlatitudes, *J. Geophys. Res.*, 101, 6713-6727, 1996.

Stolarski, R.S., S.L. Baughcum, W.H. Brune, A.R. Douglass, D.W. Fahey, R.R. Friedl, S.C. Liu, R.A. Plumb, L.R. Poole, H.L. Wesoky, D.R. Worsnop, 1995 Scientific Assessment of the Atmospheric Effects of Stratospheric Aircraft, *NASA Ref. Pub. 1381*, 1996.

Swanson, T.H., J.W. Elkins, J.H. Butler, S.A. Montzka, R.C. Myers, T.M. Thompson, T.J. Baring, S.O. Cummings, G.S. Dutton, A.H. Hayden, J.M. Lobert, G.A. Holcomb, W.T. Sturges, and T.M. Gilpin, in Climate Mo*nitoring and Diagnostics Laboratory No. 21 Summary Report 1992*, edited by J.T. Peterson and R.M. Rosson, pp. 59-75, NOAA Environmental Research Laboratories, Boulder, CO, 1993.

Thompson, T.M., J.W. Elkins, J.H. Butler, S.A. Montzka, R.C. Myers, T.J. Baring, S.O. Cummings. G.S. Dutton, J.M Gilligan, A.H. Hayden, J.M. Lobert, T.H. Swanson, D.F. Hurst, and C.M. Volk, in *Climate Monitoring and Diagnostics Laboratory No. 22 Summary Report 1992*, pp. 72-91, edited by J.T. Peterson and R.M. Rosson, NOAA Environmental Research Laboratories, Boulder, CO, 1994.

Trepte, C.R., and M.H. Hitchman, Tropical stratospheric circulation deduced from satellite aerosol data, *Nature*, 355, 626-628, 1992.

Volk, C.M., J.W. Elkins, D.W. Fahey, R.J. Salawitch, G.S. Dutton, J.M. Gilligan, M.H. Proffitt, M. Loewenstein, J.R. Podolske, K. Minschwaner, J.J. Margitan, and K.R. Chan, Quantifying transport between the tropical and midlatitude lower stratosphere, *Science*, 272, 1763-1768, 1996.

WMO (World Meteorological Organization), *Scientific Assessment of Ozone Depletion: 1994*, WMO, Geneva, 1995.

Yung, Y.L., J.P. Pinto, R.T. Watson and S.P. Sander, Atmospheric bromine and ozone perturbations in the lower stratosphere, *J. Atmos. Sci.*, 37, 339-353, 1980.

Yvon, S.A., and J.H. Butler An improved estimate of the oceanic lifetime of atmospheric CH_3Br, *Geophys. Res. Lett.*, 23, 53-56, 1996.

Zander, R., E. Mahieu, P. Demoulin, C.P. Rinsland, D.K. Weisenstein, M.K.W. Ko, N.D. Sze, and M.R. Gunson, Secular evolution of the vertical column abundances of $CHClF_2$ (HCFC-22) in the Earth's atmosphere inferred from ground-based IR solar observations at the Jungfraujoch and at Kitt Peak, and comparison with model calculations, *J. Atmos, Chem,* 18, 129-148, 1994.

6. Cooperative Programs

Evaluation of Arctic Meteorological Buoys

GERALD F. APPELL
NOAA, National Ocean Service, Ocean Systems Development Group, Silver Spring, Maryland 20910

INTRODUCTION

The United States Interagency Arctic Buoy Program (USIABP) was formed in 1991 to establish and maintain a network of drifting meteorological buoys in the Arctic. The USIABP is a collaborative program funded by nine government agencies/programs and managed by the National Ice Center in Suitland, Maryland. USIABP supports the International Arctic Buoy Program (IABP) which consists of many countries participating in the collection of meteorological data from Arctic drifting buoys.

The buoys are strategically deployed to define the surface synoptic scale atmospheric pressure, air temperature, and sea ice drift fields. The data are available in real time, via ARGOS satellite transmissions, to operational weather forecasting centers. Data are also used for research into climate change. At the inception of the program, 25 buoys were gathering temperature and pressure data in the Arctic with 72% reporting on the Global Telecommunications System (GTS). In early 1994, 47 buoys were in operation with 96% reporting on the GTS.

The IABP uses many different buoys with different sensors, configurations, and sampling schemes. Many of the temperature measurements reported by the buoys were suspect when compared with atmospheric model predictions. In 1993 it was decided by the USIABP to halt deployment of new buoys until the sources of temperature measurement errors were investigated. A program was established to evaluate the available "off-the-shelf" Arctic buoy systems being used by the IABP. As part of this evaluation, a long-term test site was established at the CMDL facility in Barrow, Alaska (BRW).

In 1995 the USIABP resumed procurement and deployment of buoys based on a buoy design derived from tests at BRW.

THE FIELD TEST SITE

In August 1993, a Coastal Climate buoy and a DSI-TAD buoy were placed at BRW. A data acquisition system was placed at the site consisting of a Telonics ARGOS uplink receiver and a Compaq notebook computer. Buoy transmissions are received and logged on the computer. Weekly interrogations of the computer are done from Silver Spring, Maryland, and data files are downloaded. In December 1993 a Canadian MetOcean CALIB buoy was added to the array, and in March 1994 a Norwegian ICEX buoy was placed at the site.

In August 1994 a meteorological station was placed at the buoy array site. This site collects temperature data from aspirated sensors at the 1 m and 2 m levels. It also collects solar radiation, barometric pressure, and wind data. The purpose of this system is to explore the horizontal and vertical temperature distribution compared with the CMDL sensors (20 m horizontal separation, CMDL sensors at 2 m and 15 m levels). Data are collected from the station via GOES satellite or dial-up phone link.

A fifth buoy was added to the site in August 1994. This buoy is a Canadian MetOcean buoy similar in design to the Coastal Climate buoy.

In May 1995 the sixth and last buoy was added to the site. This buoy was specified, designed, and built based on the experience and knowledge gained from the BRW tests. This buoy was manufactured by Coastal Climate and was based on the successful design of their original ice buoy. All of the air deployable buoys were removed from the site in 1995 with sufficient data acquired. At the close of 1995 three buoys remained at BRW, the two Coastal Climate buoys and the one MetOcean buoy.

DATA ACQUISITION AND ANALYSIS

All buoys in the test program undergo a temperature sensor calibration at the National Weather Service Test Facility in Sterling, Virginia, before shipment to Barrow, Alaska.

Each buoy has its own measurement scheme, sampling interval, data format, and data transmission interval. Data collected in Silver Spring, Maryland, is processed and reduced into a standard 1-hour averaged data format. CMDL meteorological data are sent monthly on a computer diskette for comparison with buoy data. An INTERNET link was established with BRW in 1994 for retrieval of ice buoy data. Compressed files from the buoy data acquisition system are placed on the laboratory computer for retrieval via FTP. This has saved the expense of downloading data via telephone.

Measurements are analyzed and compared with the meteorological station and CMDL standards. Temperature differences between sensors and/or standards are analyzed to learn the effects of sensor height differences, solar radiation, and wind. Results show significant differences are attributed to the measurement height of the sensors above the surface and to solar radiation effects.

In 1994, based on BRW test results, a specification was developed to procure new ice buoys. A contract was awarded to Coastal Climate Company for five new systems. The performance of the original Coastal Climate buoy placed at BRW has been superior to the others regarding accurate temperature measurements. This new specification required an improved sampling and ARGOS reporting scheme for the buoys. The ICEX, DSI-TAD, and MetOcean CALIB buoys were removed from the site in early 1995 after conclusion of tests. These buoys were

deemed unacceptable based on proximity of sensors to the ground and susceptibility to blowing snow coverage.

Analysis of data acquired in 1995 showed that the new Coastal Climate buoy performed as expected. The quality of temperature data obtained from the three remaining buoys is comparable. These buoys all measure temperature at a fixed height of 2 m above the surface and provide sufficient shielding of solar radiation. In August 1996, the original Coastal Climate buoy will have operated continuously in Barrow for 3 years, meeting its design life.

Future Plans

It is planned to discontinue the buoy test program in Barrow in August 1996. Sufficient information on buoy performance has been acquired to assure that improved sensors will be available to the USIABP.

Asian Transport of Aerosols to Mauna Loa Observatory, Spring 1994

THOMAS A. CAHILL AND KEVIN D. PERRY
Air Quality Group, Crocker Nuclear Laboratory, University of California, Davis 95616

A partial National Park Service Interagency Monitoring of Protected Visual Environments (IMPROVE) site was established at Mauna Loa Observatory (MLO) in 1989 to measure the mass and composition of fine particles (i.e., D_p <2.5 μm diameter). While this site has always produced data on the more common trace elemental species such as zinc (see previous CMDL summary reports), analytical advances in early 1993 greatly increased sensitivity and allowed a much wider suite of trace elemental species to be measured. While the IMPROVE site at MLO quickly confirmed prior findings of regular Asian dust transport each spring, it also demonstrated that elevated levels of trace elements also occur during the dust episodes. In this summary, we will compare the present results to recently published aerosol summaries at MLO, examine the intense Asian dust episodes that occurred during the spring of 1994, and outline intensive measurements being made at MLO during the spring of 1996.

Comparisons with other long-term aerosol records became possible when *Zieman et al.* [1995] summarized their high volume air sampler (Hi-Vol) data from MLO. The Hi-Vol sampler was operated for a period of 1 week during nighttime/downslope winds and collected particles <30 μm in diameter. For comparison purposes, we have summed the two weekly IMPROVE sampling periods (i.e., Wednesday through Friday and Saturday through Tuesday) to give mean weekly values during downslope winds.

The excellent agreement for sulfates in Table 1 indicates that these particles are predominantly <2.5 μm in diameter. The results for soil, however, are typically different. For example, Hi-Vols normally collect about four times more soil mass than the IMPROVE $PM_{2.5}$ air sampler. Thus, one might expect the Hi-Vol to collect ~2.9 μg m^{-3} of soil during the spring Asian dust episodes and ~0.4 μg m^{-3} during the entire year. Table 1 shows that less than half of this soil mass was observed during the dust season. This implies that the soil at MLO during the spring is much finer than typical local soils, which is consistent with transport. *Braaten and Cahill* [1986] found a mass median diameter for Asian soils of ~1.2 μm diameter, but did not measure particles above ~11 μm. Thus, while it is likely that the Hi-Vol data from *Zieman et al.* [1995] contains some local soils, most of the soil is probably transported from distant sources during the dust episodes. The data for zinc and selenium implies that most of the mass of these species is <2.5 μm in diameter, which is also consistent with transport from Asia.

The second topic involves the intense dust storms that occurred during the spring of 1994. Figure 1 shows the concentration of fine soil, soot (b(abs), measured optically), organic matter (inferred from hydrogen), and arsenic during this time period. Although the soil concentration on April 9 is about twice the maximum in most prior years, it is the other elements that make this episode interesting. For example, the maximum arsenic concentrations at MLO during the spring of 1994 were roughly equivalent to the median of the peak arsenic concentrations at the other 70 or so IMPROVE sites at mainland parks and monuments. The high arsenic concentrations at MLO were accompanied by other trace elements similar to those produced from non-ferrous smelter activity (Table 2). Ten-day backward isenotropic air trajectories for this episode pass directly over northern China, site of most Chinese smelting activity.

While we expected to find traces of Asian industrial activity in the aerosol record at MLO, we did not expect such high concentrations of arsenic. Prior research had shown that significant dilution of soil mass occurred between the Asian sources and MLO. Such high arsenic concentrations could only be achieved if either the concentrations were very high at mainland sites, or the trace elements did not suffer as much dilution as the soil dust. The former hypothesis seems unlikely. For example,

TABLE 1. Comparison of Downslope Aerosol Sampling at MLO

	Mass (μg m^{-3})	RCMA* (μg m^{-3})	SO_4 (μg m^{-3})	Organics (μg m^{-3})	Soil (μg m^{-3})	b (abs) 10^{-4} m^{-1}	Zn (ng m^{-3})	Se (ng m^{-3})
Dust Season:								
UC Davis	1.94	1.62	0.37	0.36	0.72	1.92	0.47	0.029
Zieman et al., 1995			0.37		1.27		0.51	0.038
Overall:								
UC Davis	0.84	0.68	0.29	0.22	0.10	0.62	0.18	0.021
Zieman et al., 1995			0.26		0.55		0.33	0.031

Note: All UC Davis data is from 1993 and 1994.
*Mass is gravimetric, reconstructed mass (RCMA) is the sum of measured species. The difference is mainly water.

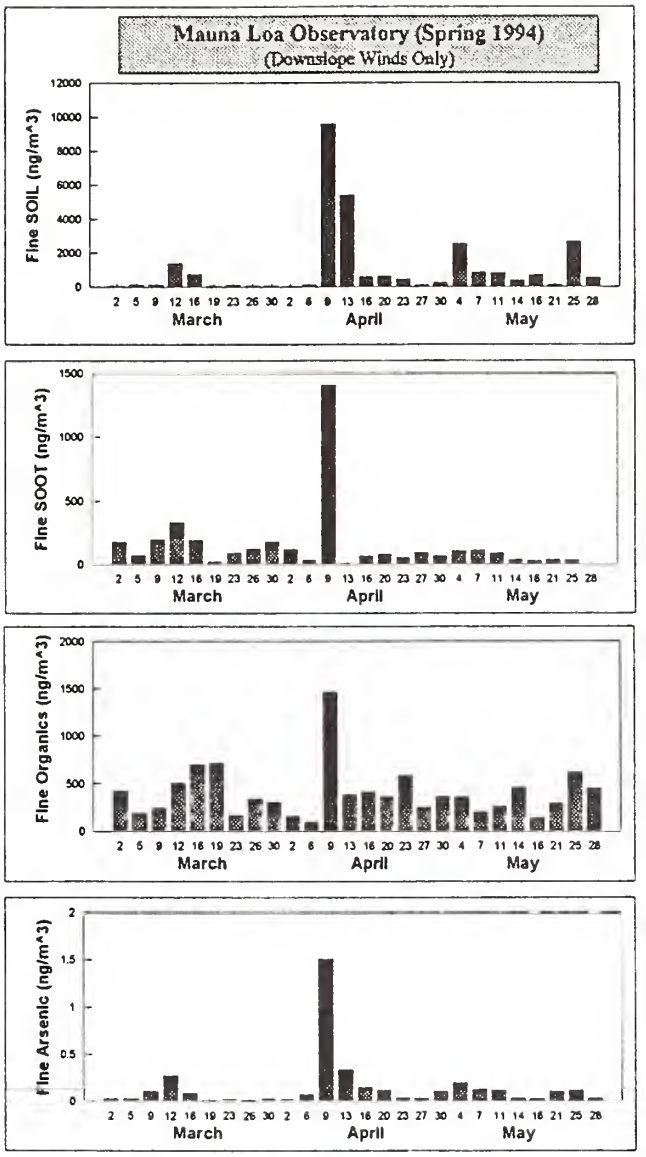

Fig. 1. Aerosol concentrations at Mauna Loa Observatory, spring 1994. All concentrations are given in nanograms m^{-3}. For details of the parameters, see *Malm et al.* [1994].

if we use typical soil dilution factors to calculate the ambient levels of arsenic and other toxic species at the source regions in Asia, we find that the concentrations would need to be in the microgram m^{-3} range over a wide area of the mainland during periods of strong ventilation and dilution associated with the dust storms. In non dust-storm periods, one would then expect arsenic levels unprecedented in western experience, levels that would likely be lethal in a relatively few years. As a result, the second explanation is probably the dominant factor. For example, using data from dust storms that occurred during the spring of 1981, we found that the dilution factor

TABLE 2. Comparison of Trace Elements From Potential Sources of Arsenic

	1000* Se/SO_4	1000* Cu/SO_4	1000* Zn/SO_4	1000* As/SO_4
Volcanoes:				
Kilauea, Nov. 21, 1992	1.9	0.39	0.37	0.32
Copper Smelters:				
Average Arizona	1.7	20.0	28.0	6.0
"Smelter No. 5"	0.02	1.0	3.8	2.3
Mauna Loa (downslope)				
April 9, 1994	<0.08	0.9	3.8	2.4

Note: All values have been normalized to sulfate.

for very fine (D_p <0.5 μm) particles was only a factor on the order of 3 (Table 3). If we use this small particle dilution factor to calculate the arsenic levels at Asian sources, the resulting arsenic concentrations are high, but not unprecedented. Thus, it is possible that other materials in the smallest size ranges (including many anthropogenic pollutants) could also be efficiently transported to MLO.

The final topic involves experiments to be conducted during the spring of 1996 to test some of the hypotheses raised by the prior work. The experiment will take place during April and May of 1996 and include the following: (a) direct measurement of organic particles by carbon combustion from quartz filters and by GC/MS from quartz filters, (b) establishment of nitrate levels via direct collection of denuded nylon filters, (c) size/time resolved sampling of optically efficient aerosol (three sizes <2.5 μm), and (d) ^{14}carbon dating of organic aerosols.

These measurements will be complemented by the IMPROVE Channel A sampler and the full suite of MLO observables, including carbon soot via aethelometer and isentropic trajectories every 12 hours from CMDL.

Acknowledgments. This work would not have been possible without the capable support of the staff at MLO who have delivered samples biweekly with an efficiency that is among the very best in the entire 70-site network. We also wish to thank Joyce Harris for both her insights and her trajectories.

TABLE 3. Comparison of Fine Soil Dust Transport Efficiencies from China (April 19, 1981) to MLO (May 12, 1981)*

	Beijing	Mauna Loa	Ratio
D_p<0.5 μm	0.6 μg m^{-3}	0.17 μg m^{-3}	31%
0.5<D_p<3.0 μm	80 μg m^{-3}	0.22 μg m^{-3}	0.3%
3.0<D_p<16 μm	136 μg m^{-3}	0.09 μg m^{-3}	0.07%

*Note that these are two different dust storms, so that the proportionality is only very approximate, but the ratios of coarse to fine dust should be reasonably similar.

References

Braaten, D.A. and T.A. Cahill. Size and composition of Asian dust transported to Hawaii. *Atmo. Environ.*, 20, 1105-1109, 1986.

Malm, W.C., J.F. Sisler, D. Huffman, R.A. Eldred, and T.A. Cahill, Spatial and seasonal trends in particle concentration and optical extinction in the United States, *J. Geophys. Res.*, 99, 1347-1370, 1994.

Zieman, J.J., J.L. Holmes, D. Connor, C.R. Jensen, W.H. Zoller, D.M. Hermann, J.R. Parrington, and G.E. Gordon, Atmospheric aerosol trace element chemistry at Mauna Loa Observatory, 1, 1979-1985, *J. Geophys. Res.*, 100, 25,979-25,994, 1995.

Ultrahigh Resolution Infrared Solar Spectra From Mauna Loa Observatory: New Results

S.J. David, F.J. Murcray, A. Goldman, and R.D. Blatherwick
University of Denver, Department of Physics, Denver, Colorado 80208

Introduction

A modified ultrahigh spectral resolution (0.0035 cm^{-1}) Fourier transform interferometer (FTIR) solar spectrometer system was installed at Mauna Loa Observatory, Hawaii (MLO) in May 1991 and was operated routinely by the observatory staff from November 1991 to November 1995. This instrument provided data on the column abundance of several atmospheric chemical compounds for the Network for Detection of Stratospheric Change (NDSC). Normal operation was one sunrise set of data each week, usually collected on Wednesdays.

During August 1995, a new, almost completely automatic FTIR system was installed at MLO. The solar tracker has a weather-tight hatch that is computer controlled. The new system requires a person to fill the detector dewars with liquid nitrogen; it then records solar spectra when weather conditions are acceptable. Weather permitting, data are collected 5 days-a-week at both sunrise and sunset. Data cartridges need to be changed weekly and desiccant changed monthly.

Here, data are presented from the complete 4-year run of the original interferometer, and comparisons between the two systems are made for data from the overlap period.

Results and Discussion

To date, we have analyzed the infrared spectra for total column amounts of several gases over a 4-year period at MLO. Gases included in this data base are O_3, N_2O, HNO_3, F22 and HCl.

The ozone spectral lines were chosen to be isolated and only weakly temperature dependent. The two fitted spectral regions, around 1146 and 1163 cm^{-1}, included two prominent ozone absorptions and a strong line due to N_2O. Nitrous oxide is reported to be increasing slightly, but is essentially constant on our scale. Infrared ozone column amounts are very consistent with the Dobson observations [*David et al.*, 1993]. Figure 1 shows the total columns measured for O_3 and N_2O. We see ozone has an annual cycle with lows in the winter and highs in the late spring to early summer. It is worth noting that O_3 hit a low in early 1995 that is consistent with a record low measured by the Mauna Loa Dobson spectrophotometer.

The HNO_3 spectral interval chosen contains three P-branch manifolds of the n_5 band located between 868.3 and 869.6 cm^{-1}; see *David et al.* [1994] for a description of the HNO_3 analysis. Figure 2 shows the total column measured for HNO_3. Currently, we are seeing a decrease of approximately 9% yr^{-1}. Our measurements started just after Mount Pinatubo erupted in July 1991; therefore, the decrease is expected, however, HNO_3 should level off soon.

We analyzed HCl using a two-step process. First, we looked at 2925.5 to 2926.5 cm^{-1} which included H_2O and CH_4 in the fit. Then we zoomed in on the $H^{35}Cl$ (1-0) band of the R(1) line at 2925 89 cm^{-1}. Our measurements show an increase in the column of HCl of approximately 2.5% yr^{-1}.

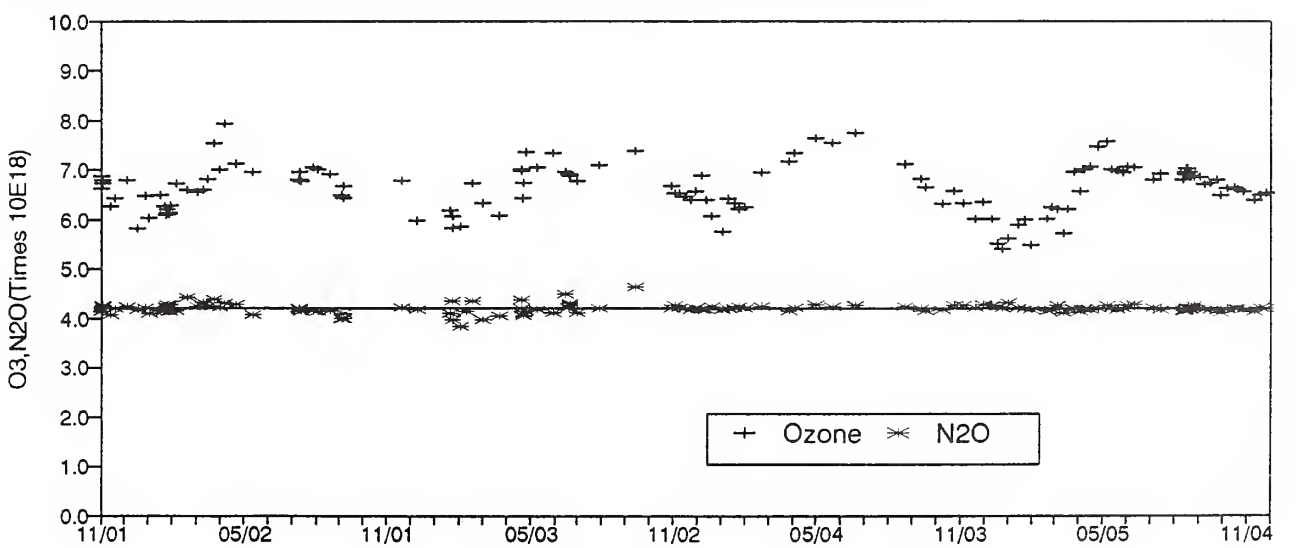

Fig. 1. Total column amounts of ozone and N_2O over Mauna Loa Observatory.

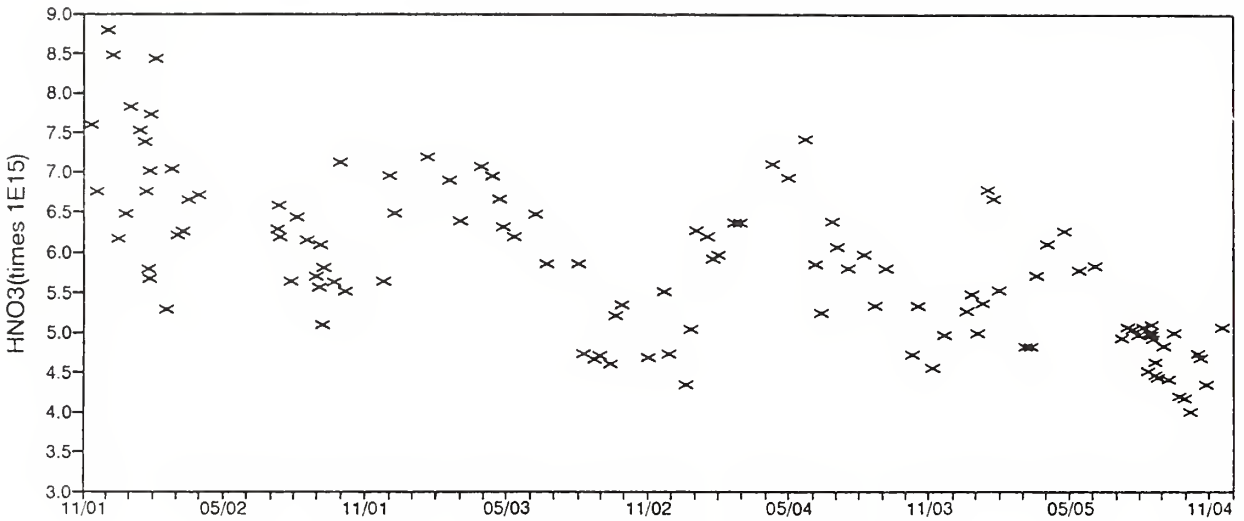

Fig. 2. Total column amount of HNO_3 over Mauna Loa Observatory.

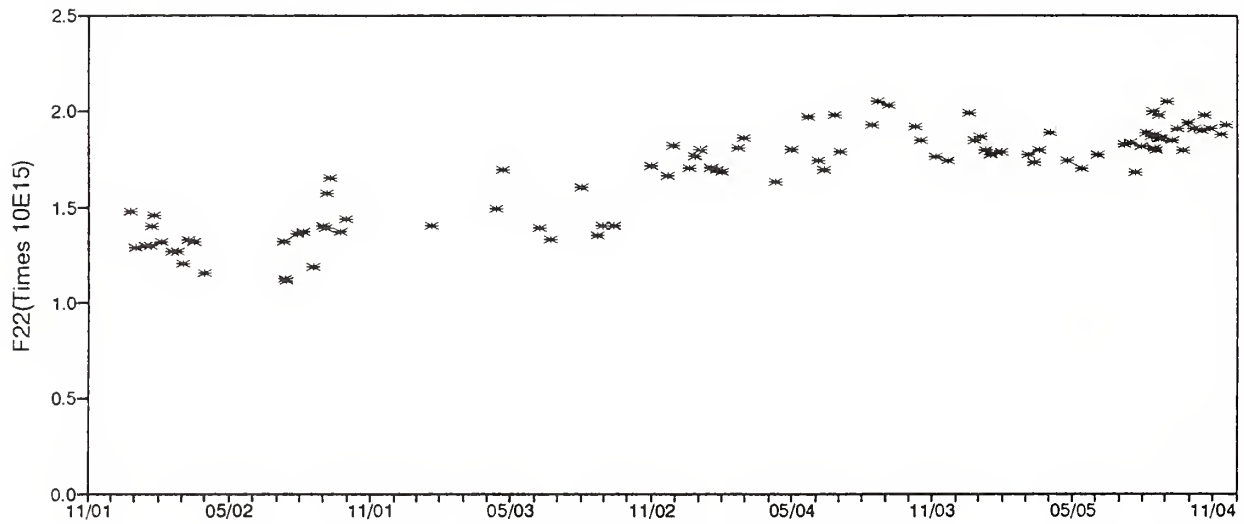

Fig. 3. Total column amount of F22 over Mauna Loa Observatory.

Finally, we measured the $2n_2$ Q-branch of CHF_2Cl (F22) at 829.05 cm^{-1}. Figure 3 shows the total columns measured for F22. Basically, we measured an increase of 20% yr^{-1} which slowed down between spring and summer of 1994.

Both instruments operated at MLO for several months. This resulted in four to six same-day data comparisons. If we look at the average of the new-to-old ratio, we find approximately 1% difference for O_3 and N_2O with the new instrument slightly higher, approximately 2% difference for the F22, and approximately 5% difference for the HNO_3 with the old instrument running slightly higher. Overall, these results have been very encouraging.

Acknowledgments. This research was partially supported by NASA under grants NSG 1432 and NAG2-351. The collection of the data was done with the support of CMDL. We are especially grateful to Bob Uchida for collecting most of this data very early each Wednesday morning.

References

David, S.J., S.A. Beaton, M.H. Anderberg, and F.J. Murcray, Determination of total ozone over Mauna Loa using very high resolution infrared solar spectra, *Geophys. Res. Lett.*, 19, 2055-2058, 1993.

David S.J., F.J. Murcray, A. Goldman, C.P. Rinsland, and D.G. Murcray, The effect of the Mt. Pinatubo aerosol on the HNO_3 column over Mauna Loa, Hawaii, *Geophys. Res. Lett.*, 21, 1003-1006, 1994.

A Preliminary Comparison of $\delta^{13}C$ Measurements in CO_2 From Mace Head, Ireland

A. GAUDRY AND P. MONFRAY
Centre des Faibles Radioactivités, LMCE, CEA L'orme des Merisiers, 91191 Gif sur Yvette, France

M. TROLIER
Institute of Arctic and Alpine Research, University of Colorado, Boulder 80309

C. FLEHOC AND P. CIAIS
LMCE, CEA L'orme des Merisiers, 91191 Gif sur Yvette, France

S.G. JENNINGS
Department of Physics, University College of Galway, Ireland

BACKGROUND

The ^{13}C composition of atmospheric CO_2 makes it possible to estimate biospheric fluxes of CO_2, as plant photosynthesis discriminates against $^{13}CO_2$, whereas isotopic fractionation during CO_2 dissolution into the ocean is small. However, to infer the partitioning of anthropogenic CO_2 between its oceanic and terrestrial sinks requires measurements of very high precision. Fluxes of CO_2 that are readily measured via changes in the atmospheric CO_2 mixing ratio have a smaller impact on $\delta^{13}C$. For instance, adding 1 ppm (analytical precision is ~0.1 ppm) of purely "biogenic" CO_2 to the atmosphere changes the $\delta^{13}C$ of that reservoir by only 0.05‰ (analytical precision is ~0.02‰). The isotopic effect of adding 1 ppm of "oceanic" CO_2 is even smaller.

Although the internal precision of mass spectrometers is about 0.01‰, systematic experimental errors may bias measurements of the $\delta^{13}C$ of air samples [*Francey et al.*, 1995]. Drift of the reference gases used to calibrate measurements can also introduce biases [*Trolier*, 1994]. Intercomparisons between different laboratories using independent calibration strategies and experimental protocols are crucial in order to assimilate their various data for use in models [*Ciais et al.*, 1995]. One of the best ways to monitor the intercalibration of independent programs is to conduct parallel sampling of whole air on an ongoing basis and at a common site.

In this paper we report a preliminary intercomparison of $\delta^{13}C$ measurements of air samples independently collected at Mace Head Station (53.43°N; -9.90°W) in the North Atlantic by CMDL and by the Centre des Faibles Radioactivités at the Laboratoire de Modélisation du Climat et de L'Environnement (CFR-LMCE; France). The CMDL samples are measured for isotopic composition at the Institute of Arctic and Alpine Research (INSTAAR) at the University of Colorado. Mace Head is located in the vicinity of the North Atlantic oceanic sink of CO_2 [*Lefèvre*, 1996], but it is also reached by continental air, especially in winter. The seasonal cycle of $\delta^{13}C$ at Mace Head has a fairly large amplitude (0.9‰), so $\delta^{13}C$ values can be compared over a rather wide range, from about -8.3‰ in winter to about -7.4‰ in spring and summer. The results of this intercomparison are summarized and discussed below.

SAMPLING AND ANALYTICAL TECHNIQUES

CFR-LMCE began continuous atmospheric CO_2 monitoring at Mace Head station in cooperation with the University College of Galway (Ireland) and International Science Consultants (United Kingdom) in July 1992. Meteorological data are also continuously recorded, enabling "background" sampling conditions to be distinguished from conditions that are influenced by local sources. Beginning in July 1993, flask samples (2-L glass flasks with Viton O-ring stopcocks, filled to 1 bar with air dried to a dewpoint of -55°C) have been measured for the ^{13}C composition of CO_2. The usual sampling frequency is two pairs of flasks per month. During the period from May 31, 1993, to June 7, 1993, the sampling frequency was about one pair per day; $\delta^{13}C$ data for these samples are not shown here. A different standard was used for the isotopic analysis which increases the uncertainty.

CFR-LMCE has operated an isotope-ratio mass spectrometer (Finnigan MAT 252) since January 1993, collaborating with CSIRO (where a similar instrument is used) to characterize the effects of instrumental artifacts on $\delta^{13}C$ measurements. The recognized effects include [*Francey et al.*, 1995] memory effects (when a sample has a very different $\delta^{13}C$ than the reference gas), size effects, which can affect linearity, and the "bleed correction," due to the fractionation that results from consumption of the reference gas. CFR recently made an accurate determination of the N_2O interference. The CFR flask measurements are calibrated against one sample of carefully purified CO_2, called SNAIL. SNAIL was calibrated against NBS-19, a carbonate provided by International Atomic Energy Agency (IAEA) [*Hut*, 1987] and two standard pure CO_2 gases, GS19 and GS20, provided by the University of Groningen, Netherlands. The $\delta^{13}C$ of SNAIL standard was determined to -9.67 ± 0.04‰ (relative to VPDB-CO_2).

NOAA began sampling at Mace Head in June 1991; the flasks (2.5-L glass flasks with Teflon o-ring stopcocks) are sampled in pairs and analyzed for the mixing ratios of CO_2, CH_4, and CO by CMDL, and for $\delta^{13}C$ and $\delta^{18}O$ of CO_2 by INSTAAR. At INSTAAR, CO_2 (with N_2O) is extracted from about 750 bar·cm^3 of whole air cryogenically, then analyzed for isotopic composition using a VG Sira Series II isotope-ratio mass spectrometer. The raw data (ratios of ion currents at masses 45 and 46 to

mass 44) are corrected for the presence of N_2O and for the contribution of species containing ^{17}O to the ion currents. The experimental technique and data analysis are described by *Trolier et al.* [1996]. The INSTAAR flask measurements are calibrated against a suite of whole-air reference gases, which in turn are calibrated against VPDB-CO_2 and V-SMOW. The estimated precision of individual $\delta^{13}C$ and $\delta^{18}O$ measurements are 0.03‰ and 0.05‰ respectively; the uncertainties in the absolute calibrations are ~0.02‰ and ~0.1‰ respectively.

INTERCOMPARISON

Figure 1 shows the time series of $\delta^{13}C$ measurements from Mace Head from both groups. Overall, the agreement appears to be good with the data sets showing no large offset and comparable seasonal cycles. We have made three quantitative comparisons of the two data sets: (1) directly comparing flask samples obtained close in time by the two programs; (2) comparing CFR data to a smoothed curve representing the entire INSTAAR data set; and (3) comparing CFR data obtained during "background" atmospheric conditions to the same smoothed curve from the INSTAAR data set. Background conditions correspond to winds higher than 4 m s^{-1} in the wind sector within 200° and 300°.

Because the two flask sampling programs are independent, their flasks are not necessarily filled close together in time. For example, there are only six instances between May 1993 and January 1995 for which flasks were obtained by both groups on the same day; in these cases, the flasks were sampled less than 1 hour apart. The average difference for these samples (CFR - INSTAAR) is -0.04 ± 0.09‰ (the error estimate is the standard deviation, 1σ, of the differences). In an attempt to compare the two records for flasks sampled on different days, a smooth curve [*Thoning et al.*, 1989] was used to represent the INSTAAR record for days on which samples were not available. The smoothed curve is obtained by first fitting a curve consisting of the sum of a third-order polynomial trend and four-harmonics to the flask data; the residuals are then filtered in the time domain using a low-pass filter with a full width at half maximum of 100 days, and the smoothed residuals are added to the fitted curve. The smoothed curve was fitted to the INSTAAR data, and differences were calculated between the original flask data (for both INSTAAR and CFR) and the smoothed curve. These differences are shown in Figure 2. The mean difference between the CFR $\delta^{13}C$ values and the INSTAAR smoothed curve is -0.05 ± 0.08‰ for 26 samples. This analysis has been repeated using only INSTAAR data obtained under "background" conditions as defined by CFR; this eliminates ~50% of the INSTAAR measurements. This comparison of background samples appears in Figure 3. In this case, the average difference is -0.03 ± 0.07‰ for 18 samples. Each comparison suggests a slight offset between the calibration scales of the two groups, although in no case is the discrepancy greater than the error of the comparison.

CONCLUSION

A preliminary comparison between the time series of $\delta^{13}C$ measurements at Mace Head, obtained by LMCE and

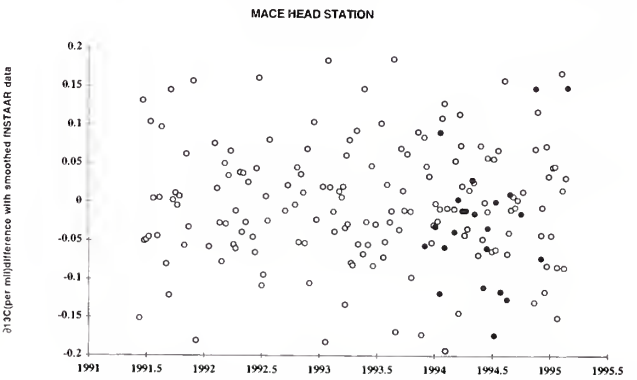

Fig. 2. Differences in $\delta^{13}C$ between the INSTAAR and CFR flask samples, and a smoothed curve fit through the INSTAAR time series. The INSTAAR data are shown with open circles, and the CFR-LMCE data by filled circles.

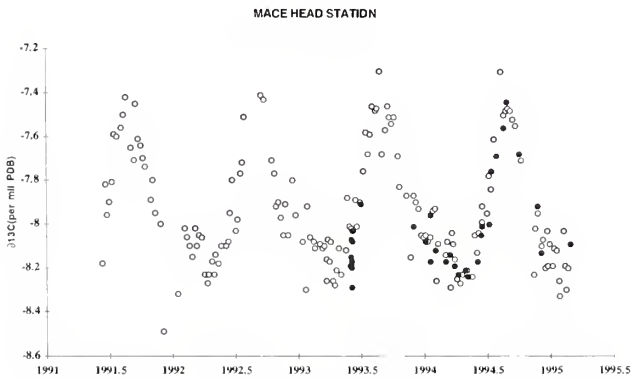

Fig. 1. Time series of $\delta^{13}C$ of atmospheric CO_2 measured from samples of air taken at Mace Head, Ireland, by the CMDL Cooperative Flask Sampling Network (open circles) and CFR-LMCE (filled circles). The CMDL samples were analyzed by INSTAAR at the University of Colorado.

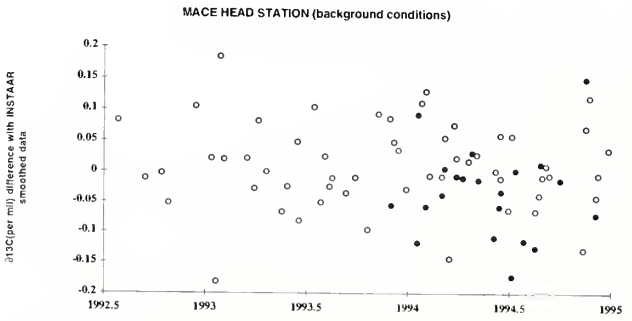

Fig. 3. Same as Figure 2, except that only CFR/LMCE data collected under "background" atmospheric conditions are used in the analysis of the differences.

INSTAAR-CMDL, covering approximately two annual cycles, is encouraging. An apparent offset of about -0.03 ±0.07‰ exists between the groups, with the CFR data being lighter. The limited duration of parallel sampling, and the small number of simultaneous samples, prevents a quantitative evaluation of drifts between the groups or a comparison of the range of the measurements observed during an annual cycle. While the intercomparison will be strengthened by continuing parallel sampling, simultaneous sampling and independent checks would be useful additions. The latter point will be partially addressed by a round-robin intercalibration being organized by the IAEA [*Allison et al.*, 1994] involving groups from Australia (CSIRO); the United States (INSTAAR, CMDL, and SIO); France (CFR-LMCE); and others.

REFERENCES

Allison C.E., R.J. Francey, L.P. Steele, and F. de Silva, The IAEA interlaboratory calibration program: Air standards for the IAEA round-robin exercise, in *Final Report on the IAEA Coordinated Research Program on Isotope Variations of Carbon Dioxide and Other Trace Gases in the Atmosphere*, edited by K. Rozanski, IAEA, Vienna, Austria, 1994.

Ciais P., P.P. Tans, M. Trolier, J.W.C. White, and R.J. Francey, A large northern hemisphere terrestrial CO_2 sink indicated by $^{13}C/^{12}C$ of atmospheric CO_2, *Science*, in press, 1996.

Francey R.J., C.E. Allison, L.P. Steele, R.L. Langenfelds, E.D. Welch, J.W.C. White, M. Trolier, P.P. Tans, and K.A. Masarie, Intercomparison of stable isotope measurements of CO_2, in *Climate Monitoring and Diagnostics Laboratory, No. 23: Summary Report 1994*, edited by J.T. Peterson and R.M. Rosson, NOAA Environmental Research Laboratories, Boulder, CO, pp. 106-110, 1995.

Hut, G., Consultant's group meeting on stable isotope reference samples for geochemical and hydrological investigations, IAEA report, Vienna, September 1985, 1987.

Lefèvre, N., A first step towards a reference ΔP map for the North Atlantic ocean, IGBP-10, working paper 11, 1995.

Thoning, K.W., P.P. Tans, and W.D. Komhyr, Atmospheric carbon dioxide at Mauna Loa Observatory, 2: Analysis of the NOAA/GMCC data, 1974–1985, *J. Geophys. Res.*, 94, 8549-8565, 1989.

Trolier, M., Calibrating the INSTAAR-NOAA/CMDL record of stable isotopic composition of atmospheric CO_2, in *Final Report on the IAEA Coordinated Research Program on Isotope Variations of Carbon Dioxide and Other Trace Gases in the Atmosphere*, edited by K. Rozanski, IAEA, Vienna, Austria, 1994.

Trolier, M., J.W.C. White, P.P Tans, K.A. Masarie, and P.A. Gemery, Monitoring the isotopic composition of atmospheric CO_2: Measurements from the NOAA global air sampling network, *J. Geophys Res.*, in press, 1996.

Measurement of Short Period Magnetic Pulsations at Barrow: A Key Location in the STEP Polar Network

KANJI HAYASHI
Department of Earth and Planetary Physics, The University of Tokyo, Bunkyo, Tokyo 113, Japan

The main objective of the Solar Terrestrial Energy Program (STEP) polar network is to realize a high time-resolution global scale network to trap disturbances induced by the solar-terrestrial links that occur somehow like earthquakes. Solar cycle effects found in occurrences of a type of short period magnetic pulsations termed as Pc1, is an unsolved and interesting target for long-term observation.

Magnetic field measurements are obtained at BRW with a highly sensitive (~ 3 pT @ 1Hz) induction magnetometer in operation almost continuously for more than 1 year when a new digital data logger was installed. The installation and the initial settings were carefully managed by the station operators.

Data status: A significant amount of DC offset and its drift in the Y component were observed in warm seasons. It was a known problem of the instrument and was reported that it settled down in the cold season. We guess that connection points along the signal cable going to the Y sensor were probably wet. Electromotive force from the sensor is very low (less than 1 Mv) and is easily overcome by battery effects at wet contacts. It will be fixed in 1996 by checking the cable.

Data release: Acquired data are primarily processed for our research but are provided for any other researchers on request and compressed data is in free access on the Internet via anonymous ftp at "hpgrl.grl.s.u-tokyo.ac.jp." The volume of high resolution data such as acquired at BRW is as much as 130 MB each month on a cassette tape. Whole-month data from about 20 sites (potentially 30 if all work well) is too much to place on the disk for free access, but will be placed on image files that contain frequency versus time display.

Total Nitrate and MSA Variation at Mauna Loa

B. J. Huebert and L. Zhuang
Department of Oceanography, University of Hawaii, Honolulu 96822

Introduction

Much of the NO and NO_2 emitted into the atmosphere is converted to nitric acid vapor or aerosol nitrate before being removed by dry or wet deposition. This conversion to nitrate is largely complete within a few days of the odd-nitrogen's emission so that in remote areas such as at the Mauna Loa Observatory, Hawaii (MLO), the total nitrate concentration (vapor plus aerosol) represents a fair estimate of the total odd-nitrogen concentration [*Atlas et al.*, 1992].

With support from NSF, we have measured nitrate concentrations at MLO for several years to help identify the important sources of odd-nitrogen compounds in remote parts of the globe. We now measure total nitrate every night from the walkup tower in collaboration with the MLO staff. We have also begun measuring methanesulfonate (MSA) aerosol.

Material and Methods

We use a Teflon/nylon filter pack method for collecting atmospheric nitrate. Since August 1988, one filter has been exposed each night from 2000 to 0800 LST. Filters are returned to the University of Hawaii laboratory for extraction and analysis by ion chromatography.

The data from August 1991 to July 1992 was, unfortunately, treated differently from the remainder. These samples were all analyzed as a batch during a brief period between the return of our analytical laboratory from a field deployment in the Azores and its shipment to its new home at the University of Hawaii. Once it became apparent that this data looked very different from previous years, it was no longer possible to replicate the analytical conditions or the standards to resolve questions of its validity. Hence, that data is excluded from the figures in this report.

Results and Discussion

In 1993 we published a description of gradient measurements of nitric acid and aerosol nitrate at MLO [*Lee et al.*, 1993]. This work showed surface-active species, like nitric acid, often have large gradients near the surface at MLO, raising the potential for underestimating free tropospheric concentrations due to depletion of material upstream of samplers. The deposition velocity of nitric acid to the lava surface varied from 0.3 to 4 cm s^{-1}.

During our intermittent MLO sampling prior to September 1988, we observed a sharp maximum in nitric acid and aerosol nitrate concentrations in the summer. The search for an explanation for this maximum continues to stimulate our science. The daily total nitrate values for 1995 are plotted in Figure 1. The lowest sustained concentrations are still evident in the winter with a mix of high-concentration events and cleaner periods in the spring and late summer.

Figure 2 shows monthly averages of 2000 to 0800 LST total nitrate concentrations from September 1988 to December 1995. The 1993 data represent the lowest

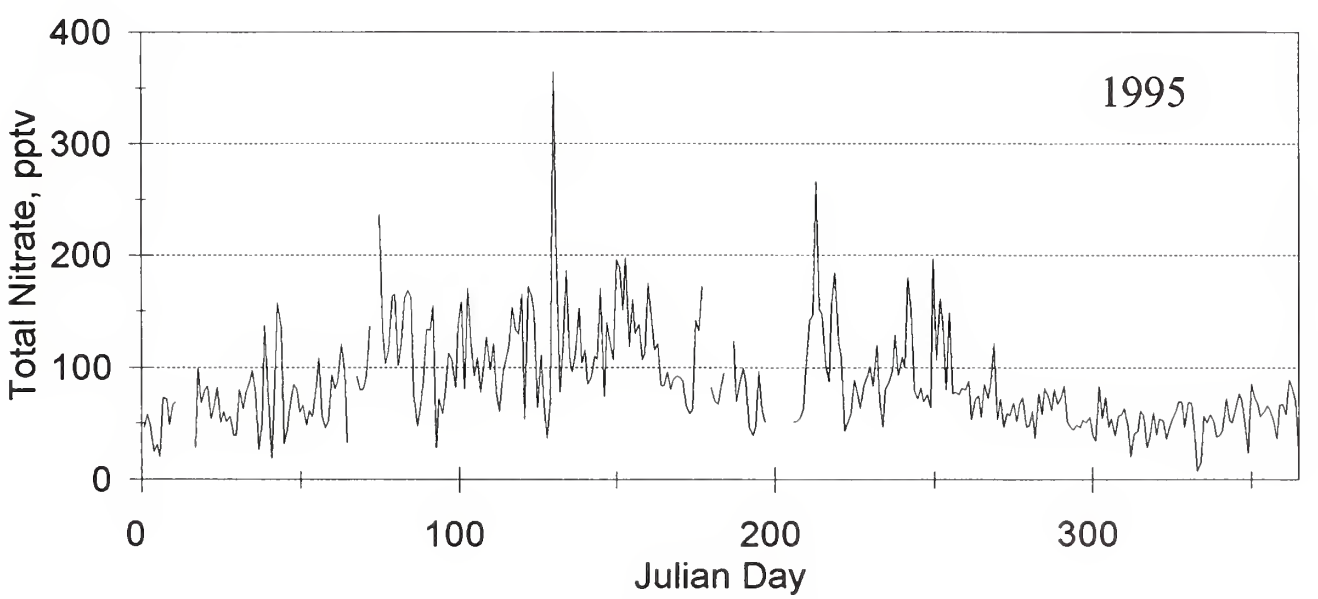

Fig. 1. Nightly concentrations of total nitrate in 1995.

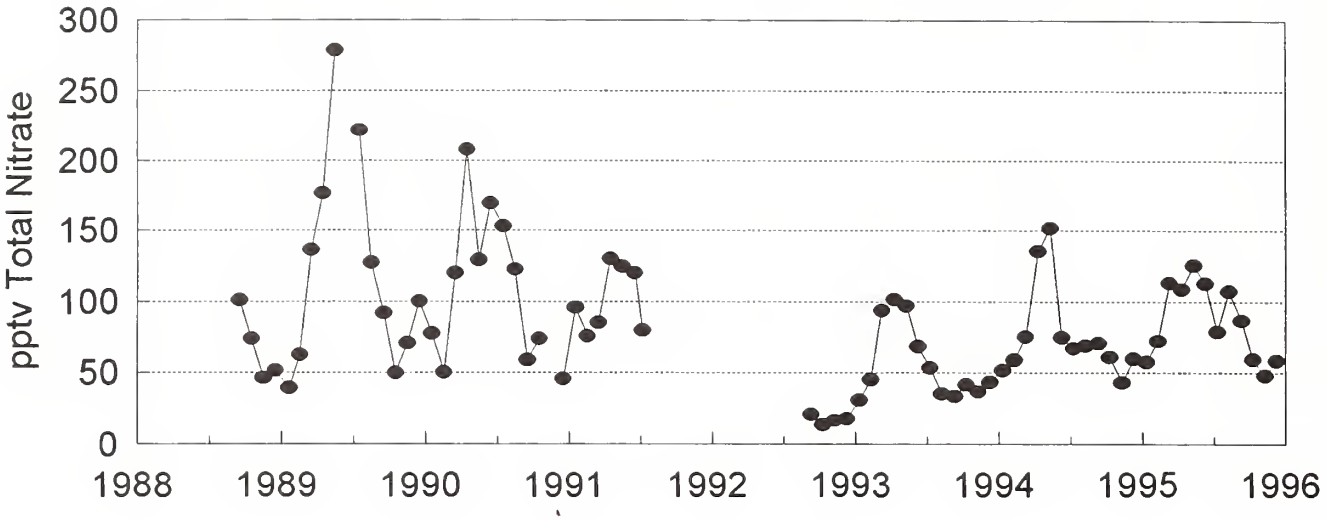

Fig. 2. Monthly average total (aerosol plus vapor) nitrate versus time.

(defendable) concentrations we have observed during our sampling at MLO.

The concentration of total nitrate at MLO is to a large extent controlled by precipitation scavenging of soluble material during transport from the continents [*Lee et al.*, 1994] so this interannual variability may be an indicator of changes in large-scale precipitation patterns. The apparently monotonic decrease in summertime total nitrate from 1988 through 1991 suggests that a cyclic process, such as the southern oscillation, may be reflected in this record. It is certainly reasonable that the transport of continental materials like mineral aerosol and fixed nitrogen (which can be limiting nutrients in certain parts of the Pacific) should be sensitive to changes in large-scale atmospheric circulation patterns. Clearly, we need to identify the climatological differences that cause this dramatic change in the annual cycle of nitrate from 1 year to the next since they may have impacts on phenomena as diverse as marine biological productivity and the earth's radiation budget.

In February 1995 we began to analyze our filter samples for MSA, since MSA is an indicator of dimethylsulfide (DMS) oxidation [*Huebert et al.*, 1996]. We are interested in the potential that DMS oxidation in the free troposphere may be responsible for much of the MSA (and some of the sulfate) found in ice cores. As Figure 3 shows, the annual cycle of MSA is both distinct and different from that of either nitrate or non-seasalt sulfate (NSS). The summer MSA minimum could be due to slower DMS transport, a change in the amount of MSA produced from DMS, or more rapid MSA removal. It is clear from the data that the MSA we see is not due to boundary-layer contamination of our samples since it is rarely accompanied by Cl or Na, which are clear indicators of boundary-layer air in our samples.

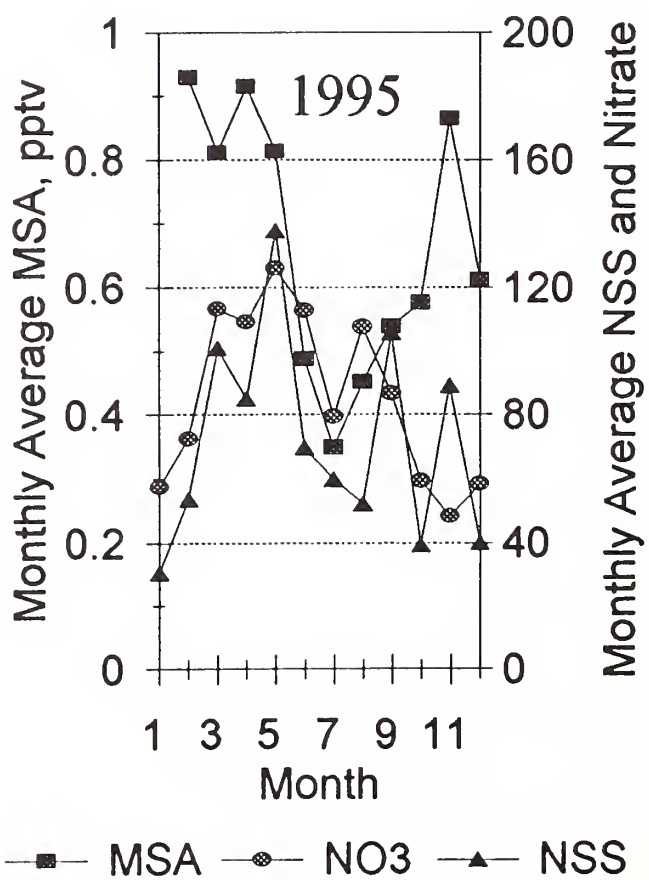

Fig. 3. Monthly average MSA, sulfate, and total nitrate for 1995.

Ongoing Research

With the help of the MLO staff, we are continuing our nightly sampling from the tower. Although equipment failures and analytical problems unavoidably cause lapses in the data, a very interesting record is emerging. We intend to continue this total nitrate data record in the hopes of identifying those factors which control the form and the range of its annual cycle.

References

Atlas, E.L., B.A. Ridley, G. Hübler, M.A. Carroll, D.D. Montzka, B. Huebert, R.B. Norton, J. Walega, F. Grahek, and S. Schauffler, Partitioning and Budget of NO_y Species During MLOPEX, *J. Geophys. Res.*, 97, 10,449-10,462, 1992.

Huebert, B.J., D.J. Wylie, L. Zhuang, and J.A. Heath, Production and loss of methanesulfonate and non-sea salt sulfate in the equatorial Pacific marine boundary layer, *Geophys. Res. Lett.*, 23, 737-740, 1996.

Lee, G., J.T. Merrill, and B.J. Huebert, Variation of Free Tropospheric Total Nitrate at Mauna Loa Observatory, Hawaii, *J. Geophys. Res.*, *99*, 12,821-12,831, 1994.

Lee, G., L. Zhuang, B.J. Huebert, and T.P. Meyers, Concentration Gradients and Dry Deposition of Nitric Acid Vapor at Mauna Loa Observatory, Hawaii, *J. Geophys. Res.*, *98*, 12,661-12,671, 1993.

Radionuclides in Surface Air at BRW, MLO, SMO, and SPO During 1994 and 1995

JOHN KADA AND COLIN G. SANDERSON
Environmental Measurements Laboratory, U.S. Department of Energy, New York, 10014-3621

INTRODUCTION

High volume air filter samples are routinely collected by CMDL personnel at BRW, MLO, SMO, and SPO for the Surface Air Sampling Program (SASP), a global network of aerosol sampling sites operated by the Environmental Measurements Laboratory. On a global scale the SASP network provides the capability to track atmospheric releases of artificial radionuclides due to nuclear weapons tests or nuclear accidents. At BRW this was most recently demonstrated by the detection of anthropogenic radionuclides released into the atmosphere by a chemical explosion and fire at the Tomsk-7 nuclear complex in Russia, 5000 km from BRW [*Larsen et al.*, 1994]. The SASP network also produces data on temporal and spatial trends in the worldwide distribution of the natural radionuclides ^{7}Be and ^{210}Pb. The SASP data has proven to be a valuable check on the transport and aerosol scavenging components of global climate models [*Rehfeld and Heimann*, 1994] and provides the bulk of the data available for this purpose.

MATERIAL AND METHODS

Air samplers drawing ~1700 m^3 of air per day through polypropylene air filters are in continuous operation at all four sites. Air filters are changed four times per month by local CMDL personnel and sent back to our laboratory on a monthly basis. Monthly composite samples are formed using half samples from each air filter, and these are analyzed for gamma emitting radionuclides using an n-type coaxial high-purity germanium (HPGe) detector. Under special circumstances, as discussed below for SMO samples collected in the autumn of 1995, monthly analyses are supplemented by individual filter sample analyses; subsamples representing about 15% of the active area of each filter are analyzed using a 1.5-cm diameter HPGe well detector. More detailed information on preparation and analysis of samples is available in reports containing data for the full SASP network [*Larsen et. al.*, 1995].

RESULTS

In Table 1 monthly ^{210}Pb, ^{7}Be, ^{95}Zr, ^{137}Cs, and ^{144}Ce concentrations in surface air at BRW, MLO, SMO, and SPO during 1994 and 1995 are decay corrected to the midpoint of the sample collection month. Concentrations reported as "less than" values reflect the lower limits of detection for the individual nuclides, which we take to be three times the one sigma uncertainty in the background counts in the region of the gamma spectrum used to quantitate each nuclide. The gap in ^{7}Be and ^{210}Pb data for the SPO site in 1994 is due to the loss of samples

TABLE 1. Average Surface Air Concentrations of Radionuclides

Date	^{7}Be (mBq m^{-3})	^{210}Pb (mBq m^{-3})	^{95}Zr (μBq m^{-3})	^{137}Cs (μBq m^{-3})	^{144}Ce (μBq m^{-3})
			BRW		
1994					
Jan.	n.d.	.74 ± .09	<87	<3	<10
Feb.	2.1 ± 0.3	.83 ± .09	<9	<2	<8
March	2.4 ± 0.3	1.12 ± .12	<6	<2	<6
April	2.3 ± 0.2	.48 ± .05	<4	<1	<5
May	2.2 ± 0.2	.24 ± .03	<6	<1	<6
June	0.5 ± 0.1	.04 ± .01	<25	<1	<7
July	n.d.	.05 ± .02	<31	<2	<11
Aug.	0.5 ± 0.1	.07 ± .01	<30	<2	<11
Sept.	0.9 ± 0.2	.10 ± .02	<56	<3	<5
Oct.	1.1 ± 0.2	.22 ± .03	<13	<2	<9
Nov.	1.6 ± 0.2	.48 ± .05	<20	<2	<3
Dec.	1.8 ± 0.2	.69 ± .07	<4	<1	<4
1995					
Jan.	2.0 ± 0.2	.84 ± .09	<4	<1	<6
Feb.	1.6 ± 0.2	.71 ± .08	<20	<1	<7
March	1.7 ± 0.2	.53 ± .06	<13	<1	<6
April	1.6 ± 0.2	.35 ± .04	<7	<1	<8
May	1.1 ± 0.2	.12 ± .02	<15	<2	<9
June	1.3 ± 0.2	.09 ± .01	<6	<2	<5
July	0.7 ± 0.1	.07 ± .01	<2	<1	<2
Aug.	0.6 ± 0.1	.06 ± .01	<6	<1	<6
Sept.	1.9 ± 0.3	.22 ± .03	<9	<2	<10
Oct.	1.3 ± 0.1	.18 ± .02	<8	<1	<5
Nov.	1.6 ± 0.2	.41 ± .05	<8	<1	<8
Dec.	1.9 ± 0.2	1.21 ± .13	<13	<2	<1
			MLO		
1994					
Jan.	6.3 ± 0.7	.26 ± .04	<17	<2	<11
Feb.	4.4 ± 0.5	.13 ± .02	<12	<3	<14
March	5.8 ± 0.6	.33 ± .05	<11	<3	<14
April	8.9 ± 0.9	.47 ± .06	<9	<3	<16
May	5.4 ± 0.6	.32 ± .04	<6	<2	<9
June	5.6 ± 0.6	.21 ± .03	<11	<3	<14
July	4.4 ± 0.5	.18 ± .03	<12	<3	<15
Aug.	4.1 ± 0.5	.15 ± .04	<17	<4	<17
Sept.	4.6 ± 0.5	.18 ± .04	<11	<3	<15
Oct.	6.0 ± 0.6	.30 ± .04	<13	<2	<10
Nov.	6.1 ± 0.6	.18 ± .02	<5	<1	<5
Dec.	8.0 ± 0.8	.30 ± .04	<28	<3	<6
1995					
Jan.	0.3 ± 0.1	.03 ±.01	<7	<2	<8
Feb.	5.6 ± 0.6	.32 ± .04	<4	<1	<5
March	7.0 ± 0.7	.43 ± .04	<13	<1	<6
April	6.8 ± 0.7	.45 ± .07	<14	<4	<18
May	7.1 ± 0.8	.45 ± .05	<11	<2	<10
June	7.8 ± 0.9	.41 ± .05	<22	<3	<18
July	5.4 ± 0.6	.20 ± .03	<45	<5	<8
Aug.	6.9 ± 0.8	.24 ± .05	<14	<3	<16
Sept.	5.8 ± 0.6	.25 ± .05	<14	<4	<16
Oct.	7.0 ± 0.8	.31 ± .05	<16	<5	<23
Nov.	3.6 ± 0.4	.18 ± .03	<11	<2	<9
Dec.	5.8 ± 0.6	.20 ± .03	<29	<4	<8

TABLE 1. Average Surface Air Concentrations of Radionuclides - Continued

Date	^{7}Be (mBq m^{-3})	^{210}Pb (mBq m^{-3})	^{95}Zr (μBq m^{-3})	^{137}Cs (μBq m^{-3})	^{144}Ce (μBq m^{-3})
			SMO		
1994					
Jan.	2.3 ± 1.2	55 ± 12	<504	<2	<6
Feb.	2.0 ± 0.2	64 ± 13	<13	<2	<11
March	1.6 ± 0.2	34 ± 12	<5	<1	<5
April	1.1 ± 0.1	27 ± 19	<6	<2	<9
May	1.7 ± 0.2	44 ± 20	<10	<2	<10
June	2.7 ± 0.3	52 ± 11	<12	<2	<3
July	2.3 ± 0.2	46 ± 11	<3	<1	<4
Aug.	3.1 ± 0.3	56 ± 21	<5	<2	<10
Sept.	2.5 ± 0.4	105 ± 20	<74	<3	<6
Oct.	1.5 ± 0.2	63 ± 15	<6	<1	<6
Nov.	2.0 ± 0.2	55 ± 11	<15	<2	<3
Dec.	0.9 ± 0.1	39 ± 10	<8	<2	<8
1995	2.2 ± 0.2	36 ± 15	<18	<4	<5
Jan.	1.7 ± 0.2	51 ± 8	<8	<1	<2
Feb.	1.7 ± 0.2	47 ± 15	<5	<2	<7
March	2.2 ± 0.2	53 ± 13	<11	<1	<6
April	1.3 ± 0.2	60 ± 14	<50	<3	<5
May	2.9 ± 0.4	69 ± 14	<10	<2	<10
June	2.5 ± 0.3	65 ± 20	<9	<2	<10
July	2.4 ± 0.3	55 ± 12	<6	<1	<8
Aug.	3.2 ± 0.4	86 ± 15	<5	<1	<8
Sept.	2.7 ± 0.3	84 ± 22	<8	<2	<11
Oct.	1.8 ± 0.2	51 ± 11	<6	<2	<8
Nov.	3.2 ± 0.3	77 ± 9	<6	<1	<2
Dec.					
			SPO		
1994					
Jan.	6.1 ± 0.7	36 ± 12	<10	<2	<9
Feb.	n.d.	28 ±1 2	<399	<2	<43
March	5.9 ± 1.0	30 ± 6	<141	<1	<12
April	4.2 ± 1.3	39 ± 18	<427	<4	<11
May	2.2 ± 0.6	34 ± 15	<72	<2	<12
June	4.1 ± 0.7	34 ± 10	<86	<3	<16
July	n.s.	n.s.	n.s.	n.s.	n.s.
Aug.	n.s.	n.s.	n.s.	n.s.	n.s.
Sept.	n.s.	n.s.	n.s.	n.s.	n.s.
Oct.	n.s.	n.s.	n.s.	n.s.	n.s.
Nov.	n.s.	n.s.	n.s.	n.s.	n.s.
Dec.	n.s.	n.s.	n.s.	n.s.	n.s.
1995					
Jan.	n.s.	n.s.	n.s.	n.s.	n.s.
Feb.	11.2 ± 1.4	51 ± 9	<41	<1	<9
March	11.3 ± 1.6	54 ± 17	<166	<5	<32
April	5.9 ± 0.8	29 ± 9	<36	<1	<12
May	5.0 ± 0.8	41 ± 19	<52	<3	<23
June	4.9 ± 0.7	48 ± 40	<56	<4	<26
July	3.8 ± 0.5	33 ± 10	<11	<1	<10
Aug.	4.6 ± 0.6	40 ± 8	<20	<1	<8
Sept.	4.3 ± 0.7	44 ± 35	<56	<5	<25
Oct.	7.1 ± 0.8	47 ± 15	<77	<4	<7
Nov.	10.9 ± 1.2	83 ± 24	<37	<5	<26
Dec.	10.8 ± 1.1	70 ± 14	<16	<3	<14

n.d. = not detected
n.s. = no sample

during shipment back to EML; occasional gaps in ^{7}Be data for other sites are the result of unavoidably long delays between collection and analysis of samples allowing the relatively short-lived ^{7}Be ($t_{1/2}$ = 53 days) to radioactive decay below detection levels.

Seasonal cycles in the concentrations of ^{7}Be and ^{210}Pb at the four sites are consistant with previous observations [*Larsen et al.*, 1995]. Concentrations of artificial radionuclides were below detection limits in all analyzed samples from the four sites. There were no known large scale releases of anthropogenic radionuclides into the atmosphere in regions likely to influence surface air concentrations at BRW, MLO, and SPO, thus the anthropogenic radionuclide data for these three sites are as expected. A potential source of anthropogenic radioactivity at SMO was a series of subsurface detonations of low-yield nuclear devices conducted by the French government at Muraroa and Fangataufa atolls, ~3000 km ESE of SMO between September 1995 and February 1996. In spite of reassurances on the part of the French government, there was widespread public concern regarding the possibility of environmental releases of artificial radioactivity from these tests. Surface air concentrations of ^{95}Zr, ^{137}Cs, and ^{144}Ce in monthly composite samples from SMO (Table 1) remained below detection limits in the last 3 months of 1995 supporting the contention that no release of anthropogenic radioactivity into the atmosphere occurred. During the period of testing at Muraroa and Fangataufa, air filters collected at SMO were returned to our laboratory by express courier service, and monthly composite analyses were supplemented by analyses of individual air filters; artificial radionuclide activities were below detection limits in all of these samples as well.

Acknowledgment. We wish to thank the CMDL staff at BRW, MLO, SMO, and SPO for the collection of air filter samples for SASP.

REFERENCES

Rehfeld, S. and M. Heimann, Three dimensional atmospheric transport simulation of the radioactive tracers ^{210}Pb, ^{7}Be, ^{10}Be, and ^{90}Sr, *Max-Planck-Institut fur Meteorologie Rep. No. 144,* Hamburg, 1994.

Larsen, R.J., C.G. Sanderson and J. Kada, EML surface air sampling program, 1990-1993 data, *U.S. DOE Rep. EML-572*, U.S. Dept. of Energy, Environmental Measurements Laboratory, New York, 1995.

Larsen, R.J., C.G. Sanderson, H.N. Lee, K.M. Decker and H.L. Beck, Fission products detected in Alaska following the Tomsk-7 accident, *J. Environ. Radioact.*, 23, 205-209, 1994.

Global Distribution of Chloroform in the Marine Boundary Layer

M.A.K. KHALIL
Department of Physics, Portland State University, Portland, Oregon 97207-0751

R.A. RASMUSSEN
Department of Environmental Science, Oregon Graduate Institute, Portland, Oregon 97291

Atmospheric chloroform comes from many natural and anthropogenic sources. We discuss its latitudinal distribution in the atmospheric boundary layer based on data taken at six sites, between January 1986 and January 1995, operated by the CMDL program. The interhemispherical ratio of concentrations is about 2.1 + 0.2 and the globally-averaged concentration is 17.3 + 1.3 pptv (+ values are 90% confidence limits).

In recent years there has been a growing interest in the global budgets of chlorine containing trace gases in the atmosphere because of their role in depleting the stratospheric ozone layer and in affecting tropospheric ozone. The most important of these gases are the chlorofluorocarbons, but other gases such as methylchloride, chloroform, trichloroethylene, perchloroethylene, dichloromethane and similar compounds also contribute to the reservoir of relatively long-lived chlorine containing gases with lifetimes between a month and several years. Little is known about the global budgets and biogeochemical cycles of these gases.

In this paper we describe the salient features of the global distribution of chloroform ($CHCl_3$). Chloroform is emitted in substantial quantities from the oceans and soils. In addition, there are many anthropogenic sources, including emissions from chlorination of water, chemical manufacturing, and combustion processes [*Graedel,* 1978; *Khalil et al.,* 1983, 1990].

Between 1986 and 1994 we obtained flask samples from eight sites distributed around the world. This sampling is part of our cooperative project with the CMDL program supplemented with our own sites. The sites are Barrow, Alaska (BRW) (71.16°N, 156.5°W), Cape Meares, Oregon (CM 45.5°N, 124°W), Cape Kumukahi and Mauna Loa, Hawaii (CK and MLO 19.3°N, 154.5°W), Samoa (SA 14.1°S, 170.6°W), Cape Grim, Tasmania (CG 42°S, 145°E), Palmer Station (PS 64.46°S, 64.05°W) and the South Pole (SP 90°S). Data from these sites are reported in Figure 1. It is important to note that these concentrations represent a long-term climatology of chloroform concentrations and that these measurements represent the marine boundary layer. There is evidence that over land, concentrations can be substantially higher at some latitudes.

Table 1 shows the concentration of chloroform at the five main sites where there are enough data to estimate mean

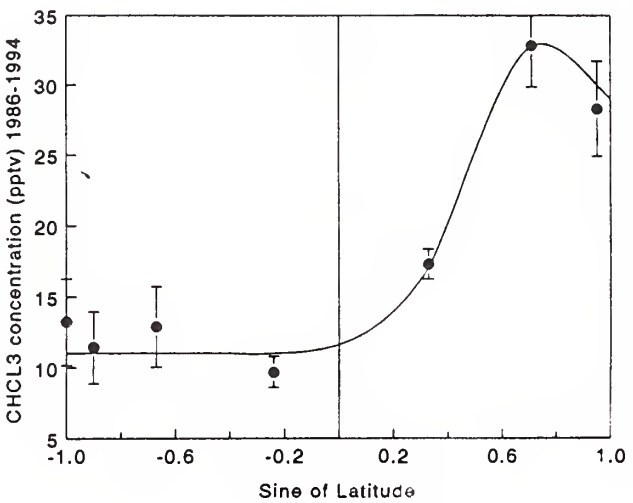

Fig. 1: The long-term concentration of chloroform in the marine boundary layer. Data shown here were taken between January 1986 and January 1995. From north to south (sine latitude = +1, the sites are Barrow, Alaska; Cape Meares, Oregon; Cape Kumukahi, Hawaii; Samoa; Cape Grim, Tasmania; Palmer Station, Antarctica; and the South Pole.

TABLE 1. Annual and Long-Term Averages of Chloroform Concentrations (pptv)

	BRW	CM	CK	SA	TA	SP
1986	26	33	15	9	8	19
1987	26	35	16	9	10	7
1988	30	35	16	11	11	8
1989	37	42	16	9	11	12
1990	36	34	19	13	24	14
1991	28	32	18	11	15	12
1992	24	30	20	8	11	9
1993	24	28	17	8	14	NA
1994	23	26	18	9	12	NA
Average	28.3	32.8	17.3	9.7	12.9	11.4
Sine latitude	0.95	0.71	0.33	-0.24	-0.67	-0.9

annual concentrations for each of the years between January 1986 and January 1995. The results show that there are no secular trends, although the concentrations do tend to increase and decrease over short periods of time. The trends, over the entire period, are generally not statistically significant at the 5% level. Concentrations seemed to have increased between 1986 and 1990 and then have been falling to the present.

Acknowledgments. This work was supported in part by grants from NSF (ATM-8109047) and DOE (DE-FG06-85ER6031). Additional support was provided by the Biospherical Research Corporation and the Andarz Co. We thank the staffs of the CMDL program, the Baseline Cape Grim Station, and CSIRO for collecting samples. We thank Don Stearns, Jim Mohan, Bob Dalluge, Rohith Gunawardena (OGI), Martha Shearer and Francis Moraes (PSU), for their contributions to the project.

REFERENCES

Graedel, T.E., *Chemical Compounds in the Atmosphere*, Academic Press, NY, 440 pp., 1978.Khalil, M.A.K., R.A. Rasmussen, and S.D. Hoyt, Atmospheric chloroform: Ocean-air, exchange and global mass balance, *Tellus*, 35B, 266-274, 1983.

Khalil, M.A.K., R.A. Rasmussen, J.R. French, and J. Holt, The influence of termites on atmospheric trace gases, *J. Geophys. Res.*, 95, 3619-3634, 1990.

NSWC Pt. Barrow Geomagnetic Observatory

DANIEL S. LENKO, JOHN F. SCARZELLO, AND DAVID TAYLOR
Naval Surface Warfare Center, Electromagnetic Fields Branch, Bethesda, Maryland 20903-5640

OBJECTIVE

The purpose of the observatory is to measure and characterize geomagnetic field variations using a sensitive magnetometer array for a period of at least one sunspot cycle.

BACKGROUND

The system was first installed in the spring of 1991. The three magnetometer sensor suites were placed on Air Force Long Range Radar Site Pt. Barrow property and cables connected the sensors to a PC in the CMDL Barrow Observatory building that controls the array and stores the magnetic information onto transportable media that is mailed to Maryland for analysis.

SENSORS

Configured to form two orthogonal gradiometer axes, magnetic N-S and E-W, with a 150 m baseline, each of the three magnetic sensor sites consists of actually two types of magnetometers. The first and most sensitive is the He-3 total field magnetometer which is an optically pumped, nuclear magnetic resonance sensing device. It provides a very accurate "absolute" measurement of the ambient magnetic field in the bandwidth from DC to about 0.1 Hz. In terms of sensitivity, the He-3 sensor can resolve submilligamma magnetic data when two sensors are configured as a gradiometer; here, a second He-3 sensor is used to cancel out earth's magnetic field. The dynamic range accommodates magnetic fields over 100,000 gamma, but the He-3 sensor is gradient sensitive which can shorten the measurement time between pumpings. The second magnetic sensor included in each location is a triaxial fluxgate magnetometer. The three orthogonal axes measure magnetic fields in a bandwidth from DC to about 1 Hz. The digital data is appended to each of the He-3 sample updates (2.34 times a second) and the fluxgate sensor can resolve about 0.1 gamma.

STATUS

The geomagnetic noise collected by the previously mentioned system has been characterized and used to develop and test noise reduction algorithms in an effort to enhance advanced detection methods. Specifically, Pt. Barrow ambient magnetic data has been "played" into detection software as a training data set. Also, on occasions, data from the observatory was used to correlate magnetic noise events at other locations throughout the world. In terms of the observatory hardware, the arctic environment is quite harsh and, therefore, cabling and sensor maintenance is in order. Also, computer and/or storage media upgrades will be performed as funds permit.

FUTURE

In order to complete the current sunspot cycle, NSWC plans to support the Pt. Barrow Observatory through the end of the decade.

Exposure Experiment, South Pole

JOHN E MAK
State University of New York at Stony Brook, Stony Brook, New York 11794-5000

CARL A.M. BRENNINKMEIJER
Max Planck Institt fur Chemie, Mainz, Germany

JOHN R. SOUTHON
Center for Accelerator Mass Spectrometry, Lawrence Livermore National Laboratory, Livermore, California 94551-9900

We are continuing with the exposure experiment for ^{14}C production rates at the South Pole.

The scope of this project is to directly detect and quantify the production rate of atmospheric ^{14}C. Carbon-14 is not only used for dating organic materials, it can also be used as a tracer of OH chemistry (in the form of ^{14}CO). In the latter case, if the inventory of ^{14}CO is measured and the production rate known, then the sink rate, which is oxidation by OH, can be calculated. Although cascade calculations have constrained the ^{14}CO production rate to 120%, it is of interest to measure this rate directly.

Carbon-14 is produced from the reaction:

$$^{14}N(n,p)^{14}C$$

which is immediately followed by:

$$^{14}C + O_2 \rightarrow {}^{14}CO + O \ (>90\% \text{ yield}).$$

The methodology takes advantage of gas-handling techniques previously developed by these authors. A known amount of CO carrier gas was mixed in with zero air and compressed into a suite of cylinders, some of which were placed 1 m above the surface at SPO. There they sit, exposed to incoming cosmic rays. After a certain length of time the cylinders are brought back to the isotope laboratory where the CO is extracted and measured for ^{14}C content at the Lawrence Livermore Center for Accelerator Mass Spectrometry.

Monte Carlo simulations are currently being performed at LLNL to estimate any effects from the mass of the cylinders used as well as the ground effect. These simulations indicate that the effect from the cylinders is small. The experimental results are still being analyzed, and preliminary analyses show that the amounts of ^{14}C produced at the South Pole would be easily detectable for an exposure time of about 6 months. To our knowledge, this is the second time direct ^{14}C detection has been achieved and the first time a ground effect has been accounted for by direct measurement. This is an ongoing cooperative project.

Investigation of the Transfer Function Between Snow and Atmosphere Concentrations of Hydrogen Peroxide at South Pole

JOSEPH R. MCCONNELL AND ROGER C. BALES
Department of Hydrology and Water Resources, University of Arizona, Tucson, 85721

INTRODUCTION

A key to understanding past and future climate lies in understanding the oxidizing capacity of the atmosphere through time. Extensive efforts were made over the past few years to use photochemical models to estimate past and future atmospheric concentrations of hydroxyl radical, ozone, and hydrogen peroxide which are the primary oxidants in the atmosphere [*Thompson et al.,* 1995]. However, these model studies of past atmospheres lack sufficient data for validation. Ice cores provide temperatures and CH_4 concentrations, but two of the oxidants, hydroxyl radical and ozone, are not preserved in the ice, and the correspondence between atmospheric and ice core hydrogen peroxide is not well understood [*Neftel et al.,* 1995]. A glacial ice record of atmospheric formaldehyde, an intermediate species in the oxidation of CH_4 by hydroxyl radical attack, could also help to lead to a reconstruction of the local hydroxyl radical concentration in the paleo-atmosphere. As with hydrogen peroxide, however, the correspondence of atmospheric and ice-core formaldehyde concentration is not known. Therefore, if the formaldehyde and hydrogen peroxide records in the polar ice cores are to be useful for oxidant modeling of both past and future climates, the transfer functions that relate atmosphere to snow to ice concentrations must be well defined.

Our research is an investigation of the atmospheric-ice transfer function for the reversibly deposited chemical species formaldehyde and hydrogen peroxide through laboratory, field, and computer modeling studies. Reversible implies that the species can be released from the snow and firn back to the atmosphere as conditions change and can be deposited back to the snow in response to further changes. The objective is to develop the capability to describe concentrations of formaldehyde and hydrogen peroxide in snow and ice, as functions of depth and time, given concentrations and conditions in the local atmosphere and properties of the snow and ice. This modeling capability will then be inverted and used to infer possible past atmospheric concentrations from observations of what is trapped in the ice, providing additional data constraints on tropospheric modeling.

PROCEDURES

As part of our cooperative agreement with CMDL, we deployed a detector for measuring H_2O_2 at the South Pole for a 3-week period in late November and early December 1994 and for a 2-week period in January 1996. Atmospheric measurements were made almost continuously during these time periods. When used for atmospheric analyses, our custom built H_2O_2 detector makes atmospheric measurements at approximately 10-minute intervals using a glass coil scrubber to transfer the peroxide from the continuous stream of air to water and then a chemical fluorescence method to determine the concentration in the water [*Bales et al.,* 1995]. When making snow and firn analyses, the samples are melted and the peroxide measurement made directly. A number of surface snow and shallow snowpit samples were collected and analyzed. In 1994, systematically and stratigraphically placed firn samples were collected from a 2.2 m backlit snowpit and a 1.0 m snowpit, both located in the clean air sector. Four snowpits, located adjacent to the snow stake accumulation field near the South Pole, were excavated and sampled at 1 cm resolution in 1996.

The CMDL winterover staff collect approximately 12 surface-snow samples each week throughout the year. This sampling started in December 1994 and continues currently. The samples collected prior to mid-January 1996 were returned to our laboratory in Tucson and were analyzed for H_2O_2 and, on a subset of the samples for $\delta^{18}O$, and some ionic species.

RESULTS

Average atmospheric H_2O_2 concentrations for the 3-week period in spring 1994 were approximately 320 pptv and, as expected, no diel cycle was observed [*Fuhrer et al.,* 1996]. Occasional rapid changes in atmospheric H_2O_2 were observed and a qualitative comparison with air parcel trajectories suggest a correlation of atmospheric H_2O_2 concentration with a source area, although there is also a correlation with local meteorological conditions. This is the subject of ongoing atmospheric chemistry modeling [*Thompson,* 1995]. Concentrations in summer 1996 were lower at approximately 100 pptv. Construction at the new clean air facility at the South Pole may have degraded these measurements somewhat.

Snowpit H_2O_2 concentrations from a pit collected in January 1996 are shown in Figure 1. Note the very obvious annual cycles in H_2O_2. Along with the other three snowpits from 1995 [*McConnell et al.,* 1995], these data will be used to parameterize and validate a snowpack model that we have developed and applied at Summit, Greenland, to investigate the atmosphere to snow transfer process [*McConnell, et al.,* 1996a]. Some revisions to the model are required because snow accumulation at the South Pole is much more sporadic [*McConnell, et al.,* 1996b].

The H_2O_2 concentrations in the surface snow samples are shown in Figure 2. Along with complimentary laboratory data [*Conklin, et al.,* 1992], these surface snow samples have been used to estimate the annual cycle in atmospheric H_2O_2 concentration [*McConnell et al.,* 1996c]. The results indicate that the surface snow provides a good proxy of the atmospheric H_2O_2 concentration throughout the year at the South Pole. Evaluation of the surface snow data continues.

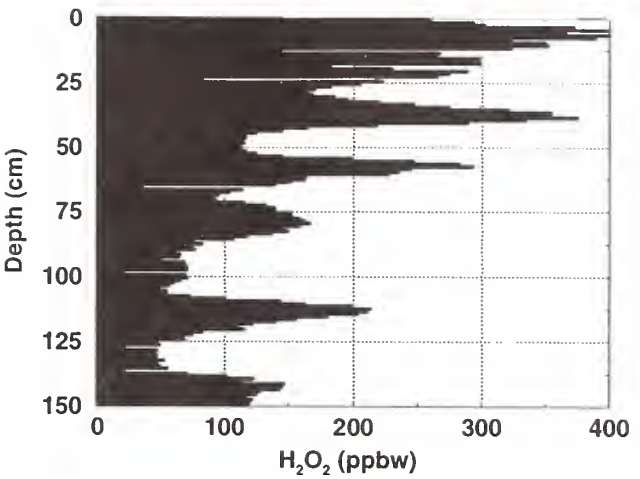

Fig. 1. Variations in hydrogen peroxide concentrations with depth at South Pole.

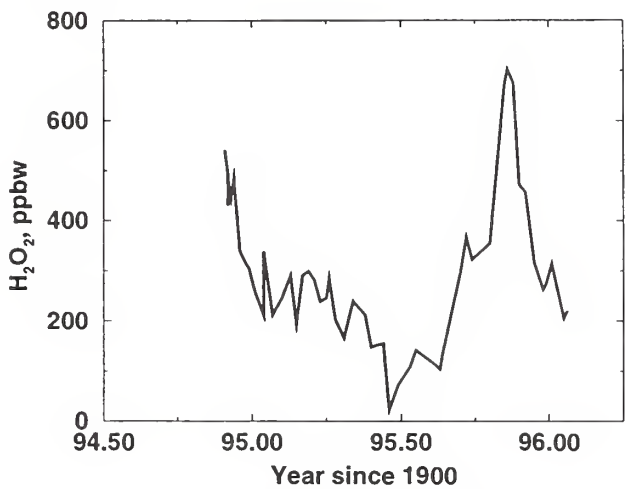

Fig. 2. Estimated atmospheric concentration of hydrogen peroxide at South Pole from a physically based inversion of surface snow concentrations.

Conclusion

A record of the oxidizing capacity of the atmosphere would improve our understanding of interactions between atmosphere and climate. This information could be used to better verify and parameterize global and local atmospheric circulation and photochemical models and so aid in predicting the impact of anthropogenic increases in greenhouse gases. However, a required step in reconstructing the oxidizing capacity of the atmosphere from polar ice cores is to fully understand the transfer relationship between atmospheric and snow/ice concentration for reversibly deposited species such as hydrogen peroxide and formaldehyde.

Based on year-round surface snow samples collected for us by CMDL staff, we conclude that the surface snow is acting as an effective archive of the atmospheric loading of hydrogen peroxide during the year. Whether or not this archive is preserved and under what conditions is the focus of ongoing work. Photochemical modeling is underway to better understand the atmospheric concentration time series measured in 1994 and 1996, especially in the context of the annual cycle inferred from the surface snow. Physical and chemical modeling of the near-surface snow and firn continues as we investigate the atmosphere-surface snow relationship and the differences in the near-surface firn profiles at Summit, Greenland, and the South Pole. The cooperation of the NOAA personnel in collecting surface snow samples and making atmospheric measurements have proven invaluable in our research into the atmosphere-to-snow transfer process, both for H_2O_2 and for reversibly deposited chemical species in general.

References

Bales, R.C., M.V. Losleben, J.R. McConnell, K. Fuhrer, and A. Neftel, H_2O_2 in snow, air, and open pore space in firn at Summit, Greenland, *Geophys. Res. Lett.*, 22(10), 1261-1264, 1995.

Conklin, M.H., A. Sigg, A. Neftel, and R.C. Bales, Atmosphere-snow transfer function for hydrogen peroxide: microphysical considerations, *J. Geophys. Res.*, 98(D10), 18,367-18,376, 1992.

Fuhrer, K., M. Hutterli, and J.R. McConnell, Overview of the recent field experiments for the study of the air-snow transfer of H_2O_2 and HCHO, in *Chemical Exchange Between the Atmosphere and Polar Snow*, edited by E. Wolff and R. Bales, NATA ASI Series I, 675 pp., Springer-Verlag, 1996.

McConnell, J.R., M. Conklin, and R. Bales, Hydrogen peroxide trends in South Pole firn, poster paper presented at the NATA ARW: Process of Chemical Exchange Between the Atmosphere and Polar Snow, Il Ciocco, Italy, 1995.

McConnell, J.R., R.C. Bales, J.R. Winterle, H. Kuhns, and C.R. Stearns, A lumped parameter model for the atmosphere-to-snow transfer function for hydrogen peroxide, *J. Geophys. Res.*, in press, 1996a.

McConnell, J.R., R.C. Bales, D.R. Davis, Recent intra-annual snow accumulation at South Pole: Implications for ice core interpretation, *J. Geophys. Res.*, in press, 1996b.

McConnell, J.R., A.M. Thompson, and R.C. Bales, Surface snow as a proxy for atmospheric hydrogen peroxide at South Pole, *EOS, Trans. AGU*, 5156, 1996c.

Neftel, A., R.C. Bales, and D.J. Jacob, Hydrogen peroxide and formaldehyde in polar snow and their relation to atmospheric chemistry, in *Ice Core Studies of Global Biogeochemical Cycles*, edited by R. Delmas, NATO ASI Series I, Vol. 30, pp. 249-264, 1995.

Thompson, A.M., Photochemical modeling of chemical cycles: issues related to the interpretation of ice core data, in *Ice Core Studies of Global Biogeochemical Cycles*, edited by R. Delmas, NATO ASI Series I, Vol. 30, pp. 265-297, 1995.

NDSC Stratospheric Ozone-Temperature-Aerosol Lidar

I. Stuart McDermid, Eric W. Sirko, and T. Daniel Walsh
Jet Propulsion Laboratory, California Institute of Technology, Table Mountain Facility, Wrightwood, California 92397-0367

Introduction

The Jet Propulsion Laboratory (JPL) lidar system, which measures stratospheric profiles of ozone, temperature, and aerosols for the Network for the Detection of Stratospheric Change (NDSC), was installed at the Mauna Loa Observatory, Hawaii (MLO) in July 1993. Since then it has been making regular nighttime measurements of these parameters, averaging more than 100 nights per year. The incidence of cirrus clouds and high winds at the observatory are the primary limiting factors on the number of measurements obtained.

A brief description of the original lidar system was given in CMDL Summary Report No. 22. Some modifications have been carried out since the initial installation to increase the altitude range over which the profiles can be measured. The impetus for these changes was the increased need to obtain ozone measurements in the upper troposphere in addition to the stratospheric measurements. To enable the increased altitude range of these measurements, the field-of-view of the telescope was increased so that the laser and telescope would overlap at lower altitudes. These changes were carried out just prior to the Stratospheric Ozone Profile Intercomparison (MLO3) NDSC intercomparison campaign (see below) and it turned out the increased field-of-view caused a saturation in the receiver at low altitudes resulting in incorrect measurements in this region. Following MLO3, the detectors in the receiver were changed to correct this problem, and since the beginning of 1996 high-quality ozone profiles are routinely obtained over the altitude range from ~13-km to >55-km. Temperature profiles, from the combined Rayleigh and Raman returns, typically cover the altitude range from just below the tropopause to about the mesopause, ~15-km to >80-km. Enhanced stratospheric aerosols from the eruption of Mt. Pinatubo are no longer observable in our lidar observations and the level of aerosols in the Junge layer of the lower stratosphere only just exceeds our detection limit indicating that this region has returned, at least, to the pre-Pinatubo levels. Since we were not operating at MLO prior to the Mt. Pinatubo eruption, we cannot comment on the suggestion that the aerosol loading is even lower than before except to say that the aerosol levels we are currently observing are very low.

Results

During the winter of 1994-1995 the CMDL Dobson spectrophotometer indicated very low ozone column content dipping below 200 Dobson Units (DU) for the first time in the measurement record. The lidar profiles are routinely integrated to obtain stratospheric column amounts and these can be compared with the Dobson results. Also the profiles can be studied to determine where the losses are actually occurring. Changes in the integrated lidar profile for both daily measurements and for monthly mean column amounts agreed very well with the Dobson data. Compared to the winters of 1993-1994 and 1995-1996 the period of low ozone in 1994-1995 extended from about September through June. Inspection of the ozone profiles showed the maximum ozone reduction occurred at approximately 30-km altitude and extended from roughly 25-km to 35-km.

MLO3

During August 1995 a formal NDSC intercomparison of ozone profiling instruments was carried out at MLO and refereed by a National Aeronautic and Space Administration-Goddard Space Flight Center (NASA-GSFC) scientist. The participating instruments included the JPL lidar, the Millitech-NASA/LaRC microwave radiometer, the NASA/GSFC mobile lidar, and CMDL electrochemical concentration cell (ECC) balloon sondes (launched from Hilo). Additionally, satellite data from the Stratospheric Aerosol and Gas Experiment (SAGE) II and the Upper Atmosphere Research Satellite (UARS) MLS were provided for intercomparison. The results from the campaign are still being evaluated and will be published sometime in the near future. Here, we just consider the preliminary conclusions for the JPL lidar. From 20-km to the maximum altitudes reported (i.e., up to 60-km) the JPL lidar results agreed very well with the consensus profile in this region. However, below 20-km the JPL lidar profile showed a positive deviation from the correct profile, increasing as the altitude decreased. As indicated earlier, this was determined to be caused by a saturation effect caused by increasing the field-of-view of the telescope. Following the campaign, this problem was thoroughly investigated and a new, different design, photomultiplier tube was installed in all of the receiver channels. The correct operation of the modified system was then verified in several informal intercomparisons with the GSFC lidar and the Millitech-NASA/LaRC microwave radiometer over the period up to the end of 1995. We are now confident that the ozone results from the JPL lidar are accurate over the range from ~13-km to >55-km.

An evaluation of the performance of the temperature measurement capabilities of the lidars is also underway and will compare the results obtained by JPL, GSFC, CMDL lidar systems, and the CMDL balloon sondes during MLO3.

Acknowledgments. The work described here was carried out by the Jet Propulsion Laboratory, California Institute of Technology, under an agreement with the National Aeronautics and Space Administration. We are grateful to the staff at MLO for continuing support of this program.

Antarctic UV Spectroradiometer Monitoring Program: Contrasts in UV Irradiance at the South Pole and Barrow, Alaska

T. MESTECHKINA, C. R. BOOTH, J. R. TUSSON IV, AND J. C. EHRAMJIAN
Biospherical Instruments Inc, San Diego, California 92110-2621

INTRODUCTION

The Antarctic Ultraviolet Spectroradiometer Monitoring Network was established by the U.S. National Science Foundation (NSF) in 1988 in response to predictions of increased ultraviolet (UV) radiation in the polar regions. The network consists of several automated, high-resolution spectroradiometers: five are placed in strategic locations in Antarctica and the Arctic, one is established in San Diego to collect data and serve as a training and testing facility (Table 1), and a portable system is used for instrument intercomparisons [*Seckmeyer, et al.,* 1995]. The network makes measurements of UV spectral irradiance and provides a variety of biological dosage calculations of UV exposure. Biospherical Instruments Inc., under contract to Antarctica Support Associates (ASA), directed by NSF, is responsible for operating and maintaining the network and distributing data to the scientific community.

The spectroradiometers used in the system are Biospherical Instruments, Inc. Model SUV-100. Each instrument contains an irradiance diffuser, a double holographic grating monochromator, a photomultiplier tube (PMT), and calibration lamps. A vacuum-formed Teflon diffuser serves as an all-weather irradiance collector, and it is heated by the system to deter ice and snow accumulation. Tungsten-halogen and mercury vapor calibration lamps are used for automatic internal calibrations of both responsivity and wavelength that occur two to four times daily. All instrument functions, calibration activities, and data acquisitions are computer controlled. Further details on the spectroradiometers can be found in *Booth et al.*, 1996.

The South Pole and Barrow, Alaska, installations of the network are in locations that also have CMDL installations. Therefore, the balance of this report will focus on these two sites. The South Pole site is located away from the influence of mountains in a region of almost constant albedo. Cloud cover is relatively infrequent and it is generally thin when it does occur. The very small hourly change in the solar zenith angle at the South Pole supports examination of changes in total column ozone (as estimated by UV irradiance) at hourly resolution [*Booth and Madronich,* 1993]. For example, in Figure 1a, a

TABLE 1. Installation Sites

Site	Latitude	Longitude	Established	Location
South Pole	90.00°S	0°	Feb. 1988	Clear Air Building
McMurdo	77.51°S	166.40°E	March 1988	Arrival Heights
Palmer	64.46°S	64.03°W	May 1988	Clean Air Building
Ushuaia, Argentina	54.49°S	68.19°W	Nov. 1988	CADIC*
Barrow, Alaska	71.18°N	156.47°W	Dec. 1990	UIC-NARL†
San Diego, California	32.45°N	117.11°W	Oct. 1992	Biospherical Instruments, Inc.

*CADIC: Centro Austral de Investigaciones Cientificas, Argentina
†Ukpeagvik Inupiat Corporation-National Arctic Research Laboratory

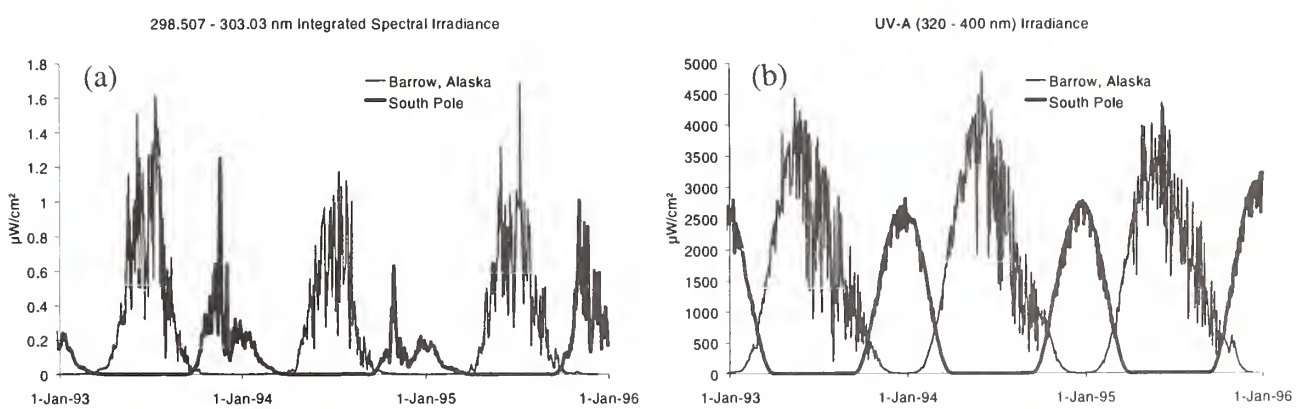

Fig. 1. Noontime integrated spectral irradiance at Barrow, Alaska, and at South Pole from January 1993 through December 1995. Panel a (left) shows the integrated irradiance around 300 nm (293.507-303.03 nm) and is contrasted with panel b (right) which illustrates the UV-A irradiance (320-400 nm). The higher irradiance values at Barrow are due to the higher sun elevation. Normally, irradiance at Barrow peaks in June, while irradiance at the South Pole peaks in December.

substantial *decrease* is seen in irradiance around the 300 nm in late November 1993. Meanwhile, Total Ozone Maping Spectrometer (TOMS) Nimbus-7 data report a substantial *increase* in the 300 nm irradiance between November 15 and November 20, 1993.

Barrow, Alaska, contrasts with the South Pole in that it is located where a significant change in surface albedo occurs due to both the springtime snowmelt [*Dutton and Endres*, 1991] and changes in sea-ice coverage. Also, Barrow experiences significant changes in incident irradiance due to Arctic storms. The contrast in irradiances between Barrow and the South Pole is seen in Figure 1b, which depicts the integrated noontime irradiances over the UV-A spectrum (320-400 nm) from January 1993 through December 1995.

The integral of spectral irradiance from 298.507 to 303.03 nm is one of the most sensitive to changes in total ozone (and solar angle). A strong correlation between the ozone concentration and UV irradiance is illustrated by the Barrow 1995 example in Figure 2. Figure 3 emphasizes that in 1994 high UV levels at South Pole were observed comparatively early in the season (at the end of October) with an early termination of influence of the "ozone hole."

Table 2 lists the maximum UV-B irradiances (290-320 nm) recorded at each site in 1990-1995. The maximum irradiance reported in San Diego happened to be elevated by cloud coverage (days of partial cloud coverage are sometimes observed to have higher irradiances than completely clear days due to reflections off of cloud surfaces). The Antarctic site measurements are enhanced by high albedo due to snow and ice coverage. During the Palmer maximum, ice coverage was heavy, increasing surface albedo.

SUMMARY

High spectral resolution scanning UV spectro-radiometers have been established at six sites and are successfully providing multiyear data sets. Resulting data were used to test radiative transfer models [*Lubin and Frederick*, 1992; *Smith et al.*, 1992], investigate radiation amplification [*Booth and Madronich*, 1993; *Madronich*, 1994], derive ozone concentrations [*Stamnes et al.*, 1992], examine the biological impact of enhanced UV [*Cullen et al.*, 1992; *Anderson et al.*, 1993; *Benavides et al.*, 1993; *Holm-Hansen et al.*, 1993] and explore geographical differences in the UV [*Booth et al.*, 1995; *Diaz et al.*, 1994; *McKenzie et al.*, 1994; *Seckmeyer et al.*, 1995].

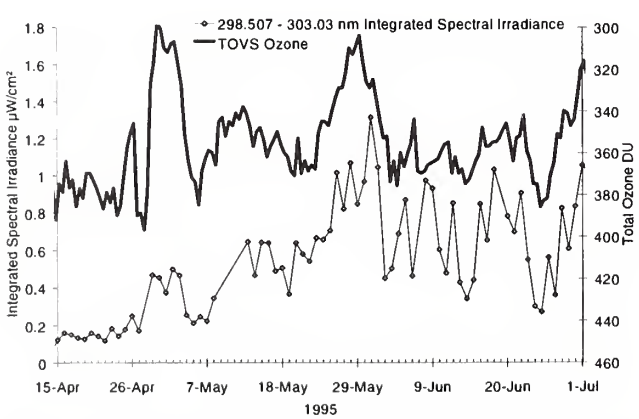

Figure 2. Comparison of the 298.507 - 303.03 nm integrated spectral irradiance and TOVS total ozone measurements made at Barrow during austral spring 1995. Note that the right axis are inverted to make the effect of decreasing ozone on increasing irradiance readily apparent.

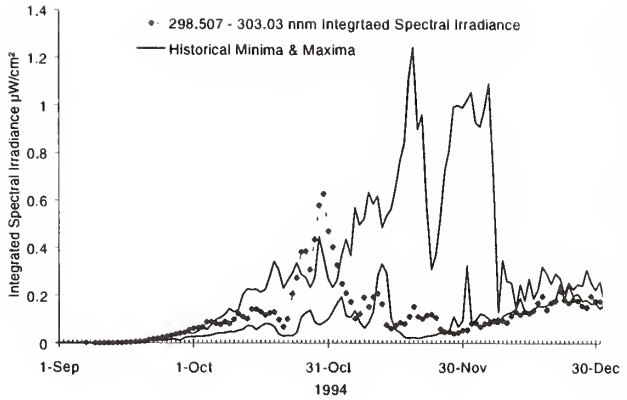

Figure 3. Integrated 298.507-303.03 nm spectral irradiance at South Pole. The thin lines represent historical (1991-1993) minimum and maximum observations, while 1994 data are expressed as diamonds.

TABLE 2. UV-B (290-320 nm) maxima (µW/cm²)

Site	Maxima	Date	Solar Zenith Angle
Palmer	382.7	Dec. 2, 1990	44.0°
San Diego	361.6	May 20, 1993	15.5°
Ushuaia	350.5	Decemer 3, 1990	35.9
McMurdo	226.5	December 1, 1992	56.1°
Barrow	199.5	June 1, 1992	49.6
South Pole	129.4	December 3, 1992	67.8°

Data, referenced to both beginning- and end-of-season calibration constants are distributed on CD-ROM and are available to any interested researcher. For more information, please contact: Biospherical Instruments Inc., 5340 Riley Street, San Diego, CA 92110-2621 (Fax: (619) 686-1887, Internet: uvgroup@biospherical.com, www:http://www.biospherical.com).

Acknowledgments. This research and monitoring activity was funded by contract SCK-M18914-02 from Antarctic Support Associates under the direction of Polly Penhale at the National Science Foundation, Office of Polar Programs. B. Mendonca of CMDL assisted in providing operators and support for the installations at Barrow. R. McPeters of NASA/GSFC provided TOMS Total Ozone data for comparison purposes. A TOMS update CD-ROM is available from the National Space Science Data Center (NSSDC), Goddard Space Flight Center. Barrow operators include D. Norton (Arctic Sivumnun Ilisagvik College), D. Endres and M. Gaylord (CMDL). The Ukpeagvik Inupiat Corporation of Barrow provided installation assistance. Operators at Palmer, the South Pole, and McMurdo were provided by ASA.

REFERENCES

Anderson, S., J. Hoffman, G. Wild, I. Bosch, and D. Karentz, Cytogenetic, cellular, and developmental responses in antarctic sea urchins (*Sterechinus neumayeri*) following laboratory ultraviolet-B and ambient solar radiation exposures, *Ant. J. U. S., 1993 Review*, 28(5), 115-116, 1993.

Benavides, H., L. Prado, S. Díaz, and J.I. Carreto. An exceptional bloom of *Alexandrium catenella* in the Beagle Channel, Argentina, Proceedings of the 6th International Conference on Toxic Marine Phytoplankton; Nantes, October 18-22, 1993.

Booth, C.R., T.B. Lucas, T. Mestechkina, J. Shmidt, and J. Tusson, High resolution UV spectral irradiance monitoring program - contrasts in UV exposure in Antarctica and the Americas, *Ant. J. U. S.*, in press, 1996a.

Booth, C.R., T.B. Lucas, T. Mestechkina, J.R.Tusson IV, J.P. Schmidt, D.A. Neuschuler, and J.H. Morrow, *NSF Polar Programs* UV *Spectroradiometer Network 1994-1995 Operations Report*, 182 pp., Biospherical Instruments Inc., San Diego, CA, 1996b.

Booth, C.R., and S. Madronich, Radiation amplification factors: Improved formulation accounts for large increases in ultraviolet radiation associated with Antarctic ozone depletion, in *Antarctic Research Series*, edited by C.S. Weiler and P.A. Penhale, 62, pp. 39-42, 1993.

Cullen, J.C., P.J. Neale, and M.P. Lesser, Biological weighting function for the inhibition of phytoplankton photosynthesis by ultraviolet radiation, *Science, 258*, 646-650, 1992.

Diaz, S.B., Frederick, I. Smolskaia, W. Esposito, T.B. Lucas, and C.R. Booth, Ultraviolet solar radiation in the high latitudes of South America, *Photochem. Photobio.*, 60(4), 356-362, 1994.

Dutton, E.G., and D.J. Endres, Date of snowmelt at Barrow, Alaska, U.S.A., *Arctic Alpine Res.*, 23(1), 115-119, 1991.

Holm-Hansen, O., D. Lubin, and E.W. Helbling, Ultraviolet radiation and its effects on organisms in aquatic environments, in *Environmental UR Photobiology*, edited by A.R. Young et al; pp. 379-425, Plenum Press, New York, 1993.

Lubin, D., and J.E. Frederick, Observations of ozone and cloud properties from NSF ultraviolet monitor measurements at Palmer Station, Antarctica, *Ant. J. U. S., 1989 Review*, 25(5), 241-242, 1992.

Madronich, S. Increases in biologically damaging UV-B radiation due to stratospheric ozone reductions: A brief review, *Arch. Hydrobiol. Beih: Ergebn. Limnol.*, 43, 17-30, 1994.

McKenzie, R.L., M. Blumthaler, C.R. Booth, S.B. Diaz, J.E. Frederick, T. Ito, S. Madronich, and G. Seckmeyer, Surface Ultraviolet Radiation, in *Scientific Assessment of Ozone Depletion: 1994, World Meteorological Organization Global Ozone Research Monitoring Project*, 37, pp. 9.1-9.22, WMO, Geneva, Switzerland, 1994.

Seckmeyer, G., B. Mayer, G. Bernard, R.L. McKenzie, P.V. Johnston, M. Kotkamp, C.R. Booth, T.B. Lucas, T. Mestechkina, C.R. Roy, H.P. Gies, and D. Tomlinson. Geographical differences in the UV measured by intercompared spectroradiometers, *Geophys. Res. Lett.*, 22(14), 1889-1892, 1995.

Smith, R.C., Z. Wan, and K.S. Baker, Ozone depletion in Antarctica: Modeling its effect under clear-sky conditions, *J. of Geophys. Res.*, 97, 7383-7397, 1992.

Stamnes, K., Z. Jin, J. Slusser, C.R. Booth, and T.B. Lucas, Several-fold enhancement of biologically effective ultraviolet radiation levels at McMurdo Station, Antarctica, during the 1990 ozone hole, *Geophys. Res. Lett.*, 19, 1013-1017. 1992.

Gamma Radionuclide Deposition at SMO During Recent French Nuclear Weapons Testing on South Pacific Atolls

M. MONETTI
Environmental Measurements Laboratory, U.S. Department of Energy, New York 10014-4811

INTRODUCTION

The Environmental Measurements Laboratory (EML) has maintained a global network of deposition sampling sites for nearly 40 years. Through CMDL support, American Samoa (SMO) and Mauna Loa (MLO) have been a part of this network for many years. This network was initiated to investigate the transport and fate of radioactivity produced from atmospheric testing of nuclear weapons. Strontium-90 was the radionuclide of primary interest due to the relatively high quantity released and its physical and chemical properties that made it a concern to human health. The global distribution and inventories of ^{90}Sr through 1990 have been determined in this program [*Monetti*, 1996]. Now that the period of atmospheric weapons testing appears to be past, EML has modified this program to meet new objectives. The most significant program change is that gamma spectrometric techniques are being used to measure the activity of several gamma-emitting radionuclides instead of the radiochemical procedure previously used to make a single ^{90}Sr measurement. Gamma radionuclides of particular interest include both anthropogenic (^{137}Cs, ^{95}Zr, and ^{144}Ce) and natural isotopes (^{7}Be and ^{210}Pb). This technique will allow EML to continue to monitor for atmospheric releases of fission products. In addition, the development of a database on ^{7}Be and ^{210}Pb deposition is valued by colleagues who can use this data to verify global circulation models. EML no longer has the resources to make these measurements in all of the samples collected from the 78 stations in the global network. As a result, samples from certain locations are analyzed and others are being archived for future interests. Whenever there is an indication of activities that can potentially release fission products into the atmosphere, EML will use the network samples to identify if a release has occurred and determine the extent and magnitude if a release is confirmed. Following announcements of France's intentions to perform a series of underground tests at the Mururoa and Fangataufa Atolls, EML conducted a special study to monitor the atmosphere in the South Pacific Ocean for radioactivity that may be released during the testing. This study involved the use of the SMO sampling station as described below.

MATERIALS AND METHODS

The first sample from SMO was collected in a 23-L polyethylene bucket that was exposed from September 1 through September 20, 1995. This sample was eluted through an ion-exchange column at EML. All other samples were weekly collections of bulk precipitation from September 20, 1995 until February 14, 1996, using EML's ion-exchange fallout collector [*EML*, 1996]. Any sample collected within 2 weeks following a French detonation was processed for analysis individually. Samples collected during intermediate periods were composited by annual quarter and then processed. Processing of the samples involved homogenizing the surface paper pulp and ion-exchange resin and sealing the sample in a 90-cm^3 aluminum can. The samples were then counted on a gamma spectrometer equipped with an n-type coaxial high-purity germanium detector, and the activities of the radionuclides of interest were determined by computer analysis of the spectral data. These spectra were also visually checked for the presence of any other anthropogenic gamma radionuclides. In all, twenty samples from SMO were analyzed.

RESULTS

Radionuclide deposition data from SMO obtained in this study is presented in Table 1. The results are shown in units of becquerels per square meter (Bq m^{-2}). A counting error is reported whenever a radionuclide was detected. The lower limit of detection (equivalent to three times the statistical variation of the background activity for each radionuclide) was used to calculate maximal deposition values for ^{210}Pb, ^{137}Cs, ^{144}Ce and ^{95}Zr when their activity was not detected. In addition, precipitation data in centimeters is provided for most sampling intervals.

DISCUSSION

The results presented in Table 1 indicate that the primary source of gamma activity in deposition from September of 1995 through February of 1996 was from natural radionuclides. In all but two of the samples the anthropogenic component of gamma activity was below the detection limit. The ^{137}Cs activity detected in two samples is only slightly higher than the detection limit. Cesium-137 has a long half-life (30 years) and it is ubiquitous because of past nuclear weapons testing. Since no other anthropogenic radionuclide was detected in the samples, it is unlikely that there was a "fresh" release of anthropogenic radioactivity from the underground French test or any other source. Deposition data from other sampling sites used for this study revealed similar observations (unpublished data). Therefore, the presence of ^{137}Cs in these two samples was probably due to resuspension of previously deposited material. Of the natural radionuclides, ^{7}Be was detected in most of the samples, but ^{210}Pb was only detected in seven of the twenty samples. Beryllium-7 is a cosmogenic radionuclide produced in the earth's upper atmosphere, while ^{210}Pb is a daughter in the primordial ^{238}U decay series and its atmospheric presence follows the release of ^{222}Rn from the earth's surface. The deposition of ^{7}Be and ^{210}Pb ranged from undetectable to 271.8 and <0.7 to 8.8 Bq m^{-2} respectively. The ^{7}Be deposition appears to be related to both the amount of precipitation and duration of the collection period. The

TABLE 1. Gamma Radionuclide Deposition at SMO from September 1995 Through February 1996

Collection Date	Precipitation (cm)	^{7}Be (Bq m^{-2})	Error (%)	^{210}Pb (Bq m^{-2})	Error (%)	^{210}Pb (Bq m^{-2})	Error (%)	^{144}Ce (Bq m^{-2})	^{95}Zr (Bq m^{-2})
3rd Quarter 1995	66.0	271.8	6	8.8	25	< 0.6		< 0.7	< 1.8
Sept. 1-20, 1995	18.1	90.8	9	< 1.5		< 1.0		< 1.1	< 2.7
Oct. 4-11, 1995	4.3	88.5	8	< 1.5		< 1.0		< 1.1	< 2.9
Oct. 11-18, 1995	0.8	14.9	16	< 1.3		< 0.8		< 1.0	< 2.2
Oct. 18-25, 1995	8.4	ND	0	< 1.7		< 1.0		< 1.2	< 2.9
Oct. 25-Nov. 3, 1995	1.0	21.4	10	5.9	40	< 0.7		< 0.9	< 2.0
Nov. 3- 8, 1995	8.0	22.4	14	< 2.0		< 1.6		< 2.0	< 4.8
Nov. 8-15, 1995	13.1	27.7	9	< 1.0		0.9	14	< 0.8	< 1.6
Nov. 15-22, 1995	3.1	21.4	11	< 0.7		< 0.4		< 0.5	< 1.2
Nov. 22-29, 1995	13.2	45.1	9	< 1.1		0.7	18	< 0.9	< 1.9
Nov. 29-Dec. 6, 1995	2.2	33.7	13	< 1.3		< 0.8		< 0.9	< 2.0
Dec. 6-15, 1995	1.1	20.1	14	3.4	36	< 0.9		< 1.0	< 2.4
Dec. 15-20, 1995	0.0	ND		2.8	37	< 0.8		< 0.9	< 2.1
Dec. 20-29, 1995	2.7	54.6	8	< 1.6		< 1.2		< 1.5	< 3.4
Dec. 29-Jan. 3, 1996	2.7	30.0	14	8.5	38	< 1.2		< 1.4	< 3.0
Jan. 3-10, 1996	8.1	46.5	7	4.7	45	< 0.6		< 0.8	< 1.8
Jan. 10-24, 1996	18.6	48.7	7	3.6	38	< 1.0		< 1.3	< 2.9
Jan. 24-31, 1996	0.9	10.1	22	< 1.5		< 1.1		< 1.4	< 3.3
Jan. 31-Feb. 7, 1996	NA	24.1	16	< 1.2		< 0.8		< 0.9	< 2.0
Feb. 7-14, 1996	NA	27.2	13	< 1.2		< 0.7		< 0.8	< 2.1

ND - Not detected
NA - Data not available

^{210}Pb data is subject to large counting errors (from 25 to 45%) as a result of the low deposition rate and high detector background counts at low energies. The concentration of ^{210}Pb in the surface atmosphere at SMO has been shown to be relatively low [*Larsen et al.*, 1995] presumably as a result of the oceanic influence. It is more difficult to identify if a similar correlation exists between the ^{210}Pb deposition and precipitation because of the large number of nondetects. Real ^{210}Pb deposition values occurred during periods of lesser precipitation which may suggest that there is a higher ^{222}Rn flux during these periods. Further measurements and comparisons with atmospheric concentrations of ^{210}Pb may reveal if this interpretation is valid. In the future, EML will analyze deposition samples collected at SMO and MLO to address this observation.

Acknowledgment. The special assistance provided by Mark Winey at SMO was invaluable to this study. The continued sampling efforts by the CMDL staff at SMO and MLO are greatly appreciated by EML.

REFERENCES

EML, *EML Procedures Manual, 28th Edition, HASL-300*, Vol. 1, pp 2.3-1 to 2.3-6, U.S. Department of Energy, Environmental Measurements Laboratory, New York, 1996.

Larsen , R.J., C.G. Sanderson and J. Kada, EML Surface Air Sampling Program, 1990-1993 Data, EML-572, 247 pp., U.S. Department of Energy, Environmental Measurements Laboratory, New York, 1995.

Monetti, M.A., Worldwide Deposition of Strontium-90 through 1990, EML-579, 56 pp., Environmental Measurements Laboratory, New York, 1996.

Early Morning UV-B During the 1994-1995 Record Low Ozone at Mauna Loa

PATRICK J. NEALE, DAVID L. CORRELL, VERNON R. GOODRICH, AND DOUGLASS R. HAYES, JR.
Smithsonian Environmental Research Center, Edgewater, Maryland 21037

INTRODUCTION

The Smithsonian Environmental Research Center (SERC) has been monitoring surface spectral ultraviolet-B (UV-B) irradiance at Mauna Loa (MLO) since fall 1984. The instrument is similar to a radiometer in operation in Edgewater, Maryland [*Correll et al.*, 1992]. The instrument measures UV-B irradiance in a series of eight, 5-nm band pass channels (290-325 nm) and records 1-minute averages. Operation is continuous except for an annual break of about 1 month when the instrument is returned to Maryland for calibration. Our primary objective is to monitor long-term changes in incident solar UV-B irradiance. Records of absolute calibration of the MLO instrument are under review, as are data from intercomparisons of the Edgewater and MLO instruments at Edgewater. We expect the results from these tests will be the subject of a future report.

While absolute irradiance is presently not available, ratios of signal intensity between instrument channels provide information on relative changes in the solar UV-B spectrum. There are several ways such data may be useful. Previously, we used the data to estimate atmospheric optical depth in the UV-B at MLO [*Neale et al.*, 1994]. Recently, there was evidence of a record low total column ozone at MLO during the winter of 1994-1995 [*Hofmann et al.*, 1996]. In this latter report, we presented UV irradiance measured in the 295-nm, 300-nm and 305-nm channels, relative to the 325-nm channel for clear days when the secant of the solar zenith angle was equal to 1.5 (about 48°). Here we present additional UV data for the winter of 1994-1995 as well as other ancillary information concerning instrument operation during this period.

RESULTS AND DISCUSSION

The instrument was calibrated at SERC and sent to MLO in July 1994 and remained in operation until April 1995. In June 1994, transmission spectra were measured for all eight interference filters in the instrument. The center wavelengths (wavelength midpoint between the upper and lower wavelengths at which transmission is 50% of maximum) calculated from these spectra for the 295-, 300-, 305- and 325-nm channels were 294.9, 300.4, 304.6 and 324.8 nm. After return of the instrument to SERC in April 1995, filter transmission spectra were again measured and these channels had center wavelengths of 295.1, 300.7, 304.9, and 325.4 nm. Apart from the 325-nm channel (0.6 nm shift), the shift in filter center wavelength was 0.3 nm or less.

Figure 1 shows measurements of 295-, 300- and 305-nm irradiance during the winter of 1994-1995 on clear sky mornings when the secant of solar zenith angle (*sec* θ_s) was equal to 2.5 (about 66°), i.e., between 0814 and 0857 LST in October and December, respectively. These are given as ratios of the irradiance in each channel to the irradiance in the 325-nm channel. The time series of Dobson spectrometer ozone measurements at MLO is shown for comparison. Over the period of decreasing ozone, November to December, there is a steady climb in the irradiance ratio in each channel. The increase from minimum to maximum irradiance was a factor of 3.0, 1.9, and 1.6, respectively, in the 295-, 300- and 305-nm channels. There is a strong correlation between ozone and the irradiance ratio in each channel. A linear regression of the 305 nm/ 325 nm ratio on total ozone (interpolating the ozone series as necessary for missing dates) had a coefficient of determination (R^2) of 0.86. The R^2 for the 295- and 300-nm ratios were 0.85 and 0.86, respectively.

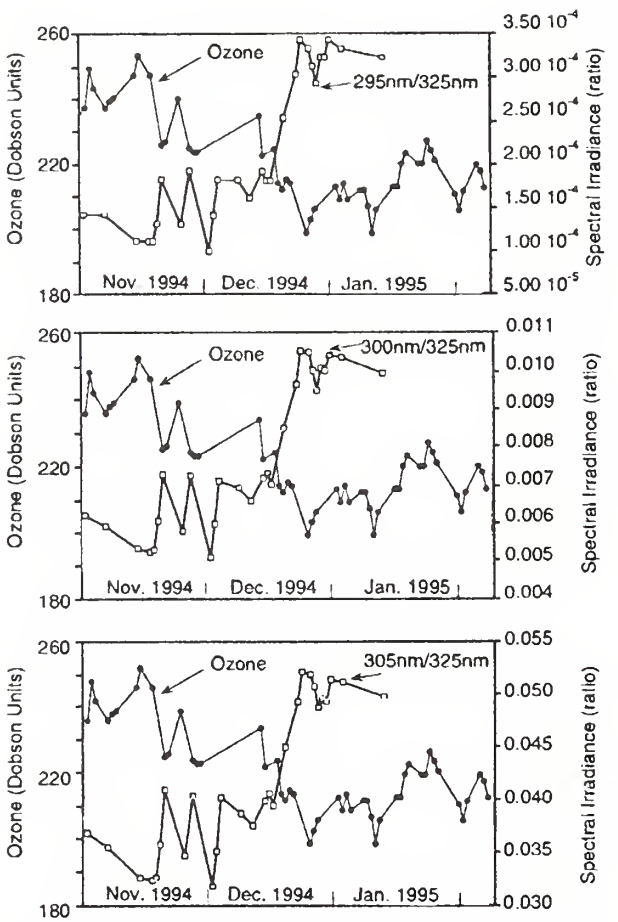

Fig. 1. Time series of total ozone and UV-B irradiance ratios at MLO during winter 1994-1995. Early morning (secant 2.5) irradiance on clear-sky days in three bands (5- nm full bandwidth at half height) with nominal center wavelengths of 295 nm (upper panel), 300 nm (middle panel) and 305 nm (lower panel) relative to 325 nm. Note different ratio scales in each panel.

These results reinforce the conclusion of *Hofmann et al.* [1996] that incident solar UV-B was significantly elevated during the record low total-column ozone event at MLO (December-January 1994). Measurements during both early morning ($sec\ \theta_s = 2.5$) and midmorning ($sec\ \theta_s = 1.5$) show specific increases in irradiance during this period that are highly correlated with the decrease in total column ozone. Since the mean optical path length of solar irradiance through the stratosphere is longer at $sec\ \theta_s = 2.5$ compared to 1.5, a given decrease in ozone should result in a larger relative increase in irradiance at higher secant. This was indeed the case for the 300- and 305-nm channels, for which there was less of an increase from minimum to maximum (factor 1.5 and 1.8, respectively) at $sec\ \theta_s = 1.5$ [*Hofmann et al.*, 1996]. However, for the 295-nm channel, the factor increase was actually higher at the shorter secant (3.2). For this channel, early morning and midmorning measurements may not be strictly comparable. This is because the effective center wavelength, i.e., the filter center wavelength adjusted for the greater proportion of longer-wavelength solar irradiance within the pass band [*Correll et al.*, 1992], is likely to be at a significantly longer wavelength in the early morning versus midmorning.

References

Correll, D. L., C. O. Clark, B. Goldberg, V. R. Goodrich, D. R. Hayes Jr., W. H. Klein and W. D. Schecher, Spectral ultraviolet-B radiation fluxes at the earth's surface: long-term variations at 39°N, 77°W, *J. Geophys. Res.*, 97, 7579-7591, 1992.

Hofmann, D.J., S.J. Oltmans, B.A. Bodhaine, G.L. Koenig, J.M. Harris, J.A. Lathrop, R.C. Schnell, J. Barnes, J. Chin, D. Kuniyuki, S. Ryan, R. Uchida, A. Yoshinaga, P.J. Neale, D.R. Hayes, Jr., V.R. Goodrich, W.D. Komhyr, R.D. Evans, B.J. Johnson, D.M. Quincy, and M. Clark, Record low ozone at Mauna Loa Observatory during winter 1994-1995: A consequence of chemical and dynamical synergism?, *Geophys. Res. Lett.*, 23(12), 1533-1536, 1996.

Neale, P.J., D.L. Correll, V.R. Goodrich, and D.R. Hayes Jr., UV-B optical depths at Mauna Loa: Relative contribution of ozone and aerosols, in *Summary Report 1993*, edited by J.T. Peterson, and R.M. Rosson, NOAA Environmental Research Laboratories, Boulder, CO, pp. 132-134, 1994.

Advanced Global Atmospheric Gases Experiment (AGAGE)

R.G. PRINN
Massachusetts Institute of Technology, Cambridge, Massachusetts 02139

R.F. WEISS
Scripps Institution of Oceanography, University of California, La Jolla, California 92093

F.N. ALYEA AND D.M. CUNNOLD
Georgia Institute of Technology, Atmospheric Sciences, Atlanta, Georgia 30332

P.J. FRASER AND L.P. STEELE
CSIRO, Division of Atmospheric Research, Victoria, Australia 3195

P.G. SIMMONDS
University of Bristol, School of Chemistry, Bristol, United Kingdom BS8 1TS

INTRODUCTION

Continuous high-frequency gas chromatographic measurements of two biogenic/anthropogenic gases (CH_4 and N_2O) and five anthropogenic gases ($CFCl_3$, CF_2Cl_2, CH_3CCl_3, $CF_2ClCFCl_2$, and CCl_4) are being carried out at globally-distributed sites to quantitatively determine the source and sink strengths and circulation of these chemically and radiatively important long-lived gases. Hydrogen, carbon monoxide, and a wide range of hydrochlorofluorocarbons (HCFCs), hydrofluorocarbons (HFCs) and other halocarbons are also measured at certain stations. The station locations are Cape Grim, Tasmania (41°S, 145°E), Cape Matatula, American Samoa (SMO) (14°S, 171°E), Ragged Point, Barbados (13°N, 59°W), Trinidad Head, California (41°N, 124°W), and Mace Head, Ireland (53°N, 10°W). The program, which began in 1978, is divided into three parts associated with three changes in instrumentation: the Atmospheric Lifetime Experiment (ALE) which utilized Hewlett-Packard HP5840 gas chromatographs, the Global Atmospheric Gases Experiment (GAGE) which utilized HP5880 gas chromatographs, and the Advanced (AGAGE) phase now underway which uses a new fully-automated system from the Scripps Institution of Oceanography (SIO) containing a custom-designed sample module and HP5890 and Carle Instruments gas chromatographic components. Also, as part of AGAGE, a new Finnigan gas chromato-graph/mass spectrometer system for measuring HCFCs and HFCs is now operating at Mace Head and a second such instrument will be installed at Cape Grim in late 1996.

1994-1995 UPDATE

The data for the seven long-lived gases measured in GAGE and AGAGE during 1994-1995 continue to be of very good quality with significant improvements in the frequencies, precisions, and accuracies of the measurements resulting from the transition from GAGE to AGAGE. Some significant conclusions have been reached over the past year as a result of analyzing the data.

First, *Prinn et al.* [1995] showed that the atmospheric concentration of the volatile anthropogenic chemical CH_3CCl_3, which was steadily increasing at 4.5 ± 0.1% per year until mid-1990, has subsequently decreased at a rate of 2.2 ± 0.4% per year (all stated uncertainties are 1σ). This recent rapid decrease is consistent with its short lifetime and recent industrial emission reductions. The observed decreases began in early 1991 in the northern hemisphere and in mid-1992 in the southern hemisphere, reflecting the predominantly northern hemispheric emissions of this industrial chemical and the approximately 1-year interhemispheric exchange time. The measurements, combined with industrial emissions, were used in an inverse method to deduce a globally averaged CH_3CCl_3 lower atmospheric lifetime (200 to 1000 mbar) of 4.6 ± 0.3 years and a total atmospheric lifetime (0 to 1000 mbar) of 4.8 ± 0.3 years. Assuming a lifetime for loss of CH_3CCl_3 to the oceans of 85 years, we deduced a global weighted-average lower atmospheric OH concentration of (9.7 ± 0.6) × 10^5 radicals cm^{-3}. The rate of change of this OH concentration is 0.0 ± 0.2% per year, implying that the oxidation capability of the lower atmosphere has not changed significantly from 1978 to 1994. Our conclusions concerning the OH concentrations and trend depend on the accuracy of the industrial emission estimates and our new absolute calibration. For methane (CH_4), these OH concentrations imply lower atmospheric and total atmospheric lifetimes of 8.0 ± 0.5 and 8.9 ± 0.6 years, respectively. The deduced lifetimes for CH_3CCl_3 and CH_4 are substantially less and the deduced OH concentrations substantially more than previous estimates. This substantially lowers the potential of these two gases (and most other hydrogen-containing gases) for affecting the ozone layer and climate compared to previous estimates.

Second, observations at the ALE/GAGE stations of CCl_2FCClF_2 have been reported by *Fraser et al.* [1996]. The observations from Cape Grim have been extended back to 1978 using archived air samples. The global atmospheric abundance of CCl_2FCClF_2 is indicated to have been growing exponentially between 1978 and 1987 with an *e*-folding time of approximately 7.6 years; it has been growing less rapidly since that time. On January 1, 1994, the mean inferred northern hemispheric mixing ratio in the lower troposphere was 84.4 ± 0.4 ppt (parts-per-trillion dry air mole fraction) and the southern hemispheric value was 80.6 ± 0.4 ppt; the global growth rate in 1991-1993 is estimated to have averaged approximately 3.1 ± 0.1 ppt per year. The differences between the northern and southern hemispheric concentrations are calculated to be consistent with almost the entire northern hemispheric release of this gas. The annual release estimates of CCl_2FCClF_2 by

industry, which include estimates of eastern European emissions, consistently exceeds those deduced from the measurements by approximately 10% from 1980 to 1993. The uncertainties in each estimate is approximately 5%. This difference suggests that up to 10% of past production might not yet have been released. The measurements indicate atmospheric releases of CCl_2FCClF_2 have been decreasing rapidly since 1989 and in 1993 amounted to $78 \pm 27 \times 10^6$ kg or $42 \pm 15\%$ of the 1985-1987 emissions.

Third, using GAGE/AGAGE observations *Cunnold et al.* [1996] showed that global concentrations of CCl_3F reached a maximum in 1993 and decayed slightly in 1994, while CCl_2F_2 concentrations increased approximately 7 ppt in 1993 and 1994. These changes suggest that world emissions decreased faster in these 2 years than industry production figures would suggest and faster than expected under the Montreal Protocol and its amendments. An analysis of regional pollution events at the Mace Head site suggest that industry may be underestimating the decline of emissions in Europe. It is argued, however, that the decline in European emissions is not biasing the background Mace Head measurements (or the GAGE global averages). Combining the chlorofluorocarbon measurements, including CCl_2FCClF_2, with GAGE/AGAGE measured global decreases in CH_3CCl_3 and CCl_4 after 1992 and with Cape Grim archived air measurements of $CHClF_2$, the measurements suggest total anthropogenic atmospheric chlorine loading from these six gases maximized in 1992 at 2.95 ± 0.04 ppb (parts-per-billion dry air mole fraction) and that it had decreased by 0.02 ± 0.01 ppb by the beginning of 1995.

During 1996, operations at the American Samoa Observatory (SMO) will make the transition from the GAGE instrument to the new AGAGE system; it is to be installed in the new laboratory building. During 1994-1995 the GAGE HP5880 continued to be operated by the CMDL station personnel in collaboration with the Scripps Institution of Oceanography (SIO) group. Operations were quite smooth and uneventful during this period with most problems being of a routine maintenance and repair nature.

The new instrument systems for AGAGE represent a significant technological advance. All operations and data acquisition are by a Sun Microsystems workstation using custom software for signal processing integration and storage of the data and chromatograms. The instrument measures its own nonlinearity for all the AGAGE gases on a regular basis using a pressure-programmed constant-volume injection system and a single gas standard. All channels of the instrument are fitted with precolumns to avoid column contamination by late-eluting gases and, as a result the frequency of measurement, has been increased three-fold versus GAGE. Precision is also greatly improved over the GAGE instruments. The system works interactively with its uninterruptible power supply (UPS). With the new installation at SMO completed, the new AGAGE instruments will be operational at all five AGAGE stations.

Another major component of the AGAGE program is the development of new absolute calibration scales. This work is being done using an extension of the "bootstrap" calibration method used earlier at SIO. In the AGAGE work, gravimetrically-determined aliquots of pure CFCs are mixed with about 12 L of gravimetrically-determined pure N_2O. A small aliquot (~0.4 cm^3) of this mixture is then introduced into a 35-L electropolished stainless steel canister to which about 10 torr of water vapor has been added to reduce wall reactions and adsorption. The canister is then filled with about 40 atmospheres of repurified "zero air" to bring the N_2O mole fraction to a near-ambient value. The resulting N_2O concentration is then calibrated gas chromatographically against existing SIO standards, and the CFC concentrations are determined by multiplying the measured N_2O mole fraction by the gravimetric CFC/ N_2O ratios of the original mixture. In this way we have been able to obtain improved accuracy for all AGAGE gases, but especially for the lower vapor pressure and more adsorptive gases. AGAGE and CMDL are now engaged in an active intercalibration program (through the IGAC/NOHALICE activity) for all of the AGAGE gases as well as for methyl halides and some HCFCs.

Data Access

The ALE/GAGE/AGAGE data are archived at the Department of Engery Carbon Dioxide Information Analysis Center, Oak Ridge, Tennessee, and are available to interested scientists. Potential users of the data may contact CDIAC on the Internet (CDP@ORNL.GOV).

Acknowledgments. The AGAGE is supported by NASA Grants NAGW-732 and NAGW-2034, NOAA Contract NA85-RAC05103, CSIRO Australia, Australian Bureau of Meteorology, the U.K. Department of Environment, and the Alternative Fluorocarbons Environmental Acceptability Study. We thank Mark Winey and the other NOAA staff at SMO for their continued excellent local support for our instrumentation there.

References

Cunnold, D.M., R. Weiss, R.G. Prinn, D. Hartley, P.G. Simmonds, P.J. Fraser, B. Miller, F.N. Alyea, and L. Porter, GAGE/AGAGE measurements indicating reductions in global emissions of CCl_3F and CCl_2F_2 in 1992-1994, *J. Geophys. Res.*, submitted, 1996.

Fraser, P., D. Cunnold, F. Alyea, R. Weiss, R. Prinn, P. Simmonds, B. Miller, and R. Langenfelds, Lifetime and emission estimates of 1,1,2-trichlorotrifluorethane (CFC-113) from daily global background observations June 1982-June 1994, *J. Geophys. Res.*, 101, 12,585-12,599, 1996.

Prinn, R.G., R.F. Weiss, B.R. Miller, J. Huang, F.N. Alyea, D.M Cunnold, P.J. Fraser, D.E. Hartley, and P.G. Simmonds, Atmospheric trends and lifetime of CH_3CCl_3 and global OH concentrations, *Science*, 269, 187-192, 1995.

The $^{13}C/^{12}C$ of Atmospheric Methane

PAUL QUAY, JOHN STUTSMAN, AND DAVID WILBUR
School of Oceanography, University of Washington, Seattle 98195

INTRODUCTION

Since 1989 we have been measuring the $^{13}C/^{12}C$ of atmospheric CH_4 on air samples collected at three CMDL sites (Pt. Barrow at 71°N, 156°W, Mauna Loa at 19°N, 155°W and Samoa at 14°S, 170°W) and on the Washington coast at 48°N, 126°W.

The $^{13}C/^{12}C$ of atmospheric CH_4 is a tracer that can distinguish between CH_4 input from bacterial and nonbacterial CH_4 sources. Bacterial CH_4 is microbially produced in anoxic environments likes swamps, bogs, rice paddies, and the rumens of cows. Non-bacterial CH_4 sources include thermogenically produced natural gas and CH_4 produced during biomass burning. Bacterial CH_4 has a $\delta^{13}C$ of about -60‰ (versus PDB) whereas the $\delta^{13}C$ of natural gas and CH_4 from biomass burning are about -40 and -24‰, respectively [*Quay et al.*, 1991].

The spatial and temporal variations in the $^{13}C/^{12}C$ of atmospheric CH_4 depend on the variations of the relative strength and $^{13}C/^{12}C$ of the CH_4 sources and sinks. Over interannual time scales the trends in the $^{13}C/^{12}C$ of atmospheric CH_4 indicates changes in the source composition, i.e., the relative strength of bacterial versus non-bacterial CH_4 sources. Changes in the loss rate of CH_4 have little effect on the $^{13}C/^{12}C$. Because CH_4 will likely contribute about 15% of the radiative forcing during the next century [*Wigley and Raper*, 1992], it is important to quantify the strength of the individual CH_4 sources and to determine whether the CH_4 source strengths are changing with time. This latter point has been underscored by the recently observed slowdown in the rate of CH_4 increase in the atmosphere [*Dlugokencky et al.*, 1994].

METHODS

The air samples are collected at approximately 2-week intervals using pre-evacuated stainless steel flasks either 15 or 30 litres in volume. The CH_4 is extracted from air in our laboratory using the procedure developed by *Stevens and Rust* [1982]. Briefly, the air is metered into a high

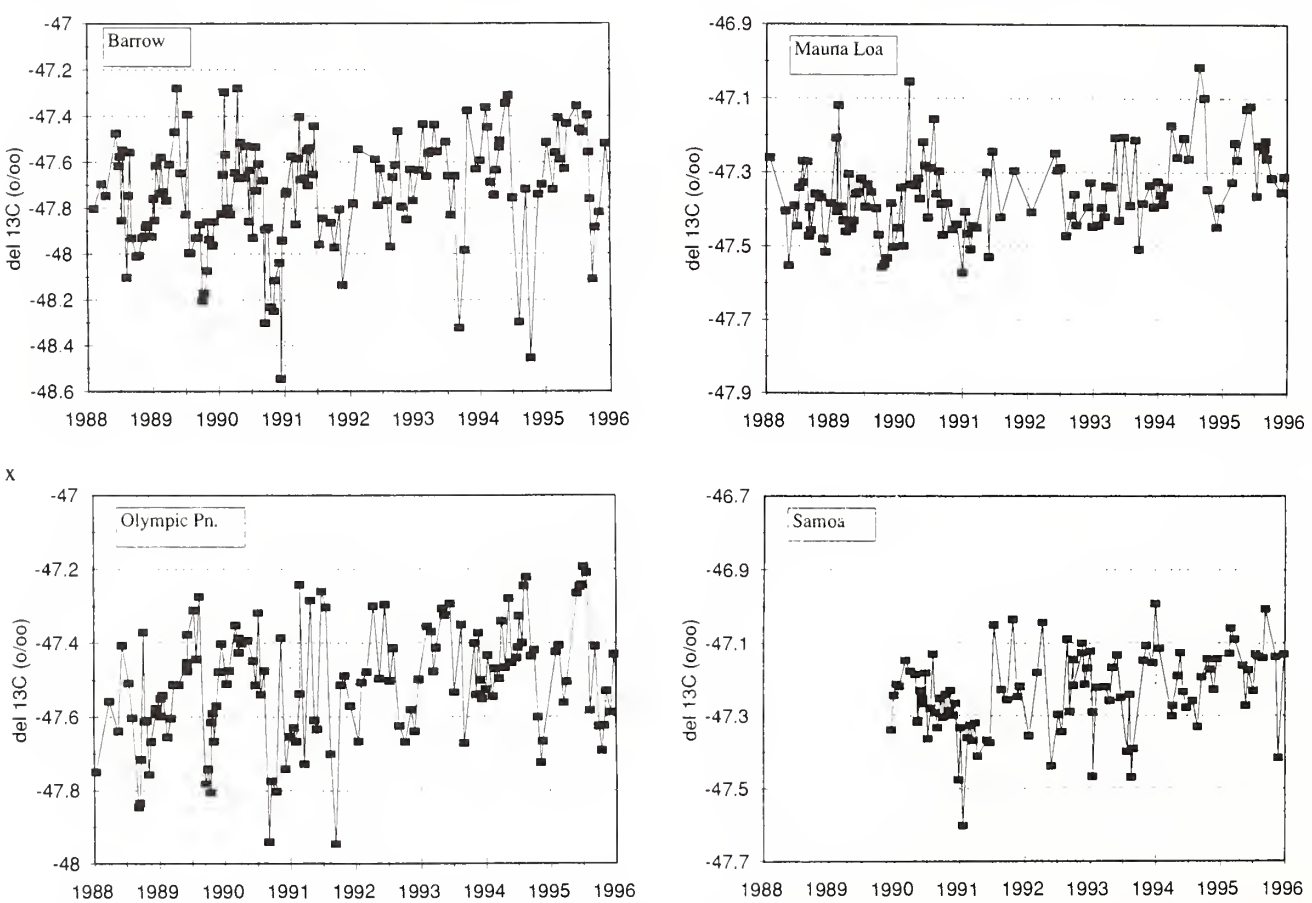

Fig. 1. The time series of the $\delta^{13}C$ of atmospheric CH_4 measured at Pt. Barrow, Olympic Peninsula, Mauna Loa, and Samoa since 1988.

vacuum extraction line through a series of liquid nitrogen traps to remove H_2O, CO_2, and N_2O. The air then passes through a bed of Schutze's reagent, I_2O_5 on silica, to oxidize CO to CO_2 which is trapped cryogenically. Then the CH_4 in the air is combusted over platinized silica at 800°C to CO_2 which is then trapped cryogenically. The yield of the procedure determined from standards is 100 ± 2% (n = 114). The $^{13}C/^{12}C$ of the CO_2 derived from CH_4 is measured on a Finnigan MAT 251 gas ratio isotope mass spectrometer. The overall measurement precision is about ±0.1‰. We obtain a $\delta^{13}C$ of -41.73‰ (versus PDB) for NBS-16.

Results and Discussion

The seasonal cycle in the $\delta^{13}C$ of CH_4 is greatest at 71°N (Barrow) with an amplitude of ~0.6‰, and decreases southward to 14°S (Samoa) where the seasonal trend is at about our measurement precision, i.e., 0.1‰ (Figure 1). The seasonal trends at 71°N and 48°N can be approximated roughly by a single harmonic with an annual period. Episodes of high CH_4 concentrations associated with very depleted $\delta^{13}C$ values occur at these two sites in September and October of each year and are due to input of bacterial methane. The trend toward higher summertime $\delta^{13}C$ values is expected as a result of increased CH_4 oxidation by OH because the $^{12}CH_4$ molecules react at a slightly faster rate (1.0054x) than the $^{13}CH_4$ molecules [*Cantrell et al.*, 1990]. It is also likely that there is seasonal change in the average $\delta^{13}C$ of the CH_4 sources. The annual mean $\delta^{13}C$ values increase southward from about -47.7‰ at 71°N to -47.2‰ at 14°S.

We calculate a global average $\delta^{13}C$ of CH_4 of approximately -47.3‰. The mean global $\delta^{13}C$ value, when combined with the ^{14}C content of atmospheric CH_4, yields estimates of the proportion of bacterial, nonbacterial, and fossil CH_4 source strengths [e.g., *Quay et al.*, 1991]. We estimate that bacterial CH_4 sources contribute about 75%, fossil CH_4 sources about 15%, and biomass burning about 10% of the total CH_4 input.

Although the seasonal cycle in $\delta^{13}C$ dominates the time series measurements in the northern hemisphere, there is evidence for a slight interannual increase. Measurements at all four time-series locations indicate an increase in $\delta^{13}C$ and, when combined and area weighted, yield a global rate of approximately 0.02‰ per year since 1989. A $\delta^{13}C$ increase indicates that the ratio of nonbacterial to bacterial CH_4 source strength is increasing slightly. The interhemispheric gradient and interannual trend in the isotopic composition of methane yields useful constraints of the magnitude of CH_4 sources and the rate at which the source strengths are changing with time.

References

Dlugokencky, E.J., L.P. Steele, P.M. Lang, and K.A. Masarie, The growth rate and distribution of atmospheric methane, *J. Geosphys. Res.*, 99, 17,021-17,043, 1994.

Cantrell, C.A., R.E. Shetter, A.H. McDaniel, J.G Calvert, J.A. Davidson, D.C. Lowe, S.C. Tyler, R.J. Cicerone and J.P. Greenberg, Carbon kinetic isotope effect in the oxidation of methane by the hydroxyl radical, *J. Geophys. Res.*, 95, 22,455-22,462, 1990.

Quay, P.D., S.L. King, J. Stutsman, D.O. Wilbur, L.P. Steele, I. Fung, R.H. Gammon, T.A. Brown, G.W. Farwell, P.M. Grootes, and F.H. Schmidt, Carbon isotopic composition of atmospheric methane: Fossil and biomass burning source strengths, *Global Biogeochem. Cycles*, 5, 25-47, 1991.

Stevens, C.M. and F.E. Rust, The carbon isotopic composition of atmospheric methane, *J. Geophys. Res.*, 87, 4879-4882, 1982.

Wigley, T.M.L. and S.C.B. Raper, Implications for climate and sea level of revised IPCC emission scenarios, *Nature*, 357, 293-300, 1992.

Aerosol Measurements on American Samoa

DENNIS L. SAVOIE AND JOSEPH M. PROSPERO
University of Miami, Rosenstiel School of Marine and Atmospheric Sciences, Miami, FL 3314-1098

An aerosol sampling program was established at the CMDL station on American Samoa in 1983 as part of the Sea/Air Exchange Program (SEAREX) network [*Savoie et al.*, 1989a]. Our data record starts in March 1983 and continues to the present. The main focus of these studies is on non-seasalt (nss) $SO_4^=$, NO_3^-, methane sulfonate (MSA) and various seasalt components. Measurements of ^{210}Pb yield concentrations that are among the lowest reported for temperate and tropical ocean regions [*Turekian et al.*, 1989], suggesting that the island is minimally impacted by continental sources Al and Sb concentrations at Samoa are among the lowest reported for tropospheric aerosols [*Arimoto et al.*, 1989; *Prospero et al.*, 1989], and concentrations of Pb are about an order of magnitude lower than those in the North Pacific westerlies [*Maring et al.*, 1989; *Rosman et al.*, 1990]. Consequently, the concentrations of nss-$SO_4^=$ and NO_3^- at Samoa should largely reflect the input from natural sources in the region.

SAMPLING AND ANALYSIS

Aerosol samples are collected by drawing air through 20 × 25-cm Whatman-41 filters at a nominal flow rate of 1.1 m^3 min^{-1}; the filters are mounted at the top of a tower at the eastern edge of the promontory where the CMDL site is located. The sampling pumps are controlled by wind sensors that activate the pumps only when the wind is off the ocean at speeds greater than 1m s^{-1}. Filters are returned to Miami for analysis; see *Savoie et al.*, 1994 for procedures. Nss-$SO_4^=$ is obtained as the difference between total $SO_4^=$ and seasalt $SO_4^=$, the latter being calculated as total Na^+ times 0.2516, the $SO_4^=/Na^+$ mass ratio in bulk seawater.

MEAN CONCENTRATIONS AND TEMPORAL VARIATIONS

The monthly mean concentrations of nss $SO_4^=$, MSA, NO_3^-, and Na^+ are presented in Table 1. The monthly

TABLE 1. Aerosol Concentrations Measured at American Samoa From March 19, 1983, to January 3, 1996

	Nitrate μg m^{-3}			Sodium, μg m^{-3}			NSS Sulfate, μg m^{-3}			MSA, μg m^{-3}		
Month	**Mean** *Med.*	**Std.** *16%*	**N** *84%*	**Mean** *Med.*	**Std.** *16%*	**N** *84%*	**Mean** *Med.*	**Std.** *16%*	**N** *84%*	**Mean** *Med.*	**Std.** *16%*	**N** *84%*
January	**0.114**	**0.057**	**38**	**6.05**	**3.72**	**38**	**0.365**	**0.213**	**38**	**24.9**	**11.1**	**18**
	0.103	*0.066*	*0.155*	*4.79*	*3.64*	*9.02*	*0.377*	*0.168*	*0.572*	*21.7*	*15.6*	*38.0*
February	**0.120**	**0.055**	**34**	**6.12**	**2.98**	**34**	**0.428**	**0.313**	**32**	**23.4**	**9.1**	**14**
	0.111	*0.069*	*0.179*	*5.42*	*3.67*	*8.39*	*0.417*	*0.197*	*0.655*	*23.7*	*13.5*	*30.6*
March	**0.091**	**0.038**	**46**	**4.70**	**1.60**	**46**	**0.381**	**0.151**	**46**	**20.6**	**8.0**	**16**
	0.087	*0.057*	*0.118*	*4.21*	*3.43*	*5.97*	*0.385*	*0.249*	*0.546*	*20.7*	*13.7*	*25.6*
April	**0.091**	**0.060**	**46**	**5.09**	**1.94**	**46**	**0.275**	**0.164**	**46**	**17.3**	**10.6**	**20**
	0.085	*0.050*	*0.116*	*4.56*	*3.35*	*6.65*	*0.265*	*0.162*	*0.396*	*13.7*	*9.8*	*28.9*
May	**0.089**	**0.036**	**49**	**5.18**	**1.84**	**49**	**0.272**	**0.238**	**49**	**24.7**	**12.8**	**19**
	0.083	*0.061*	*0.118*	*5.23*	*3.61*	*6.22*	*0.276*	*0.171*	*0.406*	*23.7*	*11.3*	*36.5*
June	**0.103**	**0.044**	**49**	**4.99**	**1.56**	**49**	**0.293**	**0.167**	**48**	**20.8**	**10.6**	**20**
	0.096	*0.067*	*0.135*	*4.75*	*3.25*	*6.73*	*0.299*	*0.206*	*0.414*	*18.5*	*13.4*	*25.9*
July	**0.103**	**0.038**	**50**	**5.46**	**1.85**	**50**	**0.272**	**0.171**	**50**	**25.0**	**12.5**	**16**
	0.092	*0.070*	*0.141*	*5.10*	*4.07*	*7.15*	*0.288*	*0.139*	*0.426*	*20.8*	*14.7*	*39.7*
August	**0.108**	**0.042**	**49**	**6.18**	**2.10**	**49**	**0.252**	**0.235**	**48**	**25.0**	**13.3**	**15**
	0.098	*0.061*	*0.149*	*5.61*	*4.53*	*8.01*	*0.276*	*0.052*	*0.476*	*27.3*	*10.2*	*31.0*
September	**0.152**	**0.054**	**50**	**5.72**	**2.45**	**50**	**0.433**	**0.195**	**50**	**31.3**	**12.1**	**17**
	0.142	*0.105*	*0.189*	*5.06*	*3.83*	*7.47*	*0.421*	*0.286*	*0.614*	*33.2*	*19.1*	*41.9*
October	**0.148**	**0.059**	**46**	**4.70**	**1.51**	**45**	**0.458**	**0.166**	**45**	**25.7**	**9.1**	**15**
	0.139	*0.093*	*0.185*	*4.53*	*3.41*	*6.00*	*0.425*	*0.281*	*0.631*	*23.2*	*18.5*	*36.2*
November	**0.128**	**0.049**	**54**	**5.13**	**1.65**	**54**	**0.328**	**0.162**	**54**	**20.7**	**5.3**	**24**
	0.123	*0.092*	*0.166*	*4.71*	*3.75*	*6.27*	*0.352*	*0.240*	*0.450*	*22.7*	*14.5*	*26.3*
December	**0.148**	**0.068**	**45**	**6.28**	**2.82**	**45**	**0.358**	**0.220**	**45**	**24.0**	**10.7**	**13**
	0.137	*0.088*	*0.215*	*5.60*	*3.97*	*8.15*	*0.368*	*0.222*	*0.528*	*22.5*	*14.5*	*32.7*
Annual-Wkly	**0.116**	**0.055**	**556**	**5.44**	**2.25**	**555**	**0.339**	**0.210**	**551**	**23.4**	**10.8**	**207**
	0.104	*0.068*	*0.165*	*4.95*	*3.59*	*7.12*	*0.345*	*0.185*	*0.497*	*22.1*	*12.9*	*33.3*
Annual-Mon	**0.116**	**0.023**	**12**	**5.47**	**0.58**	**12**	**0.343**	**0.072**	**12**	**23.6**	**3.5**	**12**
	0.100	*0.087*	*0.137*	*4.92*	*4.55*	*5.46*	*0.360*	*0.276*	*0.418*	*22.6*	*20.2*	*24.6*

Values in bold are the monthly mean concentration, the standard deviation, and the number of samples in the set. The values in italics are the median concentration and the concentrations of the samples at the 16% and 84% level in the frequency distribution.

averages listed in Table 1 and the plots of the weekly concentrations (Figure 1) show evidence of seasonal cycles. The strongest cycle is exhibited by NO_3^- for which the highest monthly mean (0.152 μg m^{-3} in September) is 71% higher than the lowest (0.089 μg·m^{-3} in April). The seasonal cycle for nss-$SO_4^=$ is similar to that for NO_3^- but the seasonal difference is somewhat less; the October mean (0.458 μg m^{-3}) is 56% higher than the April mean (0.294 μg m^{-3}). For both species, the seasonal cycles presented here do not differ significantly from those based on the 1983 through 1987 samples [*Savoie et al.*, 1989b].

There is no clearly evident pattern in the monthly averages for MSA even though there are significant month-to-month variations. This lack of a clear trend may be due in part to the fact that the data set for MSA is not as large as that for the other species. Nonetheless, the maxiumum occurs in September (mean, 31.31 ng m^{-3}) and the minimum in April (17.30 ng m^{-3}).

There is no evidence of any long-term changes in aerosol concentrations at the site. The means in Table 1 are quite similar to those previously reported by *Savoie et al.* [1989a,b] for 215 samples, 0.36 μg·m^{-3} for nss $SO_4^=$ and 0.110 for NO_3^-. Even the comparatively small data set (n = 22) used by *Saltzman et al.* [1985] provided comparable means: nss-$SO_4^=$, 0.41 μg·m^{-3}; MSA, 26 ng·m^{-3}; NO_3^-, 0.118 μg·m^{-3}; and Na^+, 5.6 μg·m^{-3}.

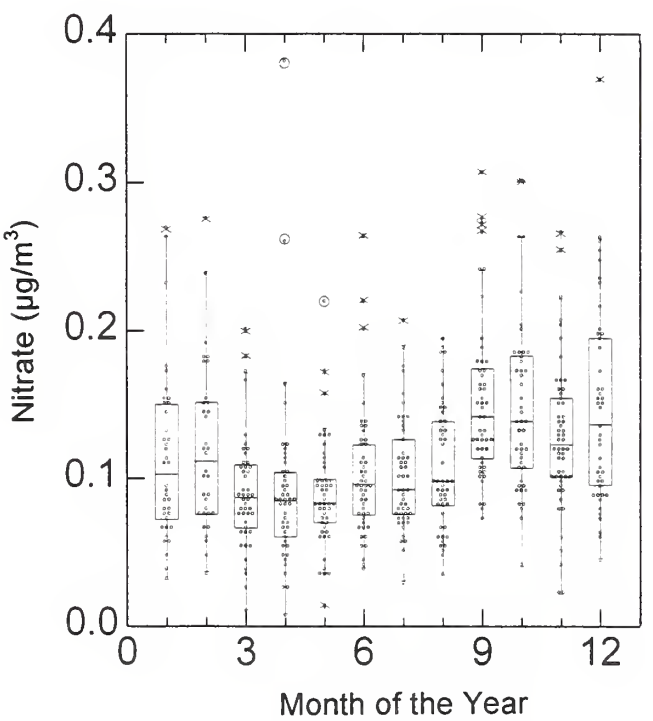

Fig. 1. Weekly aerosol concentrations for American Samoa (from March 19, 1983 to January 3, 1996) grouped by month. The data are shown with box plots. The length of each box shows the range within which the central 50% of the values fall, with the box borders at the first and third quartiles; the cross-bar shows the median [for details see *Tukey*, 1997]

The relationship between nss-$SO_4^=$ and MSA also appears to be quite stable over time. *Savoie et al.* [1994] investigated the relationships among the various species and found that the geometric mean (GM) ratio nss-$SO_4^=$/MSA (18.1 ± 0.9) is only about 7% higher than the GM ratio of 16.9 in the 22 American Samoa samples originally used by *Saltzman et al.* [1985]. As reported in *Savoie et al.* [1994] the ratio obtained at American Samoa is similar to that obtained at other ocean stations in the tropics and sub-tropics. Thus, within this region, MSA should provide reasonable estimates of the biogenic component of the total nss-$SO_4^=$.

Acknowledgments. We are indebted to the NOAA Climate Monitoring and Diagnostics Laboratory for permitting us to sample at their station and to the numerous people who have been involved in the actual field work, principally C. Farmer and E. Wilson-Godinet. The aerosol research was supported by National Science Foundation grants ATM8703411 and ATM9013125 and NASA contracts NAG8-621 and NAG8-841 to the University of Miami.

REFERENCES

Arimoto,R., R.A. Duce, and B.J. Ray, Concentrtions, sources and air-sea exchange of trace elements in the atmosphere over the Pacific Ocean, in *Chemical Oceanography*, vol. 10, edited by J.P. Riley, R. Chester, and R.A. Duce, pp. 107-149, Academic, San Diego, CA., 1989.

Maring, H., C. Patterson, and D. Settle, Atmospheric input fluxes of industrial and natural Pb from the westerlies to the mid-North Pacific, in *Chemical Oceanography*, vol. 10, *SEAREX: The Sea/Air Exchange Program*, edited by J. P. Riley, R. Chester, and R. A. Duce, pp. 84-106, Academic, San Diego, CA, 1989.

Prospero, J.M., M. Uematsu, and D.L. Savoie, Mineral aerosol transport to the Pacific Ocean, in *Chemical Oceanography*, vol. 10, *SEAREX: The Sea/Air Exchange Program*, edited by J.P. Riley, R. Chester, and R.A. Duce, pp. 187-218, Academic, San Diego, Calif., 1989.

Rosman, K.J.R., C.C. Patterson, and D.M. Settle, The distribution of lead between seasalt, dust, and lead-rich aerosols in the mid-South Pacific easterlies at American Samoa, *J. Geophys. Res., 95*, 3687-3691, 1990.

Saltzman, E.S., D.L. Savoie, J.M. Prospero, and R.G. Zika, Atmospheric methanesulfonic acid and non-seasalt sulfate at Fanning and American Samoa, *Geophys. Res. Lett., 12*, 437-440, 1985.

Savoie, D.L., J.M. Prospero, and E.S. Saltzman, Nitrate, non-seasalt sulfate and methanesulfonate over the Pacific Ocean, in *Chemical Oceanography*, vol. 10, *SEAREX: The Sea/Air Exchange Program*, edited by J. P. Riley, R. Chester and R. A. Duce, pp. 219-250, Academic, San Diego, CA, 1989a.

Savoie, D.L., J.M. Prospero, J.T. Merrill, and M. Uematsu, Nitrate in the atmospheric boundary layer of the tropical South Pacific: Implications regarding sources and transport, *J. Atmos. Chem., 8*, 391-415, 1989b.

Savoie, D.L., J.M. Prospero, R. Arimoto, and R.A. Duce, Non-seasalt sulfate and methanesulfonate at American Samoa, *J. Geophys. Res., 99 (D2)*, 3587-3596, 1994.

Tukey, J.W., *Exploratory Data Analysis*, 688 pp., Addison-Wesley, Reading, MA, 1977.

Turekian, K. K., W.C. Graustein, and J.K. Cochran, Lead-210 in the SEAREX program: An aerosol tracer across the Pacific, in *Chemical Oceanography*, vol. 10, *SEAREX: The Sea/Air Exchange Program*, pp. 51-81, edited by J. P. Riley, R. Chester and R. A. Duce, Academic, San Diego, Calif., 1989.

An Operational Intercalibration Experiment Between CMDL and CSIRO to Measure Several Atmospheric Trace Species

L.P. Steele, R.J. Francey, R.L. Langenfelds, C.E. Allison, and M.P. Lucarelli
CSIRO Division of Atmospheric Research, Aspendale, Victoria, Australia

P.P. Tans, E.J. Dlugokencky, T.J. Conway, P.C. Novelli, and K.A. Masarie
NOAA, Climate Monitoring and Diagnostics Laboratory, Boulder, Colorado 80303

J.W.C. White and M. Trolier
University of Colorado, Institute of Arctic and Alpine Research, Boulder, Colorado 80309

Introduction

Atmospheric trace species that are important to the question of global and climate change have been measured by both CMDL and CSIRO for many years through their networks of flask sampling sites. There has been some overlap of these networks, particularly at the locations of the baseline observatories. A desirable, even essential goal is to be able to "seamlessly merge" the trace species data obtained by the two laboratories, creating a larger and self-consistent data set that can be reliably used for modeling and interpretive studies of trace gas budgets, with particular emphasis on the global carbon cycle. The advantages of this approach have already been demonstrated through several studies of the carbon cycle which make use of the isotopic measurements of carbon dioxide [e.g., *Ciais et al.*, 1995a,b,c]. The initial phases of an intercomparison of stable isotope measurements of CO_2 by both laboratories has been provided by *Francey et al.* [1994].

The most commonly adopted method of determining the degree of agreement in the measurement of atmospheric trace gases by different laboratories has been the periodic exchange of standard gases, usually contained in high-pressure cylinders. This method was in use for many years by those laboratories measuring atmospheric CO_2, and is endorsed by the World Meteorological Organization [*Pearman*, 1993]. While these types of experiments can yield important information, they suffer from the disadvantages that the frequency of intercalibration is too low, perhaps occurring only once every few years, and the analysis methodology sometimes differs from that employed in the routine observing programs.

Operational Intercalibration

In an attempt to improve upon the existing methods of trace species intercalibration between CSIRO and the CMDL Carbon Cycle Group (CCG), we proposed an experiment in 1991 that was agreed upon between the two laboratories. It began in late 1991 and is ongoing. The glass flasks that are filled with air (in pairs) approximately once a week for CCG at the Cape Grim baseline station are routed through CSIRO's GASLAB on their way back to Boulder. One member of every second pair of flasks (i.e., one in every four flasks) is measured in GASLAB for several trace species (CO_2, CH_4, CO, H_2, and ^{13}C and ^{18}O in CO_2). The flask sample measured in this way is clearly marked, therefore, it can be identified when the air samples reach Boulder. All flask air samples, including the one measured in GASLAB, are then measured for the same suite of trace species in the CCG laboratories. This type of experiment is possible only because the analytical methods used in GASLAB consume relatively small volumes of air, typically less than 200 mL for the full suite of measurements. The techniques used for the GASLAB measurements are outlined in *Francey et al.* [1996]. A crucial requirement for this experiment to be successful is that the trace composition of the samples measured in GASLAB must not be altered in any way by this process. The design of the experiment should allow any such alteration to be identified.

Exchanges of data from this experiment between the two laboratories were initially sporadic. Visual inspection indicated that there was reasonable agreement for CH_4, CO, and $^{13}CO_2$. An offset of about 0.6 ppm between the CO_2 records was thought to be due to an offset in the calibration scales being used by the two laboratories. A thorough analysis of the full data set is being prepared for publication. This analysis and improvements in procedures to allow regular and systematic comparison of the results by staff of both laboratories has been greatly facilitated by support from both laboratories for an extended visit by one of the authors (KAM) to CSIRO Division of Atmospheric Research during 1996.

References

Ciais, P., P.P. Tans, M. Trolier, J.W.C. White, and R.J. Francey, A large northern hemisphere terrestrial CO_2 sink indicated by the $^{13}C/^{12}C$ ratio of atmospheric CO_2, *Science*, 269, 1098-1102, 1995a.

Ciais, P., R.J. Francey, P.P. Tans, J.W.C. White, and M. Trolier, An analytical error estimate for the ocean and land uptake of CO_2 using $\delta^{13}C$ observations in the atmosphere, *NOAA Tech. Memo. ERL CMDL-8*, NOAA Environmental Research Laboratories, Climate Monitoring and Diagnostics Laboratory, Boulder, Colorado, 13 pp., 1995b.

Ciais, P., P.P. Tans, J.W.C. White, M. Trolier, R.J. Francey, J.A. Berry, D.R. Randall, P.J. Sellers, J.G. Collatz, and D.S. Schimel, Partitioning of ocean and land uptake of CO_2 as inferred by $\delta^{13}C$ measurements from the NOAA Climate Monitoring and Diagnostics Laboratory Global Air Sampling Network, *J. Geophys. Res.*, 100, 5051-5070, 1995c.

Francey, R.J., C.E. Allison, L.P. Steele, R.L. Langenfelds, E.D. Welch, J.W.C. White, M. Trolier, P.P. Tans, and K.A. Masarie, Intercomparison of stable isotope measurements of CO_2, in *Climate Monitoring and Diagnostics Laboratory No. 22*

Summary Report 1993, edited by J.T. Peterson and R.M. Rosson, pp. 106-110, NOAA Environmental Research Laboratories, Boulder, CO, 1994.

Francey, R.J., L.P. Steele, R.L. Langenfelds, M.P. Lucarelli, C.E. Allison, D.J. Beardsmore, S.A. Coram, N. Derek, F.R. de Silva, D.M. Etheridge, P.J. Fraser, R.J. Henry, B. Turner, E.D. Welch, D.A. Spencer and L.N. Cooper, Global Atmospheric Sampling Laboratory (GASLAB): Supporting and extending the Cape Grim trace gas programs, in *Baseline Atmospheric Program (Australia) 1993*, edited by R.J. Francey, A.L. Dick, and N. Derek, pp. 8-29, Bureau of Meteorology and CSIRO, Division of Atmospheric Research, Melbourne, Australia, 1996.

Pearman, G., Survey of the results of the 1991-1992 round-robin interlaboratory intercomparison, in *Report of the Seventh WMO Meeting of Experts on Carbon Dioxide Concentration and Isotopic Measurement Techniques*, Rome, Italy, September 7-10, 1993, edited by G.I. Pearman and J.T. Peterson, pp. 104-107, World Meteorological Organization, Global Atmosphere Watch, Report No. 88, 1993.

USGS Barrow Observatory

JACK TOWNSHEND
U.S. Geological Survey, College Obesrvatory, Fairbanks, Alaska 99775-5160

The Barrow Magnetic Observatory is the northernmost of U.S. Geological Survey (USGS) 12 continuously-recording, digital magnetic observatories. As such, it serves as a singularly important site in a global network of observing stations whose combined data define the planetary magnetic field and track its secular change. Ground stations such as the Barrow Observatory are controls for field modeling by harmonic analysis, essential reference stations for airborne and satellite surveys, and absolute calibration locations for field survey instrumentation.

The primary instrumentation operated is an EDA FM-100BR Triaxial fluxgate magnetometer, an EDA PPM-105 proton free-precession magnetometer, an Observatory Magnetometer Interface System (OMIS), and several pier-mounted instruments for absolute control observations.

In late summer 1996 the USGS plans on upgrading the present fluxgate magnetometer and installing an additional instrument called a "quasi-absolute magneto-meter."

In August 1993 the USGS and CMDL negotiated a Memorandum of Agreement (MOA) to have CMDL personnel at Barrow service the USGS BRW equipment, make instrument observations, and provide some logistic support. This agreement is renewed annually.

The Barrow Magnetic Observatory receives its authorization to operate from the USGS Branch of Earthquakes and Geomagnetic Information in Golden, Colorado.

Parts of the NOAA-USGS MOA are presented below to provide some history and background of our joint Barrow operations.

For many years, the Naval Arctic Research Laboratory (NARL) was the source of electrical power, road maintenance, transportation, and lodging support. Effective October 1, 1984, this support was no longer assured as the Navy began the process of transferring ownership of NARL to the Ukpeagvik Inupiat Corporation (UIC).

Individual withdrawal applications for land occupied by each agency's project was approved by BLM and published in the Federal Register. Withdrawal file numbers are NOAA-F-81469 and USGS-F-81490. Transfer of the land to the USGS and NOAA was made effective April 2, 1991, and published in the *Federal Register*, Volume 56, Number 63, page 13413, dated April 2, 1991.

A third-party agreement was set up between NOAA, USGS, and the Department of the Air Force, now located at 11TCW/LG0X, 6900 9th St. Suite 301, Elmendorf AFB, Alaska 99506-2270, to provide support for electrical power, road service, transportation, vehicle repair, lodging, and meals through their DEW System Station at Barrow, Alaska (Pow-Main). This agreement (Inter-Agency MOA between NOAA and USGS) will be an attachment to the "Support Agreement" between USAF, NOAA and USGS. NOAA is authorized by the USGS to be signatory to the "Support Agreement" with the USAF, since they want only one signature on the document.

Subsequently NOAA and USGS agreed to get power from the Barrow Utilities and Electric Co-op, Inc., (BUEGI), through the Ukpeagvik Inupiat Corporation/ Northern Arctic Research Laboratory (UIC/NARL) facility.

NOAA and the USGS shall continue to acquire electrical power from the Barrow Utilities and Electric Co-op., Inc. (BUECI).

Under the terms of the MOA, NOAA agrees to have the CMDL personnel at Barrow do the following:

Weekly

Check facilities for any noticeable damage or unusual conditions and report anything that may seem out of the ordinary to the College Observatory, Fairbanks, check the Observatory instruments and equipment, and make routine rotations on specific forms supplied. Make four sets of magnetic absolute observations with a Declination Inclination Magnetometer (DIM); make one set of Scale Value Observations on the Observatory Magnetometer Interface System (OMIS) Fluxgate Magnetometer; change digital magnetic, and analog paper tapes; and send all data, computations, observations, and tapes to the USGS office.

Unscheduled

Perform minor trouble shooting and make adjustments to equipment when USGS technical personnel provide instructions by telephone.

For the services supplied by NOAA in the previously mentioned items, the USGS will reimburse NOAA for the time required to perform the work, travel time required to get to and from USGS facilities and instruments, and a reasonable amount for unplanned circumstances because of emergencies, weather, etc. Supplies and materials are not included in this agreement. USGS will pay for or reimburse NOAA for supplies or materials needed.

The New ANSTO Radon Detector at MLO

S. WHITTLESTONE
ANSTO, PMB 1, Menai, NSW 2234, Australia

INTRODUCTION

After 6 years, many of the questions posed at the commencement of the Australian Nuclear Science and Technology Organization (ANSTO) CMDL radon program at the Mauna Loa Observatory, Hawaii (MLO) have been answered. By 1994 the radon detector was obsolete. It is, therefore, timely to review the output from the program and describe a new radon detector designed to meet the needs of the future.

The program commenced in June 1989. Its aim was to assess the value of radon as a tracer for air masses which have been subject to recent contact with land and, therefore, not representative of the global baseline. By the end of 1991 it was evident that radon is indeed the best readily-measured indicator of perturbation of air masses by contact with land beyond Hawaii [*Whittlestone et al.*, 1992]. Because it is chemically inert, radon concentration is unaffected by the complex reactions affecting most other atmospheric species during transport. Samples of trace gases sampled in the baseline wind sector are strongly correlated with radon concentrations (Figure 1). For the first time there was a quantitative continuous measure of the influence of the Asian continent on air samples at MLO when jet streams transport air from Asia in only a few days [*Kritz*, 1990].

Radon has been useful in the study of dry deposition because its decay products are very small and highly reactive. Radon acts as a uniform source of ultrafine reactive particles that have a short half life and so indicates deposition only over a limited area. Measurements at sea level at Cape Grim, Australia, indicated very strong deposition in the lower marine boundary layer. Studies at MLO showed higher concentrations of ultrafine radon decay products were present at the altitude of MLO but that they were subject to strong deposition close to MLO in certain weather conditions [*Schery and Whittlestone*, 1995; *Schery et al.*, 1992].

Several other studies have made use of radon. For example it was valuable in validation of use of air mass trajectory cluster analysis of variations of methane at MLO [*Harris et al.*, 1992]. Data were provided for MLOPEX-II and were part of an evaluation of Pb-212 as a tracer for local ground contact [*Whittlestone et al.*, 1996a,b].

Radon has proved to be useful to other programs at MLO. However, the detector required a degree of skilled technical supervision that was not sustainable in the long term. It was desirable to be able to obtain radon measurements with no more effort than wind speed and direction. To meet this need, a new radon detector design was incorporated into the MLO detector. This design, although it was markedly simpler and more rugged than the previous one, provided improved time response, better sensitivity, lower power consumption, and freedom from routine maintenance.

Because of the simplicity of the new instrument, it is possible to obtain high-quality preliminary data in real time. Steps have been taken to make the radon data readily available from the CMDL computer.

THE RADON DETECTOR

Figure 2 is a schematic diagram of the detector. It is an implementation of the design described in *Whittlestone et*

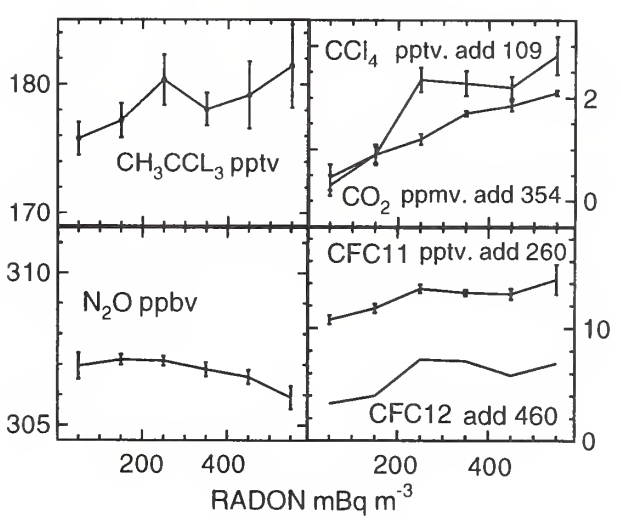

Fig. 1. Dependence of trace gas concentrations on radon concentration in the baseline wind sector at MLO.

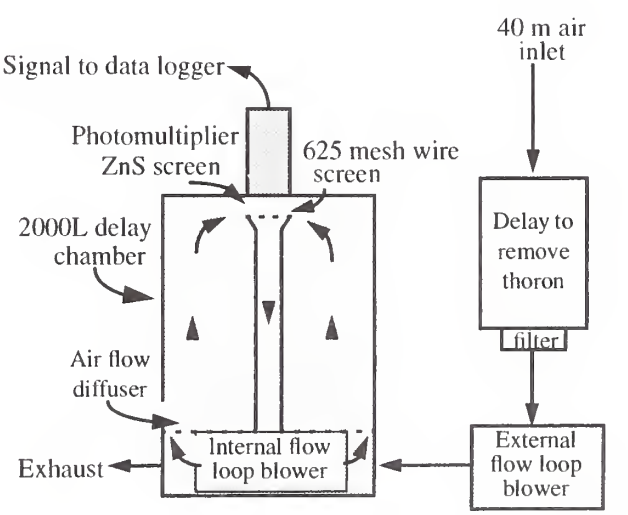

Fig. 2. Schematic diagram of the ANSTO radon detector at MLO.

[1996a] for MLO. Table 1 gives the basic specifications. As with most high sensitivity radon detectors, this design uses the two-filter principle. The first filter removes all radon decay products from the inlet air. This air moves steadily through the delay chamber and while there, a portion of the radon decays. The second filter, in this case a wire screen, collects as many of the decay products as possible. These decay products in turn decay, and the alpha radiation is detected by the zinc sulfide screen and photomultiplier. Two key features of the new design are use of a wire screen for the second filter and separation of the external flow which changes the air sample from the internal flow which acts to draw radon decay products produced inside the chamber onto the screen.

It is possible to use a wire screen as the second filter because the decay products form ion clusters about 1 nm in diameter which diffuse so rapidly that they are trapped very easily. In this detector 70% of the decay products are collected on the screen even though the flow rate is 800 L min^{-1}. The high flow rate is necessary to minimize loss of decay products through the walls of the chamber and to allow measurement of the first decay product, Po-218, whose half life is only 3 minutes.

The major benefit of using the wire screen is a reduction in power compared to that required by a conventional filter. Only 20 W are needed, compared to about 500 W for the filter. This translates to a reduction in power costs over a year from $440 to $18 at 10 cents per kW hour.

As with the use of a wire screen, the second design feature, separation of the sampling from the collection flows, results in economies in design. An 800-L min^{-1} flow would need 100 mm air lines and a large inlet filter. It is desirable to include a delay of about 4 minutes to allow any thoron gas in the inlet to decay. At 800 L min^{-1} this would need a capacity of at least 3200 L. Since the only requirement of the external flow is to achieve an average residence time of air in the chamber of 20 minutes, 100 L min^{-1} is sufficient, and 20 mm air lines are adequate.

It can be seen from Figure 2 that the only moving parts are the blowers. There are no components that require regular maintenance or that are sensitive to temperatures over the range -10 to 40°C. Only a few components would need to be adapted for arctic use.

TABLE 1. Specifications of the ANSTO Radon Detector at MLO

Item	Specification
Sensitivity:	0.5 c s^{-1} per Bq m^{-3}
Limit of detection:	20 mBq m^{-3} (30% counting error in 1 hour count)
Time response:	45 minutes to 50% after step in radon concentration
Routine maintenance:	Minimal
Power consumption:	40 W

Data Acquisition

Because of the simplicity of the detector and its insensitivity to environmental conditions, passive data logging is all that is required. A few parameters should be monitored, such as supply volts and flow rates. Since installation in February 1996, data are averaged over 30-minute intervals by a data logger. A computer downloads data automatically at preset intervals. At the time of preparation of this paper, it was not possible to operate a DOS-based download program from the pseudo-DOS accessible from Microsoft windows. The serial port was unreliable. As a result, data transfer to the computer network has to be done manually. It is hoped this incompatibility will be solved so that preliminary data can be viewed on the Internet in close to real time. Parameters needed for data quality assessment are included in the data set permitting largely automatic data editing and prompt review for general release.

Conclusion

Radon has been established as a useful tracer for tagging air recently in contact with land. In the case of air from Asia, it is the only species transported without loss by wash-out or chemical change which can indicate such contact. New instrumentation at MLO is inherently robust and simple to operate. Up-to-date preliminary data are available and a path established which should see processed data on the CMDL computer system within a few months of acquisition.

Acknowledgment. This work has been made possible by the active participation of the staff of MLO.

References

Harris, J.M., P.P., Tans, E.J., Dlugokencky, K.A. Masarie, P.M. Lang, L.P. Steele, and S. Whittlestone, Variations in methane at Mauna Loa Observatory related to long range transport, *J. Geophys Res.*, 97(D5), 6003-6010, 1992.

Kritz M. A., The China Clipper—fast advective transport of radon-rich air from the Asian boundary layer to the upper troposphere near California, *Tellus*, 42B, 46-61, 1990.

Schery, S.D., and S. Whittlestone, Evidence of high deposition of ultrafine particles at Mauna Loa Observatory, *Atmos. Environ.*, 29(22), 3319-3324, 1995

Schery, S.D., R. Wang, K. Eak, and S. Whittlestone, New models for radon progeny near the earth's surface, *J. Radiat. Prot. Dosim.*, 45, 343-347, 1992

Whittlestone, S., E. Robinson, and S. Ryan, Radon at the Mauna Loa Observatory: Transport from distant continents, *Atmos. Environ.*, 26A(2), 251-260, 1992.

Whittlestone S., W. Zahorowski, and P. Wasiolek, High sensitivity two filter radon/thoron detectors deploying a wire or nylon screen as the second filter, *ANSTO E718*, 1994

Whittlestone, S., S.D. Schery, and Y. Li, Thoron and radon fluxes from the island of Hawaii, *J. Geophys Res.*, 101(D9), 14,787-14,794, 1996a.

Whittlestone, S., S. D. Schery, and Y. Li, Pb-212 as a tracer for local influence on air samples at Mauna Loa Observatory, Hawaii, *J. Geophys Res.*, in press, 1996b.

A Comparison of CO_2 and $^{13}/^{12}C$ Seasonal Amplitudes in the Northern Hemisphere

T. P. WHORF, C.D. KEELING, AND M. WAHLEN
Scripps Institution of Oceanography, La Jolla, California 92093-0220

INTRODUCTION

To better understand the sources and sinks of atmospheric carbon dioxide, the Scripps Institution of Oceanography (SIO) continues to maintain cooperative programs of CO_2 measurements with CMDL at Mauna Loa Observatory, Hawaii (MLO, 20°N), Point Barrow, Alaska (BRW, 71°N), Cape Kumukahi (KUM, 20°N), Samoa (14°S), and the South Pole (SPO), where air samples have been collected in 5-L glass flasks on a weekly to twice monthly basis, the latter at SPO. In addition, SIO continues to record atmospheric CO_2 concentrations on a continuous basis at Mauna Loa using a non-dispersive infrared (NDIR) gas analyzer installed on site in 1958. Studies of the MLO record in the last few years include a report on changes in the rate of rise of CO_2 and its relationship with global temperatures [*Keeling et al.*, 1995].

More recently, seasonal cycle studies of data from MLO and BRW, augmented by data from Alert, N.W.T (ALT, 82°N), have been published [*Keeling et al.*, 1996] that have yielded evidence of climate induced CO_2 changes in the form of possible changes in the growth of plants on a very large spatial scale. The Alert measurements have been collected under a cooperative program between SIO and the Atmospheric Environment Service of Canada. The SIO carbon dioxide program also continues to monitor CO_2 concentrations at Christmas Island (2°N), Baring Head, New Zealand (41°S), Raoul Island, Kermadec Islands (29°S), and La Jolla, California (LJO, 33°N), the last of which started in 1969 and now includes both continuous and flask measurements.

Since 1978 the $^{13}C/^{12}C$ isotopic ratio of atmospheric CO_2 has been determined from the same 5-L flask samples of CO_2 that have been measured for CO_2 concentration. In the early years isotopic ratio was measured at MLO, SPO, and LJO and by the mid-1980s at a total of ten sites. Measurements before 1992 were determined using a VG Micromass 903 and a VG SIRA 9 mass spectrometer at the Groningen Isotopic Physics Laboratory in the Netherlands [*Keeling et al.*, 1989]. Samples since then have been analyzed using a VG PRISM Series II mass spectrometer at SIO.

Changes in the amplitude of the seasonal cycle in CO_2 concentration at MLO were first observed and reported in the early 1980s [*Bacastow et al.*, 1985]. A more recent analysis of seasonal cycle variations observed at MLO has shown an increase in amplitude of 20% since the mid-1960s, an earlier drawdown of CO_2 in the late spring and early summer by up to a week since the late 1970s, and a correlation between amplitude changes there and temperatures averaged over the northern hemisphere [*Keeling et al.*, 1996]. Here we discuss seasonal changes in the $^{13}C/^{12}C$ isotopic ratio of atmospheric CO_2 and how they compare with changes in amplitude of CO_2 concentration.

DATA AND ANALYSIS

Measurements of $^{13}C/^{12}C$ used in this study come from the same 5-L flask samples that have all been analyzed for CO_2 concentration with an NDIR analyzer of the same design as that installed at MLO. Concentrations were calibrated with our standard suite of reference gases and expressed in the X93 mole fraction scale. Air samples were rejected if pairs did not agree within 0.40 ppm of the lowest flask average (0.60 ppm at Point Barrow), if they were single analyses, or if found to be outliers having a residual greater than three sigma from our smooth curve fit. This fit, described in *Keeling et al.* [1989], uses four harmonics to describe the seasonal variations plus a cubic spline [*Reinsch*, 1967] to describe the interannual variations. A linearly-increasing gain factor was incorporated into the fitting routine when it became apparent that there were significant increases in the seasonal amplitude. This same fitting procedure has been applied to the isotopic measurements.

Isotopic data are obtained from samples of CO_2 extracted cryogenically which have passed the above 0.40 or 0.60 ppm cutoff criterion. Data for MLO and BRW are shown in Figure 1 as monthly averages and expressed as the reduced isotopic ratio, $^{13}\delta$, of atmospheric CO_2 [*Keeling et al.*, 1989, p. 170]. Similar data have been obtained at the other SIO site locations. In 16 years of MLO $^{13}\delta$ isotopic data, over 700 daily samples have been analyzed amounting to approximately 44 per year, while at BRW in 14 years, some 500 daily samples have been analyzed yielding about 36 per year. Since 1992 when samples were first analyzed at SIO, gas standards have also been run daily in order to track any changes in the spectrometer output and thereby correct for them. These standards were recently calibrated against NBS19 (in 1996), to finalize calibrations begun in 1994. Along with this set of recent calibrations, a correction of +0.095 per mil was applied to all data analyzed at Groningen and previously published [*Keeling et al.*, 1989; 1995]. This correction term is based on extensive duplicated measurements of these daily gas standards on the mass spectrometers at the Netherlands and at SIO.

RESULTS

Figures 2-4 show relative seasonal amplitudes computed annually by least-square fitting the annual function $g(1 + At_m)$ multiplied by the four harmonics derived in the overall fit to the data of each year independently. In this expression, g denotes the annual relative amplitude, t_m the midpoint time of the record, and A, a constant gain factor for the record being fit expressed in percent change in amplitude per year. The harmonic function is thus phase locked to the fit of the overall data set. Amplitudes are

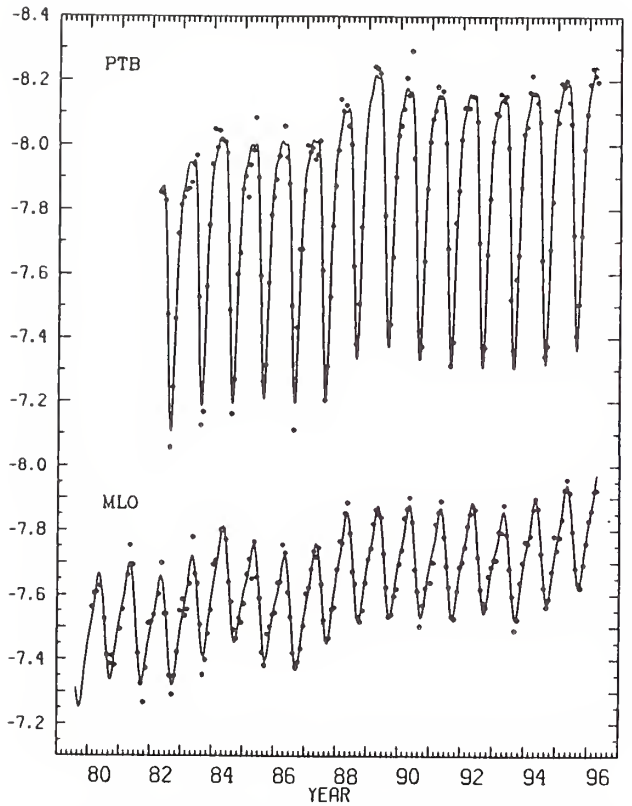

Figure 1. Time trend of the reduced isotopic ratio, $^{13}\delta$, of atmospheric CO_2 in per mil difference from the international carbonate standard, PDB, for Point Barrow (BRW) and Mauna Loa (MLO). The data are shown as monthly averages and the curve by a four-harmonic fit with spline, as described.

expressed relative to the mean annual cycle arbitrarily set at the midpoint in time of the fit [*Bacastow et al.*, 1985]. For purposes of intercomparison between stations or different time periods, the gain factor has been afterwards adjusted to a common date (see below).

Figures 2 and 3 show comparisons of seasonal amplitudes for CO_2 and $^{13}\delta$ for our northern hemisphere sites, (ALT, BRW, LJO, MLO, and KUM) in which the CO_2 station data have been fit over the same time periods as there exists data for $^{13}\delta$, typically beginning around 1980 except for ALT data, which begins later. This is so that the relative amplitudes for the two quantities are referenced to the same times to give an optimal comparison. Though the daily averages used in the isotopic fits are not identically the same as those used in the CO_2 fits, they number approximately 90% of the number for CO_2, except at La Jolla where it is about 60%. In addition, the figures showing BRW, LJO, and MLO flasks have CO_2 data extending back in time to before the beginning of the isotopic data. In these cases, fits to these longer records have yielded earlier CO_2 relative amplitudes which have subsequently been adjusted so as to be referenced to the same time as in the shorter fit and then

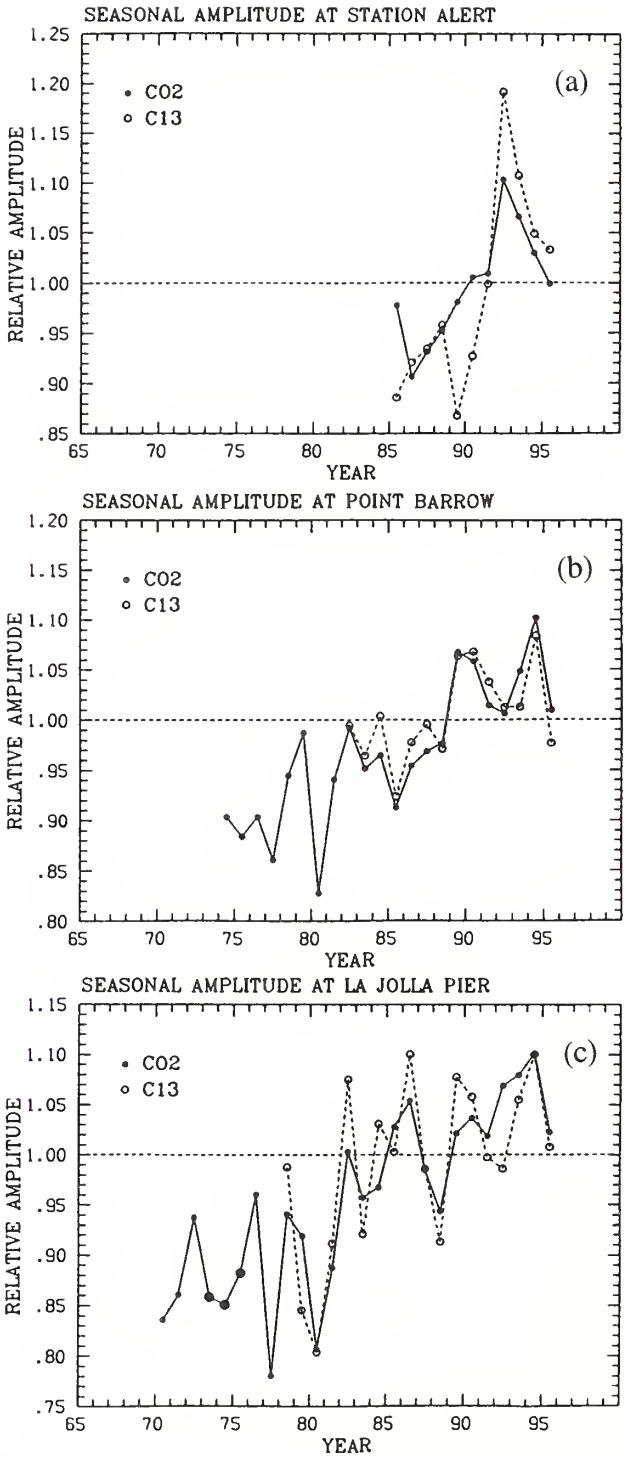

Figure 2. Comparisons of relative seasonal amplitudes for CO_2 concentration and $^{13}\delta$ at the three most northerly stations (a) Alert (ALT), (b) Point Barrow (BRW) and (c) La Jolla (LJO), each referred to the midpoint of its isotopic record (open circles). The large solid circles for LJO are continuous data.

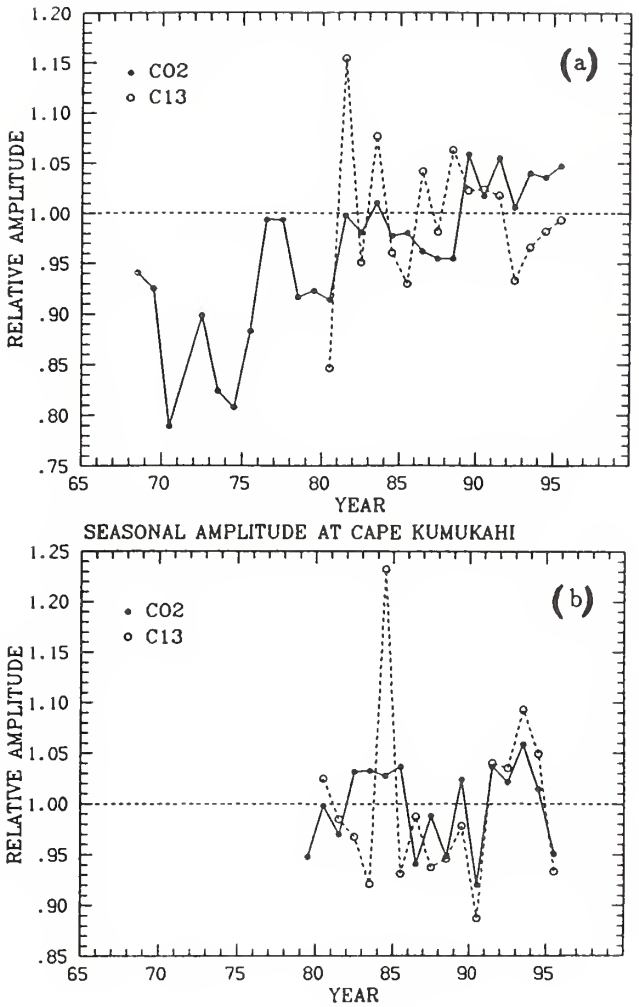

Figure 3. Comparisons of relative seasonal amplitudes for CO_2 concentration and $^{13}\delta$ at (a) Mauna Loa (MLO), flask data, and (b) Cape Kumukahi (KUM), each referred to the midpoint of its isotopic record (open circles). The large amplitude at KUM in 1984 is partly due to a strong shift in trend following the 1983 El Niño.

included in these figures. Increasing amplitudes are more apparent in these longer records. Gain factors calculated for the longer records shown at these three sites and referenced to 1970 near the start of these fits are BRW: 1.03 ± 0.16% yr^{-1}, LJO: 1.21 ± 0.17% yr^{-1}, and MLO flasks: 0.82 ± 0.15% yr^{-1}. The slightly larger fluctuations before and including 1981 for LJO and MLO flasks are attributed to there being significantly fewer annual data than in the latter part of each of these records. As an exception, the LJO record includes continuous CO_2 data in 1973-1975 (three large symbols) based on 5-hour averages of steady data subsequently converted to weekly data, so that these years are of significantly higher quality than other early years containing sparse flask data.

The fluctuations in $^{13}\delta$ seasonal amplitudes occurring over several year periods show a strong tendency to follow the CO_2 fluctuations during the same times, especially at BRW and LJO. A significant part of semi-decadal to

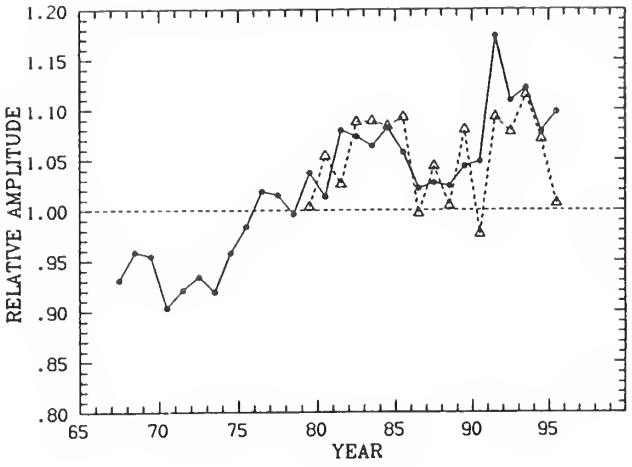

Figure 4. Comparison of seasonal amplitudes of CO_2 concentration for MLO (continuous data) and KUM, referred in this figure to the midpoint of the 1958-1995 Mauna Loa data. KUM amplitudes are adjusted to have the same mean as MLO amplitudes for the first 10 years of the KUM record (1979-1988).

decadal changes in seasonal amplitude are likely due to large scale temperature changes [*Keeling et al.*, 1996] while other fluctuations may be a result of the effect of interannual variations connected with El Niño events. Slightly larger isotopic swings in the annual amplitudes at LJO may be partly attributable to the fewer isotopic data at this site. Comparisons of the absolute seasonal amplitudes of $^{13}\delta$ with CO_2 concentration for our northern hemisphere sites show a rate of change in $^{13}\delta$ with respect to CO_2 of close to 0.05 per mil per ppm, as would be expected by a predominantly terrestrial component in CO_2. An interesting but unexplained observation is that multi-year seasonal changes at ALT in both $^{13}\delta$ and CO_2 seem to be out of phase with changes at BRW by a couple of years, particularly near 1992.

Comparison of seasonal changes in $^{13}\delta$ and CO_2 concentration do not seem to follow each other as closely at MLO as at BRW and LJO. This may stem from part of the seasonal cycle in CO_2 concentration being produced by oceanic processes that influence it without significantly affecting the amplitude of $^{13}\delta$. A difference in the trends of the seasonal amplitudes in concentration and $^{13}\delta$ is also apparent at MLO as evidenced by the differing gain factors $^{13}\delta$ and CO_2.

Gain factors for CO_2 concentration and $^{13}\delta$, compared over the same time intervals and referred to 1970, are expressed as annual rates of change in Table 1. Annual rates referred to 1980 would be about 8-10% smaller than if referred to 1970. No significant change in the seasonal cycle of $^{13}\delta$ is apparent in the MLO flask record since 1980, whereas the increase in seasonal amplitude of CO_2 concentration over the same period exceeds the standard error by more than a factor of two.

An additional observation of seasonal amplitude changes in CO_2 between MLO (continuous data) and KUM (Figure 4) where respective gain factors over the same period are shown in Table 1, shows no increase in seasonal amplitude at KUM since 1979. Also, no significant increase in amplitude is evident in the isotopic data. Since KUM,

TABLE. 1. Annual Rate of Increase in the Seasonal Amplitude of Atmospheric CO_2 and $^{13}\delta$ at Various Locations

Location	Approx. Latitude	Type	Inclusive Years of Observations	Rate of Increase* (in percent)
Alert	82°N	CO_2	1985-1995	1.21 ± 0.36
		$^{13}\delta$	1985-1995	2.48 ± 0.63
Point Barrow	71°N	CO_2	1974-1995	1.03 ± 0.16
		CO_2	1982-1995	1.10 ± 0.29
		$^{13}\delta$	1982-1995	0.58 ± 0.35
La Jolla	33°N	CO_2	1970-1995	1.21 ± 0.17
		CO_2	1978-1995	1.16 ± 0.33
		$^{13}\delta$	1978-1995	0.65 ± 0.42
Mauna Loa (flasks)	20°N	CO_2	1968-1995	0.82 ± 0.15
		CO_2	1980-1995	0.61 ± 0.25
		$^{13}\delta$	1980-1995	-0.16 ± 0.37
Mauna Loa (continuous)	20°N	CO_2	1958-1995	0.62 ± 0.04
		CO_2	1979-1995	0.34 ± 0.12
Kumukahi	20°N	CO_2	1979-1995	-0.43 ± 0.23
		$^{13}\delta$	1979-1995	0.11 ± 0.41

*With reference to January 1, 1970, except for Alert referred to January 1, 1980.

situated close to sea level, supplies principally oceanic air and MLO, at 3400 m, supplies air from aloft which is better mixed, some of this difference might stem from the sampling of different sources, MLO perhaps getting a greater percentage of air which has been influenced by passage over land.

Finally, there is a hint that whatever may be causing any divergence between the trend in seasonal amplitudes of $^{13}\delta$ and CO_2 concentration at MLO may also be occurring at BRW and LJO as shown by lower gain factors for $^{13}\delta$ over the same intervals (Table 1). These changes, however, are not significant since the isotopic records are not yet long enough to draw any firm conclusions.

Concluding Remarks

The SIO $^{13}C/^{12}C$ isotopic data have recently received final calibrations and have been analyzed to look for similarities and significant divergences in seasonal amplitude from the CO_2 concentration data. At several northerly sites including BRW and LJO, isotopic changes in seasonal amplitude appear to track the CO_2 amplitude changes quite well over periods of several years, suggesting that a dominant component in the seasonal signal of CO_2 is terrestrial plant activity. At other sites such as MLO in Hawaii, differences between trends in $^{13}\delta$ and CO_2 concentration suggest an oceanic component. At this time, when subtle changes are just becoming apparent in concurrent concentration and $^{13}C/^{12}C$ records of atmospheric CO_2, we hope to be able to continue these measurements, as in the case of concentration data in the early 1980s when an increase in seasonal amplitude first became apparent in our longest records.

Acknowledgments. This work was supported by Grant ATM91-21986 of the National Science Foundation, Grant DE-FG03-95ER62075 of the U.S. Department of Energy and Grant NAGW-2987 of the U.S. National Aeronautics and Space Administration. In addition, through Contract 50RANR100090, NOAA provided for the cost of maintaining our primary standard reference gases used to maintain accuracy in our measurements of atmospheric CO_2. We are grateful to CMDL for providing assistance in our sampling program and for maintenance of our continuous recording instrument at MLO.

References

Bacastow, R.B., Keeling, C.D., Whorf, T.P., Seasonal Amplitude Increase in Atmospheric CO_2 Concentration at Mauna Loa, Hawaii, 1959-1982, *J. Geophys. Res.*, 90, 10,529-10,540, 1985.

Keeling, C.D., Bacastow, R.B., Carter, A.F., Piper, S.C., Whorf, T.P., Heimann, M., Mook, W.G., and Roeloffzen, H., A three-dimensional model of atmospheric CO_2 transport based on observed winds: 1. Analysis of observational data, in *Aspects of Climate Variability in the Pacific and the Western Americas*, edited by D. H. Peterson, Geophysical Monograph, American Geophysical Union, 55,165-236, Washington, DC, 1989.

Keeling, C.D., Whorf, T.P., Wahlen, M., van der Plicht, J., Interannual extremes in the rate of rise of atmospheric carbon dioxide since 1980, *Nature*, 375, 666-670, 1995.

Keeling, C.D., Chin, J.F.S., Whorf, T.P., Increased activity of northern vegetation inferred from atmospheric CO_2 measurements, *Nature*, 382, 146-149, 1996.

Reinsch, C. H., Smoothing by spline functions, *Numerische Mathematik*, 10, 177-183, 1967.

7. Publications by CMDL Staff, 1994-1995

Arends, B.G., G.P.A. Kos, R. Maser, D. Schell, W. Wobrock, P. Winkler, J.A. Ogren, K.J. Noone, A. Hallberg, I.B. Svenningsson, A. Wiedensohler, H.-C. Hansson, A. Berner, I. Solly, and C. Kruisz, Microphysics of clouds at Kleiner Feldberg, in *The Kleiner Feldberg Cloud Experiment 1990,* S. Fuzzi (ed.), Kluwer Academic, Dordrecht, 59-85, 1994.

Austin, J., D.J. Hofmann, N. Butchart, and S.J. Oltmans, Midstratospheric ozone minima in polar regions, *Geophys. Res. Lett., 22(18)*, 2489-2492, 1995.

Bakwin, P.S., P.P. Tans, and P. Novelli, Carbon monoxide budget in the Northern Hemisphere, *Geophys. Res. Lett., 21(6)*, 433-436, 1994.

Bakwin, P.S., P.P. Tans, W. Ussler, III, and E. Quesnell, Measurements of carbon dioxide on a very tall tower, *Tellus,* 47B, 535-549, 1995.

Bergin, M.H., C.I. Davidson, J.E. Dibb, J.L. Jaffrezo, H.D. Kuhns, and S.N. Pandis, A simple model to estimate atmospheric concentrations of aerosol chemical species based on snow core chemistry at Summit, Greenland, *Geophy. Res. Lett., 22(24)*, 3517-3520, 1995.

Bergin, M.H., J.-L. Jaffrezo, C.I. Davidson, J.E. Dibb, S.N Pandis, R. Hillamo, W. Maenhaut, H.D. Kuhns, and T. Makela, The contributions of snow, fog, and dry deposition to the summer flux of anions and cations at Summit, Greenland, *J. Geophys. Res., 100(D8)*, 16, 275-16, 288, 1995.

Bertman, S.B., J.M. Roberts, D.D. Parrish, M.P. Buhr, P.D. Goldan, W.C. Kuster, F.C. Fehsenfeld, S.A. Montzka, and H. Westberg, Evolution of alkyl nitrates with air mass age, *J. Geophys. Res., 100(D11)*, 22, 805-22, 813, 1995.

Bodhaine, B.A., Aerosol absorption measurements at Barrow, Mauna Loa, and the South Pole, *J. Geophys. Res., 100(D5)*, 8967-8975, 1995.

Bodhaine, B.A., and E.G. Dutton, Reply [Comment on "A long term decrease in arctic haze at Barrow, Alaska" by B.A. Bodhaine and E.G. Dutton], *Geophys. Res. Lett., 22(6)*, 741-742, 1995.

Bridgman, H.A., and B.A. Bodhaine, On the frequency of long-range transport events at Point Barrow, Alaska, 1983-1992, *Atmos. Environ., 28(21)*, 3537-3549, 1994.

Buhr, M., D. Parrish, J. Elliot, J. Holloway, J. Carpenter, P. Goldan, W. Kuster, M. Trainer, S. Montzka, S. McKeen, and F. Fehsenfeld, Evaluation of ozone precursor source types using principal component analysis of ambient air measurements in rural Alabama, *J. Geophys. Res., 100(D11)*, 22, 853-22, 860, 1995.

Butler, J.H, The potential role of the ocean in regulating atmospheric CH_3Br, *Geophys. Res. Lett., 21(3)*, 185-188, 1994.

Butler, J.H., Methyl bromide under scrutiny, *Nature, 376*, 469-470, 1995.

Butler, J.H., J.W. Elkins, B.D. Hall, S.A. Montzka, S.O. Cummings, P.J. Fraser, and L.W. Porter, Recent trends in the global atmospheric mixing ratios of halon-1301 and halon -1211, in *Baseline Atmospheric Program Australia 1991*, edited by A.L. Dick and J.L. Gras Department of the Environment, Sport, and Territories Bureau of Meteorology in cooperation with CSIRO Division of Atmospheric Research, Melbourne, Australia, 29-35, 1994.

Cess, R.D., M.H. Zhang, P. Minnis, L. Corsetti, E.G. Dutton, B.W. Forgan, D.P. Garber, W.L. Gates, J.J. Hack, E.F. Harrison, X. Jing, J.T. Kiehl, C.N. Long, J.-J. Morcrette, G.L. Potter, V. Ramanathan, B. Subasilar, C.H. Whitlock, D.F. Young, and Y. Zhou, Absorption of solar radiation by clouds: Observations versus models, *Science, 267*, 496-499, 1995.

Ciais, P., R.J. Francey, P.P. Tans, J.W.C. White, M. Trolier, An analytical error estimate for the ocean and land uptake of CO_2 using $\delta^{13}C$ observations in the atmosphere, *NOAA TM ERL CMDL-8*, 13 pp., 1995.

Ciais, P., P.P. Tans, M. Trolier, J.W.C. White, and R.J. Francey, A large Northern Hemisphere terrestrial CO_2 sink indicated by $^{13}C/^{12}C$ of atmospheric CO_2, *Science,* 269, 1098-1102, 1995.

Ciais, P., P.P. Tans, J.W.C. White, M. Trolier, R.J. Francey, J.A. Berry, D.R. Randall, P.J. Sellers, J.G. Collatz, and D.S. Schimel, Partitioning of ocean and land uptake of CO_2 as inferred by $\delta^{13}C$ measurements from the NOAA Climate Monitoring and Diagnostics Laboratory Global Air Sampling Network, *J. Geophys. Res., 100(D3)*, 5051-5070, 1995.

Clarke, A., and R.C. Schnell, Black carbon variability in the Pacific free troposphere and marine boundary layer, *Abstracts, Proc., 5th Int. Conf. on Carbonaceous Particles in the Atmosphere,* DOE Lawrence Berkley Lab., Berkeley, CA, August 23-26, 1994.

Colvile, R.N., R. Sander, T.W. Choularton, K.N. Bower, D.W.F. Inglis, W. Wobrock, D. Schell, I.B. Svenningsson, A. Wiedensohler, H.-C. Hansson, A. Hallberg, J.A. Ogren, K.J. Noone, M.C. Facchini, S. Fuzzi, G. Orsi, B.G. Arends, W. Winiwarter, T. Schneider, and A. Berner, Computer modeling of clouds at Kleiner Feldberg, in *The Kleiner Feldberg Cloud Experiment 1990,* edited by S. Fuzzi, Kluwer Academic Publishers, Dordrecht, 189-229, 1994.

Conway, T.J., P.P. Tans, L.W. Waterman, K.W. Thoning, D.R. Kitzis, K.A. Masarie, and N. Zhang, Evidence for interannual variability of the carbon cycle from the National Oceanic and Atmospheric Administration/ Climate Monitoring and Diagnostics Laboratory Global Air Sampling Network, *J. Geophys. Res., 99(D11)*, 22, 831-22, 855, 1994.

Crill, P.M., J.G. Butler, D.J. Cooper, and P.C. Novelli, Standard analytical methods for measuring trace gases in the environment, in *Biogenic Trace Gases: Measuring Emissions from Soil and Water, Methods in Ecology,*

edited by P.A. Matson and R.C. Harriss, University Press, Cambridge, U.K., 164-205, 1995.

Dessler, A.E., E.M. Weinstock, E.J. Hintsa, J.G. Anderson, C.R. Webster, R.D. May, J.W. Elkins, and G.S. Dutton, An examination of the total hydrogen budget of the lower stratosphere, *Geophys. Res. Lett., 21(23)*, 2563-2566, 1994.

Dlugokencky, E.J., K.A. Masarie, P.M. Lang, P.P. Tans, L.P. Steele, and E.G. Nisbet, A dramatic decrease in the growth rate of atmospheric methane in the northern hemisphere during 1992, *Geophys. Res. Lett., 21(1)*, 45-48, 1994.

Dlugokencky, E.J., K.A. Masarie, P.M. Lang, P.P. Tans, L.P. Steele, and E.G. Nisbet, Reply to "Comments on 'A dramatic decrease in the growth rate of atmospheric methane in the northern hemisphere during 1992'," *Geophys. Res. Lett., 21(22)*, 2447-2448, 1994.

Dlugokencky, E.J., L.P. Steele, P.M. Lang, and K.A. Masarie, Atmospheric methane at Mauna Loa and Barrow observatories: Presentation and analysis of in situ measurements, *J. Geophys. Res., 100(D11)*, 23,103-23,113, 1995.

Dutton, E.G, Comparison of the solar radiative effects of El Chichon and Mt. Pinatubo long-lived aerosols, Preprints, Eighth Conference on Atmospheric Radiation, Nashville, TN, January 23-28, 1994, American Meteorological Society, Boston, 426-428, 1994.

Dutton, E.G., and S.K. Cox, Tropospheric radiative forcing from El Chichon and Mt. Pinatubo: Theory and observations, *Colorado State University Atmospheric Science Paper No. 586*, Fort Collins, CO, 217 pp., 1995.

Dutton, E.G., P. Reddy, S. Ryan, and J.J. DeLuisi, Features and effects of aerosol optical depth observed at Mauna Loa, Hawaii, 1982-1992, *J. Geophys. Res., 99(34)*, 8295-8306, 1994.

Endres, D., GPS-derived time baffles NOAA researcher, *Ocean Navigator,* 66, 22-24, 1995.

Fan, E.-M., M.L. Goulden, J.W. Munger, B.C. Daube, P.S. Bakwin, S.C. Wofsy, J.S. Amthor, D.R. Fitzjarrald, K.E. Moore, and T.R. Moore, Environmental controls on the photosynthesis and respiration of a boreal lichen woodland: A growing season of whole-ecosystem exchange measurements by eddy correlation, *Oecologia,* 102, 443-452, 1995.

Ferrare, R.A., T.J. McGee, D. Whiteman, J. Burris, M. Owens, J. Butler, R.A. Barnes, F. Schmidlin, W. Komhyr, P.H. Wang, M.P. McCormick, and A.J. Miller, Lidar measurements of stratospheric temperature during STOIC, *J. Geophys. Res.,* 100(D5), 9303-9312, 1995.

Goldan, P.D., W.C. Kuster, F.C. Fehsenfeld, S.A. Montzka, Hydrocarbon measurements in the southeastern United States: The Rural Oxidants in the Southern Environment (ROSE) Program 1990, *J. Geophys. Res., 100(D12)*, 25, 945-25, 963, 1995.

Hallberg, A., K.J. Noone, J.A. Ogren, I.B. Svenningsson, A. Flossmann, A. Wiedensohler, H.-C. Hansson, J. Heintzenberg, T.L. Anderson, B.G. Arends, and R. Maser, Phase partitioning of aerosol particles in clouds at Kleiner Feldberg, in *The Kleiner Feldberg Cloud Experiment 1990,* S. Fuzzi (ed.), Kluwer Academic Publishers, Dordrecht, 107-127, 1994.

Hallberg, A., J.A. Ogren, K.J. Noone, K. Okada, J. Heintzenberg, and I.B. Svenningsson, The influence of aerosol particle composition on cloud droplet formation, in *The Kleiner Feldberg Cloud Experiment 1990,* S. Fuzzi (ed.), Kluwer Academic Publishers, Dordrecht, 153-171, 1994.

Harris, J.M., and J.D.W. Kahl, Analysis of 10-day isentropic flow patterns for Barrow, Alaska: 1985-1992, *J. Geophys. Res., 99(D12)*:25, 845-25, 855, 1994.

Helas, G., J. Lobert, D. Schärffe, L. Schafer, J. Goldammer, J. Baudet, B. Ahoua, A.-L. Ajavon, J.-P. Lacaux, R. Delmas, and M.O. Andreae, Ozone production due to emissions from vegetation burning, *J. Atmos. Chem., 22*, 163-174, 1995.

Hofmann, D.J., S.J. Oltmans, J.A. Lathrop, J.M. Harris, and H. Vömel, Record low ozone at the South Pole in the spring of 1993, *Geophys. Res. Lett., 21(6)*, 421-424, 1994.

Hofmann, D.J., S.J. Oltmans, J.M. Harris, J.A. Lathrop, G.L. Koenig, W.D. Komhyr, R.D. Evans, D.M. Quincy, T. Deshler, and B.J. Johnson, Recovery of stratospheric ozone over the United States in the winter of 1993-1994, *Geophys. Res. Lett., 21(17)*, 1779-1782, 1994.

Hofmann, D.J., S.J. Oltmans, W.D. Komhyr, J.M. Harris, J.A. Lathrop, A.O. Langford, T. Deshler, B.J. Johnson, A. Torres, and W.A Matthews, Ozone loss in the lower stratosphere over the United States in 1992-1993: Evidence for heterogeneous chemistry on the Pinatubo aerosol, *Geophys. Res. Lett., 21(1)*, 65-68, 1994.

Hofmann, D.J., S.J. Oltmans, B.J. Johnson, J.A. Lathrop, J.M. Harris, and H. Vömel, Recovery of ozone in the lower stratosphere at the South Pole during the spring of 1994, *Geophys. Res. Lett., 22(18)*, 2493-2496, 1995.

Hofmann, D., P. Bonasoni, M. DeMaziere, F. Evangelisti, G. Giovanelli, A. Goldman, F. Goutail, J. Harder, R. Jakoubek, P. Johnston, J. Kerr, W. A. Matthews, T. McElroy, R. McKenzie, G. Mount, U. Platt, J.-P. Pommereau, A. Sarkissian, P. Simon, S. Solomon, J. Stutz, A. Thomas, M. VanRoozendael, and E. Wu, Intercomparison of UV/visible spectrometers for measurements of stratospheric NO_2 for the Network for the Detection of Stratospheric Change, *J. Geophys. Res., 100(D8)*, 16, 765-16, 791, 1995.

Hurst, D.F., D.W.T. Griffith, and G.D.Cook, Trace gas emissions from biomass burning in tropical Australian savannas, *J. Geophys. Res., 99(D8)*, 16, 441-16, 456, 1994.

Jaffe, D.A., R.E. Honrath, D. Furness, T.J. Conway, E. Dlugokencky, and L.P. Steele, A determination of the CH_4, NO_x, and CO_2 emissions from the Prudoe Bay, Alaska oil development, *J. Atmos. Chem., 20*, 213-227, 1995.

Kerr, J.B., H. Fast, C.T. McElroy, S.J. Oltmans, J.A. Lathrop, E. Kyro, A. Paukkunen, H. Claude, U. Köhler, C.R. Sreedharan, T. Takao, and Y. Tsukagoshi, The

1991 WMO international ozonesonde intercomparison at Vanscoy, Canada, *Atmos. Ocean, 32(4)*, 685-716, 1994.

Komhyr, W.D., R.D. Grass, R.D. Evans, R.K. Leonard, D.M. Quincy, D.J. Hofmann, and G.L. Koenig, Unprecedented 1993 ozone decrease over the United States from Dobson spectrophotometer observations, *Geophys. Res. Lett., 21(3),* 201-204, 1994.

Komhyr, W.D., R.A. Barnes, G.B. Brothers, J.A. Lathrop, and D.P. Opperman, Electrochemical concentration cell ozonesonde performance evaluation during STOIC 1989, *J. Geophys. Res., 100(D5)*, 9273-9282, 1995.

Komhyr, W.D., B.J. Connor, I.S. McDermid, T.J. McGee, A.D. Parrish, and J.J. Margitan, Comparison of STOIC 1989 ground-based lidar, microwave spectrometer, and Dobson spectrophotometer Umkehr ozone profiles with ozone profiles from balloon-borne electrochemical concentration cell ozonesondes, *J. Geophys. Res., 100(D5)*, 9273-9282, 1995.

Lang, P.M., E.J. Dlugokencky, K.A. Masarie, and L.P. Steele, Atmospheric methane data for 1989-1992 from the NOAA/CMDL global cooperative air sampling network, *NOAA TM ERL CMDL-7*, 49 pp, 1994.

Lobert, J.M., J.H. Butler, T.J. Baring, S.M. Montzka, R.C. Myers, and J.W. Elkins, OAXTC 92 Ocean/Atmosphere Exchange of Trace Compounds 1992: Oceanic measurements of HCFC-22, CFC-11, CFC-12, CFC-113, CH_3CCl_3, CCl_4, and N_2O in the marine air and surface waters of the west Pacific Ocean (August 3-October 21, 1992), *NOAA TM ERL CMDL-9*, 43 pp., NOAA Environmental Research Laboratories, Boulder, CO 1995.

Lobert, J.M., J.H. Butler, S.A. Montzka, L.S. Geller, R.C. Myers, and J.W. Elkins, A net sink for atmospheric CH_3Br in the East Pacific Ocean, *Science, 267*, 1002-1005, 1995.

Margitan, J.J., R.A. Barnes, G.B. Brothers, J. Butler, J. Burris, B.J. Connor, R.A. Ferrare, J.B. Kerr, W.D. Komhyr, M.P. McCormick, I.S. McDermid, C.T. McElroy, T.J. McGee, A.J. Miller, M. Owens, A.D. Parrish, C.L. Parsons, A.L. Torres, J.J. Tsou, T.D. Walsh, and D. Whiteman, Stratospheric ozone intercomparison campaign (STOIC) 1989: Overview, *J. Geophys. Res., 100(D5)*, 9193-9207, 1995.

Masarie, K.A., and P.P. Tans, Extension and integration of atmospheric carbon dioxide data into a globally consistent measurement record, *J. Geophys. Res., 100(D6)*, 11, 593-11, 610, 1995.

Montzka, S.A., R.C. Myers, J.H. Butler, and J.W. Elkins, Early trends in the global tropospheric abundance of hydrochlorofluorocarbon-141b and 142b, *Geophys. Res. Lett., 21(23)*, 2483-2486, 1994.

Montzka, S.A., R.C. Myers, J.H. Butler, J.W. Elkins, and S.O. Cummings, Atmospheric measurements of HCFC-22 at the South Pole, *Ant. J., 28(5)*, 267-269, 1994.

Montzka, S.A., M.R. Nowick, R.C. Myers, J.W. Elkins, J.H. Butler, S.O. Cummings, P.J. Fraser, and L.W. Porter, NOAA-CMDL chlorodifluoromethane (HCFC-22) observations at Cape Grim, in *Baseline Atmospheric Program Australia 1991*, edited by A.L. Dick and J.L. Gras, Department of the Environment, Sport, and Territories Bureau of Meteorology in cooperation with CSIRO Division of Atmospheric Reseach, Melbourne, Australia, 25-28, 1994.

Montzka, S.A., M. Trainer, W.M. Angevine, and F.C. Fehsenfeld, Measurements of 3-methyl furan, methyl vinyl ketone, and methacrolein at a rural forested site in the southeastern United States, *J. Geophys. Res., 100(D6)*, 11, 393-11, 401, 1995.

Moody, J.L., S.J. Oltmans, H. Levy II, and J.T. Merrill, Transport climatology of tropospheric ozone: Bermuda, 1988-1991, *J. Geophys. Res., 100(D4)*, 7179-7194, 1995.

Nemesure, S., R.D. Cess, E.G. Dutton, J.J. DeLuisi, Z. Li, and H.G. Leighton, Impact of clouds on the shortwave radiation budget of the surface—atmosphere system for snow-covered surfaces, *J. Climate, 7(4)*, 579-585, 1994.

Novelli, P.C., and R.M. Rosson (eds.), Report of the WMO meeting of experts on global carbon monoxide measurements, World Meteorological Organization, *Global Atmos. Watch No. 98*, WMO/TD-NO. 645, Geneva, Switzerland, 82 pp, 1994.

Novelli, P.C., K.A. Masarie, P.P. Tans, and P.M. Lang, Recent changes in atmospheric carbon monoxide, *Science, 263*, 1587-1590, 1994.

Novelli, P.C., J.E. Collins, Jr., R.C. Myers, G.W. Sachse, and H.E. Scheel, Reevaluation of the NOAA/CMDL carbon monoxide reference scale and comparisons with CO reference gases at NASA-Langley and the Fraunhofer Institute, *J. Geophys. Res., 99(D6)*, 12, 833-12, 839, 1994.

Novelli, P.C., and R.M. Rosson (eds.), Report of the meeting of experts on carbon monoxide, Boulder, Colorado, February 1994. *WMO Report 98*, Geneva, Switzerland, 78 pp., 1995.

Novelli, P.C., T.C. Conway, E.J. Dlugokencky, and P.P. Tans, Recent changes in atmospheric carbon dioxide, methane and carbon monoxide, and the implications of these changes on global climate processes, *World Meteorol. Bull., 44*, 32-37, 1995.

Ogren, J.A., A systematic approach to in situ observations of aerosol properties, In *Aerosol Forcing of Climate,* R.J. Charlson and J. Heintzenberg (eds.), Wiley & Sons, New York, 215-226, 1995.

Oltmans, S.J., and H. Levy, II, Surface ozone measurements from a global network, *Atmos. Environ., 28(1)*, 9-24, 1994.

Oltmans, S.J., and D.J. Hofmann, Increase in lower-stratospheric water vapor at a mid-latitude Northern Hemisphere site from 1981 to 1994, *Nature, 374*, 146-149, 1995.

Parungo, F., Z. Li, X. Li, D. Yang, and J. Harris, Gobi dust storms and The Great Green Wall, *Geophys. Res. Lett., 21(11)*, 999-1002, 1994.

Parungo, F., Y., Kim, C.-J. Zhu, J. Harris, R. Schnell, X.-S. Li, D.-Z. Yang, X.-M. Fang, P. Yan, X. Yu, M.-Y. Zhou, Z. Chen, F.-L. Qian, and K. Park, Asian dust

storms and their effects on radiation and climate, Part I, *Science and Technology Corporation Technical Report 2906*, Boulder, CO, 56 pp., 1995.

Penner, J.E., R.J. Charlson, J.M. Hales, N.S. Laulainen, R. Leifer, T. Novakov, J. Ogren, L.F. Radke, S.E. Schwartz, and L. Travis, Quantifying and minimizing uncertainty of climate forcing by anthropogenic aerosols, *Bull. Am. Meteorol. Soc., 75(3)*, 375-400, 1994.

Peterson, J.T., and R.M. Rosson (eds.), *Climate Monitoring and Diagnostics Laboratory No. 22: Summary Report 1993*, NOAA Environmental Research Laboratories, Boulder, CO, 152 pp, 1994.

Prospero, J.M., R. Schmitt, E. Cuevas, D.L. Savoie, W.C. Graustein, K.K. Turekian, A. Volz-Thomas, A. Diaz, S.J. Oltmans, H. Levy II, Temporal variability of summer-time ozone and aerosols in the free troposphere over the eastern North Atlantic, *Geophys. Res. Lett., 22(21)*, 2925-2928, 1995.

Reagan, J., K. Thome, B. Herman, R. Stone, J. DeLuisi, and J. Snider, A comparison of columnar water vapor retrievals obtained with near-IR solar radiometer and microwave radiometer measurements, *J. Appl. Meteorol., 34*, 1384-1391, 1995.

Ryan, S.C., Quiescent outgassing of Mauna Loa Volcano 1958-1994, in *Mauna Loa Revealed: Structure, Composition, History, and Hazards*, *Geophysical Monograph 92*, edited by J.M. Rhodes and J.P. Lockwood, American Geophysical Union, Washington, D.C., 95-115, 1995.

Salawitch, R.J., S.C. Wofsy, P.O. Wennberg, R.C. Cohen, J.G. Anderson, D.W. Fahey, R.S. Gao, E.R. Keim, E.L. Woodbridge, R.M. Stimpfle, J.P. Koplow, D.W. Kohn, C.R. Webster, R.D. May, L. Pfister, E.W. Gottlieb, H.A. Michelsen, G.K. Yue, J.C. Wilson, C.A. Brock, H.H. Jonsson, J.E. Dye, D. Baumgardner, M.H Proffitt, M. Loewenstein, J.R. Podolske, J.W. Elkins, G.S. Dutton, E.J. Hintsa, A.E. Dessler, E.M. Weinstock, K.K. Kelly, K.A. Boering, B.C. Daube, K.R. Chan, and S.W. Bowen, The distribution of hydrogen, nitrogen, and chlorine radicals in the lower stratosphere: Implications for changes in O_3 due to emission of NO_y from supersonic aircraft, *Geophys. Res. Lett., 21(23)*, 2547-2550, 1994.

Schmidt, E.O., R.F. Arduini, B.A. Wielicki, R.S. Stone, and S.-C. Tsay, Considerations for modeling thin cirrus effects via brightness temperature differences, *J. Appl. Meteorol., 34(2)*, 447-459, 1995.

Schnell, R.C., Are biological ice nuclei important in drought processes: Past thoughts, present perspectives, *Pro., Biological Ice Nucleation*, Laramie, Wyoming, August 4-6, 1993, University of Wyoming, Laramie, 30 pp., 1994.

Schnell, R.C., Carbon cycle species and Asian dust at Mauna Loa Observatory in relation to air mass origins, *Proc., Tsukuba Global Carbon Cycle Workshop*, Tsuka, Japan, 54-61, February 1-3, 1995.

Schnell, R.C., Recent Chinese dust storms observed at Mauna Loa Observatory, Hawaii, *Proc., WMO-IGAC Conf. on the Measurement and Assessment of Atmospheric Composition Change*, Beijing, China, 218-220, October 9-24, 1995.

Schnell, R.C., D.T. Kuniyuki, B.A. Bodhaine, and A.D.A. Hansen, The dust component of aerosol light absorption measured at Mauna Loa Observatory, Abstracts, *Proc., 5th Int. Conf. on Carbonaceous Particles in the Atmosphere*, DOE Lawrence Berkley Lab., Berkeley, CA, August 23-26, 1994.

Stone, R.S., E.G. Dutton, and J.R. Key, Properties and decay of Pinatubo aerosols in polar regions compared with tropical observations, Preprints, Eighth Conference on Atmospheric Radiation, Nashville, TN, January 23-28, 1994, American Meteorological Society, Boston, 432-434, 1994.

Svenningsson, B., H.-C. Hansson, A. Wiedensohler, K. Noone, J. Ogren, A. Hallberg, and R. Colville, Hygroscopic growth of aerosol particles and its influence on nucleation scavenging in cloud: Experimental results from Kleiner Feldberg, in *The Kleiner Feldberg Cloud Experiment 1990,* edited by S. Fuzzi, Kluwer Academic Publishers, Dordrecht, 129-152, 1994.

Tans, P.P., and P.S. Bakwin, Climate change and carbon dioxide forever, *Ambio, 24*, 376-378, 1995.

Thoning, K.W., T.J. Conway, N. Zhang, D. Kitzis, Analysis system for measurement of CO_2 mixing ratios in flask air samples, *J. Atmos. Ocean. Tech., 12(6)*, 1349-1356, 1995.

Tuck, A.F., D.W. Fahey, M. Lowenstein, J.R. Podolske, K.K. Kelly, S.J. Hovde, D.M. Murphy, and J.W. Elkins, Spread of denitrification from 1987 Antarctic and 1988-1989 Arctic stratospheric vortices, *J. Geophys. Res., 99(D10)*, 20, 573-20, 583, 1994.

Vömel, H., D.J. Hofmann, S.J. Oltmans, and J.M. Harris, Evidence for midwinter chemical ozone destruction over Antarctica, *Geophys. Res. Lett., 22(17)*, 2381-2384, 1995.

Vömel, H., S.J. Oltmans, D. Kley, and P.J. Crutzen, New evidence for the stratospheric dehydration mechanism in the equatorial Pacific, *Geophys. Res. Lett., 22(21)*, 3235-3238, 1995.

Vömel, H., S.J. Oltmans, D.J. Hofmann, T. Deshler, and J.M. Rosen, The evolution of the dehydration in the Antarctic stratospheric vortex. *J. Geophys. Res., 100(D7)*, 13, 919-13, 926, 1995.

Vömel, H., S.J. Oltmans, D. Kley, and P.J. Crutzen. New evidence for the stratospheric dehydration mechanism in the equatorial Pacific. *Geophys. Res. Lett. 22(21)*:3235-3238 (1995).

Waugh, D.W., R.A. Plumb, P.A. Newman, M.R. Schoeberl, L.R. Lait, M. Loewenstein, J.R. Podolske, J.W. Elkins, and K.R. Chan, Fine-scale, poleward transport of tropical air during AASE 2, *Geophys. Res. Lett., 21(23)*, 2603-2606, 1994.

Wobrock, W., D. Schell, R. Maser, W. Jaeschke, H.-W. Georgii, W. Wieprecht, B.G. Arends, J.J. Mols, G.P.A. Kos, S. Fuzzi, M.C. Facchini, G. Orsi, A. Berner, I.

Solly, C. Kruisz, I.B. Svenningsson, A. Wiedensohler, H.-C. Hansson, J.A. Ogren, K.J. Noone, A. Hallberg, S. Pahl, T. Schneider, P. Winkler, W. Winiwarter, R.N. Colvile, T.W. Chourlarton, A.I. Flossman, and S. Borrmann, The Kleiner Feldberg cloud experiment 1990, An Overview, in *The Kleiner Feldberg Cloud Experiment 1990,* edited by S. Fuzzi, Kluwer Academic, Dordrecht, 3-35, 1994.

Wofsy, S.C., K.A. Boering, B.C. Daube, Jr., M.B. McElroy, M. Loewenstein, J.R. Podolske, J.W. Elkins, G.S. Dutton, and D.W. Fahey, Vertical transport rates in the stratosphere in 1993 from observations of CO_2, N_2O, and CH_4, *Geophys. Res. Lett., 21(23)*, 2571-2574, 1994.

Woodbridge, E.L., J.W. Elkins, D.W. Fahey, L.E. Heidt, S. Solomon, T.J. Baring, T.M. Gilpin, W.H. Pollock, S.M. Schauffler, E.L. Atlas, M. Lowenstein, J.R. Podolske, C.R. Webster, R.D. May, J.M. Gilligan, S.A. Montzka, K.A. Boering, and R.J. Salawitch, Estimates of total organic and inorganic chlorine in the lower stratosphere from in situ and flask measurements during AASE II, *J. Geophys. Res., 100(D2)*, 3057-3064, 1995.